THEORETICAL AND EXPERIMENTAL INVESTIGATION OF A CDI INJECTION SYSTEM OPERATING ON NEAT RAPESEED OIL - FEASIBILITY AND OPERATIONAL STUDIES

Michal Tadeusz Bialkowski

Submitted for the degree of philosophy on completion of research in the School of Engineering and Physical Sciences, Chemical Engineering, Heriot-Watt University

September 2009

Abstract

This thesis presents the work done within the PhD research project focusing on the utilisation of plant oils in Common Rail (CR) diesel engines. The work scope included fundamental experimental studies of rapeseed oil (RSO) in comparison to diesel fuel, the feasibility analysis of diesel substitution with various plant oils, the definition and implementation of modifications of a common rail injection system and future work recommendations of possible changes to the injection system.

It was recognised that neat plant oils can be considered as an alternative substitute for diesel fuel offering a natural way to balance the CO_2 emissions. However, due to the differences between diesel and plant oils, such as density, viscosity and surface tension, the direct application of plant oils in common rail diesel engines could cause degradation of the injection process and in turn adversely affect the diesel engine's performance. RSO was chosen to perform the spray characterisation studies at various injection pressures and oil temperatures under conditions similar to the operation of the common rail engine. High speed camera, Phase Doppler Anemometry and Malvern laser techniques were used to study spray penetration length and cone angle of RSO in comparison to diesel. To study the internal flow inside the CR injector the acoustic emission technique was applied.

It was found that for oil temperatures below 40°C the RSO viscosity, density and surface tension are higher in comparison to diesel, therefore at injection pressures around 37.50 MPa the RSO spray is not fully developed. The spray penetration and cone angle at these spray conditions exhibit significant spray deterioration.

In addition to the lab experiments, KIVA code simulated RSO sprays under CR conditions. The KH-RT and RD breakup models were successfully applied to simulate the non-evaporating sprays corresponding to the experimental spray tests and finally to predict

real in-cylinder injection conditions. Numerical results showed acceptable agreement with the experimental data of RSO penetration.

Based on experimental and numerical results it was concluded that elevated temperature and injection pressure could be the efficient measures to overcome operational obstacles when using RSO in the CR diesel engine. A series of modifications of low- and high-pressure loops was performed and experimentally assessed throughout the engine tests. The results revealed that the modifications allowed to run the engine at the power and emission outputs very close to diesel operation. However, more fundamental changes were suggested as future work to ensure efficient and trouble-free long-term operation. It is believed that these changed should be applied to meet Euro IV and V requirements.

In memory of my Grandparents: Maria and Tadeusz,
to whom I am owe so much.

Acknowledgements

Completing my PhD was truly a marathon event and I would not have been able to complete this journey without the aid and support of countless people over the past years. However, it is not possible for me to list all the people who encouraged and helped me during my studies and research, but they will be always in my memory.

Foremost, I would like to thank my supervisors Dr. Turgay Pekdemir and Prof. Robert L. Reuben from Heriot-Watt University and Prof. Markus Brautsch for their supervision, guidance, encouragement and friendly relationship over the entire period of my Ph.D. Especially, I want to thank my prime supervisor Dr. Turgay Pekdemir for his invaluable support and guidance, which made my thesis work possible. I am very grateful for his patience, motivation, help in correcting the thesis. I warmly thank Dr. David Towers for his valuable and kind advice and for providing the guidance for the PDA system.

Also, I want to thank Prof. Guenther Elsbett and all members of the "Eslbett Company" for allowing me to carry out the experimental work in their workshop, providing me with the injection stand and the essential parts of a common rail injection system. I thank them for an excellent, inspiring working atmosphere and deep and sincere care during my work in Thalmaessing.

I want to thank present and past members of the Heriot-Watt labs and the workshop for sharing their knowledge, manufacturing of the experimental rigs and providing a great work environment. I take this opportunity to express my appreciation to Mrs. A. Blyth, Mrs. M. Thomson, Mr. A. Thomas and all those friends and colleagues who made these years very memorable.

I owe massive gratitude to two great men; Dr.Markus Gross and Dr. Krzysztof Nowak for their precious contributions and continuous encouragement as well as professional solidarity. Without your friendship, support and clever ideas my work would be much more difficult. Finally, I thank my Family for building my confidence and the drive for pursuing my PhD. Without them I would never have made it this far.

Contents

List of Symbols

α	The angle between the beams, see equation (2.4.1)
$\bar{r}$	The number averaged drop radius of a certain distribution., see equation (2.6.3)
λ	The laser wavelength, see equation (2.4.1)
Λ_{KH}	The wavelength of KH model, see equation (2.6.7)
Λ_{RT}	The wavelength of RT model, see equation (2.6.19)
μ	The viscosity of liquid phase [kg/ms], see equation (2.6.2)
μ	The viscosity, [kg/ms], see equation (2.6.12)
μ_l	The liquid viscosity, see equation (2.6.7)
ν	The relative velocity of the liquid phase [m/s], see equation (2.6.1)
Ω_{KH}	The maximum growth of the wavelength in the Kelvin-Helmholtz breakup analogy, see equation (2.6.12)
ρ	The density of gas phase [kg/m^3], see equation (2.6.1)
ρ	The gas density, see equation (2.6.7)
ρ_p	The fuel density, see equation (5.2.1)
ρ_D	The fuel vapour diffusivity, [m/s], see equation (2.6.32)
ρ_d	The liquid density, [kg/m^3], see equation (2.6.32)
ρ_g	Gas density, [kg/m^3], see equation (2.6.25)
ρ_l	Injected fuel density, [kg/m^3], see equation (2.6.25)
ρ_l	The liquid density, see equation (2.6.7)
σ	The liquid surface tension [N/m], see equation (2.6.1)
σ_ε	The constant=1.0/1.3, see equation (2.6.29)
σ_k	The constant=1.0, see equation (2.6.29)
τ_{KH}	The breakup time of the Kelvin-Helmholtz breakup analogy, see equation (2.6.13)
τ_{RT}	The breakup time of the Rayleight-Taylor breakup analogy, see equation (2.6.19)
ε	The ε - turbulence, see equation (2.6.26)
t_D	The Doppler period, see equation (2.4.2)

t_{shift} The period between the zero crossing of the signals between detectors, see equation (2.4.2)

n The molar concentration, [mol/dm^3], see equation (2.6.29)

y The length scale, [m], see equation (2.6.29)

a The major semi-axis of the ellipsoidal cross section of the oblate spheroid, see equation (2.6.22)

b Factor, see equation (2.6.4)

B_1 An adjustable constant called the breakup constant, see equation (2.6.13)

B_1 The breakup constant of KH model and equal to 60 according to Su [384], see equation (2.6.23)

c Factor, see equation (2.6.4)

C_1, C_2 Constants of order unity, see equation (2.6.25)

C_3 The RT breakup constant, see equation (2.6.19)

C_τ The coefficient related with breakup time, see equation (2.6.19)

C_d Dimensionless constant, see equation (2.6.7)

C_F Dimensionless constant, see equation (2.6.7)

C_k Dimensionless constant, see equation (2.6.7)

C_s The constant=1.5, see equation (2.6.29)

C_μ The constant=0.09, see equation (2.6.29)

C_τ Defined as 1.0, see equation (2.6.19)

$C_{\varepsilon 1}$ The constant=1.44, see equation (2.6.29)

$C_{\varepsilon 2}$ The constant=1.92, see equation (2.6.29)

$C_{\varepsilon 3}$ The constant=-1.0, see equation (2.6.29)

C_{RT} An adjustable constant according to the nozzle geometry as stated by Patterson and Reitz [312], see equation (2.6.19)

D Diffusion, see equation (2.6.29)

d The droplet diameter,[m], see equation (2.6.1)

d_0 The diameter of the nozzle,[m], see equation (2.6.23)

F The force, [N], see equation (2.6.4)

FL The focal length of the Fourier-transform lens, see equation (2.4.3)

K The constant, see equation (2.6.1)

K The liquid-gas density ratio, see equation (2.6.21)

k The k - turbulence kinetic energy, see equation (2.6.26)

L_b The breakup length, [m], see equation (2.6.23)

m Factor, see equation (2.6.4)

N The liquid-gas viscosity ratio, see equation (2.6.21)

Nu_d The Nusselt number, see equation (2.6.30)

On_f Ohnesorge number of fuel spray, see equation (2.6.2)

p Ambient pressure (back pressure), see equation (5.2.1)

p_{inj} The injection pressure, see equation (5.2.1)

$P_{k,\varepsilon}$ The production of k- and ε turbulence, see equation (2.6.29)

Pr_d The Prandtl number of he droplet, see equation (2.6.30)

r The drop radius (calculated from a spray model), see equation (2.6.3)

r The droplet radius, see equation (2.6.7)

r The radius of a parent droplet, see equation (2.6.12)

r The radius of droplet,[m], see equation (2.6.22)

r_c The critical radius, see equation (2.6.14)

r_d Droplet radius, [m], see equation (2.6.25)

r_n The new droplet radius, [m], see equation (2.6.14)

r(i) The distance of the detector element *i* from the centre of the detector, see equation (2.4.3)

Re_d The Reynolds number of the droplet, see equation (2.6.30)

Re_f The Reynolds number of fuel spray, see equation (2.6.9)

Sh_d The Sherwood number, see equation (2.6.31)

T The Taylor parameter, see equation (2.6.10)

t Time, [s], see equation (2.6.4)

T_f The fluid temperature, see equation (2.6.32)

t_{bag} Lifetime (breakup) time for bag-type disintegration, [s], see equation (2.6.25)

t_{bag} Lifetime (breakup) time for droplet stripping, [s], see equation (2.6.25)

U The velocity component normal to the fringes and in the plane of the beams, see equation (2.4.1)

u The relative velocity between the gas and droplet, see equation (2.6.7)

u_r The relative velocity between a droplet (parent or "child") and gas, see equation (2.6.12)

v_{rel} Droplet relative velocity, [m/s], see equation (2.6.25)

We_f Weber number of fuel spray, see equation (2.6.1)

x The cross section, [m], see equation (2.6.4)

x The displacement of the equator of the droplet from its equilibrium position, see equation (2.6.7)

x(i) The particle size representing the i^{th} size class, see equation (2.4.3)

y The distance from the centre of mass to its equator of the deforming half-drop, see equation (2.6.21)

y_{fv} The fuel vapour mass fraction of the fluid, see equation (2.6.32)

Z The Ohnesorge parameter, see equation (2.6.9)

Glossary

ASTM - American Society for Testing and Materials

BNC - Bayonet Neill-Concelman connector

BTDC - Before top dead centre

CDI - Common Rail Injection

CAP - Common European Agriculture Policy

CR - Common Rail

DI - Direct injection

HC - Hydrocarbons

HHV - Higher heating value

IDI - Indirect injection

EC - European Community

EU - European Union

GATT - The General Agreement on Tariffs and Trade

LEBEN - Large European Biomass Energy Network

PDA - Phase Doppler Anemometry

RSO - Rapeseed oil

SO - Standard Oil

TIFF - Tagged image format file

List of Figures

List of Tables

Published papers

1. Bialkowski M.T., Brautsch M., Pekdemir T., Elsbett G.“An approach to enable common rail engines to operate on plant oils”. 29^{th} International Scientific Conference on Internal Combustion Engines KONES 2003, Conference Proceedings 2003, Paper no. 303.

2. Bialkowski M.T., Pekdemir T., Towers D.P., Reuben R., Brautsch M., Elsbett G. “Effect of fuel temperature and ambient pressure on a common rail rapeseed oil spray”. 30^{th} International Scientific Conference on Internal Combustion Engines KONES 2004, vol. 11, no. 1-2, pp.53

3. M. T. Bialkowski, T. Pekdemir, M. Brautsch, D. Towers, and G. Elsbett, “Experimental analysis of rapeseed oil atomisation characteristics”. Photon Proceedings 2004,6-9, September 2004, Glasgow, 2004.

4. Bialkowski M.T., Pekdemir T., Brautsch M., Towers D., Elsbett G.; “Phase Doppler anemometry measurements of a dense rapeseed oil spray”. PTNSS Proceedings, vol. 1, 2005

5. Bialkowski M.T., Pekdemir T., R.Reuben, Brautsch M., Towers D., Elsbett G.; “Preliminary approach towards a CDI system modification operating on neat rapeseed oil”, 31^{st} International Scientific Conference on Internal Combustion Engines KONES 2005, vol. 12, no. 1-2, pp.31

Chapter 1

Introduction

Omnia mutantur, nos et mutamur in illis

Research study on plant oils used as a fuel in diesel engines implies a more descriptive approach and may frequently be considered not only purely as a technical problem. Some of the "technicalities" are strongly related to the non-engineering aspects extending beyond the work of mechanical professionals. These are usually present in various fields investigating such a wide spectrum of interest as alternative fuels. Often the idea of substituting conventional diesel fuel by plant oils brings out the question of the compatability of the engines, the feasibility of the process, its impact on customer driving habits, the overall economy, and finally promotes a question of the technical reliability of the recommended modification to engine systems. One can recognise that the already existing technology does not imply easy application.

This chapter outlines the main reason for the interest in plant oil as diesel substitution in accordance to the foreseen situation of diesel technology and the fuel market. A short analysis presents a potential of combined Common Rail (CR) technology with plant oils as a possible solution for upcoming challenges. The chapter also defines research objectives and describes the research stages followed to fulfil the presented objectives.

1.1 Coerced turn into environment?

The recent petroleum situation, rapidly increasing prices and uncertainties concerning petroleum availability let the scientists work on alternative fuel sources, nevertheless alternative but even cheaper and cleaner than the available ones. Hence, "green" fuel studies become current among various fields frequently overlapping issues of sustainable growth,

small communities development and long term environmental concerns. Together with the rapid development of diesel engines technology combined with the strong investigation of alternative energy sources, the last two decades reflect a significant scientific interest in using plant oils as an environmental friendly and technically balanced fuel substitution. Most of the recent studies were focused on well recognised bio-diesel composites as the result of chemical processing of plant oils or animal fat as well as the slowly growing interest in using neat plant oils. These two main streams resulted in a number of academic and technical publications and technical implementations. However, there is still a need for more research and faster engineering applications. Rapid growth of diesel cars, already in the market, and stronger public environmental concern become solid arguments to carry on such work.

The strongest impulse to investigate the application of neat plant oils as a diesel substitute was given by the crisis in supplying mineral oil as the major source for energy in the 70's, and again by the Gulf war in 1991, and present conflicts in oil rich areas. Also the current unstable political situation in the Middle and Far East and pessimistic forecasts of crude oil resources promote strong scientific interest.

There is little doubt that in the international debate on the environment, the anthropogenic greenhouse effect and the hazard relating to it have been for years a very important, if not the dominant topic. One global way of slowing the increase in anthropogenic climate gas emissions is the intensified use of fuels derived from biomass [356; 367], since it offers numerous environmental benefits. However such benefits are accompanied by a series of possible ecological drawbacks. Generally, from an ecological point of view, a necessity should be that if biomass is used for energy purposes, then ecological advantages must exceed the disadvantages or negative impacts on the natural environment and human life. Very often such assumptions are contradicting in expectations of the local business groups and lobbies. Many bio-energy projects are technically feasible and ecologically justified, but investment does not take place because other forms of energy are still more cost-competitive. Application of plant oils has suffered from similar obstacles and until now even ready-to-use technologies are only known locally.

According to the IEA there will be a need for all alternative fuels for the transport sector with special interest in the modern diesel passenger cars [10]. The European Commission (EC) proposes in the FORUM-scenario a 12% market share for bio-fuels by the year 2020 [9]. Concerning environmental damage, the transport sector has a clear

responsibility, whereas within the last 10 years its part in global warming potential has increased from less than 20% to more than 25% [225; 348]. Now bigger than those of the domestic and industrial sector, its contribution to acid gas pollution constitutes 75% of the total emissions. As one reaction the EC has developed a Directive on the Quality of Fuels [11] with new environmentally driven fuel specifications. Also, the European Car Manufacturer's Association (ACEA) has proposed, and the European Union has accepted, a Voluntary Commitment pledging to reduce greenhouse emissions "per vehicle" by 25% by the year 2008. This implies a 33% improvement in new vehicle fuel economy or a drastic contribution of bio-fuels. Furthermore, the EC has invited policy measures, which implies future increase in the stringency of emission standards (especially for particulates and NO_x), which are commonly known as Euro IV and V [1]. The European action to reduce the greenhouse emission and improve fuel economy is not isolated. In Japan, the national government has established a series of weight-class [2] fuel economy standards that require approximately a 23% improvement in the fuel economy of the petrol light-duty vehicles by 2010 (similar to these approved by the European Commission). The diesel requirements would imply a 14% fuel economy improvement (11 km/l vs. 10 km/l) compared to the 1995 fleet [14].

European car makers have a range of technologies available to them, which are quite similar to these of the Japanese carmakers [284; 328], although they have more experience with diesel technologies. While Japan is a leader in petrol direct injection technology, several European carmakers have pioneered new diesel engine systems. Lately becoming popular are the CR direct injection diesel engine systems, which are the best candidates to satisfy the environmental and fuel economy concerns presented in the FORUM-scenario as well as in the demands of the EC and the ACEA. Nevertheless, diesel technology's role in the current market depends on fuel prices of crude oil, market trends, car taxes and wealth of the society. Diesel sales in Europe are high, about a 28% market share [15] and the ACEA appears to expect to expand this share significantly in next few decades. However, the high diesel share is due in part to diesel/petrol tax differences in some selected European countries (e.g. in the UK diesel has been more expensive than petrol on 10$ on

[1] European emission standards define the acceptable limits for exhaust emissions of new vehicles sold in EU member states. The emission standards are defined in a series of European Union directives staging the progressive introduction of increasingly stringent standards. Emission standards for passenger cars are in g/km: Euro IV: CO:0.5, NO_x:0.25, HC+NO_x:0.3, PM:0.025; Euro V: CO:0.5, NO_x:0.18, HC+NO_x:0.23, PM:0.005

[2] weight-class is a car classification related to its maximum weight

average), yielding diesel prices averaging even 23% lower [15]. With lower fuel prices in those selected countries, higher efficiency, and the tendency of longer distance drivers preferentially selecting diesel, the average diesel car is driven 40-70% more than the average petrol car in Europe (e.g. Germany) [19]. The portion of this higher mileage because of the first two causes-driving stimulated by diesel lower per kilometre fuel cost should be factored into calculations of diesel environmental advantage over petrol. Increased driving tied to lower fuel prices, coupled with reduced fuel tax revenues from higher diesel shares could lead to pressure on European governments to raise diesel prices to be roughly equivalent to petrol. Such price increases would likely slow any move towards increased diesel market share and this could easily be improved by drifting toward using plant oils.

Emission standards represent only a moderate challenge to new (both diesel and petrol) technologies, but this could change soon. New European Phase IV emissions standards are likely to create no constraints on engine technology aside from some moderate development requirements for control systems in lean burn (e.g., direct injection petrol and diesel engines) for NO_x emissions and in diesel engines for particulate emissions. However, there remains potential for more stringent Phase V standards, which can be only met by CR engines. The engine technology shift that ACEA contemplates, to 90% direct injected engines [12], carries with it the potential to significantly increase emissions of ultra-fine particulates, especially when measured by the number of particles. Some scientists have become quite concerned about particles in the tiny size range emitted by direct injection diesel and petrol engines [261], and continued research into their health effects and role of it in formation of urban pollution.

Finally, it needs to be mentioned that both the European Union and Japan set their diesel standards well above their petrol standards for both NO_x and particulates (PM). In contrast, the US has set its Tier II diesel standards [3]. The differences among the three sets of standards appear likely to impact the potential of the three markets to improve fleet fuel economy and market preferences. In particular, the stringent US requirements

[3]The first federal standards for new nonroad (or off-road) diesel engines were adopted in 1994 for engines over 37 kW (50 hp), to be phased-in from 1996 to 2000. In 1996, a Statement of Principles (SOP) pertaining to nonroad diesel engines was signed between EPA, California ARB and engine makers. The 1998 regulation introduced Tier 1 standards for equipment under 37 kW (50 hp) and increasingly more stringent Tier 2 and Tier 3 standards for all equipment with phase-in schedules from 2000 to 2008. The Tier 1-3 standards are met through advanced engine design, with no or only limited use of exhaust gas aftertreatment (oxidation catalysts). Source: http://www.dieselnet.com/standards/us/nonroad.php

for diesels create the possibility that diesel cars may not be allowable in the light-duty fleet after 2007 or may not be allowable in large numbers. Further, even if the diesel standards are achievable, the control system requirements might increase costs and/or decrease fuel efficiency sufficiently to reduce this technology‘s potential market share. The US Environmental Protection Agency however has targeted a 15 ppm sulphur diesel fuel requirement as part of its Tier II requirements. The availability of ultra-low sulphur fuel does improve prospects for the use of lean-NO_x storage catalysts and PM traps for diesel cars, increasing the chances of complying with the standards. Undoubtly, low sulphur diesel fuel could be reached by broader introduction of plant oil substituting conventional diesel fuel. For instance, cold pressed rapeseed oil (RSO) consist of less than 5 mg of S per kg (for Euro IV standard a maximum of 50 ppm of sulphur in diesel fuel for most highway vehicles is required).

The extensive although essential analysis above brings out a crucial conclusion: increasing oil prices as well as the stringent environmental standards indicate that the near future of modern diesel engines will rely on seeking cheap and technically acceptable diesel substitutes and finding a way of making the switch feasible for the existing and future customers in a combination of advanced diesel solutions. It becomes very apparent that the environmental concerns are in favour of institutions and countries, however the customer’s interest is frequently neglected. Cleaner “fossil” fuels are already expensive and becoming even more expensive as the result of the situation in the fuel market. Modern diesel engines increase efficiency and reduce emissions, but their operation on conventional diesel will become more and more expensive.

1.2 Rapeseed oil - the “future” fuel of diesel engines

The potential for plant oils (replacing petroleum diesel with a plant oil fuel such as RSO or animal fat) to reduce the carbon dioxide introduced into the atmosphere as a result of engine combustion has been already suggested by several authors [32; 157; 185; 352; 358; 367; 372] and is not new. (More extensive elaboration of the topic is described in the *Chapter 2*). In this thesis rapesseed oil is considered to be a product of biomass as rapeseed is commonly cultivated crop. Because of its potential application as a diesel substitute RSO is considered to be also a biofuel although it should not be understood in the same sense as other biofuels like mixtures of ethanol and petrol or even RSO methyl or ethyl

esters with diesel. Rapeseed oil is a specific biofuel, which does not require any chemical additives nor chemical processing.

Rapeseed oil is recognised as the most feasible diesel fuel substitute in the European climate and one which would meet all requirements discussed in sections above. So, the commonly produced RSO is an example of renewable fuel, i.e. the oil is obtained from an annual plant such as a winter or spring crop. Through the process of photosynthesis the rapeseed plant fixes all of the carbon released by combustion of the plant oil. Thus, the oil plants absorb carbon dioxide from the air, which is then converted into lipids, which are processed (by mechanical and/or chemical way) into a diesel fuel substitute. Next, when the oil is used in the engine the carbon is again released into the atmosphere as carbon dioxide along with small amounts of other carbon compounds (carbon monoxide and hydrocarbons). Hence, the carbon cycle consists of the fixation of carbon and the release of oxygen by plants through the process of photosynthesis, followed by recombination of oxygen and carbon to form carbon monoxide through the processes of combustion and respiration. In comparison, the carbon dioxide released by petroleum diesel is fixed from the atmosphere during the formative years of the Earth and its present cumulative amount in the atmosphere exceeds the recombinational capability of the recent ecosystem. Carbon dioxide released by plant diesel is fixed by the oil plant and is recycled by the next generation of rapeseed crops. The process of photosynthesis and the carbon cycle has been investigated by many researchers [137; 173; 320; 378]. Replacing petroleum diesel with plant oils could result in reduced accumulation of CO_2 in the atmosphere making it circulate in a natural bio-cycle or even in removal of CO_2 from the atmosphere by the natural sequestration. Peterson et al. [322] provided data about using a screw-press to extract raw oil from rapeseed by presenting energy and mass balances. In their report the authors showed that an average engine efficiency of 78% and an energy requirement of 0.58 MJ/l was achieved.

It has also been recognised that the use of RSO as a fuel would benefit farmers and help develop rural areas (this will be broadly discussed in “Feasibility studies and economy benefits” in *Chapter 2*). Agricultural oils, in raw or chemically modified forms, have the potential to substitute a fraction of petroleum distillates and petroleum based petrochemicals in the near future while stimulating the farming sector.

Substantial and costly overproduction of agricultural crops for food has led to a reformed Common Agricultural Policy introducing a set-aside percentage for food-crops while

allowing for non-food crop production, e.g. growing rapeseed without loosing a subsidy in the European Commission. The initial amount for set-aside land of 15% declined step by step over the years to 5% today, putting the young plant fuel oil industry at a substantial risk of raw material shortage. However, there is still enough land to be cultivated for biomass purposes. The future agricultural policy will have to consider that with the enlargement of the European Union by the Countries of Central Europe tremendous opportunities of bio-fuel production are opening up. Presently these countries double the acreage per citizen compared to the European Union with an enormous potential in agro-productivity.

The information presented above has essentially indicated several reasons why the CR diesel engines fuelled with plant oils could not only be feasible but can also be technically and economically attractive. Also, it has been shown how the environmental concerns are pushing this technology towards higher standards. It is believed that the technical advantages of CR engines combined with alternative fuels would offer a perfect solution to meet such requirements.

1.3 Problem description

The use of various plant oils as fuel for diesel engines is not a new concept. During the last few decades a wealth of empirical and engineering knowledge has been developed and serves as the database for current diesel engines modifications. Development of diesel engines fuelled by plant oil has already been successfully applied in case of less advanced types e.g. Indirect Diesel Injection (IDI) engines. In spite of some similarities, plant oils and diesel fuel are different in physical properties and in chemical structure. The outstanding question regarding the use of plant oils as fuels for CR diesel engines relates to the observed durability problems [22; 93]. Investigations showed that the injection and combustion characteristics of plant oils in diesel engines are significantly different from those of hydrocarbon-based diesel fuels causing short and long-term test engine problems. Nevertheless, plant oils can be successfully applied in some diesel engines and there is a wide range of companies offering their services and know-how to convert IDI engines to be run with plant oils. These conversions vary in the sophistication of the modification, offered services and reliability.

CR system that is still waiting to be modified in order to reliably run on plant oils. Generally, conversion of the diesel direct injection engines is much less explored in comparison to the indirect diesel injection types. Taking into account existing trends within the diesel car market, modification of the CR direct injection diesel engines determines the greatest future target. This target has been defined not only by technical difficulties but also by extremely significant advantages offered by the CR technology. Regardless of the increasing customer interest in these types of diesel cars as one of the main reasons of the CR cars growing popularity, the CR injection design satisfies the very high demands for automotive diesel fuel injection systems. Being parts of modern CR systems high-speed precision actuators create preconditions for meeting future exhaust emission regulations such as Euro IV; V, Tier II; III and the new Japanese standards. The leading automobile manufacturers underline this fact by intense promotion of the CR cars.

Many users of existing diesel engines simply can not afford to replace engines until they are completely worn out and can not be longer serviced. Hence customers look for a cheap and reliable source of a diesel fuel substitute but this often requires a modification of the existing engine. Thus, the fact of the economically and technically feasible modification of CR engines operating on RSO can not be ignored as it can be offered to the customers. This is especially true in developing countries as well as in places where servicing diesel engines is particularly expensive.

The main challenge of engine modification is a lack of basic information concerning issues such as oil spray development under high injection pressure, the mechanical response of the system to the new fuel and problems in hydrodynamics of the new fuel. Therefore, prior to the modification of a CR system systematic studies of spray have to be performed which would provide enough information to modify engines. This statement has been the fundamental reason to carry out this presented PhD research.
The CR injection system is particularly sensitive to quality and type of fuel used. Therefore application of plant oil would not be as straightforward as in case of the indirect injection diesel engines. In direct injection engines, which the CR belongs to, the fuel spray characteristics have significant influence on combustion, fuel efficiency and exhaust gas emissions. Only correct spray characteristics can improve combustion of plant oils and ensure that the Euro IV and V emission standards are met. The quantitative analysis of the plant oil/air mixture formation is essential for improvement in fuel economy and NO_x

emissions. The availability of information on spray formation regarding the effects of fuel properties on the CR injection system is limited and has not been published.
Thus, before evaluating the CR engine and fuel system changes to allow satisfactory operation on plant oil it is important to find out some fundamental injection parameters e.g. injection pressure and fuel temperature for the new generation of alternative fuels including neat plant oils. To proceed with such modifications of the CR engines it is necessary to perform detailed studies on the CR injection system regarding the influence of plant oil on the injection process. This should be performed by analysing the injection system and its auxiliaries subjected to a plant oil as well as spray characteristics e.g the effect of plant oil properties on fuel flow through system parts. The spray characterisation can be evaluated using standard measurement methods involving high speed imaging techniques or laser techniques.
It is expected that the performed studies would provide enough information to define a suitable modification and consequently lead to the successful operation of the CR engine on plant oil.

1.4 Project objectives

The main and most important target of the present work was to provide sufficient information to design a modified CR injection system to operate on neat RSO in a single tank mode. The content of the presented PhD work aims to extensively explore the modification of a CR diesel injection system, which would allow it to operate on neat RSO. The presented work provides the basic understanding of RSO atomisation and its behaviour under CR conditions. In addition, both economical and technical feasibility studies have been completed.

The main objective of the thesis was to provide fundamental information on RSO spray, define and implement several changes necessary for the complete modification and las to assess these changes and make suggestion for future steps. The objectives met by this thesis are describe in more details as follows:

1. Analysis of the feasibility of the modification including economical and social aspects of RSO utilisation (*Chapter 2*).

2. Characterisation and description of plant oils with the special consideration of RSO as a potential diesel substitute (*Chapter 2*).

3. Review existing diesel injection systems, their brief description and broader characterisation of the CR system focusing on its elements, which may play an important role in the modification (*Chapter 2*).

4. Design and manufacturing of an experimental rig allowing to characterise RSO spray development and internal flow in a CR system through various experimental setups (*Chapter 3*).

5. Experimental methods, procedures associated with application of the experimental setups as well as the description of data processing (*Chapter 4*).

6. Computational verification of the experimental spray results as well as theoretical simulation of RSO sprays under engine conditions with special attention to the fuel/air mixture formation (*Chapter 5*).

7. Results of comparative characterisation of CR diesel and RSO sprays using high-speed photography, Phase Doppler Anemometry, Malvern techniques and Acoustic Emission (*Chapter 6*).

8. Definition of the essential steps required for the successful modification and their experimental verification using quantitative and qualitative methods. Preliminary assessment of the CDI engine modification using the non-intrusive method of DynoStar in engine tests (*Chapter 6*).

9. Summary of chapters together with the main conclusions. (*Chapter 7*).

10. Definition of the additional steps required and recommended for the future the modification (*Chapter 8*).

1.5 Structure of the thesis

The thesis comprises of eight chapters tackling the complex problem of application of neat RSO in CR diesel engines. This section describes three stages in which the project objectives have been implemented. The diagram in Figure 1.1 graphically depicts the research stages and the text below explains briefly the main aspects covered in each chapter.

Chapter 2 - *Literature review and background knowledge* - This chapter provides an extensive literature review of plant oils and their application in diesel engines, describes various injection diesel systems and as well as theoretical backgrounds of various experimental methods to investigate fuel sprays. The contents of the chapter also includes the background knowledge on modelling of spray formation and describes KIVA code.
In *Section 2.1* the author widely describes properties of various plant oils with special respect to their fuel properties. Various aspects of using plant oils in diesel engines including recent findings and applications are also provided. This defines the main problems of operating diesel engines on plant oils seeking analogies between conversion of the old diesel injection systems and the CR unit. Finally, the section presents the economical and social impact of substituting diesel with plant oils including development of rural areas and small communities. This section helps to understand the motivations of using neat plant oils in diesel engines and outlines the possibilities and challenges of using plant oils in CR engines. *Section 2.2* - In this section brief and basic information of diesel injection technology is presented. The text describes direct and indirect diesel engines and demonstrates that the technical complexity of an injection system is directly associated with difficulties of its modification. Finally, a presentation of the CR technology is made; its mechanical layout, functionality and way of operation. The section also includes comments on usability of plant oils with each type of injection system. The knowledge contained in this section is essential to understand the complexity of CR and challenges of modification. *Section 2.3* provides the fundamental understanding of spray characterisation using optical methods and also reviews various literature examples of high speed camera applications. Spray droplet sizing using PDA and Malvern methods from theoretical point of view are described in *Section 2.4*. This section reveals the principles of these two methods as well as demonstrates their applications for various spray characterisation tests. Principles and applications of Acoustic emission to diagnose various turbomachinery is given in *Section 2.5 - Acoustic emission technique*. The last section *Section 2.6 - Spray simulation* focuses of the background knowledge and examples of spray simulations for fuel injection.

Chapter 3 - *Experimental systems* - The chapter reveals the design and procedure of constructing a novel CR experimental stand used in the experimental part of this project. It focuses also on modifications which had been performed to accommodate different types of experimental tests using the stand. As the stand consists of genuine CR parts its construction features of modifications, which can be implemented in a real injection system.

Section 3.1 - Experimental setup of the injection stand supplies a general description of the injection stand and its similarities to a CR injection system. Later *Section 3.2 - Description of the injection chamber* gives details of the injection chamber and its connection to the injection stand. *Section 3.3 - High speed camera experimental setup*, *Section 3.4 - Phase Doppler Anemometry experimental setup* and *Section 3.5 - Malvern experimental setup* revealed details of facilitation of high speed camera, Phase Doppler Anemometry and Malvern sizing system to perform spray characterisation tests. The last *Section 3.6 - Experimental setup of the AE setup* gives details of the Acoustic Emission experimental setup.

Chapter 4 - *Experimental methods* - gathers details the experimental techniques and methods. The description directly follows the contents of *Chapter 3*. *Section 4.1 - Experimental procedures for preliminary injection tests*, *Section 4.2 - Experimental procedures of spray recording*, *Section 4.3 - Experimental procedures of spray sizing experiments* and *Section 4.4 - Experimental procedure of AE signal processing* relate to experimental methods of the preliminary injection tests, spray recording using high speed camera, spay sizing using PDA and Malvern and application of the Acoustic Emission method respectively. Description of quantitative and qualitative tests to evaluate the quality of the performed CDI modification via emission tests, engine performance, fuel economy, power output and engine reliability and durability in *Section 4.5*.

Chapter 5 - *Simulation software* - The main goal of this chapter is to present a method of modelling dense spray using RSO, which would allow to simulate a simple, cold RSO spray as well as to elaborate on injection at engine-like conditions. KIVA code has been used to compare and validate experimental and theoretical studies of standard and RSO mimicking selected injection conditions from *Chapter 4*. The modelling also utilised some results of spray injection presented below in *Chapter 6*. Finally, more complex examples of rapeseed and diesel injection inside a diesel cylinder are shown.

The chapter provides two essential elements to the overall effort of modification: verification of the existing numerical tool (KIVA) to be used to predict RSO spray development and a quick analysis of RSO development in real engine conditions. The chapter demonstrates that the tool can complement the experimental studies to provide fundamental knowledge for CR system modification.

Chapter 6 - *Results* collects all experimental and modelling results of the PhD work with the exception of some of the acoustic emission tests presented in *Chapter 8*. The chapter first show some preliminary measurements of injection quantities and oil properties. Then,

initial results of the preliminary experiments of oil injection and oil flow inside the system are shown (*Section 6.1 - Results of oil properties and preliminary injection tests*). The aim of the section is to present basic, but important results used in this PhD work and the importance of design for reliable and complex data acquisition. *Section 6.2 - Results of spray characterisation using high-speed camera* documents results of the experimental work done on spray characterisation of standard and RSO at various injection conditions using a high-speed camera. The section provides results of spray penetration and cone angle. It is expected that spray characterisation is one of the most crucial steps in gathering information of RSO spray and further alternation of the spray using temperature and pressure. These results can be directly used in modification and are a part of modification know-how. In *Section 6.3 - Results of spray sizing using PDA and Malvern* further results of studies on spray characterisation but focusing on drop sizing using Phase Doppler Anemometry as well as Malvern techniques are presented. This part is crucial for understanding differences in vaporisation and combustion of diesel and RSO. Droplet sizing, together with spray penetration, is essential for further modifications of the injection system.
Section 6.4 - Results of AE tests presents results of the acoustic emission lab. The section presents results of comparative tests of diesel and RSO flow inside a CR injector. The comparison gives information on internal flow inside the injector. These results complement data collected using the conventional spray characterisation methods i.e. high-speed camera, PDA or Malvern. And finally, *Section 6.5 - Results of CFD spray simulations* presents results of spray modelling using KIVA code. The section provides results of cold spray simulations as well as modelling of spray formation under in-cylinder like conditions.
Finally, based on the results and observations the author in this chapter defines a set of modifications which were already implemented to a CDI engine and tested. An additional, commercial , diagnostic too - DynoStar provides a mean to assess the injection performance and its impact of the running engine operation (*Subsection 6.6.5*).
Chapter 7 - *Conclusions* - This chapter summarises the theoretical and experimental work performed in this PhD research project. The chapter highlights the main findings and conclusions. For clarity, the conclusions are grouped up in sections related to previous chapters of this thesis.
Chapter 8 - *Recommendations* - As the previous chapters provided basic information about the RSO spray in comparison with diesel this chapter is written to provide a set of recommendations. These recommendations are based on the observation of the funda-

mental spray features, the modelling results and the output of the preliminary tests on the modified CDI engine. Based of some findings from previous chapters and the preliminary modification car tests the author suggest a type of changes, which should be performed for smooth operation of CR on RSO as part of the future work.

The author believes that the work presented in this thesis identifies the main issues of CR modification to operate on neat plant oils and provides fundamental data to perform such modification. It is also recognised that the work in this field is very complex and the current PhD study has not exhausted all the issues, which could be studied extensively in more detail.

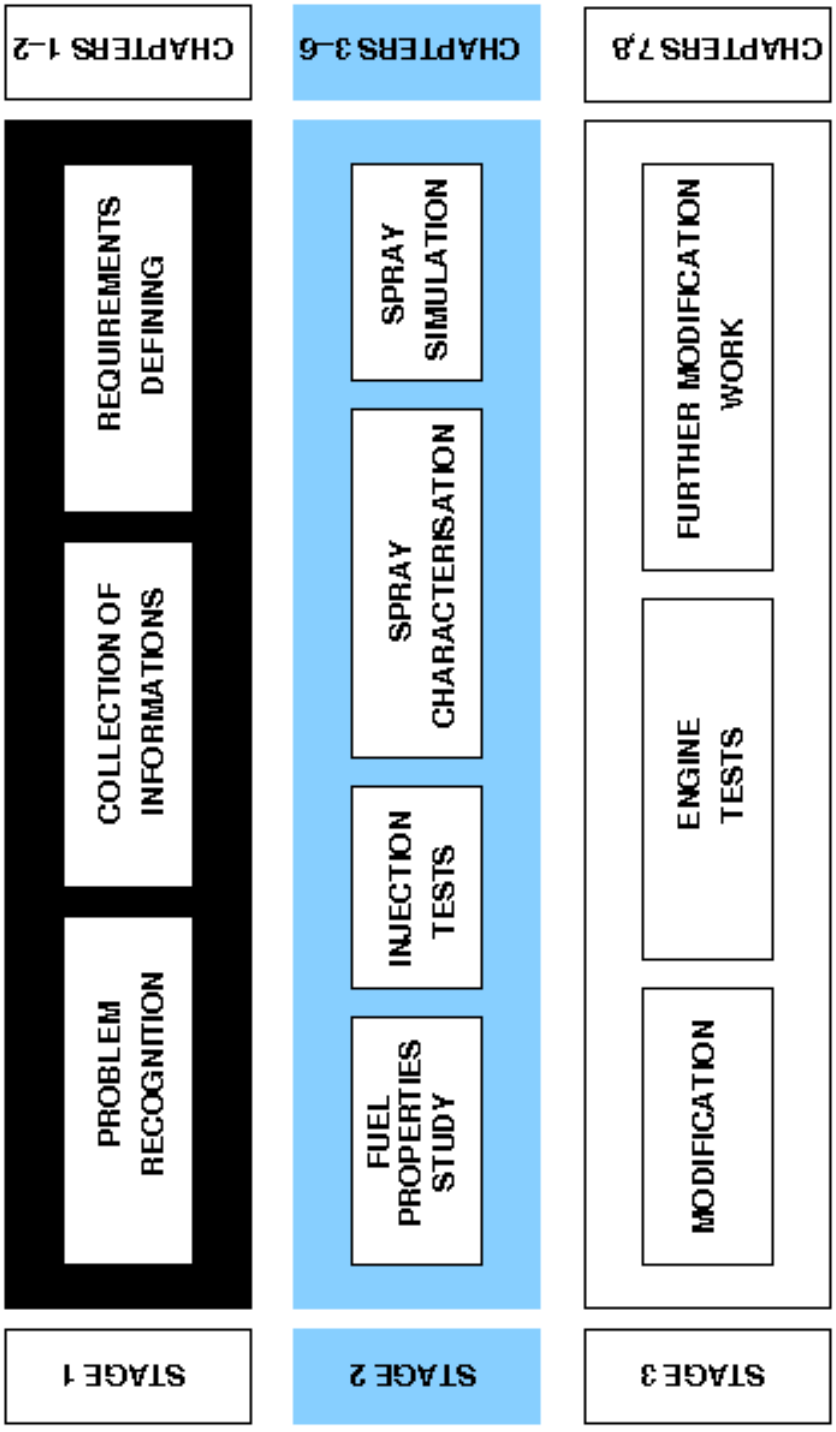

Figure 1.1: *Diagram schematically presenting the PhD work flow.*

Chapter 2

Literature review and background knowledge

Ubi dubium ibi libertas

The aim of this chapter is to collect and present a literature review, general and background knowledge needed to understand the problem of using plant oils as fuel substitutes as well as the theory of experimental methods and procedures used in this research. Therefore, the chapter is divided into six major sections presenting plant oils, diesel injection systems, spray characterisation using optical methods, spray sizing, spray simulation and acoustic emissions respectively. Each section can be considered as an individual introduction to the section topic. It is believed that the the chapter provides sufficient information for further reading of this thesis.

2.1 Plant oils as diesel fuel substitute

The idea of using plant oils as fuel for diesel engines is not new and had been initiated in the last century by Rudolf Diesel. With the advent of cheap petroleum based fuels, appropriate crude oil fractions were fractioned to serve as fuel and diesel fuels and diesel engines evolved together. In the 1930‘s and 1940‘s plant oils were used as diesel fuels from time to time, but usually only in emergency situations. Recently, because of increases in crude oil prices, limited resources of fossil oil and environmental concerns there has been a renewed focus on plant oils and animal fats to make bio-fuels and use them in neat form. Continued and increasing use of petroleum could intensify local air pollution and magnify the global warming problems caused by CO_2 [139; 367]. In a particular case,

such as the emission of CO_2 in the closed environments of plant oils have the potential to reduce the level of greenhouse gases. In fact, plant oils take away more CO_2 from the atmosphere during their production than is added to it by their later combustion. Therefore, generally it alleviates the increasing carbon CO_2 of the atmosphere.
More intense research and development of using neat plant oils as diesel substitutes took place definitely in the last 20 years of the 21^{st} century. Bartholomew [58] addressed the concept of using plant oils as fuel indicating that existing petroleum fuels should be the "alternative" fuel rather than plant oil and ethyl alcohol. He claimed that some forms of renewable energy must begin to take the place of the non-renewable, petroleum based resources.

Most of the researchers working with neat oils indicated various ranges of available oil sources, which could be used in diesel engines. More than 300 oil plant species have been identified around the World. However, the main source of plant oil as fuel still remains rapeseed, Canola [1], sunflower and soybean. Animal fats, although mentioned frequently, were not studied to the same extent as plant oils but are facing huge potential. Considerable research was done on these plant oils as fuel for diesel engines and some of the results are presented in this section. That research mainly includes RSO but also palm oil, soybean oil, sunflower oil, coconut oil, and other types of plant oils cultivated locally. As result of the present studies, existing engineering experience, considering the content of the mono-saturated oleic acid, the low level of saturated fatty acid and acceptable level of linolenic acid makes the RSO rather the ideal source of plant oil in Europe.

The aim of this section is to show the results of a literature review generally concerning the operation of diesel engines on neat plant oils but also the use of their esterified form. A special concern is paid to use of plant oils as a replacement for diesel fuel in direct injection and CR diesel engines. Although, the literature search provides a significant number of recently performed studies which evaluate plant oils as diesel substitutes, none of them investigated the CR and plant oils. The range of problems associated with diesel engines running on plant oils is the same for most diesel types. It is expected that CR engines do express similar type of problems running on plant oils and the basic information learned from the other diesel engines will help to carry out and evaluate the performance studies.

[1] In agriculture, Canola are certain varieties of oilseed rape, or the oil produced from those varieties. Its a trademarked hybrid of rape initially bred in Canada. Canola has been bred to reduce the amount of acid, yielding a palatable oil.

For a clear understanding the term “bio-fuel” is used here to describe diesel replacements including plant oils, their blends, and microemulsions, whereas the terms: “bio-diesel” or “bio-esters” are associated with esterified version of plant oils and referred to thereafter accordingly. Additionally, the term “plant oils” is preferable over “vegetable oils” due to the most appropriate description of the oil origins.

The author of this thesis is aware of some of other types of oil used sometimes in diesel engines, which are not presented here. This is because of minor research work, which was carried out on them.

2.1.1 Renewable fuels characteristics and plant crops

Plant oils have different chemical structures to petroleum-based diesel fuels, but some chemical similarities make both groups relatively close. The chemical structure depends on the type of the oilseed plant and thus results in different fuel properties. The objectives of this section are to present a variety of plant oils, show their chemical structure and analyse various fuel-related properties. In particular, fuel properties of RSO are presented. Various properties of different plant oils are compared and then compared to the standard requirements for petroleum oils.

Plant oils are produced from numerous oil seed crops, which the number has been estimated to approximately 300 species around the globe. Some of them are listed in Table 2.1. Depending on climate, soil conditions and economical circumstances, different nations may look into different plant oils for diesel fuels. Each climate region owns its own common type of plant oil. Dominant in Europe became rapeseed, in Canada - Canola, olive trees in Spain etc. Other commonly grown oil plants are coconut palm trees in Malaysia [29; 356], sunflower in France, Italy and Hungary, while Soya bean became the predominant oil source in the USA. In Nicaragua the locally available oil of Jatropha Curcas plant is processed, coconut in Philippines and Indonesia. Giannelos et al. [154] found tobacco seed as by-product of tobacco leaves production in Greece for bio-fuel production could be an attractive alternative application of the existing tobacco crops in Greece for the new fuel markets. Rapeseed, palm, sunflower and soybean oil are economically the powerful source of fuel in different parts of the World however considerable studies on their application still have to be done. Crop productions are

inconsistent according to the harvest area, climatic conditions, etc.

As can be clearly seen, plant oils are widely available from a variety of sources throughout the world, and they are renewable. However, today low cost sources of plant oil raw materials (e.g. used as frying oils collected at restaurants [225; 281; 343; 430] or even low grade beef tallow [163]) are used for bio-fuel production with improved process technologies, these can be used neat too omitting chemical processing.

2.1.1.1 Chemical structure

As far as plant oil properties are concerned, most of them express similarities in their chemical and physical specifications. Plants similarly to animals produce lipids, which constitute oils seeds. Commonly known in the animal kingdom, fats are primarily water-insoluble, complex, hydrophobic substances. These are made up of one mole of glycerol and three moles of fatty acids and are commonly referred to as triglycerides (about 95%) [375] and non-triglycerides part (about 5%) accordingly. Likewise, the triglyceride molecules of plant oils consists of three long-chain fatty acids that are ester-bonded to a single glycerol molecule. Figure 2.1 shows a typical triglyceride molecule. Plant oils

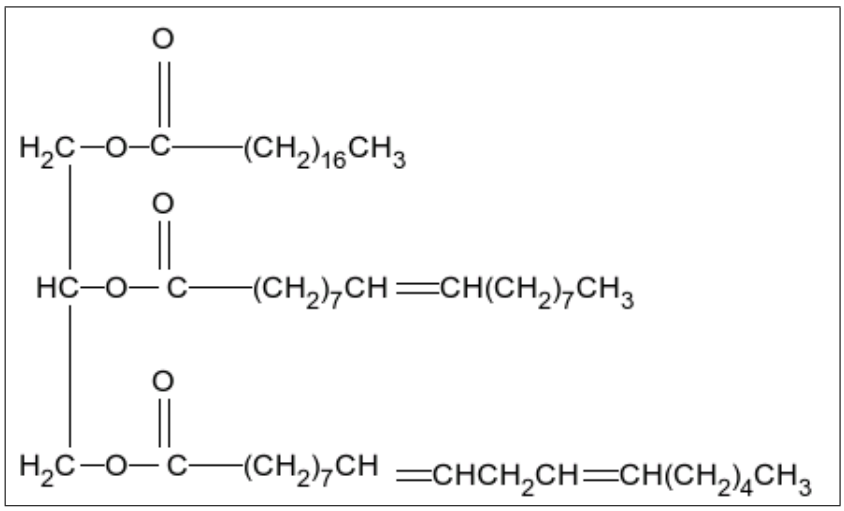

Figure 2.1: *Structure of a typical triglyceride molecule.*

comprise 90 to 98% triglycerides and small amounts of mono- and diglycerides. The proportions of these fatty acids determine the physical and chemical properties of oils. A closer examination of the molecular arrangements of diesel fuel, plant oils and a common alcohol indicates a very distinctive nature of these three chemicals. It can be recognised that a molecule of a plant oil somehow combines structure of diesel and alcohol. The plant oils with long and heavy chains (varying in length), slightly different from the structure of

Table 2.1: *Oil seeds species [29; 154; 157; 356; 375]*

English name	Latin name	English name	Latin name
Almond	*Prunus communis*	Sweet chestnut	*Castanea sativa*
Apricot	*Armeniaca vulgaris*	Syrian scabious	*Cephalaria syriaca*
Assai-palm	*Euterpe edulis*	Tallow tree	*Sapium sebiferum*
Awarra	*Astrocaryum vulgare*	Tarweed	*Madia sativa*
Bacaba palm	*Oenocarpus bacaba*	Tea-oil plant	*Camellia oleifera*
Baobab	*Adansonia digitata*	Tucuma	*Astrocaryum tucuma*
Borage	Borago officinalis	*Turpentine tree*	*Pistacia terebinthus*
Borneo tallow	*Shorea stenoptera*	Walnut	*Juglans regis*
Butter nut	*Caryocar nuciferum*	Water-chestnut	*Trapa natans*
Butter tree	*Madhuca longifolia*	Meadowfoam	*Limnanthes alba*
Carnauba wax palm	*Copernicia cerifera*	Corn	*Zea rais*
Cohune palm	*Attalea cohune*	Cashew-nut	*Anacardium occidentale*
Copaiba tree	*Copaifera officinalis*	Oat	*Avena sativa*
Corn salad	*Valerianella olitora*	Palm	*Erythea salvadorensis*
Crabwood	*Carapa guineensis*	Iupine	*Lupinus albus*
Croton	*Croton tiglium*	Rubber seed	*Hevea brasiliensis*
Earth almond	*Cyperus esculentus*	Calendula	*Calendula officinalis*
Essang	*Ricinodendron hendeloti*	Cotton	*Gossypium hirsutum*
Eth. Mahagony	*Trichilia emetica*	Soy bean	*Glycine max*
Evening primrose	*Oenothera biennis*	Coffee	*Coffea arabica*
Ginkgo	*Ginkgo biloba*	Line seed	*Linum usitatissimum*
Gorli seed	*Oncoba echinata*	Hazel-nut	*Corylus avellana*
Grape	*Vitis vinifera*	Euphorbia	*Euphorbia lagascae*
Hemp	*Canabis sativa*	Pumpkin seed	*Cucurbita pepo*
Hunters nuts	*Omphaiea megacarpa*	Coriander	*Coriandrum sativum*
Indian almond	*Terminalia catappa*	Mustard	*Brassica alba*
Jaboty Palm	*Erisma calcaratum*	Dodder-seed	*Camelina sativa*
Japanese chestnut	*Castanea crenata*	Sesame	*Sesamum indicum*
Janary Palm	*Astrocaryum Januari*	Abyssinian kale	*Crambe abyssinica*
Java almond	*Canarium comune*	Safflower	*Carthamus tinctorius*
Kagne-butter	*AIlanblackia oleifera*	Rice	*Oriza sativa*
MaIabar-nut tree	*Adhatoda vasica*	Tung tree	*Aleurites spp*
MaIabar-tallow	*Vateria indica*	Sunflower	*Helianthus annus*
Manketti nut	*Ricinodendron rautenenii*	Cocoa	*Theobroma cacao*
Mururmurupalm	*Astrocaryum murmuru*	Peanut	*Arachis hypogaea*
Narasplant	*Acanthosicyos horridus*	Opium poppy	*Papaver somniferum*
Neem	*Antelaea azadirachta*	Rape	*Brassica napus*
Niger	*Guizotia abysinnica*	Olive tree	*Olea europaea*
Nutmeg	*Myristica fragrans*	Lndaia palm	*Attalea funifera*
Oiricurupalm	*Syagrus coronata*	Gopher plant, spurge	*Euphorbia lathyris*
Pachira nut tree	*Bombacopsis*	Castor bean	*Ricinus communis glabra*
Papaya	*Carica papaya*	Bacury	*Platonia insignans*
Passion fruit	*Passiflora edulis*	Pecan-nut	*Carya illinoensis*
Pea	*Pisum sativum*	Jojoba	*Simmondsia chinensis*
Peach	*Amygdalus persica*	Babassu palm	*Orbignya martiana*
Peach palm	*Bactris gasipaees*	Purging nut	*Jatropha curcas*
Pistachio	*Pistacia vera*	Macadamia nut	*Macadamia terniflora*
Powder flask-fruit	*Afraegle paniculata*	Brazil nut	*Bertholletia excelsa*
Red pepper	*Capiscum annuum*	Avocado	*Persea americana*
Red-cotton-tree	*Bombax malabaricum*	Coconut	*Cocos nucifera*
Rose hip	*Rosa pomifera*		*Licania rigida*
Sandal beadtree	*Adenanthera pavonia*	Buriti palm	*Mauritia flexuosa*
Scotch pine	*Pinus silvestris*	Pequi	*Caryocar brasiliense*
Seje palm	*Jessenia bataua*	Macahuba palm	*Acrocomia spp*
Shea nut	*Vitellaria paradoxa*	Sourcherry	*Prunus cesarus*

diesel seems to be critical in terms of combustion in the diesel engine cycles, Figure 2.2. Hemmerlein et al. [185] reported on RSO as a fuel and concluded that the physical and chemical properties of RSO as a fuel are very similar to those of diesel fuel, and on a long term basis, it can be used in diesel engines. As esters of three fatty acids are combined with one glycerol, these contain substantial amounts of oxygen in its structure - essential for combustion properties. Fatty acids vary in their carbon chain length and in the number of double bonds. The structures of common fatty acids are given in Table 2.2 according to Goering et al. [157]. The fatty acids, which are commonly found in plant oil, are stearic,

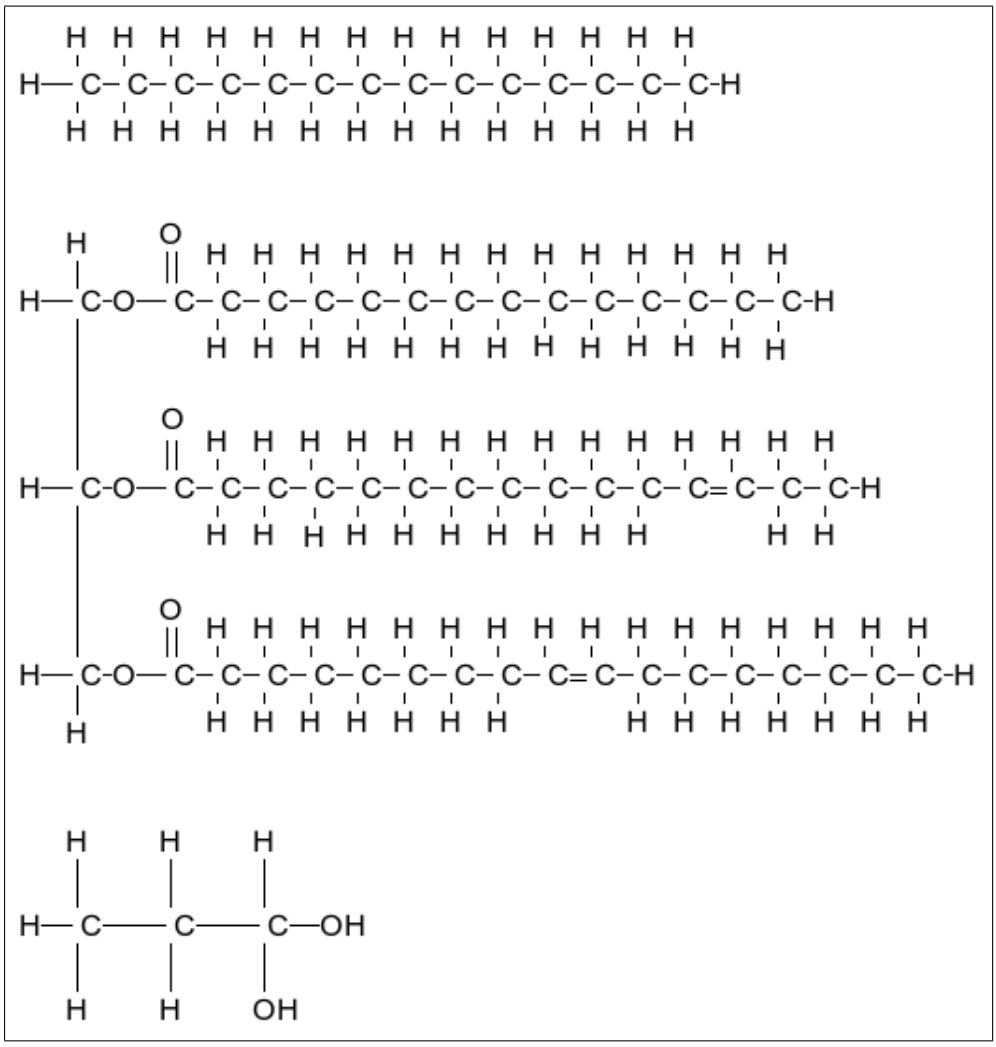

Figure 2.2: *Typical structures of diesel fuel (top), plant oil (middle), and ethyl alcohol (bottom) molecules .*

palmitic, oleic, linoleic and linolenic. Plant oils contain fatty acids (generally 1 to 5%), phospholipids, phosphatides, carotenes, tocopherols, sulphur compounds and traces of water [157]. Indeed, the sulphur content in plant oils remains at very low level. Unlike hydrocarbon-based fuels, the sulphur content of plant oils is close to zero and hence, the

environmental damage caused by sulphuric acid is very much reduced. Fatty acids differ

Table 2.2: *Plant oil composition (fatty acid compositions of plant oil, by weight, [157]).*

Plant oil	Fatty acid								Ref. no.
	16:0	16:1	18:0	18:1	18:2	18:3	20:0	Others	
Ailanthus	31.0	0	0	8.1	51.1	7.3	0	2.0	12
Bay laurel[1)]	25.9	0.3	3.1	10.8	11.3	17.6	0	31.0	13
Beech	11.6	3.5	1.2	10.4	33.3	16.4	60.0	14.6	14
Beechnut	8.8	0	3.2	30.4	48.9	0	0	6.7	15
Castor[2)]	1.1	0	3.1	4.9	1.3	0	0	89.6	11
Corn	11.8	0	2.0	24.4	61.3	0	0.3	0	16
Cottonseed	28.7	0	0.9	13.0	57.4	0	0	0	16
Crambe[3)]	2.1	0	0.7	18.9	9.0	6.9	2.1	60.4	11
Hazelnut kernel	4.9	0.2	2.6	83.6	8.5	0.2	0	0	16
Linseed	5.1	0.3	2.5	18.9	18.1	55.1	0	0	16
Peanut	11.4	0	2.4	48.3	32.0	0.9	1.3	3.7	11
Poppyseed	12.6	0.1	4.0	22.3	60.2	0.5	0	0.3	16
Rapeseed	3.5	0	0.9	64.1	22.3	8.2	0	0	11
Safflower seed	7.3	0	1.9	13.6	77.2	0	0	0	17
H.O. Safflower seed	5.5	0	1.8	79.4	12.9	0	0.2	0.4	11
Sesame	13.1	0	3.9	52.8	30.2	0	0	0	17
Soybean	13.9	0.3	2.1	23.2	56.2	4.3	0	0	18
Spruce[4)]	5.2	0	1.0	14.7	30.4	5.7	23.2	20.0	19
Sunflower seed	6.4	0.1	2.9	17.7	72.9	0	0	0	16
Walnut kernel	7.2	0.2	1.9	18.5	56.0	16.2	0	0	16

[1)]Bay laurel oil contains 26.5% of 12:0 and 4.5% of 14:0 fatty acids

[2)]Ricinoleic is the only 18:1 fatty acid which contains a hydroxyl group. Its content in castor oil is 89.6%

[3)]Crambe oil contains 58.5% of 22:1, 0.8% of 22:0, and 1.1% of 24:0 fatty acids

[4)]Spruce oil only contains 18:3 (5c, 9c, 12c) pinolenic acid (5.7%)

by the length of the carbon chains, as well as the number, orientation, and position of double bonds in the chains. Fatty acids are influencing most of the plant oil properties including viscosity and surface tension. Because of a significant number of long chain fatty acids comprising plant oils, the viscosity of oils is of the order of 10-20 times that of diesel fuel. Chemical analysis of plant oils is mainly made by determination of type and amount of free fatty acids. The fatty acids found in plant oils are summarised in Table 2.3.

Table 2.4 lists the chemical properties and determined and calculated higher heating values (HHV) [1] of the plant oils. The HHV of plant oils ranges from 37.27 to 40.48 kJg^{-1}

[1]Also known as the gross calorific value or gross energy of a fuel is defined as the amount of heat released by a specified quantity (initially at 25°C) once it is combusted and the products have returned to a

Table 2.3: *Typical fatty acid composition-common oil source presented in [375]*

Fatty acid	Soybean	Cottonseed	Palm	Lard	Coconut	Tallow
Lauric	0.1	0.1	0.1	0.1	46.5	0.1
Myristic	0.1	0.7	1.0	1.4	19.2	2.8
Palmitic	10.2	20.1	42.8	23.6	9.8	23.3
Stearic	3.7	2.6	4.5	14.2	3.0	19.4
Oleic	22.8	19.2	40.5	44.2	6.9	42.4
Linoleic	53.7	55.2	10.1	10.7	2.2	2.9
Linolenic	8.6	0.6	0.2	0.4	0.0	0.9

and it is widely presented and discussed by Goering et al. [157] and in [110]. The HHVs of different plant oils vary by <9% and in the case of RSO is 97% of a typical diesel fuel caloric value. Higher density of plant oils compensate a reduction in the calorific value if the same volume of fuel (as for diesel) is injected.

2.1.1.2 Physical and fuel properties

Since all plant oils have high energy content and fuel-like chemical structure, most require some processing to assure safe use in internal combustion diesel engines. This is mainly due to their high viscosity and inconvenient thermal properties. As it had been mentioned, most of the existing technologies process plant oils into ester form known as bio-diesel. Bio-diesel is a more convenient form of using plant oils, due to its lower viscosity and other physical properties very much resembling diesel. However, some of these oils have been already evaluated as substitutes for diesel fuels without chemical treatment. In the beginning it was rapeseed and Canola. With the higher content of the mono-unsaturated oleic acid (C18:1) of about 60%, the rather low level of saturated fatty acids (palmitic and stearic acid <6%) and also acceptable levels of linolenic acid (C18:3) RSO was found as a rather ideal raw material for the European climate and of reasonable product stability expressed by an iodine value (IV) of <115. Thus, the amount of RSO recently being esterified could be directly used in diesel engine.

Compared to standard diesel fuel, all of the plant oils are much more viscous and are much more reactive to oxygen. Oils are extremely viscous with viscosities ranging from 10

temperature of 25°C. The higher heating value takes into account the latent heat of vaporisation of water in the combustion products, and is useful in calculating heating values for fuels where condensation of the reaction products is practical (e.g., in a gas-fired boiler used for space heat).

Table 2.4: *The chemical properties and higher heating values of various plant oils taken from [157].*

Plant oil	**Iodine value** (g I/100 g oil)	**Saponification value** (mg KOH/g oil)	**HHV** (kJg^{-1})
Ailanthus	107.18	206.34	39.38
Bay laurel[1)]	69.82	220.78	39.32
Beech	105.15	202.16	39.59
Beechnut	110.64	193.52	39.82
Castor[2)]	88.72	202.71	37.41
Corn	119.41	194.14	39.64
Cottonseed	113.20	202.71	39.44
Crambe[3)]	99.83	178.59	40.62
Hazelnut kernel	98.62	197.63	39.83
Linseed	156.74	188.71	39.33
Peanut	119.35	199.80	39.45
Poppyseed	116.83	196.82	39.59
Rapeseed	108.05	197.07	39.73
Safflowerseed	139.83	190.23	39.52
H.O. Safflower seed	88.57	206.82	39.61
Sesame	91.76	210.34	39.42
Soybean	120.52	194.61	39.63
Spruced	96.08	207.79	39.44
Sunflower seed	132.32	191.70	39.57
Walnut kernel	135.24	190.82	39.56

to 20 times greatest than reference diesel fuel. The oxidative stability of uninhibited high oleic plant oils were studied in [46] where poor oxidative reactivity was found. Increased carbon chain lengths and reduced numbers of double bonds are associated with increased oil viscosity, cetane rating and reduces the induction period for oxidation. Everyone involved with the use of plant oils as diesel fuel substitute can discover that these oils have viscosities many times higher that of diesel fuel, and in addition have a low viscosity index which gives rise to very high viscosities at low temperature [57; 126]. In particular, higher viscosity makes plant oils unattractive as direct diesel substitution and causes the majority of operational problems. Most of the oils have higher cloud points and pour points than diesel fuel too. The plant oils are not directly volatile, but tend to crack during distillation into a series of hydrocarbons and carboxylic compounds. The majority of opponents of the idea of using neat plant oils in diesel engines bring out this argument stating that the non-volatile character of plant oils completely eliminate their use in engines. The full

mechanism of thermal transformation of a single plant oil in in-cylinder like conditions have not been studied yet, thus the definite conclusion cannot be made.

There are broad differences amongst the induction periods of the plant oils. Induction period is used to determine how quickly plant oil oxidises and eventually degrades due to oxidation and is related to reactivity of the oil. Linseed and safflower oil are the most reactive of the oils and castor oil is the least reactive. The increasing oxidative instability of fatty acids with increasing unsaturation was proved [269] and the instability is reflected by the induction period - the shorter the induction period, the greater the instability. Corn, rapeseed, sesame, cotton and soybean oils have the most favourable combinations of the fuel properties, which varied among the oils. Crambe, sunflower and peanut oils had slightly less favourable combinations of the same properties. Castor, linseed and safflower oils each had certain unfavourable fuel properties that weight against their use as diesel substitute. Common practice of determining plant oils viability is set of ASTM (American Society for Testing and Materials) methods. The ASTM has developed a standard to characterise fuel properties. The ASTM D975 standard is for classifying hydrocarbon diesel fuels [2]. The standard ASTM for measuring each corresponding fuel property and the ASTM limits for No. 2 diesel fuel are given in Table 2.5 below. A similar characteristic

Table 2.5: *ASTM standards for classifying hydrocarbon diesel fuels shown in [2]*

Test	ASTM test no.	ASTM limits
Distillation range [°C]	D86	282-338
Flash point [°C]	D93	52 min.
Viscosity [mm^2s^{-1}]	D445	1.9-4.1
Water and sediment [wt. %]	D1796	0.05% max.
Carbon residue [wt. %]	D524	0.35% max.
Ash [wt. %]	D482	0.01% max.
Sulphur [wt. %]	D129	0.5% max.
Cetane no.	D613	40 min.

was found in most of the plant oils in terms of their fuel properties and presented by [157]. Summary of ASTM test of some plant oils is shown in Table 2.6. Goering at al. [157] conducted a very detailed study on plant oils including ASTM tests. Eleven plant oils were identified for inclusion in a comparative study of chemical and fuel properties in work of i.e. castor, corn, cottonseed, crambe, linseed, peanut, low-erucic rapeseed, safflower, sesame, soybean and sunflower oil. This paper presents the fuel properties in relation to

Table 2.6: *Fuel properties of plant oils by Demirbas [109].*

Plant oil	ASTM tests no. for each fuel property						
	D86	**D93**	**D445**	**D524**	**D482**	**D129**	**D613**
Ailanthus	150-350	286	30.2	0.22	0.02	0.01	35.1
Bay laurel[1)]	145-345	226	23.2	0.20	0.03	0.02	33.6
Beech	155-360	242	34.6	0.24	0.04	0.006	36.2
Beechnut	155-365	260	38.0	0.23	0.03	0.008	38.2
Castor[2)]	-	260	29.7	0.21	0.01	0.01	42.3
Corn	155-365	276	35.1	0.22	0.01	0.01	37.5
Cottonseed	170-355	235	33.7	0.25	0.02	0.01	33.7
Crambe[2)]	-	274	53.2	0.23	0.04	0.01	52.9
Hazelnut kernel	160-350	230	24.0	0.21	0.01	0.02	35.8
Linseed	165-365	240	28.0	0.24	0.01	0.01	27.6
Peanut	-	270	40.0	0.22	0.02	0.01	34.6
Poppyseed	170-370	265	42.4	0.25	0.02	0.01	36.7
Rapeseed	-	245	37.3	0.31	0.006	0.01	37.5
Safflower seed	165-370	260	31.6	0.26	0.007	0.01	42.0
H.O. Safflower seed	-	292	40.8	0.24	0.01	0.02	48.8
Sesame	-	262	36.0	0.25	0.002	0.01	40.4
Soybean	-	255	33.1	0.24	0.006	0.01	38.1
Spruce	150-350	238	35.6	0.26	0.01	0.01	34.2
Sunflower seed	155-355	272	34.4	0.28	0.01	0.01	36.7
Walnut kernel	160-355	232	36.8	0.24	0.02	0.02	33.6

their chemical composition. Comparison with ASTM limits revealed that all of the plant oils met ASTM limits for carbon residue, ash, and total and active sulphur. Only crambe oil failed to meet ASTM limits for water and sediment. The flash point of all oils was far above that of diesel fuel, reflecting the nonvolatile nature of plant oils but also safer handling in comparison to diesel. It was seen that viscosity increases with an increase in chain length and a decrease with increase in the number of double bonds. The authors also investigated the cetane number of various plant oils and concluded that its value was close or exceeded the ASTM minimum of 40. The different fatty acids composition causes a considerable spread in cetane values. Presented equations include the chemical structure of oil without providing a relationship to liquid temperature.

Chemical and physical properties of plant oil substitutes were investigated by Peterson et al. [325]. Four different oils were tested and compared with No. 2 diesel. Similar to the work of Goering at al. [157], high values of oils viscosity were found. Additionally, influence of oil temperature on the kinematic viscosity was presented. Finally, some

engine tests in respect to oil properties were conducted, showing power output and fuel consumption to be equivalent to diesel fuel.

Some of the physical and chemical properties of various oils and their esters are presented in Table 2.7 regarding them as fuel.

Table 2.7: *Physical and chemical specifications of the plant oil fuels used [214]*

Fuel type	Caloric value (kJ/kg)	Density (g/dm^3)	Viscosity (mm^2/s)		Cetane number	Flash point [°C]	Average Chemical formula
			27[°C]	75[°C]			
Diesel fuel	43 350	815	4.3	1.5	47[1)]	58	$C_{12}H_{23}$
Raw sunflower oil	39 525	918	58	15	37.1[1)]	220	$C_{57}H_{103}O_6$
Sunflower methyl ester	40 579	878	10	7.5	45-52	85	$C_{55}H_{105}O_6$
Raw cottonseed oil	39 648	912	50	16	48.1[1)]	210	$C_{55}H_{102}O_6$
Cottonseed methyl ester	40 580	874	11	7.2	4552	70	$C_{54}H_{101}O_6$
Raw soybean oil	39 623	914	65	9	37.9[1)]	230	$C_{56}H_{102}O_6$
Soybean methyl ester	39 760	872	11	4.3	37	69	$C_{53}H_{101}O_6$
Corn oil	37 825	915	46	10.5	37.6[1)]	270295	$C_{56}H_{103}O_6$
Opium poppy oil[1)]	38 920	921	56	13	-	-	$C_{57}H_{103}O_6$
Rapeseed oil[2)]	37 620	914	39.5	10.5	37.6[1)]	275-290	$C_{57}H_{105}O_6$

[1)]Values for opium poppy oil were taken from Doysan Ltd. [30]
[2)]Values for RSO were taken from Paksoy Ltd.[31]

2.1.1.3 Diesel alternative feasibility

Definition of plant oil parameters determines its feasibility as diesel alternative. Companies modifying diesel cars successfully adopt such standards [93] and relates elaborated engine modifications to the quality of plant oil. Table 2.8 shows the RSO parameters accepted by Elsbett Company. Importance of properties in comparison to diesel fuel is defined by ASTM or European standards as shown already in *Subsection 2.1.1.2*. According to the information in Table 2.8 there is a group of parameters describing viability of using plant oils as fuel, and some were also described in [332] (missing numbers in the table indicate the lack of information for a particular parameter). These parameters are more related to conditions in diesel engines and are accepted by most engine designers. Most important ones for plant oils and their relevance are grouped and shown below:

1. **Density:** Most of plant oils do not express big differences in terms of density and an average deviation is about 10% higher than diesel fuel. Therefore the influence on usability is of less importance.

2. **Flash Point** As it has been stated is much higher than with diesel fuel. This makes the transport of oil safer. The influence on usability is of less importance.

3. **Calorific Value:** Is more or less the same for all kind of plant oils and 10% lower compared to diesel fuel. Because of a higher density the volumetric content of heat value is nearly equivalent to the same volume of diesel. The influence on usability is of less importance.

4. **Kinematic Viscosity:** As mentioned before most of the plant oils have higher viscosity than diesel fuel. Viscosity varies amongst the different types of oil. Kinematic viscosity is one of the crucial parameters governing engine modification. If viscosity is too high, the engine simply can not run because of incorrect performance of injection system. Heating is one of the measures to enable engines to run on plant oil. Therefore the influence on usability is important.

5. **Low temperature behaviour:** The specification of this parameter has not been defined up to now. However, the low temperature behaviour is of importance for engine cold start and low load. Viscosity is one indicator of low temperature behaviour. The influence is important.

6. **Cetane Number:** There is not a suitable testing method of cetane number. Its determination is not as straightforward as in case of octane number. The reason for this is that because the engine for the standardising test is a diesel engine itself. The cetane number influence on usability is of less importance.

7. **Carbon Residue:** There are some established methods to be used. Furthermore, it is a remarkable correlation to the residues in the combustion chamber, piston rings and valves, so carbon residue should be kept low. Influence on usability is important.

8. **Iodine Number:** Is an indicator for double bindings in the molecular structure and is defined by standards. It influences the long time stability of properties (storage). That means influence on usability is important.

9. **Sulphur Content:** Determined by standards and one of the important factors to estimate fuels environmental impact. Sulphur reduces the function of catalysts and causes SO_x emissions. The influence on usability is important.

10. **Contamination:** That is the most important property from a technical point of view. If the amount of contaminants is too high it leads to filter and nozzles blockage and is abrasive in the complete fuel circuits. Must be well controlled, the influence on usability is very important.

11. **Acid Value:** Determines the content of free fatty acids. Can affect the properties of lubrication oil if bigger quantities reach the oil sump. Therefore the influence on usability is of importance.

12. **Oxidation Stability:** Specifies the ageing process of the oil and there are standards to determine it. With progressing age the viscosity is also increasing continuously. Can also influence the engine oil. Influence on usability is important.

13. **Phosphorus Content:** Its determination is governed by appropriate standards and dependent much on how the oil is produced. Phosphorus is dangerous for the engine due to its abrasive function. Phosphorus content is strictly related to the amount of proteins present in the oil. The influence on usability is very important.

14. **Ash Content:** Methods of determination have been standardised. Provides the content of oxide- and raw-ash. Ash is abrasive. Therefore, the influence on usability is important.

15. **Water Content:** Normally it is determined through standard Karl-Fisher method. Water tends to emulsify and is not disadvantageous for combustion in the engine. However, the emulsification is not stable and coalesce into bigger drops causing problems anywhere in the fuel system then. That means the influence on usability is very important.

Generally, a first rough check of the oil quality should be focused on viscosity, contamination, phosphorus content and water content.

2.1.2 Diesel engines on plant oils

Significant number of studies have been done by different researchers involving neat plant oils as a potential diesel fuel replacement. There are some negative aspect of straight

Table 2.8: *Quality standard for RSO (Thanks to Elsbett Co., LTV-Work Session in De-central Vegetable Oil production, Landtechnik Weihenstephan, In co-operation with ASG) [22]*

Properties/Contents	**Unit**	**Limiting value**		**Testing method**
		min	**max**	
Characteristics properties for RSO				
Density [15°C]	kg/m3	900	930	DIN EN ISO 3675 DIN EN ISO 12185
Flash Point by P.-M.	°C	220		DIN EN ISO 22719
Caloric Value	kJ/kg	35000		DIN 51900-3
Kinematic Viscosity (40°C)	mm^2/s		38	DIN EN ISO 3104
Low Temperature Behaviour				Rotational Viscometer
Cetane Number				ASTM
Carbon Residue	Mass %		0.40	DIN EN ISO 10370
Iodine Number	g/100 g	100	120	DIN 53241-1
Sulphur Content	mg/kg		20	ASTM D5453-93
Variable properties				
Contamination	mg/kg		25	DIN EN 12662
Acid Value	mg KOH/g		2.0	DIN EN ISO660
Oxidation Stability(110°C)	h	5.0		ISO 6886
Phosphorus Content	mg/kg		15	ASTM D3231-99
Ash Content	Mass %		0.01	DIN EN ISO 6245
Water Content	Mass %		0.075	EN ISO 12937

application of plant oil such as declined performance of injection system and engine life in some cases will be drastically reduced. These different effects can be analysed through a type of engine test varying in time and used as a diagnostic method. As study of using plant oil in diesel engine remains very complex subject, presentation of recent results can be done by summarising the essential studies on short- and long-term problems as well as tests on different types of oils and diesel engine units. Recent publications relate to indirect and direct injection diesel engines excluding the most modern type - the CR one. Simply, the CR systems are new and application of plant oils within this group is very limited mainly to some practical trials in companies dealing with modifications. It is expected that presented results are common for the whole family of diesel engines and can be associated with the CR systems too. Understanding how diesel engines, in particular the direct injection ones, operate on plant oils is crucial for further research and modification of the CR diesel engines.

2.1.2.1 Short- and long-term problems in DI and IDI diesel engines

During the last decade many researchers have investigated the general use of plant oils in compression ignition engine fuel [164; 205; 214; 217; 377] and many others. The high viscosity and surface tension, acid composition, free fatty acid content, as well as gum formation because of oxidation and polymerisation during storage and combustion, carbon deposits and lubricating oil thickening are obvious problems [124; 181; 185; 226; 255; 318]. Therefore, the direct use of plant oils and/or the use of blends of the oils, has generally been considered to be problematic for both direct (DI), and indirect (IDI) injection diesel engines as well as for CR ones [185; 275; 295; 318; 321; 322; 336; 435; 436]. However, studies on indirect diesel engines were more successful [333] since there has already been a significant number of modified cars equipped with IDI engines properly working on plant oils are reported in following publications [185; 336]. Based on available published data, engineering experience of various companies dealing with diesel engine conversion, probable reasons for short - and long-term operational problems together with potential solutions and are shown in Table 2.9 as a guideline for enabling successful operation of diesel engines (both IDI and DI) on plant oils.

Despite the successful tests when diesel engines were working on plant oils for a short time, the actual real assessment of such success needs to be measured in long-term operational periods. Hence, two types of problems have been recognised and defined accordingly to the duration of a test: short- and long-term problems. Normally, the short-term problems are associated with engine test up to 10-15 hrs of operation. Any other conducted for longer that period are recognised as long-term tests and respectively result as long-term problems. In short-term engine tests of less than 10 hrs duration, the plant oils could perform quite well. Problems occur after the engine has been operating on the plant oil for longer periods of time and this is the crucial problem. Research on direct use of plant oil as alternative diesel fuel is based on the main idea of application and some hints are listed in Table 2.9. Then, results of the research bring some possible solutions to overcome the recognised problems. And, finally it allows the possibility to apply modifications successfully by the help of these suggestions. This methodology was described and applied in work of Ziejewski et al. [435], and Peterson et al. [325]. Plant oils are considered viable replacement fuel for diesel engines, however in order to become successful diesel fuel substitutes, problems associated with formation of deposits, incomplete combustion etc.

must be resolved, or else truly long-term engine reliability will not be possible.

According to the information presented in Table 2.9 and the summary of information from the works of Ziejewski and Peterson [325; 435] there is a limited number of engine conditions that are responsible for the majority of the problems associated with the use of plant oils as fuel for diesel engines. The low engine load, low speed modes, transition from the high loads to no load states (reduction of the fuel flow), cold start-up, and the presence of the plant oil in the injection system during the shut-off period are the most problematic aspects of using plant oils in diesel engines. Plant oils are not good for engines operating at low load, low speed conditions since they do not assure a consistently good quality injection process. Improving the injection regime would help to eliminate problems of low load and speed. During the transition from the high load, the temperature of the fuel injection system is relatively high which in conjunction with a low fuel flow rate that translates to high fuel residence time at high load, creates conditions suitable for thermal polymerisation, lacquer and deposit formation. Additionally, during these conditions a significant amount of liquid fuel is present on the nozzle tip at the end of each injection cycle, which tends to get polymerised and block up the nozzle bores. This takes place even in the case of seat-hole nozzles, where the start of the spray hole is located in the seat tapper, and with the nozzle closed it is covered by the nozzle. Problem of excessive gum formation leads to fast buildup of carbon deposit on internal parts of diesel cylinder. In the case of petroleum-based diesel fuel the temperature and air motion is sufficient for evaporation of the majority of the fuel and only small amounts of dry soot is normally present. For high viscosity plant oil the residue fuel will thermally decompose and form a carbonaceous type residue on the injection nozzle tip enhancing deposit formation. Such deposit is actually a mixture of unburned soot, lacquer and polymerised plant oil. In accordance with information in Table 2.9 one of the most obvious problems in short-term engine tests with plant oils is the formation of carbon deposits of the injection nozzles. The deposit formed by incomplete combustion of plant oils is harder than the usual one formed with diesel fuel. Another problem in the use of plant oils are the result of incomplete combustion resulting in carbon build-up inside the cylinder and rings and contamination of engine oil. Korus et al. [226] investigated the carbon deposit in direct injection diesel nozzles of John Deere T4239 four-cylinder industrial diesel engine. The fuels used were blends of high-oleic safflower oil, high-linoleic safflower and winter rape with diesel fuel. Experiments revealed that all injectors exhibited deposits in a crater-like manner on the

Table 2.9: *Known problems, probable cause and potential solutions for using neat plant oil in diesel [163]*

Problem	Probable cause	Potential solution
Short-term problems (<15 hrs)		
Cold weather starting.	High viscosity, low cetane, and low flash point of plant oils.	Preheat fuel prior to injection Chemically alter fuel to an ester.
Plugging and gumming of filters, lines and injectors.	Natural gums (phosphatides) in plant oil. Other ash.	Partially refine Filter to 4-microns the oil to remove gums.
Engine knocking.	Very low cetane of some oils. Improper injection timing	Adjust injection timing. Use higher compression engines. Preheat fuel prior to injection. Chemically alter fuel to an ester.
Long-term problem (>15 hrs)		
Coking of injectors of piston and head of engine	High viscosity of plant oil, incomplete combustion of fuel. Poor combustion at part load with plant oils.	Heat fuel prior to injection. Switch engine to diesel fuel when operation at part loads. Chemically alter the plant to an ester.
Carbon deposit on piston and head. of engine	High viscosity of plant oil, incomplete combustion of fuel. Poor combustion at part load with plant oils	Heat fuel prior to injection. Switch engine to diesel fuel when operation. at part loads. Chemically alter the plant to an ester.
Excessive engine wear combustion of fuel.	High viscosity of plant oil, incomplete to diesel fuel when operation. Poor combustion at part load with plant oils. Possibly free fatty acids in plant oil. Dilution of engine lubricating oil due to blow-by of plant oil.	Heat fuel prior to injection. Switch engine at part loads. Chemically alter the plant to an ester. Increase motor oil changes. Motor oil additives to inhibit oxidation.

outside tip, especially around the orifices. All plant oil fuel blends gave a statistically significant increase in carbon deposit relative to diesel. According to presented photographs of the four injectors the high-linoleic safflower gave significantly more deposit then either the high-oleic safflower or winter rape. Considering the presented results it needs to be stressed that the test was performed using unmodified diesel engine.
The start-up conditions, particularly at the low ambient temperature, can be an important reason for poor fuel atomisation and a significant amount of unburned fuel, which is the source of carbon residue and leads to degradation of the engine oil. The start-up problems are especially noticeable during cold seasons when firing the engine is even impossible. One of the solutions is an excessive preheating or dual-tank system.

2.1.2.2 Engine test operating on plant oils

Some basic experiments of the formation of residue were also reported by Goettler et al. [159]. He pereformed tests on suspended drops of sunflower, corn, olive and safflower oils in diesel fuel measuring residue deposit. Apart from neat oils, the methyl ester of sunflower oil was also tested for the comparative purpose. Results showed strong temperature dependence on the rate of formation of volatile components and residue coming from oils. Authors noticed that the degree of unsaturation of the tested oils would affect the outcome of the tests by degree of deposit buildup. The oils with high oleic content i.e. olive and safflower have a lower carbon-carbon double bond density and thus should produce less deposit, however this was not observed. The analysis of results showed that satisfactory long-term engine operation on plant oils would require re-tuning of the engine or/and design modification. This would prevent or deteriorate formation of the deposits. Authors did not suggest specific modification but pointed out that fuel delivery and injection system as major elements to be modified.
Some plant oils obtained from commercial producers were investigated by Peterson et al. [325] in short-term engine tests to determine their effect on engine performance. Four cycles of long-term (830 hrs) tests were also conducted to evaluate potential effects on engine life. Prior to the tests authors determined basic physical properties of investigated oil as well as chemical structure of used oils. Experimental results show again that high viscosity and tendency to polymerise within cylinder are major short- and long-term operational problems. Attempts to reduce the viscosity by pre-heating the fuel were not successful, however in short term tests engine performance showed power output and

fuel consumption to be equivalent to that for diesel-fuelled engine. Furthermore, it was observed that severe engine damage occurred in a very short term time period in tests of maximum power with varying engine RPM. In the same set of experiments, authors used a different diesel engine: Ford 4600 3-cylinder tractor to operate on 100% safflower oil. The engine continued working for 15 months and accumulated 154 engine hours, about 120 hrs doing fieldwork and 35 hrs in demonstration work. Engine inspection revealed severe piston ring seizing, stuffing of the piston onto the cylinder walls and pitting of the rod bearings. Also, excessive deposit formation was found on injectors and piston ring grooves. Researchers did not record any abnormal wear, gumming or corrosion in a diesel injection pump.

Pryde [333] performed short-term engine tests of less than 10 hrs duration, and run the engine on the plant oil for longer periods of time studying indirect-injection and direct-injection engines to examine the various problems pertinent to using oils. Pryde presented that the problems show up only after the engine had been operating on the plant oil for longer periods of time and were far more pronounced in direct-injection engines than in the less efficient engines having pre-combustion chambers (indirect-injection). The work of Pryde does not record major short-term problems as it has been showed in previous tests above. Lack of short-term problems can be explained that the engines were not properly inspected but as only performance was observed. As a result of his study Pryde defined the main advantages: liquid nature-portability, heat content-88% of diesel fuel, ready availability, renewability and disadvantages: higher viscosity, lower volatility, the reactivity of unsaturated hydrocarbon chains of using plant oil as fuel and suggested further study.

Similar to the work of Pryde [333] and Machacon [255] other articles [42; 49; 124] have reported encouraging engine performance under short-term usage, but again have faced degraded engine performance for prolonged operation with plant oils. Engine tests explored some auxiliary parts of the diesel engine and looked carefully at the combustion chamber. The problems reported included fuel filter clogging, deposit build-up in the combustion chamber, injector coking, piston ring sticking and lubrication oil thickening [42; 49; 124], which necessitate overhauling the engine with the changing of some parts. These problems are typical for diesel engine operation of plant oils and reported elsewhere.

Questions appeared only after the engine has been operating on plant oils for longer periods of time, especially with direct-injection engines. The problems include coking and soot lump formation on the injector tips. This phenomenon is caused by the polymerisation of oil at the beginning by lacquer formation to such an extent that fuel atomisation does not occur properly or is even prevented as a result of plugged orifices. Carbon deposits, oil ring sticking-thickening and gelling of the lubricating oil as a result of contamination by the plant oils are main problems revealed during experiments [295; 318; 322].
It was already recognised one major obstacle in using plant oils at room temperature was their high viscosity, which causes clogging of fuel lines, filters and injectors [42]. It was proved again that the cumulative operation hours before overhaul is needed are shorter for plant oils than for diesel. As an example a fuel filter has to be changed every 100 hrs of operation if the same as for diesel fuel is used. Therefore researchers claimed that, plant oils could not be used directly in diesel engines at room temperatures. In order to reduce the viscosity of the plant oils, three methods were found to be effective: esterification (already known process to produce bio-diesel), mixing with lighter oil (common blending with diesel) and preheating [281]. In some of the successful applications, the modifications of diesel engines were applied to the injection system parts like fuel lines, filters and pumps. Some of these solutions have been already commercially applied [93]. Especially preheating the plant oil, which is one of the basic practices performed by diesel cars modifiers to avoid the problem of clogging the fuel lines and improve atomisation. Bari et al. [57] studied filter clogging and power loss using waste cooking oil. Employing a simple experimental system parameters like flowrate through the filter the heat losses were measured. The experiment was repeated for different oil temperatures and ambient temperatures of diesel fuel. It has been concluded that a heating temperature of at least 55°C was required to prevent clogging during the start-up period and the optimum temperature of 70°C is required to overcome the head loss in the system. Compared with diesel, the head loss across the filter for oil was much higher due to higher viscosity of the oil. This work clearly showed a potential solution (technically feasible) to short- and long-term problems but the optimal temperature of 70°C seems to be difficult to maintain in practice.

As it has been shown before (*see Subsection:* 2.1.1), plant oils have heating values equivalent to diesel fuel and their combustion characteristics are nearly the same (non-engine like), but their viscosity is too high for the modern fuel injection system. As a potentially viable source of energy, plant oils face the need to modify injection system accordingly to

oils' properties. So far, the development of the modern diesel engines has been tailored to the availability of petroleum-derived fuel and its blends with bio-diesel. Followers of less radical changes to diesel injection system, suggest chemical treatment of plant oils, blending even partial distillation and filtration to make the new fuel less harmful to engines. Fuel modification may, however, improve the viscosity of plant oil fuel but other related problems may still exist. In available literature resources there is a substantial number of papers dealing with production, characterisation and application in diesel engines of the modified plant oil widely know as plant oil esters or bio-diesel. For a long time a number of application of plant oil was oriented to obtain alkyl esters from the triglyceride blends of plant oils rather than using their raw form. Direct chemical synthesis enables the solution of most of problems encountered with the use of neat plant oils in diesel engines expressed in the contents of Table 2.9.

Although, the chemical treatment of oils eliminates the idea of "short carbon chain" process [320] it makes the final product more expensive analysing the numbers presented in [418] and less safe (esters handling is more demanding that plant oils). Operational problems like fuel flow, fuel lines corrosion and start-up problems are also common for somehow "treated" plant oils and widely recognised by diesel engine drivers [258]. Even, reduced viscosity does not in fact ensure proper fuel atomisation. The paper of Krahl and coworkers [231] summarises the impact of RSO and rapeseed methyl ester on the emission of federally (according to German regulation obeying at the time of tests and cited in this paper [231]) regulated exhaust components where two types of diesel engines were used in tests: the IDI and DI ones and the emissions were compared to diesel fuel. In the case of RSO, the Elsbett engine [1] was used. In conclusion, RSO ester seems to present fewer disadvantages of the two fuels compared, level of nitrogen oxides and soot number were higher for this type of fuel, also carbon monoxide emission from DI engine was higher for the ester. Respectively, particulate matter and unburned hydrocarbons in IDI engine fuelled with neat RSO was far higher than for the ester. The authors concluded that the additional research is necessary to provide more consistent output.

In a brief summary of the remaining available publications results indicate that the esters from various plant oils are an attractive substitute for diesel fuel expressing smoother operation with reduced short- and long-term problems, with better fuel economy, generated

[1] More information about the engine in http://www.elsbett.com/us/elsbett-diesel-technology/elsbett-engine.html.

lower emissions including lower carbon monoxide, unburned hydrocarbons and particles. Bio-diesel is also essentially sulphur free and offers enhanced safety characteristics when compared to diesel fuel. It has a higher flash point and does not produce explosive air-fuel vapours. However, the main obstacle of using the plant oil esters is their price, which without government premium would not compete nowadays with diesel and relatively high cloud point. There are also examples of unattractive prices of bio-diesel. In some countries i.e. Germany, Austria, Italy, France, Sweden, Denmark and the Czech Republic [235] there is a significant reduction from excise taxes. However, cost has been a major factor slowing the commercialisation of bio-diesel. The higher cloud point of bio-diesel than diesel fuels requires engine and fuel heaters when used as a pure fuel in climates where the temperature drops below 0°C.

There are already some European manufacturers which offer bio-diesel-compatible tractors like Fendt, Fiatagri, Ford, Case, John Deere, Deutz-Fahr, Lamborghini, Lindner, Massey-Ferguson, Mercedes-Benz, Same, and Steyr [5] based on technology coming from the extensive tractor field tests done with bio-diesel in Europe [80; 230] and in the US [6; 323; 363; 419]. It is predicted that countries already producing this type of fuel will develop a bio-diesel market and therefore the use of neat plant oils will be relatively slowed down for the next few years.

Frequently, researchers have concluded that higher viscosity resulted in incomplete atomisation of neat plant oil fuel. This in turn prevents complete combustion of large fuel droplets resulting in carbon deposits and dilution of engine oil. Knocking, encountered during the test at low load and low cylinder temperature, was due to the low cetane number of plant oil and poorer air/fuel mixing. Plant oil properties examination indicate that plant oil fuels exhibit longer ignition delay and slower burning rate especially at low load operating conditions hence resulting in late combustion in the expansion stroke giving rise to a reduction of maximum peak cylinder pressure. However, as an advantage here, slower combustion restrains NO_x formation. However, some experimental results seem to be contradictive and do not prove that conclusion. Examples of the ignition delays are discussed later in this section.

The test showed [298] that plant oil fuels exhibited longer ignition delay with slower burning rates and the advanced injection timing could be proposed to compensate effect of ignition delay. This idea was investigated by Nwafor et al. [298] who employed the engine with a standard injection timing of 30° before top dead centre (BTDC). First, the injection

was advanced by 5.5° at given injection timing of 35.5° BTDC. The engine performance was noticed as very erratic on this timing. Then, the injection was advanced to 39°. The engine performance was smooth especially at low load levels, which is quite problematic once plant oils are used. The ignition delay was reduced through advanced injection but tended to a slight increase in fuel consumption. The test results showed that each alternative fuel requires injection advance appropriate to its delay period. The delay period was noted to be influenced by the engine load, speed and the system temperature. Researchers reported that at the engine speed of 2 400 RPM, there seemed to be a significant increase (by almost 40% in comparison to diesel) in brake thermal efficiency when running on RSO fuel with standard injection timing. Mechanical efficiency was observed to be reduced with advanced timing compared to the standard timing test results at 2 400 RPM. The engine ran smoothly with advance of 3.5° as compared to the standard timing. A further 1.5° advance tended to produce erratic behaviour of the engine. Nwafor [298] suggested that a moderate injection advance was recommended for operations at low engine speeds. The overall results indicated that plant oils exhibit longer combustion duration with moderate rates of pressure rise, unlike petroleum-derived fuels and the problem of ignition delay could be solved by appropriate setting of the injection timing.
Simultaneously to the evaluation of diesel engines performance in terms of their durability, research work considering emission took place. Additionally to work of Krahl [231], Altin et al. [33] comparatively evaluated the performance and exhaust emissions of a diesel engine using 100% refined plant oils and their methyl esters. Particulate emissions of plant oil fuels were higher than that of diesel fuel, on the other hand, NO_2 emissions were less, which agreed with previous observations recorded by [231; 269; 322]. Plant oil methyl esters gave performance and emission characteristics closer to the diesel fuel.

Crookes et al. [97] measured the combustion performance of plant oils, blends with diesel fuel and emulsions with water using a variety of experimental techniques including single-cylinder engine tests. Researchers examined carefully single droplets burning taking place at atmospheric and elevated pressure and compared the results with diesel. Findings showed poorer combustion of pure oils and better for emulsions. In single-cylinder engine tests at relatively low power and speed, the ignition delay was longer for the plant oils. Soot levels were generally higher for oils than for diesel fuel and oxides of nitrogen lower. Unlike most operating modifications which result in a trade-off between these components, emulsification of the plant oils with water reduced levels of both soot and oxides of nitro-

gen.
The works of Castro [87], Goring [158] and Crookes [97] revealed that the use of plant oil emulsions is one of the ways to overcome short- and long-term problems but does not provide a reliable solution.

Despite some promising results and a wide collection of experimental data, the aspect of using neat plant oils, as a source of renewable energy has not been widely applied due to well recognised short- and long-term problems and requires more detail research.
Application of neat plant oil in diesel engines is frequently determined by a type of oil and further engine modifications are subjected to these specific properties. In some cases a type of modification allows to run an engine only on a specific type of plant oil. The next subsection focus on using rapeseed (including Canola). The last subsection presents some rare application of other oils available on market.

2.1.2.3 Use of rapeseed oil

With the recent popularity of the cultivation of oilseed rape in the European Union (e.g. in UK it is currently the third most-widely grown crop), RSO is the most obvious candidate for evaluation and review of existing studies. Making RSO compatible with existing diesel engines, primarily the oil has to be readily available. The large molecular size of the component triglycerols of RSO, results higher viscosity compared with that of mineral diesel fuel (*see Subsection:* 2.1.1). There are two types of rapeseed widely cultivated in Europe: winter and spring breed and potentially available for engines. The seeds of different varieties of oilseed rape contain differing concentrations of fatty acid compounds and have different chemical and physical properties [180; 324]. As it might be expected the high viscosity of RSO affects the flow properties of the fuel, spray atomisation and air/fuel mixing and consequently vaporisation. This difference in viscosity is anticipated to have an adverse effect on the combustion of RSO in most of existing diesel engines. These properties are causing problems in the associated fuel pumps, filters and injector systems [22; 418]. There have been a number of suggestions how to reduce the viscosity of RSO and thus to alleviate these problems in [218; 295; 318; 436]. In general, RSO causes similar operational problems presented at the beginning of this section but also provides some specific to its physical and chemical properties.

Three severe problems associated with the use of RSO as fuel are: incomplete combustion, engine oil deterioration and gum formtation [322]. Additionally poor fuel flow and filter clogging would complete the list. Polyunsaturated fatty acids constituting RSO were very susceptible to polymerisation and gum formation caused by oxidation during storage or by complex oxidative and thermal polymerisation at the higher temperature and pressure of combustion and engine temperature. The gum formation is one of the most severe problems occurring in RSO exposed to higher temperature. The gum does not combust completely, resulting in carbon deposits and lubricating oil thickening. There are some methods to remove constituents enhancing gum formation and are commonly known as the degumming process. The method is widely used in the food industry, but such processing increases the price of RSO and requires additional machinery.

Winter RSO as a diesel fuel was evaluated by Peterson [322]. Because of its high yield and oil content (45%) and the high erucic acid (46.7%) content the oil is facing potential use as diesel substitute. Reported the rate of gum formation of winter RSO was five times slower than that of high linoleic (75-85%) oil. The viscosities of 50/50 and 70/30 blends of winter RSO and diesel and whole winter rape oil were much higher (6-18 times) than standard diesel. A blend of 70/30-winter RSO and No. 1 diesel was used successfully to power a small single-cylinder diesel engine for 850 hrs. No adverse wear and no effects on lubricating oil or power output were noted. Research had also shown that neat RSO promised short-term success, but in their long-term use can lead to problems, especially with the injection system, piston ring sticking etc. In the majority of short-term tests employing RSO as the fuel, peak power outputs ranged from 91 to 109% those when equivalent engines were operated with mineral diesel fuel.

Based on the work of Peterson [322] it can be concluded that winter RSOs seem to be better diesel replacement than its spring breed, however it expresses higher viscosity.

Whilst longer-term engine tests confirmed the satisfactory operation of larger-cylinder IDI engines when fuelled with RSO [131] a number of problems associated with the use of rapeseed oil in DI engines and small-cylinder IDI engines were identified in [131; 302; 403], resembling those listed in Table 2.9 largely due to incomplete fuel-combustion. Also included piston ring sticking because of deposit formation (resulting in decreased compression and leakage of unburned RSO into the crankcase and scuffing of the cylinder liners. The origins of these problems identified by researchers were the comparatively high viscosity of RSO, and the polymerisation leading to “gum” formation.

Korus et al. [227] studied the gum and deposit formation too. He suggested that thermal

rather than oxidative polymerisation is the dominant gum-forming process. According to his conclusions the formation of gums could be minimised by utilising RSO with a low fraction of fatty acids possessing conjugated double bonds (e.g. linoleic acid). However, his preliminary studies to reduce polymerisation by the addition of chemical agents (antioxidant and dispersant) had proved unsuccessful and seems be rather inviable in real conditions. In his work he did also recorded usual operational problems associated with cold starting and listed in Table 2.9.

Apart from gum and deposit formation some other diesel engine processes and the exhaust emission analysis are of great importance when deciding if a given plant oil is suitable as an alternative diesel fuel. Raubold [336] performed test-bench experiments from a swirl-chamber diesel engine using four different kinds of fuels. Diesel fuel was used as a reference, and unprocessed RSO and two other plant oils were used as test fuels. Also, the thermodynamic analysis of the measured cylinder pressure curves had been used to obtain more detailed information. In his work, Raubold [336] used a single-cylinder diesel engine but without changes to the injection system. The test engine used did not meet performance and durability requirements when fuelled with RSO. Results shown that the engine could not be started without any starting assistance e.g. preheating system. When testing RSO there was so much injector coking that long time operation with this oil was suggested as impossible. This proved the earlier suggestions of required engine modifications and presence of auxiliary equipment. It had been proposed to redesign the position of the injection nozzle so that less coking can be expected.
The CO emission for RSO was higher than those for the other fuels when running the engine on low load. This is explained that the heat level inside the combustion chamber was too low for RSO to oxidise CO completely. The low level of the NO_x emission and excess particulate emissions were confirmed and are similar to previous research [322]. When RSO was employed the thermal efficiencies of the engines were generally reported as being slightly improved. However, because of its lower energy content (see Table 2.8 and 2.4) RSO consumption was higher than that of mineral diesel fuel. The thermodynamic analysis of the engine internal process led to conclusion that when plant oil with long chained fatty acids (like RSO) have to be burnt, the injection system should be able to alter the injection timing according to both speed and load to get the best engine efficiency. The author suggested that only moderate loads and temperature in the swirl-chamber obstruct the vaporisation and start of burning of long chained fuels.

Broader research work on performance of a diesel engine running on RSO has been presented by Hemmerlein et al. [185]. Their research was aimed at getting more knowledge on operating behaviour of a wider variety of modern diesel engines under specified conditions. All combustion systems used in modern diesel engines, such as swirl chamber, pre-chamber and direct injection were represented and tests were carried out with neat RSO. Presented results revealed torque and power output with RSO were only 2% lower than with diesel fuel, which was related to the observation that with all engines the maximum combustion chamber pressures were lower causing slightly lower mechanical stresses in the crank drive and lower heat release and hence the power output. Combustion noise was lower when RSO was used. Reduced noise level is characteristic for all application of plant oil in diesel engines. All tested engines investigated fulfilled current ECE R 491 [1] regulation concerning CO, HC, NO_x and soot emissions. Carbon monoxide emissions were 100% higher with RSO compared to diesel, also hydrocarbon emissions increased depending on the operating range up to 290% compared with diesel. Similarly to previous investigations [33; 269; 318], lower maximum temperature in the combustion chamber, emission of nitrogen oxides were up to 25% lower. Soot emission decreased in the whole operating range. The reduction of particulate emissions varied from 30 to 50%. This result was in contradiction with measurements of light-duty cars in transient test procedures, where an increase in particulate emission was detected. Detailed analysis of soluble organic fraction, aromatic hydrocarbons, aldehydes, and ketones emission was performed. In most cases emissions were higher when RSO was used in [185; 230; 434]. Engine durability tests showed that pre- and swirl chamber performance was as scheduled. The DI engines and the light-duty car ones failed due to a quick build-up of carbon deposits on the injection nozzles and piston failure. Negative influence on fuel injection and in consequence on mixture preparation, ignition and combustion process caused increased amount of unburned fuel got into the lubricant oil and formation of solid residuals on the combustion chamber walls and piston ring grooves.

The second significant factor decreasing engine's performance was the rapid blocking of the fuel filters because of phosphates content. The fuel filters had to be changed more frequently, as high backpressures resulted from their blockage by phosphates in the RSO. Generally, diesel engines with divided combustion chambers and big cylinders units were able to operate permanently with neat RSO. DI engines according to authors were not

[1] European Emission Standard; max. limits (g/kWh): CO-11.2, HC-2.4,PM - not specified, NO_x-14.4

suited to operate with RSO.

The same authors also reported comparative test results of six different engines fuelled with RSO and diesel fuel. With RSO fuel torque, power and NO_x emissions of 5 engines out of 6 were better; HC emissions of 5 engines out of 6 were worse; CO emission values were worse in all engines. And two of the engines showed better endurance test results. Energy consumption values of all the engines were about the same for both fuels. Nevertheless, Hemmerlein [185] did report advantages resulting from the use of RSO. These included: lower resultant maximum cylinder pressure than that measured when using mineral diesel leading to lower mechanical stresses in the crank drive; and slower heat-release rate which ensures lower rate of pressure rise in the cylinder and a reduction in combustion noise.

Peterson [321] and co-workers carried out similar work to that by Hemmerlein [185]. Three different tests using plant oil had been explored using a farm tractor unit, 4-cylinder direct injection engine and a small single cylinder diesel unit. No modifications were made to these engines before or after using plant oil fuel. Horsepower and fuel consumption were obtained. The tractor had been operated in long-term test for over 100 hours on the plant oil and during that time the power has declined by about 10%. The short test using winter and spring rape oils and also safflower and sunflower in mixtures with diesel and alone had been conducted on this 4-cylinder diesel engine. These short-term tests indicated no decline in horsepower and virtually the same fuel consumption for various plant oils. The higher viscosity of the plant oils, particularly of winter rape, gave some engine RPM oscillation due to starving the engine of fuel when the filter restricted the fuel (possibly due to filter clogging). The fuel mixtures with diesel showed a slight increase in horsepower. Authors concluded that the results for this type of engine showed a good potential of the plant oil fuels. The endurance test was performed for 830 hours in a long-term engine run. High amounts of copper in the lube oil were found after the test. It was diagnosed as wear on the rocker arm bearing. The engine showed more carbon in the combustion chamber and on the piston rings. Also, additional varnish and carbon build-up on the injector nozzle was apparent. At the conclusion on the test, the injector in the engine had seized and the engine would no longer start. Experiments of Peterson proved usual short- and long-term problems indicated by earlier by other researchers and indicate the main obstacles.

Reviewing engine test of RSO should include similar studies on Canola. Canola is one of the most important oilseed crops in the world mainly cultivated in US and Canada.

Canola's botanical origin is rooted in rapeseed, however the deliberate breeding programs created a plant with a low level of erucic acid and glucosinolates in comparison with RSO. Nevertheless Canola oil properties are very close to rapeseed ones. A very low level of saturated fatty acids, a relatively high level of monounsaturated fatty acids and an intermediate level of polyunsaturated fatty acids characterise Canola oil. Canola oil is much more viscous than the other more commonly tested plant oils. Because of significant similarities between Canola and rapeseed some of these results of engines test on Canola are presented here too.

As with all fluids, the Canola oil viscosity is temperature-dependent. At 10°C the viscosity of Canola oil is 100 cSt; a 75-25 blend of Canola oil and diesel fuel is 40 cSt; a 50-50 blend is 19 cSt; and in comparison the viscosity of diesel fuel is 4 cSt [138]. Investigated by Engler, the flow rate of Canola was lower than diesel at the same pressure and it dropped to almost zero at 4°C, whereas at 37°C, the viscosity of Canola oil and 10% ethanol was 21.15 cSt, while that of straight Canola oil was 37.82 cSt. Because of unacceptable high viscosity of Canola oil Engler [138] proposed to lower it by blending with pure ethanol to be used as fuel. Engler's method of blending Canola with ethanol has not been tested in diesel engines.

Deposit formation and low temperature behaviour of Canola oil was studied by Strayer et al. [382]. Revealed results indicated a similar set of problems as encountered while RSO is used and presented in Table 2.9. In another study Strayer et al. [381] used Canola and high erucic RSO as a replacement extender to diesel fuel in direct-injection diesel engines - a 2-cylinder Petter diesel and a 6-cylinder John Deere turbocharged diesel. Work carried out included the documented production and refining of Canola and R500 (high erucic) plant oils, and also preparation of methyl ester and of blends of all these fuels with methanol and ethanol as potential diesel replacement. Then these fuels were evaluated by ASTM and improvised tests to determine their usefulness as a diesel fuel. Results were similar for both engines in short-term performance tests proving results already found by Engler [138].

The same author [381] performed and reported later engine tests to investigate the feasibility of using Canola and high erucic RSO as a replacement/extender to diesel fuel in direct-injection diesel engines. It seems that the output of these test was nearly identical with one performed earlier.

2.1.2.4 Use of other oils

Numerous plant oil species have been presented in Table 2.1. The major kinds of plant oils and their use as diesel replacement were shown above. To provide an additional view on nearly unlimited number of applications of plant oils in diesel engines some of the specific types of oils are presented in this section. This expresses deep interest in using plant oils even very rare ones.

2.1.3 Feasibility studies and economy benefits

Application of neat plant oil in diesel engines needs to comply with two major factors: reliability of technical modification and market availability of neat plant oil. The first issue was already discussed in the previous sections showing main stream of applications, technical problems and modifications. The second factor is discussed here focusing mainly on RSO. Feasibility of a specific crop depends on a number of factors including the suitability of the crop for local growing conditions, micro- and macro-economy, farming culture, climate, soil characteristics, and pest problems affecting crop productivity. The extent of to which RSO can be substituted for mineral diesel would depend on the quantity of oilseed rape which can be cultivated annually and, in a market-driven economy, on its comparative cost of production and conditions for this production. It does also strongly depend on government regulations and its tax policy on renewable energy sources and this is going to be shown later on.
Assessments of some of these factors are presented in this section for the use of plant oils with special respect to rapeseed and RSO esters as a diesel engine fuel in the EC as well as within the UK.

2.1.3.1 Rapeseed as a new biomass crop

New crops for the biomass markets are fundamental, strategic, and highly risky. Therefore, local and national governments see a function for themselves in stimulating these activities within the framework of their agricultural and tax policy. In defining those respective policies, the following aspects have played so far a major role: contribution to solving agricultural problems; contribution to decreasing environmental impact; and contribution to the improvement of rural structure. Now an additional component of that set can be included: beneficial production of plant oil for fuel. However, the resource base for RSO

production in the EC and the UK is limited by a number of factors which include: the amount of land available for the cultivation of oilseed rape; the seed yield per hectare; the impact of oilseed rape growth on neighbouring crops; the economic advantage that can be gathered by cultivating oilseed rape rather than alternative crops; political restrictions; and any adverse environmental impact that may arise from extending the cultivation area of oilseed rape or altering current agronomic practises. Also the fraction of RSO that can be used for the production of fuel is limited by the chemical composition of RSO (different oil-seed rape varieties are preferred by different consumers); and the economic advantage obtained by using RSO for producing fuel substitute rather than other industrial applications or edible-food manufacturing. Frequently, the domestically produced plant oils are interchangeable in food and fuel uses. Some of the plant oils are unlikely to be used for fuel given current technology because of their insufficient production, however it is assumed that advanced technologies, like development of diesel engines operating with plant oils, can promote their intense and sufficient cultivation.

2.1.3.2 Rapeseed production and supply

Satisfactory substitution of petroleum-based diesel fuels with RSO requires the development of an integrated production system, the specific infrastructure for the production (processing), and a network of oil suppliers. First of all, it is necessary to implement the end-use of the new fuels on a basis that is both technically attractive and economically rewarding to all the element of the production system. Only the development of appropriate infrastructure and close co-operation amongst farmer oil extraction plants and oil distribution will result in benefits to customers of renewable energy. Still, despite the advanced development of commercially available modified diesel engines fuelled with plant oils, the main question addressed is availability of oil sources to the owners of modified diesel cars, and national supply structure of bio-fuel distributors.

Assessing the resource base is therefore a complex and important issue, particularly as many of the factors affecting it are interrelated. In addition, agricultural practises, plant breeding and genetic modification are rapidly changing the manner in which oil plants are cultivated making the crops use questioned by public. There is already a wide collection of detailed studies assessing production of plant oils in [131; 262; 264; 285] concluding necessity to highlight the most important factor in the production: the cost of raw material cultivated rapeseed.

2.1.3.3 Rapeseed cultivation

Rapeseed, as a common example of oilseed crop is cultivated around the globe, at various latitudes and under extreme climates. For instance, it can be grown in Sweden and Finland, where it survives under snow cover for a long period of time; or even above the Arctic circle, with 24 hours of light a day in summer; or in Pakistan, where day length is less than 10 hours in winter. In some growing areas, there is almost no rainfall during the growing period, whereas in others, such as Holland and France, winter and spring are very wet. So it can be stated that European oilseed production is dominated by rapeseed, and therefore this type of oil plant is recognised as main source of renewable diesel fuel.

Yield of rapeseed varies from the location of cultivation and it is different for winter- and spring-planted breeds. Nothern and Central European winter-planted rapeseed yielded much higher than spring-planted rapeseed, i.e., about 5-6 t/ha compared with 1-1.5 t/ha under irrigation. In the Mediterranean conditions with a seasonal rainfall of 350-450 mm, a rainfed rapeseed crop might yield 2 t/ha or more when sown in winter, but only 0.7 t/ha when sown in spring.

Oilseed rape is well adapted to the climate and soils of the UK as well. Since 1990 about 470 thousand ha of oilseed rape have been cultivated annually in the UK [18]. In 2001, the exact area was 450 thousand ha, which is equivalent to 2.4% of total agricultural land and 8.5% of available cropland [17]. Popularity of rapeseed cultivation in the UK is growing as a consequence of the Common European Agriculture Policy and rising demand for RSO. Maintaining the sufficient rapeseed supply is difficult and challenging. Across Europe, the crop rotation option is potentially capable however use of set-aside land has been recently preferred as more beneficial to European farmers. The costs associated with fertilisers, seed, labour and pesticides were compiled from a group analysis [130; 264] and from a recent study by Ferchau [142]. Fertiliser is usually a major component, i.e. 28% of variable costs. Pesticide spraying costs averaged 13% of variable costs. Seed costs averaged 8% percent of variable costs. The costs associated with fertilisers, seed, labour and pesticides are not shown in this section in detail because may vary from country to country. It has been showed that the significant reduction of rapeseed cultivation can be reached by optimising the rapeseed production and combining rapeseed and animal farming together [78]. Fixed costs related to land and machinery is assumed to be the same as those for wheat. Variable costs represented 49% of total input costs.

The costs involved in production of rapeseed are competitive and there is a positive

economic return for the production with a comfortable margin for the financial risks involved.

2.1.3.4 Agriculture policy

It should be noted that the economics of the cultivation of oilseed rape in the UK (and other EC countries) are dependent now, and will continue to be in the near future, on the subsidies provided under the Common Agricultural Policy (CAP) [18]. In some regions, farmers claim that the production would not be possible without such extensive support from Brussels. The subsidies persist in maintaining kind of "regulated" market without fully revealed prices of biomass. This argument is frequently brought out by opponents of using plant oils indicating that diesel and plant oil prices are competitive.
Oilseed rape destined for European Union bio-fuel industry need not compete with other food crops for available agricultural land if it is grown on land, which the CAP has required to be "set-aside" from food production (as a measure to reduce the European Union's agricultural surplus). This land can still be used for cultivating non-food crops required for industrial applications and energy production and the production will still benefit from oilseed-specific support. Set-aside policy was introduced in the arable reform package of 1992, and one year later 702 800 ha of land were set-aside in the UK. This area rose to 736,400 ha in 2001 [20]. Some analysts predict that set-aside area may have to rise still further to adequately restrict food production to within the European Union's pledges to The General Agreement on Tariffs and Trade (GATT) [165] for either cereals or oilseeds yields.
It should be noticed that oilseeds from set-aside fields have been traded in Europe at acceptable prices of around 155 EURO per ton seed so far [165; 225]. Only cheap used frying oil and other waste oils and fats can compete with these prices.

In the UK, farmers benefit form set-aside subsidy scheme. UK production of rapeseed on non set-aside land in UK in year 2001 was 1.4 million tones (3.44 million tones in EC) and 121 000 tones on set-aside land (457 000 tones in EC) [18]. Recent production within EC of RSO consists of 3.61 million tones and it is expected that will increase up to 3.81 in 2005. Growth in production is predicted to continue over the next decade, but at a slower and steadier pace. Future growth in rapeseed production will depend on the profitability to the farmer of producing rapeseed relative to profitability of planting

substitute crops. The set-aside subsidy scheme, additional financial support e.g. the UK indicated that no national premium will supplement the EC payment to its farmers under the set-aside program. It has to be noticed that oilseed rape cultivated on set-aside land, which has been removed from agricultural production, can produce significant quantities of rapemeal and rape straw as by-products as a source of additional income to producers. Although, cultivation of rapeseed on the set-aside land is not only the way to produce RSO but one of the most attractive methods due to profits of cultivating non-edible corps on this land.

In the past, a rather inefficient structure was kept intact that protected small farmers in the EC (the Netherlands, parts of southern Germany and small parts of France). Support has shifted from product support to income support (promotion of small business, special loans for farmers etc.). Product support in the past led to a strong focus on increasing yields and, hence, to intensification and overproduction and morover to increase of degraded land due to excessive application of fertilisers. Agriculture policy attempts to combat large crop surpluses by compensating producers to idle land. In fact, each year vast area of cropland is idled either through annual set-aside programs or multi-year programs reducing that effect. So far, European policies have subsidised all or part of the commodity system to protect both production (farmers) and the political power base by keeping consumers reasonably pleased. Similar policy is applied to processors and producers of oilseeds too [82] with some exemptions coming from the Blair House Agreement.

Another common practice is diversifying agriculture to include alternative crops, particularly those that can be processed into more valuable products (value-added). This would not only reduce surpluses but also help to support the nation's industrial base and reduce imports. Opportunities exist for European farmers to employ these idled resources by diversifying beyond the traditional food, feed and fibre market of agriculture into the production of RSO to help support European Economy. Additionally to CAP directives, the competitiveness of a UK bio-fuels industry could be improved by attracting available European funding through the Alternative Energy (ALTENER) [4], through programs like so called "Intelligent Energy for Europe" and the Large European Bio-Energy Network (LEBEN) programmes of the European Commission [5]. One of the targets set in the

[4)] ALTENER: Renewable Electricity and Heat, Small Scale Renewable Applications, Alternative vehicle propulsion

[5)] It has been estimated that EC will need to take out about 20 million hectares from food production. Wishing to keep this land productive and to avoid worsening of the social problems of rural people (unem-

ALTENER programme was to expand the bio-fuels market to provide 5% of the fuel consumption of motor vehicles. This would involve non-farming sector by attracting small businesses by additional sources of investment and promote to create jobs within the oil processing industry.

2.1.3.5 Yield of rapeseed

Rapeseed has been successfully grown in Europe as an oilseed crop for over 300 years. The single most important factor influencing the economic viability of rapeseed biofuel is its seed yield. Experimental yields are often ten times higher than on-the-farm yields. Duke [121] has shown that seed yields ranging from 0.2 to 14 t/ha within wide range of oilseed crops and expected average yields of about 2.24 tones per hectare for rapeseed on a commercial scale. This amount would produce about 1350 kg high protein meal (rapeseed cake) and 894 kg oil. (The rapeseed "cake" can be incorporated as a protein source in animal rations.) Regardless previous crop estimation, an average rapeseed yield of 3.09 tones per hectare has been already reached in most of European Countries and it is expected to increase up to 3.21 in 2005. In UK RSO yield varies from 2.57 to 3.23 tones per hectare [18].

It has been estimated that in 2005 3.2 million hectares of area harvested will be used only for rapeseed [13] plus 148 thousand hectares of set-aside land and reach yield of 3.21 t/ha. It has been also evaluated [409], that the area available for industrial oil-seeds production in UK for instance, should be in the region of 200 000 ha. However Carruthers et al. [86] estimated this area of 175 000 ha, with rapeseed being cultivated according to a 1 in 4 year rotation on an area of 700 000 ha.

2.1.3.6 Farm production

The key issue in the processing of rapeseed for the production of diesel fuels is whether the processing should be conducted at the local level in relatively small units of whether the oilseeds should be processed in large-scale units resembling those now employed for the production of RSO [47; 414]. Similarities to bio-diesel production can be found whereas

ployment and lower incomes), EC decided to launch a big programme for cultivation of energy and industrial crops in that area. This programme is called "Large European Biomass Energy Network" (LEBEN) and is supporting the development of projects, at pilot and industrial scales, in many European countries (Italy, Scotland and other). LEBEN's proposal is the increasing of biomass utilisation, at regional scale, for energy production, associated with the production of industrial products like sugar, ethanol, organic fertilisers, animal feed stocks, activated charcoal and others (*source:*http://www.fao.org/docrep/T4470E/t4470e0s.htm)

generally two main models were established: local (decentralised) and centralised method of production.

On-farm liquid fuel production requires a considerable investment in capital and management, however one of the sources of supply of RSO to farmers is to process whole rapeseed on the farm. Recent concerns over the price and availability of liquid fuels have created substantial interest in alternative sources of fuel in on-farm methods of production [47; 92; 123; 348; 414]. Rapeseed crop is a well-selling product readily trading by oil producers at agricultural stock markets, this also include rapemeal. In comparison, production of traditional agricultural products is more than consumers can use. This had been the case particularly for wheat, corn, and potatoes for nearly two decades. Competition is getting more intense because production of these has increased faster than consumption. European Union forces reduction of crop acreage to prevent overproduction, which significantly effect farmer's incomes. This promotes bigger farmers' interest in industrial crops as an additional income. Therefore, it is assumed that profit is the primary motivating factor for farmers and oilseed processors. Non-monetary goals, such as energy independence, environment protection should be considered as a driving factor for some individuals but require additional investment and sometime technical skills. Over the long haul, however, the ability to generate profits is critical. Before deciding to plant a non-traditional crop, farmers must consider four factors: demand for the product as reflected in its price; availability and location of the nearest market; cost of production; and the crop's suitability to the local environment [325]. The basic question is whether returns from the crop will be more than the supply and demand and if this will comply with existing policies. Additionally, processing systems need to be developed to achieve the desired levels of purity at reasonable costs. Oilseeds crop production needs to be enhanced by selection, breeding, and improved agronomic practice for those crops that appear to be attractive on both technical and economic grounds.

There are three basic methods of extraction oils from oil-bearing seeds. These are mechanical or full-press extraction (crushing), direct solvent extraction, and pre-press solvent extraction. The latter two methods employ solvent as a means of separating the oil from the seed and are expensive. The solvent must then be distilled to recover the oil, which requires extensive capital investment in distillation equipment, and handling of highly volatile substances. The solvent extraction systems were considered to be inappropriate technology for farm scale operations and cold screw-pressing extraction is getting more

popular because of its good efficiency and its environmental friendliness. The solvent extraction method is not the most suitable one to provide quality RSO for diesel application mainly due to higher water and phosphorus contents.

The crusher and filtering equipment are necessary equipment in mechanical RSO extraction [48]. Rapeseed can be processed in most existing facilities that have traditionally been used for other oilseed crops with minimum investment. However, a study of this application should involve major outlets for the oil and meal and then potential utilisation and economic profitability of production. The technology of rapeseed processing, on farm-scale, is much simpler than that for ethanol production for instance [319]. This, coupled with the fact that most energy intensive farm operations use diesel powered equipment, has created substantial interest in RSOs as an alternative source of liquid fuel for agriculture. The time devoted to on-farm fuel production, while being a considerable drain on the farmer's efforts, is generally not enough to make an adequate return on his investment in buildings and equipment. This conflict in available time and return can probably best be resolved by going to larger off-farm plants operating full time or by creating a specific model of production and utilisation RSO and its side products. And yet the need remains for farmer controlled liquid fuel supplies. In order to achieve rurally controlled diesel fuel supplies, some types of co-operative processing plant using mechanical oil extraction are likely.

Farm RSO production promotes visible cooperation amongst agriculture and non-farming sectors. The linkage between the farm and the domestic and foreign sectors is through an industry composed of firms, which process raw oilseed commodities, manage supply, cooperate with biodiesel sector. In many cases in the European Community, firms involved in oilseed processing are also involved in raw commodity assembly and transportation to and through final export market. European Community rapeseed-processing industry has a yearly crushing capacity of approximately 9.127 million tones [13]. The RSO crushing industry has moderate excess capacity.

The decentralised method of production based on local farming community resources appears to be a sensible approach. Literature resources like [142] and existing examples of a small community based oil producers from Germany and Austria show great possibility to create a network of RSO producers at relatively low cost.

2.1.3.7 Rapeseed market

The European oilseed market is very complex, and price levels will be determined by world demand for oil and oil seed meal [397]. The net cost of RSO is highly sensitive to changes on the prices of rapeseed. Since 1980, rapeseed market prices have varied quite substantially from a peak of about £225 [1] per tonne in 1984, to as low as about £112 per tonne in 1987. In 80's, it was anticipated that rapeseed prices would remain within the range of £115 per tonne to £200 per tonne over the next decade, and within $\pm 10\%$ of £180 per tonne for the next 2-3 years [409]. However, the RSO price in June 2002 had already reached £276 and growing until nowdays.[2]

From an economic standpoint, the potential of using RSO as fuel depends on the relative costs of producing and processing plant and RSO and its ability to compete in conventional fuel markets. Until this oil can be purchased at competitive prices, its wide spread adoption under normal market conditions seems doubtful. Usually the selling price is oriented at the fossil diesel prices and compete under the condition of mineral oil tax relieves [225; 367]. Alternatively, the competitiveness of RSO could be encouraged by adjusting the cost of mineral diesel to take account of the externalities associated with its production and consumption.

The cost of RSO production is also moderately sensitive to the price of rapemeal. In 1994, rapemeal was trading at £113 per tonne [409]. Whilst it is difficult to see the price of rapemeal changing radically from current levels, it was predicted that it would rise to about £125 per tonne early in the next century [157] however current price is £88 per tonne [375] [3]! The UK is currently a net importer of about 208 191 tonnes per annum of rapemeal (which may be obtained from the yield of about 100 000 ha of rape) [17]. It is, therefore, evident that extended UK RSO production of the scale envisaged would reduce imports and improves the national balance of trade figures [408].

Still, the major determinants of demand worldwide for plant oils are price, (relative to non-plant sources of fats and oils), incomes, and population. The dominant determinant in any particular market is related to the level of development of a country and the consumption. Industrialised countries generally have high diets, high income, and low population growth. These factors combine to create a rather stable demand for fats and oils, which is somewhat insensitive to swing in plant oil prices. Developing and underdeveloped countries typically

[1] All prices are Raw Materials Price Index.
[2] It has reach a value of £338 per tone at the beginning of 2007
[3] In 2005

have higher population growth rates, low incomes, and low levels of fats consumption in their diets. Demand for fat and oils in these countries tends to be most unstable, more subject to changes in prices, exchange rates, and shortages of hard currency. Potential growth in demand for fats and oils is the greatest in these areas. Non-food application of oilseed crops is already directed into application of plant oil in small stoves and ovens to replace fossil fuels like kerosone.

The impact of the use of plant oils as fuels must be viewed the same way as all other potential uses of plant oils from a demand analysis perspective. The amount of plant oil used as a fuel will be a decreasing function of plant oil price. Since plant oils can provide only small portion of total fuel requirements, increases in the price of plant oil relative to the price of diesel would cause large decrease in the quantity of plant oil demanded for fuel use.

2.2 Diesel injection systems

Diesel injection system are complex and mechanically sophisticated systems. Over the years injection systems were evolving into more advanced and efficient integrated parts of diesel engines. Diesels hold significant inherent performance advantages over gasoline engines in fuel efficiency, power, durability and certain emissions, and therefore their popularity is steadily growing. Such excellent efficiency is partly due to the way fuel is mettered and injected. Generally, diesel injection systems depend on the particular way of forming air/fuel mixture (direct or indirect injection) and consequently on combustion process.

In the last decades the direct injection engines became the top solution within the diesel technology. Successful development and implementation of these engines benefits from very efficient preparation of combustible air/fuel mixture and thus the improvement fuel economy and the reduction of emission. In order to ensure efficient air/fuel mixture formation, the latest injection system inject the fuel into the diesel engine's combustion chamber at a pressure between 350 and 2 000 bar (the pressure actually utilised in systems), whereby the injected fuel quantity must be metered with extreme accuracy and the fuel quality must comply with the design requirements of the injection system. This implies implementation of very complex and advanced electronic control unit, which can fast and precisely control the injection process as well as control of combustion process. The last generation of diesel injection system comply with these requirements.

This section briefly presents and characterises existing types of diesel injection systems as an integral part of diesel engines. The presentation aims to show the complexity and variety of diesel injection systems, which had been developed specificly for the diesel fuel and evolved throughout the decades.
The final section specifically focuses on CR diesel injection (CDI) system, and formulates some desirable properties of this system including its advanced injection regime and a short information of its exhaust-gas reduction system. The CDI description also includes an overview of its design with a special attention paid to the separate CDI components.
At the end of each section (describing a group of injection systems), some aspects of utilising plant oils as diesel substitute for each injection system are briefly presented.

2.2.1 Diesel engines and injection systems

A brief comparison of diesel and petrol engines performance is given in Table 2.10 and their emissions in Table 2.11. It can be clearly seen that diesel system are highly advantageous and exhibit good fuel economy. With the diesel engine, load and speed are controlled by the injected fuel quantity, and there is no intake-air throttling characteristic of the petrol engines. The majority of the conventional vehicles, locomotives and ships are still controlled by mechanical (flyweight) governors nevertheless the diesel market gradually and readily orients on modern designs of electronic control. Therefore, in diesel passenger cars (and already in some commercial vehicles e.g. min-vans and power generators), these mechanical governors are increasingly being superseded by electronic diesel control systems characterised by very precise fuel metering and higher torque at relatively moderate engine revolution. These systems are much more efficient and exhibit high fuel economy. In line with the latest state-of-the-art of the diesel engine technology, it is mainly the high-pressure injection systems that are used for motor-vehicle diesel engines.

Over the years, a wide variety of different requirements, such as the installation of direct-injection engines in small delivery vans and passenger cars, led to the development of various diesel fuel-injection systems which are aligned to the requirements of a particular application. Of major importance in these developments is not only the increase in specific power, but also the demand for reduced fuel consumption, and the demand for lower noise and exhaust-gas emissions [190; 211; 223; 284; 289; 328]. These factors have always played a crucial role in advancing the existing diesel injection system or re-designing the

Table 2.10: *Comparison of the overall performance of diesel and petrol engines [344; 373; 380]*

	DI engines	**IDI engines**	**Petrol engines**
Engine compression ratio	14:1-25:1		8:1-12:1
Average thermal efficiency, [%]	43	33	30
Torque output	More torque at lower engine speeds (1600-2000 RPM)		Torque at higher engine speeds (2500-4000 RPM)
Noise level	Reduced or close to petrol	High	Low
Average fuel consumption	15% less than IDI	30% less than petrol	1[1)]
Average fuel economy peak rating, [kW/litre]	80-100	50-70	40-85

[1)] Fuel consumption as a change in comparison to petrol (=1)

Table 2.11: *Emissions for diesel and petrol passengers cars (g/km test cycle). Values in brackets represent expected emission, which will be reach in future [24; 196; 280; 373; 410]*

Operational Date	**IDI engines**	**DI engines**	**Petrol engines**
CO	0.64(0.50)	0.64(0.50)	2.30(1.00)
HC+NO_x	0.56(0.30)	0.56(0.30)	0.35(0.18)
NO_x	0.50(0.25)	0.50(0.25)	0.15(0.08)
PM_{10}	0.05(0.025)	0.05(0.025)	-

combustion chambers. The detailed description of all diesel designs is beyond the scope of this thesis, thus Table 2.12 lists only the main diesel fuel-injection systems and provides their brief characteristics.

2.2.1.1 Diesel engines types

There are two major types of diesel engine designs, which can be distinguished in terms of fuel injection type: indirect (IDI) and direct diesel injection (DI) engines. In practice, majority of drivers as well as manufacturers refer to diesel engines using the terminology of indirect and direct diesel engines.

But surely the injection system is not only the main feature of these types. The diesel engines can have divided or undivided combustion chambers which is another feature defining the indirect and direct injection engines. Here some of the main features of these two types of engines are briefly presented and some characteristic advantages are outlined below.

Table 2.12: *Diesel injection types and their injection condition [203] in the ascending order in terms of technical advancing.*

Inj. type	Injection				Engine - related data			
	Injected fuel quantity/ stroke [cm^3]	Max.nozzle pressure bar	Type of governing/ control[1)]	Type of injection[2)]	Pilot injection(VE)/ Post injection(NE)	No. of cylinders	Max. speed [min^{-1}]	Max. power per cylinder [kW]
In-line fuel-injection pumps								
M	0.6	550	m,e	IDI	-	4-6	5000	20
A	0.12	750	m	DI/IDI	-	2-12	2800	27
P 3000	0.25	950	m,e	DI	-	4-12	2600	45
P 8500	0.25	1300	m,e	DI	-	4-12	2500	55
H 1	0.24	1300	e	DI	-	6-8	2400	55
H 1000	0.25	1350	e	DI	-	5-8	2200	70
Axial-piston distributor injection pumps								
VE	0.12	1200/350	m	DI/IDI	-	4-6	4500	25
VE..EDC[3)]	0.07	1200/350	e,em	DI/IDI	-	3-6	4200	25
VE..MV	0.07	1400/350	e,MV	DI/IDI	-	3-6	4500	25
Radial-piston distributor injection pumps								
VR...MV	0.135	1700	e, MV	DI	-	4,6	4500	37
Single-plunger injection pumps								
PF(R)...	0.15-18.0	800-1500	m,em	DI/IDI	-	arbitrary	300-2000	75-1000
UI 30[4)]	0.16	1600	e,MV	DI	VE	8[5a)]	3000	45
UI 32[4)]	0.4	1800	e,MV	DI	VE	8[5a)]	3000	80
UI-P1[5)]	0.062	2000	e,MV	DI	VE	8	4000	35
UI(PF[R])	3.0	1400	e,MV	DI	-	6-20	1500	500
CR accumulator injection system								
CR[7)]	0.1	1350	e,MV	DI	VE[7a)] /NE	3-8	5000[7b)]	30
CR[8)]	0.4	1400	e,MV	DI	VE[8a)] /NE	6-16	2800	200

[1)] m:Mechanical; e:Electronic; em:Electromechanical; MV:With solenoid valve;
[2)] IDI Indirect Injection (Pre-chamber injection); DI Direct Injection;
[3)] EDC Electronic Diesel Control;
[4)] UI unit injector for commercial vehicles;
[5)] UI unit injector for passenger cars;
[6)] UP unit pump for commercial vehicles and buses;
[7)] CR,1st generation for passenger cars and light commercial vehicles;
[7a)] Up to 90° crankshaft BTDC, freely selectable;
[7b)] Up to 5500 min^{-1} during overrun;
[8)] CR for commercial vehicles, buses, and diesel-powered locomotives;
[8a)] Up to 30° crankshaft BTDC.

2.2.1.2 Indirect Diesel Injection Engines (IDI)

Indirect Diesel Injection (IDI) Engines were one of the first in the market and their popularity goes along with the simplicity of the injection system and the overall engine layout implemented. This type of diesel engine was developed in the late 1970's when the interest in improving the fuel economy of light duty vehicles had started to intensify.
In this type, the fuel is injected into a small pre-chamber (frequently called a pre-mixed chamber) attached to the main cylinder chamber. In a pre-chamber engine design, there is a relatively small volume separate from the main combustion chamber, but connected to it via one or more connecting passages. The connecting passage and volume can be designed to produce good swirling and mixing of the fuel and air, hence better fuel utilisation. The fuel is forced through an injector at a moderate pressure and "sprays" into a pre-combustion chamber where the fuel is mixed and begins the burning process. The flame front is well established when it enters the centre of the main chamber (cylinder) and its propagation is gradual and less rapid. The design is called indirect injection, since the fuel is not introduced into the main combustion chamber above the piston but into a pre-chamber, ignites and then flows through the passages down to the combustion chamber. Thus, the indirect injection combustion engines use the pre-chamber to promote intense fuel-air mixing with short ignition delays to provide adequate levels of specific power output at high speeds and relatively low levels of exhaust emissions.
Start of ignition is aided by a high compression ratio (resulting in compression heat), up to 27, and a glow plug installed in the pre-chamber. The glow plug is an aiding device, operating as a heater, to elevate the temperature of the combustion volume at cold start. Indirect injection system usually allows for a lower overall fuel-to-air ratio and lower pollutant emissions, since it is easier to control the process for the smaller pre-chamber volume.

IDI engines provided approximately 30% improvement in fuel economy relative to the petrol engines in production at time IDI engines entered the market (see Table 2.10). Such revolutionary change in fuel economy started the era of highly efficient diesel engines and their long-term development. However, nowadays this design having the advantage of less noise and faster combustion, typically suffers from poorer fuel economy in comparison with more advanced petrol and direct injection diesel engines. Presently indirect diesel engines are "squeezed out" by more advanced diesel engines: the direct injection ones.

Most of indirect diesel engines have been successfully modified to operate on plant oils. It has been proved that plant oils work without the long-term problems in pre-chamber system [22]. This can be explained by the way the air/fuel mixture is prepared in IDI engines. The pre-chamber provides enough volume for mixing plant oil with air in a hot surroundings hence evaporation of oil is more likely to take place and secondary droplet brake-up occurs. Therefore, in a such way the air/fuel mixture is well prepared and can be easily ignite. Also, combustion in IDI engines partly takes place in the pre-chamber and then moves on towards the cylinder. The process provide enough time to evaporate the remaining plant oil droplets and thus enhances the overall combustion.
IDI engines do not exhibit the same scale of problems to operate on neat plant oils as their successors. This is due to a simple way of preparing the air/fuel mixture as well as metering the fuel.

2.2.1.3 Direct Injection (DI) Diesel Engines

Direct Injection (DI) Diesel Engines are also frequently named as Open Chamber Engines. Basically, in this type, the fuel is injected at high pressure (which can reach extremely high value up to 2000 bar) directly into the cylinder chamber above the piston. So, in DI diesel engines the idea of injection into a combustion pre-chamber had been replaced by implementation of a direct booster into cylinder. These engines are also characterised by high-swirl designs with a deep bowl in the piston. The engines can also operate at low-swirl or quiescent type characterised by having a shallow bowl in the piston, a larger number of holes in the injector and higher injection pressures. Nevertheless, the most modern DI diesel engines utilises high-swirl as well as very high injection pressures.

Two factors, in particular, determine the quality of a direct injection system: the fuel pressure injected into the cylinder and the extent to which the cycle of an individual injection can be formed. Some of the modern DI diesel engines inject multiple times during one combustion cycle, starting a short combustion (pilot injection) and building to the power stroke through the main injection. Since the fuel spray distribution in a DI diesel engine with pilot injection is actively controlled by pilot and main injection at different piston positions it allows to prevent the main fuel injection from hitting the pilot flame. This is one of promising countermeasure for reductions in exhaust gas emissions in diesel

engines [272]. Also, it has been shown that using a desired quantity of pilot injection with an optimised timing was crucial to improve the initial firing and then to achieve a good cold startability [401]. The multiple injection feature and direct fuel into cylinder differ the DI diesel engines from the IDI. Such injection regime promotes quiet engines and has a significant effect on emission.
The older DI diesel engines had a tendency to produce greater amounts of noise because they did not incorporate a slowly controlled combustion feature as present in the IDI (IDI utilises the pre-chamber to initiate combustion). Initially, the combustion was too sudden and led to local detonation of the air/fuel mixture. Presently, DI diesel engines generate less heat and less volume of exhaust gas. There is also further reduction of emissions and this has been reached by implementing the EGR (Exhaust Gas Recirculation), which improved the air intake utilisation. The improved fuel economy of the DI diesel engine results also from the following: lower heat losses - because of lower in-cylinder air charge velocities and reduced surface to volume ratio; improved mechanical efficiency stemming from the elimination of the pre-chamber pumping losses and faster burn rates resulting from the absence of the two stage combustion process as present in the IDI engine. The DI diesel engines are presently most advanced group of diesel models gradually developed towards higher efficiency and lower emissions due to a constant improvement of the fuel injection pressure.

The DI diesel engines are generally more economical, the injection can be more precisely controlled, and they can be made quieter and more dynamic at lower torque (see Table 2.10). DI diesel engines have got a greater efficiency than indirect injection engines using a pre- or swirl chamber. By converting from indirect injection to direct injection combustion system, a 10 to 15% average improvement in the fuel economy of a diesel engine has been obtained. Fuel consumption, torque, emissions and engine noise all strongly depend on injection quality and the way of air/fuel mixture is formed and distributed inside a combustion chamber (see Table 2.11).

A vast majority of DI diesel engines do not operate straightforwardly on neat plant oils for long time without a significant modification. However, the engine short-test performance reveals successful operation and a space for a successful modification. More detailed description of modifications and operation of DI diesel engines on plant oil has been described in the *Section 2.1* and are not presented in this section.

A summary of some advanced DI diesel engines features are presented in Table 2.10 and their designs are described in the next sections. The description has been outlined in increasing order of engine advance and it finishes off with the most advanced and the latest model amongst DI diesel engine - the CR injection system.

2.2.2 Diesel fuel injection systems

The injection systems can be distinguished in terms of the way in such the fuel injection is controlled i.e. mechanically or electronically.

The oldest and most common type of diesel injector is the separate pump system. In its most basic explanation, this uses a separate injection pump, commonly indexed off of the timing chain. The timing chain turns what could be described as a mini-piston engine that pumps fuel to the various injectors that “pop” open when a specific or set pressure is reached. So, in the fuel injection systems the volume control is controlled in conventional mechanical injection pumps. The control sleeve position is adjusted according to the ratio of the tension of the governor spring and the centrifugal force in the flywheel and this is a purely mechanical way of controlling the injection process. In the electronically controlled injection pumps, however, the control sleeve position is fixed, by employing signals from an engine control unit (ECU), to control an electronic governor [286]. The electronic system are very sophisticated, more accurate and still evolving towards more advanced solutions. Already, the diesel fleet equipped with the electronic systems is a top shelf product within the diesel market.

Fuel injection systems vary in the maximum utilised injection pressure. IDI injection pumps have a normal output fuel pressure of 2000-4000 psi (0.14-275.79 bar). The latest style of injector is where there is no specific injection pump, but a pre-pump or helper-pump is used to bring the fuel at relatively low pressure to the injector itself and the injector has its own internal pump that increases the pressure to extremely high levels (up to 30 000 psi (2 068 bar) and more!) These are used in DI engines. Due to different design of fuel-injection system there is a broad range of systems, which have been briefly described below in the following subsections.

2.2.2.1 In-line fuel injection pump

One of the most widest group of injection type is the in-line fuel injection pump [76]. All in-line fuel-injection pumps have a plunger-and-barrel assembly for each engine cylinder. As the name implies, this comprises the pump barrel and the corresponding plunger, which is forced in the delivery direction by the engine-driven camshaft, and returned by the spring. The assembly is fitted in a single unit depicted by a typical diesel injector layout. The term: "in-line" indicates that the plunger-and-barrel assemblies are arranged in-line. The in-line pump turns at half the engine speed and is always synchronised to the diesel engine's piston movement. The fuel is forced through high-pressure lines to the nozzle-and-holder assemblies from where it is then injected by the nozzles. The injection pressure may vary from 750 up to 1 300 bar. Plunger lift can not be varied by controlling the delivery quantity of the fuel. Slots have a shape of the plunger with its diagonal edges known as helixes. The rotating plunger is forced by the control rack and the helixes permit the selection of the required effective stroke. Placement of delivery valves depends on the fuel-injection conditions and normally take place between the pump's pressure chamber and the fuel injection lines.

Traditional pump-line-nozzle injection systems on large truck engines, buses, off-highway (e.g. stationary engines, construction and agricultural machinery) typically use an in-line injection pump with a pumping element for each injector. The systems are also employed in passenger cars.

The in-line fuel injection pump are a relatively simple assembly and could be modified to accommodate neat plant oil. It is expected that by re-designing the plunger-and-barrel assemblies it is possible to make the system operate on plant oil in the almost same way as on diesel. However, it has to be highlighted that the successful operation of the in-line fuel injection pump is subjected to appropriate pre-heating of plant oil prior to injection.

2.2.2.2 PE standard in-line fuel injection pump

The PE standard in-line fuel injection pumps are a subgroup of the in-line injection pumps. The PE group is characterised by start of fuel delivery defined by an inlet port which is closed by the plunger's top edge. The fuel quantity is determined by this inlet port being opened by the helix. The control rack is controlled by a mechanical (normally flyweight)

governor as well as in modern version an electronic actuator.

The PE injection pumps are expected to work on neat plant oil under same conditions as the in-line pumps. Although, it has to be noted that the purity of the plant oil is essential. Any suspended solids can cause malfunction of the plunger and helix assemblies.

2.2.2.3 Control-sleeve in-line fuel injection pump

More advanced group of in-line fuel injection pumps is the control-sleeve one. It allows to produce a high injection pressure and a precise start of injection. A difference of the control-sleeve in-line fuel-injection pump in comparison to a conventional in-line injection pump is a "control sleeve", which slides up and down controlling the pump plunger. Operation of an actuator shaft vary the plunger lift to closing and fuel delivery position. The control sleeve's setting is adjusted as a function of different influencing variables. The control-sleeve version allows a further degree of freedom and makes this type more flexible in comparison to the rest of the in-line fuel-injection pump. With the newly developed control sleeve pump, the start of injection and the delivered fuel quantity can be freely selected by means of maps on commercial vehicle diesel engines. The precise start of injection and the fuel delivery is electronically controlled by linear solenoid valves. Within a predetermined range, the sleeve riding on the plunger can be adjusted to vary the start of injection.

The control sleeve pump can be mounted on engines without any difficulty as they are separate injection units. The classical in-line pump can be easily replaced by the new control sleeve pump which in addition to injection pressures of up to 1 400 bar at the nozzle offers precise start of injection.
This new system also opens up the possibility of integrating diesel injection into a network of electronic controls gathering signals from across the vehicle. For example, the combination of electronically controlled control sleeve pump with traction control (ASR) - an important feature for heavy commercial vehicles - is especially useful and advisable.

Operation of the control-sleeve in-line fuel injection pump on neat plant oils can be subjected to some problems, particularly if the oil has not been pre-heated accordingly or it contains some particles. The control-sleeve mechanism combines relatively precise

hydraulic assembly together with the electronically controlled valves. Therefore, it has to be ensured that the plant oil delivery is taking place at appropriate temperature to reduce its viscosity (to reduce mechanical delays due to increased hydraulic friction) as well as the electronic system can respond accordingly to different fluid properties of the plant oil.

2.2.3 Distributor fuel injection pumps

The main feature of this group is a mechanical (flyweight) governor, or an electronic control with integrated timing device. The distributor pump has only one pumping element for all the engine cylinders [74; 75] and distributes a high-pressure fuel charge to each injector in the firing sequence. The delivery is achieved through fuel passages are drilled in the plunger which not only moves up and down in the barrel but also rotates. The fuel passage is drilled partway through its core, with the open end at the top of the plunger. Also, a perpendicular passage is drilled all the way through the plunger near the bottom end. These two passages join to form a "T" inside the plunger. Somewhere, along the core passage is a branch passage that leads to a hole in the side of the plunger. This is the plunger's distributor port. When the plunger blocks the fill port, pressurised fuel flows through the core passage and to the distributor port. With each stroke, the plunger also rotates to align the distributor port with the next delivery passage in the pump head [76]. The passage that forms the "T" at the end of the core passage, called the cutoff bore, is the spill port. A control sleeve slides along the plunger to open or close the spill port. When the spill port opens, fuel pressure is vented from the pumping element and injection ends. Opening the spill port early in the plunger's stroke makes injection end sooner, so less fuel is injected. Opening the port later in the stroke increases the amount of fuel injected. The pump's governor controls fuel delivery by controlling the position of the spill port control sleeve.

An example for the distributor fuel injection pumps is an electronically controlled VP 44 high pressure radial piston distributor pump produced by Bosch. It is capable to generate pump pressures of more than 1 000 bar and nozzle pressures of over 1 500 bar. The high atomisation energy thus produced at the nozzles, plus the variable delivery rate and pre-injection lead to a very clean burning engine with a smooth and consequently quiet combustion process. The fast-response adjustment of injection timing and high precision metering of the fuel by fast acting solenoid valves form the basis for the high power output

and low fuel consumption of modern diesel engines.

An assessment of the distributor fuel injection pump operation on neat plant oils can be done jointly for the all types (listed below). The presented fuel pumps employ a sophisticated hydraulic system of fuel metering, which consist of fine fuel channels and passages. It can be easily foreseen that any plant oil of higher viscosity would noticeably affect the fuel injection, as its flow through the passages would be different. The method of oil pre-heating is one of the ways to overcome the problem, however it has to be remembered that at the start-up and engine shut-down the injectors are filled with plant oil, which if not preheated might cause a serious deterioration of the injection process. Hence, the distributor fuel injection pumps would require a careful modification of the injectors and the fuel delivery system.

2.2.3.1 Axial-piston distributor pump

The conventional distributor pumps deliver the fuel by means of a central, axially aligned distributor plunger. In this injection type, a vane-type pump delivers fuel to the axial-piston of the high-pressure pump chamber. A central piston running on a cam plate generates pressure individually delivered to engine cylinders [76]. The piston strokes per one revolution of the driveshaft correspond to the number of engine cylinders. The rotating-reciprocating movement is imparted to the plunger by the cams on the underside of the cam plate, which ride on the rollers of the roller rig. In the conventional VE axial-piston distributor pump with mechanical governor, or electronically controlled actuator, a control collar defines the effective stroke and with it the injected fuel quantity. In the solenoid-valve-controlled axial-piston distributor pump, instead of a control collar an electronically controlled high-pressure solenoid valve controls the injected fuel quantity. The open and closed-loop control signals are processed in two ECU's (injection-pump ECU and engine ECU) [75]. Still there is a wide range of the axial-piston distributor pumps varying in term of the control from mechanical distributor pump VE mechanically (flyweight) controlled, and P30 (by Bosch) distributor pump with integral PSG5 (by Bosch) pump fully governed by an ECU.

Even with an electronically controlled governor in place of the old spring-and-lever mechanical governor, distributor-type injection pumps are amazingly complex pieces of

equipment. Springs and check valves, retraction collars, metering slits, cam plates, pressure regulating valves and orifices and a number of other items have to be carefully matched to produce a controlled injection event.

But after 80 years of development, the mechanical fuel injection pump is fast becoming obsolete for on-road applications with the introduction of electronically controlled CR injection. It will still be used in industrial engines for a long time, and its need for extremely high precision and extremely fine surface polishing has pushed the limits of the manufacturing art further than anything else. The technology introduced by Bosch in 1927 will be important for some time to come.

2.2.3.2 Radial-piston distributor pump

In this type of injection system, fuel is delivered by a vane-type pump to the high-pressure pump which is in the form of a radial-piston pump with cam ring and two to four radial pistons. The pump creates the high pressure for fuel delivery. Quantity of fuel is metered by a high-pressure solenoid valve and the timing device rotates the cam ring in order to adjust the start of delivery. The way how the fuel is metered resembles some similarities of a conventional petrol injection system.
As in case of axial-piston distributor pump system, the opening and closing loops are controlled by ECU's, while speed is controlled by a triggering mechanism of the actuator. The main features of the radial-piston distributor pumps are:

1. Radial-piston configuration for pump pressures up to 100 bar.
2. Fuel injection system optimised for high atomisation energy at the nozzle.
3. Rapid fuel-quantity response and rapid spill through fast high-pressure solenoid valve.
4. Extended durability due to multi-point calibration in ECU.
5. Start-of-delivery control without needle movement sensor.

2.2.4 Single-plunger fuel injection pumps

The single-plunger fuel injection pumps is another advanced group of injection units. The single-plunger design makes the pumps smaller and less expensive than multi-plunger

types. This group encloses a significant number of injection types listed in Table 2.12. Three main types are briefly described below.

2.2.4.1 PF single-plunger pumps

The PF single-plunger pumps term describes a pump type produced by Bosch and the 'PF"-term represent a technical type. The stroke of the plunger in the PE single-plunger pumps is constant, however, the amount of fuel actually pumped at high pressure is varied by moving a control collar that opens a port to relieve pressurised fuel during part of the plunger's stroke. Plunger's back and forth movement is driven by the turning injection pump toothed pulley. The movement of the control collar adjusts how much fuel is pumped per stroke.
The governor mechanism controls the collar displacement. The governor is adjusted by movement of the lever connected to the throttle cable. There is a mechanical way (an adjustment screw) which can control how the outside throttle lever affects the governor mechanism. The governor adjusts fuel-quantity and transfers the information by a rack integrated in the engine. The injection timing is not implemented by rotating the engine camshaft since the actuating cams for the individual PF single-plunger pumps are located on the engine camshaft for each injector respectively. To adjust an advance angle, an intermediate element like a rocker is installed between camshaft and a roller tappet. Also, there is a fuel distributor on the end of the pump, to select which injector gets the portion of fuel. Due to the construction, the single-plunger injection pumps are readily used with viscous and heavy oils or in case of fluctuating fuel viscosity. They have no camshaft of their own, although they correspond to the PE in-line injection pumps regarding their method of operation.

A classic example of the PE single-plunger pump is a Perkins EPVE pump or the Volkswagen (VW) Bosch pump. It uses a single plunger and cylinder to create high pressure. But also these pumps are used in small diesel engines, big marine engines, construction machinery as well as in diesel locomotives. In case of large engines, there is a mechanical-hydraulic governor or an electronic controller, attached to the engine block.

There are numerous examples of successful modification of the PE pumps running on cold pressed RSO [22]. Especially, engines equipped with a VW Bosch pump type were

modified and offered to customers. Briefly, the modification is based on replacement of the existing injector assembly with a new made insert. This allows to increase the opening injection pressure and therefore to enhance RSO atomisation.

2.2.4.2 Unit injector (UI)

This is the injection system design used on the modern diesel vehicles although the idea has been around for some time. The Unit Injector (UI), also named as the Unit Injector System (UIS), combines the injection pump and the injection nozzle in a single assembly recognised as an unit injector. The injector pump and the injection nozzle form such unit, which is installed in each engine cylinder head [73]. Fuel again is directly injected into the cylinder of the engine. In addition to the unit injector, the system also comprises the low-pressure system with pre-supply pump, filter, pressure-control valve and the ECU with sensors and user-diagnosis interface [73]. Each unit injector is driven directly by a tappet or indirectly from the engine camshaft through a valve lifter.
In comparison to in-line and distributor injection pumps, UI are able to produce considerably higher injection pressure (up to 2 200 bar for passenger cars and 1 800 bar on commercial vehicles). Such high injection pressure is fully controlled by electronic device adjusting injection duration, fuel quantity in a flexible injection mode. Since the UI has no high-pressure lines, depending upon rotational speed, injection pressures can be flexible altered.

Unit Injector Systems for commercial vehicles are installed in engines with output powers of up to 80 kW/cylinder, with the maximum number of cylinder of 8. However, by increasing the number of ECU's it's possible to fit the system up to 16 cylinders. A classical example of the UI is a Volkswagen - Audi engine equipped with what is named as the system Pumpe-Düse (pump injector). The flexible injection mode and an independent injection control result in significant reduction of toxic emissions as well as engine knocking.
Currently these engines cannot be converted with an Elsbett [22] one tank system and like the CDI engines require special two tank conversion systems [168]. Nevertheless, the UI engines are expected to be modified for a single tank mode if more fundamental study is done on plant oils injection.

2.2.4.3 Unit pump (UP)

The Unit pump type is similar in its principle and operation to that of the UI one. Frequently it is referred to as the Unit Pump System (UPS). The main difference is that the unit pump is connected to the nozzle by a short high-pressure delivery line precisely matched to the pump-system components. A typical unit system consists of a high-pressure pump with integral solenoid valves, a short high-pressure injection line, a pressure fitting, and a conventional nozzle-and-holder assembly (a nozzle holder). A Unit Pump is allocated to each engine cylinder [77] equipped with such assembly. The pumps are driven by the engine camshaft with a relatively low power demand. It has to be pointed out that injection of UP is controlled by an electronic unit (ECU) triggering a solenoid valve, which permits precisely defined characteristics of the individual injection.

The main advantages of the UP are as listed below [77]:

1. High injection pressures of up to 2 100 bar.
2. No cylinder-head design changes when converting from in-line or distributor pump to UP. This allows flexible upgrade of the in-line/distributor system to UP.
3. Easy handling in the workshop. The access and therefore the replacement of the pump is an easy matter.
4. Low maintenance and servicing.

Unit Pump systems are installed in commercial-vehicle engines with up to as many as 8 cylinders, but also are used in passenger cars. However, if the appropriate ECU configuration is used (combining a master/slave switching mode), UP units can be used on engines with more than 8 cylinders.

As described above in the pervious section, the UP engines exhibit a similar scale of problems when operating on neat plant oils. Generally, it can be stated that the delivery and injection process of UP have to be significantly modified to deliver the same performance as for diesel.

2.2.4.4 Accumulator injection system

This group includes the most modern and advanced type of injection systems - the CR diesel Injection (CDI). As started in late nineties [271; 346] CR system has been modified

and improved to deliver better performance on diesel. Development of the CDI system was a response to a need for a flexible fuel injection system offering variation of fuel quantity and start of injection, permission to choose freely injection pressure within a pressure range and be capable to inject fuel in several portions. These significantly contributed to further improvements of DI engines concerning noise, emissions and engine torque.
In 1997 the first CR system in the world for passenger cars was fitted in production by Alfa Romeo and Mercedes-Benz. The maximum injection pressure of 1 350 bar was utilised. Then in 1999 the CR system for trucks was introduced by Renault (RVI) utilising the maximum injection pressure of 1 400 bar. Finally in 2001 the 2^{nd} generation of the CR for passenger cars started to be manufactured. It makes engines even more economical, cleaner, quieter and more powerful. The maximum injection pressure increased up to 1 600 bar. The system was employed in Volvo and BMW. In the year of 2002 the same 2^{nd} generation provided lower emissions, improved fuel consumption and more power for heavy vehicles (MAN). And finally in 2003 the 3^{rd} generation CR equipped with rapid-switch piezo in-line injectors (piezo element integrated very closely to the nozzle needle in the injector shaft) has been introduced for cars.
The main advantages of the latest CR system are: up to 20% lower emissions, 5% more power, 3% lower fuel consumption and up to 3 dB(A) less engine noise. The innovative, 3^{rd} generation CR provides low exhaust emissions in the new V6 diesel engine of the Audi A8. A car with the new 3.0-litre diesel engine has met the exhaust emission norm Euro 4, which had become mandatory in 2005. For its 4^{th} generation of CR for passenger cars the developers are currently exploring designs using even higher injection pressures of more than 2 000 bar, as well as injectors with variable injection geometry and faster solenoid valve.

The following sections describe in details the “philosophy” and beauty of the CR system i.e. its main features and functions.

2.2.5 Common-rail Diesel Injection (CDI)

If a single sentence must be used to describe the main feature of CR, it would be the separation of pressure generation and the actual injection process. Independently generated - from engine speed and injected fuel quantity - injection pressure is stored and ready for each injection in the fuel accumulator described as “the rail”, which is basically a thick

wall metal tube. The rail a pressure, which is determined by the injection pressure setting in the ECU and EDC. It takes place independently of the engine speed and the quantity of fuel injected. The fuel is fed through rigid pipes to the injectors, which inject the correct amount of fuel in a fine spray into the combustion chambers. The engine management systems controls extremely precisely all the injection parameters, such as the pressure in the rail and the timing and duration of injection as well as performing other engine functions. Figure 2.3 presents the system schematically, whereas Figure 2.4 shows a layout of the CR system components fitted in a Mercedes E220C car.

The start of injection is controlled and independently calculated for each cylinder by the

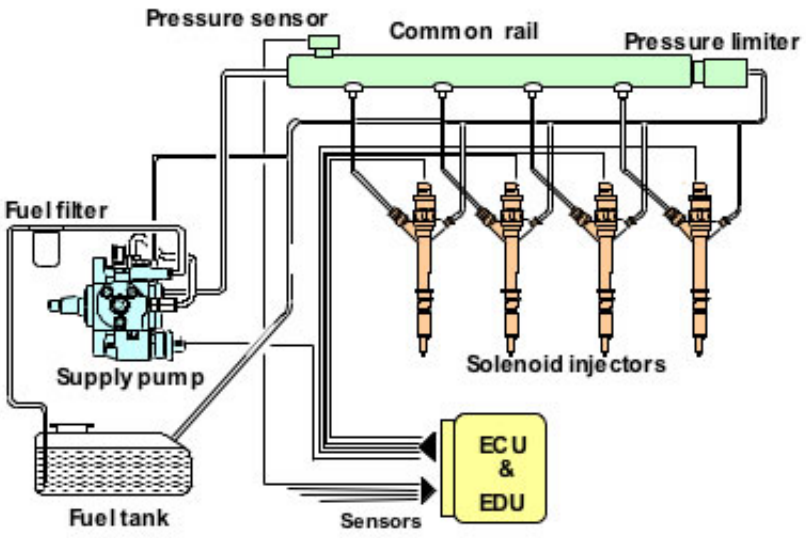

Figure 2.3: *Depiction of a CR injection system implemented by DENSO Co,. (With courtesy of ©2002DENSO)*

Electronic Control Unit (ECU) and the Electronic Diesel Control (EDC) with respect to the actual driving conditions and demands. The ECU and EDC are electronic circuits with a pre-loaded software acting as the electronic engine management units. So, the ECU and EDC trigger a solenoid valve of each injector accordingly to required power demand. This electronic engine management network is a critical element of the CR system because only the speed and spontaneity of electronics can ensure immediate pressure injection adjustment and cylinder-specific control of the injector solenoid valves.

Compared to conventional cam-driven systems the CR injection system for direct-injection diesel engines provides for considerably higher flexibility in the adaptation of the injection systems to the engine, for instance [383]:

- Extensive area of application (for passenger cars and light commercial vehicles with output powers of up to 30 kW/cylinder, as well as for heavy duty vehicles,

locomotives and ships with outputs of up to approx. 200 kW/cylinder;

- High injection pressure of up to approx. 1 500 bar);
- Variable start of injection with possibility of pilot injection, main injection and post injection;
- Matching of injection pressure to the operating mode.

The CR system in particular gives engine developers the freedom they need to reduce exhaust emissions even further, and especially to lower engine noise.

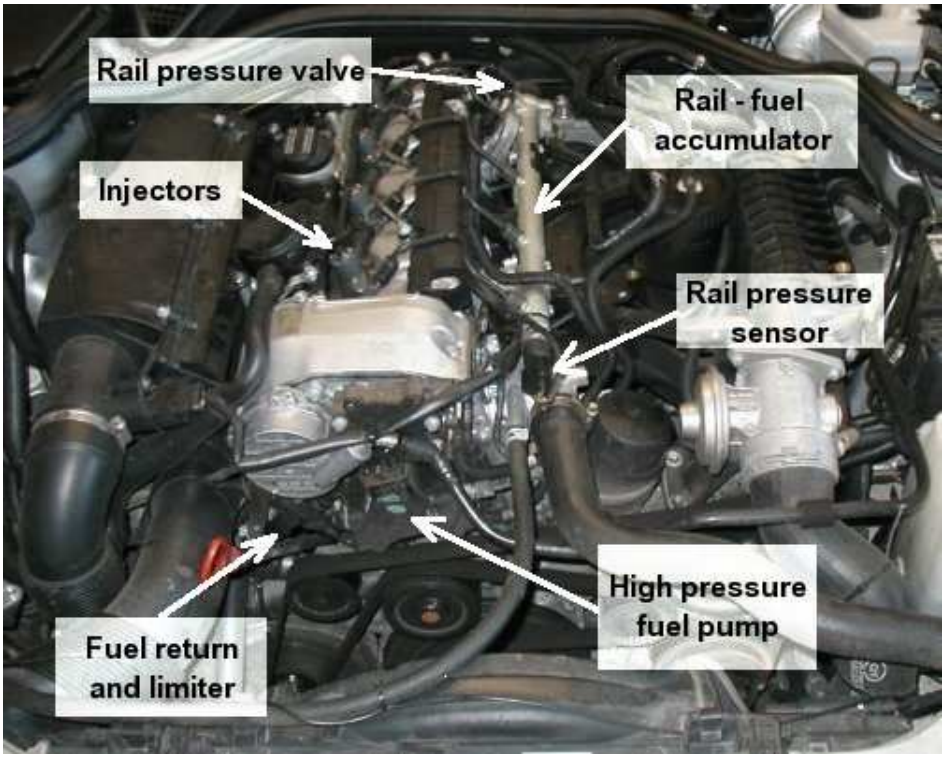

Figure 2.4: *An overview of a Mercedes E220 CR Bosch injection system.*

2.2.5.1 Design and functions

The CR system alters the injection of the diesel fuel at the right moment, in the right quantities and with the correct injection pressure. It also has to be pointed out that such control ensures that the engine not only runs smoothly, but also economically. Hence, the injected fuel quantity is defined by the driver, and the start of injection pressure are calculated by the ECU and EDC using the stored programme.

The main control unit is the ECU, which triggers the solenoid valves so that the injector at

each engine cylinder injects accordingly. The EDC plays an auxiliary role and controls other function of the engine and the whole car.
Briefly, the controlling loop of the system comprise: ECU, crankshaft-speed sensor, camshaft-speed sensor, accelerator-pedal sensor, boost-pressure sensor, rail-pressure sensor, coolant sensor, and air-mass and temperature sensor. In case of low outside temperatures and/or with the cold engine, the ECU applies the data from the coolant-temperature and air-temperature sensor to adopt the setpoint values for start of injection, post injection and further parameters to the particular operating conditions. The crankshaft-speed sensor measures the engine speed, and the camshaft-speed one determines the firing sequence (phase length), so the gathered signals are sent to the engine management unit and processed accordingly to the pre-loaded program. So, the way how the firing sequence is set up is different from the conventional, mechanical governing of the ignition. The accelerator-pedal module informs the ECU about how far the driver has depressed the pedal, and including the input signals from the above sensors defines the instantaneous operating performance of the engine and the vehicle as a whole, which indicates directly the torque requirement. Hence, engine running condition is monitored by sensor signals, where fuel injection volume and injection timing are optionally controlled to ensure maximum driving performance and minimum levels of noise, vibration and black smoke emission [203]. The ECU can then intervene with open and closed-loop controlling action (a synchronised management of electronic signals) at the car and particularly at the engine.

These auxiliary functions, described as closed- and open-loop control functions, serve to improve both the exhaust-gas emission and fuel-consumption figures, or are used for increasing safety, comfort and convenience. Examples here are Exhaust Gas Recirculation (EGR), boost-pressure control, vehicle-speed control (cruise control) and electronic immobiliser etc. The detailed description of these can be found elsewhere [76; 203].

The CR system comprises the three major elements: a low-pressure stage for the low-pressure delivery of fuel, a high-pressure stage for the high-pressure delivery, and the ECU. The low-pressure stage is engaged to prepare fuel prior to compression whilst the high-pressure stage produces and stores the compressed fuel at the appropriate injection pressure. Both stages are monitored and governed by the ECU. A brief description of the stages excluding ECU is given in [267; 383].

2.2.5.2 Low-pressure delivery

The low-pressure stage of CR fuel system incorporates: fuel tank with pre-filter, pre-supply pump, fuel filter and low-pressure fuel lines. The fuel tank is made of non-corroding material and remains free from leaks at double the operating pressure, and in any case at 3.0 bar. The tank is fitted with a safety valve with a pressure sensor and a pre-supply pump. Fuel lines for the low-pressure stage are often made of flame-inhibiting steel-braid-armoured flexible material or in the latest vehicles of a specially treated polymer tubes. These line exhibit excellent durability and, for instance, in the case of engine movement, there must have no adverse effect on fuel-line. All fuel lines are normally protected against the effect of heat and are highly durable to corrosion and changing atmospheric conditions. The pre-supply pump is either an electric fuel pump (used more readily) with pre-filter, or a gear-type fuel pump. Its job is to maintain an adequate supply (in the Bosch CR system, the pre-pressure has to be maintained at 4 bar) of fuel to the high-pressure pump in every operating stage and at the necessary pressure. The electric fuel pump is only used in passenger cars and light commercial vehicles but its use has got more advantages over a gear-type one. Despite of its major job, within the framework of system monitoring it must also interrupt the flow of fuel in case of an emergency accordingly to the signal provided by the pre-pressure sensor and the ECU. Beginning with the engine cranking process, the electric pump runs continuously independent of engine speed and its operation requires a low amount energy. The pump delivers fuel permanently from the fuel tank, and through the filter to the high-pressure pump. Excess fuel can flow back to the tank through an overflow valve. There are variety of different pumping element types available and fitted into the pump and the most common units are provided by Bosch, Denso and Delphi. The pump has two valves: a non-return one in order to prevent the emptying of the circuit and a safety one which limits the pressure to a maximum value of 5 bar in case of obstruction of the diesel fuel circuit. It depends on the pump's field of application and the detailed description of them can be found in [203] or any of these manufacturers web pages.
The fuel filter is normally fitted just before the hight pressure pump and plays a crucial role in fuel delivery. It guarantees the fuel to be free of water and solid impurities above 5 μm.

2.2.5.3 High-pressure delivery

The high-pressure stage of CR fuel system incorporates: high-pressure pump, rail (fuel accumulator), rail high-pressure valve, rail pressure sensors and high-pressure fuel lines.

The high-pressure pump is used for compressing the fuel at high pressure and sending it at pressurised stage towards the rail (described below). The high-pressure pump is powered by the engine through the toothed distribution belt or directly sits on a shaft. The supplied force is equivalent to about half speed of the engine. The high pressure is obtained from the action of three small pistons being arranged in radial position at an angular distance of 120°. Due to their action a pressure from a minimum of 150 to 1 350 bar is generated. One of the main advantages of the pump is that it does not require the phasing since the time and duration of injection are managed by the ECU

The fuel loop section between the high pressure pump and the injectors is named as the rail which serves as an fuel accumulator. The rail is a thick wall metal tube equipped with the nozzles, a high-pressure valve, and sensors on its both ends. The fuel is compressible and is subjected to oscillations initiated by the pulsating delivery of the high pressure pump and especially by the abrupt extraction of fuel via the injectors. The rail pressure oscillations and pressure waves are a separate and important issue. Uncontrolled fuel waving and oscillating may cause a serious obstruction of the atomisation process and make the injection control difficult [28; 256].

A pressure sensor measures the fuel pressure in the rail and its signal is compared to a desired value stored in the ECU (determined by an algorithm embedded in a pre-loaded computer program stored in the ECU). If the measured value and the desired value are different, the high-pressure valve is opened or closed accordingly. In case the pressure is too high, the valve opens in order to make part of the fuel flow from the rail to the fuel tank. This is realised by the return line, which is also connected to each individual injector to collect the fuel being bled during the operation. In case of too much low pressure in the rail, the valve is closed separating the high pressure side from the low pressure.

2.2.6 CDI injection characteristics

In comparison with conventional injection systems, delivery is practically uniform (see Figure 2.5). This means that not only is the high-pressure pump smaller, but also that its drive is not subject to such high pressure-loading peaks. A typical injection pattern for a conventional DI engine is presented in Figure 2.6. Presuming constant pressure, the injected fuel quantity is directly proportional to the length of time the solenoid valve is energised. The required high-speed solenoid switching is achieved by using high voltages and currents. The start of injection is controlled by the angle-time control system of the

ECU which uses a sensor on the crankshaft to register engine speed and a sensor on the camshaft for phase detection.
In comparison to conventional injection characteristics, the following demands are made on and ideal injection regime:

- Independently of each other, injected fuel quantity and injection pressure should be definable for each and every engine operation condition (provides more freedom for achieving ideal air/fuel mixture)
- At the beginning of the injection process, the injected fuel quantity should be as low as possible (i.e. during the ignition lag between the start of injection and the start of combustion)

These requirements are complied with in the CR injection system with its pilot and main-injection features. In conventional injection systems using distributor and in-line injection pumps (this applies to all IDI and majority of DI engines), fuel injection comprises only the main injection phase(Figure 2.6). In conventional systems, pressure generation and provision of the injected fuel quantity are coupled to each other by a camshaft and a pump plunger. The injection pressure increases together with increasing speed, load and injected fuel quantity. This can be clearly seen in Figure 2.6 where the injection pressure increases gradually with time to reach peak pressure and then drops rapidly. In CR the main fuel portion could be injected as a single amount or divided as well as combined with pilot and post-injection. The pilot injection, split injection and multiple injection were introduced as a one of the methods to improve the emission characteristics [270; 287; 398]. The initial phase of injection and the quantity are programmed by the control unit - ECU, through an electronic instruction towards the electronic injectors.

Injection fuel amount is set as function of many variables e.g. engine speed and accelerator opening angle, and compensated in accordance with engine coolant and air temperature, fuel temperature and transient running conditions. Injection timing is set and compensated in accordance with engine parameters too. Limits on maximum injection fuel amount are maintained in accordance with engine speed and intake air volume as regulated by an air flow meter. Desired idle speed is set in accordance with engine coolant temperature, air conditioner, transmission shift and warming-up conditions, and feedback control is applied to maintain the desired speed in accordance with existing conditions.

The system accordingly controls and correct the engine revolution cycle time to maintain a uniform injection level in each cylinder. Also, control on maximum injection volume by intake air volume prevents the exhaust pipe smoke emission which occur at high levels as a result of excessive injection volume.
In addition, the actual injection timing is monitored by a nozzle equipped with a newly-developed needle -lift sensor, thus eliminating the negative effect of changes in fuel characteristics, nozzle valve opening pressure etc. This makes it possible to maintain optimum injection timing under all driving conditions [286].

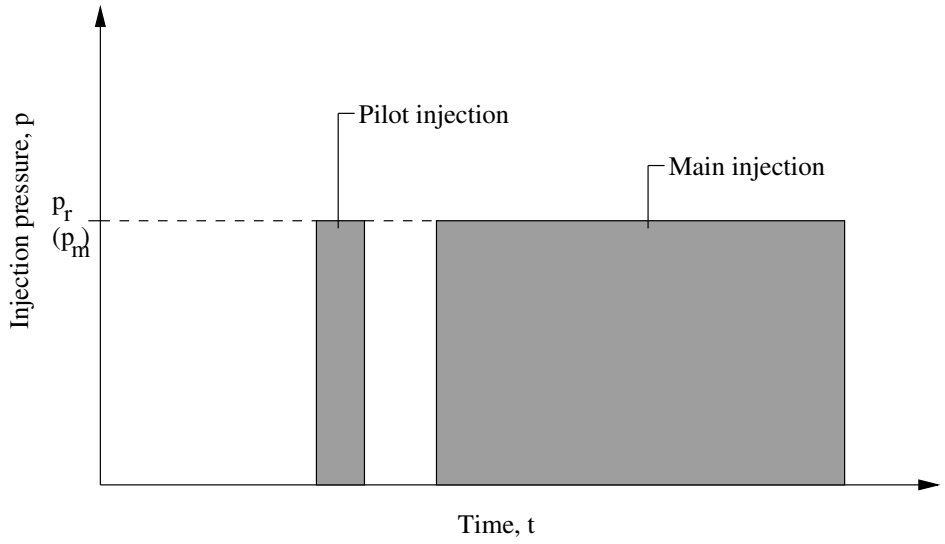

Figure 2.5: *Ideal rate of discharge curve for CR fuel injection; p_m - mean injection pressure, p_r - rail pressure.*

2.2.6.1 Pilot injection

The high combustion pressure and the rate at which this pressure rises during the combustion process normally produce higher noise levels. This is a well recognised occurrence in DI engines and does not take place in their pre-chamber (indirect injection) counterparts. The CR system employs a piece of technical wizardry known as pilot injection to overcome this problem. Pilot injection is also named as pre-injection. Pilot injection consist of a small amount of fuel injected into the cylinder and being ignited. The process take place some time before the main fuel injection. Pilot injection is regarded as a very good strategy for reducing fuel consumption but tends to exhibit a slightly higher NO_x emissions [64; 388].

Pilot injection can be advanced up to 90° of crankshaft referred to TDC (Top Dead Centre). If the start of injection occurs less than 40° BTDC (Before TDC), fuel can be

deposited on the surface of the piston and the cylinder walls, and can lead to unwanted dilution of the engine oil [203; 388]. With pilot injection, a small amount of diesel (varies from 0.8 up to 4 mm^3) [388] is injected into the cylinder to "precondition" the combustion chamber. Combustion efficiency can be improved as a result, and the following effects are achieved:

- The compression pressure is increased slightly due to pilot reaction and partial combustion;
- The main-injection ignition delay being reduced;
- A reduction of combustion-pressure rise and of the combustion-pressure peak (softer combustion, reduction of knocking).

The effects are to reduce the combustion noise, the fuel combustion, and in many cases the exhaust gas emission, especially soot formation. Since it reduces the ignition delay, pilot injection makes an indirect contribution to the generation of engine torque. When using a pre-injection, the following main injection ignites almost without any ignition delay.
The specific fuel consumption can increase or decrease as a function of the start of main injection and time between the pilot and main injection sequences.

2.2.6.2 Main injection

The main fuel amount is injected as main injection at almost linear velocity. Main injection can be divided into a couple of separate events as frequently called split injections. During the main injection, the fuel jet penetrates the combustion chamber with almost a constant linear velocity (see Figure 2.5). The following main-injection is injected into the burning pre-injection and ignites almost without any ignition delay. Recent studies have provided that NO and particulate emissions can be markedly reduced by using appropriate split injection schemes [150; 432].

The energy for the engine's output work comes directly form the main injection sequence. This indicates that essentially the main injection is responsible for the development of the engine's torque. In the CR, the injection pressure remains practically constant throughout the whole of the injection process and is controlled by the ECU. However, constant injection pressure during main injection does not result in a constant fuel rate. Changes of the injected fuel are characterised by the rate of discharge curve, which defines

the variations in fuel mass flow during a single injection cycle (from start of injection until end of injection). Typical presentation of discharge curves are shown in Figures 2.5 and 2.6. The rate of discharge curve determines the mass of fuel delivered during the combustion lag (between start of injection and start of combustion). Furthermore, since it also influences the distribution of the fuel in the combustion chamber it also has an effect on the efficiency on the air utilisation. The curve must rise slowly in order that fuel injection during the combustion lag is kept to a minimum. The fuel combust suddenly as soon as combustion is initiated with the achievements of negative effects on engine noise and NO_x emissions. The rate of discharge curve must drop off sharply in order to prevent poorly atomised fuel leading to high hydrocarbon (HC) and soot emissions, and increased fuel consumption during the final phase of combustion.

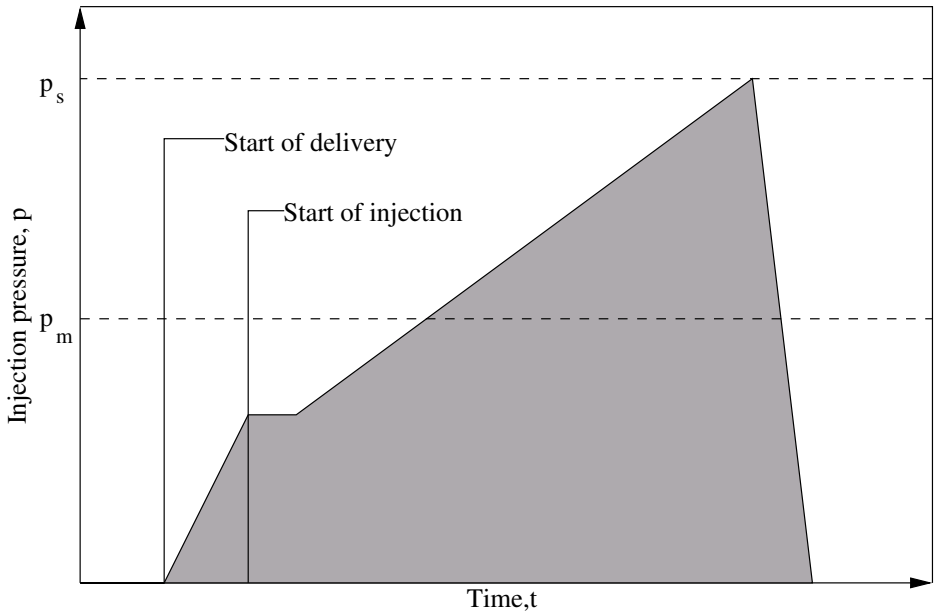

Figure 2.6: *Rate-of-charge curve for conventional fuel injection. p_m - mean injection pressure, p_s - peak pressure.*

2.2.6.3 Post injection

Post injection or secondary injection, follows the main injection process and is timed to take place during the expansion or exhaust cycle up to 200° after TDC. Secondary injection introduces a precisely metered quantity of fuel to the exhaust gas. In contrast to the pilot and main injection processes, the injected fuel does not combust but instead vaporises due to the residual heat in the exhaust gas. Such process had been found to be applied for NO_x reduction with certain types of NO_x catalytic converter. Post injection had turned out also

to be an efficient way to reduce soot emissions, with no change in NO_x emissions and only small increase in fuel consumption [64].

During the exhaust cycle, the resulting mixture of exhaust gas and fuel is forces out through the exhaust valves and into the exhaust gas system and to the catalyst. Part of the fuel is returned for combustion via the EGR system and has the same effect as very advanced pilot injection. Provided suitable NO_x catalytic converters fitted, these utilise the fuel in the exhaust gas as reduction agent to lower the NO_x content in the exhaust gas. Since very late pilot injection leads to dilution of the engine lube oil, it must be carefully designed and controlled.

2.2.6.4 Influence of high-pressure injection

Start of injection, type of injection, rate of discharge curve, and atomisation of the fuel do have an influence on fuel consumption and on exhaust gas emissions in CR cars. Due to lower process temperatures, as a consequence of more enhanced control of injection, retarded fuel injection reduces the NO_x emissions. But if it is too far retarded, HC emissions and fuel consumption increase, as do soot emissions especially under high loading conditions. This is caused by shorter time to complete the combustion of all hydrocarbons. Therefore, retarded fuel injection are precisely controlled and take place in situations when for instance car's catalyst requires regeneration. High sensitivity to injection time demands high accuracy when adjusting the start of injection and the way how the injection progresses. CR system adjusts precisely and quickly all required injection parameters accordingly to the collected signals.

As it has been recognised, finely atomised fuel promotes the efficiency mixing of air and fuel. It contributes to a reduction in HC and soot emissions. High injection pressure, optimal cylinder design and optimal geometrical configuration of the nozzle injection orifices lead to good atomisation. To prevent visible soot emissions, the injected fuel quantity must be limited in accordance with the intake air quantity. This necessitates excess air in the order of at least 10-40% (λ=1.1$\pm$1.4) [267]. Once nozzle needle has closed, the fuel in the injection orifices can vaporise (in the case of sac-hole (blind-hole) nozzles the fuel vaporises in the sac-hole volume) and in the process increase the HC

emissions. This means that such (unwanted) volumes must be kept to minimum.

High-pressure injection and its precise control is highly advantageous, but has not been studied for plant oils. CR system has been design and optimised for the diesel fuel and application of diesel ensures the correct and optimal system operation. It is assumed that, in case of significantly different (from diesel) fuels, the system may be subjected to numerous injection obstruction. Therefore, studies on plant oils in CR system should carefully consider the information presented in this section with special attention paid to the main CR features and function potentially being affected by a new type of fuel.

2.2.6.5 CDI operating on neat plant oils

As it can be noted from the description of the CDI system above, its operation of plant oils has not been fully recorded. There are some separate examples where companies were offered modifications of CDI cars, but it has to be emphasised that these changes were related to a double tank convertion. The double tank convertion is not convenient for the driver but it is a common practice of companies offering conversions to ensure trouble-free operation. A single tank, i.e. an engine starting and shutting off on pure plant oil has not been made commercially available The main technical obstacles are due to a sophisticated way of fuel delivery and injection, but also the complexity of the CDI injectors. These are practically impossible to be modified even at an advanced car workshop. As it can be relatively easy to do in case of the distributor and some single-plunger fuel injection pumps, the CDI injector nozzles are too advanced to be re-assembled off production line. It is expected that the modification of the CDI injectors could be performed in a injector producer factory as a mass order.

Apart from the injectors, the CDI system is precisely controlled and tuned for a specific type of fuel i.e. diesel. This is done by means of the ECU and EDC units, specifically programmed by a manufacturer. It is expected that the accommodation of a new fuel would require changes to some parameters of the original program to alter the injection regime for the new fuel accordingly. A separate problem is the presence of pilot- and post-injections, which are strictly designed for diesel and linked with operating conditions. A speculation based on the reported problems with the CDI [22] can be made that the split injection may cause some obstruction of plant oil combustion due to the prolonged injection ignition

delay of plant oils and the presence of post-injection can be responsible for unburned oil build-up in the engine.

Summing up, it can be stated that CDI must be modified to operate on neat plant oil in a single tank conversion. It can be achieved by very careful and complex study of the system running on plant oil as well as by investigation some fundamental features of injection pattern.

2.3 Spray characterisation using optical methods

Spray characterisation term is mainly used to describe sprays macro- and microscopic structure developed in a closed vessel under various injection conditions. Often, it is described by penetration of the liquid spray tip, its cone angle and by a spectrum of drop sizes within a spray. The spray penetration rate from a diesel injection is essential to assess fuel spray process and therfore air-fuel mixing. The depth of spray penetration is strictly function of injection parameters as well as engine design and cylinder geometry. If an injection results in a short penetration a possible advantage may occur by reducing fuel impingement which is essential especially during the start-up as well as can be recognised as a serious problem when plant oils are used. However, in this case formation of air-fuel mixing may be inhibited by poor utilisation of air intake. This issue was reported by Bergstrand et al. [66], van Basshuysen [59] and Rhim [342]. On the other hand an excessive penetration of fuel spray may lead to generally unwanted impingement against cylinder walls or piston head. Apart from the pure scientific interest, diesel engineers utilise spray penetration data to design and modify injection systems, so the work on penetration is essential. As it is crucial for air-fuel mixing process to know key spray parameters like penetration, cone angle or the break up length a reliable spray characteristic method and a setup need to be chosen.

This section presents work on rapeseed (RSO) oil and standard oil (SO) spray characterisations. The work was inspired by a lack of RSO spray characterisation data and the recognition that RSO spray characterisation is essential for the work on CDI modification. The study was performed in a comparative manner between RSO and SO. Partly, the existing methods and related issues are reviewed. Then, a description of the experimental technique and the experimental set up is presented. Special attention is paid to outline the

way of selecting the experimental procedures and the specific methods of data extraction. The chapter finishes off with results and discussion of the collected data.

2.3.1 Background

A recent collection of scientific papers deals with spray characteristics varying from experiments of spray characterisation to different types of correlation to predict a spray pattern. Some papers offer standard methods of spray characteristics and others present more advanced, recently developed techniques.

Some of the fuel penetration tests were conducted and various correlations were proposed in literature as early as work of Hay and Jones [183]. The authors discussed a disagreement between their experiment and a proposed correlation and made an effort to elaborate a new correlation suitable for diesel spray at a moderate injection pressure. Their work inspired others for further investigation of spray penetration and correlate it with injection and ambient conditions.

Kuniyoshi et al. [232] performed spray tests in ambient and low pressure using a high speed photography method. A similar method was used by Reitz et al. [339] to work with diesel spray and investigate mainly its cone angle in relationships with varying injection conditions. The fundamental work in spray characteristic was performed by Hiroyasu and Arai and presented in [192] and [193]. The authors produced an empirical model with the dependence on fuel and ambient pressures. Their correlation became one of the most frequently cited in literature and applied in spray studies. Also, the authors showed a significant effect on spray penetration of the in-cylinder temperature causing reduction of the penetration in comparison to the non-evaporating conditions. Hiroyasu and Arai applied the two-zone theory that sprays comprises liquid jet and a gas jet. Also, appropriate equations describing these two regions for the spray penetration were given.

Tabata et al. [387] investigated the effect of liquid viscosity on the spray angle and the Sauter mean diameter over the range of injection pressures and viscosities of fuel at the fixed ambient pressure. It had been found that the increasing fuel viscosity decreases the spray angle, whilst the Sauter mean diameter decreases. Also, the researchers found an upper limit of the viscosity for a fine atomisation of a spray. It has been stated that at a high injection pressure, viscosity has no effect on the spray angle.

For limited geometry and injection conditions Dent [111] suggested a model with the jet mixing theory considering the ambient temperature effect. As concluded by Hiroyasu and Arai in [193] that the in-cylinder temperature reduces the penetration, Dent proposed a term to compensate this effect. However in work of Naber and Sieberts [283] and also Morgan et al. [277] it has been shown that the Dent's model does not completely counterbalance the temperature effect. Wakuri et al. [407] evoked a spray model based on the momentum theory that air entrained into fuel produces mixed gas together with fuel drops for the density ratio range 40-60. Models produced by Schihl [357] and Naber and Sieberts [283] describe the spray penetration in a more conventional manner without including additional coefficients and as functions of physical fuel parameters and ambient conditions.

A Delphi CR injection system was used by Shao et al. [365] who applied digital imaging and image processing to investigate characteristics parameters of the sprays including tip penetration and spray cone angles. The authors concluded that the top penetration under a lower injection pressure is shorter than that under a higher injection pressure for the same chamber pressure. A higher chamber pressure results in greater spray angles than those under a lowest ambient pressure. The influence of in-cylinder charge density and injector nozzle geometry on the behaviour of diesel sprays were examined using high-speed camera and a CR injection system by Kennaird et al. [219]. The penetration results showed similar trends found in [193; 283] for different injection pressure and in-cylinder conditions. Some pressure fluctuations in the injector nozzle and hence a delay at the beginning of the spray development was also found. Spray hesitation at the opening phase of the VCO nozzle was reported and its effect on the needle lift. A similar, fundamental spray characterisation work was done by Yu and Bae [427] investigating the dimethyl ether sprays produced using a CR system. A charge coupled device camera was employed to receive spray penetration and cone angle. The study revealed that the dimethyl ether forms a mushroom-like shapes of the spray tip in atmospheric pressure conditions and becomes diesel like with elevated ambient pressure.

Arai and Amagi [7] investigated experimentally the structure of multi-stage injection spray. The spray tip penetration and spray angle were measured using a high speed camera and the total spray volume and mean equivalence ratio were also evaluated under various conditions of injection intervals between split sprays. Two typical injection patterns

between split sprays were described. The authors named them “catch up” type and “push away” patterns. Also, the work showed that the injection interval of the split sprays affected the spray angle and the total spray volume.

For a multi-hole nozzle, it is difficult to determine which one better represents the characteristics of fuel spray. Majority of CDI experiments employed a single hole injector, which does not fully represent a real injecting device. Selection of a hole in the sac[1] remains problematic. In accordance to the number and position of holes on the sac injector were experimentally tested by Hosoya and Obokata [195]. Spray flow characteristics including drop size distribution were presented. Summarised findings showed that the spray injected from the single-hole nozzle having a hole located at the tip of the sac has very different characteristics to sprays injected from multi-hole nozzles.

The alternative method for testing diesel sprays is a large-scale model giving some possibilities to overcome the difficulties in measurements in a small-scale by means of optical methods. Mainly, determination of droplet velocities becomes more easier to complete and this approach offers a great help in avoiding multiple droplets in the measurement volume due to decrease in the number concentration of the droplets. Rantanen et al. [335] measured diesel sprays using a large-scale model and compared the results with a normal size nozzle tests (two rigs scaled 4:1). Modelling of the spray tip penetration was also performed with the successful application of the correlation of Hiroyasu and Arai in [193]. Differences between small and large scale were about the same as measurement accuracy. Authors observed some differences and indicated that more factual research needs to be done. Nevertheless, the authors recognised the method as valuable in testing the break up and atomisation mechanism.

A heavy duty multi-hole injector was studied using high speed camera technique to obtain the spray formation parameters in the work of Klein-Douwell et al. [222]. A CR system delivering a fuel pressure of up to 200 MPa and the maximum ambient pressure of 6.1 MPa was used. It was found that the spray length was proportional to time (duration of the injection from start) in power of 0.4. The final correlation included the cone angle and hence differed from the previous works reported in the literature.

[1]The term “sac” refers to the volume between the needle tip and the inside of the nozzle tip.

Stationary diesel jets were studied in the work of Eisfeld [133] mainly focusing on the mechanism of the breakup process. Tip velocities as well as cone angle were investigated. The author also presented samples of the spray images showing cavitation and its effect on the spreading of the injection jet by improving the atomisation. The effect of cavitation was created by choosing a right injection pressure for the phenomena to happen. Eisfeld highlighted the importance of the cavitation at the end of the injection when the injection velocity is low and large drops are formed, resulting in poor combustion.

Often, spray penetration and the cone angle were investigated focusing on effects of different injector configuration on diesel spray shapes. As showed by Bergstrand and Denbratt [66] a reduction in the nozzle orifice diameters has an effect on combustion and thus the emissions. Following the general rule that the combustion is strongly affected by the quality of air-fuel mixture, it can be concluded that the smaller droplets produced by a smaller nozzle, creates more readily the air-fuel mixture. Small droplets evaporate faster and reduce the ignition delay. Nozzle diameter is one of the parameters influencing the droplet size, but also the hole shape has a significant effect on discharge coefficient and the breakup close to the injector tip. Work of Dodge et al. [115], tested twelve different hole shapes for diesel injector tips. They showed that the hole shapes had a little effect on either the volume fraction (air-fuel ratio) or drop sizes. This finding appears to be in contradiction to the general effect of the hole shape and it would required a similar set of tests to confirm that.

Bae et al. [52] investigated the multi-hole injection and found no significant variation related to hole-to-hole changes of a VCO (Valve Covered Orifice) nozzle, however some changes in spray angle were reported testing a sac type nozzle. These results were different from findings of Campanella et al. [83] who also investigated a five hole VCO nozzle. Despite the same type of nozzle used in both tests the difference occurred due to a different nozzle configuration. Bae [52] tested more extensively the development of diesel spray from a VCO CR nozzle. The macro- and microscopic images of sprays revealed the structure of a dense diesel spray consisting of thick ligaments or membranes. Describing the mechanism of droplet creation the authors concluded that majority of the liquid droplets are formed at the tip of ligaments from spray surface due to the waves developed on it. Moreover, it had been found that as injection pressure increases the interaction between spray and ambient air becomes important or the liquid penetration and spray angle, and

the rate of penetration is proportional to injection pressure. Similarly, Ohnishi et al. [300] conducted an experimental study on the behaviour of the fuel spray and the nozzle needle in a multi-hole valve cut orifice. The time lag for fuel discharge among individual holes and the photographic observation of fuel sprays were carried out using a video camera. The collected results showed that the earliest fuel spray appeared from an opposite hole to the the radial displacement of the nozzle needle and therefore the spray development was not equal to all five injector nozzles.

The mixture formation and the combustion process of small direct-injection diesel engines, equipped with a high pressure CR fuel injection systems was investigated by Ofner et al. [299] at several engine operating and injection conditions. Different sac hole and VCO nozzles types with a variable number of holes were examined. Irregularities in the spray structure of VCO nozzles, similar to those recorded in [300] were recorded. The VCO nozzles showed an acceleration of the spray tip at the beginning of the injection. Also, cavitation was found to have an important influence on the fuel jet break up.

From the cited literature it can be concluded that the spray irregularities of VCO nozzles (including the CR nozzles) seems to be important and require further investigation. Although in some cases the nozzle geometrical configuration is not clearly described, the CR nozzles equipped with two needle guides should be more closely investigated and verified against the hole-to-hole variation spray data. Also, validation of sprays produced in multiple orifices against single orifice nozzle should be performed.

Since bio-fuels have been emerging as a potentially viable alternative to conventional fossil fuels, need for understanding of the basic bio-fuel spray characteristics had become quite apparent. Furthermore, rapid development of DI diesel especially the CR ones enforced to examine bio-fuel sprays in these new system. A key problem in the use of these fuels is spray atomisation, a phenomenon that aids proper combustion after fuel injection. Recent literature does not offer enough information in comparison to the standard diesel fuel. Although, there are some information about bio-esters and some plant oils used to produce fuel sprays in conventional DI diesel engines, such information for the CR system almost does not exist. In this part of the section the review of some publications on spray characteristics using bio-fuels is presented.

The influence of viscosity, surface tension and other physical parameters of several plant oils, on the droplet formation after injection into the engine were tested by Dunn and Perera [125]. Photographs of spray produced by a single hole diesel injection revealed that the spray angle of plant oils was only half of the spray angle for diesel oils and under atmospheric conditions is dependant upon both the viscosity and surface tension. Also, the authors concluded that the smaller angle of plant oils can lead to poorer air-fuel mixture formation and thus causing incomplete combustion. Such basic experiments carried out by Dunn and Perera [125] did not provide appropriate information about spray characteristics at higher chamber pressures and spray drop sizes.
Msipa et al. [278] made an attempt to develop equations as function of surface tension and viscosity as critical parameters in predicting whether or not proper atomisation will occur for a given fuel. Soyabean and sunflower oils blends with diesel were examined and viscosities and surface tension were correlated to calculate permissable concentrations of plant oil in blends with diesel fuel. Allowable concentrations ranged from zero to 34% depending on injection parameters. Despite practical manner of the investigation the authors did not investigate the basic spray characteristic parameters.

Extensive work on methyl ester sprays was carried out by Jimenez et al. [207] using a Phase Doppler Anemometer (PDA) and a high speed camera. Spray results obtained at ambient pressure and two different temperatures were compared with those of a diesel fuel and the spray penetration data was used to generate an empirical equation. Results presented noticeable similarities between the ester and diesel in terms of droplet diameter and penetration. Slightly higher axial velocities of methyl ester were reported and the authors interpreted this as the result of higher ester viscosity. Also, higher droplet mean diameter was obtained at spray tip for the ester than for diesel.

Similar experimental work on five types of bio-fuels was conducted by Allen and Watts [31] using a Malvern analyser and focused on droplet size distribution. Amongst tested esters only the coconut oil methyl ester revealed the same statistical atomisation characteristics as diesel. The rest of esters provided higher Sauter mean diameters. The results can be explained by looking at viscosities of used ester, which the coconut one is the lowest. Presented results are comparable with the previous work of Jimenez et al. [207], however the type of ester used there was not provided.

Goering et al. [157] investigated eleven different plant oil in terms of their physical properties and capability of alternative fuel substitute. Selected ASTM tests were performed to examine the oils and compare their properties with diesel. Also, the formulas correlating viscosity and surface tension had been worked out. Authors indicated that higher viscosity and surface tension of plant oil may lead to poor atomisation and recognised a need for the further spray studies. Similar suggestions were made by Peterson at al. [327] evolving the potential of plant oils based fuels. Further concerns about using unmodified plant oils and their poor atomisation were reported in the work of Jones and Peterson [209].

Direct engine tests on plant oils conducted by Peterson and co-workers [325]. Observation proved that high viscosity of plant oils noticeable reduced engine performance due to spray atomisation poorer than those of a diesel fuel. Authors suggested using a blend of RSO and diesel for more successful engine operation.

Nwafor [296] tested pure plant oil in an indirect injection engine, concluded that application of plant oil in a direct injection engine is not recommended due to the high degree of atomisation required for this type. He suggested that the problem was related to increasing droplet size following the fuel injection into the cylinder which resulted in poor combustion. The results showed that fuel pre-heating increased peak cylinder pressure and was also beneficial at low speed and under part-load operation. The method of oil heating was suggested as one to enhance plant oil atomisation.

From the literature reviewed above, it appears that most of the research investigating spray characteristics had been conducted on diesel spray with a special interest on the spray tip penetration and the spray cone angle. The data available in the literature permit to collect enough data of diesel spray to evaluate and simulate spray penetration and therefore air-fuel mixture formation. From the avaliable literature source it is relatively easy to determine the appropriate spray testing method and validate it against collected experimental data. Although, investigation of diesel spray provided essential correlation to evaluate spray tip penetration, there is still some need for further development. As far as plant oil are concerned, spray characterisation has not been extensively investigated.

It can be recognised that the successful application of plant oils requires range of data describing spray especially under high pressure injection conditions. Such information can obtained by using high speed camera imaging and drop sizing techniques. It is expected that the spray characterisation data of RSO generated in this work will aid alter RSO

spray by changing injection temperature and/or pressure. And following the rule that the combustion is strongly affected by the quality of air-fuel mixture, it can be concluded that the smaller RSO droplets should create more favourable the air-fuel mixture and therefore improve combustion.

2.3.2 Spray characterisation

The quantitative information on the diesel spray is of significant importance both in understanding the process of fuel mixture formation and in examining its effect on combustion characteristics in diesel engines. The high pressure diesel spray structure is quite complex. A significant number of method have been used to characterise the diesel spray. Determination of macroscopic characteristics like spray tip penetration, cone angle and air entrainment by the spray is usually based on imaging techniques. In this section some of spray characterisation techniques are briefly described.

2.3.2.1 High speed imaging methods

Spray characterisation requires capturing spray images at maximum optical conditions and then perform a snapshot analysis. This can be done by means of the high speed photography frequently named also high speed cinematography or high speed imaging. The method is commonly used in a combination of a light source (a flash lamp) which can be setup as a back, front or side illumination or a laser illuminating sheet.

Spray illumination can be done using a collimated beam of light which illuminates the spray. There are three ways how individual rays of light may be affected passing through the spray: unaffected passing without loosing the light intensity, light being scattered by the liquid phase and refraction of light by the vapour fuel phase. The last effect is frequently described as Schlieren effect. The sensitivity of the technique depends on detecting the light rays steered by refraction using a camera with an adjustable aperture. Examples of different spray illumination types and certain applications are presented further down in the *Section 2.3.2.1*. The test arrangement typically consist of three parts: the light source, the image capturing device and the image processing system. Captured spray images can then be analysed to determine the tip spray penetration, the spray cone angle. The accurate measurement of these parameters depends strongly on the quality and criteria followed to determine the spray contour. It is necessary to provide an appropriate automatic processing method with objective criteria to define the spray contour and it should not be

dependent on the particular image characteristics. A range of different image-processing techniques presenting various procedures to process spray images can be found in the literature [161; 241; 309].

Different approaches exist to extract (segment) the diesel spray form the background [161]. Most of them are applied only to gray-scale images. The processing method is crucial for the accuracy of the measurement of spray parameters. There are three basic methods to process spray images: the threshold method, the model-fitting method and the pattern recognition method.

In the threshold method a proper threshold is selected to separate spray images from the background. The threshold level is very often chosen arbitrarily and sometimes underestimates the spray contour. In principle, the threshold is chosen as the pixel value that provides a contour of the spray captured on an image. The threshold has a direct effect on the results of the spray parameters. It is important to eliminate the image noise prior to the processing to avoid underestimated contour size. Some of the application of the threshold method are given in [99; 222; 355; 431].

The model-fitting method involves edge detection based on recognition and fitting of pixels into a model describing the spray boundary. Pixels are analysed and transformed to provide the best fit into the model which is explicitely taken from the previous investigations or mathematically modelled. The method is not suitable for highly distorted sprays and requires high level of spray symmetry.

The pattern-recognition method utilises a procedure to analyse the origin of a pixel. i.e. if belongs to spray background. The method still relys on the optimal threshold value to extract the diesel spray. There is a number of algorithms to perform spray segmentation involving examination of the brightness, probability density function, and image restoration. Generally, all of them work if the spray and background distributions are non-overlapping. Segmented images can be processed using appropriate sizing algorithm to obtain spray features from the spray outline. Although there are some commercial packages which may be used to analyse segmented pictures, in most cases, researchers develop their own way to perform measurements.

The procedure of the high speed imaging can also be applied using laser sheet illumination. In this case, pulsed laser source is used to provide required image resolution and quality. The illumination can be performed with a high-power copper vapour laser emitting

light pulses in the green and yellow spectral range. Normally, the laser is triggered by the camera. This approach readily combines the traditional way of spray capturing and an advance method of spray illumination. The method based on laser scattering images is also recognised as laser elastic scattering LES [306; 400] from liquid surfaces and droplets. The technique works well in media that are optically thin, where the laser in attenuated by only 10% or less after passing through the spray. Hence, with this method the liquid in the spray needs to be completely transparent for the laser light to avoid absorption and extra attenuation. Captured images can be analysed in the same way as in the case of the flash light illumination.

2.3.2.2 Laser-induced exciplex fluorescence (LIEF)

Air-fuel formation, as an important feature of spray characteristic are one of the most frequently observed parameters in diesel spray development. There is a range of methods based on the fluorescence signal emitted by dopant in diesel fuel. One of them is the Laser-induced exciplex fluorescence (LIEF) technique. Originally developed to observe air-fuel formation, the technique is also used to obtain the spray penetration and the cone angle.

The method was initiated by Melton et al. [265] and since then it has attracted considerable attention for the simultaneous measurement of liquid and vapour phases in a diesel spray [60; 116; 149; 219]. The method had been also used to evaluate emissions from diesel engines and examples can be found in [191; 212; 274]. The fluorescence phenomenon used by Laser-induced exciplex fluorescence can be briefly described by combination of Einstain's equation and the two level model and the Beer-Lambert law. The method of using measured fluorescence intensity change with the density of fluorescent substance is presented in [425].

Despite being very successful in spray characterisation, the LIEF method has several disadvantages. One is the appropriate thickness of the spray. The method works well with thin sprays allowing the laser plane pass through the spray without significant intensity lose. In case of dense sprays the method may not provide reliable results. Another problem frequently reported is the ability of obtaining the absolute concentration under suitable calibration. The calibration process is highly demanding and subject to well known dense spray structure which frequently needs to be investigated in the first instance. It needs to

be highlighted that in some case the LIEF method works only with precisely chosen and appropriate dopant with known characteristics and use of diesel fuel is very limited. The drawbacks of using reference fuels are that measurements are not performed under real conditions because of the change in the properties of the fuel itself i.e. important effects such as cavitation in the nozzle and chances in the penetration length and cone angle can depend on fuel properties.

One of the variations of modified LIEF is the Planar Laser-Induced Fluorescence (PLIF) which is an imaging technique that allows measurements fuel concentration and relative Sauter diameters distribution by combining PLIF with Mie scattering. It is possible to determine the geometric characteristics of the spray, as in other imaging optical techniques such as shadowgraphy, but with a higher signal to noise ratio. Le Gal et al. outlined the use of the ratio of fluorescence intensity and Mie intensity to measure the surface volume and the Sauter mean diameter for studies of fuel injection and mixing in gas turbines and internal combustion engines [244].

Similar to LIEF method the problem appears if fuel concentration and its fluorescence properties are not known. Additionally, the method suffers from difficult fluorescence intensity calibration and the loss of the laser beam travelling across the spray. In both methods a spray is expected to be axisymmetric, however any laser sheet based image of sprays presents higher intensity on the side of the beam entry. Thus there is a need for any accurate method correcting and improving the image symmetry.

Both methods work well with sprays in isothermal conditions. Recently there has been a number of publication presenting some compensating methods to overcome problems associated with LIEF methods [25; 26; 310].

2.3.2.3 Spray acquiring using a high speed camera

Image processing is highly depended on the quality of images obtained from the high speed camera as well as the way how the image was taken. Parameters like spray illumination type, optical setup, quality of glass used are crucial and affect the choice of processing method. Therefore, it is essential to design spray acquiring procedure which would provide the best snapshots quality. The selection of the method is not only based on the type of spray (e.g dense spray, non-uniform spray shape, etc.) but also on the type of the fuel injected. It has been recognised throughout the literature review that [112; 200; 266; 315], the majority of the spray penetration measurements have been performed by using back-

light or a laser sheet illumination. It needs to be highlighted that the choice of the method isn't only up to the experimenter but is very much determined by the system itself. In the current experimental work, the spray is produced periodically and determined by a injection frequency parameter. As presented in the cited literature above, in most of the tests, a continuous spray was used, which provides a flexible and relatively easy way to setup the spray illumination. In case of non-continuous spray, its varying nature creates serious experimental problems of precise illumination of the spray. For instance, a possible offset of the illumination laser sheet would result in incorrect spray snapshots ie. smaller spray shape or high distortion of a spray edge. The problem is graphically presented in Figure 2.7. From the figure it can be seen that the left hand side of the spray is not

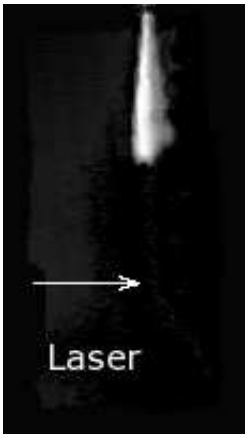

Figure 2.7: *Spray image using the laser sheet (after compensation).*

sufficiently illuminated and therefore the "cloud" of small droplet at the left edge can not be seen. Such situation takes place when the laser sheet (as indicated by the arrow in the figure) does not cut the spray across its centreline. In the presented case the lack of illumination was likely caused by changing shape of the spray from injection to injection. It is essential to chose a right illumination method and setup correctly the way of acquiring the spray. Next section describe the way of setting up the hight speed camera system and the procedure of recording and analysing of spray images.

2.4 Spray droplet sizing using visible laser methods

In order to achieve a uniform mixture distribution of RSO within the CDI engine cylinder, the atomisation characteristics of the fuel spray must be known. This plays an important role in modification of the CDI engine concept. It is also well known that high-pressure CR injection systems, mainly used in diesel engines, achieve poor mixture formation because

of the possibility of direct fuel impingement on the combustion chamber surfaces [249]. On the other hand it has been recognised that atomisation is the first process encountered during the combustion of fuels in a compression ignition engine and is largely determined by the fuel‘s viscosity and surface tension [30]. In the case or RSO, it is expected that poor atomisation can lead to incomplete combustion. However, a rough assumption can be made that if by altering RSO temperature at least the same droplet distribution of RSO as for SO can be achieved, the combustion process could be improved. Hence, it is essential to perform comparative studies of RSO and SO atomisation at various injection and ambient conditions.

There is a wide range of optically based droplet size measurements techniques which together with methods exploring spray tip penetration and spray cone angle fully assist to characterise fuel sprays. In this section a group of methods used to determine droplet sizes and velocities are reviewed. These methods are based on light scattering and refraction, and are considered, at the moment, the most accurate for spray characterisation. A special attention is dedicated to a Laser Doppler Anemometry (LDA) variant method i.e. Phase Doppler Anemometry (PDA) applied in this work.

2.4.1 Spray liquid phase measuring

There has been tremendous change over the last few decades in the operating conditions of diesel fuel injection systems and engines, and in the diagnostic tools and numerical models available to evaluate them. Systems like PDA or LDA have inevitably changed the direction of diesel spray studies and helped to develop more quantitative analysis of the drop formation mechanism. Improvements in the diagnostic techniques coinciding with changes in diesel injector technology have brought about an entirely different view of the breakup of liquid in current diesel sprays and thus helped to understand, develop and model diesel sprays. Despite the very fast grow of these diagnostic techniques, the spray diagnostic area is still developing and new methods are offered to researchers. It has to be stressed that application of LDA techniques is more readily found in studies of petrol sprays and only the resent research had been focusing on the diesel sprays. Examples of PDA in petrol direct injection engines are not discussed here and can be found elsewhere [90; 246; 347; 417] for more information.

Smallwood et al. [374] reviewed diagnostic methods to investigate the structure of transient diesel sprays. A detailed examination of the history and current understanding of the structure of the dense core region in transient diesel sprays was presented. Methods like tomography was recognised as the the most appropriate for determining the structure of the dense core region. Also, the line-of-sight techniques were recommended by the authors but only for studying the periphery of the spray whereas the high-intensity Mie scattering is preferred over line-of-sight methods for liquid spray penetration distance measurements due to its greater contrast. Smallwood discussed the structure of the spray, its atomisation near the nozzle tip and the dominant breakup mechanisms. The results of recent research on the liquid spray penetration distance and drop size were also summarised. Work of Smallwood and coworkers shows a need for better understanding the breakup mechanism by using combination of avaliable techniques.

Behrouz [61] used a single-holed round nozzle to produce hexane, solid cone sprays in nitrogen at 1.46 MPa. A differential pressure of 13.6 MPa was used to generate a narrow, fast, steady diesel-type spray. Effects of instrument variables of a PDA on the mean and the root mean square (RMS)[2] of the drop axial velocity and Sauter mean diameter (SMD) were investigated. It was found that a seemingly good choice of instrument parameters based on SMD may not necessarily be appropriate for velocity measurements. Influence of the photo multiplier voltage was investigated which revealed that all measured quantities tended to level out at sufficiently high voltage values but the same tendency was not recorded in the shift velocity. Optical arrangements with smaller measurement volume showed less sensitivity to the instrument parameters and produced mean and RMS velocities in agreement with 8% with those obtained with a single-component, dual Bragg cell LDV (Laser Doppler Velocimetry, is described in more details in 2.4.3) system. It was found the SMD decreased radially and then increased where the mean velocity was virtually zero. Work concluded further necessary drop size and velocity measurements at various axial locations, particularly closer to the nozzle where the spray becomes denser, possibly using different instruments such as the PDA, the Malvern particle analyser and LDV.
Similarly to Behrouz [61], Wu et al. [421] performed measurements of axial and radial components of the drop velocity for n-hexane/nitrogen sprays from single-hole cylindrical nozzles at room temperature. The gas/liquid density ratio, the injection velocity, and

[2]The root-mean-square velocity is defined as the square root of the average velocity-squared of the droplets in a gas.

the nozzle length and diameter were varied. The dual beam LDV argon-ion laser based was used to conduct the tests. Authors reported that that beyond 300 nozzle diameters from the nozzle so much ambient gas has been entrained by the drops that the subsequent structure of the spray is dominated by the entrained ambient gas, and the fully developed incompressible jet structure and drop-gas equilibrium are being approached. The total error in the measured mean and fluctuation drop velocities was less than 10% from the centreline to the half-radius and larger and more uncertain beyond it. It was found that the velocity bias was the most difficult error to quantify.

In his work Hardalupas et al. [178] applied a PDA to measure spatial and temporal velocity profiles of the entrained air and diesel droplets, together with the associated fluxes using a 5-hole nozzle exhausting into atmosphere. The work recorded that the SMD decreased from a maximum centreline value of around 80 μm at 100 diameters from the nozzle to 38 μm at 780 diameters, and a similar decrease was observed between 1 and 2 ms after the start of injection at the upstream location. The mass flux carried by the 30 μm droplets was up to twice that associated with the 60 μm droplets. Although the velocities of the larger droplets were consistently higher than those of the smaller droplets. Authors concluded that the measured decrease in the mean diameter was due to small droplets, generated by breakup at the leading edge of the spray, losing velocity due to aerodynamic drag and falling behind the leading edge. Authors claimed that droplets generated later in the injection schedule were likely to overtake those generated earlier and together with the fan-spreading effect. However, the explanation of that claim was not given in the paper. The author of the thesis assumed that larger droples had higher velocities due to higher jet momentum towards the end of the injection as a result of more developed spray.

Hosoya and Obokata [195] investigated the best number and position of holes on the injector sac using a laser Doppler anemometer and a phase Doppler anemometer. Spray flow characteristics, such as mean and fluctuating two component velocities, the two dimensional distribution of particle diameter were tested in four different nozzle configurations and then compared with each other to identify the differences in spray characteristics between them. A wide range of droplet diameters were obtained with the maximum value of 500 μm which seems be quite large for diesel. Furthermore, the results show that the spray from the original single-hole nozzle on the top of the sac is distinct from the other types of nozzle.

High validation of PDA measurement of diesel sprays have always been problematic and presence of large droplet sizes were not always validated. Araneo and Tropea [44] used a PDA to characterise diesel sprays produced in a CR system. Setup used provided a high validation which was compromised by very low sphericity factor of 30%. This would result in sizing of non-spherical droplets favouring a low rejection rate. The limitation of the PDA technique in testing dense sprays was widely discussed by Ficarella et al. [143]. A dense spray of CR system was investigated and the velocity and diameter validations analysed in connection to the PDA setup and power. Different approaches to establish the LDA/PDA technique that would allow measurements to be made over a wide drop size range with confidence are presented in paper of Wigley et al. [416] and Kashdan et al. [215]. The papers concentrate on applications of PDA under quasi-steady conditions and dense spray discussing the possible solutions.

Lacoste and his colleagues [240] used Phase Doppler anemometry to explore a diesel spray produced using a CR injection system at three feeding pressures (100, 140 and 160 MPa). Authors discussed the fundamental principles of PDA and the main difficulties in application of the technique in diesel sprays. In addition to the errors affecting the measurement of spray in general, like defocusing, shape irregularities, some other factors in making measurements of the dense diesel spray were presented. An overlapping signal due to a “multiple occupancy” in the measuring volume is one of the obstacles. A possible solution recognised by the authors was to reduce the control volume, which would lead to decreasing the size of the measuring volume and thus the increased number of fringes. The small measurement volume would also result in distortion of signal by a drop passing through close to the measuring volume. It has been shown despite the difficulties, that PDA can provide valuable results of the spray velocity and droplet sizes. However, the results might not be fully satisfactory.

In another similar work Lacoste et al. [239] concentrated on characterisation of dense diesel sprays in a CR system. The PDA technique was applied to measure droplet seizes and velocities in the Proteus engine. Authors carefully investigated influence of various setup parameters on the spray characterisation. Parameters like laser power and photomultiplier voltage need to be adjusted to the measurements revealing significant effects on measured droplet diameters. The effect of injection pressure and in-cylinder pressure showed an increase in mean droplet velocity. Increasing the in-cylinder pressure led to improved spray atomisation. Similar results of the injection pressure effect were found by Araneo

and Coghe [43]. Additionally, they recognised difficulties in collecting reliable data at 30 mm from the nozzle tip.
Kurachi et al.[236] used a LDV system to investigate diesel sprays injected into a high pressure vessel at room temperature. Spray tip penetration was measured by the delay time of Doppler signals from injection start to spray tip arrival at each measuring point and spray breakup length was estimated by measuring the standard deviation of the delay time which indicated dispersion of the time form injection start to Doppler signal rising. Each measured data was compared with the data estimated from spray photographs. Results of the Doppler method were in good agreement with the conventional high speed camera technique.

Cossali et al. [96] investigated the air entrainment in a transient non-evaporating diesel spray using LDV to provide information on the mixing properties in the near-field region. The spray was injected into confined quiescent air at ambient pressure and temperature. Authors applied two injection conditions and examined their influence on the entrainment. In the near field zone investigated, the air entrainment in transient liquid jets appears to be lower than that in steady gaseous jets, but larger than that in steady liquid jets.

Park and Watkins [307] compared of wall spray impaction models with experimental data on drop velocities and sizes provided by PDA measurements. Several spray/wall impaction models were tested. Authors recognised a need to establish the ability of models to predict the internal structure of the sprays and their validation by means of the PDA method. They concluded that the agreement is far from complete, and it is evident that further work is required to enhance the predictive capabilities of the model.

A fundamental work on a comparison between conventional and bio-derived fuel spray characteristics was described by Jim*é*nez and others [207]. Radial distributions of drop size, axial and radial velocity components were measured sing a PDA for methyl ester and diesel fuel. Same effect of spray injection and ambient pressure as presented in [239] were found for the both fuels. Additionally, the droplet mean diameter decreased with increasing ambient temperature due to reduction of methyl ester viscosity. Axial mean velocity of methyl ester were found slightly higher than for diesel. Such effect was explained as a consequence of the higher viscosity leading to the poorer atomisation. Spray penetration results were fitted to an empirical equation. The paper of Jim*é*nez is a rare example of

studies on bio-fuels where PDA had been applied.

Generally it can be concluded that the avaliable literature sources do not offer a selection of scientific works presenting the application of PDA with plant oils. It has been recognised that the lack of data is due to absence of scientific activity in drop sizing of various plant oils, which is a consequence of relatively low interest to investigate combustion properties of plant oils.

2.4.2 Particle Image Velocimetry (PIV)

The Particle Image Velocimetry method is a full field non-intrusive technique being applied since mid-1980‘s in fluid flow metrology. PIV is a method for obtaining instantaneous whole field velocities and it is based on the simple equation that distance equals speed multiplied by time. The property measured by PIV is the distance travelled by droplets in the flow within a known time interval. The measurement is achieved by illuminating a spray field by a light sheet, which is generated by a laser and detecting the Mie-scattering signal. To detect the position of the illuminated particles, a camera is located at right angles to the light sheet. The spray droplets are illuminated twice in a same area of flow by two pulsing light sheets. In order to resolve the droplet speed shots are recorded on one or two images. Signal processing involves dividing the image into rectangular interrogation regions, and for each of these regions the images from first and the second light pulse are correlated to produce an average droplets displacement vector. By analysing all the regions a vector map of average droplets displacement can be produced.
The PIV technique is robust due to applied method of correlation of the displacement of the particle images whether they be from tracers added to a flow or naturally occurring drops in a spray [27]. There had been some solutions to overcome the directional ambiguity using the image-shifting techniques based on birefringence[1] optics [242], a rotating mirror [243; 305] and on grey-scale classification [422].

PIV method based on the image-shifting technique is still limited due to the complicated mechanism itself and its limitation in measuring flow speed. This is especially noticeable measuring very uneven spray flows where it is difficult to provide a sufficient

[1]Crystalline materials may have different indices of refraction associated with different crystallographic directions. Birefringent materials are used widely in optics to produce polarising prisms and retarder plates such as the quarter-wave plate. Putting a birefringent material between crossed polarisers can give rise to interference colours.

number of images servicing the whole flow field. The PIV technique has got lower spatial resolution than single-point measurement methods like these based on the Laser Doppler Anemometry and requires expensive cross-correlating camera and the interrogating system.

2.4.3 Laser Doppler Velocimetry (LDV)

Laser Doppler Anemometry (LDA) is a non-intrusive optical technique for measuring in-cylinder spray fluid velocities. LDA is also known as Laser Doppler Velocimetry (LDV) and is a single point optical measuring technique. This technique was first reported by Yeh and Cummins in 1964 [424] and since than its application to the study of fuel sprays has been steadily growing. The measurement is based on the Doppler effect, where the motion of a particle causes reflecting laser energy to change wavelength in proportion to its velocity. Therefore, the local velocity of the spray is determined by analysing the Doppler equivalent frequency of the laser light scattered by the droplets within the flow in a probe volume.

There are two types of scatter the forward and the back one. Figure 2.8 presents a “one component dual-beam system”, dual because of two laser beams of equal intensity. In this simple and specific example the system measures one velocity component U. The forward scatter LDA requires a line of sigh path through the cylinder volume. A quartz spacer, window through the side of the cylinder are normally used. The laser beams are generated in a laser source and them split using the “beam splitter” and focused using a sending lens. Unfortunately, very often it is necessary to have all the equipment on the same side of the window. Therefore it is possible to collect the light that scatters back towards the laser and in this case the system is called the LDA back scatter and show schematically in Figure 2.9. In the back scatter which is more common and advantageous, the LDA uses a single window. The scattered laser light is reflected back through the same window. Application of a single window makes the optical access to the cylinder more convenient but on the other hand makes the measurement more difficult. The main obstacle of this configuration is the high level of background noise and high influence of fuel buildup on the window on laser beams.

The LDA measures the velocity at a point in a flow. This is obtained by using two laser beams intersecting in the probe volume creating a fringe pattern (light and dark

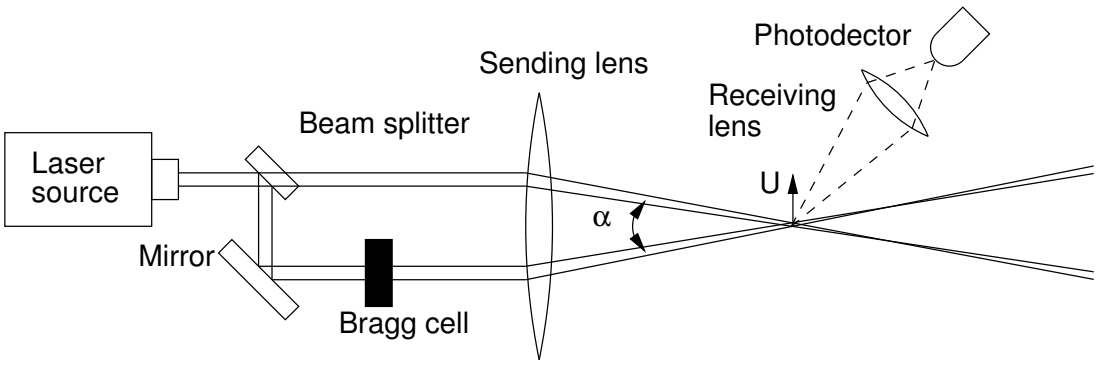

Figure 2.8: *A single-component dual-beam LDA system in forward scatter mode*

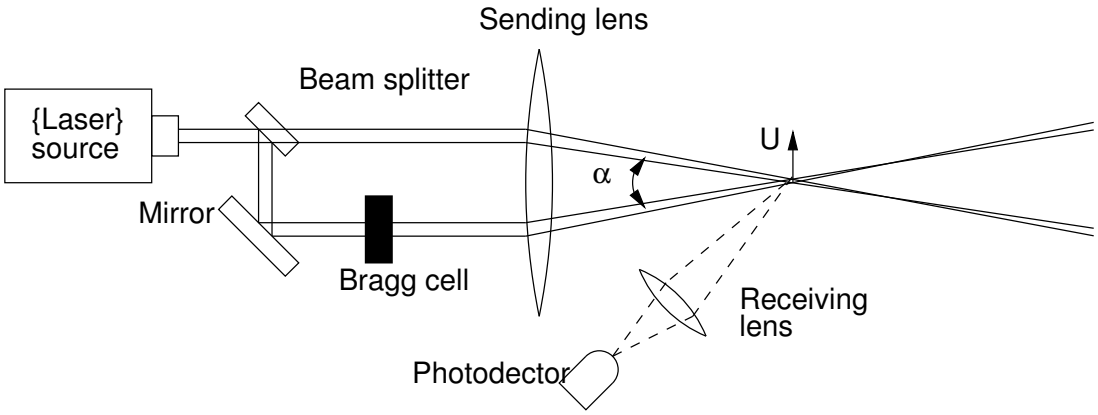

Figure 2.9: *A single-component dual-beam LDA system in back scatter mode*

bands) parallel to the bisector of the beams showed in Figure 2.10. This can be created since the laser beams are monochromatic and coherent. The interfering light waves are in phase add up creating a bright fringe and those out of phase are cancelled creating a dark fringe. Droplets passing the fringe patterns reflect the laser light at each fringe creating the Mia-scattering signal which fluctuates accordingly to the droplet fluctuation. The frequency of this fluctuation is proportional to the velocity of the droplet normal to the fringes. To detect this frequency, the light scattered by the droplet is collected by the receiving lens and focused on a photodetector which converts the fluctuations in light intensity into fluctuations in a voltage output signal.

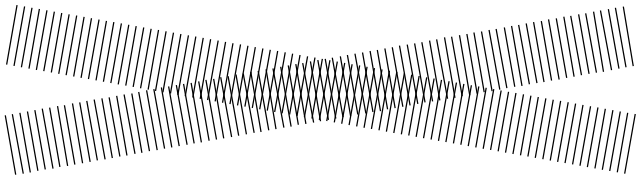

Figure 2.10: *Schematic presentation of the measurement volume consisting of the laser fringes*

In order to calculate the spacing between the fringes the laser wavelength λ needs to be known together with the angle between the beams α. The enlarged region of fringes is shown in Figure 2.11.

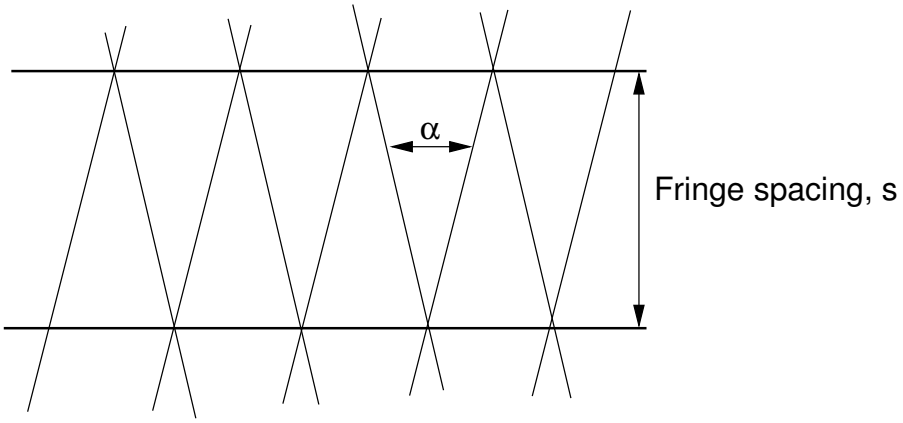

Figure 2.11: *Schematic presentation of the measurement volume consisting of the laser fringes*

Using trigonometry the height of the triangle i.e. the fringe spacing s is equal to $\lambda/(2sin(\alpha/2))$. Considering the velocity component U normal to the fringes and in the plane of the beams, then the droplet crosses a total of U/s fringes per second. The droplet generates a signal frequency of fluctuations known as the Doppler shift frequency [128] and is given by:

$$f = \frac{2U sin\left(\frac{\alpha}{2}\right)}{\lambda} \tag{2.4.1}$$

The Doppler frequency f can be determined by measuring the period of the Doppler signal, if the laser wavelength and the angle of intersection of the two beams are known. To process the Doppler signal a droplet must be present in the measurement volume. It is important that the droplet is small to accurately follow all the movement of the flow (at given fringe spacing). Considering the way how the signal is detected it can be seen that the technique has two main limitations: a stationary droplet does not provide a signal and also two droplets with the same speed but travelling in opposite directions give two indistinguishable signals. The both problems may be solved by shifting the frequency of one of the laser beam causing the fringe to move at a constant speed in the velocity U direction. Hence, a stationary droplet is present it now produces signal of constant frequency. The directional ambiguity is solved because two droplets of different directions now produce higher and lower frequency. The device used to produce the frequency shift

is called a Bragg cell.

By analysing the electronic signal given out by the photodetector it can be observed that it contains periods of silence where there is not droplet in the measuring volume and randomly interspersed with bursts of signal created by a droplet passing through the measuring volume. Figure 2.12 presents a idealised signal burst.

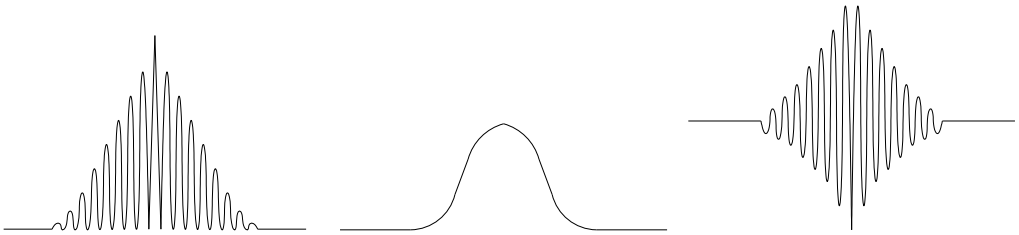

Figure 2.12: *A typical set of LDA signals burst generated when a droplet passes through the measurement volume: (a) Burst; (b) Pedestal; (c) Doppler*

A droplet passing through the edge of the measurement volume where the fringes are weakly illuminated produces also a weak fluctuations signal. It can be noticed that the overall shape of the burst (Figure 2.12 (a)) is a consequence of the fact the laser beams producing the measurement volume are obviously stronger at their centre than at their edges. Whilst a droplet travels throughout the measurement volume centre the signal fluctuations become larger and then get weaker. A frequency signal consequently can be divided into two parts: a low frequency part described as the "pedestal" (Figure 2.12 (b)) and a high frequency part which contains the Doppler signal (Figure 2.12 (c)). Due to the positive light intensity the fluctuations are never centered about zero. In modern setups of LDA there is a special, sophisticated digital processor allowing to analyse burst and extract the frequency and hence velocity at the instant.

Other types of LDA system are also available. Reference beam systems use only a single laser beam to illuminate particles in the flow. For instance, light scattered by the droplets is combined at the photodetector with a second beam that comes directly from the laser source. The resulting heterodyning makes the Doppler frequency measurable. Reference beam systems are less common than dual beam systems since they are more difficult to set up producing noisier signals and suffer from greater errors.

The Phase Doppler anemometry (PDA) was developed and demonstrated by Bachalo and Houser [51] and Durst et al. [127]. It is an extension of the laser Doppler anemometry that usually uses two receiving lenses and photodetectors. To determine the drop size it is necessary to measure the spatial frequency of the interference fringe pattern produced

by the scattered light. Basically, the technique relies on measuring the time delay that occurs when the light scattered by a droplet traversing the intersection of two coherent laser beams arrives at two spatially separated photo detectors, hence it name related to the Doppler effect. This can be achieved by using a second photodetector to collect light simultaneously form a different part of the interference pattern. A Doppler burst signal is produced by each photodetector but with a phase shift between them. Therefore, the signal from the two photodetectors have the same Doppler frequency f and similar amplitude, but are separated by a phase shift ϕ, which is described by the formula:

$$\phi = \frac{t_{shift}}{t_D} \times 360^{\circ} \tag{2.4.2}$$

where:

t_D - is the Doppler period;

t_{shift} - is the period between the zero crossing of the signals between detectors.

The phase shift is directly related to the particle size by a linear calibrations curve for a given optical configuration of the PDA system. The slope of the linear response curve is a function of parameters like the laser wavelength and power, the collection angle, the refractive index of the droplet and the laser beam intersection angle. Through proper set-up of the PDA the method has the potential of collecting accurate data at extremely high data rates with good statistical certainty. However, measurement accuracy is dependent on a number of factors already discussed. One of the fundamental limitation of the PDA systems is the inability to accurately measure non-spherical droplets discussed by Damaschke et al [100] and Kashdan et al. [215]. Presence of non-spherical droplets is a common problem in spray characteristic tests. Such conditions are observed in near-orifice flows. This creates problems for data certainty, since only a fraction of the spray droplet population is spherical. The additional photodetector is used to eliminate sizing errors due to non-spherical particles.

Principles of the PDA system has been described in this section using a one-component dual-beam example, however it can be extended up to three one-component units. Then, two or three velocity components can be measured simultaneously with droplet sizing. It is believed that through good design and proper set-up the Doppler method has the potential to gather accurate data at extremely high data rates with good statistical certainty.

2.4.4 Malvern laser-diffraction

Laser diffraction is probably the most widely used technique for fuel spray analysis equally for diesel and petrol sprays [370; 413]. A classical example of the laser diffraction method is the Malvern instrument, hence the term Malvern is frequently used to refer to the laser diffraction technique. Unlike other optical techniques, laser diffraction does not require single droplets to be measured successively to obtain a size distribution. Instead the interaction between light and the ensemble of all illuminated droplets in analysed. The method is based on inverting measurements of the angular distribution of near forward scattering from a collimated beam [345]. Inversion of the recorded signal is made according to a mathematical algorithm and frequently engaged into a Malvern instrument setup. Basically, the method reports the number of a particle of a given size, since the light energy reported by the detector system is proportional to the volume of the measured droplet. This contrast with counting-based techniques, which records the number of droplets of a given size.

The optical arrangement of a Malvern assembly is shown schematically in Figure 2.13. Droplets are allowed to move across a parallel laser beam. The scattered is focused by a Fourier transform lens onto 30 semicircular photosensitive, concentric, annular rings (in employed experimental setup) placed at predetermined radii in the detector plane. The annular rings are approximately log spaced, and their distribution on the detector are fixed by the manufacturer. The size classes used in the laser diffraction instrument are defined by the detector dimensions and focal length through the relation [237]. Each detector ring effectively measures the energy of the scattered light in the forward direction at a particular angle to the incident beam.

$$x(i) = \frac{\lambda}{\pi \cdot sin\left[arctan\left[r(i)/FL\right]\right]} \cdot K \tag{2.4.3}$$

where:

r(i) is the distance of the detector element *i* from the centre of the detector;

λ is the wavelength of laser light;

x(i) is the particle size representing the i^{th} size class;

FL is the focal length of the Fourier-transform lens;

K is the constant.

The particular benefits of laser diffraction are: range of applicability; dynamic range of

sized spray i.e. measurements can be made across a range from 0.02 μm to a few millimetres; speed of measurement - single measurements can be made in 400 μs; measurement repeatability. The method delivers excellent repeatability due to the ability to acquire data rapidly and ease of verification as laser diffraction generally requires no calibration.

However, spray investigation using Malvern are frequently subjected to errors in size measurements arising from poor sampling and spray dispersion. Sampling and dispersion are often overlooked when assessing the potential of different spray diagnostic techniques. The assumption of sphericity, upon which laser diffraction droplet size is based frequently can lead to experimental errors. Therefore, alternative techniques being reported [54; 106; 220; 345] as providing a better assessment of the droplet size of non-spherical particles. Droplets are three-dimensional objects and, therefore, cannot be described by a single number that equates to the "particle size". For this reason, all techniques measure some property of a particle and provide the diameter of the equivalent sphere as the droplet size.

Since the particle distribution is inferred through a mathematical procedure that attempts to match the measured and calculated energy distribution over the detector rings and the fitting procedure in a model-dependent iterative technique, the procedures are subjected to the fitting error. Basically, the values of the parameters describing the size distribution are adjusted until the best fit between measured and calculated energy is archived. It is clear that if a wrong model is applied the magnitude of the error can be significant.

One of the main drawback of the Malvern technique is a need to use a procedure (deconvolution) by which measured line-of-sight averages can be converted into the actual radial variation of number density and droplet-size distribution. The procedure can be extremely sensitive to inconsistence in the line-of-sight averages. Perturbations of 2.5% points in extinction or 20% in droplet-size distribution can be produced in the de-convoluted droplet number density and size distribution especially near the centre of the spray [175]. The deconvolution procedure is often subjected to the unique preferences of a measurement and therefore to the certain level of inconsistency throughout various measurements performed by different investigators.

A brief review of the literature provide some examples of the laser diffraction technique to investigate diesel sprays. The technique has also been applied to study dense spray and measurements have been compared with other techniques. Kihm at al. [220] investigated droplet-size characteristics near the spray tip of intermittent sprays of diesel fuel from an

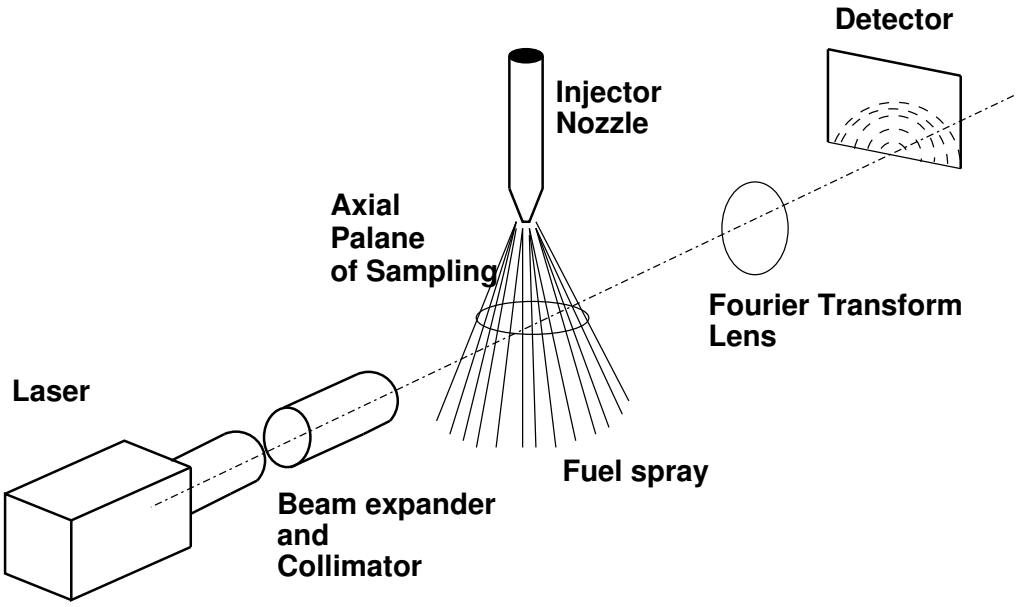

Figure 2.13: *Sketched presentation of the Malvern instrument setup.*

electronically controlled accumulator injection system using a modified laser-diffraction particle-analysing technique. The Sauter Mean Diameter was measured at low obscurations without multi-scattering bias. Measurements were made at various axial locations at different injection pressures upto 83 MPa in pressurised and depressurised chamber conditions.

De Risi and co-workers [106] looked closely at the spray produced by a CR single-hole injector under different conditions of pressure and temperature of the injection chamber environment. Back-lighting technique together with the diffraction method (Malvern Spraytec) were employed to study spray development for two different values of the injection pressure and injected quantity. Droplet size data obtained at high temperature and pressure were compared to those acquired at ambient conditions.

A complex measurement of drop size in dense diesel spray was performed by Baisot and Yon [54]. One of the employed methods was a diffraction-based granulometer. Authors concluded on the atomisation process and the shaped of the drops at 30 mm downstream from the nozzle outlet. It has been stated that the the atomisation process is not totally established at this position in opposition to what can be deduced from the drop size distribution alone.

Lee et al. [249] described the spray characteristics of a low-pressure CR injector using optical diagnostics including laser diffraction and phase Doppler, and high-speed camera photography methods. The effect of fuel properties on the spray characteristics was investigated using n-heptane, Stoddard solvent (gasoline surrogate), and diesel fuel. Malvern results provided quantitatively similar trends as PDA.

Cossali and Hardalupas [95], using the laser diffraction and the phase Doppler techniques, investigated a small diameter dense sprays, such as those produced by diesel and petrol injectors. They reported significant differences between the laser diffraction technique and the PDA. It has been stated that the differences were due to the lack of spatial resolution of the laser diffraction technique, the influence of beam attenuation, and non-spherical droplets in both instruments. Also, problems and sources of sizing errors in the application of both instruments were discussed.

Allen et al. [30] used the the laser diffraction to study bio-fuels atomisation as potential sources of varying results of engine tests. The Malvern technique had been also used to investigate atomisation difference of fifteen bio-diesel fuel types and results were related to their viscosity and surface tension. Atomisation studies revealed that except for coconut and rapeseed bio-diesel fuels, the rest of the bio-diesel fuels had similar atomisation characteristics.

2.5 Acoustic Emission technique

The background knowledge of spray characterisation methods presented in this thesis so far were focusing on the investigation of fuel sprays from the moment the fuel enters the high pressure chamber. But, there is also a need to provide a method to study quantitatively the effect of a different fuel and its properties on injection development inside the CR injector. Also, it is required that this tool would be suitable to investigate such effect in bench tests and during engine runs. An additional necessity for the method that is should have a non-intrusive feature particularly if the whole injection process needs to be studied. The method should also provide a way to study the effect of performed modification on the CDI system.

There is not a universal single method providing sufficient information of the performance of a diesel injection system and the engine altogether. Normally, couple of techniques are

combined like emission tests, investigation of the specific fuel consumption, the power output, engine oil analysis etc. However, in this work there was a need to concentrate more on the injection process and the influence of a different fuel since the importance of the injection was recognised as crucial for the performance of the CDI engine. It was thus accepted that the successful modification of the injection system would be the key for correct and efficient engine performance.

Most of the continuous condition diesel engines monitoring techniques are intrusive thus non-specific (e.g. a temperature change at a probe location could be associated with different sources). There is a group of the non-intrusive methods namely vibration analysis or airborne sound radiation. These are used to diagnose rotary machinery including diesel engines [55; 170; 171; 254] featuring of simple hardware and instalation. However, both methods are sensitive to low frequency environmental noise originates resonance or the noise of ancillary equipment.

This section relates to monitoring the condition of CDI injection with diesel and RSO by using a method known as Acoustic Emission (AE). The AE method is based on recording waves attenuating as they propagate through structures and determining the relationship between attenuation of AE wave energy and its propagation path. In this thesis the AE technique was applied to study diesel injection to develop a generic empirical approach to AE wave propagation which can then be used to determine AE events in a CDI injector and reconstitute their timing and amplitude.

2.5.1 Background

This subsection covers very general description of the AE technique as well as present only some examples of its application mainly in engine diagnosing. It has to be highlighted that the AE is relatively new technique and it has been steadily developed since its first implementation.

The AE technique is based on a high frequency stress wave that propagates in materials and therefore can be detected directly by using external sensors mounted on a surface of an engine, an injector, a fuel pump etc. The method is non-intrusive and features high

sensitivity and hence acquired signals require very careful post processing, frequently involving filtering and appropriate normalising. As far as application of the AE is concerned, it is often coupled with crankshaft position and thus the well defined time domain can be established.

The detected AE signal is normally filtered with a preamplifier within a frequency band of 0.1 to 1.0 MHz and thus is free of airborne noise and a whole body vibration. The frequency band is also defined by the frequency bandwidth of the sensor and its sensitivity. The AE carrier frequency offers very high temporal resolution (often between 2 and 5 MHz), which can be utilised to locate the source of even the shortest mechanical events if a sensor is placed close to the source. Determination of the diagnosed events is normally performed in combination of signal analysis and pattern recognition algorithms. However, the acquired AE signal is very complex, particularly if representing such complex systems as a diesel engine. One would say that AE measurements are simple and robust but the later signal processing is difficult and require appropriate knowledge of signal processing.

A vast majority of AE application has concentrated on diagnosing faults and malfunctions in reciprocating and rotating machinery but also on successful monitoring a number of diesel engine conditions, for example combustion [155; 156], head gasket leakage [135; 136], exhaust valve leakage [145; 146], injector faults [156] and liner scuffing [369]. Some detailed examples of these are covered in this section. Application of sophisticated signal analysis methods allows to develop a generic empirical methodology to correlate AE wave propagation with engine events and reconstitute their timing and amplitude.

AE wave propagation in a complex structure like a diesel engine is affected by various occurrences similar to these characteristic for an acoustic wave e.g. attenuation, reflection, refraction and mode conversion [329] because of multiple signals of bearings, exhaust valves, combustion etc. and its quality depends on a location of the sensor (as close as possible to the source). Interaction of signal and the sensor itself should also be considered. Resonance frequency, i.e. sensor characteristics, has to be known to avoid undesired signals being analysed. Especially, deconvolution method could be applied to obtain a real signal. The interference can distort the AE signal or make it particularly difficult to recognise if signal overlapping takes place. Nevertheless a signal amplitude processed with time windowing and pattern recognition has been reported to be an efficient method in diesel engines [145; 155; 366].

The AE methods allow recognition and recording of unbalanced inertia and pressure forces associated with faults in a system. An example of such application is the work of Schultheis et al. [362] where a leaking valve was diagnosed with respect to the piston position. The valve leak was determined by the amplitude of the vibration and by the proportion of the stroke occupied by leakage signal. The author also applied AE to investigate bearing faults and wear in reciprocating compressors by analysing the crankshaft displacement relative to the main bearing and also by measuring bearing temperature. A fault can be recognised by comparing vibration displacement amplitude produced by a bearing clearance of a working bearing with a signal of existing vibration. AE method is frequently applied to diesel engines operating on slow speed and featuring in conventional (mechanically governed) fuel delivery system. Therefore studies of marine engines and big diesel generators becomes naturally in favour. Lately Douglas et al. [119] investigated piston ring/cylinder liner interaction of a large two-stroke, marine diesel engine under normal operation using AE. Raw AE signals acquired at a sampling frequency of 2.5 MHz from two AE sensor located on the exposed area of the upper and lower part of the cylinder liner were used to detect sliding contact between the piston rings and the cylinder liner and related blow-by or exhaust valve leakage during the compression and expansion strokes. Additionally, event associated with fuel injection start and end with mechanical impacts during the injection period, attributed to the piston ring/cylinder liner contact were observed. The authors found the AE signal increased accordingly during the compression and expansion strokes. It was observed due to increasing the in-cylinder pressure and the sealing forces exerted on the piston rings during the compression the combustion respectively. Separate AE signal peaks were also detected due to oil flow through the oil groove located on the inner surface of the cylinder where the circumferential spread of injected lubricating oil was taking place. The event was seen at both sensor positions. Douglas et al. [119] showed that the AE method could be successfully applied to detect and study the combustion process. Thus it has been proven that the AE is a valuable method for monitoring the performance of diesel engines. The most valuable observation is the presence of AE signals associated with fluid flow. This fact indicate that the AE technique can be used to detect and monitor not only lubricant oil flows but also fuel movement.

In a work enclosing the investigation of two large, low-speed, two-stroke, marine diesel engines of a similar design, Douglas et al. [120] studied the power output and correlated it

between AE energy and the variation of the Instantaneous Crankshaft Angular Velocity (ICAV) waveform. AE signals (RMS) were acquired simultaneously with a sampling frequency of 20 kHz over a range of engine operating conditions. An AE sensor was placed on the cylinder cover, at a position close to the injectors, the exhaust valve housing and the combustion chamber. Additionally, a position in relation to a top dead centre (TDC) was references using a shaft encoder. It was found that the ICAV waveform exhibited cyclic variation about the mean engine speed and the ICAV decrease indicated the compression stroke of each cylinder whereas an increase in angular velocity indicated the expansion stroke (combustion). A series of peaks in the frequency spectra of the ICAV waveform were determined and associated with different events and a number of peaks was related to the number of cylinders in the engines. RMS signals in the time domain were mapped onto the crank angle domain so that the AE events associated with the entire engine process could be identified. The work showed that the standard deviation calculated from the ICAV waveform of each cycle for both engines increased with load.
Gill et al. [155] have investigated the fuel delivery process in a four-stroke, high speed direct injection (HSDI) diesel engine with two induced fault conditions. The engine was exposed to fuel starvation in one cylinder and reduced injector discharge pressure and resulted directly in changes of the power output of the engine. AE data was acquired from AE sensors placed at various positions with a sampling frequency of 50 kHz along with an engine timing signal. It was found that a sensor positioned on the camshaft side of the engine, as close to the point of combustion as possible, could be used to examine the valve mechanism movement and fuel combustion characteristics. Authors suggested splitting the entire AE signal into four time bands relating to the combustion events, then calculating the energy content of each band and averaging over ten cycles, which results provided remarkably consistent energy signal between cycles.

Various types of AE signals associated with the fuel injection/combustion event; diesel fuel pressure build up prior to injection, the opening/closing impacts associated with the injector spindles, high-pressure discharge of fuel into the chamber, and fuel ignition and combustion were analysed by Douglas et al. [120]. It was found that that timing of the beginning and end of the injection event changed with load and that AE energy in the injection event could be used as an indication of power output. The RMS AE energy of the injection/combustion event was calculated over a crank angle window of 40 degrees relative to TDC of each cylinder and the energy increased with power output. The study

concluded that both the RMS AE energy and standard deviation of the ICAV waveform could be used as power output indicators.

The injection and the combustion process were examined by Gill et al. [156] who studied mechanical and fluid flow phenomena occurring during these two events. Studies were performed using a small HSDI (a 76 kW, four-cylinder, Perkins T1004-4 HSDI with the Bosch KD fuel injectors operated by a Bosch EPVE rotary fuel pump) diesel engine and involved AE examination of the fuel injection equipment faults together with data acquisition from a needle lift sensor, an in-cylinder pressure sensor and a shaft encoder. The engine speed was varied from 1000-2500 RPM. Two different fault conditions were examined: reduction of the injector discharge pressure from 258 bar to 165 bar and the injector discharge pressure reduction to 100 bar in cylinder 4. The comparison of the mean and standard deviation of the RMS energy of all tests revealed that the timing of the increase of fuel line pressure and the time at which the injector needle became fully open could be detected using AE and these times advanced while injector discharge pressure reduced.

In all of the above mentioned work, it has been noted that attenuation of some events can be seen relative to others in the AE signals and that higher signal amplitudes are obtained from a sensor placed closer to the source and this offers the possibility of source location.

2.6 Spray simulation

Spray dynamics and the interaction between fuel and gas phase are crucial in the DI diesel engine design and modelling. Currently, the combined experimental-computational approach represents a relatively cost effective way of investigating the diesel systems. This allows researcher quickly and in a cheap way evaluate the spray characterisation and feed data into a preliminary design stage. Optical techniques provide the necessary insight into spray as well as data for the validation of computational models. Numerical simulations can give detailed information on spray and guidelines to measurements and therefore to reduce the number of experimental test cases. Spray modelling is therefore essential and a critical part of the fuel spray studies, especially when dealing with high-pressure and dense sprays like those produced by a CR system [69; 391]. Although, the existing numerical implementation of spray models can replace experiments to certain extent, simulations still

has to be validated against experimental data.

It appears that petrol simulations have been explored more extensively. Some of the simulations are based on analytical solutions employing a set of equations while others on a typical Eulerian/Lagrangian calculations involving thousand lines of programming codes. However, one of the most common way of numerical simulation of fuel spray has its origin in the KIVA code. This section presents basic information about spray development and some selected examples of KIVA simulations mainly at higher injection pressures and for real geometries.

2.6.1 Breakup process of fuel jets

Spray atomisation is a complicated physical phenomenon, which is critical in diesel engine combustion, as well as it can be expected for a fuel like RSO. The main occurrence that takes place in the diesel spray is the breakup of the droplets. Other phenomena, such as collisions or coalescence also influence the final atomisation. The spray characteristics depend on fluid properties, ambient conditions, the fuel-injector design and operating conditions. Therefore, the RSO atomisation is expected to be different from diesel and a different group of parameters may play the major role in the atomisation.
The breakup of the injected fuel is caused by the aerodynamic liquid-gas interactions and the nozzle flow effects. The atomisation process of liquid jets and sheets can be usually divided into two consecutive stages: the primary and the secondary breakup. During primary breakup, the liquid jet or sheet exhibits large scale coherent structures, frequently described as “ligands”, that interact with the gas phase and break up into drops of various sizes. During secondary breakup, these drops break up again into smaller drops (droplets) that finally form the drop size spectrum or may evaporate.

Fuel jet primary breakup is the physical process leading to the detachments of drops and ligaments from the liquid jet surface. There have been a numerous theories explaining the diesel fuel core atomisation [45; 340; 349; 353], but unfortunately none of them fully explain the breakup phenomenon for a wide range of fluids, injection and ambient conditions. Basically, the primary breakup can be divided into different regimes as a function of the jet velocity. Figure 2.14 represents schematically the breaking up process of a hypothetical spray. The first stage, described as a dripping, relates to the low jet velocity, at which a separate drops can be formed at the end of the nozzle. The second stage is referred

to as the Rayleigh regime in which the breakup is caused by the instabilities. Fuel property like surface tension contribute in amplifying the forces of the jet instabilities. At this stage, the effect of aerodynamic sources become more apparent. In case of RSO atomisation, the Rayleigh regime should be mainly governed by the higher surface tension of the oil and its viscosity. The Rayleigh regime is followed by the transition stage where the spray breakup is practically only function of surface tension. The next stage is described as the turbulent regime and is associated with a typical low-pressure injection diesel systems. The fuel particles gain a radial component of velocity, which assist them to overcome the surface tension forces and break away from the main fuel jets. The source of the radial component is the turbulent flow in the injector holes. In this regime, the surface perturbation are described by the characteristic length scale, which is proportional to the integral length scale of turbulence. The ambient conditions become a significant factor promoting the growth of the surface perturbations. The instabilities, commonly referred to as Kelvin-Helmholtz instabilities, simply can be described as kind of "waves" created on a jet surface parallel to the fluid motion and caused by the shear forces.

The last recognised stage of the spray breakup is the atomisation regime, which consequently features sprays of high-pressure. It can be described by a situation when a high speed fuel jet emerges from the nozzle hole in a compact continuous form and disintegrates closely to the nozzle tip. This can be visualised as the fuel jet surrounded by varying size drops. The actual breaking up mechanism is caused by the internal stress. Turbulence and cavitation are the most relevant factors contributing to the stress. In fact, the description of the mechanism is quite complicated but here can be summarised in the way of three main components: the aerodynamic-induced, the jet turbulence-induced and the cavitation-induced atomisation. These three components are included in different atomisation models, however, the cavitation-induced part has not been yet fully implemented.

The primary breakup occurs at the end of a injected liquid core and results in a atomised drop population that the droplets may undergo the secondary breakup. Secondary breakup is due to the interactions between the surrounding gas and the droplets. The interactions lead to droplets deformation and finally to secondary breakup. Fuel properties such as surface tension, viscosity and those of the ambient gas are responsible for droplets deformation. The deformations are commonly described as waves and are Rayleigh-Taylor instabilities. Similarly like in a case of the transition regime of the primary

breakup, the shear forces acting on droplets create a second type of instabilities named the Kelvin-Helmholtz ones. In practice, the "quality" and direction of droplets deformation is described by Weber and the Ohnesorge numbers defined by Equations (2.6.1) and (2.6.2), respectively:

$$We_f = \frac{\rho \nu_{rel}^2 d}{\sigma} \tag{2.6.1}$$

ρ - density of gas phase [kg/m^3];
ν - relative velocity of the liquid phase [m/s];
d - droplet diameter,[m] ;
σ - liquid surface tension [N/m].

$$On_f = \frac{\mu}{\sqrt{\rho d \sigma}} \tag{2.6.2}$$

μ - viscosity of liquid phase [kg/ms].
The Weber number refers to the strength of aerodynamic forces relative to surface tension forces, whereas the Ohnesorge number measures the damping effect of viscous friction in the drops against surface tension. The Weber number is commonly used to distinguish amongst different stages of drops deformation. Detailed description of the different deformation stages as a function of Weber number can be found in literature [349]. Table 2.13 presents a summary of each region in the relation to Weber number.

Table 2.13: *Classification of breakup mechanism [349; 360].*

Weber value	**Regime description**
We$\leq$12	Vibrational-deformation amplified by vibrational resonance of liquid surface
12<We<45	"Bag" regime-deformation is like a bag structure
45<We<100	Chaotic-transitional stage where breaking of filaments occurs
100<We<350	Stripping-the K-H instabilities causing droplet disintegration (stripping)
We>350	Catastrophic region of spontaneous droplet breakup

In a high pressure injection system such as CDI, the injection velocities are very high. The droplet evaluation can, therefore, go through various stages related to higher Weber

numbers. This is expected to be govern by the K-H instabilities as well as a presence of the deformations described by the Rayleigh-Taylor instabilities. The mathematical description of such complex phenomenon is complicated. The description of high-pressure spray may, thus, require a revision of the breakup mechanism particularly of the primary breakup. Additionally, if a high viscosity fuel like RSO is atomised, effect on instabilities can be difficult to evaluate. The next section presents some of the formulation of breakup models which can be applied to simulate high-pressure sprays.

2.6.2 Breakup phenomena for high-pressure droplet atomisation

One of the main problems to simulate spray evolution is a choice of a breakup model. Therefore it is essential to understand the breakup phenomena and select a right model according to fuel properties and ambient conditions. Usually, the atomisation process takes place in turbulent conditions and mathematically is described using time and length scales. Primary droplet breakup is a process of spray disintegration due to hydrodynamic forces and properties of the spray jet. This stage of droplet formation is well described mathematically, whereas the secondary breakup is more complex and difficult to be described.

The time and length scales were used to develop various models to describe the secondary breakup process. It was observed that the droplet deformation response depends not only on the relative intensity of the aerodynamic forces, but also how they are applied to the droplet. The effect of different deformation scenarios is reflected in the value of the critical Weber number, We_c, widely used to describe breakup process as presented in the Table 2.13. The number We_c=20 characterises gradual load and We_c=13 features sudden loading and negligible viscosity effects [199; 359].

"Visualisation" of the breakup process can be performed using a computational volume frequently described by the characteristic length scale l (Herrmann [188]) shown schematically shown in Figure 2.14. Characteristic length is the length of a spray jet just before atomisation. Such representation is frequently applied in different computational models of spray breakup. It can be assumed that the characteristic length scale of the drops, l, is much smaller than the available spatial grid resolution Δx used in calculations. There,it can be assumed that the characteristic length scale of the drops is much smaller than the available grid resolution and that the liquid volume fraction in each grid cell l is small. Therefore, the liquid volume fraction in each grid cell Θ_l is small. Furthermore, assuming

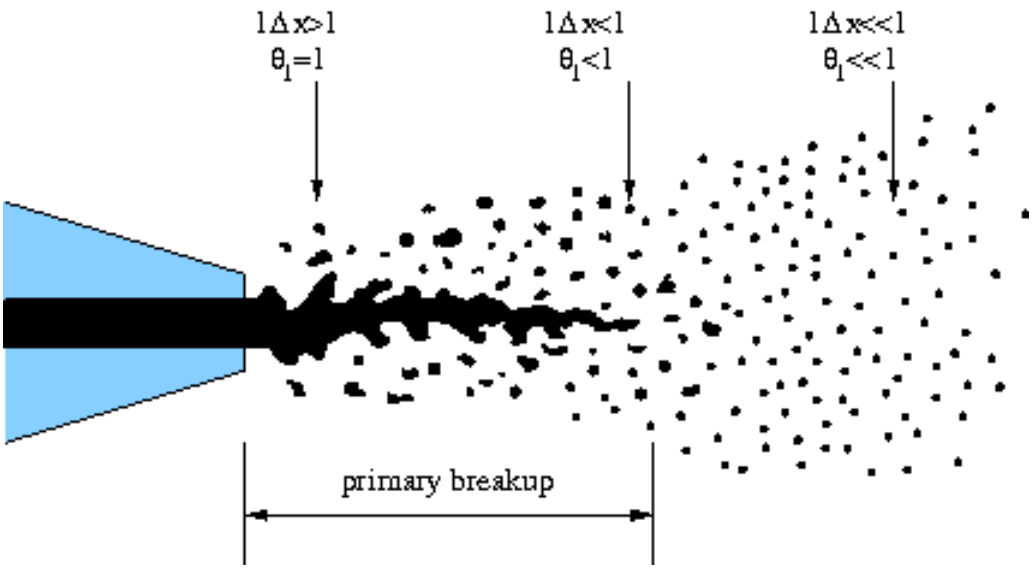

Figure 2.14: *Diagrammatic presentation of breakup of a liquid jet [188]. l-the characteristic length scale (as explained in the text), Δx-the available grid resolution,Θl-the liquid volume fraction in each grid cell.*

simple geometrical shapes of the individual drops, like spheres or ellipsoids, the interaction between these drops and the surrounding uid can be taken into account. The breakup process shown in Figure 2.14 includes the definitions of lengths. Moreover, assuming simple geometrical drops shapes, the interaction between drops and the surrounding fluid can be mathematically described. Using a simple description of the breakup, as presented in Figure 2.14 some statistical models describing the secondary breakup were derived ([340; 390; 392; 433]). It needs to be highlighted that this simple description of the breakup is not true for the primary breakup, where the turbulent liquid flow interacts with the surrounding turbulent gas phase on scale larger than Δx. This results in highly complex interface dynamics and individual grid cells that can be fully immersed in the liquid phase. In most practical models, the loading scenario is mathematically described using the the spatial variables of the drop and its physical properties. It has to be noticed that the existing models are complex as they include the flow field inhomogeneity and transient character. Furthermore, the flow conditions continuously change depending on the time and length scales involved. Nevertheless, the existing models are efficient and robust and have been used to describe the breakup process in the fuel injection simulations.

With respect to droplet breakup, several modelling approaches were proposed for the use in spray simulations and were based on the concept described above. These models take into account the flow configuration, a variety of operating parameters such as fuel and

ambient gas flow rates, pressure of temperatures and droplet size and velocity. Models assumes that the breakup process is subdivided into two stages: initial droplet deformation and further deformation followed by disintegration. Regarding the mathematical description of the breakup processes in *Section 2.6.1*, different approaches have been used in literature. Some do not distinguish between primary and secondary breakup assuming that the atomisation of injected liquid and the subsequent breakup of drops are indistinguishable phenomena (TAB, DDB, WAVE). Others distinguish between the two processes using various approaches (WAVE+TAB). The next subsection presents some of them available in KIVA. These were successfully applied in simulations of high-pressure diesel sprays and are expected to be in use (to certain extend) for RSO.

2.6.3 Review of the studies employed KIVA simulation code

The spray model in KIVA has been based on the discrete droplet model of Dukowicz [122] implemented in KIVA. The model utilising the Eulerian/Lagrangian approach employs computational particles that represent parcels of spray droplets with uniform properties. Since the scale of a typical grid cell is much larger than an average droplet, each particle is assumed to occupy a single point in space, neglecting the volume occupied by the droplets and simplifying calculations. Levý et al. [251] applied KIVA-II code, which proposed and applied the model of the Assumption of a Fully Atomised Jet (AFAJ) to avoid the break-up description and based that model on a jet fully atomised when leaving the nozzle. The computational results of such primitive approach were successfully compared with some of the PDA results. Authors did not provide the details of the injection pressure and hence it can be concluded that they investigated medium and high-pressure diesel sprays. The model utilised a simple approach of "boosted" droplet velocity at the nozzle exit. This allowed small droplets to penetrate into the gas like a liquid core. A good agreement has been shown with the PDA experiments. Although, its application is limited to cases where significant information about the droplet distribution is known. Furthermore, the model has not been validated for high pressure ambient conditions.

High pressure diesel sprays produced in a CDI system have been investigated by Bianchi et al. [71]. The authors implemented the KIVA-3 code to investigate the effect of diesel split injection as well as the shape of the combustion chamber on reduction of NO_x and soot emission. A customised version of KIVA implemented the submodes of the hybrid

breakup approach for the primary breakup and the Taylor Analogy Breakup (TAB) [4] model for the secondary breakup. Also, the RNG k-ε model (Renormalisation Group k-ε model) [393] was applied to describe the turbulence. The research showed a relatively good agreement with the experimental results and proved a capability of the KIVA code to optimise and simulate a CDI injection and combustion. Some suggestions on emission reduction and performance were presented based on numerical simulations. The study also presented a new combustion chamber for improving the mixing and hence emissions.

In a further numerical work Bianchi et al. [69] concentrated on the extended modelling of the high-pressure diesel sprays injected by a CDI system. The simulations reproduced the real cylinder density of a DI diesel engine at injection time. A non-evaporating spray was investigated using three different spray models - the TAB, the hybrid and the modified hybrid model. The modified model included the cavitation-induced sub-model and imposed that in a very early period of the injection. The fuel "blobs" were not treated using the TAB model but by Kelvin-Helmholtz (KH) instabilities. The numerical calculations were carried out for different injection and ambient conditions. The results provided good agreement of the hybrid model with experiments.

Improved KIVA code was also applied by Rotondi and co-workers [349] to simulate low- and high-injection pressure diesel sprays. As already presented above, the hybrid model for the atomisation was employed. The simulations successfully distinguished between jet primary breakup and droplet secondary breakup. For the high pressure spray, the effects of jet turbulence and cavitation on liquid core and the primary breakup has been considered. Presented results included the tests for high injection pressures in a vessel and various ambient conditions. The results were also compared with the experimental data. The hybrid model provided impressive agreement with the experiments, however, it implemented some parameters evaluated from the experiments for the model tuning.

Interesting numerical studies on fuel atomisation characteristics on high-pressure CDI sprays were carried out by Lee and Park [245]. The authors followed already implemented approach of Rotondi et al. [349] considering a difference between primary and secondary breakup using the Kelvin-Helmholt - Rayleigh-Taylor (KH-RT) hybrid model. The hybrid model was constructed and implemented in a similar manner as it had been developed previously by Bianchini et al. [69]. The numerical results were compared with the experimental data of PDA measurements. The numerical results showed fairly good agreement with the experiments, with a tendency to overestimate the spray penetration and underestimate the

Sauter mean diameter. It was confirmed that the hybrid model required determination of breakup parameters and its quality highly governed the accuracy of the final results. Also, the model did not show the potential to generate acceptable mean diameters in the region of less than 40 mm from the injector tip.

Some selected experimental results were compared with numerical simulations utilising a modified KIVA-II code by Yeom and Fujimoto [426]. The effect of change in the injection pressure on the spray structure in high temperature and pressure conditions was investigated. In a contrast to the previous studies this work examined the evaporating spray structure in a constant volume vessel. The original TAB breakup model was modified and its results compared with the experimental data. The preliminary parameters tuning was required to obtain satisfactory numerical results. It is assumed that the authors modified the model specifically to fit into the experimental data, because normally such good agreement can not be received using the TAB model without distinguishing between the breakup regions. The penetration results were more accurate for the initial spray development but over-predicted the penetration as the spray further propagated. It can be concluded that the TAB model its not sufficient for the prediction of the vapour phase penetration.

Equally to the interest of spray penetration, numerical research has also focused on spray atomisation with a special attention paid to droplet formation. De Risi et al. [102] investigated variable density diesel sprays and analysed fuel compressibility on the spray produced by high-pressure injection system of CDI. The authors introduced a new set of equations to the KIVA code to calculate liquid density as well as modified the existing Kelvin-Helmholtz and Rayleigh-Taylor breakup model. A comparison between experimental and numerical data obtained in a constant-volume vessel at ambient pressure and temperature revealed good agreement. Calculated drop size distribution proved successful modification of the breakup model however the results were shown only for a single injection pressure.

Further breakup model development has been performed by Park and Lee [308] to simulate the high-pressure spray issued from the CDI system. The TAB model was replaced by the KH-DDB competition model, which assumed the competition between the wave instability and droplet deformation causes the droplet breakup above the breakup length. The KH-DDB model provided good agreement for both: the spray penetration and the overall Sauter mean diameter. However, the effect of the axial distance from the nozzle

tip on the Sauter mean diameter revealed a significant differences between the experiment and the simulation. It can be concluded that simulation of droplet distribution close to the nozzle tip is highly difficult. The same conclusion were found in the previous work of Lee and Park [245]. Also, it is expected that the KH-DDB model would require appropriate parameters which can be derived from the experiment prior to simulation, and this has not been indicated in the paper. Nevertheless, the proposed KH-DDB model could be successfully applied for future simulation of high-pressure sprays.

Despite a wide literature review done on various fuel spray simulation, only a few of available sources present results of a non-hydrocarbon based fuel and mainly relate to the use of dimethyl ether and bio-diesel. The author is aware of some separate attempts to simulate plant oil sprays, however only one trace of these works has been documented. Griend et al. [166] investigated numerically alternative fuels in a direct injection diesel engine using KIVA code. A simple unmodified TAB breakup model was applied. Details of combustion kinetics for RSO were not given nor the injection conditions. The spray characteristic has not been carefully investigated. Moreover, the capability of the existing breakup models has not been checked for plant oils. Therefore it is considered that simulation of RSO sprays is particularly challenging and novel in the field of spray simulation.

It was also recognised that spray development simulation at engine conditions would provide a chance to find the conditions at which the combustion of RSO would be the most feasible. Thus, the simulations should be done including the effect of cylinder temperature and as well as fuel injection pressure and fuel temperature. The statement can be directly connected to findings presented in *Subsection 2.1.2.3* (influence of fuel temperature and in-cylinder pressure) and of work of Raubold [336]. The aspects of engine simulations are covered later on in this section.

2.6.4 Background of KIVA package

The original KIVA code was released in 1985 [3; 39; 40] by the Los Alamos and was replaced by the improved KIVA-II version in 1989 [3; 38]. These earlier versions worked well to calculate in cylinder flows and a variety of open combustion systems, but were quite inefficient when applied to complex geometries that included such features like long transfer ports or diesel pre-chambers. KIVA-3 [252] brought out a significant improvement

by the use of a block-structured mesh that entirely eliminated the need to create regions of unused cells. When KIVA-3 was developed, the immediate applications was to Internal Combustion (IC) engines with port in the cylinder walls. The KIVA-3 code version became popular with the availability of increased computing power on high-end platforms.

The next version of the KIVA code, named KIVA-3V, was introduced and included a significant increment in capability through the additions of the effective model for intake and exhaust valves as well some other improvements [35]. KIVA-3V retained the distinct three-part structure of KIVA-3, in which the grid generator and graphics are separated from the main simulation. The KIVA-3V code included both a pre-processor (*k3prep*), which has been expanded to support the generation of grids with valves, and a post-processor (*k3post*).

The latest version of KIVA (KIVA-3V2) code was introduced in May of 1999 [36]. A number of corrections for improving accuracy had been implemented. One of them allowed to correct the 2-D planar option to make it properly independent of the third dimension. Additionally, extensions to the particle-based liquid wall film model make the model somewhat more complete. In response to research in fuel injected diesel engines, a split-injection option had been also added.

2.6.4.1 Fuel spray breakup in KIVA

Prior to description of the available breakup models it is essential to understand how the breakup process is governed by KIVA. The fuel spray procedure of KIVA includes multi-hole nozzle capability with continuous or pulsed hollow or solid cone sprays. Pulsed sprays may be described by different velocity profiles (defined by the PULSE variable) within either a fixed particle radius or a distribution of radii.
The number of computational particles injected per second or the total number of computational particles to be injected is set up by the variable TNPARC. KIVA automatically calculates the mass per computational particle to ensure that the correct total mass or mass flow rate is injected. This is independent from a choice of TNPARC, which is managed solely by computer time and storage constraints. Computational particles are injected with speed described by the variable VELINJ and with either a distribution of particle radii or particles of a fixed radius. If a breakup model is used a spectrum of sizes is created according to the mechanism specific for each breakup model and described in the next

subsections. A new radius of the product drops (a child droplet) is then chosen randomly for a χ-square distribution with Sauter mean radius according to the formula:

$$f(r) = \frac{1}{\bar{r}} e^{-r/\bar{r}} \tag{2.6.3}$$

Where:

r - is the drop radius (calculated from a model);

$\bar{r}$ - the number averaged drop radius of a certain distribution.

Each of the breakup models consists of a specific equation describing a radius of a product drop, which then is used in calculating a χ-square distribution. To conserve mass, the number of drops associated with the computational particle is adjusted. It is important to understand that KIVA breakup is governed by a probability function, which operates on a droplet population rather than on a single evolving droplet.

2.6.4.2 The TAB model

The Taylor Analogy Breakup (TAB) [4] model is a classic method for calculating droplet breakup, which has been applicable to many (but still limited) diesel sprays at various conditions and injection pressures. The TAB model has been the first and is the most primitive breakup description implemented in KIVA and the most widely applied. The droplets are represented by the computational parcels with de-formable surfaces. The droplet deformation or shape is affected by external aerodynamic forces as well as surface tension and viscous forces of the liquid. The TAB model is based upon Taylor's analogy [394] between an oscillating and distorting droplet and a spring mass system. The spring represents a fuel ligament and its evolution is similar to the interactions inside a spring wire. The drop deformation in terms of the radial cross-section change, x, is described by the forced, damped harmonic oscillator:

$$m\frac{d^2x}{dt^2} + b\frac{dx}{dt} + cx = F \tag{2.6.4}$$

Where:

m,b,c - factors;

t - time, [s];

x - cross section, [m];

F - force, [N].

Droplet distortion is a non-dimensional parameter. The forcing term, F, arises from the aerodynamic drag and the restoring force, cx, is given by the surface tension. $b\ dx/dt$, called the damping term, is analogous to liquid viscosity. Equations (2.6.5),(2.6.6),(2.6.7), given below, present analogy between the appropriate forces included in the equation describing oscillation and the breakup description. Drop breakup occurs when $x>a/2$, where a is the drop radius, which corresponds to $We>We_{crit}=6$. The product drop size is determined by an energy consideration which equates the surface, oscillation and radial kinetic energies of the parent and product drops. Thus, in this model, the droplet is idealised as a dynamic spring mass system described in terms of a single deformation coordinate. Modelling implementations employ the resulting TAB model equation set, which governs the oscillating and distorting droplet.

$$\frac{F}{m} = C_F \frac{\rho u^2}{\rho_l r} \tag{2.6.5}$$

$$\frac{k}{m} = C_k \frac{\sigma}{\rho_l r^3} \tag{2.6.6}$$

$$\frac{d}{m} = C_d \frac{\mu_l}{\rho_l r^2} \tag{2.6.7}$$

Where:

C_F, C_k, C_d are dimensionless constants

ρ, ρ_l are the gas and liquid densities

σ is the surface tension

μ_l is the liquid viscosity

$u$is the relative velocity between the gas and droplet r is the droplet radius

x is the displacement of the equator of the droplet from its equilibrium position.

Equations (2.6.5), (2.6.6) and (2.6.7), which represent the amounts of deformations due to the gas aerodynamic force, the surface tension, and the liquid viscosity, are solved analytically in the frame of Lagrangian droplet tracking schemes to determine the droplet oscillation and distortion at any given time. As it can be recognised the system has the analytical solution assuming constant coefficients. Hence, when the droplet oscillations grow to a critical value the "parent" droplet will break up into a number of smaller "child" droplets. The "child" droplets are frequently assumed to be the same diameter, hence a single droplet produces a twin droplets pair. Otherwise, a liquid "conglomerate" is broken up abruptly when the distortion parameter x exceeds unity. As a droplet is distorted from a spherical shape, the drag coefficient changes. The TAB model is more accurate for low-Weber-number droplets. The effect of the aerodynamic drag force on the droplet is taken into account by interpolation between the limiting geometries of spherical and disk shaped droplets. Extremely high Weber number sprays result in shattering of droplets, which is not described well by the spring-mass analogy. In the CR spray, most of the atomisation process is occurred in the catastrophic regime due to the high injection pressure [308] and therefore resulting in high Weber numbers. Hence its applicability can be limited if the high pressure sprays are considered. Therefore, the detailed description of this model is omitted. The main deficiency of the TAB model is the underestimation of the product droplet sizes and its poor performance for evaporating sprays. This was supported by the work of Kim et al. [221] who studied dense diesel sprays atomisation using the TAB model without vaporisation.

Later, Tanner [389] proposed an improved version of the TAB model, which was named as the Enhanced TAB (ETAB) Model. The approach utilises the standard TAB model to calculate the drop breakup criterion, but the product drop size is determined through a drop breakup cascade from an exponential law, where the exponent factor depends on the drop breakup regime. The droplet breakup criterion is left unchanged compared with the standard TAB model. The simulation of a fragmented liquid core is achieved with the droplet breakup cascade in combination with the appropriate choice of the initial droplet deformation rate determined from experimental jet breakup correlations. The radial product droplet velocities, responsible for the spray angle formation (shape) are determined by equating the surface, deformation and kinetic energies of the parent and product droplets. The ETAB model has been implemented into one of the respective CFD spray packages:

STAR-CD and applied in diesel spray simulations by Tanner and Weisser [391].

An alternative to the TAB model are the Wave Breakup model (and its modifications) based on work of Reitz [337] and the Rayleigh-Taylor model presented in Patterson's PhD thesis [311]. The Wave Breakup model considers the breakup of the injected fuel to be induced by the relative velocity between the gas and liquid phases . After the fuel injection, the liquid fragments break into droplets due to aerodynamic forces as a result of instabilities on the gas/liquid interface. The Wave Breakup model includes three types of droplet evaluation i.e. bag breakup, where $6< We <80$, the stripping (shear) breakup for $80< We <350$ and the catastrophic (surface wave) breakup for $We >350$. As it can be compared to Table 2.13 the breakup regions in the Wave Breakup model are different and cover wider ranges of Weber numbers. The regions were specifically defined by Patterson.

Two main mechanisms of such instability reveal themselves in the spray atomisation, Rayleigh-Taylor (RT) instability due to inertia of more dense fuel opposing the liquid acceleration, and Kelvin-Helmholtz (KH) instability due to viscous forces causing the relative motion of the liquid layers are included into the Wave atomisation model. Originally, it has been assumed that the time of breakup and the resulting droplet size are related to the fastest-growing Kelvin-Helmholtz instability, derived from the jet stability analysis. Thus, the wavelength and growth rate of this instability were used to predict details of the newly-formed droplets. As it can be observed that the droplet velocity is very high within the breakup length in comparison to the velocity of droplet beyond the breakup region. In majority of studied cases the Reitz's theory has been developed and used as the KH and RT models. They are commonly used for simulation of the liquid atomisation and breakup processes. The models were combined in one the KH-RT model. The KH instability and the RT instability are compared and the breakup process is calculated by the dominant one. More detailed description of the models is given in the following subsections.

2.6.4.3 Kelvin-Helmholtz breakup analogy

In the catastrophic secondary breakup regime, model based on Kelvin-Helmholtz (KH) instability theory (WAVE) is applied.

This model simulates the stripping of droplets from the surface of the liquid core. It is based on the Reitz-Bracco stability analysis [340]. A wave-like disturbance on the surface of a stationary, round, liquid jet injected into an inviscid, incompressible gas leads to a dispersion relation between the disturbance frequency and its wavelength (Figure 2.15). The product drop size is determined from the wavelength of the fastest growing disturbance wave. The fastest growing disturbance on the surface of a liquid droplet determines how and when a droplet breakups. With this method small new droplets are created while the large parent drops continually decrease in size.

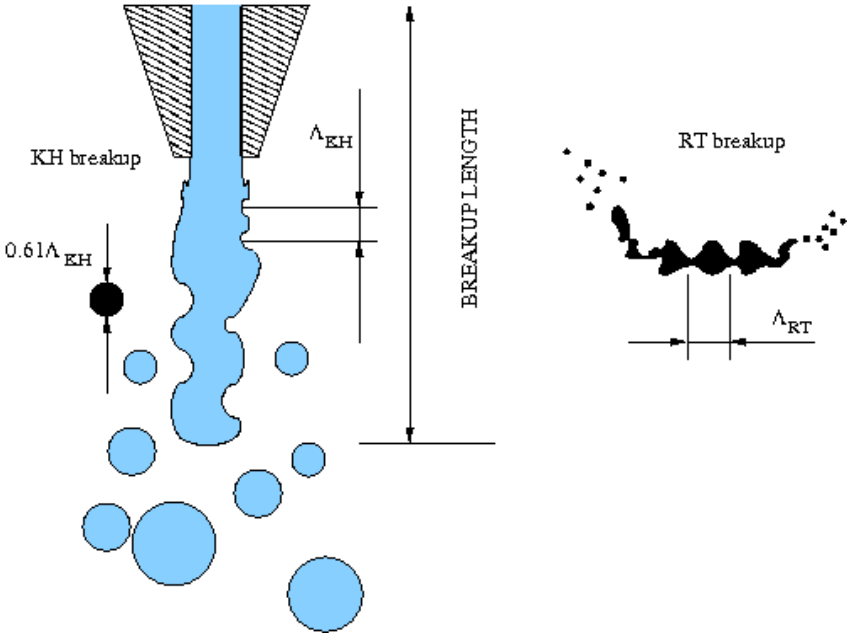

Figure 2.15: *Schematic presentation of the KH and RT breakup mechanisms in a nozzle-spray configuration.*

The wavelength Λ_{KH} corresponding to the surface disturbance of the highest probability to breakup is given as:

$$\frac{\Lambda_{KH}}{r} = 9.02 \frac{1+0.45Z^{0.5}\left(1+0.4T^{0.7}\right)}{\left(1+0.87We_g^{1.67}\right)^{0.6}} \tag{2.6.8}$$

where Z is Ohnesorge parameter and described as:

$$Z = \frac{\sqrt{We_f}}{Re_f} \tag{2.6.9}$$

and the Taylor number (or Taylor parameter) is given:

$$T = Z\sqrt{We_g} \tag{2.6.10}$$

The definition of th Reynolds number follows the expression for fluid:

$$Re_f = \frac{\rho_f u_r r}{\mu_f} \tag{2.6.11}$$

The maximum growth of the wavelength (or its rate) Ω_{KH} can be described by the equation below and determines when breakup occurs:

$$\Omega_{KH}\left[\frac{\rho_f r^3}{\sigma}\right] = \frac{\left(0.34 + 0.38We_g^{\frac{3}{2}}\right)}{(1+Z)(1+1.4T^{0.6})} \tag{2.6.12}$$

Where:

r is the radius of a parent droplet

u_r is the relative velocity between a droplet (parent or "child") and gas

μ is viscosity

σ is liquid surface tension.

The sub-symbols g and f refer to gas and liquid phase respectively.

Non-dimensional parameters characterising the bag breakup phenomena mechanism are the Weber number specifying the intensity of aerodynamic forces relative to the stabilising surface tension forces and the Ohnesorge number quantifying the effect of internal viscous forces:

Liquid breakup is modelled by postulating that new drops of radius r are formed from parent drop or "blobs". The breakup time or breakup timescale used for calculations, which determines the time that should pass between breakup events is given:

$$\tau_{KH} = \frac{3.726 B_1 r}{\Omega_{KH} \Lambda_{KH}} \tag{2.6.13}$$

Where:

τ_{KH} - breakup time of the Kelvin-Helmholtz breakup analogy.

B_1 is an adjustable constant called the breakup constant that should be determined based on the characteristics of the nozzle applied in simulations. The procedure for adjusting the B_1 parameter is described by Patterson and Reitz [312].

The radius of the droplet is determined by the relationship between the calculated wavelength, the maximum growth, and the radius of the parent droplet. Depending on the size of the parents drop radius, two droplets formations can be distinguished. The drops are assumed to be disintegrated from the liquid ligament in the centre of the spray and the drop radius is smaller than some fraction of the breakup wavelength. If the radius is larger than some fraction of the breakup wavelength, a new droplet is formed from the original parcel. Because KH breakup occurs with uniform radius reduction rate, new droplet radius r_n is calculated using following equations, according to [341]:

$$\frac{r - r_n}{dt} = \frac{r - r_c}{\tau_{KH}} \tag{2.6.14}$$

During the breakup, the droplet radius, r, reduces to critical radius r_c with uniform rate. In this case critical droplet radius and breakup time τ_{KH} are given as described in [338]:

$$r_c = 0.61 \Lambda_{KH} \tag{2.6.15}$$

The value of 0.61 is a constant according to Reitz [337], however there is a certain range of the constant and its value can be found using experimental data.

2.6.4.4 Rayleigh-Taylor breakup analogy

As far as the secondary breakup is considered, for high pressure sprays, the inclusion of Rayleigh-Taylor (RT) accelerative instabilities is necessary. This is due to high droplet velocities. The RT breakup model determines how and when droplets will breakup by predicting the wavelength of the fastest growing instability (Figure 2.15). Particularly, the RT approach describes the instabilities due to acceleration distortion rather than aerodynamic instabilities.

In RT instability mode, the maximum growth rate and its corresponding wavelength of the RT wave that is induced by accelerative instability. The equations for the wavelength, Λ_{RT} and frequency, Ω_{RT} of the fastest-growing wave are given according to [63] and [194]:

$$\Lambda_{RT} = 2\pi\sqrt{\frac{3\sigma}{a\rho_f}} = \frac{2\pi C_{RT}}{K_{RT}} \tag{2.6.16}$$

$$K_{RT} = \left(\frac{U_r\left(\rho_f - \rho_g\right)}{3\sigma}\right)^{0.5} \tag{2.6.17}$$

$$\Omega_{RT} = \sqrt{\frac{2a}{3}}\left(\frac{a\rho_l}{3\sigma}\right)^{\frac{1}{4}} \tag{2.6.18}$$

The breakup timescale calculated from the frequency of the fastest growing wavelength is given by:

$$\tau_{RT} = C_\tau \Lambda_{RT} \Omega_{RT} \tag{2.6.19}$$

Where:

C_{RT} is an adjustable constant according to the nozzle geometry as stated by Patterson and Reitz [312];

C_τ is the coefficient related with breakup time;

C_3 is the RT breakup constant;

C_τ is normally defined as 1.0.

τ_{RT} - breakup time of the Rayleight-Taylor breakup analogy.

The combination of the Equations (2.6.16) and (2.6.18) allows to calculate the breakup timescale of the fastest growing wavelength. Thus, the timescale defines the period between breakup events. The new droplet radius is calculated according to:

$$r_n = \frac{C_3 \Lambda_{RT}}{2} \tag{2.6.20}$$

The superposition of the KH and RT models has been explored in details and revealed significant improvement in the spray simulation [312]. Practically, when the catastrophic secondary breakup occurs, both instabilities KH and RT are utilised based on the competition between these two approaches. When the two models are used together, the calculations of the Rayleigh-Taylor approach are conducted first. The recent studies on diesel spray are focusing on applications of the KH and RT analogies and their combinations to elaborate more accurate breakup models [249; 339; 353; 384].

A combination of the KH and RT models was implemented in the Large Eddy Simulation (LES). The LES approach has been suggested by Herrmann [188] where all interface dynamics and physical processes occurring on scales larger than the available grid resolution Δx are fully resolved and all dynamics and processes occurring on sub grid scales can be modelled.

2.6.4.5 The Droplet Deformation and Breakup model (DDB)

Ibrahim et al. [202] formed the Droplet Deformation and Breakup (DDB) model, which allows to study large spray distortions. The model is a nonlinear formulation of the TAB model equations (the non-linear effect are not considered by the TAB model). The droplet

breakup is based on the drop dynamics of excessive deformation of the droplet. It is assumed that the initial droplet is deformed by a pure extensional flow. The main equation governing the DDB model is given by:

$$K + \frac{4N}{Re}\frac{1}{y^2}\frac{dy}{dt} + \frac{27\pi^2}{16We}y\left[1 - 2\left(cy\right)^{-6}\right] = \frac{3}{8} \tag{2.6.21}$$

where:

K - the liquid-gas density ratio;

N - the liquid-gas viscosity ratio;

y - distance from the centre of mass to its equator of the deforming half-drop.

The critical condition of the drop breakup is given by (Ibrahim et al. [202]):

$$\frac{a}{r} = \frac{We}{6\pi} \tag{2.6.22}$$

where:

a - major semi-axis of the ellipsoidal cross section of the oblate spheroid;

r - radius of droplet.

In comparison to the TAB model the DDB approach predicts the initial spray penetration with higher accuracy as shown by Ibrahim et al. [202]. Nevertheless, the DDB model has not found wide application yet. This is because of the necessity of sacrificing the accuracy of time-resolved numerical iteration over an essential improvement in physical accuracy. Furthermore, if the secondary breakup is not important then there is no need to implement the more complicated DDB model which can be replaced by the simpler TAB approach.

2.6.4.6 The KH-DDB competition model

The KH-DDB breakup model was presented by Park and Lee [308] to simulate high pressure spray diesel sprays produced in a CR injection system. It has been assumed that in the case of catastrophic breakup regime, the wave instabilities on the droplet surface are known as a reason of droplet breakup. In comparison to the RT and KH models, at

high relative velocities between droplet and ambient gas, in this model droplet flattening is taken into account as the origin of further breaking. It can be concluded that for the CR spray, most of the atomisation process occurres in the catastrophic regime due to high injection pressure and the high deformation of liquid blobs. To improve the mathematical description of the atomisation process within the breakup length, it is assumed to be affected by both wave instability and droplet deformation (flattening). Since, the high pressure spray develops, the major part of the atomisation process is governed by the deformation of the droplet.

The KH-DDB model describes the spray evolution after the fuel jet is issued from the nozzle in a way that the droplets are disintegrated by the result of competition between the instability of KH wave and the deformation of the droplet. As the spray time progresses, the deformation and the wave instability are increased. Additionally, Park and Lee [308] assumed that the KH breakup does not occur if the DDB breakup occurs. Also, it has been accepted that beyond the breakup length droplets are affected by the deformation since the velocity of droplet at that region is relatively low (the wave effect is reduced). Thus, the atomisation of the spray beyond the breakup length is only governed by DDB model. The breakup length of the KH-DDB model is calculated according to the formula [308]:

$$L_b = \frac{1}{2} B_1 d_0 \sqrt{\frac{\rho_f}{\rho_g}} \tag{2.6.23}$$

where:

B_1 - the breakup constant of KH model and equal to 60 according to Su [384];

L_b - the breakup length;

d_0 - the diameter of the nozzle.

The KH-DDB model was applied in [308] to simulate CR diesel sprays and the results were compared with phase Doppler measurements. The results showed good agreement between experiments and simulations, however the same model has not been applied by other investigators and therefore can not reliably validated.

2.6.5 Reitz-Diwakar (RD) model

Reitz and Diwakar [341] utilised the KH-RT model to construct a new approach to describe secondary droplet breakup called RD model. The RD model was included in KIVA code

and follow the criteria for bag and stripping breakup: We>6 and We·Re^{0}.5 >0.5.
The corresponding lifetimes for unstable droplets are given as

$$t_{bag} = C_1 \sqrt{\frac{\rho_l r_d^3}{\sigma}} \tag{2.6.24}$$

$$t_{strip} = C_2 \frac{r_d}{v_{rel}} \sqrt{\frac{\rho_l}{\rho_g}} \tag{2.6.25}$$

where:

t_{bag} - lifetime (breakup) time for bag-type disintegration, [s];

t_{bag} - lifetime (breakup) time for droplet stripping, [s];

r_d - droplet radius, [m];

C_1, C_2 - constants of order unity;

ρ_l - injected fuel density, [kg/m^3];

ρ_g - gas density, [kg/m^3];

v_{rel} - droplet relative velocity, [m/s].

Whenever one of the breakup criteria is satisfied for a droplet class for longer than the respective breakup time, it is assumed that the original droplet is disintegrated into a number of small droplets. All child droplets are of equal size. It is determined from equating the respective breakup criterion of Webber numbers (as above) to its critical value and by solving it for the droplet diameter. Thus, it is assumed that the new child droplet are initially in a state that is just stable.

2.6.6 Other KIVA submodes

Breakup models play a vital role in spray simulation, but KIVA code is also equipped with several submodes mathematically describing turbulence, evaporation, droplet collision and coalescence. These equally contribute to a final mathematical output and the computational time of spray simulation, therefore, can not be neglected. As the main aim of this section is to focus on breakup models, the turbulence and evaporation are shortly described in this section only. It has been accepted that these have a significant influence on spray development and droplet formation. More extensive description of KIVA models can be found in the documentation of the code [3; 37; 39; 40].

2.6.6.1 Turbulence model

There are two major turbulence models available in KIVA code: the standard κ-ε model [392] and the RNG linear variant of the κ-ε model [176]. It has been recognised that the RNG model works better when high strain rates are present in the mean flow [69], however the model has not been checked for non-diesel fuels. Therefore, the standard κ-ε model was applied in the present work. The selection was based on the model features, which indicate its application for robust, engineering applications and especially good for trend analysis. The model also provides good results for flows of low Mach numbers without a chemical reaction.

The standard κ-ε model consist of two turbulence components described as k and ε turbulence. The turbulence sub-model, as detailed in O'Rourke [303], uses the k and ε fields to generate fluctuating velocities that are then used in all spray model calculations that involve the relative velocity between a particle and the surrounding fluid. The k-turbulence equation is expressed by:

$$\frac{D(\rho k)}{Dt} = D_k + P_k - \rho\varepsilon \tag{2.6.26}$$

and can be shortly rewritten as the kinetic energy of turbulence [m^2/s^2]:

$$\nabla\vec{k}\cdot\vec{n} = 0 \tag{2.6.27}$$

The ε-turbulence equation is described as:

$$\frac{D(\rho\varepsilon)}{Dt} = D_\varepsilon + P_\varepsilon - \rho D_\varepsilon \tag{2.6.28}$$

and is commonly known as the turbulence energy dissipation rate [m^2/s^3]:

$$\varepsilon = C_{\mu\varepsilon} \frac{k^{3/2}}{y} \tag{2.6.29}$$

Where D is diffusion, k-turbulence kinetic energy, $P_{k,\varepsilon}$ production of k- and ε turbulence, n is molar concentration, ε dissipation rate and y is the length scale. The epsilon-Production part includes the empirical constants which for the purpose of the presented simulations were established as follow: $C_{\varepsilon 1}$=1.44; $C_{\varepsilon 2}$=1.92; $C_{\varepsilon 3}$=-1.0; C_{μ}=0.09; C_s=1.5; σ_k=1.0; σ_ε=1.0/1.3 according to [38].

From the Equations (2.6.26) and (2.6.28) it can be concluded that the effect of the particles on the turbulence fields is determined from the work done by the turbulence to disperse spray droplets. Also, each fluctuating velocity is effective for the length of the time corresponding to the minimum of time it would take the particle to cross a characteristic eddy or the time it would take the eddy to breakup.

2.6.6.2 Evaporation model

Evaporation of droplets involves simultaneous heat and mass transfer processes; heat of evaporation is transferred to the droplet surface by conduction, convection and radiation from the surrounding hot gases, while fuel vapour is transferred by convection and diffusion back into the gas stream. KIVA accommodate simple models of elaborating heat transfer between droplets and surroundings which are briefly described here.

In order to simulate a real complex phenomenon like diesel fuel spray evaporation a lot of assumptions have been commonly used. A classic droplet vaporisation model is the Spalding mode as originally introduced in the KIVA II code. The droplet evaporation model accounted for the processes that occur due to heat transfer between the droplets and the surrounding fluid. Energy conducted from the fluid to the particles resulted in a combination of droplet temperature change and fuel phase change from liquid to vapour. Inter-droplet effects on the evaporation process were neglected and the liquid fuel temperature is assumed uniform throughout the droplet. The existing KIVA evaporation sub-model is based on the original approach and a combination of the Frossling correlation [152], detailing the change in droplet radius during evaporation, the Ranz-Marshall correlation

detailing the heat conduction rate, and basic energy conservation principles. This model is based on many over-simplified assumptions. The Frossling and Ranz-Marshall correlations are given below:

$$Nu_d = 2 + 0.6 Re_d^{\frac{1}{2}} Pr_d^{\frac{1}{3}} \tag{2.6.30}$$

where:

Nu_d - the Nusselt number;

Re_d - the Reynolds number of the droplet;

Pr_d - the Prandtl number of he droplet.

$$Sh_d = 2 + 0.69 Re_d^{\frac{1}{2}} Sc_d^{\frac{1}{3}} \tag{2.6.31}$$

where:

Sh_d - the Sherwood number.

The evaporation of a particle results in a change of the particle droplet radius and droplet temperature. The rate of change of a single droplet radius is given by:

$$\frac{dr_d(t)}{dt} = \frac{-\rho D\left(T_f\right)}{2\rho_d r_d(t)} y R_{fv} Sh_d \tag{2.6.32}$$

where:

ρ_d - liquid density;

ρ_D - the fuel vapour diffusivity [m/s];

T_f - the fluid temperature;

y_{fv} - the fuel vapour mass fraction of the fluid;

Sh_d - the Sherwood number of the droplet.

More details of the mathematical presentation of the evaporation sub-model can be found in [3; 3; 302].

The evaporation procedure for a single time-step is sub-cycled in time. This sub-cycling results in better evaporation behaviour, allowing the evaporation process to respond to the changes in the fluid resulting from the evaporation. Within each sub-cycle, the change in droplet temperature is first solved for in an implicit fashion. The corresponding change in droplet radius is then determined, as is the resulting changes in the local fluid properties. The existing KIVA evaporation sub-model had been applied in spray evaporation by Senda and Fujimoto [364]. Gemci [153] verified the existing KIVA-3v model with the experiments. A summary of the existing literature studies on the evaporation model implementation indicate its high accuracy only if the accurate physical parameters for the investigated fuel had been correctly implemented. The droplet evaporation is also affected by the ambient conditions, of which definition is particularly difficult in complex engine conditions. Evaporation of a RSO droplet is expected to be determined by the oil's physical properties namely the latent heat of vaporisation as well as the value of the diffusion coefficient.

Chapter 3

Experimental systems

Non omnia possumus omnes

This chapter includes description of the experimental setups, which were used in the work. It presents first the origin of the experimental rig i.e. the injection stand. This part was then upgraded and coupled with other experimental elements like the injection chamber, a high speed camera or sizing equipment Growing complexity of the rig was done to facilitate various experimental test, which were selected to provide a concise set of data needed for technical assessment of a CDI injection system operating on RSO. The setup consisted of injection stand and a high pressure chamber. Its fundamental parts and the way how they were fitted into the system are described in this section. The setup modifications in accordance to different experimental requirements are also presented.
The chapter aims systematically introduce various setups in an increasing order of complexity and advance level. Six main subsections presents the injection stand, the injection chamber, the high speed camera setup, the Phase Doppler Anemometry, the Malvern sizing unit and finally the acoustic emission device.

3.1 Description of the injection stand

Consideration of neat plant oils as potential fuel for CDI engines should include studies of spray characteristic in a similar way the conventional fuels were investigated. Therefore it was required to provide an injection setup, which would closely reflect on a real CR system and would allow the study of the injection process.
Diesel spray characteristics is generally measured by considering the macroscopic and microscopic structure of the spray at the defined ambient and injection conditions. Since

diesel fuel injection under high pressure is a highly dynamic and transient process an experimental spray setup should maintain a suitable way to provide high quality measurements for quantification of the spray characteristics. As it can be found in the literature the previous studies were performed in the open atmosphere [31; 88; 236; 245; 249] and the vast majority of the experiments on the high pressure diesel injection, have been performed in a closed vessel coupled with auxiliaries to pre-condition the injected fuel. For the results to be useful for practical application, high pressure atomisation studies should be performed in a pressurised vessel so that the ambient pressure should be as close as possible to the operational engine conditions .

Furthermore, the injection system should have a good repeatability so that it can reproduce sprays under a constant set of conditions to reveal the relationships between the spray characteristics and the injection conditions. A good repeatability of the injection setup is thus an essential criterion for the design of the experimental setup. As far as the design of a suitable system is concerned it is challenging and influences quality of the results. There is a large number of experimental setups presented in the literature varied in complexity and functionality. As stated already, some equipped in a CR or in other Direct Injection systems worked in the open atmosphere [31; 213; 245; 249] conditions. Others accommodating injection into a constant volume spray vessel [79; 140; 236; 273; 330; 365; 426] with thick glass or quartz windows and frequently filled with an inert gas [61; 91; 111; 204]. Also, a partly open system can be found in the literature where a low speed continuous-flow gas tunnels have been applied [115; 207].

As far as the way of pressurising the fuel is considered, in most of the tests setups a motor-driven high pressure pump has been used [7; 85; 134; 207; 387; 426; 431] often fed by a smaller pre-pressure pump. This type of the injection setup is widely designed and readily used. Recently, applications of pneumatic systems have been reported [115; 200; 245; 249; 427], in which operation resembles closely the first group but differs in a way of pressurising the fuel. Instead of a mechanical high pressure pump, the system consists of a fuel reservoir kept under the constant pressure using highly compressed inert gas. The system features of strong advantages over the mechanical setups due to reduction of mechanical parts often being a source of the fuel pressure instability and leaks [256].

Spray characteristics had also been studied in systems that strictly mimic the engine conditions. Specially designed glass engines or transparent diesel engine cylinders can be found in the literature used to test diesel sprays [149; 186; 191; 233; 239; 276; 350; 368].

The main drawback of these systems is a significantly high cost and a narrow operational mode. However, glass engines always provided the most realistic engine conditions.

Finally, there are some other literature examples of spray studies employing specially made devices to study the spray injection rate in a micro [257] or macro scale [174] or under specific injection regime.

3.2 Common Rail injection experimental system

The experiments presented in this thesis were conducted using several variations of the same experimental setup. The construction of the experimental setup was based on the modified bench-scale Elsbett injection stand [22], which incorporated genuine CR parts. The experimental work in the order of the experimental setup modification progressed as: investigation of the injection quantities including the overall flow performance of the injection setup; spray characterisation using optical methods which involves spray penetration studies and spray droplet sizing using laser methods, and finally acoustic emission tests of the spray development. The injection quantities and system performance test were performed using the stand and an injection measuring panel. Spray characterisation, droplet sizing and the acoustic emission experiments were conducted using the stand coupled with the high pressure spray chamber.

The Elsbett injection stand was originally designed and built at Elsbett Company [168], Germany to examine the diesel injection event at the conditions that were thermodynamically similar to that encountered in a real injection system. In its original configuration the system was not suitable to accommodate a CR injection unit and had to be redesigned, modified and also upgraded. Figure 3.1 shows of the final configuration of the injection stand coupled with the high pressure injection chamber. The central part of the experimental rig is the injection system which consist of two major parts: the CR and the auxiliary fuel delivery unit.

The CR was an electronically controlled Bosh-Mercedes system (10) driven using a variable-speed electric motor (9) coupled to the high pressure pump (7) through a shaft assembled in a mechanical transmission (8). One purpose for applying the transmission was to provide enough power to drive the high pressure pump within revolution range.

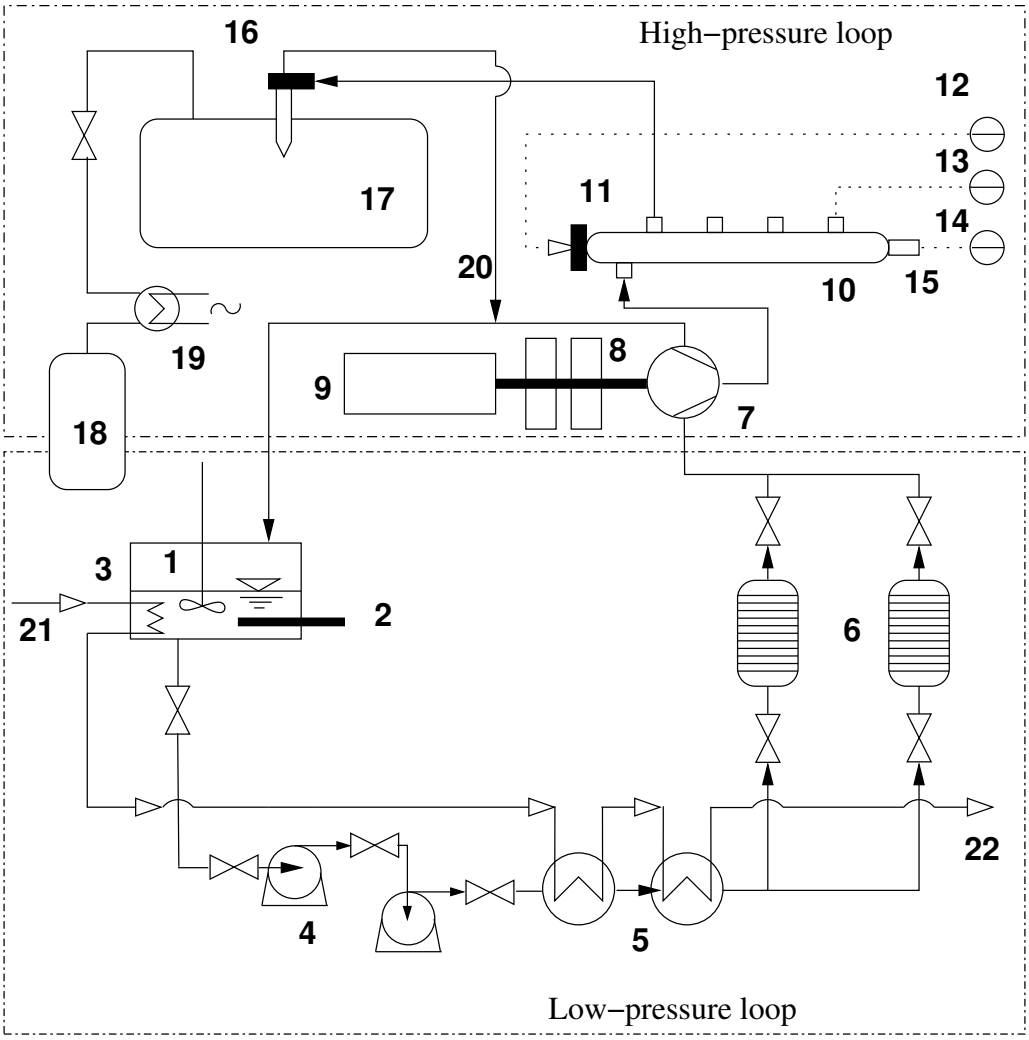

Figure 3.1: *Schematic presentation of the experimental rig (the injection stand and the spray chamber):(1) fuel tank, (2) fuel electric heater, (3) fuel water cooler, (4) low pressure fuel pumps, (5) heat exchangers, (6) fuel filters, (7) high pressure pump, (8) transmission, (9) electric motor, (10) rail, (11) rail pressure control valve, (12) pressure valve controller, (13) rail fuel temperature indicator, (14) rail pressure indicator, (15) rail-pressure sensor, (16) nozzle port, (17) spray chamber, (18) gas cylinder, (19) in-flow gas heater, (20) fuel return, (21) cooling water inlet, (22) cooling water outlet.*

The system also was able to count and control the number of shaft revolutions. The fuel delivery system operated as a closed hydraulic circuit and was composed of two pressure varying flow loops. Namely, the low pressure delivery loop and the high pressure rail part directly corresponding to the original CR injection system layout present in a car. Detailed descriptions of these two loops are presented in the next two subsections.

The injection stand was utilising the three phase power which required a specially designed control panel. The panel incorporated a system of switches, relays and automatically tripping fuses backing up each electric part of the system. The central part of this

panes was a unit managing speed of the electric motor.

3.2.1 Low-pressure loop

The main function of the low-pressure loop was to precondition fuel before feeding the high pressure pump. The design of the low-pressure loop of the experimental setup directly reflects on the elements described in *Subsection 2.2.5.2*, although some of its parts had to be simplified. Nevertheless, the arrangement is similar to the low-pressure stage of the original CR fuel injection system [203].

Correct and efficient operation of a CR system relies on the performance of fuel delivery directed to the high pressure pump. According to Bosch specification, the high pressure pump must be fed with correctly filtered fuel at an appropriate pressure. Almost a constant pre-pressure of 0.41 MPa had to be kept to maintain required performance of the high-pressure pump [203], otherwise the high pressure pump fails to produce the high injection pressure. Thus the low-pressure loop of the experimental setup incorporated two in-line pre-supply pumps of different pressure output (4) to avoid the pressure overload of a single pump. To ensure almost homogenous temperature of the fuel the fuel tank was equipped with a mixer working continuously throughout experiments. Temperature of the fuel inside the tank was automatically setup and regulated by a self controlled system consisting of an electrical resistance heater (2) and a set of thermocouples (not shown). Additionally, a water cooling coil (3) was build in to control fuel temperature in the case of an excessive heat release for faster cooling. Almost all parts of the low-pressure loop were insulated to maintain the system at required and constant temperature.

Then, from the pumps, fuel was transferred to a battery of plate heat exchangers (5). Cooling water leaving the fuel tank coil was utilised in the battery. To avoid heat losses, the fuel lines, the filters and the heat exchangers were insulated using two types of an insulating tape. The pre-heated fuel was transferred to the fine fuel filters (6). Each filter was equipped with a manual pump to assist fuel filter filling operation and to help remove the air from the system. To ensure the required fuel pre-pressure, an in-line pressure gauge was installed (not shown). A “T” type junction ensured almost pressure drop free flow. Next, fuel was directed to the the high-pressure pump (7) in the high-pressure loop.

3.2.2 High-pressure loop

This is where the preconditioned fuel is utilised to obtain the actual (operating) injection pressures. Pressurisation takes place in the high-pressure loop and in its integral part, the CR system - the high pressure pump. The loop comprises a Bosch high-pressure pump (7), driven by a variable-speed electric motor (9). As presented at the beginning of *Section 3.2*, the driving force was transmitted from the electric motor onto the high pressure pump using the transmission gearbox. Revolution of the electric motor could be manually controlled from the stand panel and allowed to vary the shaft rotation up to 3 500 RPM. However, the motor speed depends on the load applied on the high pressure pump and should not exceeded 3 000 RPM as recommended according to [203]. The injection pressure buildup

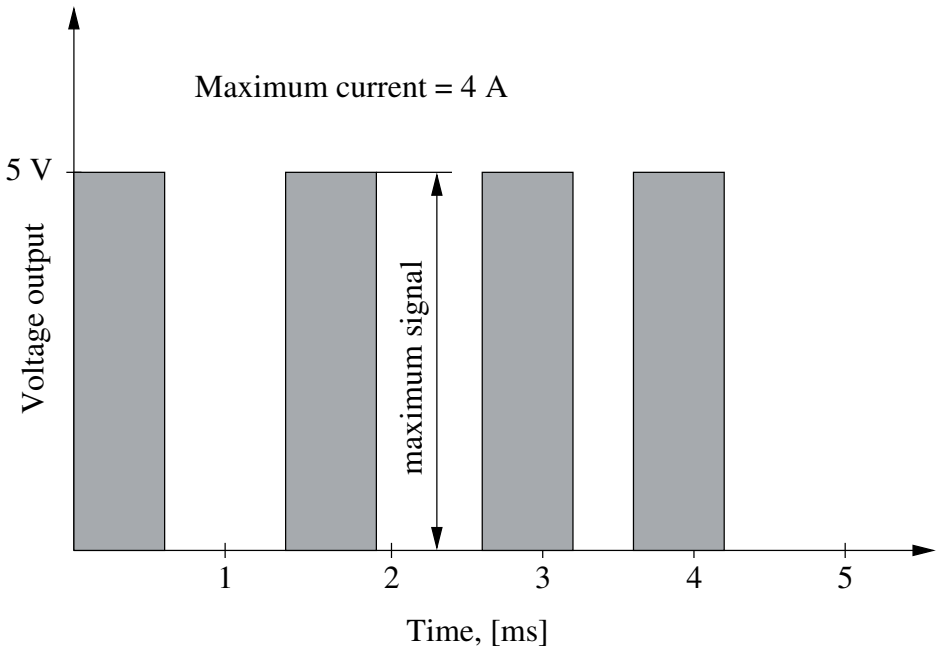

Figure 3.2: *Rail high-pressure regulator power supply signal.*

starts in the high pressure pump where fuel enters through the safety valve's throttle bore. Then fuel is compressed above the delivery pressure and leaves the pump through the outlet valve. The pressurised fuel passes through a high-pressure line and into the tubular high pressure accumulator called here the rail (10). The maximum pressure utilised in experiments was 1350 bar[1]. Process of the pressure buildup was controlled through the pump itself but the main role was given to the pressure-control valve (Bosch 0281002241) (11). The valve incorporates a by-pass-collecting system allowing fuel from the rail (not shown in the figure), the injector fuel return nozzle and the high-pressure pump to be sent

[1]Pressures of experimental parts are given as gauge pressure

through the same collector line (20).

In a real engine, the pressure-control valve sets the correct pressure in the rail as a function of the engine load and does it accordingly to the ECU signal. A typical response to the ON/OFF signal is shown in Figure 3.2, which illustrates a measured signal sent to the valve in a Mercedes C220 equipped with a CR system. The maximum signal voltage can reach 5 V and provide 10 up to 70% of the signal strength within very short time intervals (usually the frequency of 1 kHz is enough to operate the valve without unwanted pressure fluctuations). A linear switching power supply (DPS4005) (12) and an in house made electronic board unit were used instead of an original rectangular electric signal modulator. By varying the power signal from the power supply (12) the valve could be closing gradually and an excessive portion of the fuel could return from the rail to the fuel tank through a collector line.

In order to monitor the internal rail pressure the rail-pressure sensor (Bosch 0281002498) (15) was fit on the opposite side of the rail. An amplifying circuit was designed to produce the amplified sensor signal varying from 0.5 upto 4.5 V and measured using a digital multimeter (14). The signal output and the pressure-control valve power supply were applied to control the rail pressure.

Once the pressurised fuel enters the rail it can be distributed through four injector ports. Although, in the present system 2 ports were blanked off. One open injector port was connected to an injector and the other one, the closest to the fuel inlet, was fitted with a temperature sensor (13) measuring the rail inlet temperature. The high-pressure fuel was directed from the rail to the injector mounted in the high-pressure chamber injector port (16). The injector was triggered by a CR Signal Unit (Hartridge HK850) by applying a single injection pulse within a frequency range of 0 - 10.0 Hz and the injection duration of 0 - 5.0 ms.

A seat-hole Mercedes (A6110700587) CR injector was mounted in the high pressure spray chamber. Figure 3.3 shows a picture of the injector and Figure 3.4 illustrates its details schematically. The specification of the injection nozzle was six holes with 0.2 mm bore-diameter and bore length of 0.92 mm . It needs to be noted that the injector was not new and had been operating in an engine fuelled with diesel. The injector was located in the injector port as shown in Figure 3.8. The construction of the high pressure chamber imposed the way for optical spray access. Two different injector ports were designed to produce two different spray projection. In the presented work an in house

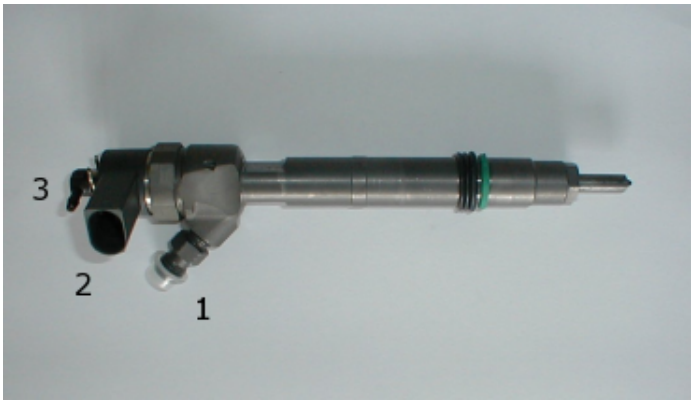

Figure 3.3: *A Mercedes (A6110700587) CR diesel injector: (1) the fuel inlet port; (2) the control cable connector; (3) the fuel return exit.*

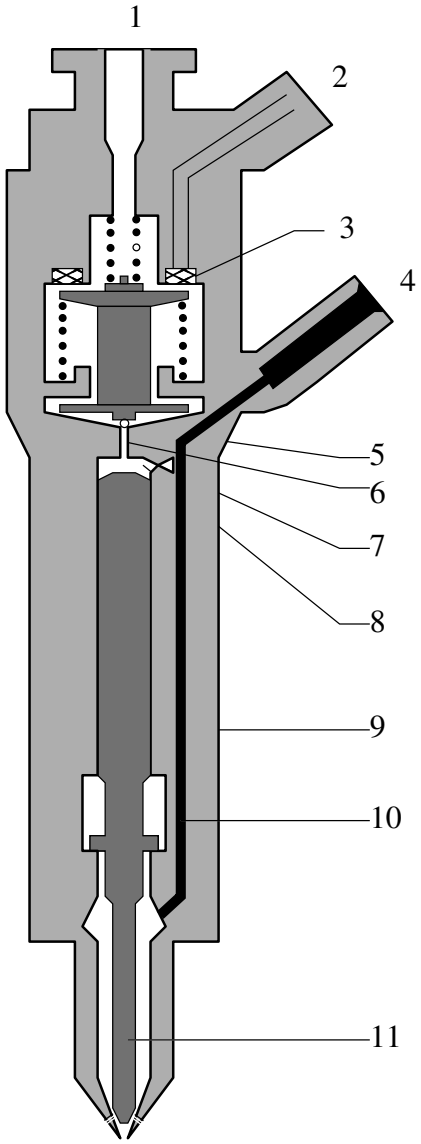

Figure 3.4: *Injector (schematic). (1) fuel return, (2) electrical connection, (3) solenoid valve, (4) fuel inlet from the rail, (5) valve ball, (6) bleed orifice, (7) feed orifice (8) valve control chamber, (9) valve control plunger, (10) feed passage to the nozzle, (11) nozzle needle*

made nozzle sleeve was designed and constructed to overcome a problem of multiple jets in a measuring volume. A schematic presentation of the sleeve is shown in Figure 3.5. Some other attempts performed to block off the nozzle holes led to serious damage of a nozzle. Application of the sleeve was a result of a compromise between having a single spray jet and also preserving the nozzle hydrodynamics. The sleeve spray pass (Figure 3.5) (5) allowed a single spray jet to travel through a gap without interfering with other jets, at least until the injection was terminated. The sleeve was tested using the high-speed camera to adjust the position of the sleeve slot and to gain the confidence that it worked optimally. Rest of the five holes were operating without any obstacle to the internal flow and the excessive fuel flow was diverted away through the fuel outlet (6). Practically, only a single, free travelling jet contributed in the mist buildup, whereas the other jets were captured before fully developed. Nevertheless, the sleeve application was not free of

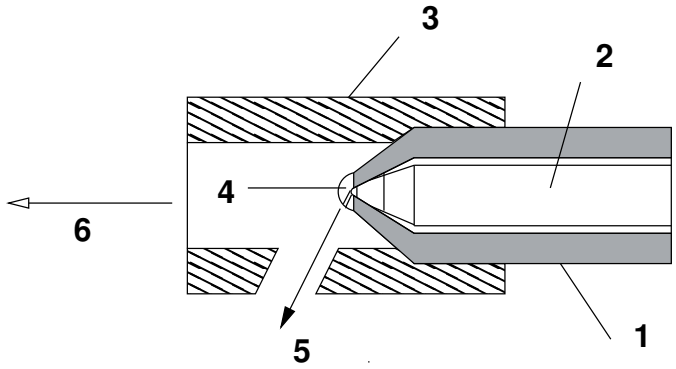

Figure 3.5: *The nozzle sleeve. (1)nozzle-body shaft, (2) needle shaft, (3) plastic sleeve, (4) nozzle tip, (5) sleeve spray pass, (6) excessive fuel outlet.*

drawbacks. Firstly, it was difficult to have a close observation of the surroundings next to the nozzle tip. This was especially important when penetration was investigated, however the unaccessible area was about couple of milometers from the hole end. The second was a presence of a fuel drop remaining at the sleeve spray pass after the last injection was terminated. Therefore, the image processing always excluded a first injection from the final results for some experimental runs. This practice came along with observation that each first injection features of a certain level of distortion and should be excluded from an experimental set [427].

3.2.3 The high-pressure spray chamber

Second integral part of the experimental setup was a high-pressure spray chamber.The chamber was made to be used together with the existing injection stand and to allow

conduct various experiments involving spray characterisation and acoustic emission tests. Its design and testing was novel and did not correspond to any system reported in the literature before.

A schematic presentation of the spray chamber is shown in Figure 3.8 and its pictures are presented in Figure 3.6 and in Figure 3.7. The size and shape of the spray chamber provided sufficient space to develop a spray without impinging the walls and the interference with other parts of the chamber. The vessel incorporates three glass windows - two "end" windows and one side window (Figure 3.8) (4,5) equipped with the spray devices to keep them droplet-free, two nozzle ports (2), three window cleaning spray devices, gas inlet/outlet ports (7,8) and pressure (3) and temperature control point (9). Visilume circular sightglasses were fitted on circular flange sets complete with relevant matching seals. Viewing diameters were 150 and 48 mm for the big and the smaller windows accordingly.

Figure 3.6: *The high pressure injection chamber - injection ports and the side window layout.*

The system was designed to be pressurised up to 16 bars and allowed the gas temperature up to 200°C, however most of the experiments were conducted at 20°C.
The gas inlet was incorporated into a gas supplying system consisting of gas lines, valves, a heater, a pressure gauge and a thermocouple. The gas inlet permitted a flexible operation with or without using the spray devices, switching between two gas sources (SF_6, N_2), gas purging and monitoring of gas temperature and pressure. Figure 3.9 shows a diagram of the window accommodating a spray device. Two different injector ports (Figure 3.8 (2)) were

Figure 3.7: *The high pressure injection chamber - a side view.*

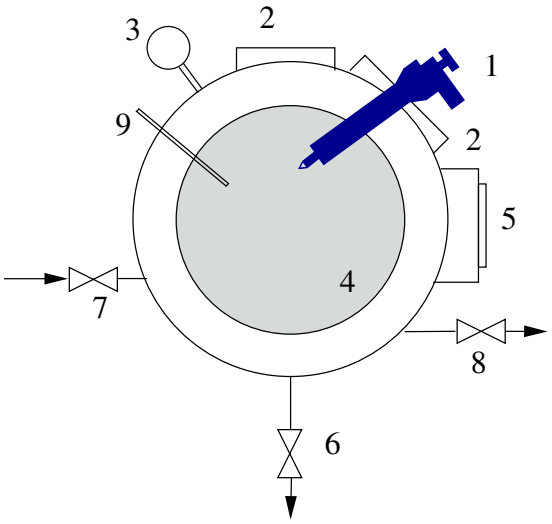

Figure 3.8: *Schematic of the high pressure chamber. (1) injector, (2) injector ports, (3) pressure gauge, (4) end window, (5) side window, (6) drainage valve, (7) gas inlet (8) gas outlet (vent), (9) temperature sensor*

accommodated in the chamber. The top one allowed to mount the injector vertically and a side one which was used to produce a single vertical spray. Only one port was utilised for the work presented in this thesis, whereas the unused one reminded sealed off. The injector port was manufactured to accommodate a thermocouple to control temperature of the injector right up to the fuel inlet. To maintain a required gas temperature inside the

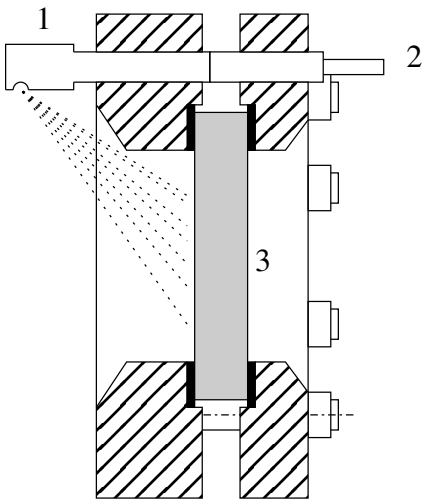

Figure 3.9: *Window assembly and a spray device. (1) spray head, (2) gas inlet, (3) glass.*

chamber an in-line gas heater (200 W, RS AH37-4MF) was installed. The constant gas flow was regulated using needle valves (Figure 3.8, elements (7) and (8)). The gas heater was fitted in a bypass gas line due to safety instead of operating on the main gas line.

The chamber also had a drainage valve (Figure 3.8 (6)) to remove fuel collected at its bottom during experiments. In order to avoid interaction between exhaust fuel and the spray an absorbing pad was placed at the bottom of the chamber which is shown in Figure 3.7. The chamber was equipped with a safety valve which was rated to 12 bars.

3.2.3.1 Chamber pressurising

Two types of inert gasses were used to pressurise the spray chamber, nitrogen and sulphur hexafluoride (SF_6) accordingly. Nitrogen was used for testing and pressurising the chamber at 2.5, 5.0 and 7.5 bars. Sulphur hexafluoride was applied at 2.5, 5.0, 7.5 and 10.0 bars. Because of its high density (60 kg/m^3), SF_6 allowed to perform experiments under significantly lower pressure than if air were to be used. For example, for 51 bar equivalent in cylinder pressure with SF_6 the regular pressure in the chamber was only 10 bar. SF_6 in commonly used in non-combustion spray tests in gas turbine industries as well as in diesel spray studies. In addition, SF_6 as an inert gas did not have the corrosive effect on the rig and provides non-combustive atmosphere. The gas viscosity and its optical properties are very similar to those of the air. Detailed information of the SF_6 are given in Table 3.1. Similar application of SF_6 and N_2 used in spray experiment were reported in [310; 316] where CR diesel sprays were tested. Also, Powell et al. [330] applied SF_6 and N_2 in their work investigating diesel sprays using X-rays as well as McPhee et al. [256]. Application

of SF_6 in spray penetration studies was also described by Pastor et al. [309]. Gas pressures

Table 3.1: *Physical properties of sulphur hexafluoride (SF_6).*

Property	**Value**
Relative gas density, (air=1)	5
Molecular weight	146 g/mol
Specific Gravity (H_2O = 1) @ -50°C	1.91
Boiling Point	-64°C
Vapour pressure @ 20°C	2 MPa
CAS No	02551-62-4

applied in experiments and the equivalent air in-chamber densities are listed in Table 3.2. Taking into account the physical properties of SF_6 and N_2 it has to be noted that the sonic speed in SF_6 was found much less than of N_2. The speed was estimated to be $\sim$137 m/s. As long as the effect on spray dynamics caused by the sonic velocity of the ambient gas is not studied the higher value of the sonic speed of SF_6 can be neglected. The application

Table 3.2: *Experimental ambient in-chamber conditions.*

Ambient pressure	**Density [kg/m^3]**	**Equivalent air pressure @ 20°C [bar]**
atmospheric (air)	1.1981	1.013
2.5 bar N_2	3.0	2.5
5.0 bar N_2	6.0	5.0
2.5 bar SF_6	15.0	12.5
5.0 bar SF_6	30.0	25.0
7.5 bar SF_6	45.0	37.3
10 bar SF_6	60.0	51.0

of SF_6 is highly advantageous due to its high density and there is no need for high pressures in the spray cylinder. Although, the lower pressures do not contribute in the back-pressure effect in the same way as the same density is obtained using the compressed air. This effect is discussed in more details in *Subsection 4.1.1*.

3.2.3.2 Optical characteristics of the windows

The experimental setup has been designed to work extensively on spray characterisation which involved different optical methods. Since the glass quality remains essential for both high speed camera recording and PDA measurement, selection of suitable glass discs

of big clear aperture was crucial. In similar setups quartz type of glass has been used and quite often BK7 glass type is utilised. Quartz glass offers excellent properties, but it is expensive and the most common cuts normally offer small aperture. The existing windows sizes and ambient conditions required a considerably large glass disk with good strength and resistance. Toughened borosilicate glass discs to DIN 7080 were tested and finally selected. An extract from the DIN 7080 standard regarding the surface finish and tolerances featuring the glass discs is presented in Table 3.3. A comparison of the borosilicate glass

Table 3.3: *Surface finish and tolerances of the DIN 7080 borosilicate glass according to Visilume.*

Diameter of bubbles	Permissible number of bubbles
Less than 0.3 mm	3/cm^2
From 0.3 mm to 0.5 mm	10/pane
Over 0.5 mm up to 1 mm	4/pane
Over 1 mm up to 2 mm	2/pane
Knots and streaks	not permissible
Solid inclusions	No more than 3 solid inclusions are permissible per pane not be greater than 0.2 mm in diameter and shall be at least 10 cm apart
Tolerances	Diameter for discs from 150 to 200 mm $\pm$1 mm Thickness over 20 mm +0.8 mm -0.4 mm
Geometrical tolerance	Flatness of panes over 150 mm up to 200mm diameter = 0.12 mm Parallelism of top and bottom face of panes over 150 mm up to 200 mm diameter = 0.25 mm

with the quality crown optical glass like BK7 features in a good optical transmittance. In order to verify the transmittance range the absorption spectrum of the glass disks was tested using a spectrometer. Figure 3.10 shows the transmission curve which is almost linear within the visible range of wavelength. It has been proved that the glass quality is appropriate to conduct planned experiments.

3.2.4 Injected volume measuring tray

In addition to the spray characterisation experiments, the series of tests in which the injected volume of fuel was measured were performed. The aim of these experiments was to test the capability of the system to mimic CR-like conditions and investigate differences in the injection maturation between the standard and RSO. Additionally, some simple

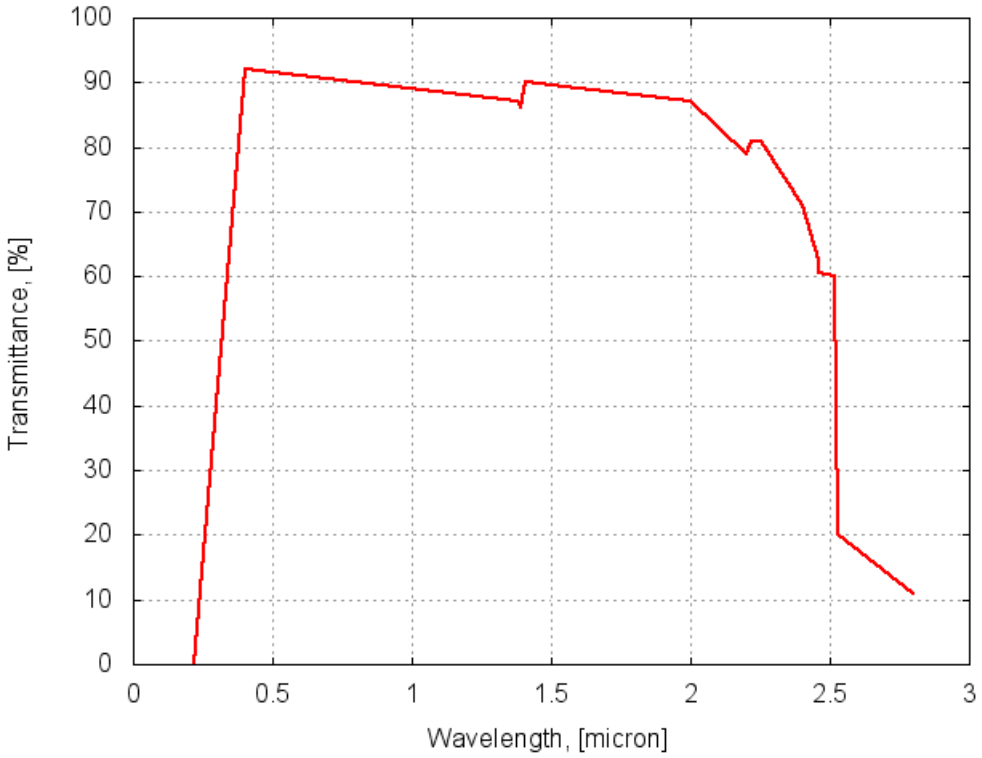

Figure 3.10: *Transmittance test results of a 20 mm borosilicate glass disc.*

investigation of hydrodynamics and heat flow inside the system for these two oils was performed.

It has to be emphasised that rate of injection in a CR system has not been extensively described in the literature. Only few papers report studies on injected quantity of fuel regarding injection profiles and pilot injection [210; 383; 396]. However, none of them concentrated on variation of injected amounts as function of injection pressure, fuel temperature. No study to the date has tested neat RSO. Quantities of injected fuel may limit performance of injection system and effect the overall engine effectiveness. Hence some comparative, preliminary studies on standard and RSO had to be performed. Thus it has been accepted that the injection quantity of RSO requires more thorough studies of fuel metering as a function of the injection pressure conditions.

The injection stand was originally designed to measure fuel amounts delivered through the different diesel nozzles. In the upper part of the assembly were series of plastic bowls located right above a movable tray. The tray comprises of the automatic system to collect fuel for a required number of injection or the motor revolutions and the glass burettes wherein fuel was collected. As the system was not originally setup to accommodate a

CR injection system it had to be modified. Therefore, for these tests the fuel line and the injector were mounted inside a metal port assembled in the injection tray of the Elsbett stand. The injector was fed with oil through a metal tube which was longer than the original one and its length has been scaled to provide the lowest pressure drop. The port was fixed in the tray and insulated to reduce the heat losses from the injector. The end of the injector was placed in a plastic bowl to enable the complete collection of the fuel and to capture the fuel mist. The plastic bowl was finished off with a plastic stopper and additionally a rubber tube was placed on the stopper. The photograph of the port is shown in Figure 3.11 and the plastic bowl and the injector is presented in Figure 3.12. The rest of the system remained unmodified and allows to produce the appropriate injection pressure and temperature of the tested oil.

Figure 3.11: *The nozzle metal port (prior to fitting the insulation).*

3.3 High speed camera experimental setup

After testing various position of the light source, the final method of illumination used in this work was chosen as a front light positioned at 10° relatively to the camera-injector centreline. However, prior to the experiments, series of test were performed to select the best spray lighting method. Three methods were tested: back light, laser illumination sheet

Figure 3.12: *The nozzle plastic collecting bowl.*

and the front light. All three methods were used in a combination with the spray chamber and the injection stand described in details in the *Section 3.2*. As the final one the front light illumination approach was chosen for the later of test.

The laser sheet illumination method employed used the water cooled green (509 nm) laser of New Wave Model Solo II (15 Hz repetition rate). A pulse laser sheet was produced and used to illuminate the spray perpendicularly to the spray path. The laser beam was brought in through the side window of the spray chamber and appropriately positioned to ensure that the laser sheet passed through the spray at its centreline. Setting up the laser sheet in that way for each test (varying spray size and structure) was found to be very difficult as it was required to illuminate the spray exactly through its centreline and thus provide a spray picture at its widest planar exposure. A typical snapshot of a single spray jet laser illuminated is shown in Figure 2.7 (similar to the one shown in [26]). The arrow indicate the direction origin of the laser light. A closer analysis of the snapshots taken in this manner, revealed that the spray is not fully illuminated and due to a high density of the spray produced by the CR. Similar problems were recorded and presented elsewhere, such as in [26] where the authors discussed degradation of the quality of images when

the medium is not optically thin, as in the core of the fuel spray. They also described a modified laser-based experimental setup which was used to work with high speed camera imaging . A similar discussion of laser dissipation in a dense spray was carried out by Eckbreth [132] and Ossler et al. [306] in case of dense spray.

Moreover, during the preliminary tests, it has been found that the laser spray illumination results in a lack of fully lit up spray due to varying spray size - wider spray cone angle results in dissipation of the laser light after passing a spray core. Due to varying injection pressure and thus wider or denser spray, adjusting the laser sheet would require a fine tuning at each experimental run. Also, even the slightest dislocation of the chamber (e.g. during the window cleaning) caused serious dislocation of the laser sheet and hence an offset from the centre. And finally one of the main problems was to illuminate a single spray whilst the injector produced several of them significantly interfering with the laser sheet. Therefore this method was found to be difficult to deal with and it was concluded that it might cause inconsistency during the measurements.

The second method which was applied in the preliminary test was the back light illumination that was successfully applied in previous works [245; 277]. In comparison to the laser illumination, this method does not involve such difficult adjusting of the light source, and moreover, the light does not have to pass the sprays and its centreline.

A halogen lamp - Ianbeam 800 working in flood mode, was used to light up sprays and

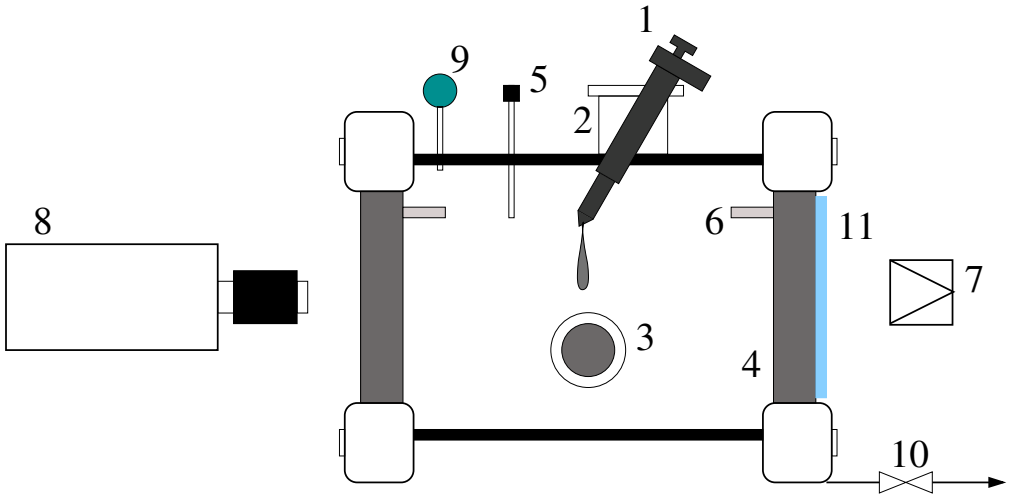

Figure 3.13: *High speed camera set-up with the back light illumination (not scaled): (1) the CDI injector; (2) the injector port; (3) the side window; (4) the end window; (5) the temperature sensor; (6) the gas spray device; (7) the back light source; (8) the high speed camera; (9) the pressure gauge; (10) the gas outlet valve; (11) the light diffuser.*

positioned approximately 25 cm away from the window. The light was introduced through

the the rear chamber window, and the recording took place at the opposite side to the halogen lamp (see Figure 3.13). Finally, the front light illumination approach was tested. The same source of a halogen lamp as applied during the back light illumination was positioned in a front of the chamber next to the window. The details of the lamp set-up is illustrated in Figure 3.14. A similar method was utilised by Sazhin et al. [355] working with the initial stage of spray penetration produced by a CR and compering the results with three different theoretical models. Authors used photoflood lamps and recorded at 27000 fps. The front-lighting was also used by Morgan et al. [277], however these authors used a diffused back light too for more homogeneous illumination. The global characteristics of spray including spray angle, spray tip penetration and spray pattern produced in VCO nozzle were measured by Kang [213] from the spray images which were frozen by a spark light source in a front light setup. A similar approach was applied by Sovani et al. [376] measuring cone angles of diesel sprays formed by a high injection pressure effervescent atomiser. The spray was illuminated evenly from both sides and a video camera was used to capture spray images. Sazhin et al. [354] studied the effects of droplet evaporation, break-up and air entrainment of diesel fuel spray penetration in the Bosch CR system using a side and front halogen lamps. Finally, flash source was used to illuminate the sprays produced by a Delphi CR fuel injection system using a front ring light [365]. It has been found that the front light method does eliminate some of the

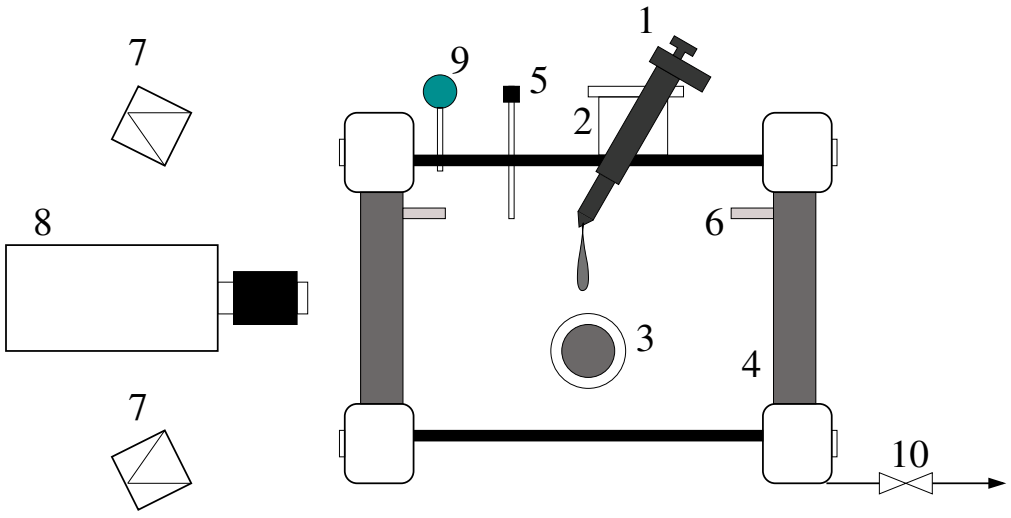

Figure 3.14: *High speed camera set-up with the back light illumination (not scaled): (1) the CDI injector; (2) the injector port; (3) the side window; (4) the end window; (5) the temperature sensor; (6) the gas spray device; (7) the back light source; (8) the high speed camera; (9) the pressure gauge; (10) the gas outlet valve.*

measurement obstacles present in the first two methods, nevertheless brings others. The light entering the chamber travels through the volume of the spray, and finally reaches the

end of the chamber, i.e. the rear window. To avoid any reflection from the back window, the black filter was placed on the outside of the rear window. Later on, it was found that by placing the same filter inside the chamber, close to its end provides the best results. The filter was a home made piece of plastic sheet painted with a mat black paint. The painting of the plastic was done several times to ensure a uniform paint cover. Additionally, the surface of the paint was specially treated to enhance oil absorption and therefore to eliminate collection of reflecting oil on the filter. It was crucial to paint mat black the inner side of the chamber including flanges.

At this point it's important to comment on an issue which clarification in most of the recent publications or reports has been generally omitted. This is, the choice of light strength for the front or the back light spray illumination. It can be concluded that for the sprays of dense core and significantly wide cone angle, spray edges quite readily let light go through due to less dense structure. Even if it is assumed that spray edges terminates at a line of still compact and concentrated droplets, it can be seen that too strong light leads to reduction of that sharp line resulting in what is here as the "loosing edge" effect. The effect is a combination of over illuminated droplets and brighter background. Such unwanted effect is particularly important at the beginning of spray penetration where a small spray jet exists close to a nozzle tip and its snapshot needs to be analysed. This plays an important role as far as the cone angle is concerned because any distortion or unreal spray image can cause error. The problems becomes even more apparent if the tests are carried out at varying injection conditions. In this case, the spray structure changes in its density and influences its edge transparency too. Taking into account all these factors it is extremely difficult not to face the "edge loosing" effect throughout the experiments. Nevertheless, in these test some procedures were applied to reduce the problem.
Firstly, at each injection conditions a series of spray pictures were taken with gradual increase of the light intensity. It could be seen that there was a certain level of intensity beyond which the spray edges become reduced. This boundary light intensity was used as an appropriate one for experiment at the same injection conditions. Secondly, a numerical procedure was written to analyse pixel brightness of the background and the spray and then equalising process was applied to the spray picture prior to penetration/cone angle value determination. Further details of the image processing and used methods are described in the *Subsection 4.2.3.*

3.3.1 Experimental conditions

The high speed camera spray acquisition was performed at different ambient and fuel conditions for both standard and RSO. The ambient chamber conditions are presented in Table 3.2 and other experimental details are given in *Chapter* 4. The fuel injection conditions are showed in Table 3.4. The injection pressure values were selected to represent

Table 3.4: *Experimental conditions for standard and RSO*

	Standard oil	**Rapeseed oil**
Oil temperature [°C]	25,30	25,40,60
Oil injection pressure[1)] [MPa] ([V])	37.50 (1.5) 56.25 (2.0) 75.00 (2.5) 93.75 (3.0) 112.50 (3.5) 131.25 (4.0)	

[1)] Values in bracket show an effective pressure sensor voltage output used to control the injection pressure.

a wide range on the operational conditions taking place in a real engine but taking into account some limitation of the experimental setup. It has been found that the injection pressure above 1350 bars creates a significant level of vibration in the system and hence difficulties to maintain the rail pressure at constant, required pressure. In practice, the injection pressure above that value is hardly utilised in a low and intermediate engine load. Therefore all observation at such high pressures are not as crucial for the engine modification as those up to 1000 bars. All measurements were performed at an injection duration of 1.0 ms and frequency of 1 Hz.

3.4 Phase Doppler Anemometry experimental setup

Droplet sizes and velocities of a SO and RSO spray were measured simultaneously with a Dantec Dual PDA system using the experimental injection setup and the high pressure chamber described in *Section 3.2*. The system consisted of an emitting optics based on components of the *55X Modular LDA Optics* system in 2D or 3D configuration; a scattered light receiving optics of *57X80 Dual-PDA Probe*, a signal processing electronics of *58N81 Dual-PDA Detector Unit* with the signal processor: *58N80 Multi-PDA* equipped with two velocity channels; a traversing system and an acquisition system including a computer. The

experimental PDA optical arrangement is shown schematically in Figure 3.15. Photographs shown in Figure 3.16 and 3.17 present a general look over the PDA arrangement in the lab. The emitter and the collecting optics were mounted on a traversing system, which allowed to control the position of the optics in relation to the spray chamber. The position was controlled by using a motored 3D traversing table. The light source was an Argon-Ion

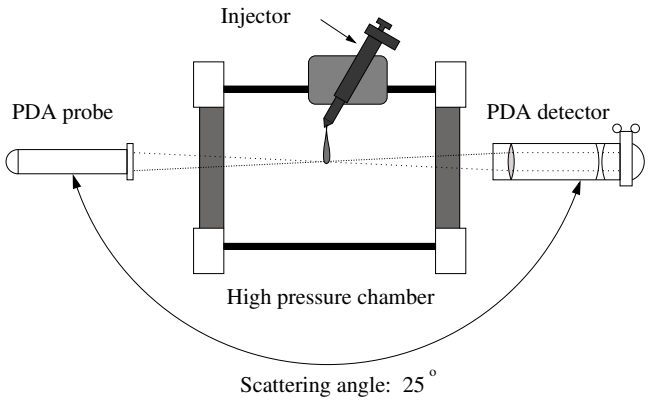

Figure 3.15: *Representation of the setup for PAD measurement.*

Dantec 500 mW laser providing beams at two wavelengths, green (λ=514.5 nm) and blue (λ=488.0 nm). Both wavelength were used in the size measurement and the green beam was used for the measurement of the main velocity component (U) and the blue beam was used for the second velocity component (V).

The beams were transmitted to the PDA probe through an optical fibre and then focused at the measurement volume at a focal length of 600 mm from the PDA transmitter. The PDA system was operating at the scattering angle of 25°. The scattering angle commonly used with the PDA system falls within the range of $20^\circ < \varphi < 50^\circ$ and is the most applicable. At a scattering angle around 50° the measured size will be relatively independent of smaller changes in the refractive index. However, the intensity of the scattered light is greater at a lower angle, (e.g. 30°) and therefore favourable in situations of poor signal-to-noise ratio, which is expected for dense sprays. Due to the construction of the spray chamber and the position of the nozzle, the adjustment was limited to using up the main big chamber windows. The final selection of the emitting and collecting optics offsets was based on the guidelines provided by Dantec, but the final setup was determined by a trial and error method attempting to achieve the best possible acquisition and droplet validation under existing geometrical constrains. Further details of the PDA setup is given in Table 3.5. The alignment, focus of the PDA, and validation of the measurements were checked with a water nebuliser resulting in a droplets spectrum of Sauter mean diameter

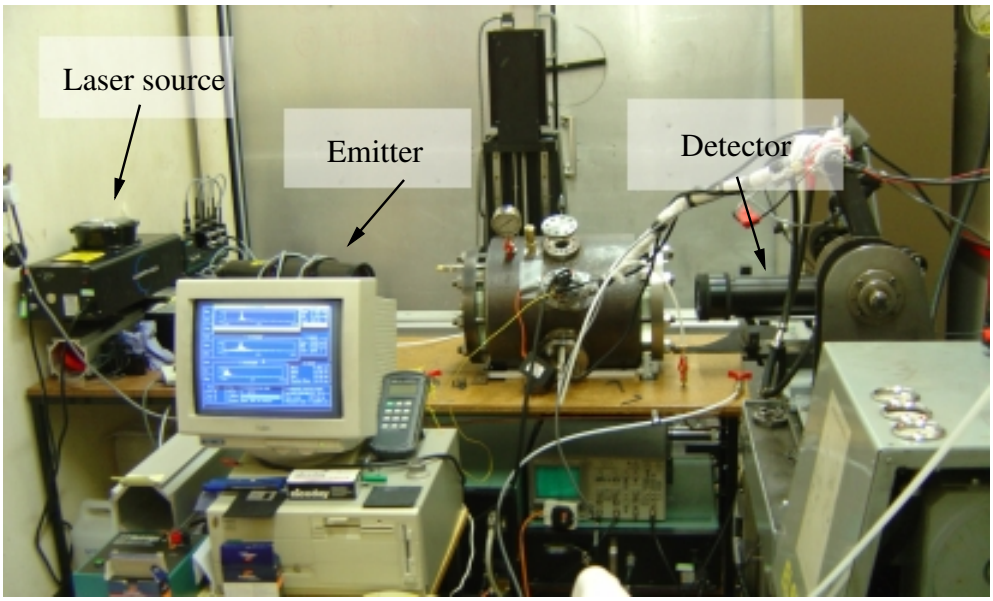

Figure 3.16: *Experimental arrangement of the PDA system.*

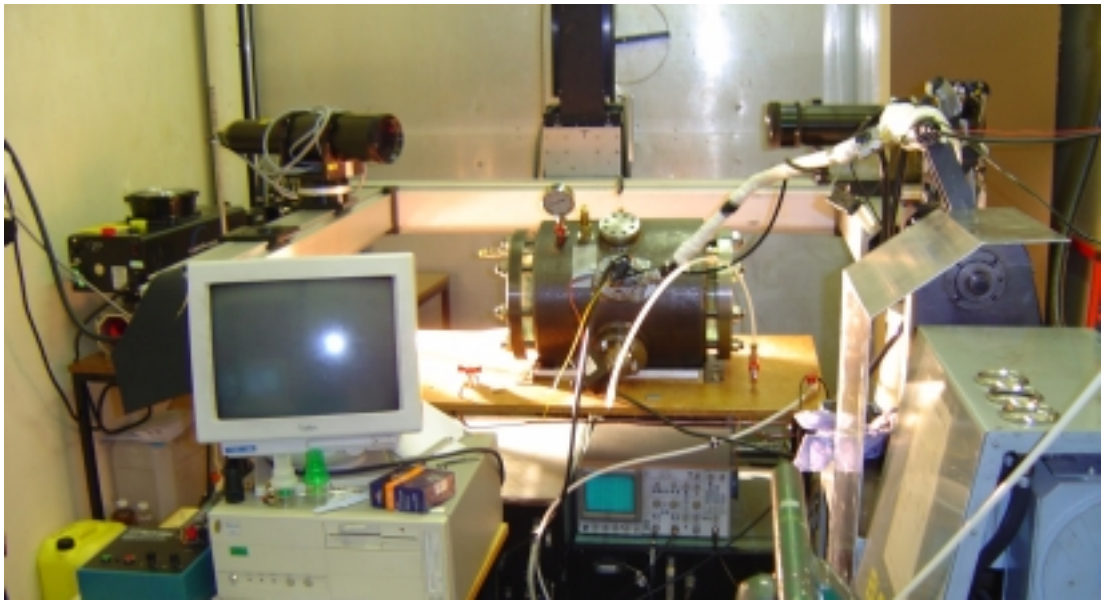

Figure 3.17: *View of the PDA and the traversing system.*

of $\sim$10μm, which agreed with the similar measurements performed before [399]. The same nebuliser was used for the fine tuning of the PDA setup described in *Subsection 4.3.1*.

The measurements were taken at different ambient and injection conditions shown in Table 3.6. For each injection and ambient condition measurement was repeated 3 times at the same point for 7 consecutive injections. Thus each PDA measurement resulted in 21 separate measurements of a spray. The final results were averaged over each set. Spray measurements were taken along the spray centreline at two axial distances of 30 mm and 40 mm from the nozzle tip (as shown in Figure 3.18), consecutively to obtain 21

Table 3.5: *Parameters of the PDA setup*

Beam separation [mm]	25
Fringe spacing [μm]	12.350 11.714
Number of fringes	12
Velocity bandwidth [m/s]	-37.0 to 111.1
Maximum diameter [μm]	178.82
Particle/medium refractive index	1.41-1.47/1
Validation level [dB]	-3
Max. spherical deviation [%]	15

Table 3.6: *Ambient and injection condition of PDA SO and RSO test.*

	Standard Oil	**Rapeseed oil**
Injection pressure [MPa]	37.5, 56.3, 75.0, 93.8, 112.5, 131.3	
Oil temperature [°C]	25, 30	30, 40, 60
Ambient density [kg/m^3]	1.2,3.0, 6.0, 15.0, 30.0, 45.0, 60.0	
Injection frequency, [Hz]	1.0	1.0
Injection duration, [ms]	1.0	1.0

measurements and repeated twice for the lowest and the highest injection pressure. It was found that measurements at 30 mm were likely too close to the injector and that 30 mm could be the distance where the primary breakup occurs. Hence, only results of at 40 mm were used and showed later.

A measurement volume was located in the centreline of the spray with the maximum deviation from the centreline of $\pm$ 1mm. The centreline of a spray was found by scanning of spray velocities in X,Y and Z direction downstream from the nozzle tip as presented in Figure 3.19 at 10, 20, 30 and 40 mm (along X axis). As finding of the spray centre can be easily done by scanning spray in the radial direction, the axial distances need to be measured differently. A specially made scale was prepared and mounted vertically on the spray nozzle. The tool allowed to find the axial distance by pointing the laser beam onto it in relation to the scale. The experiments were conduced in a similar manner like those where the high speed camera has been applied (compare *Section 3.3*). A gentle gas flow throughout the chamber was retained to remove fuel mist. More frequent chamber evacuation, higher inert gas flow, and more frequent and longer breaks during experiments (to allow the chamber reach the desire temperature and reduce internal gas motion due to fresh gas introduction) were also applied. On average, the procedure of pressurising and depressurising the chamber took place after every 4 consecutive measurement sets. One

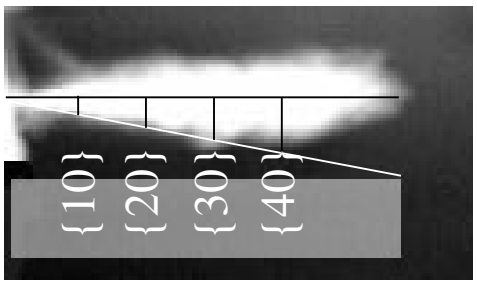

Figure 3.18: *PDA test and measurement locations (only the distance at 40 mm was utilised to obtain the final results)*

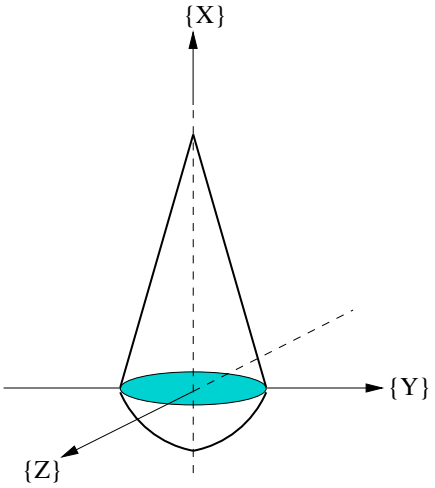

Figure 3.19: *Spacial orientation of spray applied in PDA measurements.*

of the important issue was the effect of oil drops splashing against the windows on the quality of the laser beam. It has been noted that even small amounts of oil residue would reduce acquisition rate and affect validation similar as in [106]. A consequence of window fouling was the reduction of the spray measurements only to a single-shot injection. A set of plastic tubes were fitted on the inner side of the glass windows to protect the windows from oil deposit as well as reduce the beams interaction with droplet residue. The tubes does not allow small drops to accumulate to the inner side of the windows. The tubes were only used for the PDA tests otherwise spray devices as shown in Figure 3.9 were used. A photograph in Figure 3.20 shows one of the chamber window with the plastic tube covering a laser beam.

3.5 Malvern experimental setup

The laser-diffraction instrument used was model Insitec of Malvern Instruments Limited, high speed, real time, and high concentration sizer. The setup consisted of the optical

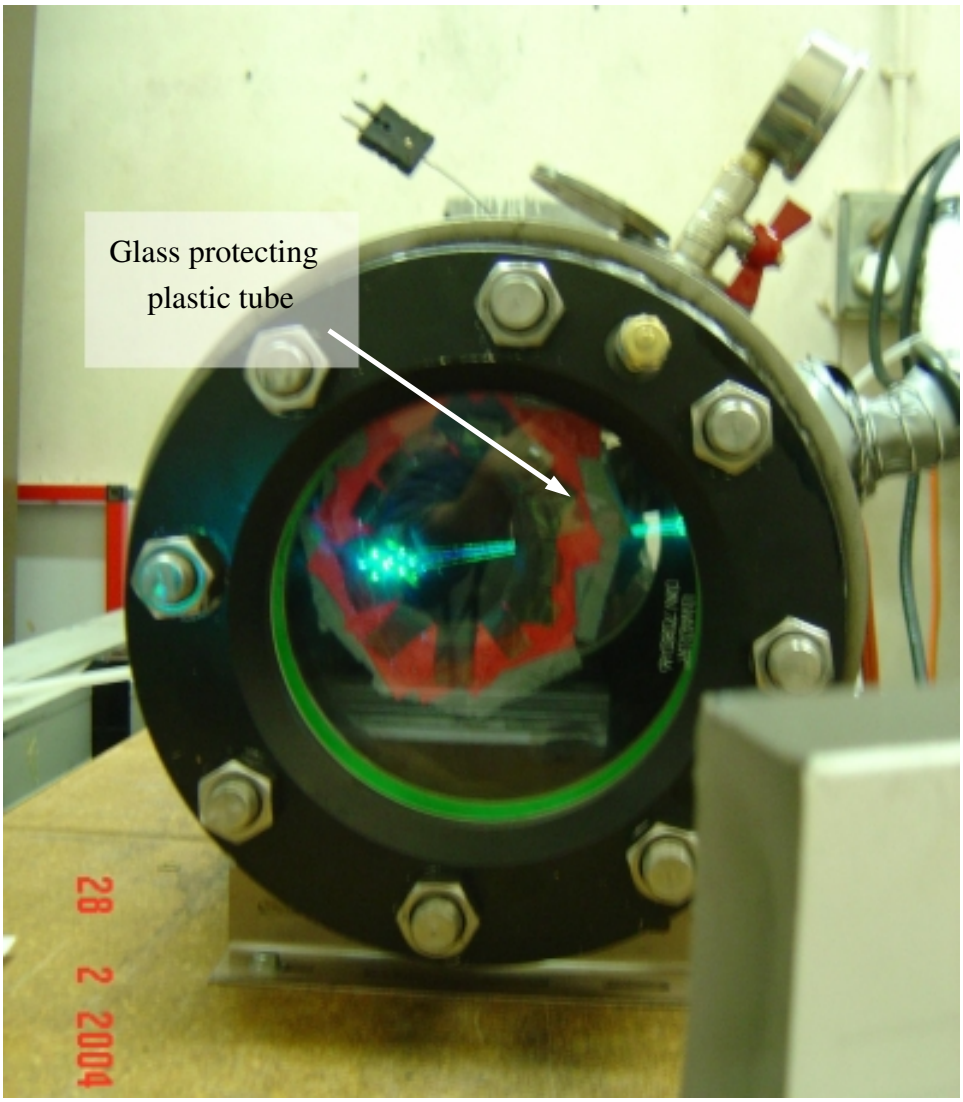

Figure 3.20: *Plastic tube converging of the "laser" path mounted on the window facing the PDA emitter.*

unit, the electronic interface (a processing unit), and computer equipped with the interface card. The optical unit accommodated the emitter and receiver optics canister attached to a mounting bridge. The bridge was a long base providing standard 450 mm distance between the emitter and receiver optics. For the receiver, the 300 mm focal length *f/7.3* lens was used and the laser beam diameter was reduced from 10 to 3 mm as it was required to work with a narrow (small) spray.

The system was fitted with the high pressure chamber to characterise the fuel sprays. Because of the generic properties of the high pressure chamber setting the unit upside down allowed to perform required test in the most desirable way. A similar approach was used by De Risi et al. [106]. A specially made stand was constructed to accommodate the Malvern instrument in upside down position. The system was levelled and positioned

to provide the best alignment. The measurements were performed on horizontal planes located at the axial distance of 40 mm from the nozzle exit to be consistent with the location of the PDA measurements. The same house-made scale that was used in PDA measurements was employed to position the laser beam at the desired distance from the nozzle exactly at the spray centreline. The laser scanned horizontally through the spray at different radial positions, from the centre to the edge of spray to find the exact centre of the spray. Figure 3.21 presents a picture of the experimental setup and other auxiliaries. Parameters and setup details of the Malvern instrument are presented in Table 3.7. The

Table 3.7: *Malvern's Spraytec instrument parameters.*

Parameter	**Value**
Light source	Laser Diode 670 nm
Laser beam diameter	10, 6 and 3 mm $1/e^2$
Measurement rate	1 to 2500 Hz (giving 1 measurement every 400 microsecond)
Concentration rate	Sprays with obscuration from 2% to 95%
Accuracy	3% (using RS-3 reference standard reticle)
Precision	0.5% (using RS-3 reference standard reticle)
Droplet size range	2.25 to 850μm

instrument was capable to work at the maximum data acquisition rate of 2500 Hz. For this work, the data acquisition rate between 1250 and 2500 Hz was chosen to measure drop size distribution of spray at 1.0 ms duration. For each test this meant that there were at least 1250 records of drop size distributions and 1250 values of drop size distribution parameters. Sampling procedure included measurement of seven consecutive injection which was similar to testing using PDA to ensure consistency of the procedure. The average drop size distribution were calculated from these seven samples.

Sampling errors associated with the Malvern measurements have different origin and have been widely discussed in [113; 114; 268]. Generally, sampling errors can be related to the measurement of a dense spray and beam wander when the instrument acquires particle sizes while the deflected mean is outside the trigger window. First source of errors was reduced by following the optimal setup suggested by the Malvern manufacturer. The second type of error was minimised by minimising the instrument response time as low as possible for the existing setup. However, it has been recognised that the conditional sampling circuitry and the Malvern electronics have finite bandwidth hence the error is unavoidable. It has been accepted that the measurements features the maximum experimental errors and precision listed in Table 3.7.

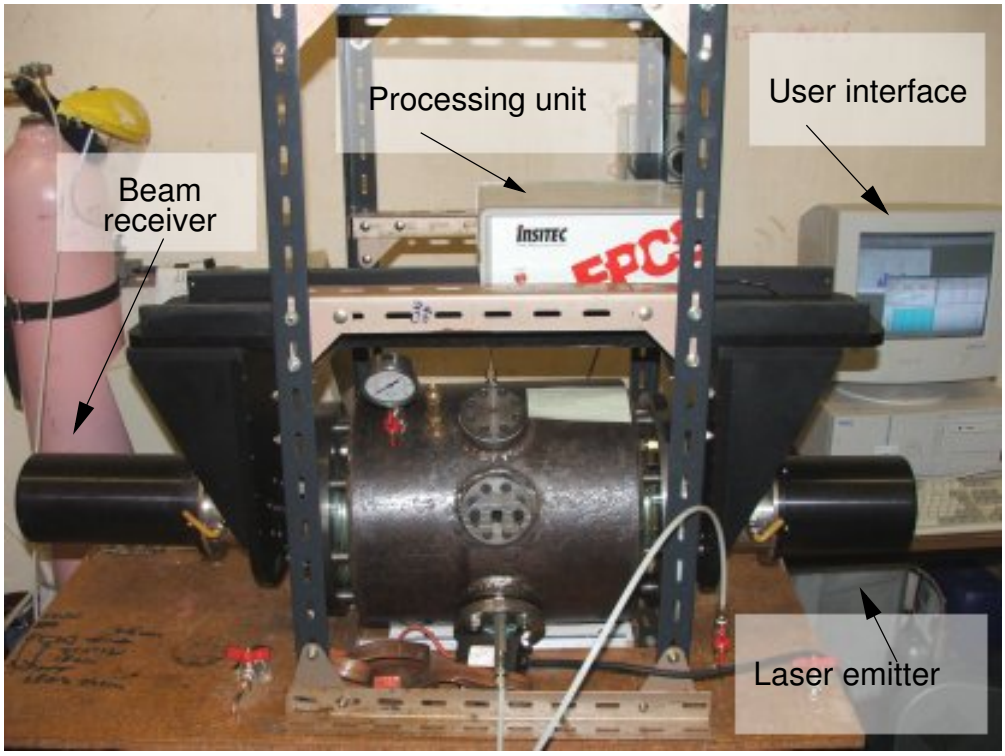

Figure 3.21: *A snapshot of the experimental setup - the instrument layout in the lab.*

3.6 Experimental setup of the AE setup

Figure 3.22 shows a typical AE acquisition system and experimental set-up used to gather AE signals from two different sources. In general the system comprised a tested source of AE signal, a set of two AE independently connected to signal preamplifiers, a data acquisition card (DAQ), and a user interface which is a computer with software for controlling the acquisition and data storage. The lab bench scale spray experiments employed a 4-channel AE system. The setups had appropriate software to control the acquisition process and record the AE signal into a file for later analysis.

3.6.1 AE sensors and sensor mounting

Each AE acquisition experiment required two AE sensors, which were selected from commercially available, broadband AE sensors. Micro-80D sensors manufactured by Physical Acoustics (PAC) were used. The sensors were able to convert detected waves propagating through the material under examination into a time varying voltage signal. The Micro-80D sensor is omnidirectional and produces a relatively flat frequency response in a range of 175 - 1000 kHz within a temperature range from -65 to +177°C.

The micro sensors are convenient in application where a small contact has to be investigated.

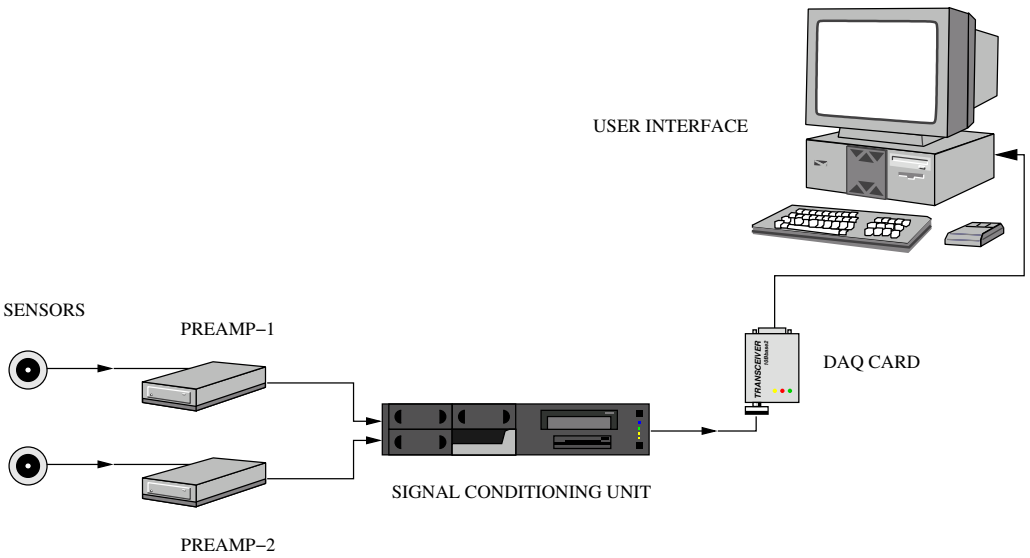

Figure 3.22: *Schematic presentation of a AE acquisition setup.*

The sensors are 10 mm in diameter and 12 mm hight and allow to be mounted on a flat surface of a limited space around. The AE senor gathering signal from the CDI injector was mounted on the injector upper body as shown in Figure 3.23.

The sensor body was secured onto the injector using a metal clamp. The second sensor was placed on the surface of the high-pressure chamber by means of a magnetic clamp. Figure 3.24 presents the location of the AE sensor mounted on the chamber shell. The surface quality is essential in order to obtain good transmission of the AE signal. Therefore, in each experiment the surface was prepared smooth and kept clean. Silicone grease was used to fill any micro gaps of surface roughness and also to eliminate air gaps. The application of the grease prevent dissipation and deterioration of AE signal transmission. The sensitivity of sensor at each mounting point was checked by breaking a pencil close to it so amplitude of the signal at each position was the same level (around 4-5 V).

3.6.2 Signal preamplifying

Raw AE signal acquired through sensors has to be “strengthen” to o a level that can be easily transmitted and converted by an Analogue to Digital Converter (ADC). Two preamplifiers of type PAC 1220A were used to amplify the AE signal before carrying it to the signal conditioning unit. The preamplifiers were equipped with a a switchable 40/60 dB gain and a built-in an internal bandpass filter capable to filter out signal in a range of 0.1-1.0 MHz. It has been found that the 40 dB gain was applicable to all investigated changes. The preamplifier was powered by a +28 V power supply and used a single BNC

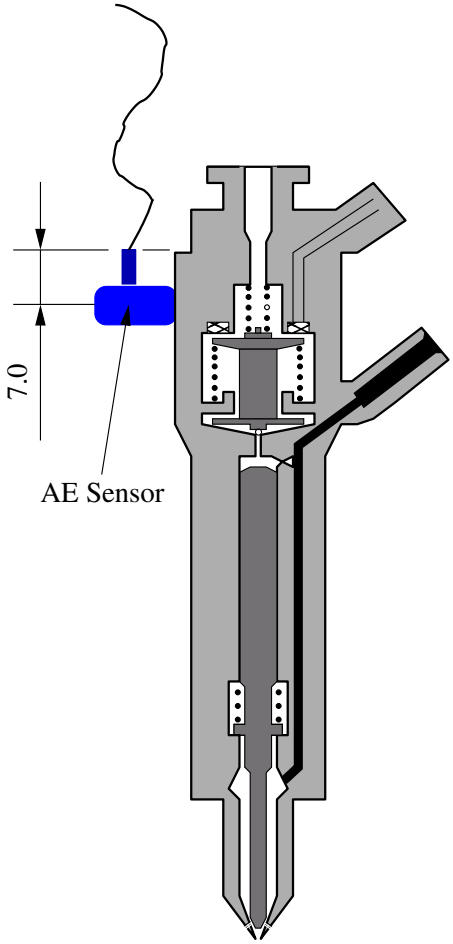

Figure 3.23: *Graphical depiction of the mounting point of the AE sensor on the injector body.*

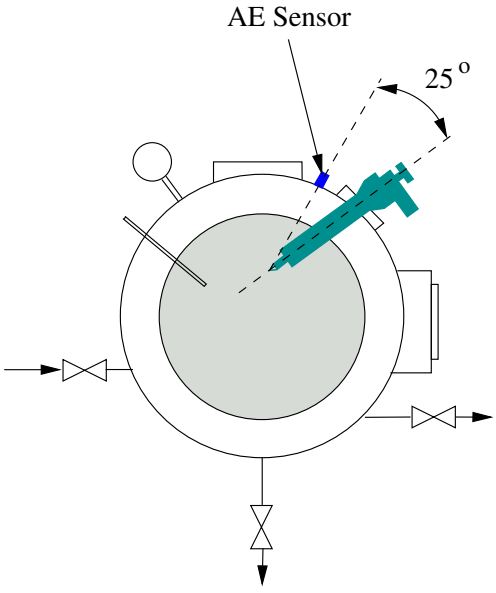

Figure 3.24: *Schematic presentation of the mounting location of the high-pressure chamber AE sensor.*

connection for both power and signal. Preamplified signals were transmitted then to the signal conditioning unit.

3.6.3 Signal conditioning unit

Signal conditioning unit was an essential part of the acquisition signal. The unit can be used to perform analogue RMS processing and it is capable to amplify or attenuate the signal if necessary. Despite a number of commercially available units, the existing system was designed and constructed at Heriot-Watt University. More details on its construction can be found in Nivesrangsan [290].
Basically, the signal conditioning unit was used to power the AE sensors and pre-amplifiers (+28 V) and allowed to work independently with a number of input AE signals.

3.6.4 Data acquisition (DAQ) unit and user interface

The Data acquisition system had a construction served by an in-house built desktop PC with a 12 bit, National Instruments (NI), PCI-6115 board placed into a PCI slot, which has a better transfer rate of data than the ISA slot. This board can acquire simultaneously the raw AE signal for 10 MHz for up to four channels and is a multi function analogue, digital and timing device. This board acquires only differential input and has an over-voltage protection at $\pm$42 V. It was equipped with on-board switches or jumpers so that it could be configured and calibrated by software. This feature provides programmable means to set up signal gain 0.2, 0.5, 1, 2, 5, 10 or 50 in an input range from $\pm$200 mV to $\pm$42 V with data sampling from 20 k samples per second up to 10 MHz at each channel. This DAQ utilised board memory of 32 MB. Two of our source location were used to record raw AE signals, sampled at 5 MHz for the lab injection experiments.

An in-house user interface (programme) based on LabVIEW software from National Instruments was used to control the PCI-6115 electronic card at its maximum performance. Parameters like sampling frequency, number of acquired data per channel, number of records, input range, pre-trigger data and trigger channel were controlled using the programme. More details on the programme and the signal gathering can be found in [290].

3.6.5 Lab AE tests of CDI injection

The main goal of the lab testwas to investigate single CDI injection at various fuel and ambient conditions. Measurements were collected to preform comparative studies between the conventional diesel fuel and RSO. One of the prime aims was to check if the AE could be used to diagnose fuel injection in CDI system. Thus the investigation also included setting up the diagnostic system and providing the best method of triggering the AE setup. The lab test focused on how the sprays develops and therefore the AE measurements were combined with simultaneous examination of spray development using a high speed camera. The details of the camera setup can be found in the previous section (3.3) describing spray characterisation techniques.

Chapter 4

Experimental methods

Quidvis recte factum auamvis humile praeclarum

This chapter consist of information on the experimental procedures and methods employed in this PhD work. Its structure follows the layout of *Chapter 3* where corresponding experimental hardware was presented. Some elements of the presentations are also related to *Chapter 2* where the background knowledge of these methods was presented.
The chapter does not include a presentation of the modelling procedures and data processing, which are relevant to spray simulation. Relevant information is presented separately in *Chapter 5*.

4.1 Experimental procedures of the preliminary injection tests

The procedure of obtaining samples of the injected oil was essentially the same for all combinations of the injection parameters i.e. injection pressure, injection frequency, duration and fuel properties. The measurements were initially performed at different frequencies and injection durations for SO and RSO as listed in Table 4.1. The ambient pressure was atmospheric and the ambient temperature was 22°C. More measurements were performed at the injection frequency of 5 Hz. This frequency was chosen as a compromise between the experimental variables and the accuracy of the measurements. It has been noted that frequencies lower than 5 Hz resulted in a very slow increase of collected amounts and therefore lower accuracy of readings and led to the noticeable overheating of the circulated oil. On the other hand, frequencies higher than 5 Hz led to excessive heat released in the injector due to on and off energising of the solenoid valve and

thus heating up of the solenoid coil. Such excessive heat release significantly contributed in the final oil temperature changing it by 3.5°C per 75 injections. Thus finally it was accepted that the later experiments would be performed at 5 Hz.

For each set of the injection, 5 consecutive measurements were taken consisting of a set of consecutive injections yielding in an oil volume of 5 ml. Prior to the measurements, the experimental system was operating to reach the desired tank oil temperature and then the injector was triggered accordingly. A first sample was taken on the average 10 minutes after starting the injection process. Collected oil amounts were measured using the glass burettes of the accuracy ± 0.5 ml. Then the samples were weighted using an electronic scale of the repeatability of ± 0.0001 g. The final, average results were calculated as the output of five measurements in grammes. After each measurement the burettes were cleaned and dried using an organic solvent and compressed air. Some of the recognised experimental errors associated with the measurement of injected oil are presented in the Table 4.2. As is it is shown in the Table 4.1, the oil temperatures is referenced to the

Table 4.1: *Experimental conditions of the injection test.*

Parameter	**Standard oil**	**Rapeseed oil**
Injection pressure, [bar]	300,500,600,800,1000	300,500,600,800,1000
Oil tank temperature[1)], [°C]	20,30,40,50,60	20,30,40,50,60
Injection frequency, [Hz]	3,5,7,10	5
Injection duration, [ms]	1,1.75,2,3	1,1.75,2,3

[1)]The effective oil temperatures in the rail were higher than these set up in the tank.

temperature in the tank, whereas the real oil temperatures should be measured in the rail. Although, it was found challenging to maintain the constant oil temperature in the rail preferably identical as in the fuel tank. Nevertheless, the results refer to the temperature readings taken at the closest point to the injector.

4.1.1 Accuracy and calibration

This section analyses sources of different experimental errors associated with the operation of the injection system together with the high pressure chamber and also describes basic oil properties. A summary of the errors associated with the use of the injection stand is presented in Table 4.2. The table includes magnitudes of the recognised errors and methods used to evaluate the accuracy values. Additionally, three separate subsections discuss the main factors influencing injection pressure, temperature and ambient pressure

control of performed experimental runs. Some of the factors influencing the accuracy of

Table 4.2: *Summary of errors including delays effecting performance of injection.*

Recognised type of error	**Error degree**	**Method of determination**
Rail pressure sensor (full-scale reading)	±2.0%	B
Electric motor speed fluctuation (idle)	±0.3%	TM
Electric motor speed fluctuation (full load)	±1.3%	TM
High pressure pump compression fluctuation	±0.2%	GM1
Pressure drop of the injector fuel line	±5.4 bar	GM2
Gas pressure in the chamber	±0.5 bar	GM3
Injection rate and duration control	±2.0%	HM+OM
Pressure drop in the fuel line in the injection quantities test	±7 bar	GM2
Temperature control in the low-pressure loop	±1.0°C	TC
Temperature control in the high-pressure loop	±3.0°C	TC
Injector temperature control	±0.1°C	instrument specification
Oil volume readings	±1 ml	instrument specification
Oil mass readings	±0.0001 g	instrument specification

measurements was evaluated separately for standard and RSO (e.g. pressure drop in the fuel line). Although, the magnitudes of these factors was marginally effected by the oil type and therefore the values of the errors are common for both types of oil and given in the Table 4.2.

Methods used to determine the errors magnitude are described below:

B - The pressure rail sensor had been calibrated by Bosch and the calibration was given in [203].

TM - A Check-Line™ manual tachometer, model MT-200 was used to test the electric motor revolutions. Reading were compared with the reading of a tachometer incorporated in the injection stand.

GM1 - An additional pressure gauge was used to test the injection pressure delivered to the rail at the fully opened rail pressure control valve and constant motor speed at 2 500 RPM. Using this setup changes in pressure produced by the high pressure pumps were measured.

GM2 - An additional pressure gauge was connected to the end of the delivery fuel line

serving the injector. Recorded pressure was compared with the reading of the pressure rail sensor to work out the pressure drop.

GM3 - An additional pressure gauge was connected to the gas outlet of the high pressure chamber. Four different pressures (of N_2 and SF_6) were tested. Recorded pressure was taken over the period of 30 minutes and compared to the reading of the pressure gauge mounted on the chamber.

HM - Accuracy of the injection frequency and duration was provided by the Hartridge Manufacturer and additionally checked using the oscilloscope (Hameg™ HM1507) for the dry and the fuelled injector. The injector load should not have a reversed effect on the Hartridge control unit, nevertheless the increased temperature of the injector body affected the injection duration. The magnitude of this influence was studied qualitatively only and a multimeter (Voltronic type VC840 MultiMate™ with enabled PC interface) controlled the accuracy of the injection signal unit between the runs.

TC - Oil temperature leaving a loop was measured using a digital thermometer and compared with the temperature reading. In case of the high pressure loop the comparison was made at constant flow from the low-pressure loop of fresh oil.

It has been also noticed a frequent "misfire" of the injector as a result of the CR Hartridge Signal Unit overload during the experimental runs. It was caused by the interaction of the unit and the injector mainly in a form of the electrical induction between the solenoid valve and the unit's sampling circuit. In a real engine, the effect is overcome by applying a filtering unit synchronised with the Electronic Control Unit which has not been employed in the Hartridge unit. An effort has been made to eliminate such unwanted unit behaviour, but a suitable solution had not been found.

Additionally an external triggering unit was applied to energise the high speed camera accordingly to a signal from the CR Hartridge Signal Unit. As it states in the camera documentation [8], a TTL[1] open collector electronic circuit can be used as a trigger, although the required current was not specified. Therefore an additional signal processor was build to tune up the trigger sensitivity and the opening drive current. To avoid recording of a misfired injection (due to random signal unit overload), a certain threshold level of these two parameters was set up. This allowed a smooth synchronisation of the signal unit and the camera at the minimum camera delay (in details described in *Section 3.3*).

[1]Transistor-Transistor Logic - a type of digital circuit in which the output is derived from two transistors.

There have been series of minor errors affecting the results which are not presented in the Table 4.2 but were recorded in sections describing other experimental methods separately and can be found there accordingly.

4.1.2 Injection pressure

The accuracy of the injection pressure was essential throughout the conducted experiments. Some sources of the experimental errors associated with the construction of the injection system was already presented in Table 4.2. Adjustment of the injection pressure during a run could not be done *ad hoc* but had to be dynamically controlled over a certain period of the experiment.

Mainly, the injection pressure was influenced by the quality of pre-pressure supply and performance of the high-pressure loop. As showed in the *Subsection 3.2.2* the injection pressure was monitored using the linear power switch combined with the digital meter (14) (in Figure 3.1) and the pre-pressure delivery by a pressure gauge (not shown in Figure 3.1). To provide a required level of oil compression the high pressure pump had to be fed with initially pressurised oil supplied by a set of pre-pressure pump. The stability of that delivery was crucial of the final injection pressure output. Since, these two pump units were working independently their control was primarily determined by the pre-pressure set. There have been some rail pressure fluctuations which were associated with a sudden deterioration of the pre-pressure pumps due to overheating. It also has to be recorded that the high pressure pump exhibited a random disruption due to overload of the electric motor. As soon as one of these two obstacles was detected an experimental run was repeated until a free of failure run had been reached.

An additional factor affecting the injection pressure and already recognised by Ahlin in [28] is pressure waves inside the rail. This phenomenon is recognised as a possible reason contributing in a significant difference of the injected fuel quantities among the injectors. Measurements in [28; 105] showed that the pressure at the injectors differ in behaviour, which may explain the varying injected amounts. Generally, the pressure in the rail can be described by superposition of many different pressure waves which cause such instability. In the present work the phenomenon was not studied but recognised as in consequence of several changes differing the injection system from the real engine (e.g. a presence only one of the injector). The pressure waves were strictly determined

by interactions between the rail and the high pressure pump subjected to the high back pressure. The maximum error associated with the fluctuation was difficult to elaborate and finally has been evaluated as $\pm 3\%$ of required pressure. It needs to be highlighted that the error was not systematic and was more apparent at higher injection pressures. It's occurrence was random and had a dynamic character.

4.1.3 Fuel temperature control

As presented above fuel temperature was altered using heating elements operating and being controlled independently. Working with oils impose a need for uniform heat distribution due to higher heat capacity and viscosity of the oils. Firstly, to ensure uniform heating of fuel and to avoid its local overheating a stirrer was incorporated in the fuel tank. Fuel temperature in the tank was altered and controlled by a heating element ((2) in Figure 3.1) and a thermocouple fitted into the tank accordingly. As far as oil heating is concerned the desired oil temperature could not be reached only by providing heat. Therefore, a cooling water coil was also fitted in the tank and working in the countercurrent mode. Due to very low oil circulation in the high pressure load a circulating loop was designed to provide higher oil turbulence. The maximum temperature error of this such arrangement was evaluated at ± 1.0°C. The rest of the temperature control points incorporated in the low-pressure loop expressed the same magnitude of errors within the working temperature range.

It is important to point out that the main source of inaccuracies of the temperature control was the excessive heat produced in the rail pressure control valve i.e. in the high pressure loop. Since, fuel was returned to the fuel tank through the fuel return line it was inevitable to absorb heat in the high pressure valve. Even, very accurate temperature control in the low-pressure loop could not prevent temperature buildup associated with the valve in the high-pressure stage. Hence, it had been evaluated that the actual fuel temperature in the system might have been different by ± 3°C from the desired ones. In addition to the heating system incorporated in the low-pressure loop a separate heating of the injector was applied. This allowed to minimise heat loses and maintain the injector body at the same temperature as oil. The temperature sensor located at the injector body was the nearest measurement point to the nozzle tip and therefore the oil temperature was

accepted as indicated by the sensor. The temperature sensor reading featured the maximum error of ± 0.1°C.

4.1.4 Spray chamber temperature and pressure control

The spray chamber was pressurised using an inert gas at constant temperature of 20°C throughout the whole set of experiments. The chamber temperature was monitored and the appropriate gas temperature was adjusted according to the temperature reading. The maximum temperature error evaluated from the heater test was ± 1°C. It needs to be noted that some contribution to the chamber temperature was made by the fuel sprayed inside the chamber. At the fuel temperature of 60°C there was a gas temperature increase by 2°C within 10 min of an experimental run. This effect was difficult to be controlled and therefore while working with the highest fuel temperature more frequent gas purge was applied.

Pressure control of the spray chamber was performed by means of a pressure regulator engaged into the cylinder gas and a pressure gauge installed on the chamber with the maximum error of ± 1 bar. To maintain the constant pressure during the experiments a gas flow across the chamber was applied so the system remained at a desired constant pressure, and the procedure was applied whereas the high injection pressures were used. At the low injection pressures, the chamber was pressurised and the gas flow was closed. Pressure drop due to leakages was negligible and resulted in 1 bar pressure drop per hr for the highest tested chamber pressure of 12 bars.

As presented in *Subsection 3.2.3.1* the high density of SF_6 does not require high ambient pressure and in comparison to real in-cylinder conditions has a different back-pressure effect. Since the in-cylinder density remains the same as for compressed air, the pressure driving force between the injection and ambient pressure is different. This can be illustrated by analysing the effect of ambient pressure on spray tip penetration employing the empirical corelation of Hiroyasu and Arai [193] as one which most studies for the prediction of spray tip penetration have introduced [200]. The tip penetration before and after the breakup time accordingly is described as follow:

$$S = 0.39 \left(\frac{2\Delta p}{\rho_l} \right)^{0.5} \tag{4.1.1}$$

and

$$S = 2.95 \left(\frac{\Delta p}{\rho_a} \right)^{0.25} (d_o t)^{0.5} \tag{4.1.2}$$

where:

S - the tip penetration, [m]

Δp - injection pressure differential, [Pa]

ρ_l - the fuel density, [kg/m^3]

ρ_a - the ambient density, [kg/m^3]

d_o - the nozzle diameter, [m]

t - time, [s]

It can be seen from the equation 4.1.1 describing penetration before the breakup time that the spray penetration using SF_6 can be higher than one at the same ambient density but using air due to bigger pressure difference. In a similar way, the spray penetration will be affected after the breakup time as it can be evaluated from the equation 4.1.2. The magnitude of this effect is presented in more details inclusively with spray penetration results.

4.1.5 Density, viscosity and surface tension measurement

Oil densities were measured with the AP Paar Digital Densimeter DMA 35 thermo-balanced with quartz tube, with accuracy of $\pm 1 \cdot 10^{-3}$ g/cm^3. A 2 ml of oil was used at appropriate temperature for density determination. The temperature of measurement was obtained by heating oil at a hot plate. Oil temperature was controlled and reported using a standard laboratory thermometer. Constant oil stirring was applied to ensure the same bulk temperature. Then an oil sample was injected into a quartz tube of the densitometer. Measurements were replicated three times and provided values varying by 2% from the mean density value.

Viscosities were determined with a Carrimed Rheometer (TA Instrument Model CDL 100) viscometer. Measurements were taken according to the method described by German and US standard. A circulating water bath was used to maintain constant experimental temperatures from 5 to 90°C with the accuracy of $\pm 0.1\%$. Viscosity tests were replicated three times and showed an average precision of 0.2%.

Surface tension of the samples was determined over the temperature range -5 to 80°C by using a torsion balance method. Measurement was performed by means of White Elec Inst. Coltd., apparatus with the accuracy of ± 0.01 mN/m. A sample of oil was poured into the flask and it was placed on the heater. Temperature was controlled in the same way as for density measurements. Then the surface test was performed and repeated three times. Results were elaborated as an average value of three experimental sets.

4.2 Experimental procedures of spray recording

A Kodak Ektapro HS Motion Analyser Model 4540mx was used to capture images of spray produced over a range of injection conditions. The system consisted of two parts: the HS Processor and Imager. Specification of the system is given in Table 4.3. A 50 mm Nikkon lense (1:1.8) type 4042514 was attached to the camera. Two other types of Kodak lenses were applied, but the Nikkor lense was finally chosen as giving the best picture quality at the widest setting range. Additionally a Cosmicar TV lens extension tube set was used to provide flexibility in focusing.

The camera is capable to acquire images at several frame rate modes listed in Table 4.3.

Table 4.3: *Specification of Kodak Ektapro HS Processor and HS Imager*

HS Processor	
Video output	NTSC or PAL compatible output
Signal input	Trigger in: BNC connector TTL level
Recording Technique	Digital images stored in Dynamic Random Access Memory
Record Rates	30,60,125,250,500,750, 1125,2250,4500(full frames per second), 9000,13500,18000,27000,40500 pictures per second
Playback rates	2,5,10,15 or 30 pictures per second (NTSC), 2,4,8,12 or 25 pic. per second (PAL) plus single step, freeze frame forward or reverse
HS Imager	
Sensor	256 x 256 pixels
Sensitivity	Equivalent to ISO 3000 at high gain settings
Gray scale	256 levels
Lens Mount	C-Mount

In modes from 30 up to 4500 frames per second (fps), recording takes place at full screen mode. Gradual increasing the frame rate leads to significant reduction of the recorded viewport and it is called the segment frame mode. For instance at 9000 fps the reduction is about 25% in the top and bottom of the image whilst at 13500 the same level of reduction is applied equally around the viewport. Also, the exposure duration is the reciprocal of the recording rate. At 4500 fps the exposure is 1/4500 seconds or 222 μs. Therefore it is required to open the aperture as the frame rate is increased. In the work aperture around 22 was set up and kept throughout the experiments.

It can be found in [53; 222; 248] that the most common framing rate starts from 4500 fps, although much lower rating can be found too, like 30 fps [195], or even a static photography (f/8.0) used by Rhim in [342]. Rapid development of the high-speed imaging techniques and their commercial availability now allows ratings between 4500 - 18000 [276] and even at 25000 fps [330]. In this work recording frame rates were adjusted to 9000 fps with progressively reduced resolution. The framing area was set as such to allow the entire injection phase to be recorded. The choice of such recording rate was made after taking into account all technical constraints of the existing experimental setup as well as minimum required number of recorded events. The same frame recording rate can be found in [423] where authors investigated split injection in similar CR system. Hentschel et al. [186] used 8000 fps and measure the diesel spray formation and penetration in a glass cylinder. More recently Lee et al. [250] used an optical system working at 9000 fps to look into the spray characteristics of alternative fuels in the CR system. Therefore it had been concluded that selection of such recording rate was reasonable for the purpose of the work.

The exposure of a single frame used in this work was 0.11 ms. Further increase of the frame rate would result in incomplete projection of spray and hence incomplete measured data. To enable a view of the development of a single spray a single source of white halogen floodlight with a diffuser was applied as described in *Section 3.3* above. A full view of the experimental setup is shown in Figure 3.14.

The recording operation was controlled manually directly from the keypad and by a trigger. An internal or an external trigger could be used to synchronise the recording with the injection event. More details about triggering the system can be found in [8]. As listed in Table 4.3 the Image Processor stores picture in the Random Access Memory and there are four modes how the data is stored there: Start, Centre, End and Random. Choosing a record mode is guided in the reference manual of the system [8]. In this work the Start mode was selected as the most appropriate for the observed injection event. The beginning of the

recording can be set up through the trigger and in this work a home made triggering system was used to initiate the recording. The trigger was energised by the injection management unit described in the Chapter *3* and connected to the HS Processor through a BNC type connector. The input was connected to an optoisolator requiring roughly 10 miliamps drive current from a 5 Volt source. The general layout of the TTL collector can be found in [8]. The trigger system was calibrated accordingly to the signal level of the injection management unit. Available memory buffer allowed to record continuously five complete injection.

Due to non-continuous manner and varying geometry of spray, keeping the spray in focus was a substantial issue. Closer analysis of the 3D presentation of a solid cone spray reveals that there are two main regions which need to be in the focus for correct spray penetration and cone angle measurement: the outer surface of a spray shape defined by a plane crossing the centreline of the spray and the spray front, which in most of the cases of real spray lies in the centreline of the spray too. The schematic presentation of a spray and its part being in the focus is presented in Figure 4.1. The easiest way to focus the camera at the plane

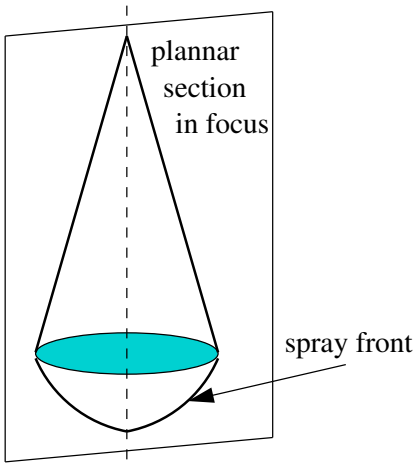

Figure 4.1: *Planar "slicing" of spray volume indicating focusing region.*

crossing spray centreline is to place a reference planar object and adjust the focus. In this case the camera was brought to focus using a specially designed nozzle sleeve. This was a piece of thin plastic, sheet, and was fixed vertically, directly below the nozzle orifice. A milimeter scale created on the surface of the sleeve helped to bring it into focus.

For calibration purpose some images of the millimeters scale (additionally to a picture of the nozzle sleeve) in focus were taken and used in further processing. The calibration was performed at the same lighting conditions and optical setup. Later, the calibration images were transferred into a computer to extract a scaling factor. A series of 7 images were

processed to get an average value of the scaling factor. However, it is inevitable not to disrupt the system and cause small dislocation between the camera and the high-pressure chamber. Therefore, the calibration was done at the same frame rate every time before the image acquisition was carried out.

4.2.1 Recording operation

Prior to spray recording the Motion Analyser needed to be calibrated. The gamma correction needed to be set to 1 and the appropriate gain was chosen. The electronics, starting with the sensor in the Imager, may cause fixed pattern noise and shading errors in the pictures seen on the monitor and then transferred into the memory buffer. These unwanted artifacts can be corrected using of the Aux Mem record modeaccording to the correction method described in [8].

The recording process followed preparation of the injection system and conditions inside the high pressure chamber. The injection management system energised the trigger which then initiated the recording process. The acquisition was terminated automatically once the memory buffer was filled with spray frames and was completed in roughly 6 seconds after triggering the Analyser. The procedure was repeated for different chamber pressures and fuel temperatures accordingly.

4.2.2 Downloading images

Once the recording process was completed whole set of recorded frames can be transferred directly onto a computer. The TIFF (Tagged Image Format File) was used to save the images. Sessions were saved in the format “S001TM.1” in case if a download was made with the ID of 1. The extension was incremented accordingly to number of recorded injections. Because the injection events were taken place in 1 Hz intervals, there was a significant time gap between collected series of frames. To avoid high consumption of storage space and also to optimise further image processing procedure only essential parts of the injection series was transferred.

4.2.3 Image processing

Determination of spray penetration and its cone angle using series of taken spray images is a procedure involving several steps. In this work home-made processing scripts were

employed to work out spray penetration and cone angle form recorded spray images.

Raw spray snapshots are not fully ready for the processing. Due to many obstacles, like light intensity distortion, droplets concentration inside the chamber, windows dirt the quality of snapshots varied. A consistent processing method which would improve the image quality in the same manner for all injection series is crucial and can affect the final result. Amongst methods of determination of spray penetration, the threshold method seems be most widely used [133; 276; 277]. As presented in [316], this method offers a high level of reliability and repeatability. It is based on image conversion from a gray scale (or colour) into highly contrasted black and white picture at a given level of intensity threshold. A converted picture can be easily used with a specialised software or numerical scripts to find out spray parameters. Most of recent processing was done in time consuming and a manual way. The main image processing was done using a bash based script and Image Magic - the image manipulation and processing Open Source package. The overall processing process is presented schematically in Figure 4.2. The processing involves five main steps starting from image correction through image processing and finally finishing off with elaboration of spray penetration (cone angle) values.

At the first stage of the processing an image correction procedure was applied. This is described in Figure 4.2 as “image correction”. This step involves a series of image adjustment procedures to correct its orientation, quality, normalise the image and finally apply a threshold conversion. Firstly, an image is rotated to obtain a vertical spray. A Image Magic build in function was used to perform such rotation. At this stage the jet orientation is not yet fully vertical and is going to be finally fixed in a later stage of image processing. In a next stage, image background and spray brightness are sampled. If the values are in ballance, i.e. there is no excessive light in comparison to the original light matrix, this step is terminated and the image processing is carried over to the next one. In case of brightness inconsistency between an existing snapshot and the matrix a correction procedure is applied. This procedure involves a numerical correction of a single pixel in the image matrix accordingly to the probing output values. The procedure mostly involves light intensity of the background rather than a spray itself. Since the light intensity had been corrected it is unlikely that parts of a spray will loose their sharpness and hence their overall quality. Therefore in the next step i.e. in “spray pixel analysis” the quality correction is applied. Numerical analysis of a snapshot provides a new pixel matrix which can be compared with the initial one and used for further corrections. The output values are sent to another processing stage called here “gamma correction”. It results in improved

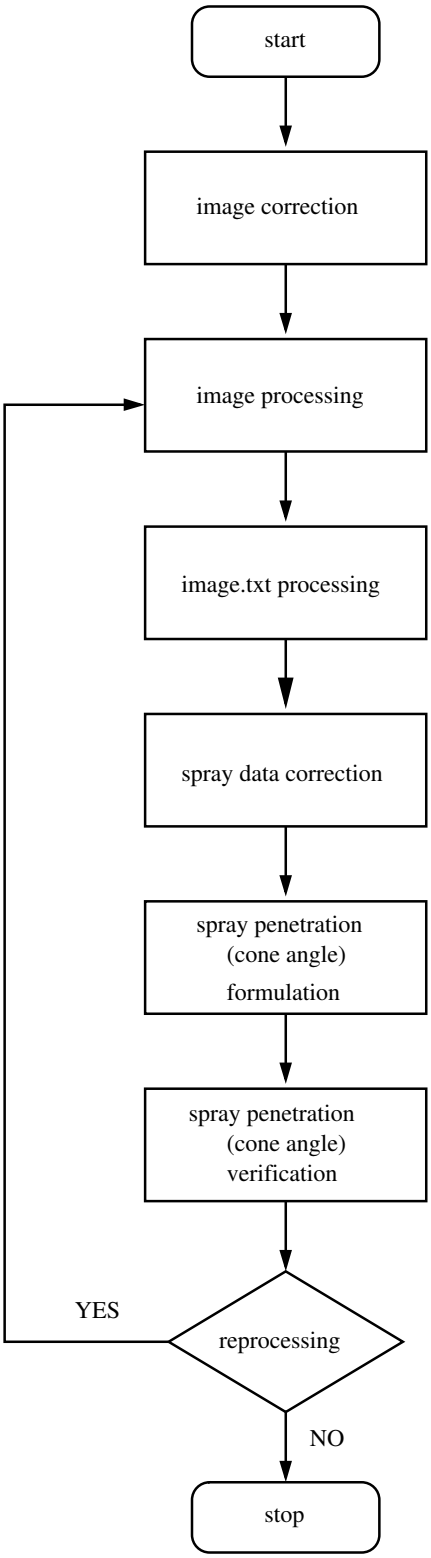

Figure 4.2: *Schema of the image processing procedure.*

image quality with already numerically enhanced light intensity. The gamma correction is based on a indication that the same colour image displayed on two different workstations may look different due to differences in the display hardware and also pixel processing. Use of gamma correction lets adjust for this quality difference and is mainly used for colour

pictures. Reasonable values extend from 0.8 to 2.3. Separate gamma values to the red, green, and blue channels of the image with a gamma value list can be applied, nevertheless in this work this method was adopted to work with grey scale images with an optimised gamma values of 1.7 (in a gray scale mode only). As there is no clear guideline for such optimisation, a trial and error method was used. Finally, utilisation of the Image Magic script performed the gamma correction. In a next and the final step of image correction

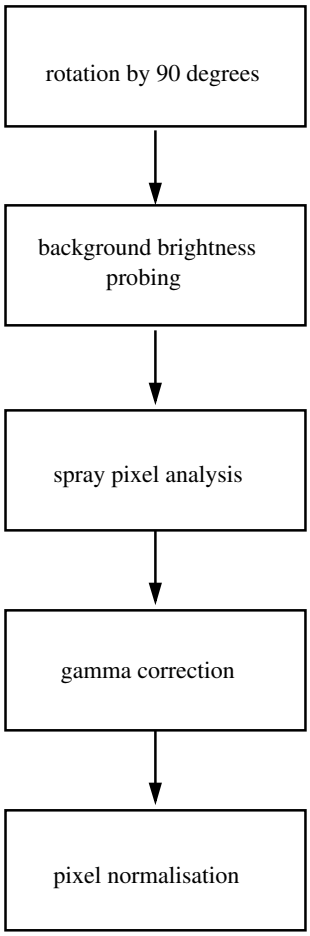

Figure 4.3: *Schematic presentation of spray penetration processing details.*

a normalisation procedure was applied. This is a contrast enhancement technique and was used to ensure the equal (normalised) contrast distribution amongst pixels as well as amongst series of images taken at varying experimental conditions. The procedure originally transforms image to span of the full range of colour values and in this case does the same to the gray scale. The process of normalising was done using a Image Magic script in combination with the convert function. Such modified image is almost ready to be transformed and used to evaluate the spray parameters.

Prior to the actual determination of spray penetration (cone angle), the image has to be thresholded. This method creates an image such that any pixel sample that is equal or

exceeds the threshold is reassigned the maximum intensity otherwise the minimum intensity. Otherwise, a black and white pixel matrix is created with equal white and black intensity. Originally, if the green or blue value is omitted, these channels (colours) use the same value as the first one provided. If all three colour values are the same, the result is a bi-level image which was utilised in this work. If the opacity threshold is omitted, OpaqueOpacity (a default variable of Image Magic) is used and any partially transparent pixel will become fully transparent. Such transformation is applied to produce a spray picture of high contrast and therefore excellent sharpness. This makes any further processing steps easier and eliminate risk of measurement inconsistency. The final output of the image correction (a thresholded picture) is highly dependent on each step of the process and requires very careful snapshot analysis and choice of processing values. Some of the aspects of this are discussed in the *Subsection 4.2.5*. Figure 4.3 and 4.4 present graphically summary of the flowpath of image processing to obtain values of spray penetration and cone angle.

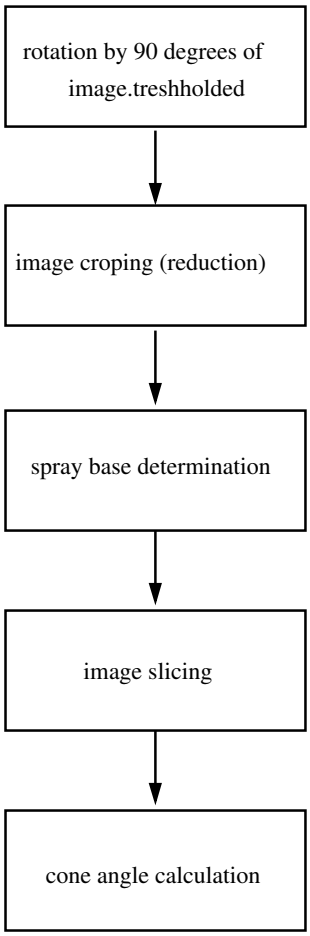

Figure 4.4: *Schematic presentation of spray cone angle processing.*

4.2.4 Cone angle evaluation

The cone angle evaluation is a more demanding. In general, the spray cone angle has been defined at $60d_o$ (hole diameter) and frequently it is referred to as "the far spray angle". Some variations from these values can be found in the literature and are imposed in applications of non-diesel fuels [200]. However, in majority of works the cone angles are obtained by measuring the angle formed by two straight lines drawn from the nozzle tip to the outer edge of the spray. The edge of the spray is defined as the border outside which can be detected by an user defined processing method. The same approach was used in this work using a combination of image processing scripts and manual checking/correction. The threshold level that is related to the transmittance of the illuminating light is used to separate spray area from the background in the raw images. For instance, Tennison et at. [396], Payri [316] and Chiu [89] accepted the local transmittance of the image greater than 95% as a factor defining the outer edge of the spray, but also defined a constant distance from the injector tip where the cone angle was measured. The edge of diesel sprays was also defined 80% [101; 200] transmittance in the measurement of spray angle. Such approach seems be reasonable however, the cone angle tends to vary throughout the injection event due to the transient nature of the spray. Hence, some authors present an average value of a cone angle rather than a local one.

Morgan and coworkers [277] used a modified method described by Naber and Sieberts [283] to calculate the diesel spray cone angle even if the tip of the nozzle was not visually accessible and the beginning of the injection could not be observed. Firstly, the maximum spray penetration was calculated by finding the spray pixel furtherest from the nozzle and then this value of penetration was used to calculate the spray angle at half the maximum penetration length. Although Morgan's method provide consistent results. It can be questioned due to non-conical shape of the spray in the longitudinal direction. A half of the maximum penetration length may correspond to the local, lower value of the cone angle.

In case of non-diesel fuel spray injected at various ambient pressures the defined angle are not appropriate due to a small curvature of the spray. This causes problem with establishing two lines to define the spray angle following the spray boundary. The problem has been identified by Yu and Bae in [427] and [428]. A similar situation was found in the present work for RSO spray. Nevertheless, a consistent method of analysing the spray cone angle had to be developed both for standard and RSO.

It needs to be highlighted that measurement of the cone angle is particularly challenging

in the denser in-cylinder atmosphere which readily promotes enhanced turbulence at the spray boundaries.

4.2.5 Accuracy and errors

Accuracy of the high-speed camera test derives directly from the efficiency of the whole experimental setup. Sources of the experimental errors have been listed in *Section 4.1.1* already and here the uncertainty associated with the actual recording process is discussed. The exposure of a single frame was 0.11 ms resulting in an uncertainty due to spray development during the exposure of ± 3 mm (this would be the maximum error associated with the calculated length of spray). The error had been evaluated by analysis series of the same injection taken in 10 consecutive tests at the same time interval. It was found that during the early stages of injection the spray penetration may yield in a length of maximum 3 mm. The injection pulse sent from the injector activator triggered off the camera and it was found out that the pulse delay associated with the triggering device was negligible in comparison to the velocity of the fastest developing spray.

4.2.6 Data reliability

From the detailed analysis of the literature review presented at the beginning of this thesis it can be concluded that many of the experiments studying spray characteristics had been undertaken using specially manufactured or modified CR nozzles. Some of these nozzles were the commercial types proceeding a developing stage [236; 396; 426] or the commercially available but specially modified to facilitate spray data gathering [249; 349; 432]. Often this indicates use of a special single orifice nozzle (non-commercially available [68], or that all bores but one orifice discharge was captured. In the last case a measurement was performed on one particular hole and therefore validity of such experiments could be questioned according to [105]. Furthermore, the vast majority of published data were collected at various nozzle geometry and types, i.e. sac-hole or seat-hole nozzle, different spray-cone offset angles, a cone type, a bore diameters and L/D ratio. Frequently nozzle information is not given or incomplete to perform a meaningful comparison. Details like the way how a nozzle was manufactured or weather had been used in an engine or not are greatly important. Summing these up, information available in the literature does not provide an easy base for comparison and validation.

Despite the difficulties in finding data collected at the same conditions, a brief comparison

of selected data has been performed. Figure 4.5 shows four different cases of injection and ambient conditions, corresponding experimental data and data collected by other researchers facilitating the most resemble CR system to the one used in this project. Summary of the cases is given in Table 4.4 and details presented below. The selected literature results were compared with SO injected at 25°C for 1.0 ms using the injector described in *Chapter 3*. The oil density was 841.3 kg/m^3. It should be highlighted that the injector used in this work had been already used in a CR engine for a significant period of time to accommodate deposit and experience a certain level of wear between the needle and the injector tip seat. It is assumed that all nozzles used in test showd in Table 4.4 were new and not used in engines before.

Table 4.4: *Injection conditions for various experimental data used in comparison.*

	Reference	**Injection pressure [MPs]**	**Ambient density [kg/m^3]**	**Nozzle diam/type**
Case 1:	Pastor et al. [309]	120.0	$\sim$28.0	-
p_{inj}=112.5MPa	Kennaird et al. [219]	100.0	28.0	0.2mm, VCO
ρ_{amb}=30.0 kg/m^3	Laguitton et al. [241]	100.0	30.0	0.2mm, L/D=5
Case 2:	Morgan et al. [276]	60.0	15.0	0.2mm, VCO
p_{inj}=56.25MPa	Yeom et al. [426]	72.0	12.3	0.2mm, DLL-p
ρ_{amb}=15.0 kg/m^3				
Case 3:	Kennaird et al. [219]	100.0	49.0	0.2mm, VCO
p_{inj}=112.5MPa				
ρ_{amb}=45.0kg/m^3				
Case 4:	Rotondi et al. [349]	70.0	1.2	0.18mm,VCO
p_{inj}=75.0MPa	Kurachi et al. [236]	50.0	$\sim$1.2	0.16mm, UMS
ρ_{amb}=1.2kg/m^3				

Case 1: Penetration of SO injected at 112.5 MPa and into 5.0 bars of SF_6 (ρ_{amb}=30.0 kg/m^3) was compared with data of Pastor et al. [309], Kennaird et al. [219] and Laguitton et al. [241]. In all literature cases, a similar nozzle type was applied. Pastor performed their experiments in very similar ambient conditions using SF_6 gas which produced an in-cylinder density of 28.0 kg/m^3. The penetration results were gathered at higher injection pressure and unknown fuel temperature or density. The injector was a modified single hole type and more details were not provided. In the work of Kennaird the diesel fuel of density ρ_f=840.0 kg/m^3 was injected into compressed air at minimum temperature of 297°C.

The injection pressure of 100 MPa was lower from that which SO was subjected to. The injection duration was about 3.41 ms. Laguitton utilised the same injection pressure but the diesel fuel was injected into denser ambient conditions at temperature higher than 277°C for 3.1 ms. The comparison of penetration curves is presented in Figure 4.5(a). From the figure it can be seen that results of Kennaird and Laguitton are very close and different from these of Pastor and SO. The SO penetration shows lower penetration results and a very similar trend. The SO results were recorded at different time reference point, i.e. from the time when the injector was triggered and includes the injection hesitation. Although, the results of Kennaird and Laguitton start from t=0 which indicates a different time reference point . It can be clearly seen that if the injection hesitation was subtracted form the injection time, the SO curve would much closer to these of Kennaird and Laguitton. It should to be noted that higher in-cylinder temperature readily effect the penetration too. A certain degree of similarity between the results of Pastor and SO can be expected. The results become similar 1.5 ms after triggering the injector. However, the more detailed analysis is difficult since the nozzle geometry and fuel properties are not known. ***Case 2:*** Two literature sets of data were compared with SO injected at 56.25 MPa and 2.5 bars of SF_6 (ρ_{amb}=15.0 kg/m^3). Morgan et al. [276] performed the spray characteristics experiments using a VCO injector to atomise diesel of density ρ_f=840.0 kg/m^3 into compressed air of 15.0 kg/m^3. The injection took place at higher ambient temperature of 297.0°C. The injection conditions were very similar to these applied by Kennaird et al. [219]. The second set of data provided by Yeom et al. [426] were collected for spray atomisation at 72.0 MPa into compressed air featured by a density of 12.3 kg/m^3. As it can be seen from Figure 4.5(b) the experimental results of SO perfectly match the data of Morgan. Both experiments were performed at nearly the same conditions varying in a nozzle type and ambient gas. It could be expected that results of Yeom would resemble the SO and Morgan's because of similarities in the injection pressure and ambient conditions. It seems to be more apparent that a type of the nozzle may influence the penetration. This case is a common example of lack of consistency amongst spray characteristics data collected even at similar injection conditions.

Case 3: In this case penetration of SO injected at 112.5 MPa into a dense SF_6 atmosphere (ρ_{amb}=45.0 kg/m^3) is compared with results of Kennaird et al. [219]. The literature penetration was gathered at the injection pressure of 100.0 MPa and the ambient density of ρ_{amb}=49.0 kg/m^3. The fuel properties and the ambient temperature were similar to

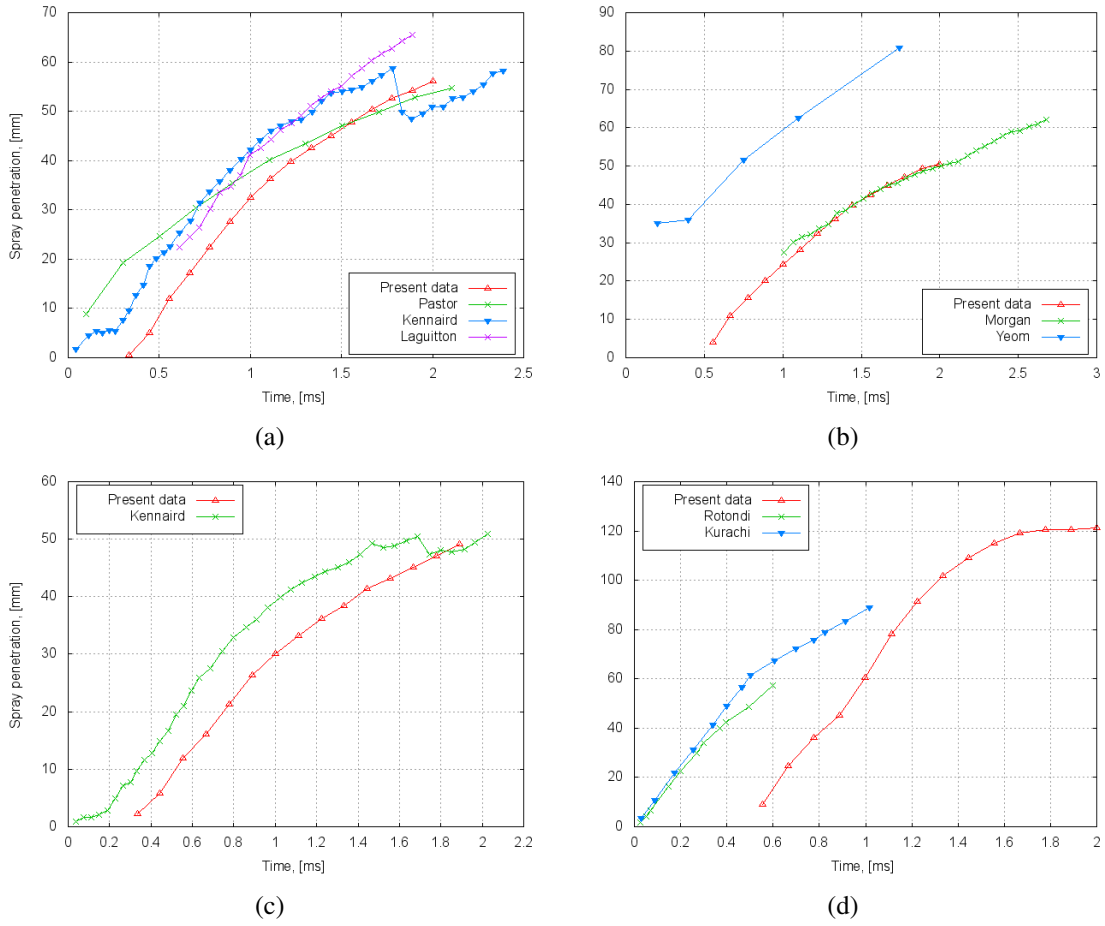

Figure 4.5: *Comparison of penetration between selected experiments of SO and various literature data. (a) Case 1: p_{inj}=112.5MPa, ρ_{amb}=30.0 kg/m^3; (b) Case 2: Case 2 p_{inj}= 56.25MPa, ρ_{amb}=15 kg/m^3; Case 3: p_{inj}=112.5 MPa, ρ_{amb}=45kg/m^3; Case 4: p_{inj}=75.0 MPa, ρ_{amb}=1.2 kg/m^3.*

these presented in *Case 1*. The difference between two penetration curves is presented in Figure 4.5(c). Similar to the *Case 1*, the penetration curves exhibit identical trend but the results of SO show an injection delay. Hence, the same discussion like in the *Case 1* can be carried. An average deviation between these two sets is 30% and more apparent in the middle of the penetration period.

Case 4: Results of spray penetration at 75.0 MPa into nitrogen is presented in Figure 4.5(d) together with the results of Rotondi et al. [349] and Kurachi et al. [236]. Both authors used nearly the same injector type, the diesel fuel and the same ambient conditions identical to the experiment of SO (ρ_{amb}=1.2 kg/m^3). Rotondi conducted the experiment for density of 821.0 kg/m^3 and kinematic viscosity 3.188 mm^2/s. The actual injection duration was four times higher than used for SO. In the work of Kurachi, a single hole nozzle accommodating diesel was applied but more detailed information were not given. Form Figure 4.5(d), a noticeable difference can be seen between the literature and the experiment.

The SO curve is time shifted regardless similar penetration values (the tip penetration distance). Such difference can be explained by higher hesitation in the experiment and differences in nozzles and the injection duration. In general, injection characteristics at ambient conditions (ρ_{amb}=1.2 kg/m^3) were found problematic in terms of spray development and its acquisition. Such low ambient density conditions result in the reduced shear forces and uncertainties in evaluating a correct spray front penetrating the injection vessel. Some of these problems were encountered by other researcher but unfortunately not recorded in the literature.

From the above it can be concluded that the experimental data for SO follow the expected trend of the penetration characteristics. The injections took place within the same time scale, and despite a spray hesitation, can be used to compare the spray penetration at different injection and ambient conditions. The comparison with the literature shows differences in the absolute values of penetration in some cases and can be explained by the different injection and ambient conditions as well as differences in injectors. It is concluded that the spray development characteristics carried out for RSO will follow the same trend and could have been validated if the appropriate data had been available.

4.3 Experimental procedures of spray sizing

This section jointly present the experimental methods of Phase Doppler Anemometry and Malvern sizing. Section mainly focussing on PDA procedures because PDA was used as a prime method to size sprays, whereas Malver provided and additional mean to check up results. Also, the Malver setup and methods are less complicated and more straightforward in comparison to PDA. It is recognised that PDA setup is specific to the application and required careful adjustment for each type of measurement.

4.3.1 Tuning and calibration of PDA

It is recognised two pairs (two green and two blue) of crossing beams should emerge from the front lens of the transmitting optics to create the microstructure of fringes (see Figure 2.10). Measurement tests were performed in a close vessel therefore beam alignment had to be corrected due to refraction. The refraction effect changed direction of the laser beams hence the original beam positioning has to be readjusted.
Fine adjustment of the beam crossing was made by adjusting the micrometer screws of the probe support mounted on the traverse arm. It was found that the beam crossing alignment tended to get dislocated and the alignment had to be checked prior to each test and readjusted if required. Figure 4.6 presents a picture of the beam crossing looking into the eyepiece of the PDA probe in a chamber right after a RSO measurement. Prior to

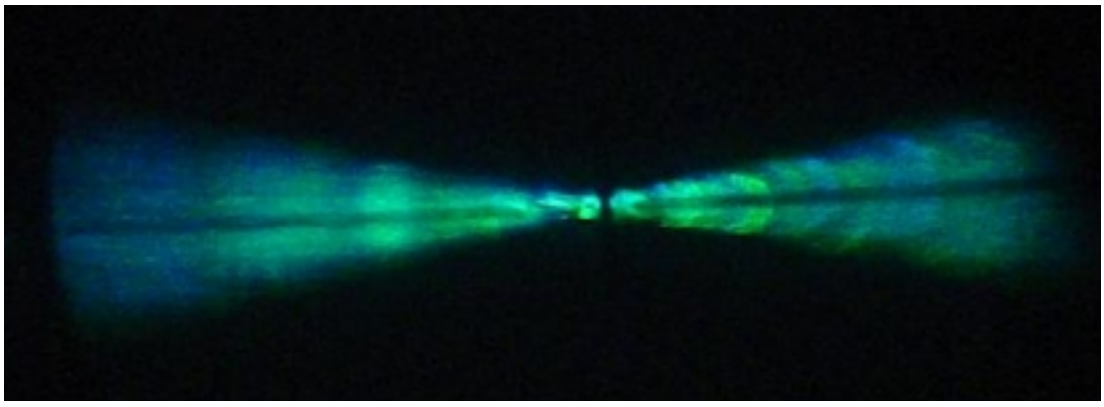

Figure 4.6: *The focusing of the beam crossing through the view port of the PDA probe.*

the spray measurements the system required calibration to chose suitable photomultiplier (PMT) voltage. The SIZEware programme provides the high voltage setup to control simultaneously the value of the PMT tube voltages. The range of PMT voltage (typical value: 800 and 1600 V) was scanned. The Doppler monitor outputs were used for

monitoring the signals on an oscilloscope during final alignment and for judging the quality of the Doppler burst. Additionally for each adjustment drop mean diameter was recored and compared. Additionally, the number of successful measurements (without signal saturation) for each seat of PMT voltage was recorded and analysed. The sensitivity of the PMT was finally set to 1000 V whereas the voltage for successful completion of the test varied between 900 V and 1200 V. Randomly at 1000 V the PDA signal got saturated and it was necessary to re-stabilise the PMT.
Figure 4.7 presents the effect of the PMT voltage on mean droplet diameter. It can bee seen that the increasing of the PMT voltage leads to relatively stable droplet diameter. The PMT voltage was selected to maximise the data acquisition but also to avoid signal saturation. The final voltage of 1000 V was chosen as the best fit between the droplet acquisition and the count of successful measurements. The last parameter is depicted in Figure 4.7 and describes the percentage of PDA runs fulfilling the following criteria of featuring a run:

1. The lack of signal saturation
2. The number of drops in a population greater then 2000
3. Droplet diameter differ by a maximum $\pm 10\%$ of standard deviation for the overall value for all ten runs for a selected injection conditions

The presented criteria were derived from the experimental experience of the author as well as from problems reported already by De Risi [106], who investigated diesel spray produced by a CR system. The fine tuning of the PMT‘s was performed for SO and for a reason of consistency was carried over to RSO measurements. It has to be noted that the quality of RSO signal was deteriorated in comparison to the signal produced during SO experiments.

4.3.2 Data processing of PDA results

PDA measurements were gathered by the Dantec SIZEware software. In the first step stored, raw binary data was reorganised to the converted binary form, which included only validated data. In the second step the converted binary data was exported. All sizing tests were performed using two dimensional PDA setup, whereas the raw data processing was carried out with 1D configuration. A similar approach was described in the method applied to a dense CR spray analysis performed by Doudou [118] and Lacoste et al. [240].
The final result presentation was based on the average drop population derived from the

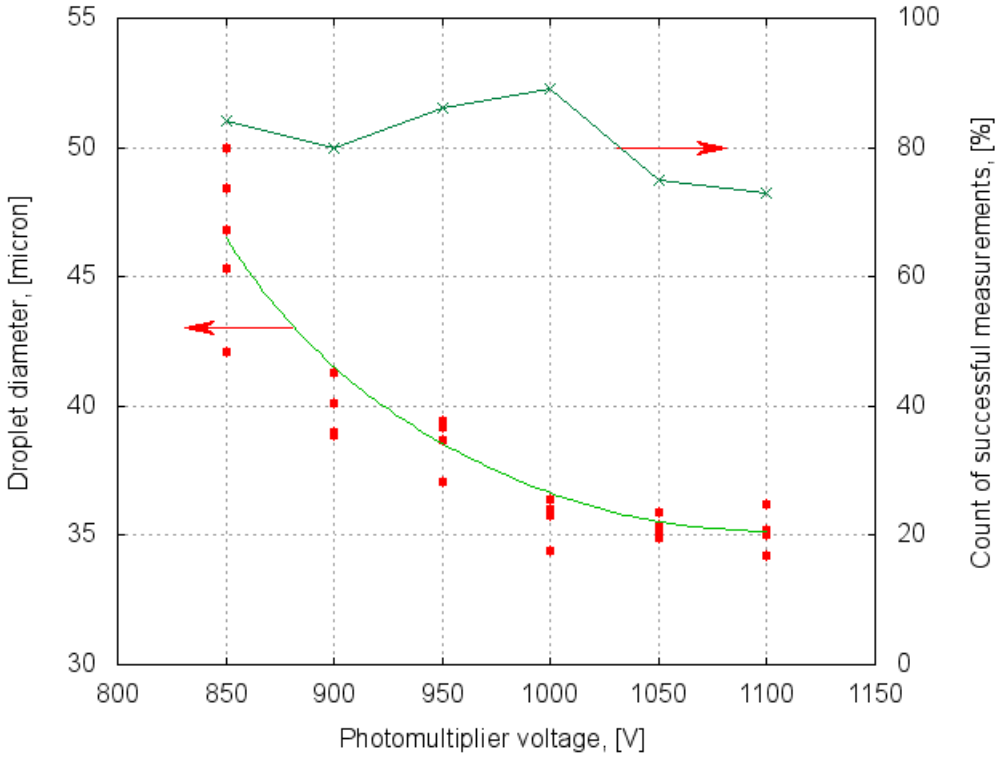

Figure 4.7: *Variation of the mean Sauter SO droplet diameter with the photomultiplier voltage.*

processed raw output data of 21 injections. A statistical filter was established to separate abnormal drop sizes to improve data reliability. The filter was build based on statistical analysis of drop populations fitting into the Gaussian distribution. It has been accepted that drop larger than 3σ+mean (σ: the standard deviation) and of lower attendance than 2 % in a population were rejected. A similar approach has been reported by Lacoste et al. [239]. Filtered drop populations were processed using user made scripts to obtain arithmetic, Sauter, and De Broukere mean diameters as well as an average droplet velocity of SO and RSO. The three types of mean diameters are briefly described below.

Arithmetic mean diameter, D_{10} - The simple average diameter of all the droplets in a spray. D_{10} is equal to the sum of the diameter of all the droplets divided by the quantity of droplets and used mainly for comparison:

$$D_{10} = \frac{\sum_{i=1}^{n} N_i d_i}{\sum_{i=1}^{n} N_i} \tag{4.3.1}$$

Sauter mean diameter, D_{32} - This diameter is calculated using the concept of the volume to surface area ratio. It is equal to the sum of the cube of all diameters divided by the sum of the square of all diameters. This yields a characteristic droplet diameter that

has a volume-to-surface-area ratio equal to the volume-to-surface-area ratio of the entire spray. This diameter is particularly important in engine applications because the mass transfer happens at the interface of the droplets and the surrounding air i.e., at the droplet surface. To enhance the evaporation of a population of droplets, one has to maximise the active surface areas and minimise the internal volumes. D_{32} is used to describe a droplet population in terms of its combustion and mass transfer features:

$$D_{32} = \frac{\sum_{i=1}^{n} N_i d_i^3}{\sum_{i=1}^{n} N_i d_i^2} \tag{4.3.2}$$

De Brouckere or Harden's mean diameter, D_{43} - a term used to relate mean diameter to combustion and equilibrium, which corresponds to the centre of gravity of the volume (mass, if the density is constant) distribution:

$$D_{43} = \frac{\sum_{i=1}^{n} N_i d_i^4}{\sum_{i=1}^{n} N_i d_i^3} \tag{4.3.3}$$

where:
N_i is thus the number of droplets in a bin; d_i is the middle diameter of its size range.

4.3.3 Spray symmetry

Once the PDA setup is ready for measurement and a location of the measuring volume is fixed it is important to verify the spray symmetry. Contrary to the expectation that the spray should exhibit high degree of symmetry, it has been found that the spray may have rather unsymmetrical nature. Spray asymmetry as well as the hole-to-hole variations have been described and investigated already by De Risi et al. [105]. Thy provided some useful information to design a spray experiment. The assessment of spray asymmetry can be made after finding the spray centreline through velocity profile measurement. Several SO sprays were experimental tested. Figure 4.8 indicates spray deformation (an example) as the radial velocity of the recorded spray is not symmetrical. Hence, it is expected that the spray characterisation could be done only on one side it becomes clear that its radial scanning (measurements on both sides of the centreline) should be taken into account. In this work it has been assumed that spray sizing method should be performed on both sides of the spray at the same distance from the nozzle tip and then the results should be averaged. It has to be noted that the measurement should be performed for each pair instantaneously for the best representation, however such approach is practically infeasible. Performing the

sizing in two separate measurements requires a sufficient number of measurements to be statistically representing. It has been achieved by repeating measurements at least 5 times.

It has to be highlighted that the practice of spray sizing is even more complicated. Spray to spray repeatability is frequently not maintained as it was observed that the spray shape is changing from injection to injection.

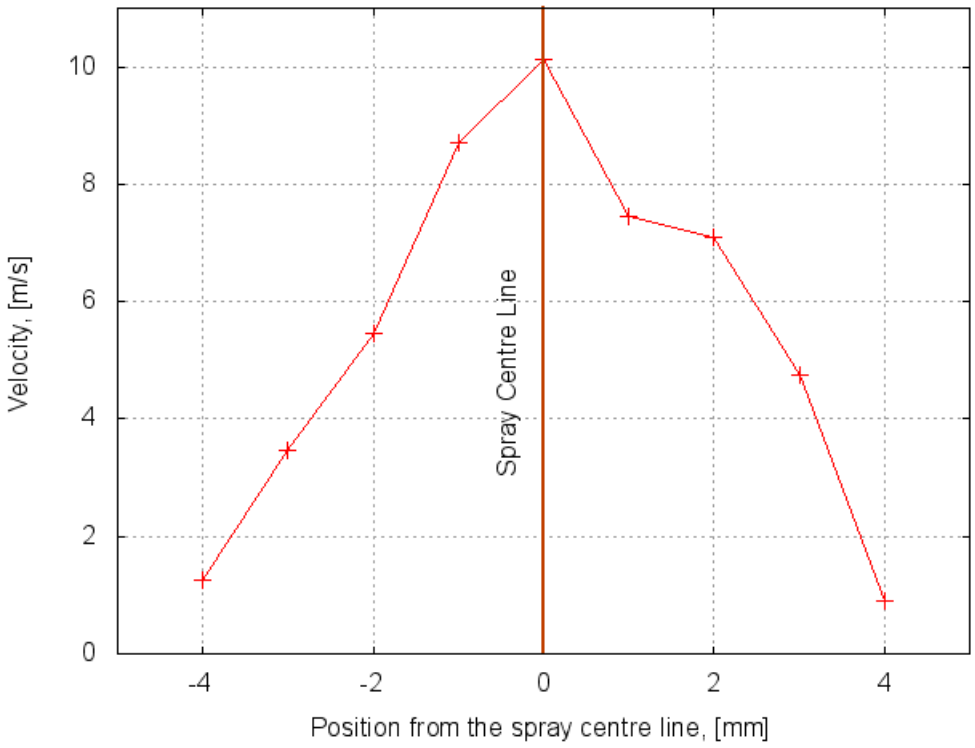

Figure 4.8: *Presentation of the radial profile of the spray velocity.*

4.3.4 Accuracy and errors of the PDA tests

The PDA system include a fragile and sensitive opto-mechanical assembly. The size measurement range and accuracy depends on numerous optical factors and on certain input parameters that are specified by the user. Accuracy of the measurements is deeply affected by the laser setup but it can change during a test due to many factors. For a type of spray and ambient conditions there is a limited level of validation and data rate. It has been accepted that PDA measurements might feature uncertainties up to 15% due to fluctuations of the intensity and the temporal changes of the droplet surface area [1; 177; 179]. However, it is expected that the final uncertainties are lower (around 8%) and constant. Table 4.5 presents measurement ranges and accuracy at system level.

In this part of the experimental work two types of oils were investigated. The accuracy and errors sources are evaluated separately for each of them. This is due to different physical properties of the oils resulting in variation of spray density as well as due to different atomisation mechanism. The sprays of the both oils exhibit the typical range of problems associated with measurement of the dense spray. However, it can be concluded that the measurement of RSO spray is particularly difficult. It results in lower validation by about 10% on average in terms of sphericity. In the present work the minimum validation for SO droplet was found to be $\sim$86% $\sim$48% for RSO. It was noticed that the validation level increased with rising ambient pressure and oil temperature. The measurements employing the atmospheric conditions were characterised by the lowest validation.

Sine, the PDA alignment relies on the hardware setup, it is essential to position the measuring volume exactly at the point of required measurement, otherwise measurements will be subjected to much higher level of uncertainty and lack of repeatability. This was done by means of the traversing system operating in the X, Y and Z directions. The replacement in the 3D direction was controlled by a metal scale attached to each arm of the traversing system. The maximum error of the arm shift was estimated to be at $\pm$0.5 mm. As shown in Figure 4.6, the beam crossing on the middle of the slit is essential for measuring. Despite the system had been mounted on a rigid traverse system, which should have ensured its stability, some distortion of the system were noticed from time to time. This resulted in a sudden drop of validation and poor acquisition. To eliminate disfocussing, when happened the beam crossing alinement was immediately checked prior to each measurement. It has been estimated that the maximum inaccuracy error of positioning due to a random distortion of the traverse system could reach $\pm$1 mm. A typical

Table 4.5: *Measurement range and accuracy at system level*

Recognised parameter	**Magnitude**
Diameter range	0.5-13 mm
Diameter range accuracy	$\pm$0.5%$\div\pm$1%
Diameter range resolution	8 bit=1.41°
Dynamic range	1:40
Maximum velocity. [m/s]	470
Velocity accuracy	$\pm$0.5%
Velocity resolution	0.03%

injection signal presenting the instantaneous droplet velocities is shown in Figure 4.9. It

can be seen that PDA detection collects droplets of arrival time and velocity not only during the injection but also after the injection pulse. The figure indicates the presence of drops collected after the scavenging process and those of "satellite drops" in the chamber. Such droplet residue is carried over from one injection onto another as a result of gas motion caused by spray, which also forms a "tail" consisting of slow motion floating droplets. The occurrence is similar to the findings reported in [240] and [239]. The presence of the residual drops can be excluded by applying a "windowing" procedure if a triggering time is known. However the expulsion of drops close to the injection pulse is difficult. In the present results only the "satellite drops" have been removed from the final distribution sets. It needs to be highlighted that the RSO measurements could be effected by a number of "abnormally large" drops present especially close to the measuring point. This might lead to the higher number of large drops present in nearly each drop population. In general the RSO drop population consisted of a significant number of larger drops within a range of 60-100 μm in comparison to the expected diesel spray. Contribution of these large drops in values of D_{32} and D_{43} is significant. Thus the increased number of small drops does not result in reduced values of mean drop diameters since the noticeable number of large drops are present in the population. However, an earlier study [240] indicates the presence of droplet diameters of a diesel fuel as large as 500 μm for much lower injection pressures. It needs to be stressed that measurements of dense sprays of RSO remains very difficult.

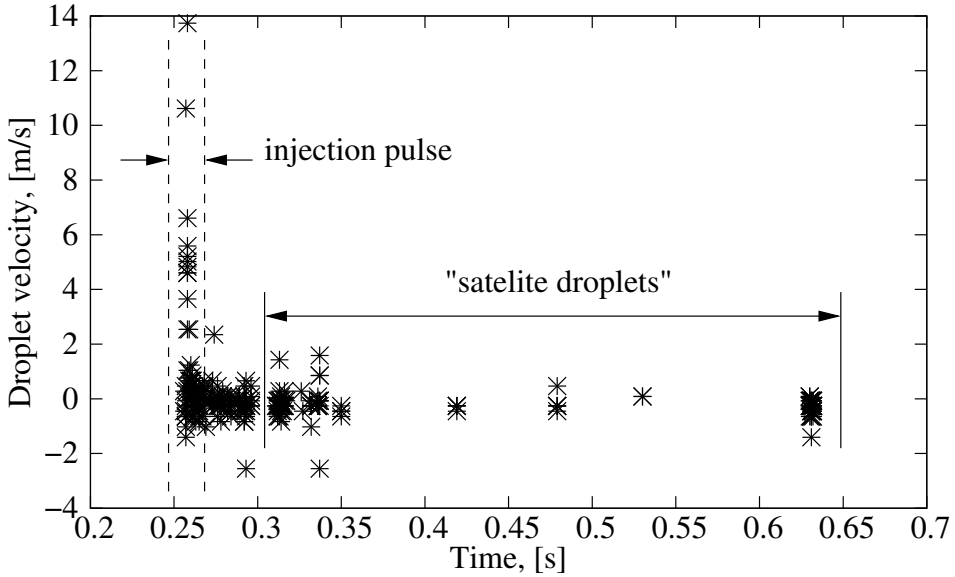

Figure 4.9: *Presentation of the axial droplet spray velocity component (U) with the acquisition time.*

Reduction of some errors is highly demanding and some of them are even unavoidable. Nevertheless, the PDA measurements can provide essential information about RSO spray

and a good starting point for further studies. Concerning the experimental errors and the equipment capability in observing dense sprays, the PDA results have been verified against those from the laser diffraction technique.

4.3.5 Experimental conditions and data processing of the Malvern tests

In this part of study, sprays of RSO were investigated using the fuel injection system described in *Section 3.2 and 3.3*. RSO was maintained at 40°C throughout the test. The experimental procedure involving chamber pressurising and producing a desired injection pressure was identical with that presented in *Section 4.1* for spray penetration and in the section describing PDA measurements (*Section 3.4*).

It has to be highlighted that running the Malvern instrument at desired experimental conditions was less demanding then the PDA unit and the measurements were relatively more straightforward. Although it has been accepted that measurements of the intensity of scattered light to determine drop size does not require calibration, as it is inherently calibrated from basics diffraction principles without resorting to a reference standard [113], the instrument has been checked and the calibration according to the manufacturer had been performed. Prior to each measurement the background and noise sampling were performed. Details of the experimental runs are presented in Table 4.6. For each set of

Table 4.6: *Ambient and injection condition of Malvern RSO test.*

	Rapeseed oil
Injection pressure [MPa]	37.5, 56.3, 75.0, 93.8, 112.5, 131.3
Oil temperature [°C]	40
Ambient density [kg/m^3]	15, 30, 45
Injection frequency, [Hz]	1.0
Injection duration, [ms]	1.0

experimental conditions approximately 7 or more injections were collected. The data raw was was initially processed using the Insitec software, which automatically averaged the data and performed the statistical analysis. Then, results were plotted and manually checked for any abnormal measurements or errors.

4.4 Experimental procedure of AE tests

It is essential to ensure that signals gathered have been properly post processed and interpreted. Utilisation of the AE technique implies that its users must utilise appropriate signal processing techniques. Signal analysis of AE data could be considered as a separate and difficult area of research, thus in this work only essential techniques were applied to allow perform comparative studies between SO and RSO injections. Utilisation of more sophisticated techniques was very much limited by the research time as well as the limited knowledge of the author.

Since the time domain of the measured CDI AE signals was difficult to be established, very specific approach had to be applied. This included signal pattern recognition and mapping the CDI injection behaviour with AE signals. AE signal was analysed using user made Scilab codes based on Fourier transformation, Hanning function, Time-Frequency Analysis using the Wigner-Ville Distribution and periodogram and power spectral density. Theory of these standard mathematical signal processing tools is not presented here and can be found elsewhere.

4.5 Experimental procedures of engine tests

A range of tests was conceived to evaluate the quality of the performed CDI modification and its output. The modification included changes of the delivery system and the high pressure loop and are described in more details in 6.6.2 and 6.6.3. Both quantitative and qualitative tests were used to collect data of emissions, engine performance, fuel economy, power output and engine reliability and durability. Qualitative observations and observations were considered to be of value as well, and were useful in examining operational characteristics and potential user interest. A CDI Mercedes C-class, 2.2 was subjected to the modifications.

Experimental procedures were performed at various weather conditions with a special consideration paid to the cold weather conditions and the startup period. Duration of tests varied from a short period of time up to long term operations lasting for 10 months. The overall milage performed on RSO amounted to $\sim$250 000 km. The test involved:

- Cold weather tests including start up
- Emission tests, visible smoke and exhaust smell

- Power output, fuel economy and driveability
- Lubricating oil test and injector inspection

Cold weather is generally problematic for diesel engine in general but of a different scale for IDI and DI engines. Laurikko [144] showed that ambient temperature has the major impact on DI engines hydrocarbon and smoke emissions at cold start and the IDI type of engine was less sensitive. Ambient temperature had also a slight elevating effect on CO and hydrocarbon emissions at warmed-up operation.

For diesel car driver it does not have to be explained that there is a range of problems associated with a cold start of the diesel engine. Even the conventional diesel and bio-diesel are subjected to "clouding" (the formation of wax crystals) at low temperatures. Analysis of the RSO density graph (see *Subsection 6.1.1*) clearly shows that the oil will also plug fuel filters at low temperatures. Clouding can cause the fuel filter to become plugged and the engine to stop running. Bio-diesel and RSO tend to cloud at higher temperatures than the conventional diesel. Cloud point and "pour point depressants" (petroleum based additives) are used in the conventional diesel to combat the formation of wax crystals [172]. It is also important to take into account the increase of the fuel cloud point due to injection under high pressure. The influence of the pressure on the wax formation in diesel showed an increase in the diesel cloud point of about 25°C at the operation pressure of a CR engine (100 MPa) [313]. The same effect is expected for RSO has to be considered in the modification of the engine where RSO and is injected under high pressure. Thus, cold weather and high injection pressure may significantly contribute in the wax formation of RSO.

In theory, the CDI engine could avoid or reduce this cost of the above RSO "cloud point" problem. The start-up/shut-down cycle could be performed with the conventional diesel and then RSO would be heated prior to use. In an effective modified diesel engine, RSO that had solidified from cold temperatures in the auxiliary tank would be liquefied and made ready for use after a short period of time, since the modification uses waste heat from the engine. However, the discussed modification has been based on a single tank mode only thus such solution can not be applied.

It become essential to perform some cold weather runs to test a quality of the implemented modification. Therefore, presented results were collected at low ambient temperatures varying from -20 to 15°C. Cold weather operability test were devised from the conventional diesel and RSO and included:

- Cold start with and without use of a block heater. Cold starting characteristics using glow plugs and the block heater were compared against the use of glow plugs only. Such tests were performed after the vehicle had been parked outside overnight.
- Normal operation in cold weather. In this case testing consisted of the researcher's observations of the engine operation on RSO.

It has to be noted that cold weather tests were subjected to the available ambient temperatures in the researcher's region. During the test period, the coldest temperature was approximately -20°C. The start-up tests (at different ambient temperatures) were performed with and without pre-heating. Test where stable engine conditions were required were conducted in a way that the engine was brought to operating temperature by operating the vehicle in idle for at least 10 minutes.

4.5.1 Emission tests

Certain emissions are included in the standard engine tests, and these are CO, NO_x, HC, particulate matter (PM) and CO_2. These are normally expressed in grams per kilometre. In this work results or comparative tests between diesel and RSO are presented.

The test were performed by the local Mercedes car emission test representative using a ECOM A-Plus portable emission analyser. Because the unit can not measure particulates and an additional particulate probe was used. The emission unit is easy to use and provides quick emission analysis. The A-PLUS features an advanced Sample Conditioning system, incorporating an optional heated sample line, thermoelectric Peltier Gas Cooler, and peristatic pump for continuous moisture removal. The unit was fitted with sensors to measure O_2, CO, NO_x, and Combustibles (HC and CO_2).
It was found during the test that the oxygen measurements did not represent reasonable results and were not repeatable. The problem was not solved and thus the oxygen measurement was not included in the test.

4.5.2 Visible smoke and exhaust smell

The next engine test was performed on visible smoke and exhaust smell. The parameters which are not normally quantitatively assessed although their observation tells a lot about combustion. Also, the aspect of smog creation and general driveability are functions of these two parameters.

The smell of RSO exhaust is distinctive and it has often been characterised as having a "fish and chips" smell. Despite most people reportedly find this to be more pleasant than the conventional diesel exhaust RSO exhaust can be very intense and cause eyes, nose and throat irritations. Visible smoke is one of the factors which can indicate the quality of combustion and also is considered as an important factor as far as the environmental impact is considered.

In these test visual observations of visible smoke emissions from the exhaust pipe were made while starting the engine at different ambient temperatures. Also, similar observations were conducted when driving the vehicle. Observations were made primarily by observing the amount of visible smoke released from the exhaust pipe under conditions that normally cause diesel engines to emit significant amount of visible smoke i.e. cold starts, hard acceleration from start and ascensions for steep grades. The observations were made in a comparative way between the conventional diesel and RSO.

4.5.3 Power output and fuel economy

The excellent power and economy characteristic provided by the combination of energy density of conventional diesel fuel, and the efficiency of the CDI engine is desirable and should not be sacrificed by using RSO. Power output of the diesel engine is very important to the driver and correspond to the successful assessment of the CDI modification. Horsepower and torque on RSO fuel would have to be very close to that of conventional diesel for market acceptance of RSO as a fuel. Literature review provided examples that bio-diesel offers similar fuel economy to conventional diesel [6; 84; 235; 408] but much less information was found for RSO. Therefore, fuel economy tests of RSO are essential and need to be analysed.

To assess the power and engine performance the DynoStar kit was employed, which works like an electronic dynamometer. A dynamometer is basically a device that measures the amount of power being developed by an engine however DynoStar is a unique

combination of INS (inertial navigational systems), a high performance GPS (Global Positioning System) receiver and powerful data logging [169]. The unit measures the entire performance of a vehicle continuously from the INS and GPS data, and automatically maps racetrack, road etc, as a car is driven. DynoStar measures the power of the engine directly by making precise measurements and can analyse the entire power band of any engine. It can do measurements of power and torque in one gear, or power and speed/time through the gears. Then it calculates speed, distance, power, and more against time, speed or RPM. Measurements of power, cornering forces, handling and braking efficiency are performed and correlated to position on the road.
A similar test had been performed for the unmodified (on diesel) and modified engine running on RSO.

4.5.4 Lubricating oil

In all diesel engines a certain amount of lube oil contamination takes place from fuel products, therefore lube oil for diesels must be specially formulated. It is necessary to ensure that any alternative fuel does not degrade the lube oil to a greater extent than does diesel. Some studies showed that plant oils can cause ring sticking and lubricating oil thickening over the longer term [321; 322; 325; 326]. Test of using a conventional, mineral type of lube oil and diesel fuel revealed [321; 322; 325; 326] that the fuel pushed to the oil pan by piston rings evaporates from the hot lubrication oil, whereas plant oil remains there and due to its acid structure it tends to esterify the lubricant. This changes the properties of the lube oil making it very thick so it can no longer be pumped to the lubrication passages. Therefore, the conventional synthetic 5W/40 lube oil had to be replaced by the enhanced engine oil (PlantoMot, SAE 5W/40) suitable for diesel engines working on plant oils [21]. The composition of PlantoMot is based on RSO, which means the lubricant is compatible to fuels like bio-diesel or plant oil. The selection on the oil was based on periodical examination of oil samples withdrawn from the engine roughly after 20,000 km of operation..
The parameters like density and viscosity values were measured and compared with a corresponding mineral oil sample. The measurements were performed using the same equipment and procedures described in 4.1.5.

4.5.5 Acceleration test, drive-ability and fuel consumption

Diesel cars acceleration is considered to be barely adequate at its best. From a driver point of view any reduced acceleration capability that may result from RSO fuel use it would make driving the diesel car less attractive to customers. Acceleration tests were therefore considered to be useful and also necessary. A stopwatch was used to record 0-100 km/h acceleration for standard diesel and RSO. Each test was performed once in each direction under calm conditions on a level, paved surface. Prior to each test the vehicle was driven for approximately five minutes at approximately 90 km/h. Results were very similar for both fuels and it can be concluded that RSO acceleration times were very close to those for diesel. The test were performed at the same road conditions and ambient temperatures were approximately the same. The difference in acceleration might have been because of a small decrease of the power recorded for RSO.

The Mercedes car was subjected to several driving tests to evaluate the drive-ability after making the modification. The test took place over a short and long period of time as well as in cold and warm weather. The test were especially focused on comfort of driving and ease of car operation when the new fuel was used. The test had qualitative manner but are a standard part of any car tests before its commercialisation. The overall impression of drive-ability was very positive. The car provided sufficient torque in all gears. Acceleration and tackling of routes of different grade did not show noticeable power losses in comparison to diesel. Practically, the car drove very smooth and served sufficient power under the full load conditions.

4.5.6 Injector and cylinder inspection

Twicely, i.e. after several months and approximately 250 000 km of various driving on RSO, the injectors were removed and inspected. The injectors were compared with an identical CDI injector performing for a significant period of time on the conventional diesel fuel. The inspection was made using a standard microscope linked to a camera and a computer. The deposit measurements were done using the specialised software dedicated to the microscope.

Cylinders were examined using an endoscope and a camera. Two cylinders, on both sides of the engine were inspected.

4.5.7 Cold weather performance

Cold weather test were essential to assess a scale of short-term problems mainly related to the cold weather start. Cold starts on RSO were almost impossible without the use of the block heater and the pre-heating system. Even at temperatures above freezing and without heating aids starting was very difficult. Also it has been found that a separate use of the glow plugs slightly improve engine startup, but repeated use of glow plugs and the block heater was essential for a smooth engine start. The block heater was applied and equipped with a programmer which allowed to start up pre-heating remotely.

Chapter 5

Simulation software

There is no one great ability without a mixture of madness

As it was presented in *Section 2.6* it is very beneficial to predict the mixture formation process inside diesel engines for investigation of possible fuel utilisation and engine performance. In the diesel engine, combustion and emission characteristics are influenced by fuel atomisation, nozzle geometry, injection pressure, shape of inlet port, and other factors. In order to improve fuelair mixing, it is important to understand the fuel atomisation and spray formation processes. In this chapter, numerical simulations of free sprays formed by a CR injector are carried out using KIVA code and employing different models for the breakup of the liquid sheet and that of droplets downstream. The breakup of the liquid sheet is modeled using according to models presented in *Section 2.6* and for diesel and RSO. The objective of this part of the PhD is to investigate the effect of injection pressure on the macroscopic spray behaviour and atomisation characteristics of high-pressure rapeseed spray in the CR type diesel injection system. In this study, the predicted characteristics such as spray development, spray penetration, and the distribution of mean droplet diameter obtained by the KIVA-3 code are compared with the experimental results for diesel and RSO.

5.1 Fuel library

As it is crucial to work with various fuels, the original release version of KIVA-II offered 12 chemical species in a fuel library file [37; 40]. This number can be increased or decreased as needed. A KIVA user can change the contents of the *fuelib.f* file to define a new type of a fuel or modify the existing one. What remains is to define the fuel, species 1, which

requires a number of other properties in addition to its enthalpy. For both gaseous and non-gaseous fuels the molecular weight, critical temperature and heat of formation have to be defined. If the fuel is a liquid, several more quantities need to be set. These are the tables of liquid latent heat of vaporisation and liquid vapour pressure, for use in droplet vaporisation, along with a table of liquid viscosity, for use in droplet breakup. In addition, the slope and y-intercept of the surface tension versus temperature linear fit are defined. Normally, these are based on the surface tension at 350°K, which is a typical fuel temperature, and the critical temperature of the fuel. Data is used in the surface tension linear fits in droplet collisions and breakup. It has to be highlighted that in KIVA-II and KIVA-3, the surface tension was treated as a linear fit between two data points: the surface tension value at 350°K and a value of 0.0 at the critical temperature. Later examination revealed that they depart noticeably from being a straight line. Accordingly, the linear fit procedure has been replaced by tabular interpolation of actual surface tension values, specified at intervals of 10°K. Furthermore, the coefficient for duel diffusivity in air is set, for use in droplet evaporation. Finally, the library contains a complete set of tables of liquid thermal conductivity, which is required in the heat transfer calculations for evaporating of a liquid wall film.

The tabular information on fielib.f file has been drawn from a number of sources and very often implemented for a particular user application. In the present work two types of fuels have been used: diesel and RSO. The diesel property data were taken and modified directly from the fuel library implemented in KIVA-3 version, where two typed of diesel are available: diesel #1 labelled DF2 and #2 labelled as DI. The DF2 model was assembled by T. L. McKinley of Cummins Engine Company [34]. It uses diesel #2 vapour pressure, but the critical temperature, latent heat of vaporisation, and liquid viscosity are set equal to those for n-hexadecane, with the remaining quantities set equal to those for n-dodecane. DF2 is described by the following chemical formula: $C_{12}H_{26}$ (dodecane) as defined in [34]. The DI model, contributed by Constantine Varnavas of the University of Illinois at Urbana [404] offers an alternative to the DF2 model. The DI model was compiled from tables, graphs, and correlations from various sources, which Varnavas believes to be more representative of diesel #2, and uses the chemical formula $C_{13}H_{23}$. Finally, the author applied a diesel model based on a chemical formula of $C_{14}H_{28}$ as the closest representation of the diesel fuel available in the European market. Both formulas of DI and DF2 were constructed for the purpose of KIVA simulations.

5.1.1 Diesel and RSO fuel library

Since two different fuels were used in calculations the physical and chemical properties had to be provided. In case of SO and diesel simulations properties of standard diesel fuel had been used. These were provided in the fuel library implemented in the original [35] and modified KIVA code [36].

As far as simulation of plant oils is considered, KIVA fuel library does not offer any type of data. Therefore, an additional RSO section was created to overcome the absence of that species. The section was build as a compilation of physical and chemical properties provided by Writh et al. [420], the experimental results presented in *Chapter 6*, computer simulations using HYSIS and finally the information published by Griend et al. [167]. The tabulated data of density, surface tension and viscosity were implemented directly from the physical properties results reported in *Chapter 3*. Table 5.1 lists properties and sources respectively used to build the RSO fuel properties library. It has to be noted that due to

Table 5.1: *RSO physical properties implemented in fuelib.f module.*

Property	**Source**
Molecular weight	282.5 Wright et al. [420]
Critical temperature	809.0 Wright et al. [420]
Heat of formation	-22.6 Griend et al. [167]
Density	experiment (see *Chapter 3*)
Diffusion in air coefficients	Wright et al. [420] and Griend et al. [167]
Enthalpy	THERGAS[279]
Latent heat of vaporisation	The approximated heats of vap. from octadecane have been scaled through the (estimated) critical temp. of oleic acid
Vapour pressure	Landolt-Boernstein [129]
Viscosity	experiment (see *Chapter 3*)
Surface tension	experiment (see *Chapter 3*)
Thermal conductivity	Vargaftik [402], HYSIS

a lack of the fundamental physical properties of RSO some of them have been evaluated using properties of oleic acid and octadecane. The approach has been applied when thermal conductivity was calculated using HYSIS. A similar approach has been already accepted in [167; 278] and [125].

5.2 Simulation procedure and startup files

The KIVA3 code was developed by means of the Arbitrary-Lagrangian-Eulerian (ALE) method, which is essentially an operator-splitting technique that solves the finite difference equations in two phases: a Lagrangian phase, and a Eulerian phase. The trajectory model of spray droplets performs Lagrangian tracking of the trajectories of a large number of computational particles to simulate the dispersal phase. Each computational particle represents a certain number of real droplets with the same properties. Eight ordinary differential equations for momentum, internal energy and mass of the computational particle, together with three terms for its location, are solved numerically. The solution obtained gives the required particle velocity vector, as well as its location, diameter and temperature as a function of time. The spray droplets are assumed to be spherical and the droplet oscillations take place around its equilibrium spherical shape. Owing to the large density ratio of the liquid fuel to the ambient gas, the dynamic behaviour of droplets is mainly governed by aerodynamic drag. Equations governing spray simulations are collected in a set of subroutines controlled by a short main program. There are a number of supporting subroutines that perform tasks for the primary subroutines. Subroutines are written in FORTRAN and can be modified by a user and recompiled.
As most of the CFD packages KIVA simulation can be divided into three parts: a pre-processing, a main run and a post-processing. Pre-processing involves grid preparation and grid check which results in mesh structure which can be used in a run. A typical KIVA simulation includes the following running procedure described by four general steps:

1. Generation of a grid files *otape11* and *itape17* from an input file *iprep* using the **k3prep** script

2. Generation of user input files of *itape5* (consisting of the engine conditions), *itape18* (with valve motion specification), *itape7* (with definition of restarting)

3. Execution of the mail KIVA script **kiva3v** and generation of the output files: *dat.** (data files of in-cylinder conditions), *otape8* (data for restarting), *otape9* (detailed results for postprocessing) and *otape12* (with general inforation about the run)

4. Post processing of output files using the **k3post** script and further data elaboration using own made GMV scripts

An input file is needed to proceed pre-processing and is called *iprep*. *iprep* file is basically a collection of computational cells reflecting on a real cylinder design and assembled

to create a geometrical structure, which will represent a calculation volume. The main run program *kiva3v* is the output of specificly compiled FORTRAN files and some input files. The input files relate to a type of fuel, its chemistry, and the chemical kinetics of combustion if any takes place. These files have to be presented in a main file path whilst the KIVA compilation proceeds. The main input file, which describes a case being simulated is called *itape5*, and must be present to initiate a simulation. A user utilises the contents of this file to build up a case or control the output.

Despite KIVA produces a good range of output files which can be used by other external post-processing packages, the code provides a separate post-processing programme. The appropriate files can be compiled and as the *k3post* executable file employed to plot or display results. It is a common practice amongst KIVA users to use an external post-processing programme, which normally offers better flexibility, and the independence from a working machine architecture.

5.2.1 Grid definition and pre-processing

As already described above, a KIVA simulation consists of preparation of a grid which will be used in calculations and definition of an input file which incorporates operational parameters. Generally, a grid defines the "space" or the geometry over which a simulation takes place and an input file determines how. Both parts are integrated and equally important.

As described above, the *iprep* file defines the structure of the computational grid. This structure can be fully static or have of moving parts like piston or valves. Grid preparation is widely described in [35], and must be started from a clear definition of space boundaries. KIVA contains no grid generation capability of its own, and instead relies on a *iprep* file to be provided by a separate grid generator or manually defined by a user.
The K3PREP pre-processor which is provided in KIVA translates a grid into mesh. The mesh generator creates an *otape17* file to be read by the main program that contains all the grid coordinates x,y,z, flags (cell attributes), six neighbour connectivity arrays, three cell-face boundary conditions arrays and a region identifier array. The main program completes the setup by sorting the storage, generating all other arrays required to describe the problem, and creating the tailored boundary conditions tables. Whole process is quite

complicated especially if a complex structure is defined. An *otape7* file is produced which then can be used in simulations (also for restarting) as long as the same geometry is used. In many cases after the processing a modification of several KIVA files is required. It is due to different numbers of cells allocated for simulation which is changing depending on mesh type as well as to mesh quality (density).

5.2.2 Definition of input variables

The operational parameters of a simulation are provided by means of the *itape5* input file. Details describing the ambient and injection conditions, the operational parameters of the injection system, even thermal state of a fuel, have to be defined in this input file. Each computational run is defined by a separate itape file. The structure of the file and its integration with the main KIVA code allows the user flexibly and instant control of a simulation without the major changes of the main Fortran code. The *itape5* file also consists of strict control variables governing the computational flow. These are variables affecting the accuracy, convergence, and the output format of the simulation.

Input parameters include mean spray velocities calculated according to the procedure described in *Subsection 5.2.6*. The mean velocities have been implemented with a relation to the NUMVEL and PULSE parameters defining number of velocities values in a velocity table and a type of a velocity profile. Additionally mean Sauter diameters as an average value at the injector bore are included and associated with the a SMR (Sauter mean radius). It should be the radius of the injector hole, however to provide more accurate results the SMR value has been verified against the average D_{32} values from the PDA results (since, it was essential to perform droplet sizing experiments in *Section 3.4* and *3.5*). It is expected that the SMR parameters could be used in a combination of the nozzle diameter and the appropriate breakup model, nevertheless such procedure is more suitable for a neat injector bore. To complete a set of input variables the spray cone angle has to be defined. For the studies CDI injector parameter of the cone angle is taken as a solid type and identically defined for both variables CONE and DCONE. Values of cone angles were taken from the high speed camera experimental results and averaged over the spray duration.

As far as the cold spray simulation is concerned, there is group of variables directly affecting calculations: the injected mass (TSPMAS), the number of computational parcels (TNPARC), the breakup model type (BREAKUP), the injection profile mode (PULSE),

the evaporation model (EVAPP) , the turbulence model (TURBSW) and number of injection velocities (NUMVEL). More details on the input variables and the way of their implementation are given in the KIVA manual [3; 38].

Two breakup models, namely Reitz Kelvin-Helmholtz Rayleigh-Taylor (KH-RT) and Reitz-Diwakar (RD)(In Subsection 2.6.5), were selected and implemented into the main KIVA code in the present work. Table 5.2 lists the main breakup parameters used in breakup sub-models. The values were defined in accordance to descriptions in [35], Lee et al. [245], Gonzalez et al. [162], Bianchi et al. [69], Levý and coworkers [251], and Rotondi et al. [349].

Table 5.2: *Breakup model parameters*

Reitz Kelvin-Helmholtz Rayleigh-Taylor (KH-RT)	**Reitz-Diwakar (RD)**
B_0=0.61 Eq 2.6.15	r_{lim}=0.05
B_1=1.0 Eq. 2.6.13	C_{bag}=6.0
C_τ=1.0 Eq 2.6.19	C_{strip}=0.5
C_{RT}=0.1 Eq 2.6.16	C_{sprayb}=0.785
We_{lim}=6	C_{sprays}=10.0

5.2.3 Post-processing

After a simulation is completed results can be analysed and presented using a post-processor. Despite the fact that KIVA is providing post-processing tool, in the most cases this post-processor is not used by KIVA users. They can choose amongst a wide selection of available post-processing packages. In this work two non-commercial postprocessors were used: GMV [304] and openDX [23]. GMV can directly present and analyse a content of an output file exported in an appropriate format during a simulation. Using GMV, the overall presentation of spray including detailed analysis of particular cell is available to a user. In case of calculation including combustion or vaporisation, profiles of combustion produces can be presented for each chemical species. GMV is able to represent visually a drop population in a spray shape as well as to analyse a singe cell or set of cells. In order to perform more detailed analysis of a drop population, other suitable post-processing package needs to be used. It has to be pointed out that processing of results can be done in time intervals strictly defined by a user or in crank angle intervals. Originally, the KIVA-3V2 code was compiled for a HP computer. The compilation was performed without code

splitting and several HP system libraries had to be added. Due to significantly long time of computational runs, it was decided to recompile the code on faster computers. Finally, the Intel Fortran Compiler has been chosen to compile the split code (The code splitting is the operation of separating up the KIVA subroutines into individual Fortran files.) The compilation process was performed at two architectures: the Suse Linux Pentium 4 PC and the multiprocessor Dell 650 series Premium unit.

5.2.4 Grid types

As it can be found in literature, the spray simulation is highly grid dependent [41; 291; 292; 361]. Hence, grid construction must be carefully performed prior to any spray computation. It has been reported that the final calculated values of mean diameter and penetration of diesel sprays can be severely mesh-dependent [41]. This is mainly due to the size of a computational cell, which in overall results in a density of a computational grid. As it can be suspected, the cell size must be sufficient to accommodate the whole spectrum of the spray.
Numerically, the main problem is that the point of injection is essentially a singularity since in reality the injection point has got a certain volume and its size is comparable to the size of a liquid core. Frequently, it is the size (diameter) of an injector. As far as the numerical calculations are concerned, the sampling used for droplet evolution calculations should take place on length scales (size scales) that are shorter than the length scales of the spray (the length scales used by a breakup model). The natural polar symmetry of the singularity is not consistent with the 90° resolution of the Cartesian cells, as the correlation between parcel location and velocity is not resolvable on a Cartesian grid. Therefore, at the initial period of injection, a single point concentrates a large amount of fuel and this region does not represent the real situation. Frequently, it is visualised as a thick liquid core or a liquid structure build of large aggregates. Such drawback of KIVA simulation needs to be taken into account when the near-tip studies should be performed as well as viscous liquids are investigated.

Generally, two types of uniform Cartesian cells grid types were used in the present work simulations: a full 3D rectangular and a generic sector block. A schematic presentation of the grids is shown in Figure 5.1. Details of the computations mesh produced out of the grids are given in Table 5.3. A rectangular grid is preferred for sprays modelling [361] and has

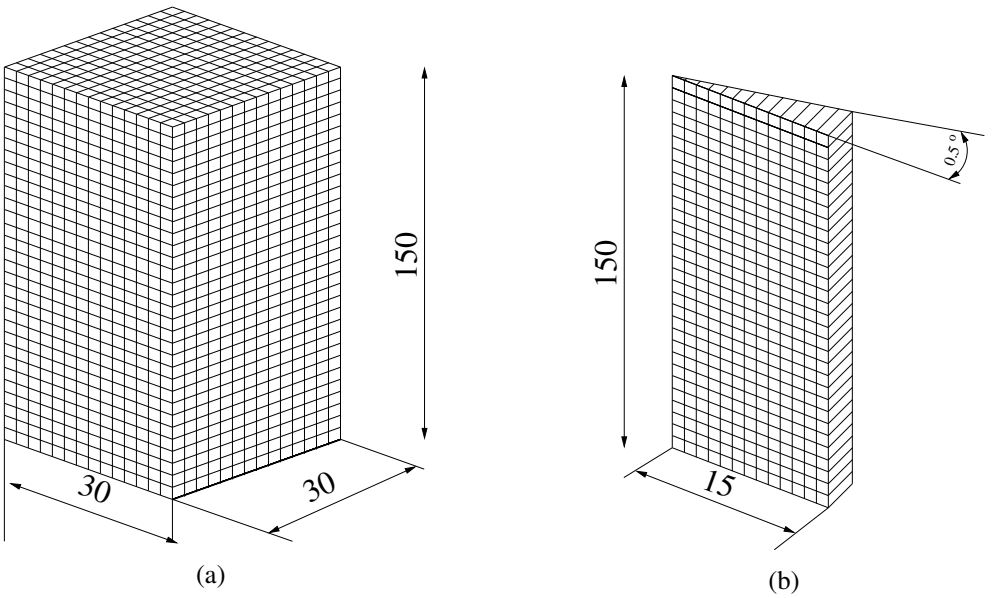

Figure 5.1: *Schematic presentation of the computational grid (dimensions in millimetres and scaled accordingly): (a) rectangular mesh, (b) generic sector.*

Table 5.3: *Description of the computational grid*

Featuring variable	**Cylindrical mesh**	**Generic sector**
Height,[mm]	150	150
Diameter/width,[mm]	30	15
Type of KIVA grid	full cylinder, thsect=360	generic sector, thsect=0.5
Number of computational cells	3 00 000	15 000
Node numbers	3 23 200	16 160

been already proved working better for diesel sprays [166; 251; 405; 406]. Its geometry compromised between the accuracy of the calculations and longer computational time. Additionally, the rectangular grid allows to observe a full spray including its asymmetry. The rectangular grid is oriented around the injection axis, and sized just large enough to accommodate all of the parcels within a breaking up length. The grid resolution was set as fine and balanced a sufficient sample size in the cells near the spray centre and the number of parcels that were used in the simulation. This has been done by performing a series of runs where the injected amount of fuel corresponded to the highest injection pressure and only the grid resolution and number of parcels were changed to obtain the normal run termination without the numerical overflow. Detailed grid analysis has not been performed but it has been accepted that the grid has been optimised for accuracy by controlling both spatial and statistical resolution. The acceptance was based on assumption that the maximum parcel numbers should not exceed 8000 and the grid resolution would

accommodate a fuel sample of the maximum possible size present in a population (here equal to the nozzle diameter).

The generic sector grid was used for some preliminary simulations mainly to test inputs files. Though the generic sector grid can be used for the full range simulation it does not provide enough information about spray in a full spatial resolution. Basically, the sector grid represents only a "slice" or a sector of the full spray. Also, if the sector grid is used, the results can be only evaluated assuming the full symmetry of a spray, which does not represent the real conditions. However, application of the sector grid was mainly due to reduction of the simulation time.

Finally, in order to analyse a more realistic spray chamber, a diesel chamber profile has been developed using available Volvo cylinder data. Despite the extensive effort, the author could not base the grid on a real Bosch CDI geometry due to lack of the cylinder data. Therefore, the grid was based on a Volvo D12C diesel engine piston bowl. The engine grid is different from the geometry of the Mercedes cylinder therefore the simulations were performed for the cooperative analysis only. The calculations were developed in an axisymmetric bowl-in-piston engine. The D12C engine is used in light truck and represents a typical DI piston geometry [386]. It was expected that the grid would help to understand behaviour of RSO in DI engine in general and could be used especially in the comparative studies. Figure 5.2 presents the geometry of the D12C grid. Additionally, Table 5.4 includes the geometrical parameters of the grid and the final mesh. Details of the injection parameters are specified in Table 5.5 according to [160].

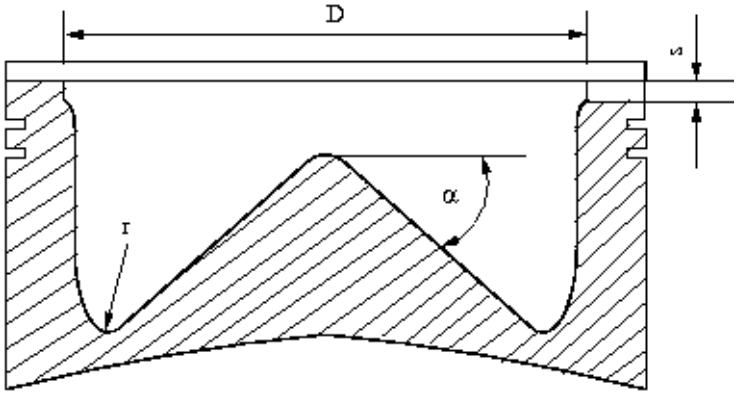

Figure 5.2: *Combustion chamber geometry*

Table 5.4: *Parameters values of the D12C grid.*

Parameter	Value
D,[mm]	130.0
α,[°]	40
s, [mm]	3.0
r, [mm]	3.0
Stroke, [mm]	150.0
Squish[1], [mm]	1.0
Mesh type	thsect=0.5[2], 3 blocks
Number of computational cells	6355
Numbers of vertices	6462

Table 5.5: *D12C engine injection specification.*

Parameter	Value
Injector nozzle diameter,[mm]	0.235
Engine speed, [RPM]	1500
Injection velocity, [m/s]	200-500
Inclination angle of spray, [°]	79.0

5.2.5 Operating conditions

Simulations were divided into two groups: modelling in a constant-volume vessel simulating the spray chamber experiments for SO and RSO, and these real engine cylinder-like conditions. Since ambient conditions were kept constant and low temperature, vaporisation could be considered negligible for the first group of simulations. Nevertheless, all the simulation were performed with vaporisation model being active. This was in order to observe droplets evolution and trace fuel concentration changes in the gas phase. The numerical results of non-evaporating spray were compared with experimental data collected in the spray characterisation studies described in *Chapter 3*. In the second group of spray simulations, the effect of in-cylinder conditions on RSO was evaluated and compared with diesel simulations (SO - the test oil used in experiments instead of diesel - was replaced by diesel fuel). The simulation tests were focused on the cold spray only without combustion on other chemical reactions.

The first group of the spray simulations were performed in a constant-volume vessel filled with an inert gas at constant atmospheric ambient pressure and temperature of 20°C.

The ambient pressure was selected to ensure availability of the discharge coefficient for the CDI injector used in experimental study and correct calculation of the injection velocity (see *Subsection 5.2.6*). The investigated operating conditions are shown in Table 5.6 and 5.7 for SO and RSO respectively. SO simulations were carried out at single fuel temperature: 25°C, whereas RSO calculations were performed at fuel temperature of 40°C. The injection parameters were implemented in the input file (*itape5*) required for a KIVA simulation. The injection time of all simulations was accepted as 1.0 ms and corresponded

Table 5.6: *Operating conditions for SO spray simulations*

Parameter/Case	**SO1**	**SO2**	**SO3**
Total fuel mass, [mg]	4.5	6.4	8.6
Injection time, [ms]	1.0	1.0	1.0
Ambient pressure, [MPa]	0.1	0.1	0.1
Ambient temperature, [°C]	20.0	20.0	20.0
Injection pressure, [MPa]	56.25	93.75	131.25
Fuel temperature, [°C]	25.0	25.0	25.0

Table 5.7: *Operating conditions for RSO spray simulations*

Parameter/Case	**RSO1**	**RSO2**	**RSO3**
Total fuel mass, [mg]	4.0	6.1	6.4
Injection time, [ms]	1.0	1.0	1.0
Ambient pressure, [MPa]	0.1	0.1	0.1
Ambient temperature, [°C]	20.0	20.0	20.0
Injection pressure, [MPa]	56.25	93.75	131.25
Fuel temperature, [°C]	40.0	40.0	40.0

to the injection time used in the experimental spray investigations described in *Chapter 4*. For each simulation a number of computational parcels was defined and varied from 3100 upto 5000. Parcels definition is arbitrary and was made to ensure the normal termination of calculation. If calculation was terminated due to the exceeding parcels number in the computational volume, the parcel numbers were reduced and the calculation was restarted.

In addition to the constant-volume vessel simulations, KIVA was used to simulate the diesel and RSO spray development in a real engine conditions using the computational grid presented in the *Subsection 5.2.4*. Diesel simulations were based on a KIVA built-in fuel of the chemical formula of $C_{14}H_{28}$. The physical properties were defined according to [36]. The engine parameters and injection variables were taken for Volvo D12 DI diesel

engine [386]. Tables 5.8 and 5.9 shows the details of the computational runs. It has to

Table 5.8: *Cylinder and injection parameters used in the engine simulations.*

Parameter	**Diesel and Rapeseed oil**
ATDC, [°]	-180.0
Initial swirl ratio	0.4
Initial swirl velocity profile	3.11
Crank angle to initiate fuel injection, [°]	-8.1
Duration of the injection in crank angle, [°]	26.0
Total fuel mass, [mg]	212.0
Initial in-cylinder pressure, [bar]	2.4
Initial in-cylinder temperature, [°C]	27.0
Cone angle, [°]	10.0
Compression ratio	∼17.6

Table 5.9: *Cylinder and fuel temperatures implemented in the engine simulations.*

Parameter/Case	**ED1**	**ED2**	**ERSO1**	**ERSO2**	**ERSO3**	**ERSO4**
Wall temperature, [°C]	10.0	227.0	10.0	227.0	227.0	227.0
Head temperature, [°C]	10.0	227.0	10.0	227.0	227.0	227.0
Piston temperature, [°C	10.0	227.0	10.0	227.0	227.0	227.0
Initial fuel temperature, [°C]	10.0	60.0	10.0	10.0	60.0	77.0

be recognised that the actual combustion of RSO in engine can not be simulated because of the lack of a RSO combustion chemistry kinetics. Nevertheless, the author performed several computational runs where the new RSO kinetic had been included. However the results of the runs could not be experimentally validated and therefore do not provide fully valuable verified data. There exist a need to develop appropriate RSO combustion kinetics for full simulation of the engine cycle.

The engine simulation were deeply simplified for the sake of comparative studies of spray development inside the combustion chamber only. Diesel and RSO simulations utilised the same injected amounts as well as velocity profiles (see the next subsection). So, it has been assumed that the injected fuel amounts are identical for both fuels as a result of a preliminary modification of the injection system.

5.2.6 Estimation of injection velocity

To simulate a fuel spray KIVA code requires an initial velocity profile or an averaged cross-section fuel velocity (bulk velocity) at the nozzle exit. Since, the velocity profile in the nozzle is not known, the bulk velocity can be evaluated from the injection experiments using the injected fuel amounts or the value of the discharge coefficient, C_d. Very accurate velocity profile can be found only if an injection profile rate is known as the function of time and injection conditions. The injection rate profile has not been measured in this work. Unfortunately, the author's attempts to utilise the original injection profile taken from the manufacturer were not successful. Values of the discharge coefficient had to be evaluated and compared with similar types of CDI nozzles used elsewhere [64; 411].

The discharge coefficient is frequently accepted as constant [201] however it's time and injection pressure dependent. Wang et al. [411] showed a difference between the steady-state coefficient and the dynamic one as well as its variation with the injection pressure and time. A similar discussion has been carried out by Kong et al. [224] and confirmed by KIVA simulations. A typical variation of the dynamic C_d include three segments corresponding to three phases of the needle namely: opening, full lift and closing [64]. Hence, in the first range the C_d increase can be observed which last until the full lift position is reached and then the same value is maintained until the needle start to close. Measurements of the dynamic C_d revealed needle bouncing which results in local fluctuations of the C_d with the injection time [411; 412]. In evaluation of the injection velocity it is easier to use a constant C_d value which represent a mean value of the dynamic C_d. Normally, the dynamic C_d at needle full-lift state is lower than the steady state value.

To improve accuracy of the simulations the coefficient was estimated using the procedure based on methodology described by Levý et al. [251] but without calculating mass flow rate which was already known. The procedure was feasible only for injected fuel quantities measured at atmospheric ambient pressures.

The procedure applied to calculate C_d used the equations of mass and momentum balance described below by Equations Equations (5.2.1) and (5.2.2). The averaged velocity

can be also calculated using the following expression:

$$\bar{V} = C_d \sqrt{\frac{2\left(p_{inj} - p\right)}{\rho_p}} \tag{5.2.1}$$

Where:

p_{inj} - the injection pressure

p - ambient pressure (back pressure)

ρ_p - the fuel density.

The averaged cross-section velocity or bulk velocity can be calculated using the recorded signals of injection pressure and needle lift according to the Equation (5.2.4). The maximum needle lift of the nozzle used in the test was 0.31 mm. The mass flowrate of injected fuel is given by:

$$\dot{m}_{inj} = C_d A \sqrt{2\rho_p \left(p_{inj} - p\right)} \tag{5.2.2}$$

Combination of Equations (5.2.1) and (5.2.3) together with the relevant experimental data (giving the amount of injected fuel at certain ambient conditions and the injection pressure) allow to calculate the mean injection velocity. However, the calculations of the mean injection velocity and the presented literature results [216; 251; 301] show that at simulations based on the bulk velocity according to Equation 5.2.1 underestimate the spray penetration. This is thought to be caused by irregularities of the injection due to the mechanical operation of the injector as well as the additional effects like cavitation not being included in the estimation of mean velocity. A deviation from the experimental values appear either at the beginning or at the end of the penetration. The author has investigated the influence of the discharge coefficient of spray penetration and found a necessity to modify the original equations. It can be concluded that the discharge coefficient is changing with time (as far as an injection is analysed) and also is affected by the quality of the injector bores. This could be seen as a difference if a brand new and used injector was investigated (all experiments were performed using an used injector as already described in *Chapter 3)* and *4*.

The approach described above and use of Equation (5.2.1) leads to the overestimation of C_d and thus higher mean velocity values. A sample of the calculations presenting this occurrence in shown in Figure 5.3. The figure shows a comparison of spray penetration for three different values of C_d (calculated using the experimental data and Equations 5.2.1

and 5.2.2). In this case experimental values at atmospheric pressure were shown, but a similar trends were found for other ambient pressures. A noticeable difference from the experimental data can be seen especially at the end of the injection where values are by 30% higher from the experiment. The C_d coefficient calculated from a similar set of equations was applied in the work of Kuo [234] where it was found that the calculated injection velocity over predicted the early phase of the penetration and under predicted that of the later phase. It has been brought to the author's attention that cavitation, in particular, may significantly affect the final bulk velocity (feedback on paper [67]). Experimental calculations were based on the specific shapes of spray penetration curves for high injection pressure presented in the *Section 6.2*. As the equations 5.2.1 and 5.2.2 do not include the non-linear effect of velocity caused by th injection delay, the final bulk velocity was based on the modified version of Equation (5.2.1) and rewritten as:

$$\bar{V} = C_n^* \sqrt{\frac{2\left(p_{inj} - p\right)}{\rho_p}} \tag{5.2.3}$$

where C_n^* is the modified discharge coefficient and defined as:

$$C_n^* \equiv C_n = min\left(\frac{h}{h_c}, 1\right) \tag{5.2.4}$$

Where h is the needle lift and h_c is the critical lift (obtained from the injector vendor). Details of the method to include the cavitation and viscous effect is presented in [251].

Figure 5.4 presents selected data of the mean values of the discharge coefficient for different injection pressure evaluated using the experimental data and calculated according to the method outlined above. It should be noted that the values of the discharge coefficient varies with a fuel type. Taking into account that the Reynolds number is a function of the flow velocity in the injector orifice, and therefore it is dependent on the injection pressure, these parameters are directly proportional. The effect can be seen for SO as a gradual increase of the C_d with the injection pressure. For low values of the injection pressure the C_d increases up to a certain value of the injection pressure (76 MPa) and then the increases noticeably slower. It has been shown that the rapid increase of the C_d value depends strongly on the injector geometry [148]. Whilst, the SO discharge coefficient gradually increases with the injection pressure, values of RSO are following the same pattern only

for the injection pressure upto 93 MPa. Beyond this pressure the C_d the RSO curve show the inflexion point where very likely cavitation starts to take place. It is assumed that cavitation starts due to the high pressure drop and thus C_d drops rapidly. According to Nurick [294], it can be assumed that the nozzle is collapsed or under choke state. RSO presented curve indicates the start of cavitation, however this has not been verified with other experimental method. The fact that the RSO pattern is different than that of SO might give useful insight in designing or modifying CDI injector to operate with RSO fuel.
A very similar set of C_d values for diesel data, in comparison to those presented in Figure 5.4, was presented for a similar CR injector by Benajes et al. [64].

For each KIVA run, simulating SO and RSO spray penetration a separate velocity value was provided based on a calculations involving the injected mass, the injector geometry and the calculated, mean discharge coefficient value. Such approach simplifies the injection profile rate into a single velocity value representing a mean spray velocity in the injector tip. Equation (5.2.1) was used further to find values of C_d for SO and RSO. For the engine

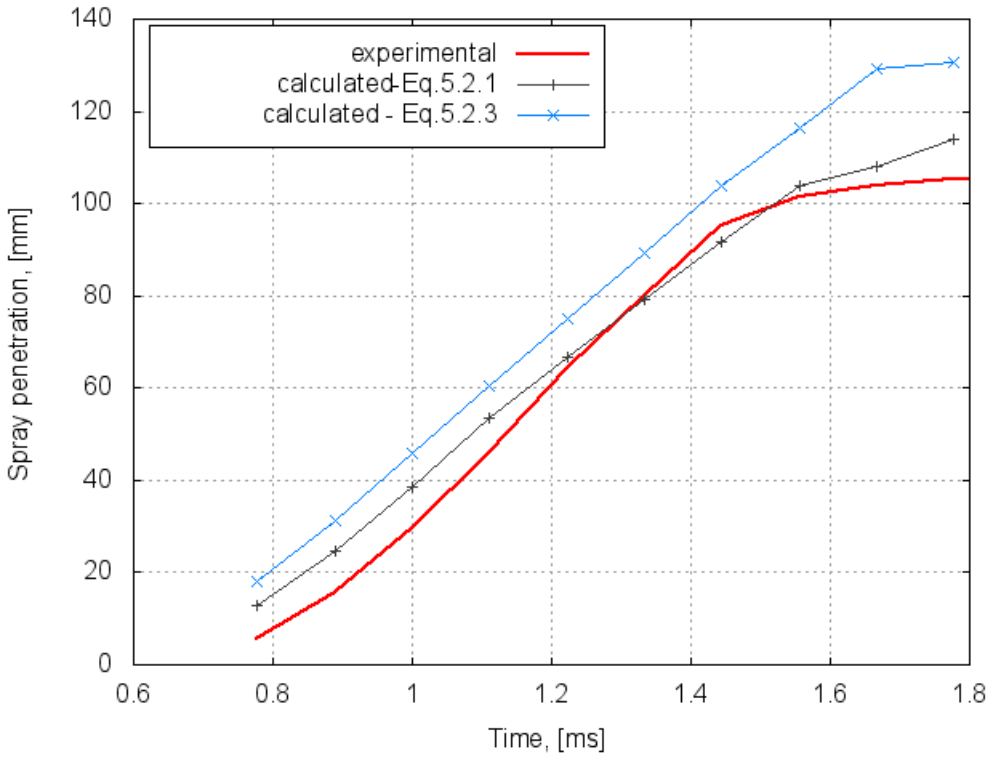

Figure 5.3: *Comparison of the C_d effect calculated according to the Equations (5.2.1) and (5.2.3) on RSO penetration at 131.25 MPa and atmospheric pressure. (Penetration calculated using the KH-RT model).*

spray simulations, velocity profiles were not calculated but accepted as provided by [386].

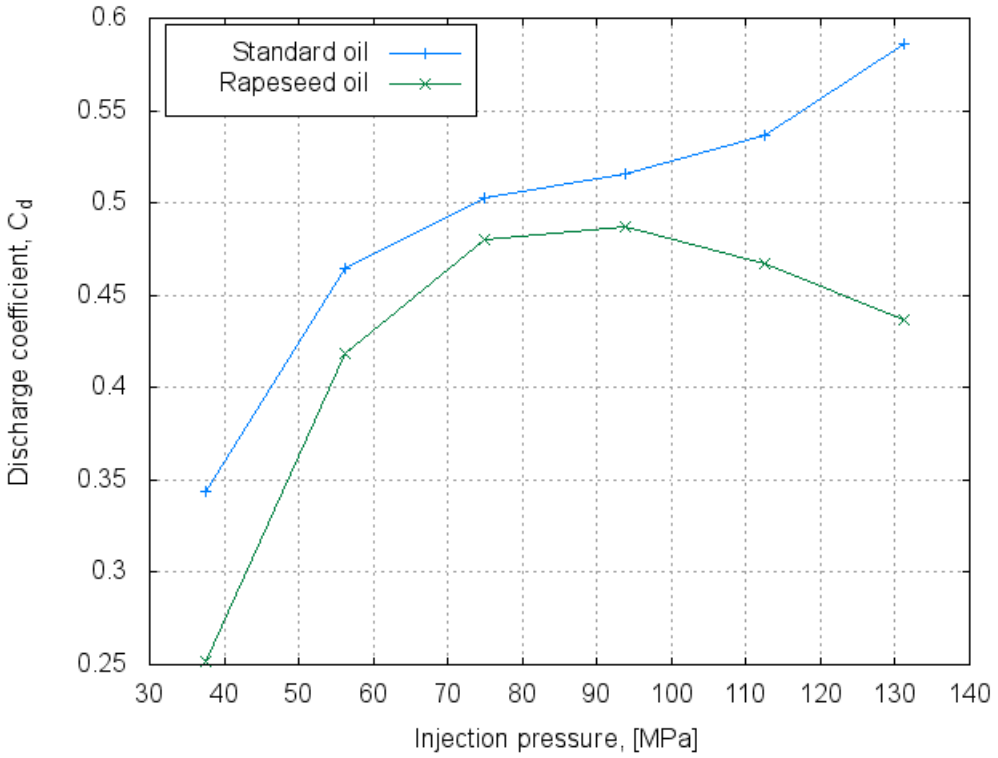

Figure 5.4: *Variation of the discharge coefficient with the injection pressure at the atmospheric pressure for standard and rapeseed oils.*

It is concluded that in the case of engine simulations, the methodology to calculate velocity profiles or C_d and used for a simple cold spray would not provide valuable results and the experimental data need to be used instead.

5.2.7 Accuracy and errors

There are several factors influencing KIVA spray simulations as well as the quality of results. Some do have a typical numerical origin others are related to the use of KIVA submodes and fuel properties and some, like velocity profiles and the discharge coefficient, are influencing whole injection process. The detailed discussion of the numerical problems in KIVA simulations can be found elsewhere [39; 166; 361; 385] and it is not discussed in this subsection. Here, the author will concentrate only on those that are specific to RSO simulations and considered as interesting for further discussion, in terms of plant oil spray simulations.

There are two basic instabilities most likely to interrupt the full spray simulations: (i) the unstable criterion of the conjugate gradient solver in the main KIVA loop and (ii) the increase of the diffusion field due to turbulence resulting from exceeding of the maximum setup limits. Additionally the development of the spray is dependent on the cell size. This

effect is also important and crucial.
The instability of a run due to a disruption of the conjugate gradient solver origins from setting up the tolerances of the time step routines and are not directly related to a type of simulated spray. It can be seen that by decreasing the time step it eliminates the instability due to a smaller step of iterations. This is common for all numerical calculations involving the iterations. The decreased time step results in a smooth iteration flow however increases the overall time of simulation. In case of RSO, the time step values were lower by the factor of 10 in a comparison to diesel. Value of $1 \cdot 10^{-5}$ was the most common one used in present simulations. The setup of the time step values tend do decrease with the increasing injection pressure.
The second instability type occurs when the turbulent diffusion field increases beyond the maximum limit. The fluctuations of the diffusion field during a calculation is typical, however its sudden increase beyond the maximum limit causes the termination of calculations. It was seen that the increase was fairly common for RSO simulations. The problem was alleviated by reducing the size of the time steps and increasing the relative error in the implicit solution for the dissipation of turbulent kinetic energy diffusion as well as by allowing relative error in implicit solution of heat diffusion. The errors step (the maximum tolerance accepted in a single iteration loop) had been increased to $1 \cdot 10^{-4}$.

The turbulent diffusion instability is also influenced by the presence of coarse boundaries crossing areas of steep gradients in the turbulence fields. This problem can be reduced by refinement of the cell. The development of the spray is dependent on the cell size of the finest grid containing part of the spray. The finest grid ensures higher accuracy and reasonable stability but prolongs the calculating time. In this work, diesel and RSO calculations were performed in a coarse-fine grid which has been already tested in the Aachen bomb system [228]. It has been accepted that the type of the grid provided appropriate stability and accuracy.
The quality of the grid affects the collision process and may result in larger droplets and fewer particles as the collision grid cell size decreases. The effect was not investigated in this work. The RSO calculations did not show the numerical overflow due to the collision error. Such investigation should ideally be considered to ensure better drop size accuracy.

The problems of the injection delay has been already outlined in the *Chapter 3* and consequently affected results throughout this research (see *Section 6.2*). As presented in the

Subsection 5.2.6 the needle lift has been used to calculate values of the discharge coefficient. The pressure in the nozzle, the back pressure as well as the pressure applied to the top of the needle, determine the needle lift behaviour. In the case of presented simulations the pressure applied to the top of needle was equivalent to atmospheric pressure therefore the pressure in the nozzle pressure chamber dominated the needle lift pattern. Therefore, the rail pressure determined the injection delay which varied with a fuel line length. In the existing experimental system the injection delays were found between 0.35 and 0.6 ms. Similar delay values were evaluated in the work of Wang et al. [412]. These delays detected in a real system are not included in KIVA code. Therefore the final results of simulations were corrected accordingly to the injection delay recorded for a rail pressure.

Results of the simulations described in this chapter are presented in *Section 6.5* of Results chapter.

Chapter 6

Results

No man is more deaf than he who will not hear.

This part of the PhD thesis presents results of experimental tests described in previous chapters. The results were grouped up in sections which directly follows the layout of *Chapter 3*. For clarity, results of CFD simulations described in *Chapter 5* are placed at the end of this chapter.
Additionally, at the end of this chapter results of the modified engine tests are presented. The results are based on the preliminary modifications of the CDI engine performed at the end of the project. The output is utilised for the direct support of the future work on CDI modifications shown and discussed in *Chapter 8*.

6.1 Properties and preliminary injection tests

In this section three sets of results are shown: investigation of density, viscosity and surface tension of RSO in comparison to SO and diesel, the injection tests focusing on the analysis of injected oil quantities under different injection conditions, and studies of filter clogging at RSO flow. The main aim of this part of the research was to determine the main physical properties of RSO and investigate the influence of the injection frequency, duration and oil temperature on the injected oil amounts in the comparative studies. Also, performed injection experiment confirm usability of the injection stand to mimic a CR injection system.
The comparison between injected amounts of standard and RSO had been conducted at different injection conditions, fuel temperature and atmospheric pressure (if not specified, the presented results were taken at the injection frequency of 5 Hz).

6.1.1 Oil properties

The relevant plant oil properties are usually directly related to the spray formation. Current theory of the spray atomisation occurring in diesel engines emphasises the influence of surface waves on droplet break-up. The surface tension of the fuel is important because of its influence on the stability of these waves. Also parameters like density and viscosity of the liquid. In dense sprays, which are often created by plant oils, it has been shown [302] that the coalescence of the droplets competes with droplet break-up to determine the size distribution in the spray. Surface tension and viscosity play important roles in these two processes.

Three main oil properties (density, viscosity, surface tension) were investigated, which frequently are recognised as the most influential on spray development and fuel flow in diesel injection systems. The tests were carried out on three liquid samples: a standard diesel fuel, SO and RSO. Standard oil is used and recommended by diesel nozzle developer as substitute for diesel. The oil resembles closely diesel properties and is much safer to health. The RSO sample came from a Bavarian RSO mill and represented a most common RSO type used as diesel substitute in that region. The oil was neat, cold pressed, filtered and chemically unprocessed.

Analysis of the physical properties of RSO in comparison to SO is relatively straightforward. Results of density, viscosity and surface tension as functions temperature are presented. The comparison has been done not only to recognise differences between standard and RSO but also to find out how elevated RSO temperature would aim to make these properties similar to SO. In adition to rapeseed and SO each graphs includes several point representing ordinary diesel. Points were added to show that SO and diesel have almost identical physical properties.

Figure 6.1 compares the density values of rapeseed, diesel and SO at varying temperature. Presented experimental results agree with the previous studies reported in [125; 185; 298] where the similar temperature dependence was obtained. The literature results included the ordinary diesel and a sample of RSO. The obtained results show that the density of RSO is higher than diesel oil at any temperature, whereas SO and diesel correspond to almost the same density. The density of RSO was decreased remarkably with increasing temperature and is considerably high at low temperatures. It can be seen that the density of RSO at 0°C is 930 kg/m^3 and therefore may lead to serious obstruction of

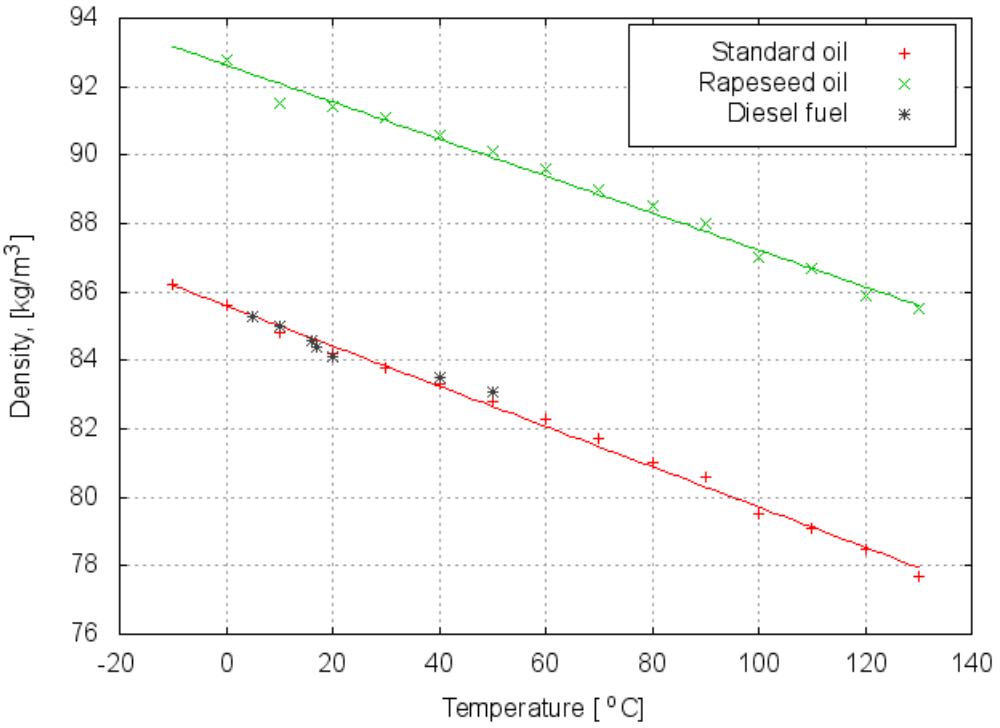

Figure 6.1: *Oil densities.*

the fuel flow inside the injection system. By extrapolating the existing density values it can be concluded that RSO density would become close to diesel (at 20°C) at temperature above 190°C. Typical diesel exhibits a density of 850 kg/m^3 (ASTM D-287). Various RSO densities are reported to vary between 900 and 930 kg/m^3 and the typical value is 920 kg/cm^3 [185; 298].

Presented density values of RSO indicate that volumetric metering of RSO (as in the unit injectors used in modern diesel engines) will result in the delivery of a slightly greater mass of fuel, about 5% on weight at the same temperature as diesel. However, if a CR injector delivers the same volume of fuel, the actual energy will be similar to standard diesel. In general, RSO has lower energy content on mass basis [185]. Discussion on RSO calorific value including its density is briefly covered in work of Hemmerlein et al. [185]. Authors proved that lower calorific value of RSO was almost compensated by greater injected mass of the fuel and measured power output was 2-5% lower in comparison to diesel fuel. Density values of RSO found in this study were similar to those found in work of Hemmerlein and other studies [185; 297; 298; 434].

The variation of viscosities is shown in Figure 6.2 and compared with the values of standard diesel. From the results it is observed that viscosity values of RSO are much

higher than diesel. This is especially apparent for the temperatures lower than 60°C. The ASTM D-445 specification of maximum 4.1 cP viscosity at 40°C is not met by RSO, as shown at Figure 6.2 and presented also by Dunn et al. [125]. Viscosity values of RSO exceed this value significantly at any practical temperature which could be utilised in practice to preheat the oil. In any case, the viscosity of neat plant oils is higher than for typical diesel. Similar results have been already reported earlier by Hemmerlein at al. [185] and Dunn et al. [125]. The viscosity of RSO decreases remarkably with increasing temperature and becomes close to diesel (at 20°C) at higher temperatures. A reasonably similar viscosity value of RSO can be reached above 120°C. Figure 6.3 presents a

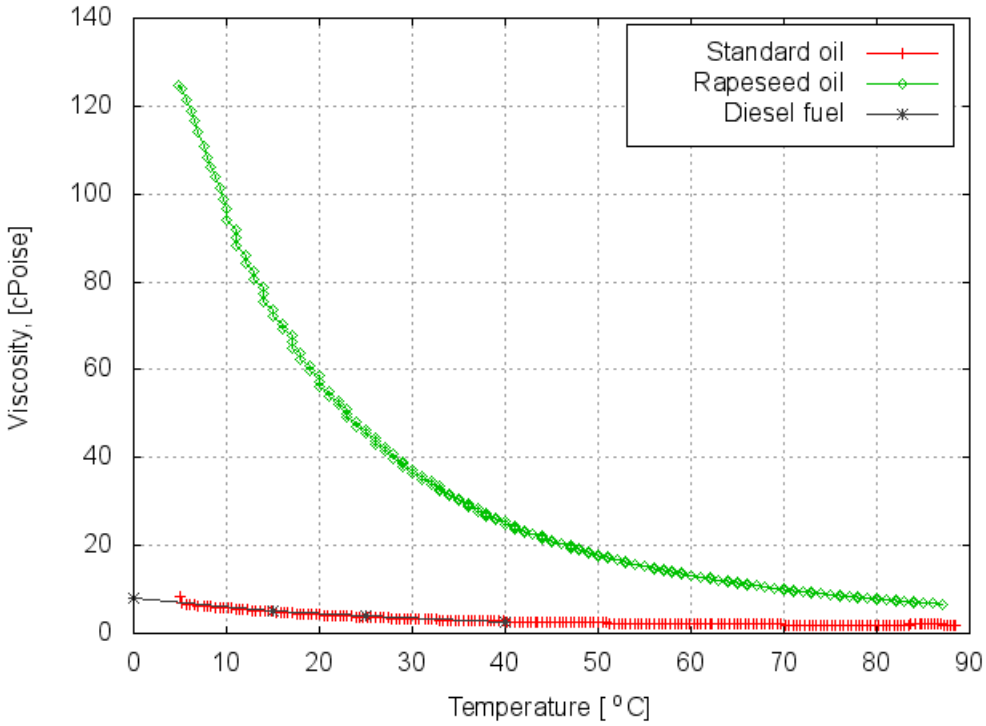

Figure 6.2: *Oil viscosity.*

comparison of surface tension data for two different oils and diesel fuel. Only very limited data on the surface tension of neat plant oils is available in the literature, and none of ASTM or DIN methods is associated with measurement of surface tension. In most cases reported values do not present the surface tension variation with temperature but relate to the room temperature. Surface tension is an important fuel property that affects spray atomisation, droplet size, and fuel flow behaviour within an injection system. Surface tensions play the crucial role as one of the parameters, which should be considered in modification of the CR injection system. It has been established that the spray pattern from

the injection nozzle is adversely affected as surface tension increases. Some researchers [125; 325] discussed the influence of surface tension on the spray cone angle, based on spray experiments performed using a single-hole diesel injector at moderate injection pressure. The observations proved that higher value of surface tension resulted in inferior combustion and contributing to cylinder deposits, particularly in direct injection engines. A typical surface tension value for an ordinary diesel is 22.5 mN/m at 100°C. However,

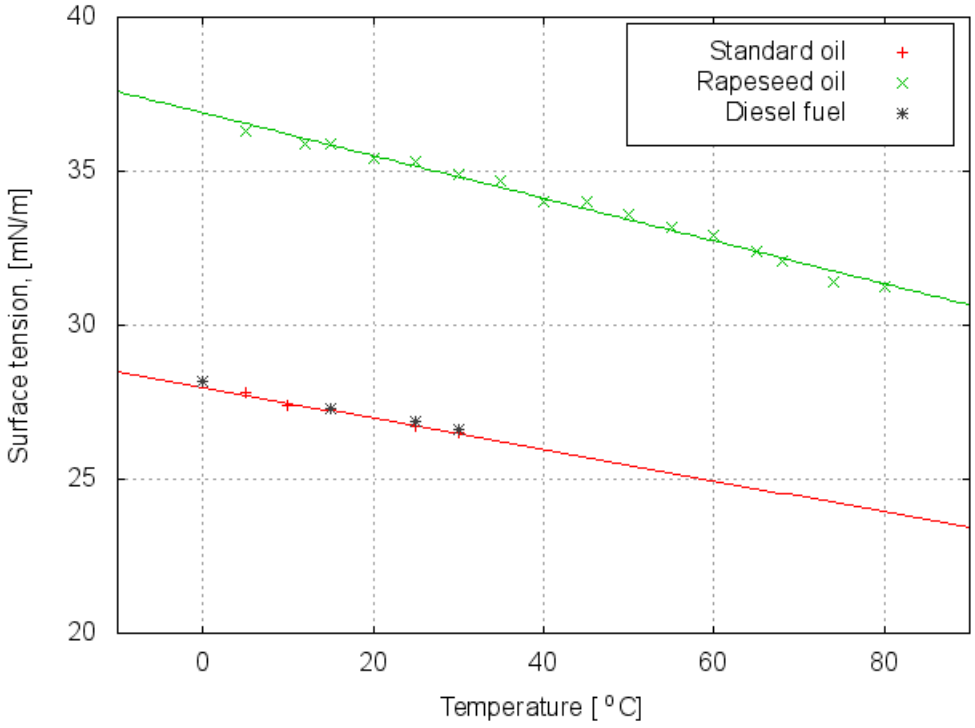

Figure 6.3: *Surface tension*

the diesel surface tension varies and depends on diesel quality and is mainly affected by presence of various additives (in modern diesel fuel a wide range of surfactant additives can be found [172]). The minimum value of 10 mN/m at this temperature was found in literature [16], but the sample constituents were not listed.

As it was expected, temperature has noticeable effect on the surface tension of RSO. The variation with oil temperature is linear. Heating up the RSO to 142°C would render its surface tension to the same as that for standard diesel (27.12 mN/m) at 20°C. Similar results were recorded by Dunn et al. [125]. Figure 6.3 shows that surface tensions of diesel are almost the same. It is recognised that surface tension of diesel is different due to a different concentration of additives.

Presented results confirm the main drawback of using neat plant oils. It is expected that higher density, viscosity and surface tension will effect the characteristics of the fuel spray and will deteriorate engine performance as already recognised in [125; 325]. Hence, these higher values will strongly contribute in the cold start problem and the long-term problems category. It is expected that the situation will effect any type of DI diesel engine including a CR type.

It has been recognised that the high RSO properties can be reduced by oil pre-heating [56; 258]. This is a very common way of adopting an existing injection system to allow diesel engine to operate on neat plant oil . It is believed that the same methodology could be applied to CR injection. Determination of the practically applicable and effective temperature remains an open question and requires further investigation of injection and spray pattern. The results also confirm that the SO represents almost identical properties as diesel. Therefore the oil can be used instead of diesel in further experiments.

6.1.2 Influence of the injection frequency and duration

Following the implication of the previous section, an investigation on injection quantities of RSO in comparison to SO was conducted. The injection tests were performed assuming the proportionality of the increasing amounts of injected oil and the injection frequency. Investigation of injection quantities as a function of injection frequency and duration is important to find out if injected amounts of RSO and SO are similar or different for various combinations of frequency and duration.

As it can be expected, the experiments conducted at the same injection duration and different injection frequencies should result in the same oil volume injected per injection pulse. This can be concluded taking into account the way how the CR system operates. At the increased engine revolution and the constant load the injection frequency is risen but the amount of injected fuel should remain constant as far as the main injection is concerned. Firstly, the SO injections have been studied and analysed. Presented charts refer to injected fuel mass per injection pulse.

Figure 6.4 shows the effect of the increasing injection frequencies on amounts of injected SO at 30°C. As it can be seen the values change in a linear order. The plot consist of three curves practically overlapping each other with a slight value variation at 800 bars of $\pm 1.6\%$. Increasing injection frequency creates excessive heat release and the final oil temperature rise due to more frequent operation of the solenoid valve. It is expected that the deviation

of the results are cause by a difference in the oil temperature as well as injection pressure instabilities. However, as this effect is not significant, it can be seen that the injected amount of the oil are almost the same. As it was expected the injection pressure led to the linear increase of the injected oil amounts for all injection frequencies. Therefore, it had been concluded that the injection amounts can be scale up/down accordingly with the increasing/decreasing injection pressure. Figure 6.5 presents quantities of SO heated up to

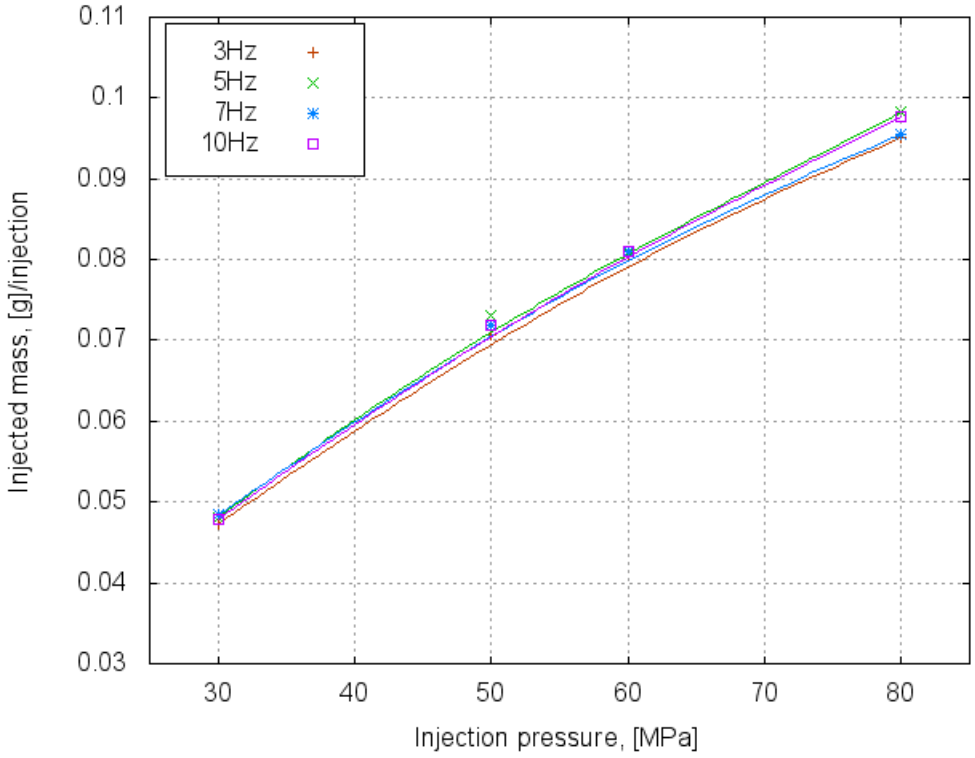

Figure 6.4: *Injected mass of SO for different injection frequencies. (Injection duration - 1 ms, the injection temperature 30°C)*

30°C and injected at different injection durations for three various injection pressures: 30, 60 and 100 MPa respectively. It can be seen an increase of the injected oil with increasing injection pressure. As it one could expect 3 times longer injection time does not result in 3 times higher injected quantities. As it can be seen from the figure, the values at 3 ms are slightly lower for 60 and 100 MPa and higher for 30 MPa. It is concluded that injected quantities are affected by disruptions taking place at the beginning and the end of injection, which have implications on the fuel flow through the injector. It can be also seen that the injector delay is very non-linear with respect to injector pressure.

A similar investigation is shown in Figure 6.6 where RSO was used. The results express almost linear trend of increasing injected amounts with the increased injection duration. In comparison to SO, values for RSO are lower thus the plots are featured by

lower slope values. Additionally, the quantities at 30 MPa can not be simply scaled up to obtain corresponding values for 60 and 100 MPa accordingly. It has been accepted that the flow of RSO at 30 MPa is still deeply affected by much higher viscosity and the temperature of 30°C is too low to alter the viscosity. Thus, there is a very small amount injected for 30 MPa and 1 ms. Comparing the results collected at 60 and 100 MPa it can be seen that the injection pressure has more significant effect leading to almost proportional values. The effect of varying duration was investigated for higher oil temperatures i.e.

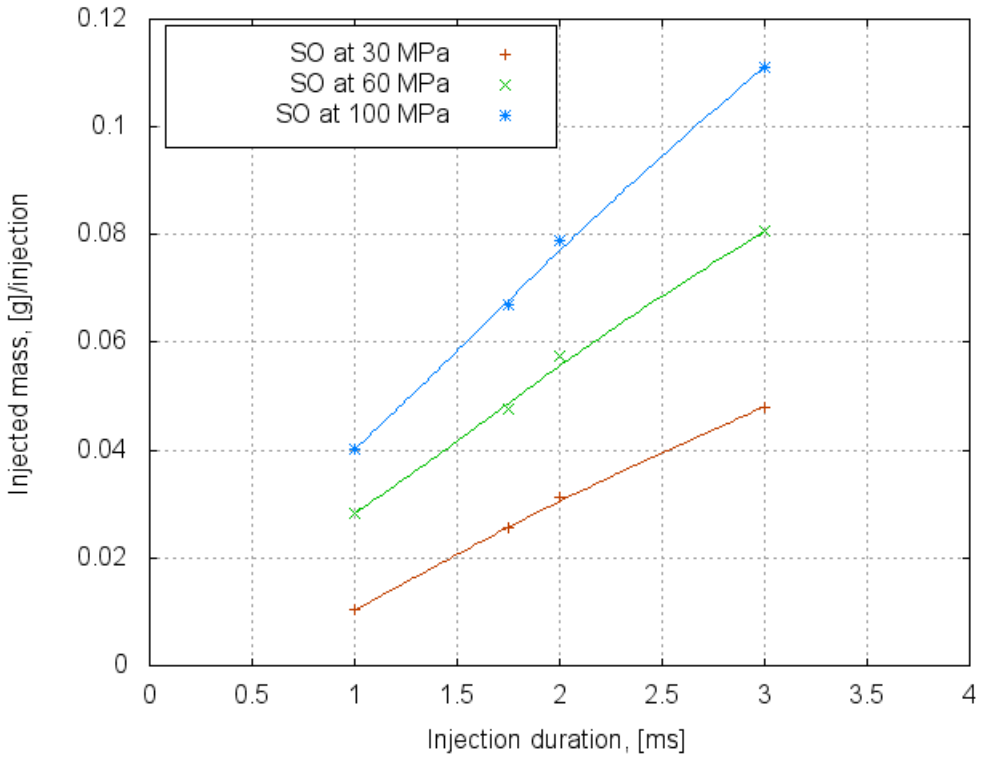

Figure 6.5: *Injected mass of SO for different injection durations. (Injection frequency - 5 Hz, the injection temperature 30°C)*

46 and 72°C. The results are shown in Figures 6.7 and 6.9 and 6.8 and 6.10 for standard and RSO, respectively. From a first glance of Figures 6.7 and 6.9 it can be found that the injected quantities of SO follow a similar trend as for 30°C. The plots exhibit the same linear trend with the significant higher slope accounted for the oil injected at 100 MPa. Despite that it can not be clearly seen from the graphs that the increased oil temperature leads to considerably increased amounts of injected oil. This is due to the fact that the temperature effect is not so apparent since the SO viscosity is not considerably altered within this temperature range. The data of Figures 6.5 and 6.7 are almost identical. A close analysis of the RSO quantities injected at the same temperature revealed a similar linear trend of the increasing oil amount with higher duration of injections. The data of

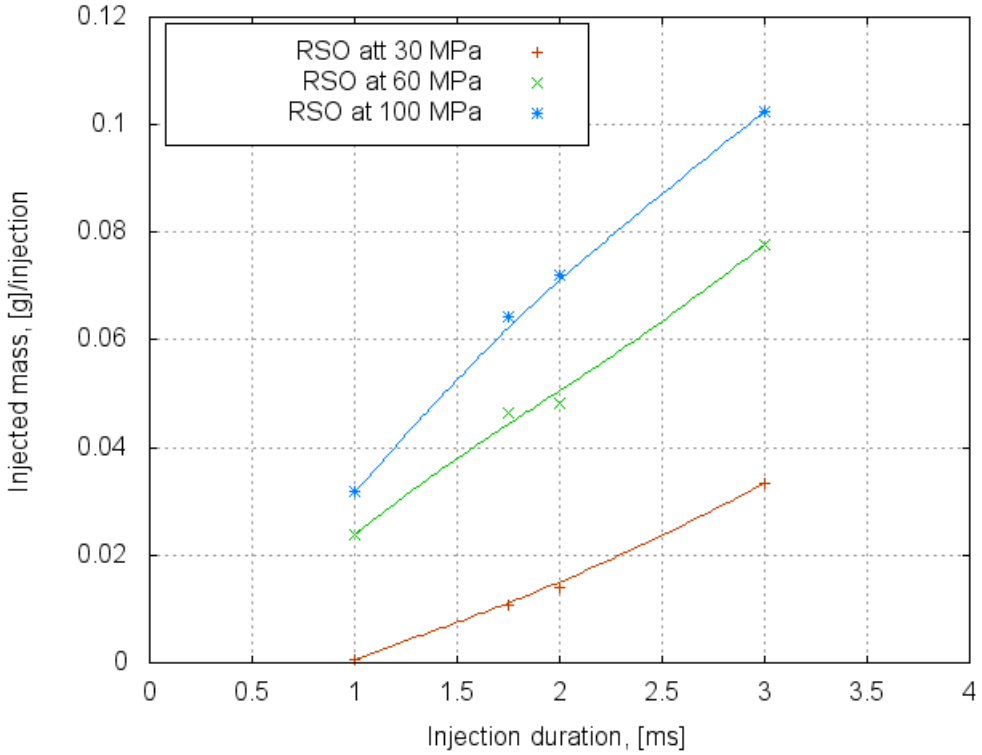

Figure 6.6: *Injected mass of RSO for different injection duration. (Injection frequency - 5 Hz, the injection temperature 30°C)*

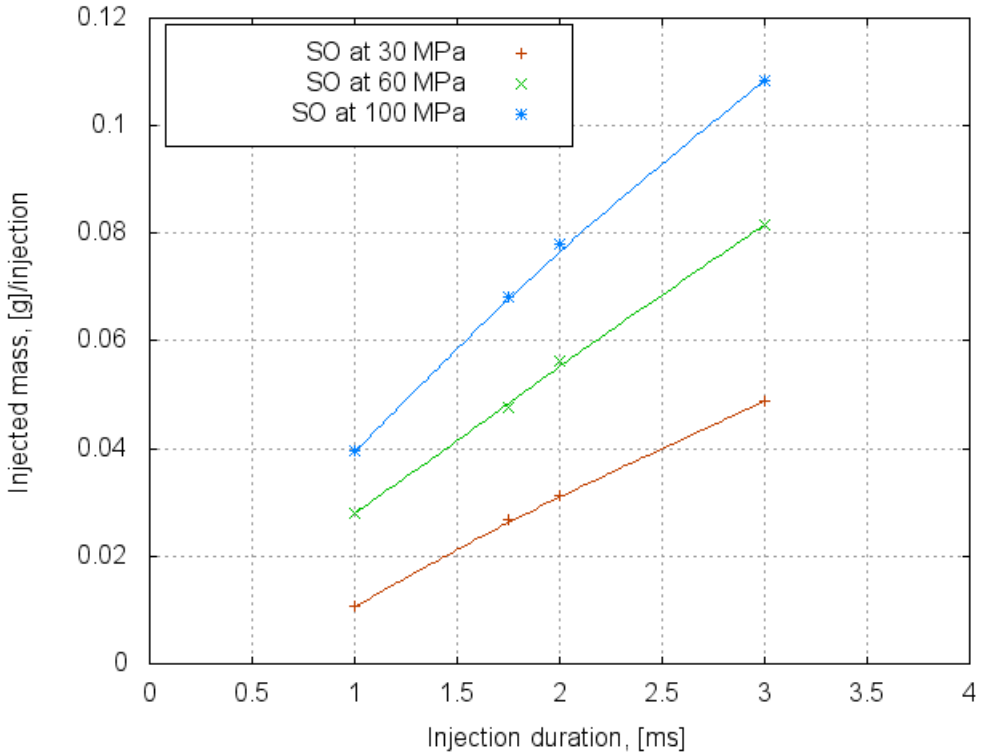

Figure 6.7: *Injected mass of SO for different injection duration. (Injection frequency - 5 Hz, the injection temperature 46°C)*

Figures 6.8 and 6.10 clearly show the increased values of the injected oil in comparison to these obtained at 30°C as well as "lower" degree of delays at 1 ms, which reflects on higher injected volumes at this duration. It is expected that the temperatures higher than 40°C should successfully contribute in reduction of oil viscosity and therefore in the improvement of the internal flow inside the injector. A comparison of Figures 6.5 and

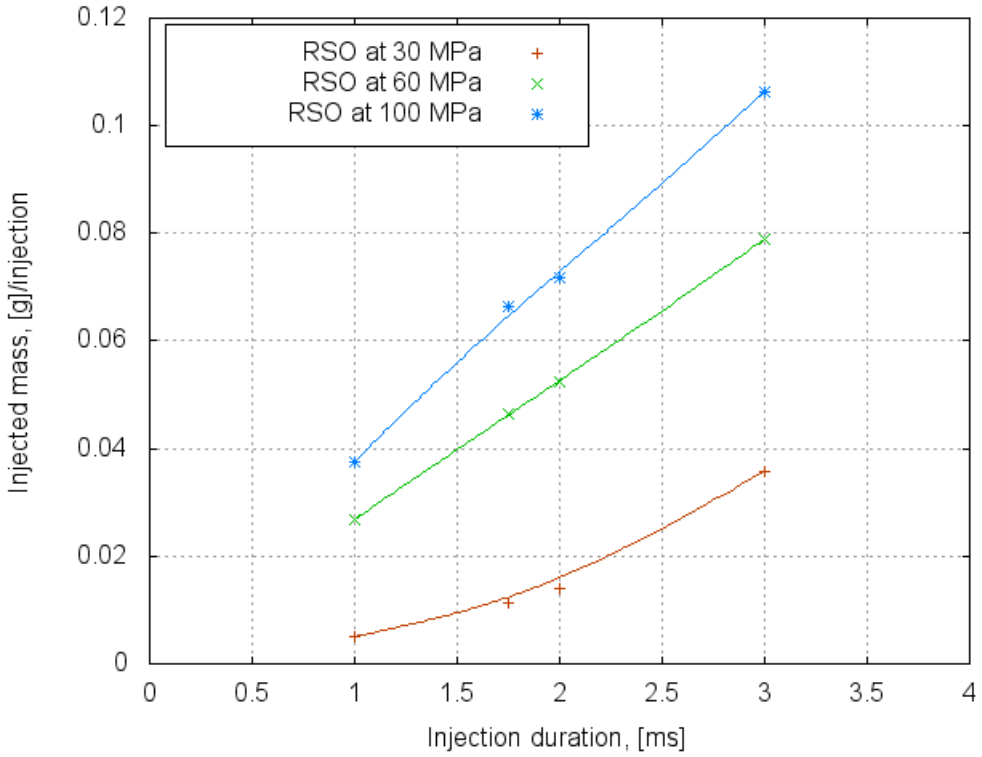

Figure 6.8: *Injected mass of RSO for different injection duration. (Injection frequency - 5 Hz, the injection temperature 46°C)*

6.10 brings out a conclusion that the amount of the RSO injected at 72°C approach the value recorded for the SO. The conclusion can be drawn based on the information provided by the viscosity graph where temperature close 70°C reduces the oil viscosity. Also, it has to be taken into account that increasing RSO temperature contributes in reduction of its density and surface tension. Since, the injected quantities are mainly determined by a constant volume of the injector pressure chamber it can be expected to receive lower quantities (on weight basis) at higher oil temperatures. However, the temperature effect on density is not as decisive as a flow enhancement inside the injector. Therefore the final injected amounts are higher for higher oil temperatures. From the presented results it can be concluded that increased injection pressure and duration lead to increased injected oil quantities. The effect is almost linear and practically can be scaled proportionally to the elevated injection time. A special care needs to be taken if values corresponding to the

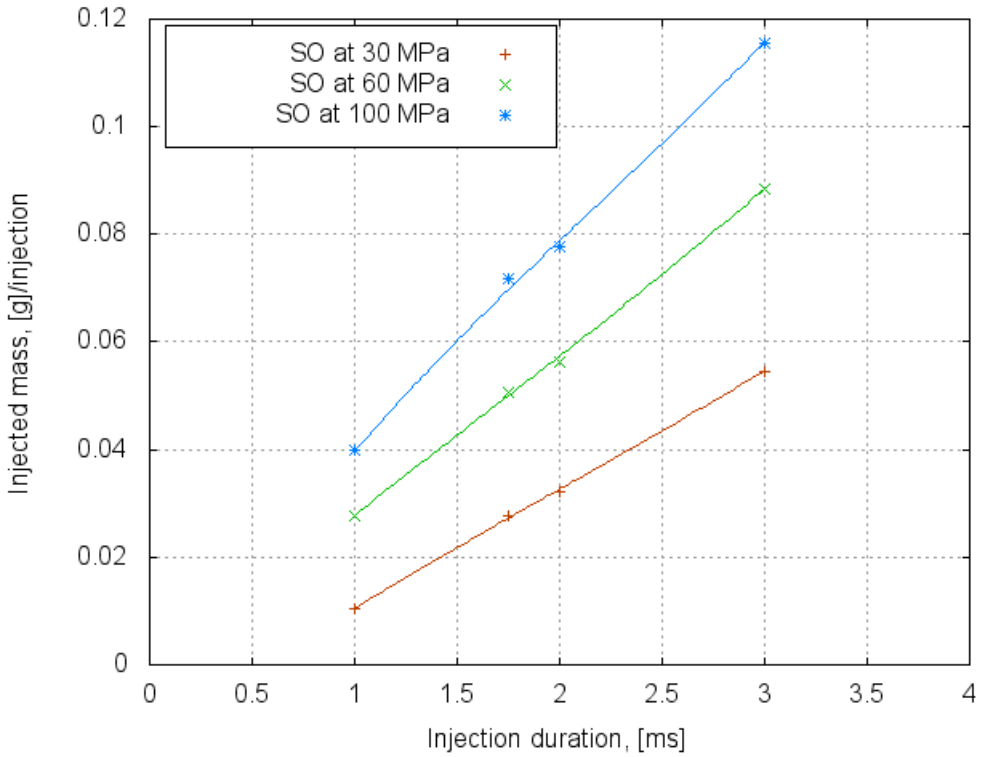

Figure 6.9: *Injected mass of SO for different injection duration. (Injection frequency - 5 Hz, the injection temperature 72°C)*

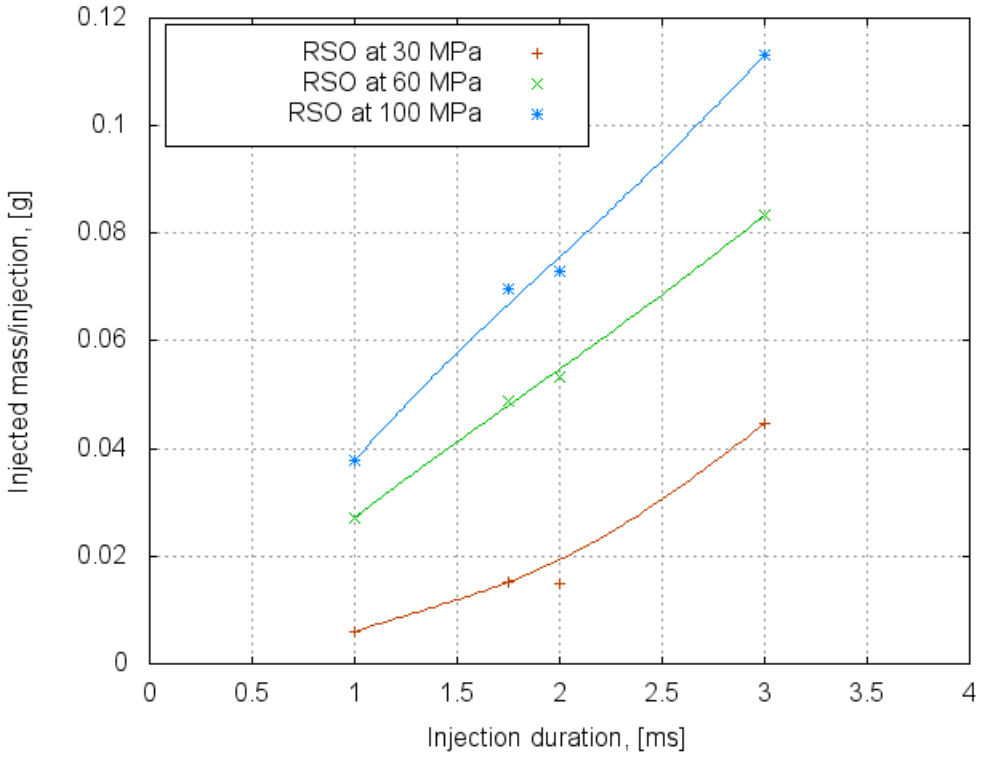

Figure 6.10: *Injected mass of RSO for different injection duration. (Injection frequency - 5 Hz, the injection temperature 72°C)*

injection duration of 1 ms are used. It has been shown that RSO injection lasting for such short time are particularly affected by oil temperature released in injection delays. This noticeably reduces the effective injection time.

6.1.3 Influence of the oil temperature

As it can be seen form the results presented above, the increased fuel temperature increases the injected quantities of RSO. Clearly, oil pre-heating becomes a prospective solution to overcome the short- and long-term problems associated with application of plant oils in CR diesel engines. Therefore, the temperature effect on the injection process seems to be crucial for further investigations. In this section the effect of oil pre-heating studies are shown in more details.

Figures 6.11 and 6.12 provide a comparison of injected quantities of oils at the constant injection duration and frequency, but only altered by injection pressure and oil temperature. In a comparison to the last four graphs presented in the previous subsection, the figures provide the essential information which is required to assess if modification of CR injection system should be based on the fuel pre-heating. Figure 6.11 demonstrates monotonically

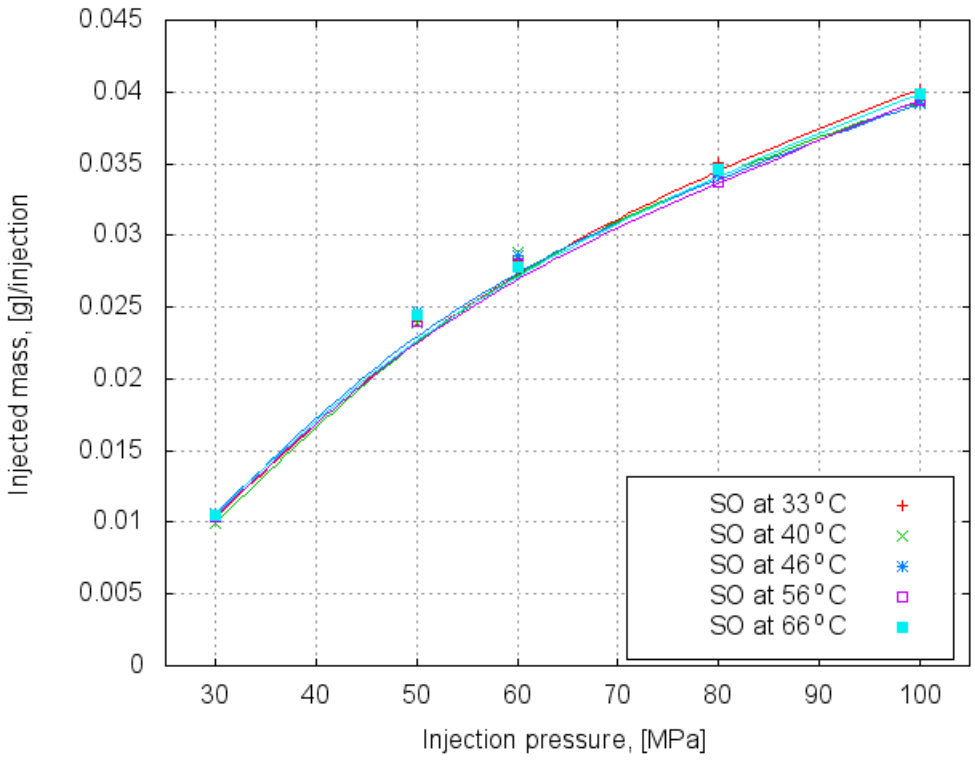

Figure 6.11: *Injected mass of SO for different injection pressures and oil temperature. (Injection duration - 1 ms, injection frequency 5 Hz)*

increasing trend of injected SO quantified for the injection pressures in the tested pressure range. However, the amounts collected at 30 MPa does not fit particularly into this linear trend and that is expected due to the depreciation of the oil flow taking place inside the injector and caused by friction between the oil and the injector. It is concluded that the injection pressure does not provide adequate impact to overcome the initial injection delay. Although, the injection pressure exceeding 30 MPa are high enough to weaken this effect and it can be noted that injection pressures above 50 MPa contribute in the linear injection trend.

The data displayed in Figure 6.12 shows that the quantities of RSO are more sensitive to the oil temperature and also lower than those for SO. It can be seen that the oil temperature of 33°C provides lower values by 10% on average. The increased RSO temperature results in the increasing measured oil quantities. The points pattern of the graph can not be described linearly at least not in the whole range of the injection pressures. Again, it leads to a conclusion that the linearity of data may be affected by the obstruction of internal flow due to friction which can be overwhelmed after applying a certain level of the injection pressure. This level is a function of the oil temperature and higher in comparison to the SO. The linear trend can be accepted for the injection pressures higher than 60 MPa. Figures 6.13 and 6.15 present a closer analysis of injected quantities of both oils. Presented data had been organised using the bar chart type (graphs do not follow the stack type). Values of SO are depicted in red and RSO data is associated with a withe and the green pattern. In all presented charts RSO values are overlapping SO data which is always higher. The bars show differences in the injected amounts at four different injection pressures and the constant injection duration and frequency. The results placed in Figure 6.13 manifest lower values of injected RSO particularly apparent at the injection pressure of 30 MPa. As frequently stated it is assumed that at 30 MPa and 33°C the injection delay lowers the injected quantity. It needs to be commented that the SO quantities are also much lower in comparison to the values for more elevated injection pressures. From 36 MPa onwards the quantity differences between these two oils remain approximately constant.

Figure 6.14 show the same trend and a difference between standard and rapeseed. However, it is expected that the temperature effect becoming more influential on the injected RSO as a result of reduced viscosity. Also, a deviation between these two oil at 30 MPa is lower than the data one recorded at 33°C. Further increase of the oil temperatures leads to less apparent differenced in the injected amounts of the oil (Figure 6.15). A gradual

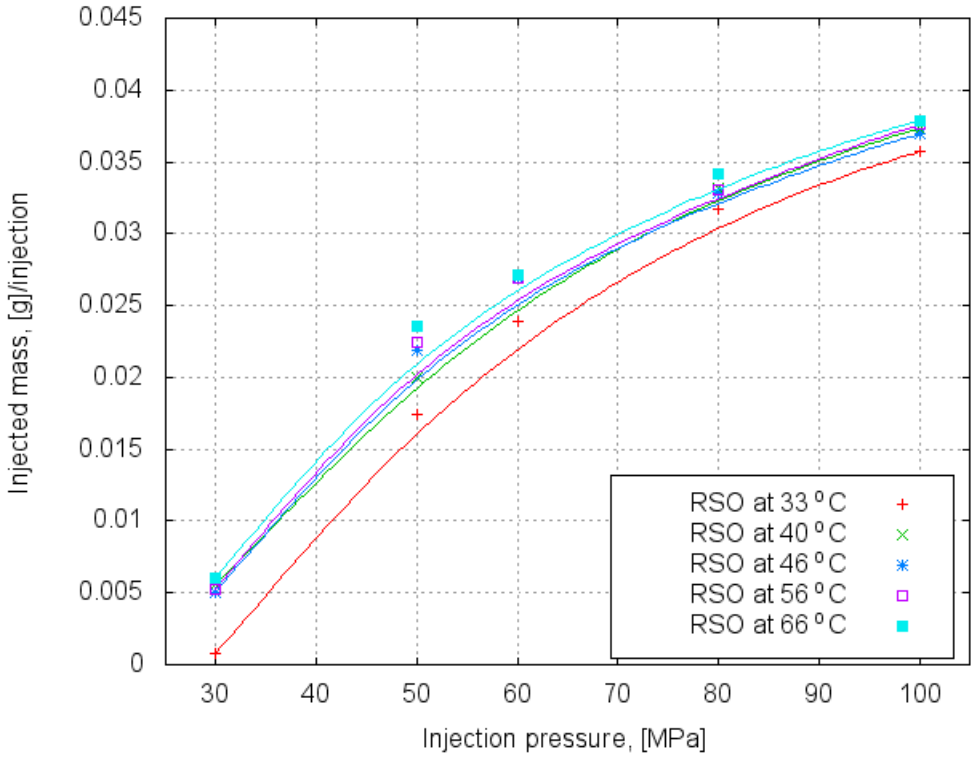

Figure 6.12: *Injected mass of RSO for different injection pressures and oil temperature. (Injection duration - 1 ms, injection frequency 5 Hz)*

reduction of the difference can be seen at 30 MPa and it is caused by lowering the RSO viscosity. An abberations at 100 MPa bar does not reveal further expected reduction but it can be explained by inaccuracies in the measurement and the experimental errors. Form Figures Figures 6.13 and 6.15 can be seen that the temperature effect is more pronounced for RSO, whereas the SO quantities are almost temperature independent. This confirms that elevation of the oil temperature can be used to alter injected quantities of RSO. It is clear that RSO injection taken place at 30 MPa and 33°C may lead to a lack of fuel utilised in air/fuel mixture and delay of the combustion.

6.1.4 Influence of the injection pressure

From the result above, alteration of the oil temperature lead to an improved flow inside the injector, however the temperature effect seems be less pronounced at low injection pressures. Although, such low injection pressures are frequently utilised at engine start-tup [22; 187] it is expected that it could be elevated to improve injection. This section presents influence of injection pressure on oil quantities.

The injected quantities of standard and RSO are compared in Figure 6.16 for the selected injection pressures and in a range of oil temperatures. Three pairs of curves

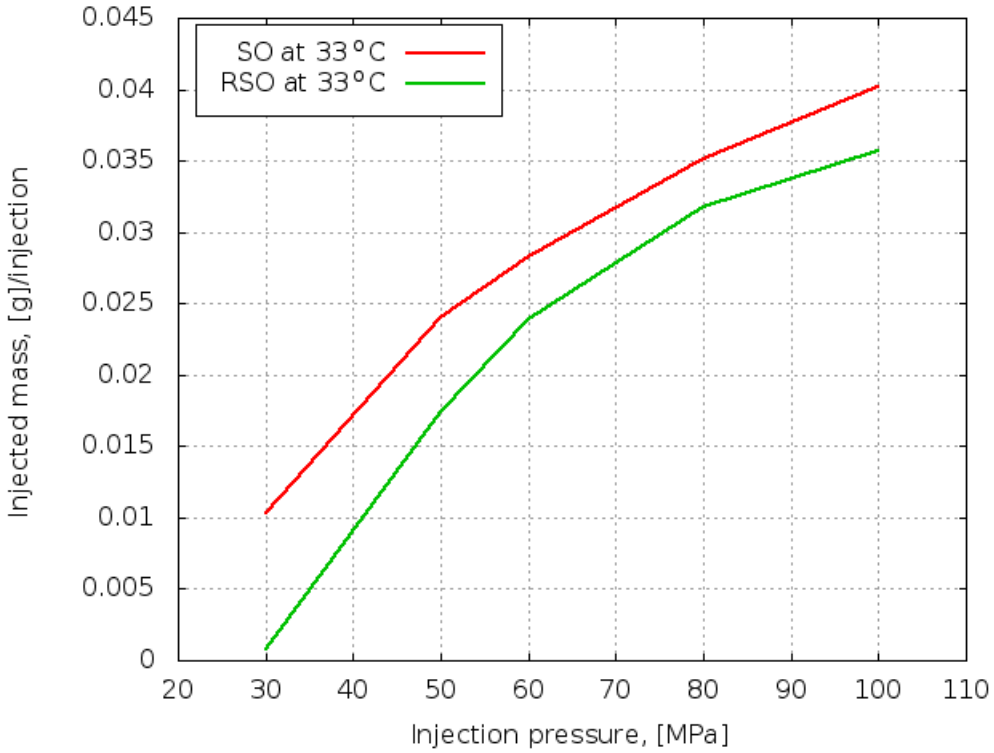

Figure 6.13: *Injected mass of standard and RSO for different injection pressures and oil temperature of 33°C. (Injection duration - 1 ms, the injection frequency 5 Hz)*

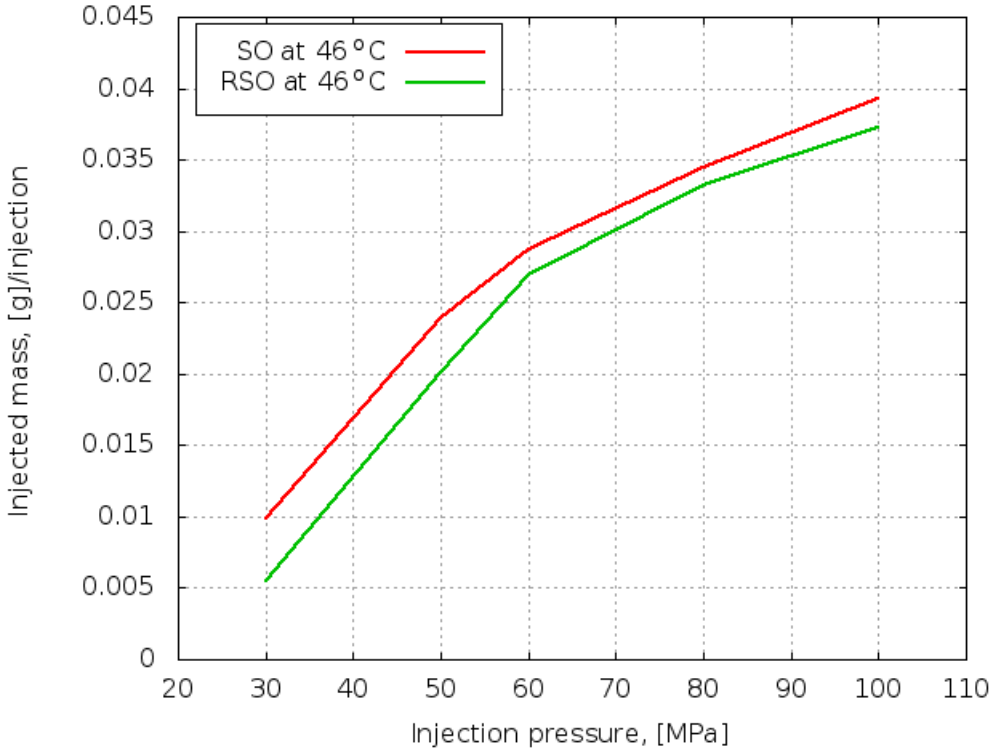

Figure 6.14: *Injected mass of standard and RSO for different injection pressures and the oil temperature of 46°C. (Injection duration - 1 ms, the injection frequency 5 Hz)*

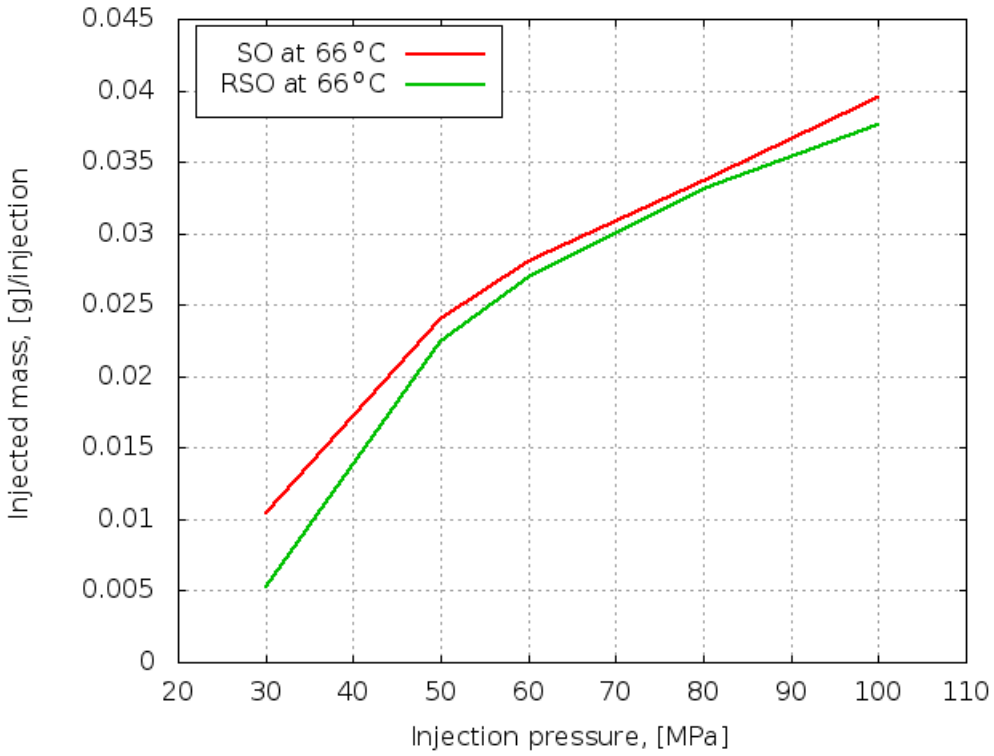

Figure 6.15: *Injected mass of standard and RSO for different injection pressures and the oil temperature of 66°C. (Injection duration - 1 ms, the injection frequency 5 Hz)*

exhibit a general overlook of these two types of oil and changes of injected quantities. The figure shows the rise of injected RSO quantities with fuel temperature and injection pressure, but also illustrates a combined effect of these two parameters on injection. As the injection pressure and temperature increase the points are getting closer and the pressure effect seems be dominant over the temperature effect. This is manifested in the closed oil curves for each pressure set. Values for SO are approximately constant. Next two graphs presented in Figure 6.17 and 6.18 provide more detailed information in a wider pressure range. As it can be seen, the quantities of SO are not immensely affected by the temperature increase which manifests in almost flat curves. It can be seen that within the bound of expected experimental error these curves are flat. As far as the same effect on RSO is analysed it can be noticed from Figure 6.18 that the injected values are gradually increasing with injection temperature for temperatures <40 30°C. Such rise of the curves manifests reduction in the physical properties like viscosity and the surface tension and is more apparent for the lower injection pressures. Both trends of data for standard and RSO caused by temperature and pressure reveal a greater magnitude of changes associated with increasing injection pressure whereas the temperature effect is more apparent for RSO between 30 and 40°C. From the presented graphs it can be seen that the injection

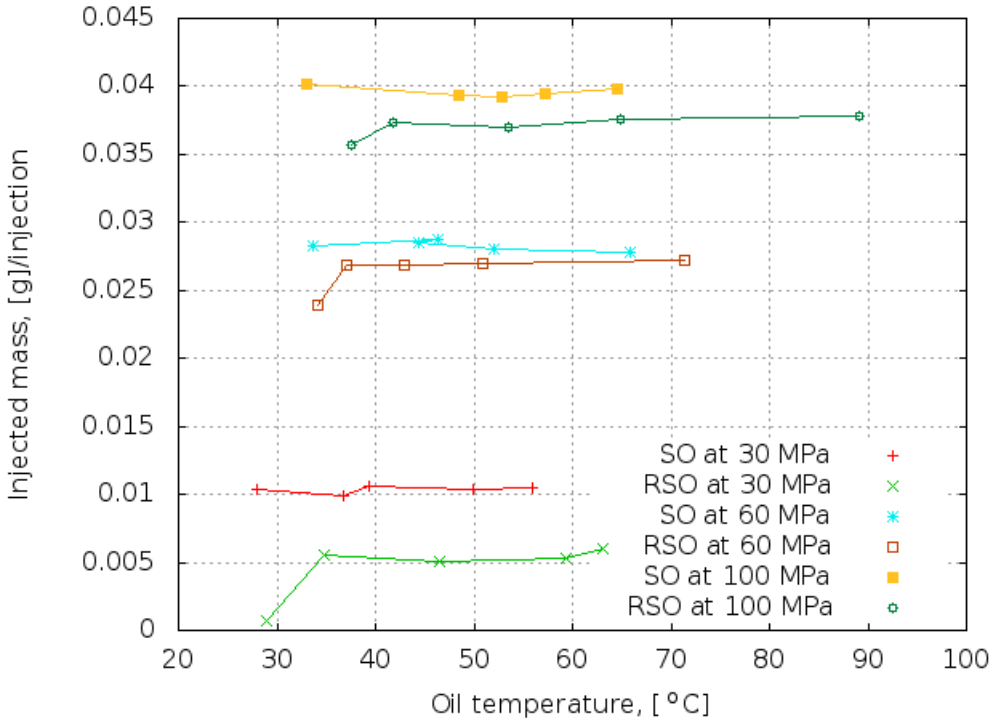

Figure 6.16: *Effect of the oil temperature on injected mass for standard and RSO at different injection pressures and oil temperature. (Injection duration - 1 ms, injection frequency 5 Hz)*

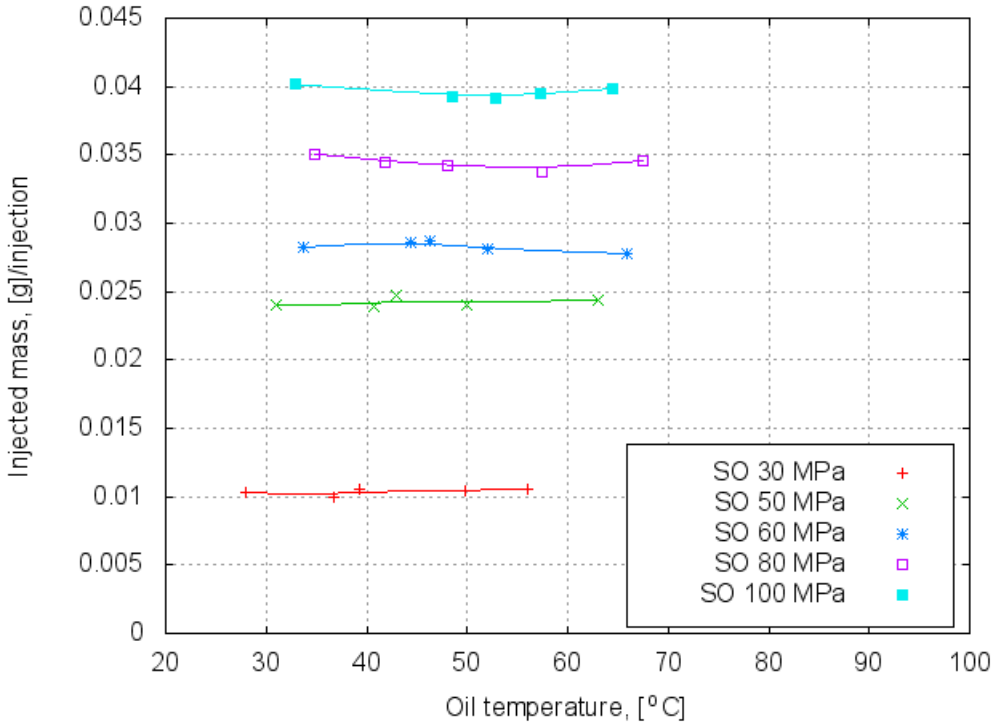

Figure 6.17: *Effect of the oil temperature on injected mass for SO at different injection pressures and oil temperature. (Injection duration - 1 ms, injection frequency 5 Hz)*

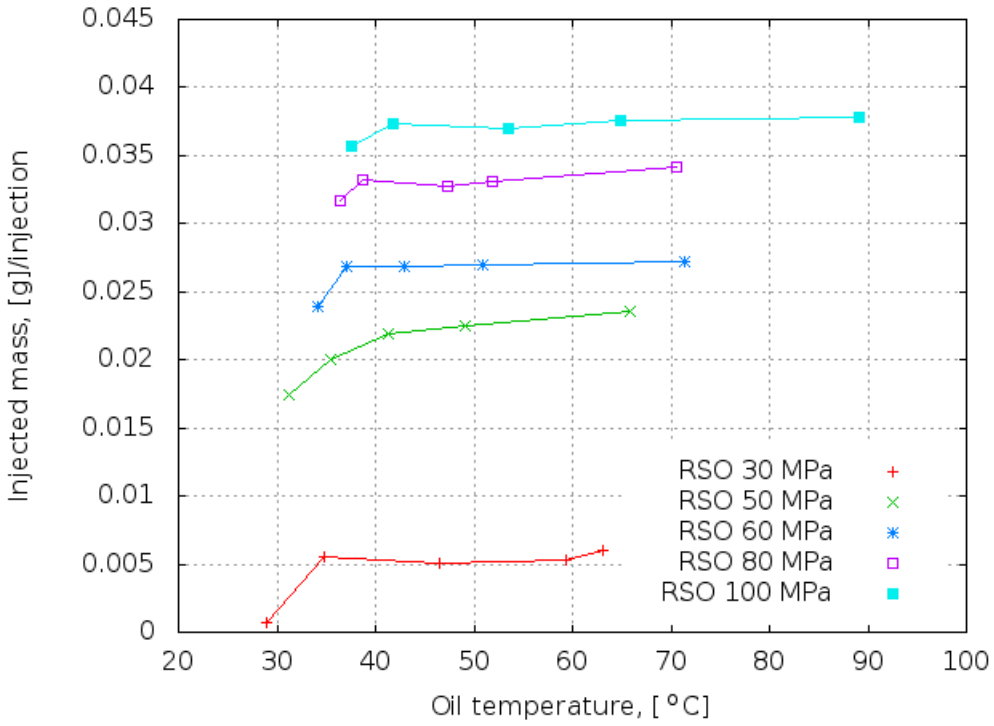

Figure 6.18: *Effect of the oil temperature on injected mass for RSO at different injection pressures and oil temperature. (Injection duration - 1 ms, injection frequency 5 Hz)*

pressure alters injected amount of RSO in a higher magnitude than temperature. The explanation of such finding can be sought in a detailed analysis of oil flow inside the CR injector. Since, the diameters of the injector channels are very small, effective driving forces produced by the pressure differences are significantly affected by interactions governed by viscosity and the surface tension of RSO. Surface tension enhanced adhesion forces whereas viscosity proportionally increases friction factor. Since, these two properties of RSO are higher than for diesel and the diameter reamins the same, the resistance to the flow is higher (the effect can be analysed using Darcy-Weisbach Formula). Higher temperature of the oil reduces these forces in a "static" manner however an increased injection pressure creates greater "push" and enhances the oil flow. However, altering of RSO injection can be reached by combining oil heating and injection pressure. It seems that due to different physical properties RSO injection results always in smaller injected quantities.

6.1.5 Fuel filter clogging

The use of RSO as fuel poses a few challenges to injection system operation and the filter clogging is one of the common problems. Hence, several experiments were performed to investigate the influence of RSO on fuel filter at different fuel temperatures. The problem

of filter clogging due to reduced flow properties is a consequence of the temperature dependencies of properties like density and viscosity (see *Subsection 6.1.1*) but also indicated by researchers investigated filtered frying oil (Zaher [430]).

The injection stand was re-arranged to measure oil flow across a fuel filter. Heating elements installed in the fuel tank and the in-line heat exchangers were used to ensure appropriate oil temperature. The experiments were performed at two different ways: firstly, prior to the start, of the flow RSO was preheated up to 30, 40 or 60°C and then pumped through the filter. In the second experiment, a cold start was mimicked. The oil had initial temperature of 5°C and was simultaneously pumped through the heat exchangers towards the fuel filter. The high pressure pump was running at 900 RPM and the rail was not pressurised. The flow rate as well as oil temperature were measured after the fuel filter. The readings were taken every 10 minutes. Two brand new Bosch NG172(1St) fuel filter were used separately for each oil.

Figure 6.19 illustrates results of a test where RSO was subjected to 3 different oil temperatures. At each case, the oil was preheated in the fuel tank, pumped through the filter and diverted to a discharge tank. The figure compares RSO results with the flow of SO at three different tank temperatures i.e. 30,40 and 60°C. The figure shows that pre-heating RSO increases the flow rate across the filter. Rapeseed oil flow at 30°C is much lower than in case of SO. The flow is nearly 3 times lower as result of noticeably high viscosity i.e. 35 cP. Therefore, for heating temperatures above 30°C, the increasing flow rate was mainly the results of the decreased RSO viscosity. At 60°C, RSO is close to the SO flow at 30°C. In this case the plant oil viscosity was approximately 12 cP in comparison to 4 cP of SO. At the beginning of the tests, the flow rate was not stable because the fuel lines, pumps, valves were cooler than that of the flowing oil hence absorbed the heat of the oil that passed through them. This can be seen at the beginning of each curve of Figure 6.19. After certain time the oil and system reached a stable (equilibrium) stable temperature and subsequently the flow rate became constant. The experiments were finished after 250 minutes and the fuel filter was inspected. A similar results for waste cooking oil were presented by Bari et al. [57]. The author investigated oil flows at different temperatures through a filter and compared with diesel. The waste cooking oil flow was about 240% lower than the conventional diesel. Figure 6.20 shows the graph of oil flows and temperature measured when standard and RSO were heated from 5°C up to 30°C. The experiments was designed to simulate a cold start conditions where 50 litres of oil are stored in a fuel tank and

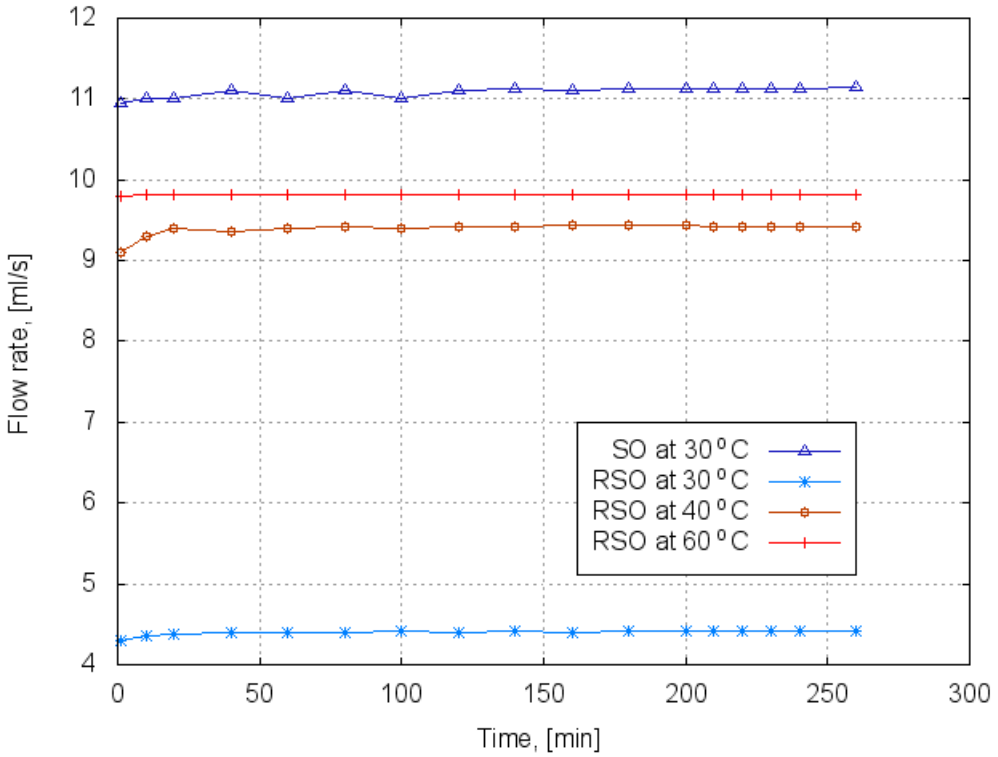

Figure 6.19: *Flow rate of standard and RSOs through the filter at different constant fuel temperatures.*

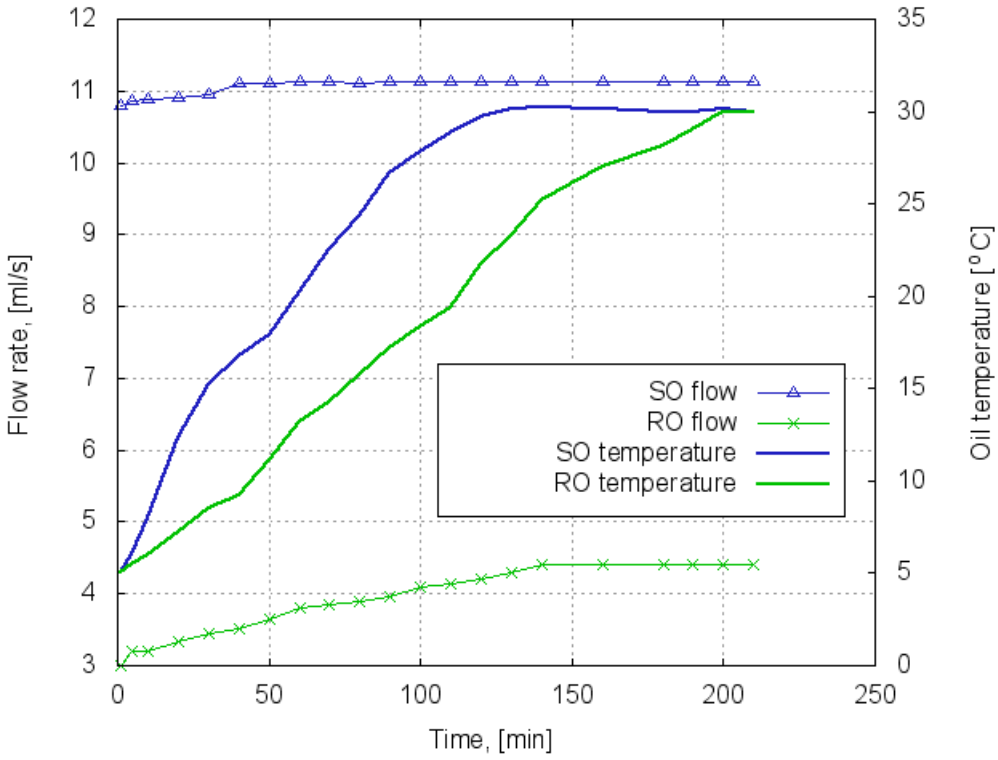

Figure 6.20: *Flow rate of standard and RSO circulating at constant heating.*

gradually pumped into a CR system. Since, high oil volume is not utilised in injection it returns back to the fuel tank whilst its temperature gradually rises. Only a warm water-RSO heater was used to increase oil temperature.

It can be seen that SO flow reaches it maximum value (at 30°C) quicker than RSO. It takes approximately 2.5 hours for RSO to provide the constant flow whilst the SO remains already constant after 1 hour. Additionally, the figure shows temperature profiles recorded in this experiment. Both temperature curves have the similar profile, but it can be seen that the SO temperature curve rises up faster. The temperature profiles strictly correspond to the flow curves and it can be seen that the rising temperature is followed by the rising flow rate. Also it can be seen that SO reaches faster the constant temperature which reflects on a stable flow rate.

The results indicate serious filter flow deterioration of RSO at temperatures lower than 40°C. Oil pre-heating improves radically the flow but the similar flow can not be reached. Rapeseed oil subjected to the constant heating and recirculating in the system gets heated slower than SO. This can be due to higher flow properties and poorer heat transfer. Generally, RSO requires longer pre-heating period to reach desired temperature and this may indicate that an extra pre-heating system must be fitted to provide fast and efficient oil heating. It can be concluded that a separate filter heater should be considered to ensure enhanced oil flow through filter.

6.2 Spray characterisation using high-speed camera

In this section results of the high speed camera spray acquisition tests are presented, which include spray penetration and spray cone angle data. The results were extracted from sets of spray snapshots. The series were processed to include only spray pictures, which consist of a start of an injection until the spray disintegrated from the nozzle tip. Thus, the final snapshot was accepted as a picture showing a breakup point of a jet.

It is known that the injection pressure, drag force, physical properties of injected fuel, and the ambient pressure govern spray characteristics. Amongst these factors, the drag, which is governed by the relative magnitude of the kinetic energy and the aerodynamic resistance of the surrounding gas is very important. The following section presents the influence of these parameters on standard and RSO spray characteristics.

In each subsection results of SO and then a comparison with RSO are presented. It should be noted that due to a large number of results only selected data of injection and

ambient pressures of Table 3.4 were used in the following section. It has been assumed that presented results represent the most fuel and ambient conditions taking place in a real CR injection system.

6.2.1 Injection pressure effect on penetration

The injection pressure has a significant effect on the development of diesel spray. The general trend of increasing the injection pressure and therefore enhancing fuel/air mixture formation led to commercialisation of injection systems utilising gradually higher injection pressures than their predecessors. Therefore, the knowledge of the injection pressure effect is crucial for understanding of either diesel or RSO spray development.

Figure 6.21 presents a spray penetration of SO at 25°C recorded for three different injection pressures at the same ambient conditions of 15 kg/m^3. The penetration curves exhibit a typ-

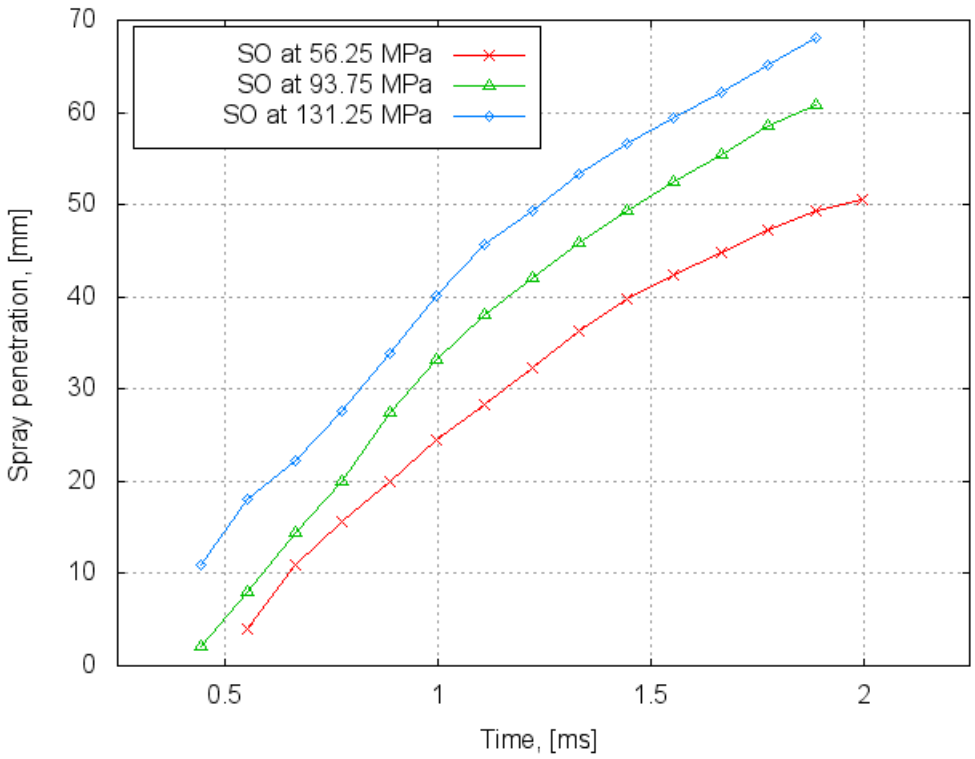

Figure 6.21: *Spray penetration of SO for different injection pressures. (Oil temperature of 25°C) at* ρ_{amb}*=15.0 kg/m*^{3} *of ambient density.*

ical profile of a diesel spray which can be found in the following works [108; 282; 314; 396]. This could be expected since the properties of SO are similar to the diesel ones. All three curves follow the same pattern and it can be seen that the penetration of 56.25 MPa and 93.75 MPa are close at the beginning of the injection. Despite the shape similarities, the curves are less steep in comparison to these recorded in the cited literature. It can be due

to much higher ambient pressure which successfully deteriorates fast spray development. Also, it can be concluded that the shear forces for such high ambient pressures are more pronounced and result in a greater reduction of the tip penetration. In comparison to the literature, the penetration data in Figure 6.21 features of a longer time after which the spray was detected. This indicates slower development of the spray than these recorded in the literature but more likely due to the greater spray delay between the injection start and the optical detection of the spray. The same phenomena was described in [219].

As it can be expected increased injection pressure promotes more enhanced spray penetration. It is showen that a spray penetration for the injection pressure of 131.25 MPa provides almost 5 times higher penetration at the beginning of the injection in comparison to the other two taken at the lowered injection pressures. The initial spray tip penetration from 0.4 ms after start of injection, increases sharply with time up to 0.9 ms and then increases smoothly with time. In all cases, the penetration curves exhibit spray delay which graphically can be found as a lack of the detectable penetration between time zero and the actual beginning of penetration curves. Such hesitation of spray is mainly due to flow retention, hesitation taking place in the injector. The delay of the recording system can be accepted as negligible, i.e. max. 0.11 ms. The spray delay is discussed later in the following section. Figure 6.22 illustrates a set of snapshots of SO injected at 131.25 MPa and ambient density of 15.0 kg/m^3. The snapshots represent a series of five penetrations used to calculate the final penetration for the highest injection pressure presented in Figure 6.21. The first picture shows an initially detected SO jet (within the camera time resolution) recorded at 0.44 ms. The following pictures were taken every 0.11 ms. The last snapshot shows the SO spray just before it disintegrate from the nozzle tip. Spray changes such as those shown in Figure 6.22, revealed that the higher injection pressure makes the leading edge of the sprays slightly distorted. Due to the higher degree of air entrainment and the presence of small vortices at the edge of the sprays. The presence of turbulence indicates a “fuzzy region” at the edge along the spray. Shear forces between the stagnant gas and liquid sprays result in such a phenomenon which would contribute to an increase in the mixing and evaporation of SO droplets as concluded previously by Laguitton et al. [241]. Figure 6.23 shows the effect of increasing injection pressure of SO at ambient density at 30.0 kg/m^3 i.e. the doubled ambient pressure in comparison to the previous chart (Figure 6.21). Similarly to the data collected at 15.0 kg/m^3, higher injection pressure leads to the increased spray penetration. Differently to the previous graph, the curves of 93.75 and 131.25 MPa are not having the same initial values of the penetrations. The penetration at 93.75 MPa at

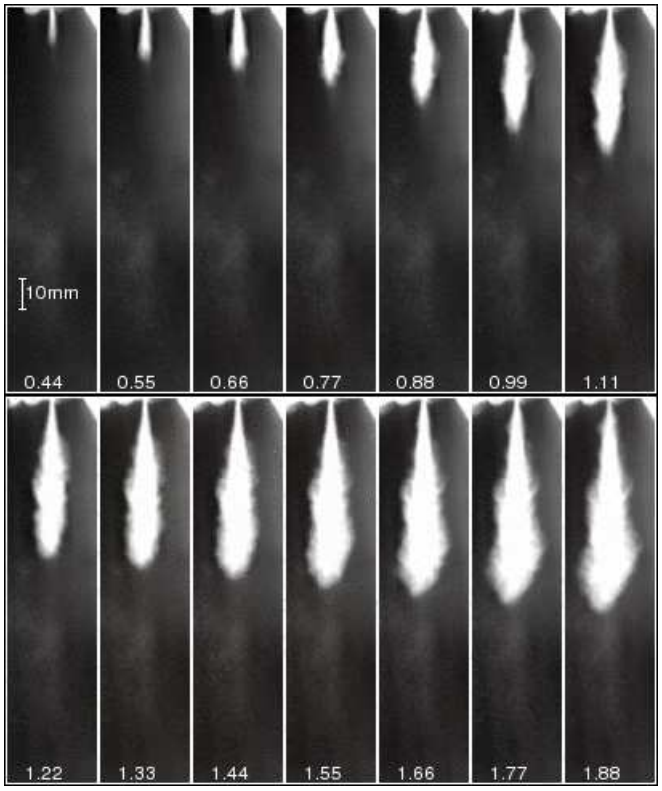

Figure 6.22: *A series of injection snapshots presenting the SO jets at the injection pressure of 131.25 MPa and at ambient density of 15.0 kg/m^3. The times are shown in milliseconds after the injector was triggered. (unprocessed and not scaled)*

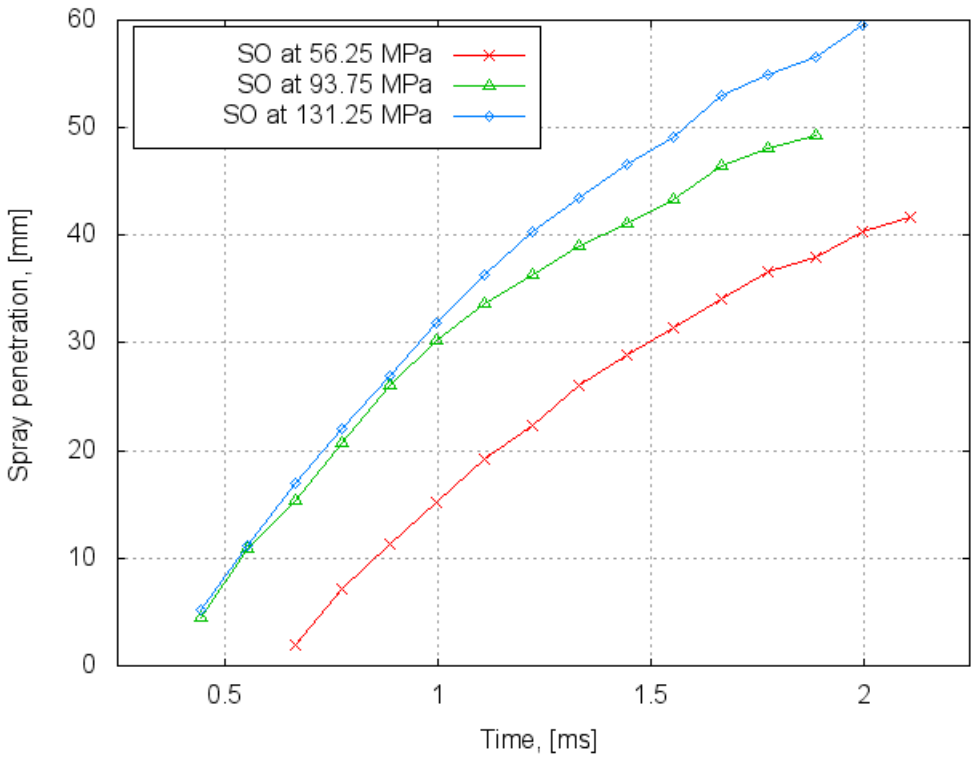

Figure 6.23: *Spray penetration of SO for different injection pressures. (Oil temperature of 25°C) at ρ_{amb}=30.0 kg/m^3 of ambient density.*

its initial stage is almost identical to the highest presented injection pressure. Then, the penetration is getting slowly reduced towards the end of the injection period. This can be due to lower momentum carried on by the spray in comparison to the curve of 131.25 MPa. As the ambient pressure increases the spray penetration becomes more reduced and results in lower final values of penetrations than these presented for the ambient density of 15.0 kg/m^3. For the injection pressures of 93.7 and 131.25 MPa the penetration curves exhibit two distinctive parts: the sharper penetration increase, which can be associated with time period before the break-up takes place approx. at 1.1 ms, and the second part of less steep and lasting increase for the rest of the spray development. The second stage of the penetrations exhibit a detectable ambient density effect. Finally, Figure 6.24 presents

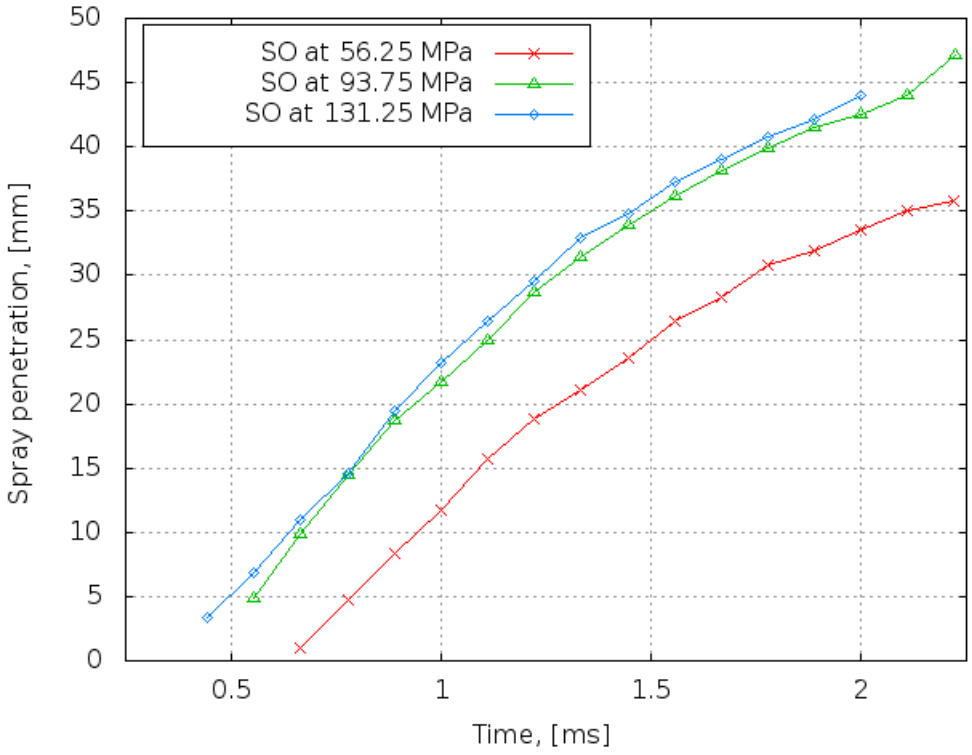

Figure 6.24: *Spray penetration of SO for different injection pressures. (Oil temperature of 25°C) at* ρ_{amb}*=60.0 kg/m*^{3} *of ambient density.*

spray penetration results for the identical set of injection pressures but for the highest ambient pressure of 60.0 kg/m^3 . The penetration is deeply affected by the noticeably high ambient pressure and results in values, which are almost 30% lower than these presented in Figure 6.21 accordingly. This effect can be expected as the ambient pressure was increased by four times. Lower gradients of the penetration curves indicate slower spray development which can be explained by considerably high shear forces acting against spray. The penetration patterns of the highest injection pressures do not feature in distinctive two

stages as it has been recognised for the ambient density of 30.0 kg/m^3.

The lack of significant difference between two curves corresponding to the injection pressures of 93.75 and 131.25 MPa is more apparent. It is concluded that the shear forces produced by the ambient gas are having a similar adverse effect on the spray, and its strength can not be overcome by neither131.25 nor 93.75 MPa. Also, the initial values of penetration show a reduction in the length and the slopes are lower than these for the lower ambient pressures. It also needs to be noticed that there is no clear primary breakup point in comparison to Figure 6.23. Despite the measurements were repeated several time the same trend was observed. Therefore, author can not explain why the figure does not show a clear breakup. A set of SO jets progressing with time is presented in Figure 6.25. The snapshots

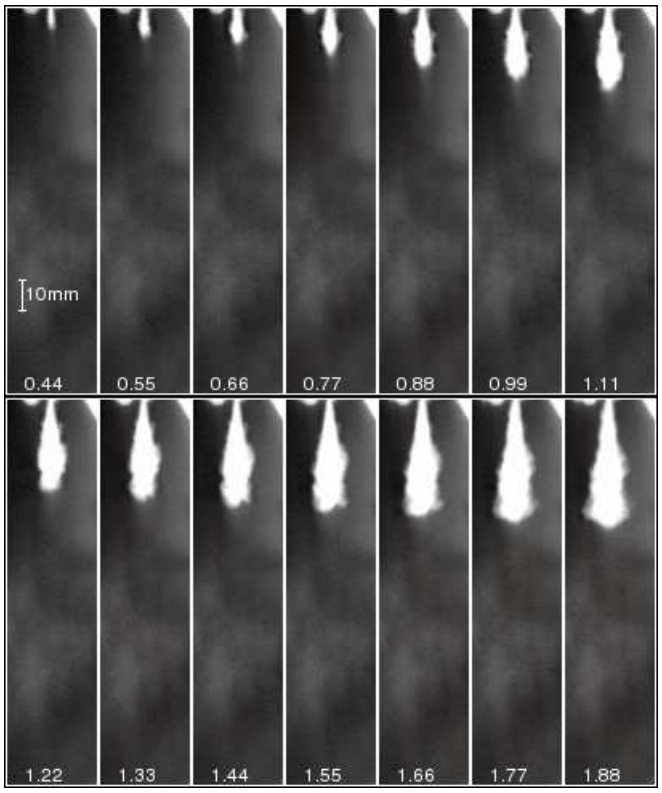

Figure 6.25: *A series of injection snapshots presenting the SO jets at the injection pressure of 131.25 MPa and at ambient density of 60.0 kg/m^3. The times are in milliseconds after the injector was triggered. (Pictures unprocessed and not scaled)*

were taken at the injection pressure of 131.25 MPa and the highest ambient density of 60.0 kg/m^3. The figure adequately supplements the penetration chart of Figure 6.24. The increased ambient pressure results in reduced penetration and "richer" and denser fuel spray. The front edge of the sprays appears to be more rounded and slightly demonstrates sign of regularity as the whole spray becomes more symmetrical. This is particularly

noticeable at the beginning of injection from 0.44 up to 1.11 ms and can be compared with less rounded and more needle like sprays presented in Figure 6.22. It also has to be highlighted that the spray snapshots revealed a very dense and compact structure of sprays. It could be concluded that the dense ambient conditions could contribute in the secondary breakup of the oil drops due to enhanced friction between drop and the gas.

For all presented cases one can clearly notice that the increased injection pressure generates more enhanced SO spray tip penetration regardless the ambient pressure effect. The similar situation was previously recorded in the literature [98; 108; 219; 314; 396] others.

As the injection pressure effect on spray penetration was discussed for SO, a similar analysis can be performed for other non-diesel fuels including RSO. It is vital to recognise difference and define parameters which influence spray penetration of RSO in comparison with SO. Figure 6.26 and 6.28 present the influence of the injection pressure on RSO spray penetration at ambient density of 15.0 kg/m^3 for two different oil temperatures. As seen from Figure 6.26 despite the typical trend of the penetration curves, for a temperature of 25°C RSO, due to the high density and viscosity (see Figure 6.1 and 6.2 in *Section 6.1*), exhibit substantially deteriorated flow inside the injector. Hence the spray development of RSO, especially for low injection pressures, may not represent a fully atomised spray. It was observed that at an injection pressure of 37.5 MPa RSO did not form a proper cone shape spray and oil metering was practically not present. This is due to high RSO viscosity (46.0 cP) and surface tension (35.2 mN/m), which are, in comparison to SO 32% and 1050% higher, respectively. Therefore, the spray penetration at 37.5 MPa injection pressure was not studied for all ambient pressures at 25°C. It can be also noticed that the beginning of penetration does not follow a typical trend recorded for SO i.e. a straight line. The initial period is described by a slow penetration increase which lasts for approx. 0.11 ms and then is followed by a typical sharply rising curve. Such different and very initial period of spray development can be explained as a consequence of noticeable flow obstruction inside the injector and hence very reduced spray penetration. After a short period of time the momentum forces overcome such obstruction enhancing a better flow. Also, the cooling effect of the injector has to be taken into account. Since, the nozzle tip is not heated, oil entering the injector tip is rapidly cooled down and thus influences the beginning of injection. It can be seen from Figure 6.26 that the rapeseed penetrations at 93.75 and 131.25 MPa resemble the similar curves taken for SO at the same oil temperature. Injection of RSO features a longer injection delay than SO. It can be seen that RSO at 56.25 MPa shows a meaningful spray penetration value only after 1 ms. Such large delay

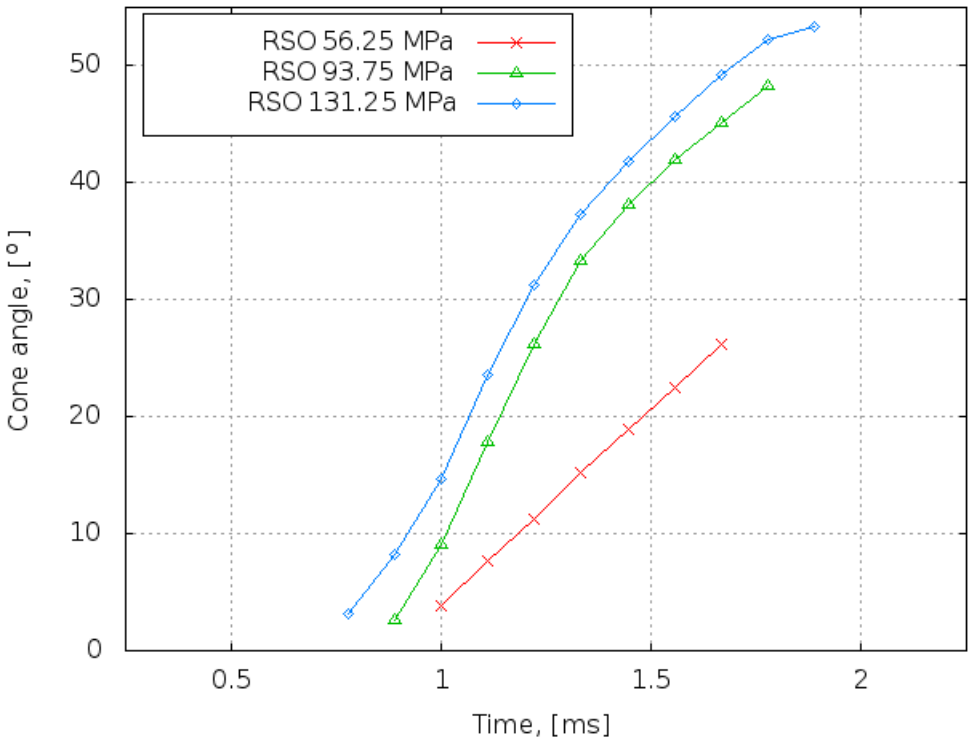

Figure 6.26: *Spray penetration of RSO for different injection pressures. (Oil temperature of 25°C) at* ρ_{amb}*=15.0 kg/m*^{3} *of ambient density.*

can be related to the poor oil flow inside the injector which also reflects on the slower spray penetration. This is manifested by low gradient of the penetration curve which is almost perfectly straight. A similar penetration characteristics was found by Jimenez et al. [207] who investigated RSO methyl ester and compared with diesel (viscosity of the ester was 7.0 cSt at 25°C). The methyl ester results followed the similar straight linear trend of penetration and authors noticed not as good penetration of the ester as in the diesel case which could be associated with 30% higher viscosity. It has to be recalled that the viscosity of methyl ester is lower compare to RSO and at its average value at 25°C is ten times lower. Therefore, it can be concluded that at lower injection pressures and 25°C RSO atomisation is incomplete. At such RSO temperature, injection pressures higher than 56.25 MPa should be utilised. A visual presentation of RSO spray development is presented in Figure 6.27. A series of RSO jet pictures illustrate spray propagation produced at 131.25 MPa and 25°C. The jets can be described by a needle-like shape and feature a reduced cone angle in comparison to SO jets presented in Figure 6.22. Spray-shape can be noticed further down the spray as it becomes more rounded. Close analysis of the spray indicates the formation of vortices due to the enhanced entrainment of the ambient gas. However, the turbulence is less apparent than for SO which indicates a reduced oil dispersion and possibly larger drops. The jet core of RSO spray is narrower and surrounded by the oil deficient dispersed

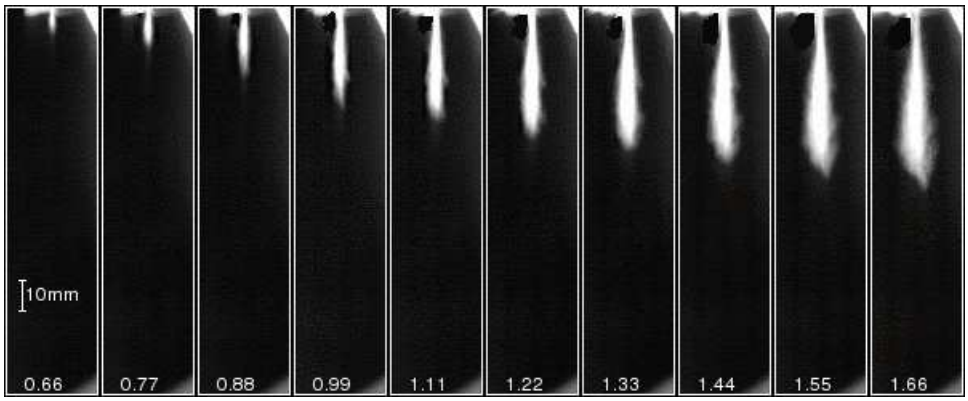

Figure 6.27: *A series of injection snapshots presenting the RSO jets at the injection pressure of 131.25 MPa at 25°C. The ambient density of 15.0 kg/m^3. The times are in milliseconds after the injector was triggered. (Pictures unprocessed and not scaled)*

phase.

Figure 6.28 illustrates penetration curves of RSO at the same ambient density of 15.0 kg/m^3 but for an oil temperature of 60°C. Each of the penetration curve follows a similar trend already observed at 25°C for 93.75 and 131.25 MPa. Here the penetration at 56.25 MPa exhibits the same curve pattern as the remaining two. The spray delay has been significantly reduced (almost 0.5 ms in comparison to the penetration at 25°C) due to lower oil density and viscosity and thus improved oil flow inside the injector. The penetration curves for 93.75 and 131.25 MPa represent very similar penetration results which may indicate a resembling oil flow inside the injector. The injection pressure effect is not as distinctive as in a case of lower temperature of 25°C. Also, the maximum tip penetration for the 93.75 and 131.25 curves is almost the same as observed in the figure for 25°C. Some images of RSO spray are presented in Figure 6.29. The recording was conducted at the injection pressure of 131.25 MPa, the oil temperature of 60°C and the ambient density of 15.0 kg/m^3. Presented RSO sprays had been developed in the same way as is presented in Figure 6.27. The comparison of both figures reveals some difference in the spray shape and the entrainment of the ambient gas. Higher oil temperature produces richer spray of more rounded structure. Even at the early stages of the penetration oil sprays have a typical rounded shape. The spray core is wider and the spray edges consists of oil vortices which may indicate higher turbulence due to better fuel dispersion. Especially the snapshot taken at 1.77 ms reveals a distinctive two region, the inner dense spray core and the outer less dense but well mixed spray.

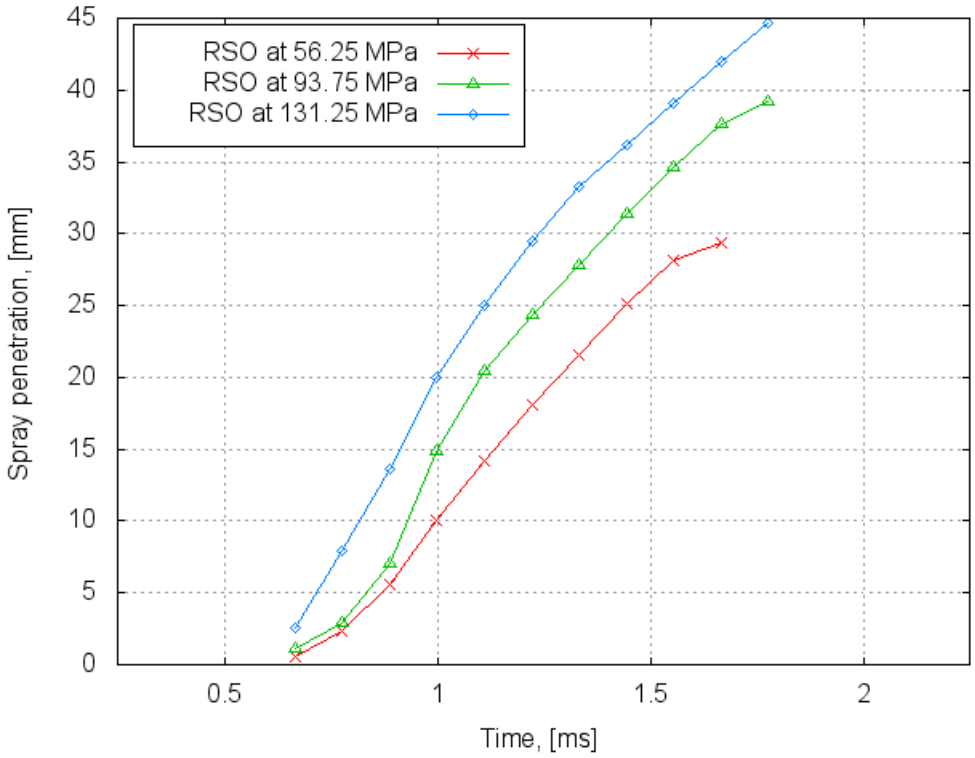

Figure 6.28: *Spray penetration of RSO for different injection pressures. (Oil temperature of 60°C) at* ρ_{amb}*=15.0 kg/m*^{3} *of ambient density.*

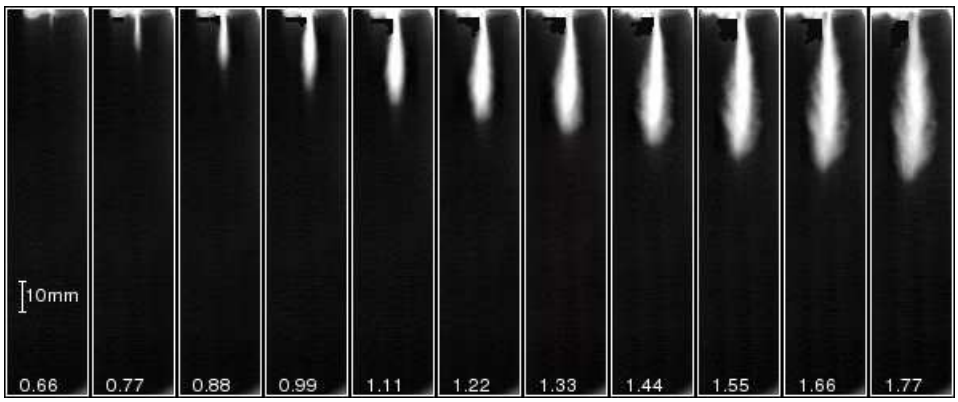

Figure 6.29: *A series of injection snapshots presenting the RSO jets at the injection pressure of 131.25 MPa at 60°C. The ambient density of 15.0 kg/m*^{3}*. The times are in milliseconds after the injector was triggered. (Pictures unprocessed and not scaled)*

6.2.2 Injection pressure effect on cone angle

The cone angle results were evaluated according to the method described in Subsection 4.2.4 at common ambient and injection conditions as for the penetration results presented above. Results of standard and RSO are presented in a similar orders as penetration results.

Figure 6.30 shows changes of SO spray cone angle with the injection time. It can be seen from this figure that the angle values sharply increased at the beginning of the

injection and oscillates around 20 ° for 56.25 and 93.75 MPa. For the injection pressure of 131.25 MPa the cone angle values are gradually decreasing from 1.5 ms onwards. Within the first part of the cone angle pattern values are changing from 12.5 ° (for 93.75 and 131.25 MPa) up to 22.5 ° for 93.75 MPa. The similar trends of spray angle was recorded for diesel in [396] and in [200] where dimethyl ether was used and it is associated with a very initial formation of the spray. In case of dimethyl ether, the angle curves expressed an initial rapid rise and then a gradual fall towards almost a constant value at the end of injection. The presented results feature the same initial trend, whereas at the end the cone angle values do follow almost a constant value. It may be concluded that the presented data describe a continuous development of a spray and increasing penetration is not always followed by an increasing width of the spray. The cone angle increases faster than penetration at the beginning and then changes are proportionally to the change of the spray length resulting in an almost constant value.

The cone angle shows rather little reduction with the injection pressure. This is demonstrated by the slightly lower values of the cone angle at 131.25 MPa in comparison to the lower injection pressures presented. A similar observation was recorded by Payri et al. [314] who investigated diesel fuel at low and moderate injection pressures and the work of Yu and Bae [427] who investigated dimethyl ether in a CR injection system. In both of the literature cases, the authors did not observe a proportional increase of the cone angle with the injection pressure. The observed fluctuations were rather within a certain value band with a tendency of increased cone angle for higher injection pressures. However, this observation contradicts conclusions made by Delacourt et al. [108] who did not record influence of the injection pressure diesel spray angles (they did not use a high speed camera technique for the spray studies). The authors stated a lack of quantitative validation of the results with others but confirmed a satisfactory match with the theory developed by Reits and Bracco [340]. It needs to be noted that the values of spray cone angle presented by Delacourt remains nearly constant during the whole injection and do not vary a lot with a changing injection pressure. This observation has not been recored in other works. Delacourt results start at 0.6 ms which also indicates a considerable injection delay. As already discussed above the presented cone angles appear to agree with the near cone angle results reported by Tennison et al. [396] where characteristic diesel sprays were reported in a CR injection at 1200 bars. Tennison considered two types of the spray cone angle: near and far. The results of the near cone angle compares better with the present

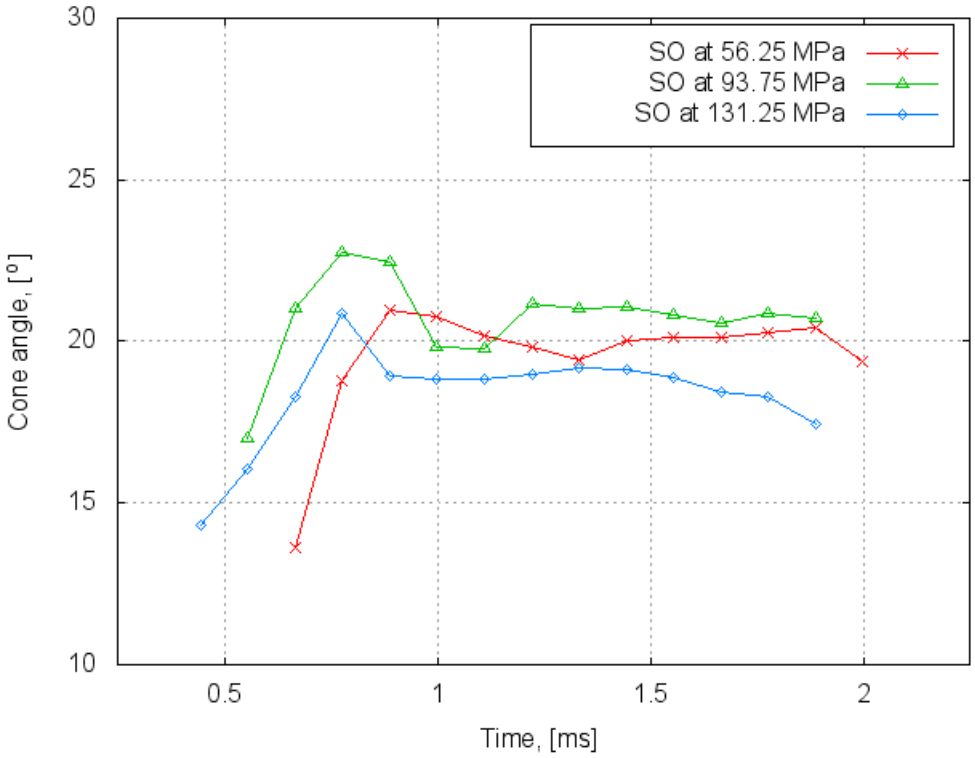

Figure 6.30: *Spray cone angle of SO for different injection pressures. (Oil temperature of 25°C) at* ρ_{amb}*=15.0 kg/m*^{3} *of ambient density.*

data presented in Figure 6.30. The present results are lower in comparison to the literature on average by 10%. It is assumed that the literature data were generated using a different method as well as injection pressures were not exactly identical to those used here.

Variation in the spray cone angles for SO injected into denser ambient gas is presented in Figure 6.31. As it can be expected denser ambient conditions result in wider cone angle due to the greater drag forces acting against the spray front. In comparison to the previous figure, the angle values are higher by 10% on average as already observed from the figures presented above showing the appropriate snapshots. The denser is the atmosphere in-cylinder, wider is the cone angle. A similar conclusion was found by Hwang et al. [200]. However contradicting comments on the effect of ambient conditions were found in [376] and in [427]. It can be concluded that higher ambient density (pressure) creates higher drag force by reducing the spray penetration but also providing better fuel dispersion due to stronger shear forces This can be seen in Figure 6.25. The wider spray at the reduced penetration should result in the larger cone angle values. The contradictive results presented in [376] and in [427] may have the origin in the way of processing snapshots with the special attention paid to the threshold level. It can be concluded that in the case of very thin and turbulent spray edges, the threshold level has to be chosen to define a reliable spray contour.

Next figure, Figure 6.31, presents results of cone angle for SO injected at three different injection pressure but elevated ambient gas density i.e. ρ_{amb}=30.0 kg/m^3. It can be seen from Figure 6.31 that the lowest injection pressure produces the highest cone angle after 1.4 ms. This can be explained by the reduced penetration and hence short longitudinal spray dispersion at relatively wide spray curvature. The curves feature the same trend and a pattern. However, a characteristic feature of Figure 6.31 is a wider difference between the final cone angles of the lowest and the highest injection pressures. Further increase of

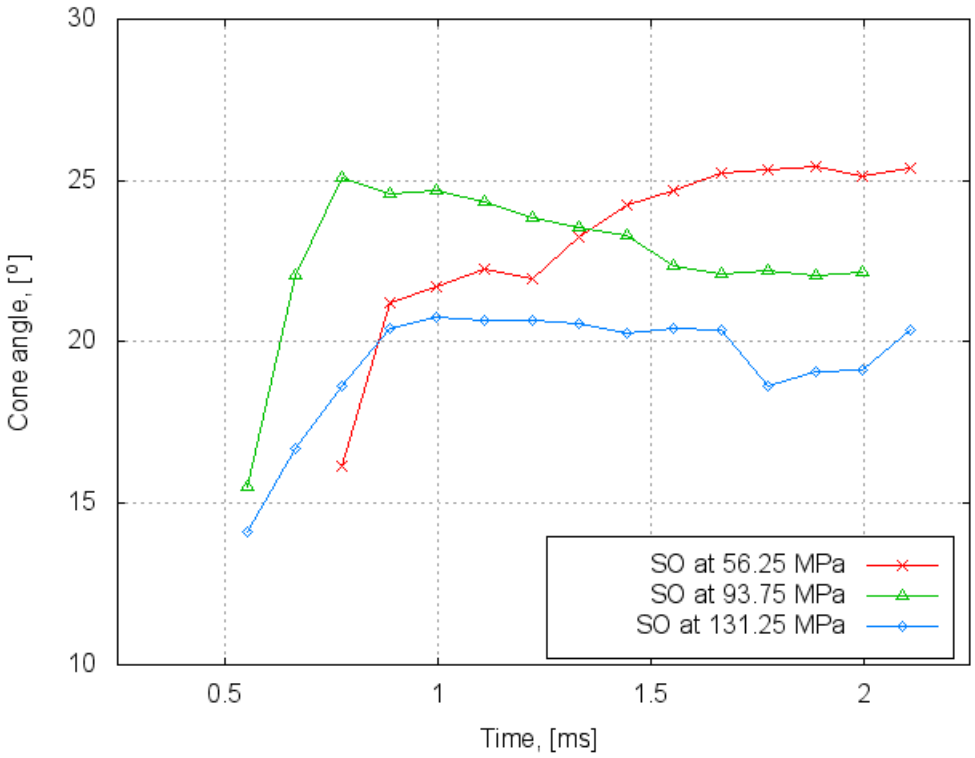

Figure 6.31: *Spray cone angle of SO for different injection pressures. (Oil temperature of 25°C) at* ρ_{amb}*=30.0 kg/m*^{3} *of ambient density.*

the ambient pressure up to 60.0 kg/m^3 leads to richer spray shapes and thus to increased cone angles as shown in Figure 6.32. Sovani and co-workers [376] investigated effect of ambient pressure on spray cone angle and indicated that the cone angle rises as ambient density increases. Similarly to the previous figure, as the injection pressure increases the cone angle continues to decrease gradually. Again, the injection pressure effect on the cone angle can be considered as relatively week as the values vary by 10% on average.

Figure 6.33 illustrates the effect of the injection pressure on the RSO spray cone angle. The results were collected at the oil temperature of 25°C and therefore can exhibit a high degree of uncertainty and can be questioned as the corresponding values of penetration presented above. From the figure it can be seen a significant difference of cone angle values between the lowest and the highest ambient pressure which reaches 40% on average.

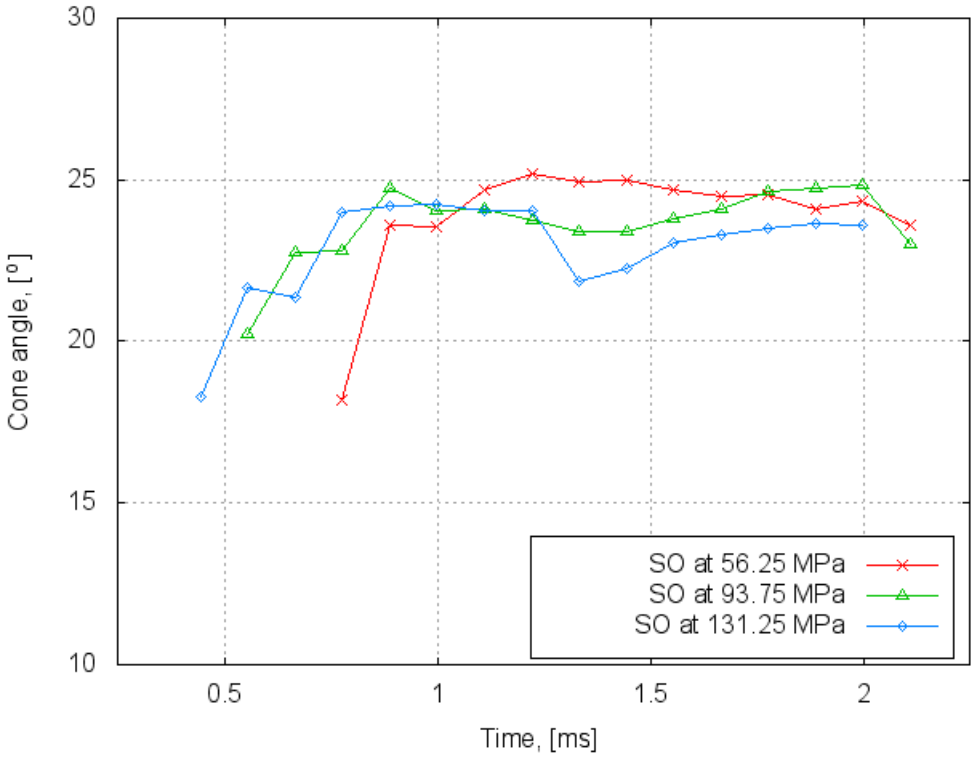

Figure 6.32: *Spray cone angle of SO for different injection pressures. (Oil temperature of 25°C) at* ρ_{amb}*=60.0 kg/m*^{3} *of ambient density.*

It is recognised that the width of the spray at the reduced spray penetration results in a wide cone angle, nevertheless may not represent the actual angle due to deteriorated oil flow. A general trend of the cone angle curves observed for the results presented for SO is not followed here. Also, a higher time delay and faster cone angle decreases with time can be observed from the graph. As it can be seen from Figure 6.27, corresponding to the cone angle data in Figure 6.32, the RSO spray development is characterised by relatively rapid increase of penetration, whilst the cone angle remains almost constant after 1.2 ms. This may explain the trend of the rapeseed curves presented in Figure 6.33. Corresponding data to the spray penetration results presented in Figure 6.28 for oil temperature of 60°C, cone angle is given in Figure 6.34. It can be seen that a small difference in the trend and pattern exists in comparison to the curves obtained at 25°C (shown in Figure 6.33). Figure 6.34 reveals a characteristic trend of increasing values of cone angle with time, especially at the very beginning of the injection process. But then the values gradually decrease. These patterns and trends differ from those of SO presented above. Results obtained for the highest injection pressures are higher from those at 56.25 MPa. This could indicate more developed spray resulting in a wider cone angle. It can be concluded that higher oil temperatures increase cone angle for higher injection pressures.

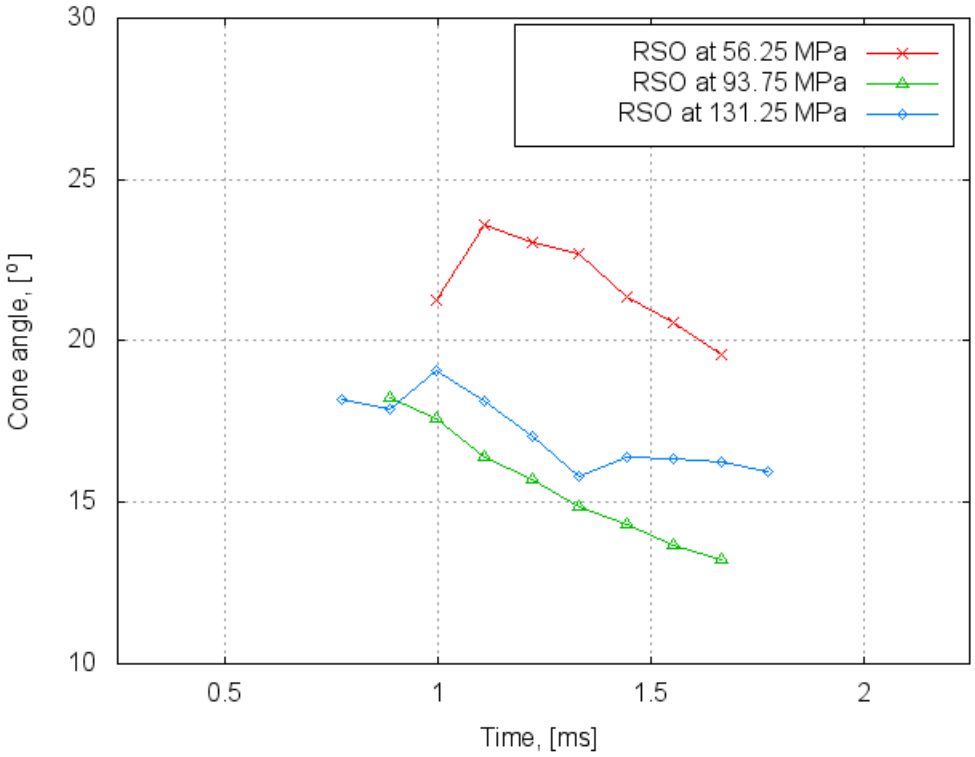

Figure 6.33: *Spray cone angle of RSO for different injection pressures. (Oil temperature of 25°C) at* ρ_{amb}*=15.0 kg/m*^{3} *of ambient density.*

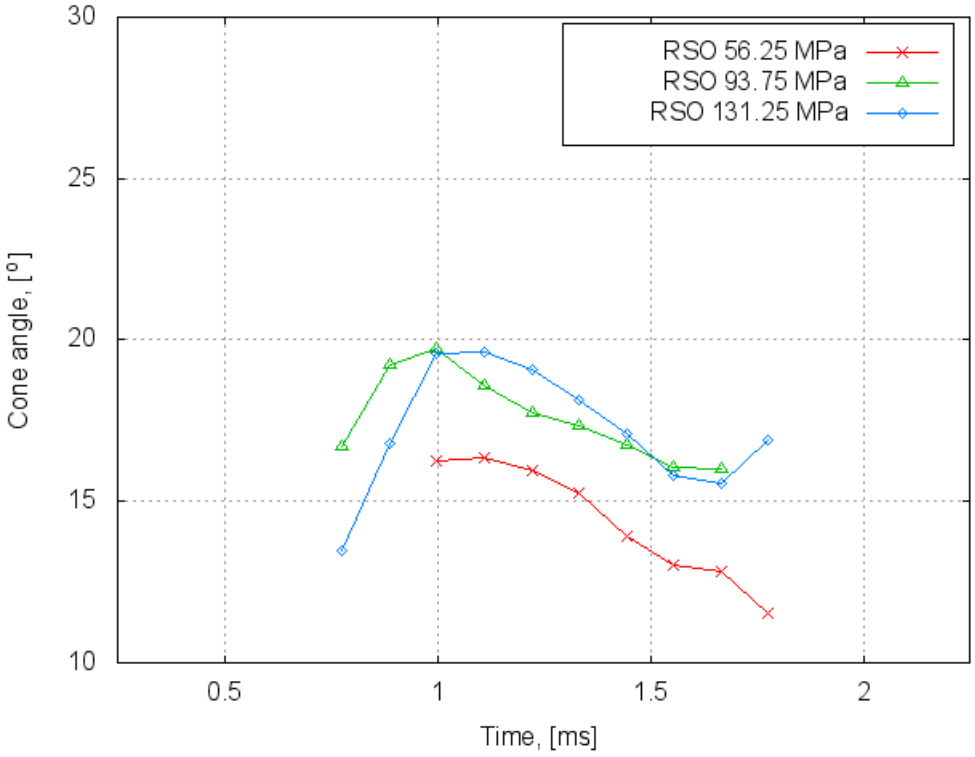

Figure 6.34: *Spray cone angle of RSO for different injection pressures. (Oil temperature of 60°C) at* ρ_{amb}*=15.0 kg/m*^{3} *of ambient density.*

6.2.3 Oil temperature effect on penetration

Amongst the fuel properties higher viscosity of RSO is considered as the crucial factor affecting the characteristics of spray. It could be seen from the result of spray penetration and cone angle that at temperature of 25°C RSO sprays are noticeably different from SO and provide more reduced values. It is well recognised that the high viscosity of fuel produces a poorly atomised fuel spray with a reduced penetration and a small cone angle [125]. This may result in large fuel droplets causing reduced air entrainment and fuel/air mixing rate. One of the methods to improve the RSO spray characteristics is to decrease oil viscosity, density and surface tension. In this part of the chapter, the fuel temperature effect on RSO spray is presented for the injection pressure of 56.25 MPa. It can be concluded from the previous results that the use of this pressure for RSO could be questionable because the spray may not be well developed. Although, it was assumed that this injection pressure is very important because the start of a CDI engine takes place at pressures around 50 MPa, therefore capturing a temperature effect in this case is essential. It can be accepted that at higher injection pressures the temperature effect must only beneficial. Presented results are compared with the corresponding data of SO taken at 25°C. It is believed that the result will aid to enhance RSO spray making it similar to SO.

Figure 6.35 shows a variation of the RSO spray penetration for a constant injection pressure of 56.25 MPa and different oil temperatures. As far as physical parameters are concerned the RSO viscosity is reduced from 46 down to 12 cP for 25 and 60°C, respectively whereas the viscosity of the SO at 25°C is about 5 cP. As it is expected the rapeseed, oil penetration values remain lower in comparison to SO and exhibit longer injection delays. The injection delay is particularly significant at 25°C and the penetration at this temperature is greatly reduced. As the oil temperature increases the RSO penetration approaches values of SO. Rapeseed oil sprays at 60°C represents the closest values to SO. It can be concluded that the temperature has enhanced the spray development and reduced the injection delay. Variation of RSO penetration within the same oil temperature range but higher ambient density of of 45.0 kg/m^3 is shown in Figure 6.36. The injection pressure of 56.25 MPa had been selected for comparative studies. As it is be expected increased ambient density imposes reduction in values of the spray penetration but the temperature effect significantly enhances RSO penetration. It can be seen that RSO at 25°C lacks full atomisation and its curve is different from the rest of the cases. Similar

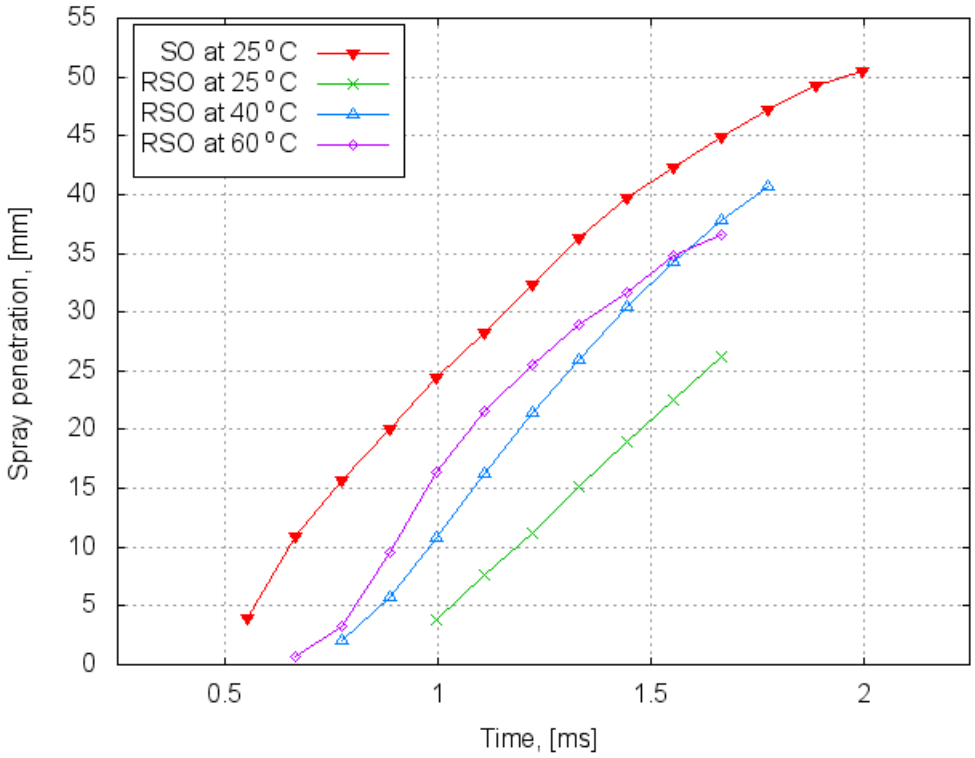

Figure 6.35: *Spray penetration of RSO for the injection pressures of 56.25 MPa at* ρ_{amb}*=15.0 kg/m*^{3} *of ambient density for three oil temperatures: 25, 40 and 60°C compared with SO at 25°C.*

to the previous figure, the penetration exhibit a noticeable injection delay, almost 1.0 ms after triggering the injector. The observation is specific to RSO injection. The reason of such trend can be seek again in a higher viscosity and density of RSO as well as the effect of the backpressure. Curves for 25°C in both figures are almost straight lines and finish abruptly, which was associated with the time when the jet disintegrated from the nozzle tip. Figure 6.37 presents the penetration curves for the injection pressure of 56.25 MPa and ambient pressure for three different RSO temperatures. As it can be recognised the oil temperature effect is almost identical as presented in Figure 6.36. Penetration curves of 40 and 60°C follow almost the same trend and the maximum penetration value is almost identical, however the initial penetrations are higher by approximately 100%. Penetration curve of 25°C features of the same trend as for the rest of the curves.

6.2.4 Oil temperature effect on cone angle

The oil temperature effect has been already presented for spray penetration. It is expected that elevated fuel temperature should affect spray cone angle increase the spray width. Figure 6.38 presents variation of cone angle as function of RSO temperature. It can be seen that as the oil temperature increases, the spray cone angle rises. Values of 40 and 60°C are

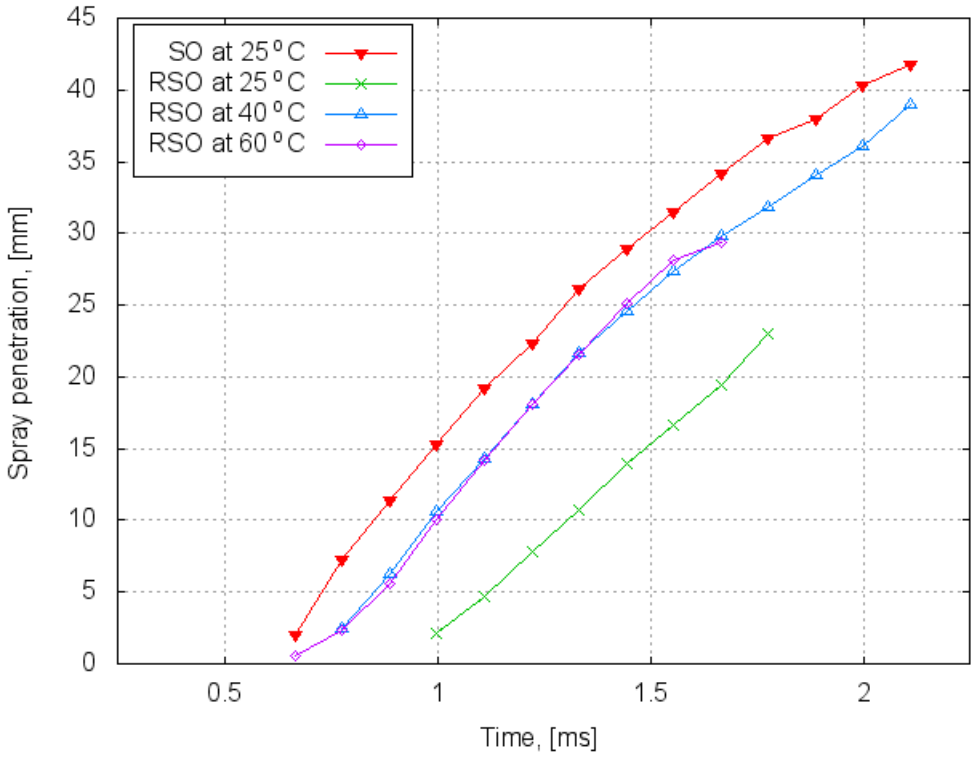

Figure 6.36: *Spray penetration of RSO for the injection pressures of 56.25 MPa at* ρ_{amb}*=45.0 kg/m*^{3} *of ambient density for three oil temperatures: 25, 40 and 60°C compared with SO at 25°C.*

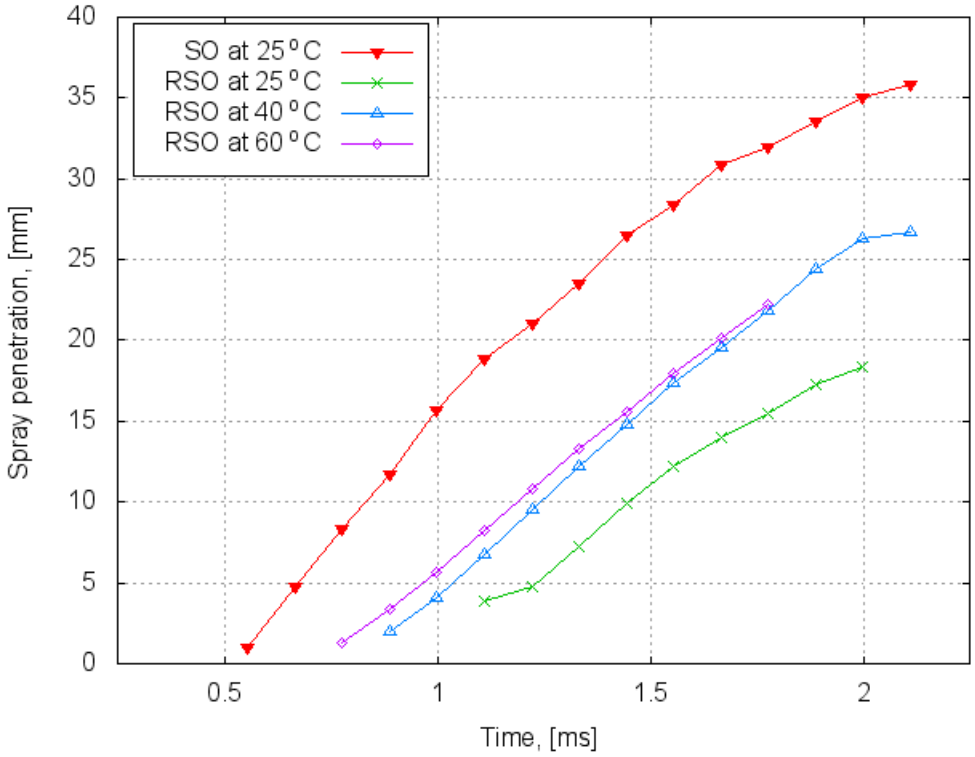

Figure 6.37: *Spray penetration of RSO for the injection pressures of 56.25 MPa at* ρ_{amb}*=60.0 kg/m*^{3} *of ambient density for three oil temperatures: 25, 40 and 60°C and of SO at 25°C.*

relatively close to the data of SO cone angle collected at 25°C. It can be seen that at 25°C the cone angle of RSO is reduced. Additionally, all RSO curves exhibit a decreasing trend with the injection time. Figure 6.39 shows changes of spray cone angle with temperature

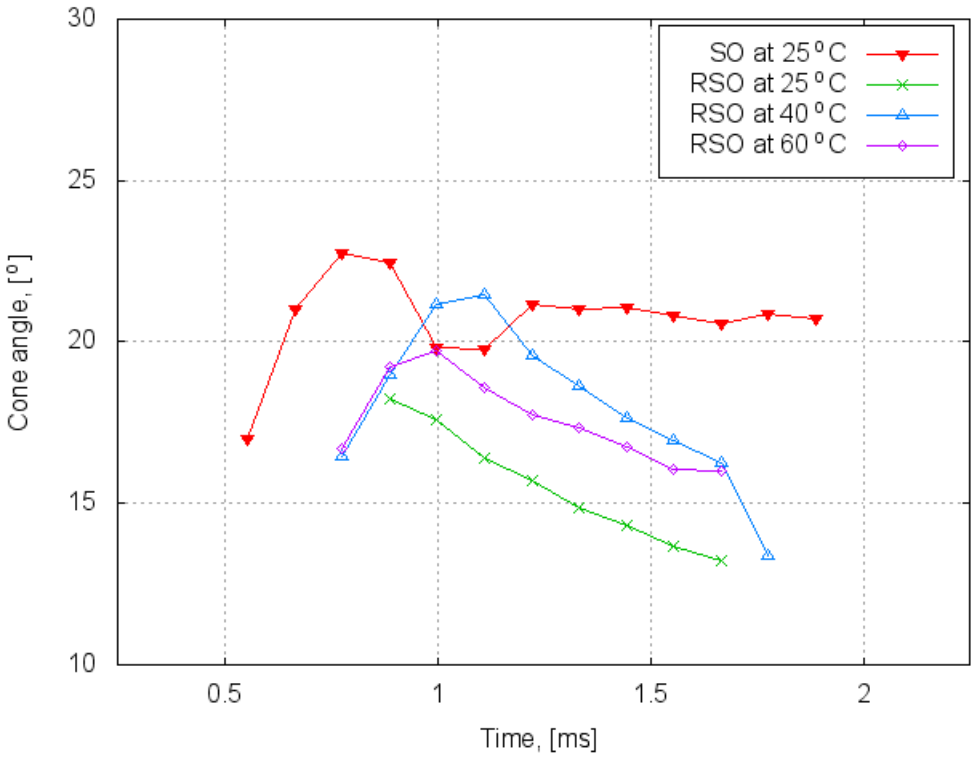

Figure 6.38: *Spray cone angle of RSO for the injection pressures of 93.75 MPa at* ρ_{amb}*=15.0 kg/m*^{3} *of ambient density for three oil temperatures: 25, 40 and 60°C.*

but at lower injection pressure and higher ambient density of 45.0 kg/m^3. As it can be seen from the figure elevated oil temperature of RSO successfully decreases values of spray cone angle. At 60°C RSO expresses almost the same cone angle as SO at 25°C. It can be seen that RSO injection features higher injection delay and therefore the spray cone angle values are considerable shifted in time. Figure 6.40 show the temperature effect on RSO spray cone angle produced at the highest ambient density and the highest injection pressure. It is seen that the temperature effect has been reduced by the ambient pressure effect. It can be found that injection of RSO at such high ambient pressure promotes reduction of spray cone angle even for lower RSO temperatures. The effect shows that the common practice of oil pre-heating needs to be assessed more carefully when RSO is injected into a considerable high in-cylinder density.

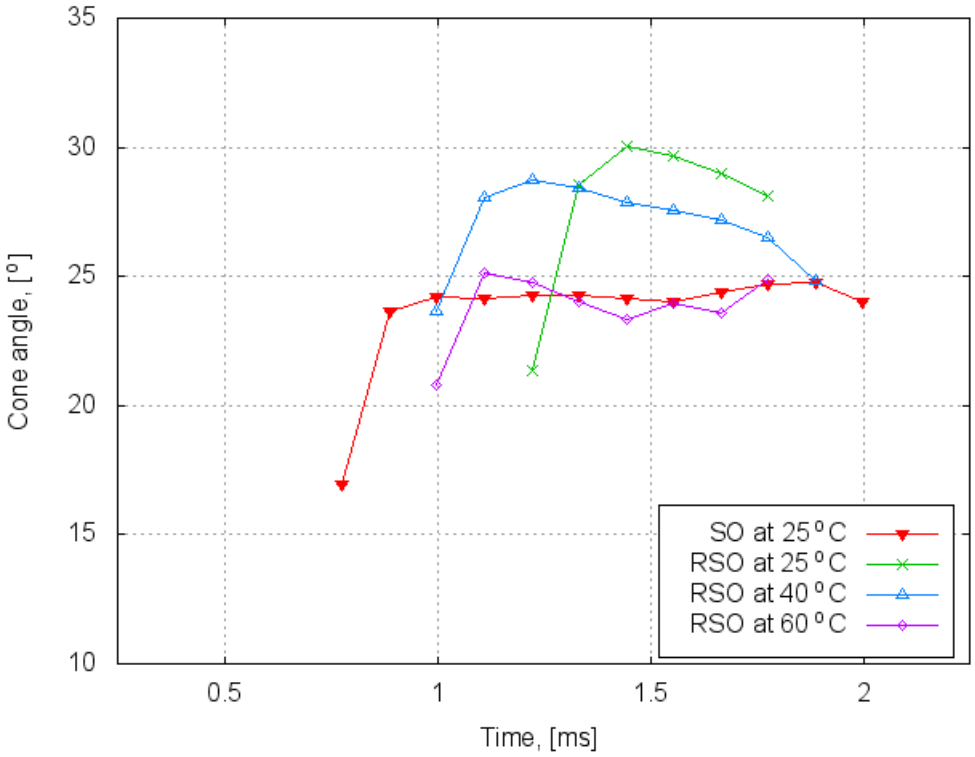

Figure 6.39: *Spray cone angle of RSO for the injection pressures of 56.25 MPa at* ρ_{amb}*=45.0 kg/m*^{3} *of ambient density for three oil temperatures: 25, 40 and 60°C.*

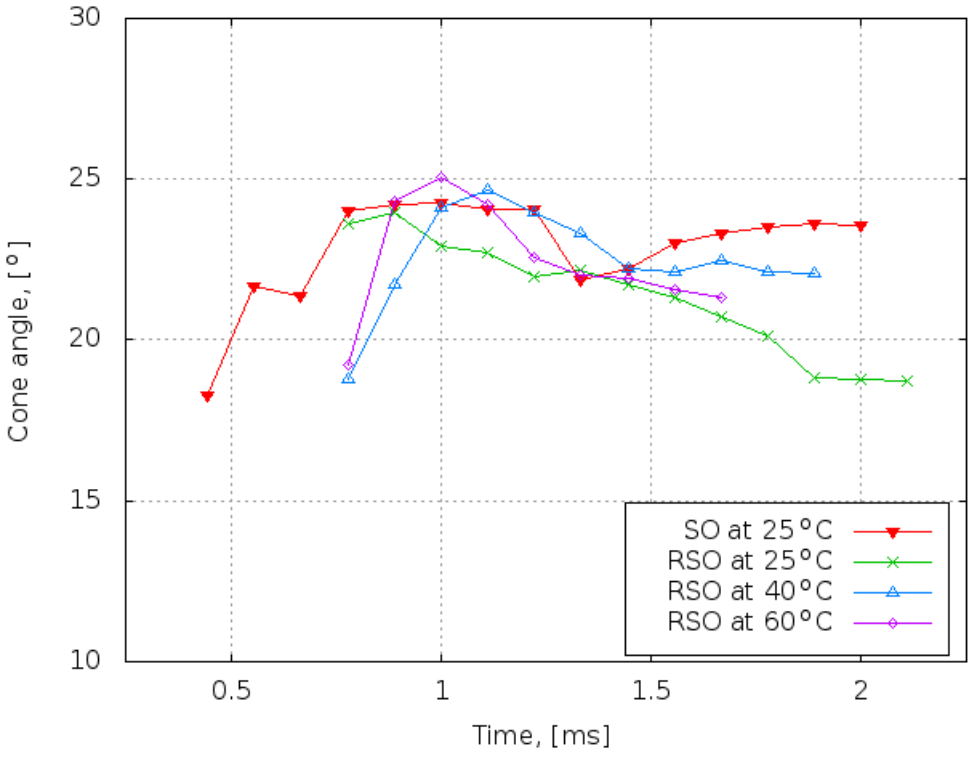

Figure 6.40: *Spray cone angle of RSO for the injection pressures of 131.25 MPa at* ρ_{amb}*=60.0 kg/m*^{3} *of ambient density for three oil temperatures: 25, 40 and 60°C.*

6.2.5 Spray delay

Throughout the presented results of SO and RSO spray penetration development it has been noticed that one of the significant occurrences is the spray delay. In the literature the delay is called as the "spray hesitation" and its description for diesel can be found in [396]. A similar problem was recognised by Kennaird et al. [219] who observed some pressure fluctuations of diesel in the injector nozzle and hence a delay at the beginning of the spray development showed. They reported a spray hesitation at the opening phase of the VCO nozzle and its effect on the needle lift. The hesitation depends on a type of injector, injection pressure and ambient conditions. For instance, Delacourt [108] presented results starting at 0.6 ms which indicated an obvious and considerable injection delay.
The RSO injection delay may result in serious drawback of CDI modification. Mainly it may lead to the ignition delay and miss-adjusting of the injection timing. On the other hand it is believed that the problem can be overcome by the self-adjustable feature of the ECU if the system is operating on diesel but it is not clear that would take place for RSO. It has to be highlighted that the issue of spray delay or RSO has not been yet investigated nor discussed. It is believed that this section outlined and address this problem for the first time.

Processing of the spray development images obtained in this work showed discrepancy between the solenoid valve activation and start of the penetrations. Playback of an image sequence presented time delay between time when the injection signal activated the high-speed camera and the first sight of fuel appearing at the nozzle tip as previously found by Laguitton et al. [241] for diesel and using a similar technique. In his work this phenomenon was noted for all the injection rates of tested fuels however the delay phenomenon was longer for RSO. The nozzle needle opening speed is determined by the difference in the flow rate through the bleed and feed orifices i.e. by a cushion of fuel stopping the nozzle control plunger. Higher viscosity of RSO results in slower flow within the feed passages and therefore higher hesitation. In case of low injection pressure ($\sim$30.0 MPa) and fuel temperature (25°C), in some cases, injection did not result in atomisation at all. This was also found in [187]. It has to be recalled that the penetration data shown in this paper are referenced from the time the injector is activated.

From the present data it can be concluded that RSO reveals longer injection delay. The delay is directly related to higher physical properties (viscosity, density, surface tension) of

the oil. Thus properties like viscosity and density directly reflect on the delay. Therefore, by increasing oil temperature the spray delay can be reduced but still remains longer than that for SO. It is believed that a modification of a CDI system should include a way of reducing the injection delay by pre-heating oil prior to feeding the injector or/and directly heating the injector and the rail.

6.3 Spray sizing using PDA

This section includes only selected results of SO and RSO spray droplet sizing performed using PDA. Malvern results are show in the end of this section in 6.3.5 to verify PDA measurements.

Most of the results had been presented in a comparative manner grouped together with SO data. The aim was to highlight the differences between spray atomisation for both oils as well as to define key factors governing RSO atomisation. This was expected to be useful in modification of CR system to provide appropriate RSO atomisation.

The measurements of RSO have been undertaken at three different oil temperatures, however it has been found that the best atomisation was reached at 60°C for the full range of injection pressures. Nevertheless, the results at lower temperaturesare also included in this section. All measurements were taken at 40 mm from the nozzle tip. More details regarding the distance from the nozzle, at which measurements were taken and the data processing procedures are described in *Section 3.4* and *Subsection 4.3.2* for PDA and *Section 3.5* and *Subsection 4.3.5* for Malvern.

6.3.1 Comparative studies of temperature effect

As commonly recognised oil pre-heating is one of the most common ways of altering plant oil sprays to be utilised in diesel engines. The temperature effect on RSO physical properties is very advantageous thus a similar effect on oil atomisation can be expected. A series of figures presented in this subsection show the temperature effect on RSO atomisation in a comparative manner. The charts consists of blue band of which widths represent the area of SO mean diameters within the limits of a maximum (upper edge) and minimum (lower edge) values corresponding to the lowest (37.5) and maximum (131.25 MPa) injection pressure. Corresponding RSO data had been drawn over the band in a form of lines with

experimental points. The layout allows to easily recognise whether RSO values fall into SO limits, which would be desirable as far as the pre-heating effect and combustion are concerned.

The first set of results were recorded for the ambient density of 15 kg/m^3 and a whole range of injection pressures. Figure 6.41 represent changes of Sauter mean diameter with oil temperature compared with the equivalent SO range at 30°C. SO diameters are represented by a blue band indicating a relatively narrow mean diameter range of 15-20μm. The effect is noticeable but particularly strong for diameters measured between 30 and

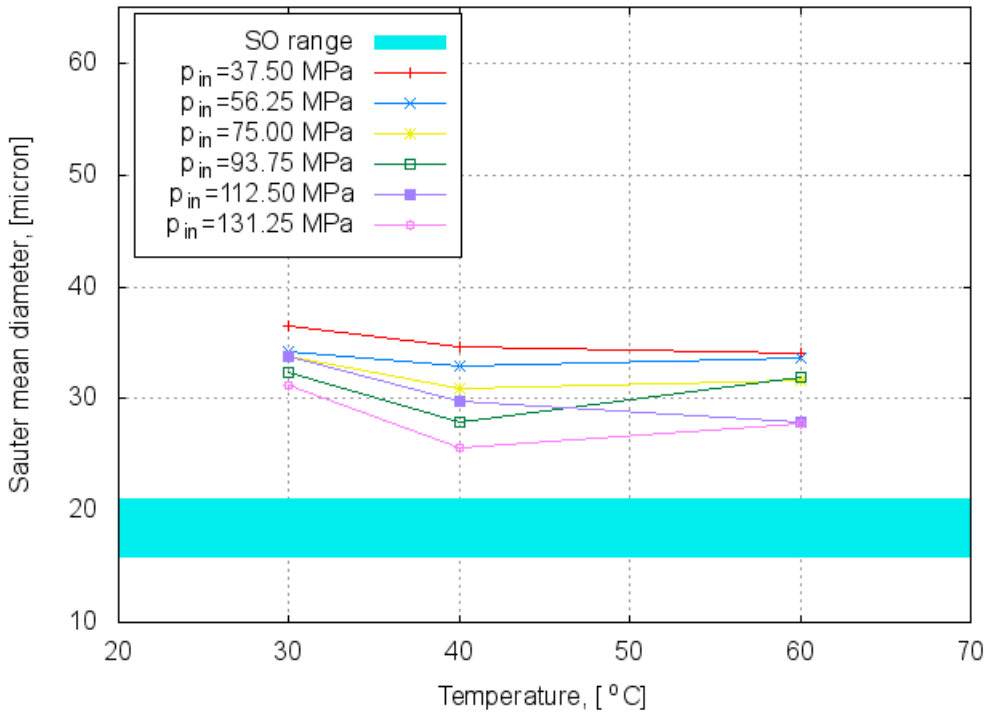

Figure 6.41: *Temperature effect on the Sauter mean diameter (D_{32}) of RSO and comparison with SO. Ambient density 15 kg/m^3*

40°C and higher injection pressures, where the reduction is approximately by 15%. From 40°C onwards, the temperature does not have a significant effect and except 112.5 MPa diameters are slightly decreasing. It has been accepted that a weak increase of diameters was caused by more enhanced evaporation of smaller drops, whereas the large drops remain unchanged. Comparison of RSO with SO data clearly show higher values of the plant oil within the whole range of oil temperatures. It can be seen that the experimental points at 40 and 60°C are located close to the upper diameter limit of SO but still higher by ∼25% on average.

The same ambient conditions were used to analyse the influence of RSO temperature on

the arithmetic mean diameter as shown in Figure 6.42. The arithmetic diameter values have been significantly reduces at 40°C in comparison to 30°C. Beyond 40°C a gradual increase can be observed as it has been already seen in Figure 6.41. As it can be expected

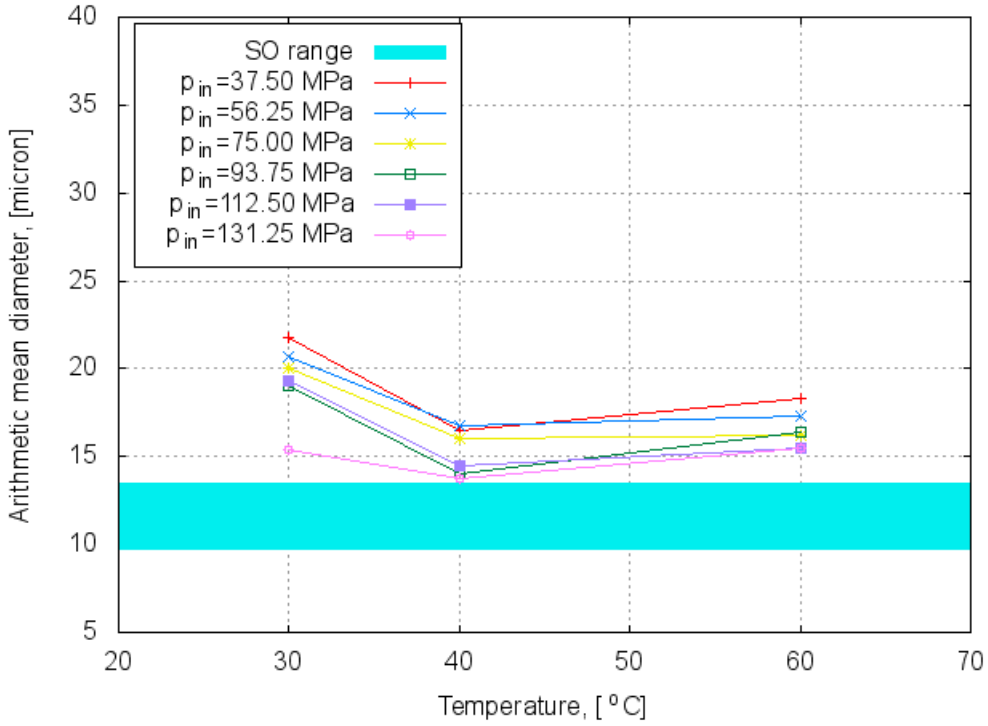

Figure 6.42: *Temperature effect on the arithmetic mean diameter (D_{10}) of RSO and comparison with SO. Ambient density 15 kg/m^3*

values of D_{10} are higher than for SO and for temperatures higher than 40°C progressively approaching the upper limit of SO. Only diameters obtained at the highest injection pressure (131.25 MPa) and 40°C are closely located to the upper SO limit.

Figure 6.43 presents changes of De Broukere mean diameters with RSO temperature for different injection pressures. A noticeable gap between the RSO and SO can be seen. The De Broukere diameters of RSO are much higher for the whole range of temperatures as well as injection pressures. Presented curves indicate the lowest mean diameter values of the highest injection pressure and the largest diameters recorded for 37.50 MPa. As it can be observed, the SO diameter range is represented by a narrow range and indicates that the SO De Broukere mean diameters are lower than 25 μm. The effect of changing fuel temperature has been also investigated for the ambient density of 30 kg/m^3 and presented in the following figures. In the first Figure 6.44 changes of Sauter mean diameters are shown. The injection curves initially decrease values and then increasing with oil temperature. The largest Sauter diameters were recorded for the lowest injection pressures, whereas the SMD for RSO approachthe upper limit of SO data only for the last highest injection pressures

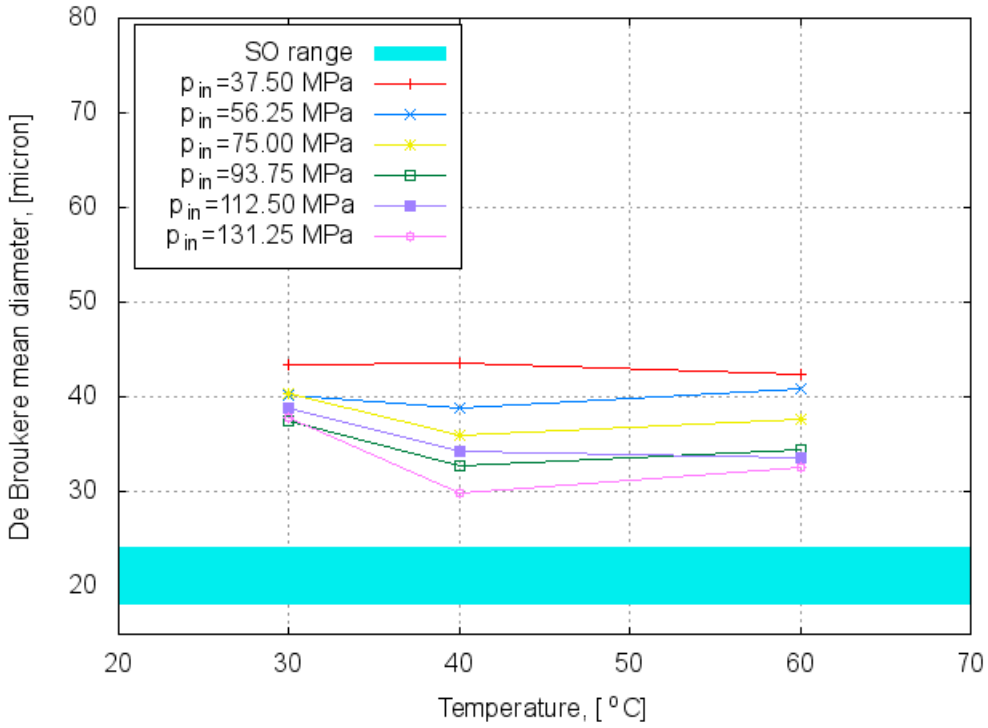

Figure 6.43: *Temperature effect on the De Broukere mean diameter (D_{43}) of RSO and comparison with SO. Ambient density 15 kg/m^3*

112.50 and 131.25 MPa and 40°C. It can bee seen that higher ambient density improves atomisation resulting in diameter values more resembling the SO data. Corresponding arithmetic mean diameter values for RSO recorded at varying injection pressure and ambient density of 30 kg/m^3 are shown as function of oil temperature in Figure 6.45. It can be seen that almost all diameters are within SO ranges and for the highest injection pressures and 40°Care even smaller. Nevertheless, the mean diameter values of the lowest injection pressure are still close to the highest values of SO. Presented curves show initial decrease of diameters with temperature and then gradual increase almost back to the values recorded at 30°C. In the next Figure 6.46 a variation of De Brouckere mean diameter with RSO temperature is revealed. It can be seen that for the whole set of the data RSO values are above SO range and only at the highest injection pressures and 40°C RSO diameters reach the upper SO diameter limit. The diameters values recorded at 60°C are almost identical for the all injection pressures except enormously large value for the injection pressure of 37.50 MPa. The last sets of figures present temperature effect for the highest ambient density of 60 kg/m^3 on three different mean diameters. Figure 6.47 reveals changes of the Sauter mean diameter for six injection pressures. It can be seen that increasing oil temperature does not lead to significant reduction of mean diameters and rather has the adverse effect e.g. for the lowest injection pressure. The overall pattern is different from

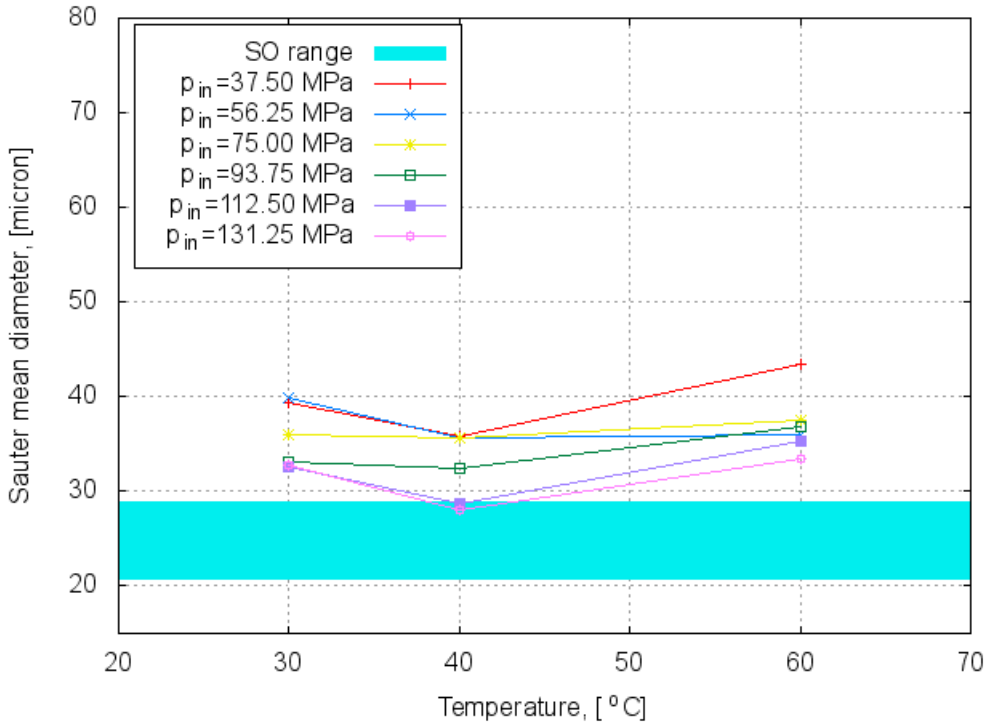

Figure 6.44: *Temperature effect on the Sauter mean diameter of RSO and comparison with SO. Ambient density 30 kg/m*^{3}

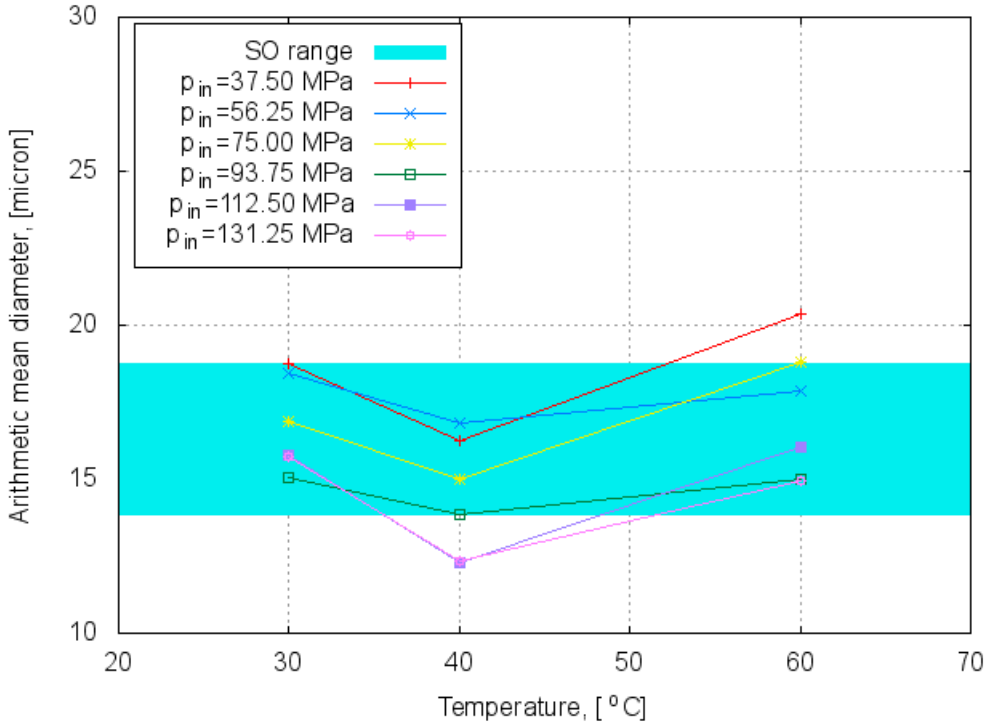

Figure 6.45: *Temperature effect on the arithmetic mean diameter of RSO and comparison with SO. Ambient density 30 kg/m*^{3}

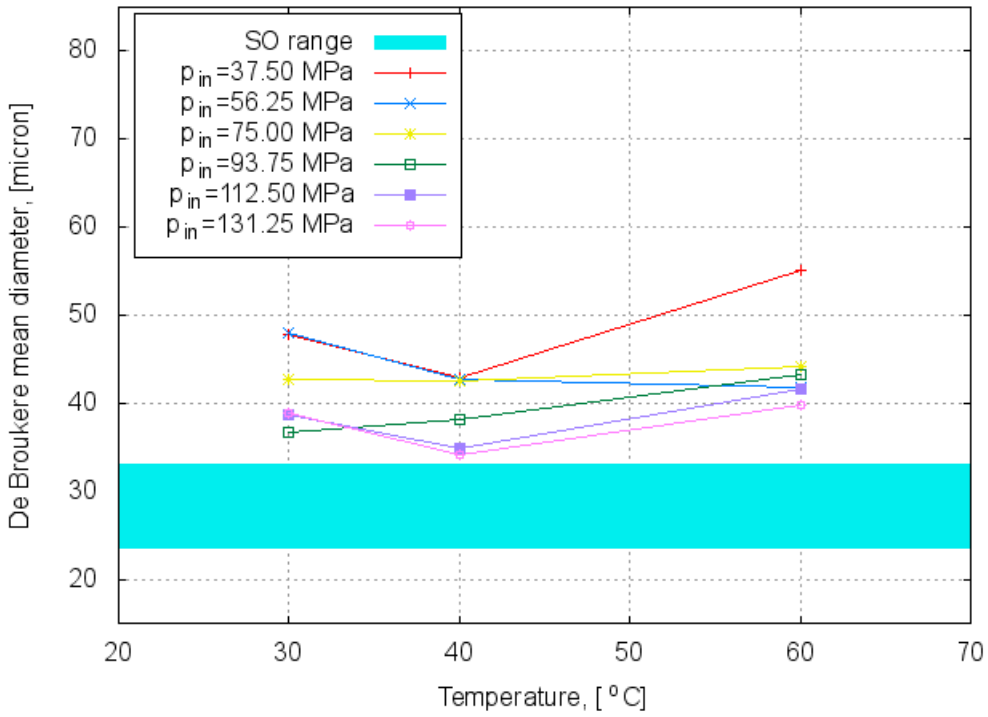

Figure 6.46: *Temperature effect on the De Broukere mean diameter of RSO and comparison with SO. Ambient density 30 kg/m*^{3}

the previous charts, thus the presented trends of various injection pressures exclude a general conclusion that elevated oil temperature results in decreased mean diameters for the whole range of ambient densities. It can be seen that the RSO values are within a wider droplet range (from 25 up to 45 μm).

Practically, the injection pressures of 93.75, 112.50 and 131.25 MPa represent Sauter diameters within SO limits. The lowest injection pressure of 37.50 MPa relates to the highest Sauter diameters far above the SO range for the whole range of oil temperatures. These values are approximately 50% higher than the SO ones. The effect of temperature on the arithmetic mean diameter and the same injection conditions is presented in Figure 6.48. As it can be seen the increasing oil temperature causes a gradual increase of the mean diameter for 37.50 and 112.50 MPa. RSO data for almost whole range of injection pressures do not exceed the SO range. The "worse case" is represented by the lowest injection pressure. It can be seen that this injection pressure produces the arithmetic mean diameter larger that the upper limit of SO and shows a rapid increase along the whole temperature range. Furthermore, within a temperature range of 30 up to 50°C the mean diameter are lower than for SO. Variation of the De Broukere mean diameter with RSO temperature is shown in Figure 6.49. The increasing oil temperature leads to larger values of D_{43} for 37.50 and 112.50 MPa, which steadily increase approximately by 5%. The

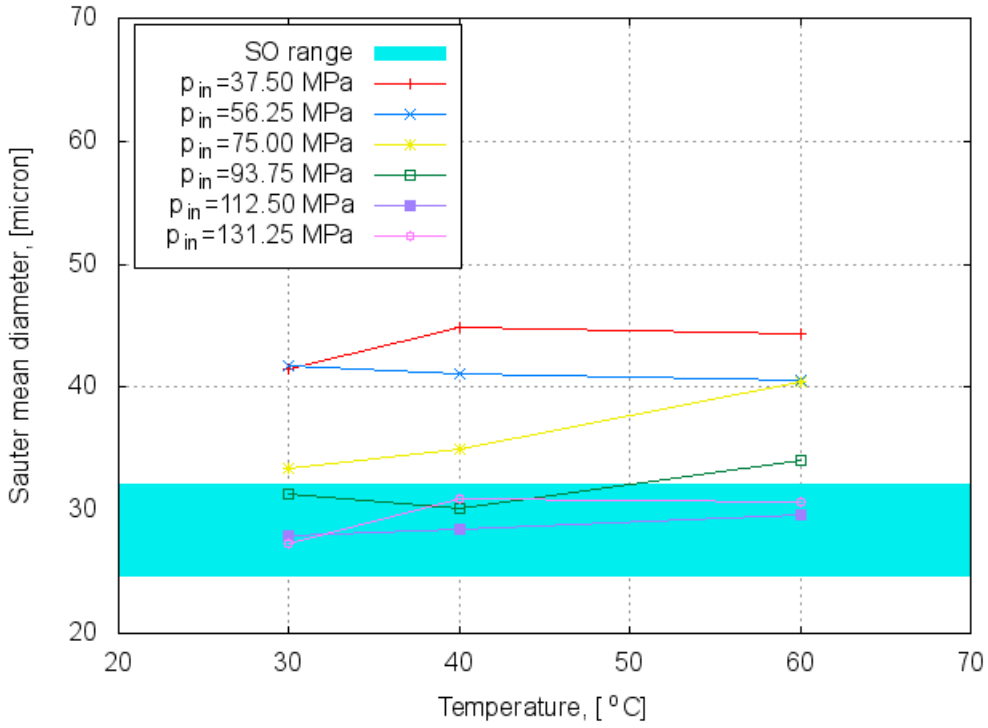

Figure 6.47: *Temperature effect on the Sauter mean diameter (D_{32}) of RSO and comparison with SO. Ambient density 60 kg/m^3*

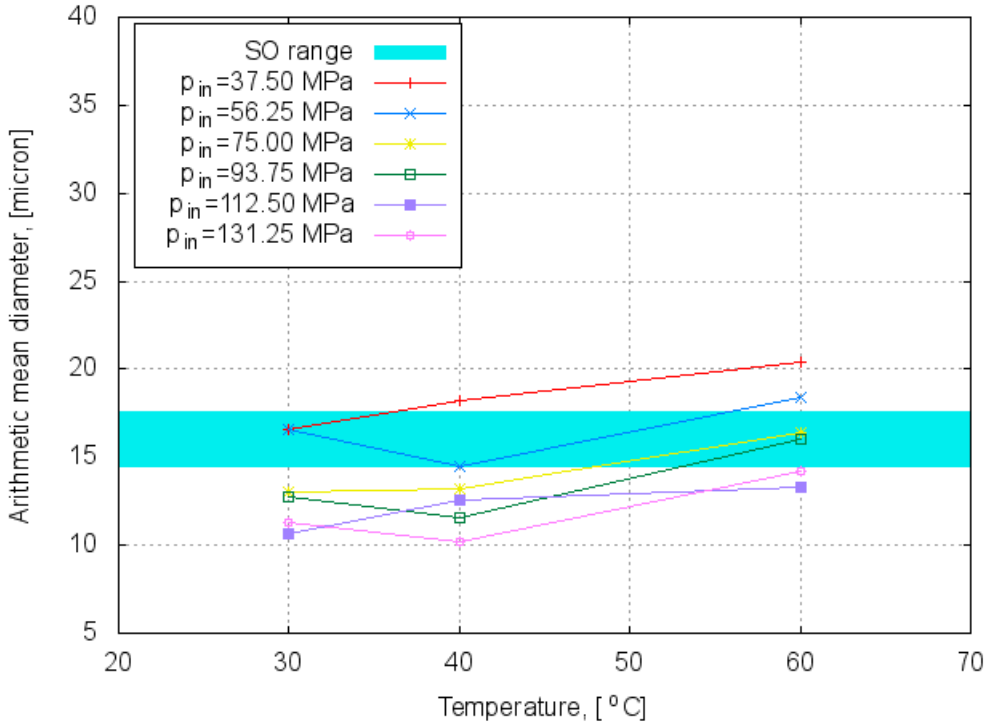

Figure 6.48: *Temperature effect on the arithmetic mean diameter (D_{10}) of RSO and comparison with SO. Ambient density 60 kg/m^3*

curves feature a similar trend and similar slope except for the lowest injection pressure. As it can be seen, the spread of RSO diameters are relatively wide and is within a range of 35 to 55 μm. The highest ambient density certainly enhances creation of a smaller diameters for higher injection pressures whereas injection at lower pressure still results in drops of higher diameters than that of SO. It can be seen that injection pressures higher than 93.75 MPa provide mean diameters falling within the SO limits. Presented results

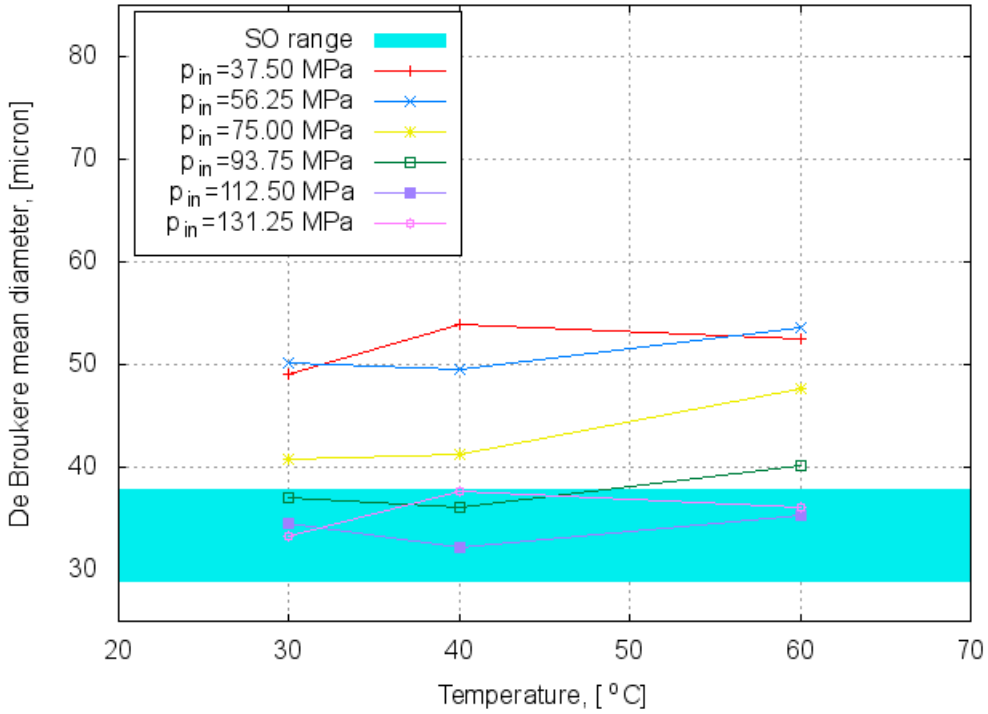

Figure 6.49: *Temperature effect on the De Broukere mean diameter (D_{43}) of RSO and comparison with SO. Ambient density 60 kg/m^3*

of the temperature effect do not indicate a steadily decrease of diameters with the whole range of RSO temperature and injection pressures. The effect can be analysed within two different temperature ranges. In the first one, from 30°C to 40°C, in all cases a noticeable reduction of diameters can be observed. Changes of RSO viscosity and density within that temperature range is significant, which is reflected on the presented results. In the second temperature case, from 40°C onwards, the temperature effect is less noticeable leading rather to stable diameter values or a slight increase. The explanation of the event can be associated with the internal structure of spray and the vaporisation effect. RSO subjected to elevated oil temperatures tends to atomise more readily. However the enhanced breakup may occur along with coalescence compensating creation of smaller drops. Additionally, there is more enhanced heat transfer between the ambient gas and spray, which may lead to greater temperature gradient between the spray centreline and the outer cone surface.

The temperature effect is expected to be more pronounced for higher ambient densities and this has been recorded in Figures 6.47- 6.49. Also, it is recognised that the effect was more likely caused by increased shear forces between the gas and spray.
The second and the most reasonable explanation of such occurrence can follow the suggestion made by De Risi and his co-workers who stated that the number of bigger diesel droplets increases at high temperature, probably due to vaporisation of smaller droplets, especially at the spray periphery. In their work it was found that mean diameters obtained at high temperature were substantially different from those measured in ambient, lower temperature condition. Although, vaporisation of RSO is significantly reduced in comparison to SO, still the effect should be taken into account and can explain the variation of droplet sizes with oil temperature.

6.3.2 The ambient pressure effect on Sauter diameter

Since the oil temperature effect has been already discussed it is also interesting to look more carefully at the influence of the ambient pressure. In a real engine situation internal pressure in cylinder changes with the piston move and reaches its maximum at the TDC therefore it is not constant, whereas the following experiments were performed at constant ambient pressure. Nevertheless, it is important to analyse the effect of ambient pressure on spray atomisation to see what is the optimal combination of injection and ambient pressure on RSO. The author believes that the ambient pressure effect on spray may be utilised in modification of CDI system by changing the compression ratio or adjusting the injection timing to benefit form ambient pressure effect.

The ambient pressure in this work up to this point has been expressed in terms of the ambient density. However, in this section, due to more practical engineering approach, the pressure is presented as function of ambient air equivalent pressure instead. To provide easy to read graphs and a retrospective view of a results already presented only three different injection pressures have been selected for this analysis.
Firstly, atomisation of SO is looked at to provide an overview of the behaviour of a conventional fuel. Figure 6.50 presents variation of Sauter diameter of SO with varying ambient pressure for three different injection pressures: 56.25, 93.75 and 131.25 MPa. The data was collected for the fuel temperature of 30°C which is very likely to be found in the fuel lines after the cold start. As it can be seen from the figure the Sauter values rise up with

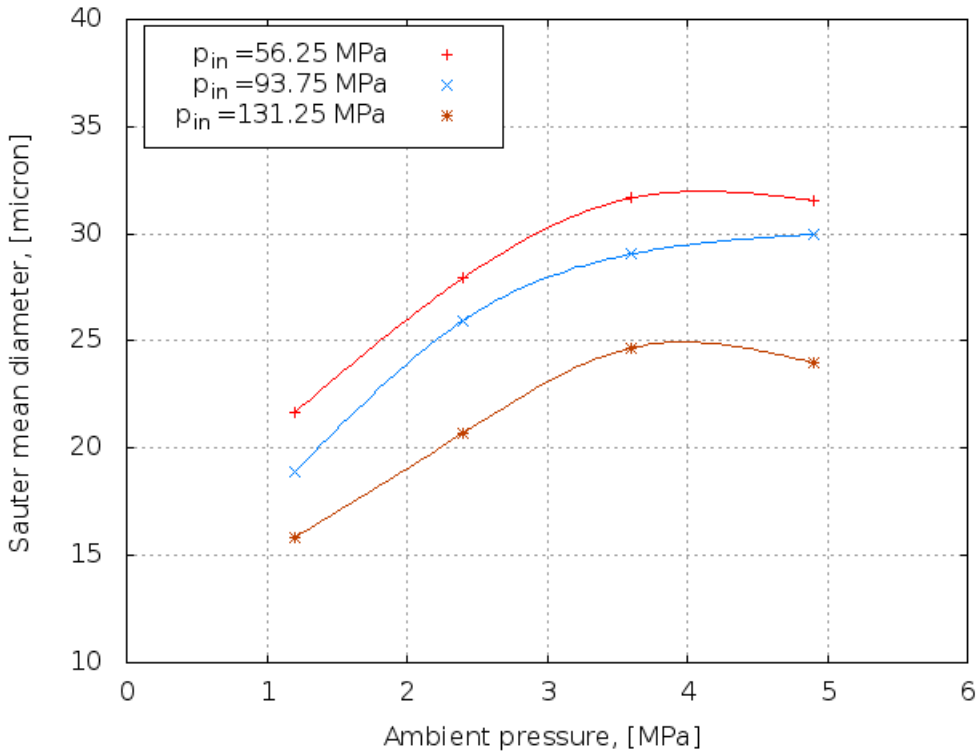

Figure 6.50: *Influence of the ambient pressure on Sauter mean diameter of SO injected at 30°C*

increasing ambient pressure up to approximately 4 MPa. The steep slopes indicate a quick increase of the mean diameter values. It can be observed that for 56.25 and 131.25 MPa the curves feature a similar slope demonstrating a very comparable effect on Sauter mean diameter. It can also be noted that the ambient pressure beyond 4.0 MPa causes slow decrease of mean diameters. Overall, within the analysed ambient pressure range the diameter increases by approximately 40% with the increase in the ambient pressure from a range approximately 1.0 MPa up to 5 MPa.

Next RSO was subjected to the same injection and ambient conditions as SO. Changes in Sauter diameters with ambient pressure for RSO are shown in Figure 6.51. Initially, RSO Sauter diameters increase with ambient pressure up to approximately 3.5 MPa and then sharply decreases as it is shown for 56.25 MPa or sharply decreases as for 93.75 and 131.25 MPa but keep gently increasing for 56.25. Comparison of SO and RSO (Figures 6.50 and 6.51) measurements at the fuel temperature of 30°C revealed slower increase of diameters for RSO and then rapid decrease of diameters after 3.5 MPa, whereas the SO values do not decrease in the same way. The explanation of the RSO trend could be related to the atomisation of RSO at 30°C, which is rather poor and the results may suffer from the incomplete breakup of RSO droplets. A higher fuel temperature of RSO at 40°C

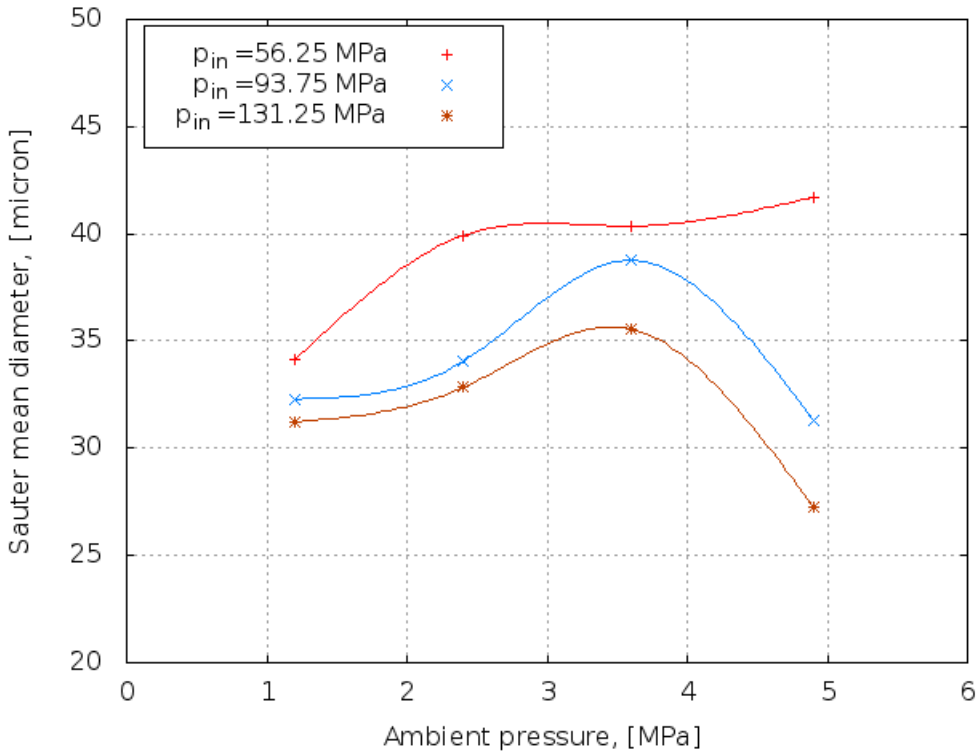

Figure 6.51: *Influence of the ambient pressure on Sauter mean diameter of RSO injected at 30°C*

was selected to investigate ambient pressure effect on RSO Sauter mean diameters. The results are shown in Figure 6.52. Presented curves feature an initial increase of diameters for the injection pressures of 93.75 and 131.25 MPa. For the highest and medium injection pressures Sauter diameters increase with ambient pressure, up to about 4.0 MPa, thereafter it decreases as already been observed for RSO at 30°C, but the decrease is not so sharp. Then, these curves at the ambient pressure of 3.5 MPa start showing decreasing trend. On the other and the curve for 56.25 MPa demonstrates an increasing trend within the whole range of the investigated ambient pressure. Similarity between the injection curves for 56.25 MPa at 30 and 40°C of RSO can be observed. Both curves are described by a linear trend and tend to increase throughout the whole range of ambient pressures. Curves constructed using data of 60°C for RSO are shown in Figure 6.53, which display a trend similar to the data presented in Figure 6.52. The lowest injection pressure results (56.25 MPa) in a linear increase of Sauter mean diameters with ambient pressure. The linear trend resembles the slope similar to that already presented for 40°C. For the injection pressure of 56.25 MPa a gradual increase of Sauter diameters within a whole range of ambient pressures can be observed, whereas the higher injection pressures initially produce droplets of gradually increasing Sauter mean diameters with a maximum approximately at 3.5 MPa. Then, the values start decreasing. A similar behaviour can be seen for 93.75 MPa.

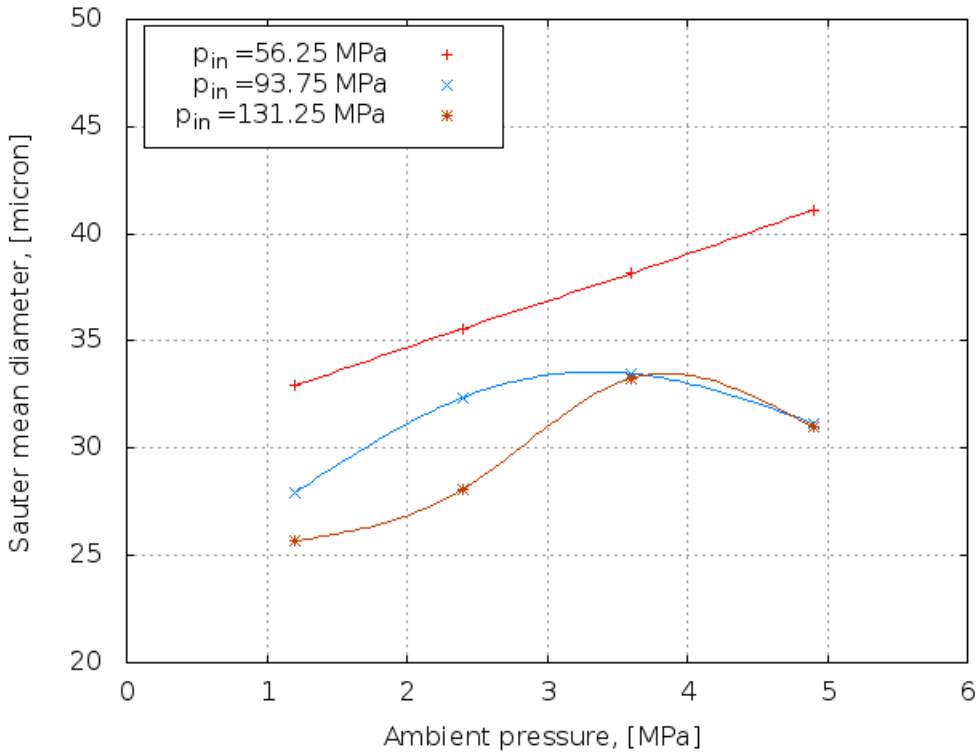

Figure 6.52: *Influence of the ambient pressure on Sauter mean diameter of RSO injected at 40°C*

It can be concluded that as far as the effect of ambient pressure on SO and RSO diameters is concerned both oils behave rather differently especially for higher ambient pressures i.g. >3.5 MPa. Both oils show increasing trend up to this pressure, which was much sharper for SO and then decrease, but the decrease was much more pronounced for RSO diameters.

6.3.3 The injection pressure effect on mean diameter

It is important to study the effect of the injection pressure on the droplet diameters as the injection pressure is expected to have significant and strong influence on atomisation. It has been recognised that increased injection pressure produces finer drops thus enhances fuel atomisation. It is expected that the injection pressure together with fuel pre heating will play a crucial role in modifying the CDI system.

Firstly, results of SO are shown for the investigated injection pressure range and selected ambient pressures. SO results were collected at the fuel temperature of 30°C and three different ambient densities. Figure 6.54 shows influence of the injection pressure on Sauter, arithmetic and De Broukere mean diameters at the lowest ambient density of 15 kg/m^3. As it is expected, the diameters decrease with elevated injection pressures by 25% on average in comparison to their initial values at 37.50 MPa. The presented curves

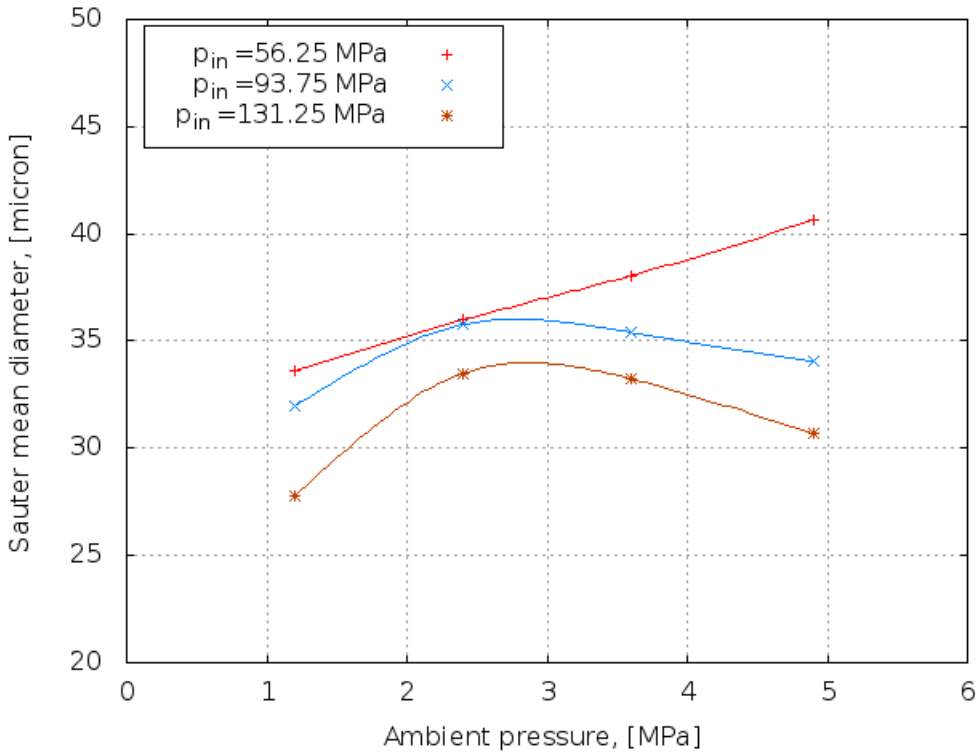

Figure 6.53: *Influence of the ambient pressure on Sauter mean diameter of RSO injected at 60°C*

have similar trends. As it is expected the D_{43} values are the highest amongst presented in the figure. Results of the investigation of the injection pressure on diameters at higher ambient density of 30 kg/m^3 are shown in Figure 6.55. Curves are characterised by a similar trend as described for the lower ambient density in Figure 6.54, however, the data point are more scattered, which could be associated with a kind of oscillations. All diameters decrease with increasing injection pressures. It is seen that the fastest reduction of diameters is between 110 and 140 MPa. Generally, values are higher than those obtained at 15 kg/m^3 and it can be explained by a higher density of the spray and therefore more prompt formation of larger drops due to much diminished spray atomisation. The effect can be concluded directly from the equations describing spray atomisation and the influence of the back pressure (Equation 4.1.1 and 4.1.2). Figure 6.56 shows results of SO mean diameters recorded for varying injection pressures and 45 kg/m^3 of the ambient density. The values follow a general trend of increasing mean diameters due to elevated ambient pressure (ambient density) however the injection pressure effect has a typical descendancy. Curves representing D_{32} and D_{43} variations are almost parallel and do have almost the same slope. It can be seen that the values instantly decrease from around 40 μm down to 30 μm for D_{43} and from 32.5 μm to 27 μm for D_{32} respectively, whereas the fluctuations of D_{10} are less pronounced. It can be explained that in the whole range of injection pressures the

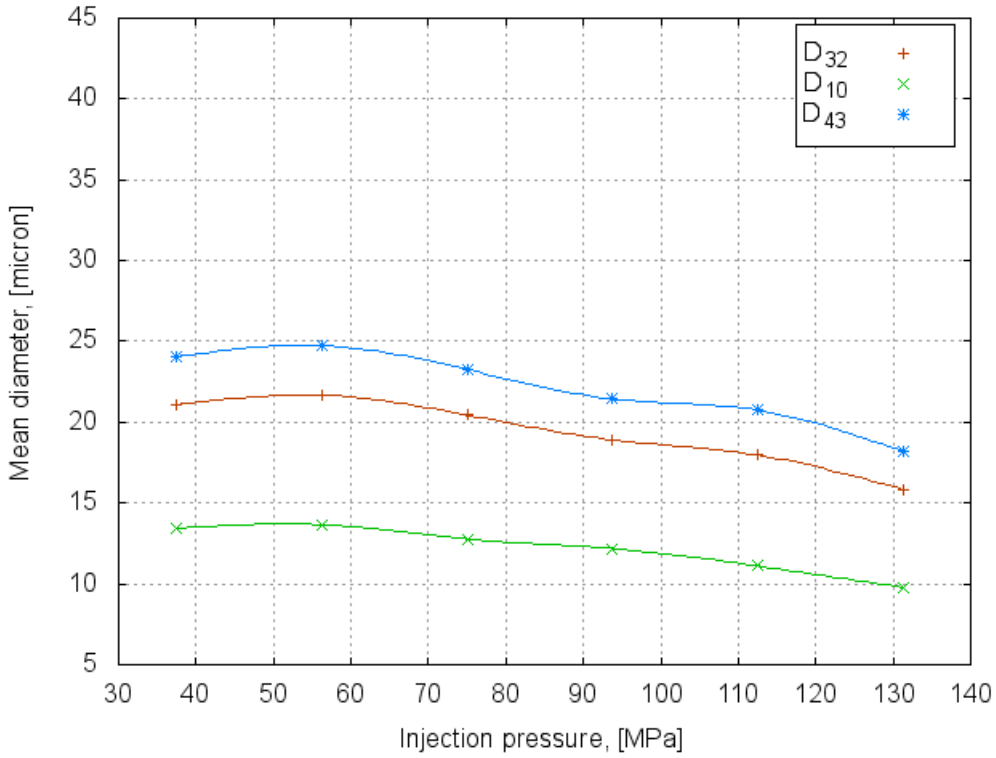

Figure 6.54: *Effect of injection pressure on SO at 30°C and the ambient density of 15 kg/m^3*

droplet populations consist of equally distributed droplet ranges or droplet class numbers contributing adequately in almost stabilised D_{10} values. The injection pressure effect on values of D_{10} is marginally weakened but still causes reduction of SO drop sizes. As shown in Figure 6.57, when the ambient density increases to 60 kg/m^3, mean diameter values become higher in comparison to data at 15 kg/m^3 and but similar to values recorded at 45 kg/m^3. Figure 6.57 shows that the curves for Sauter, arithmetic, and De Broukere mean diameter are significantly influenced by increasing injection pressure. This is manifested by steep slopes of D_{32} and D_{43} curves associated with the diameter drop by approximately 20%. The effect is particularly noticeable for injection pressures higher than 90 MPa. The change of D_{10} values is more noticeable than for already presented lower ambient densities and similar to the trends of the D_{10} curve in Figure 6.56. As it can be seen the injection pressure effect on SO mean diameters is common for all ambient densities. For a full range of injection pressures a gradual values drop can be observed and it becomes more apparent for the injection pressures higher than 90 MPa. This trend is especially distinctive for D_{32} and D_{43} curves and the magnitude of the decrease is a function of the ambient density. It can be seen that higher ambient density promotes larger diameter decrease for the same changes of injection pressure.

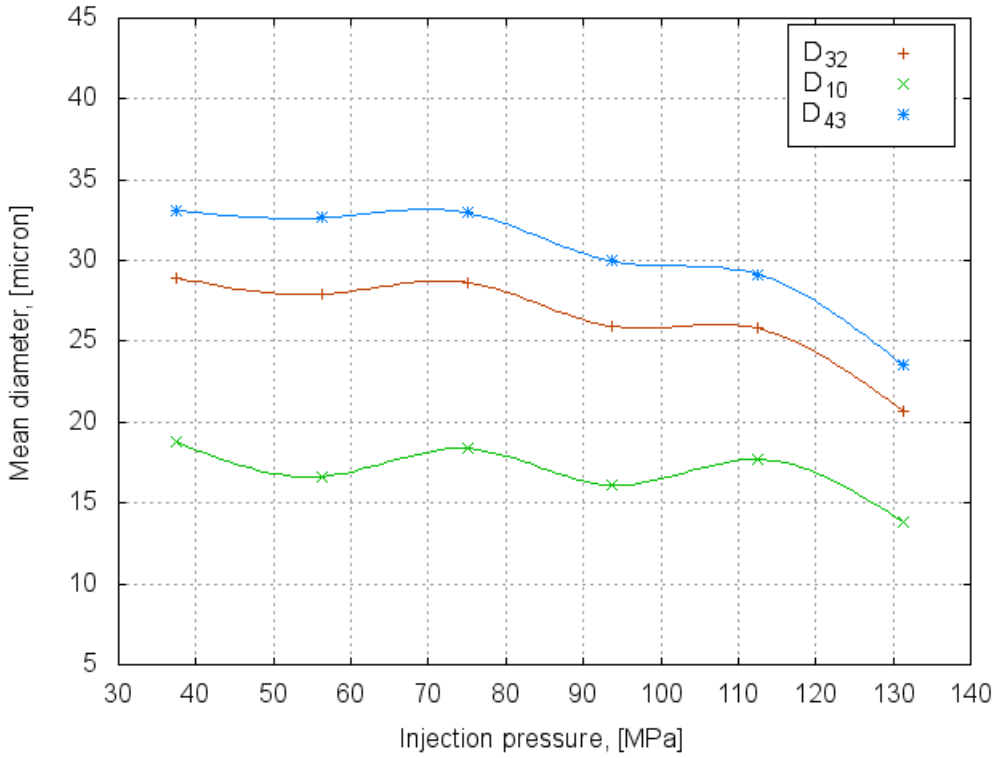

Figure 6.55: *Effect of injection pressure on SO at 30°C and the ambient density of 30 kg/m^3*

A similar analysis of the injection pressure effect was performed for RSO at two separate oil temperatures, i.e. 30 and 60°C. These two temperatures represent the most extreme RSO conditions as far as the a reduction of flow properties is concerned. The investigation was chosen to study differences between SO and RSO and to check if both oils would follow the same experimental trend and the magnitude of reduction. A set of four figures (6.58, 6.59, 6.60 and 6.61) present results of the injection pressure effect on mean diameters of RSO injected at 30°C and various ambient densities.

Experimental data shown in Figure 6.58 were collected at 15 kg/m^3 of ambient density. The drop sizes decrease gradually with increasing injection pressure. The D_{32}, D_{10}, and D_{43} curves exhibit a similar fluctuating decrease. A similarity between RSO data and results of SO tests (Figure 6.54) can be found as far as the linear trend is concerned, however, diameter changes seems to be less noticeable for RSO. RSO oil drop size decreases and generally the effect of injection pressure is weaker. An average size reduction of approximately by 25% is observed. The curves are almost parallel and the lowest values can be seen for the D_{10}. Figure 6.59 shows the results of RSO injections collected at the ambient density of 30 kg/m^3. RSO diameters are getting reduced with the injection pressure. It can be observed that the diameter decreases and reaches almost to constant

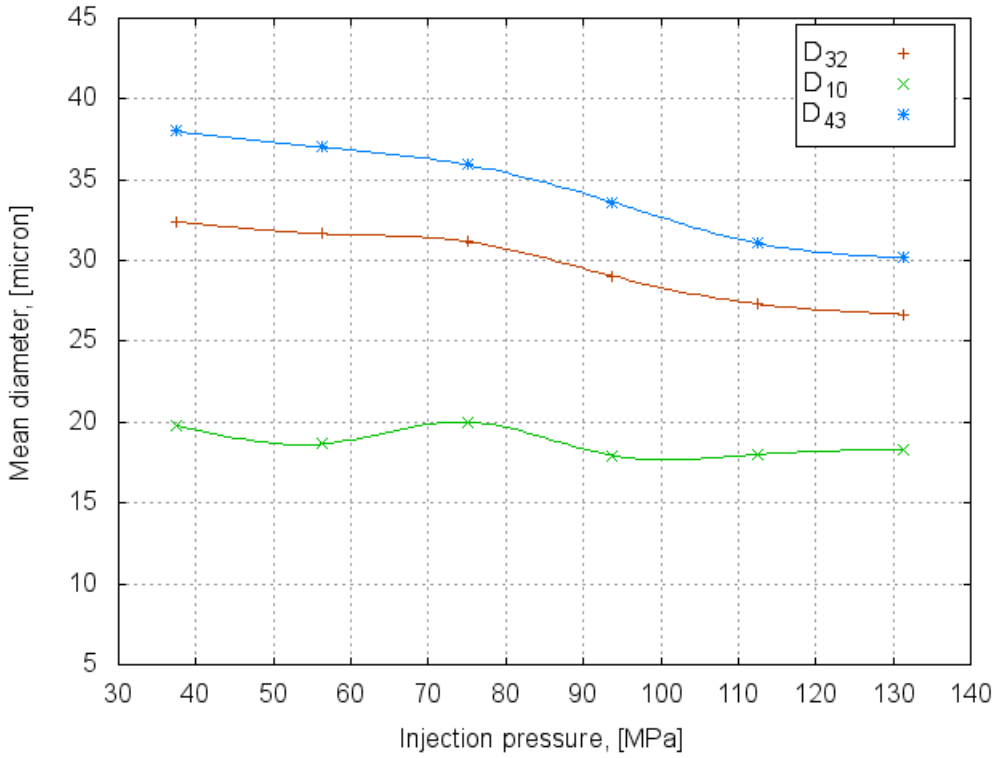

Figure 6.56: *Effect of injection pressure on SO at 30°C and the ambient density of 45 kg/m^3*

values of 39 μm and 34 μm for D_{43} and D_{32}, respectively, as the injection pressure goes beyond 110 MPa. Such effect together with the much higher values of mean diameters are major differences between the RSO results and the corresponding SO results presented in Figure 6.55. Further comparison of these two data sets recorded data reveals less modest increase of diameter values with ambient density. Further increase of the ambient density to 45 kg/m^3 and its effect on the variation of the mean diameters with elevated injection pressures is shown in Figure 6.60. Presented curves describe an expected gradual decrease of the mean diameters with injection pressure. It is observed that the curves feature a different trend to those for SO presented in Figure 6.56. The curve slopes are less steep, which indicates a lower reduction of the mean values in the comparison to SO. It can be seen that D_{43} and D_{32} values are much higher that mean arithmetic data. A gap between D_{10} curve and the rest of mean diameters remains almost constant throughout the whole range of investigated injection pressures. The overall values of mean diameters are higher than the data of SO and also slightly higher than those of RSO at 30 kg/m^3 shown in Figure 6.59. Mean diameters recorded for the highest ambient density of 60 kg/m^3 as a function of injection pressure is shown in Figure 6.61. Similar to the SO results, the data show the most dynamic decrease with injection pressure. The absolute values of RSO diameters are the lowest within the utilised ambient density range. A reduction by almost

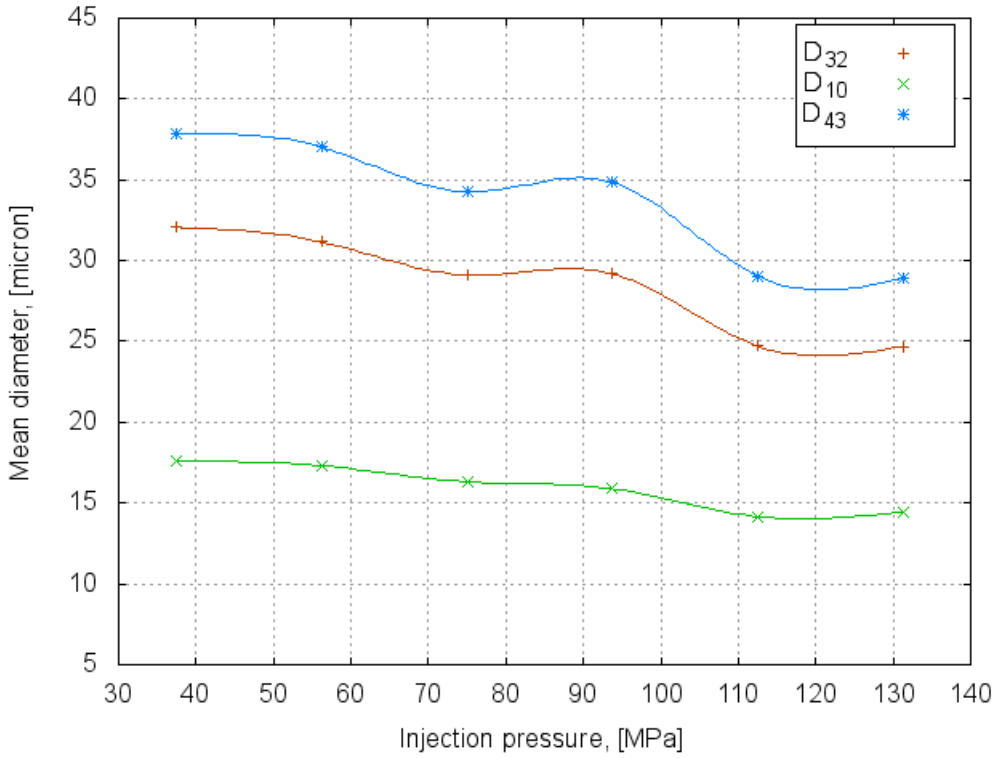

Figure 6.57: *Effect of injection pressure on SO at 30°C and the ambient density of 60 kg/m*^{3}

30% can be observed for the values of D_{43} and D_{32}. The presented results reflect on a significant reduction of mean diameters since RSO has been subjected to a combined effect of high injection pressure and the active shear forces of the ambient gas. As it can be seen, the values of D_{43} and D_{32} are decreasing particularly at the end of the injection pressure range, whilst the D_{10} reduction is not so strong.

6.3.4 Effect of ambient pressure on RSO droplets validation

As the injection pressure alters the spray density one can conclude that the ambient density should influence the spray concentration too. Therefore, a study of the ambient density effect is naturally interesting and would provide some hints for investigation of plant oil sprays at different ambient densities. The effect of ambient density (pressure) on the number of validated RSO drops is shown in Figure 6.66.

The RSO droplet were studied at two different oil temperatures of 30 and 60°C. The presented data were collected for the injection pressure of 131.25 MPa. As it is seen from Figure 6.66, denser ambient conditions lead to decreasing validation almost in a linear manner. This effect could be associated with the increasing ambient causing higher shear forces stripping off the spray. It is seen that the effect is more noticeable for the higher oil temperature, which weakens oil viscosity, density and surface tension. Thus the stripping

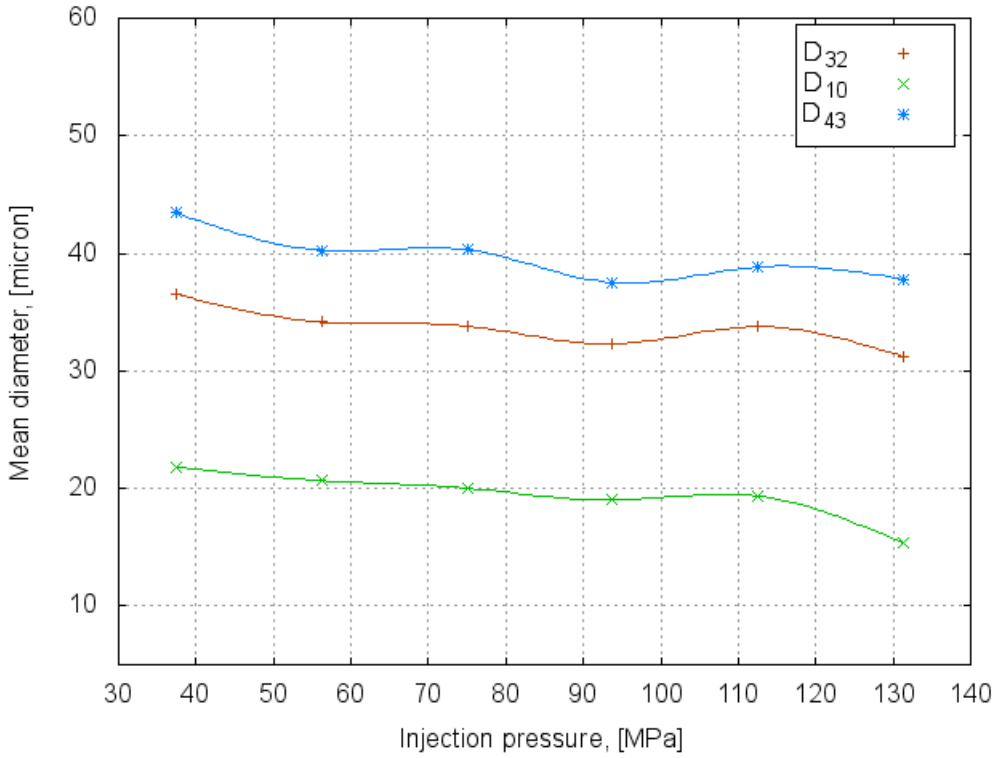

Figure 6.58: *Effect of injection pressure on RSO at 30°C and the ambient density of 15 kg/m*^{3}

process is more pronounced and the "droplet" cloud is more readily formed. The lower ambient density enhances higher drops validation. It should be commented that the influence of the injection pressure and ambient density on the validation is deeply affected by number of satellite drops always present in a spray vessel particularly at higher injection pressures and oil temperatures. The satellite drops tend to float across the vessel and mask the laser signal which then leads to a lower validation. The effect is random and can only be eliminated by a more frequent evacuation of the vessel contents.

6.3.5 Verification of the accuracy of the PDA measurements

As it has been shown above, the PDA results were obtained for highly dense SO and RSO sprays. Questions may arise concerning the accuracy of these measurements. Also it may be a question how well results obtained with the PDA compare with results for the same spray using a different instrument. The purpose of this subsection is to verify the drop sizing results of the PDA setup with those of a Malvern instrument. Here, only the essential and most important element of the comparison will be presented as a detailed comparison of PDA and Malvern is beyond the scope of this thesis.

PDA method, as it has been described in the introduction, employ the phase-shift principle and provides the largest dynamic range in sizes at a single setting, whereas Malvern is

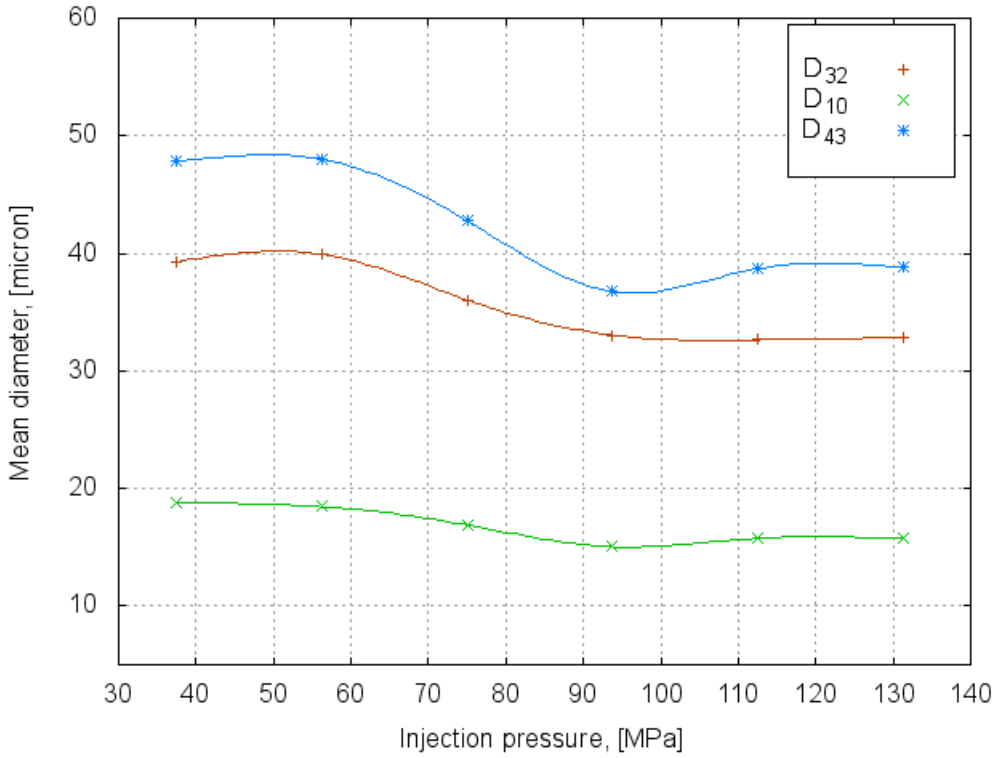

Figure 6.59: *Effect of injection pressure on RSO at 30°C and the ambient density of 30 kg/m*^{3}

based on the laser-diffraction principle offering a line-of-sight average droplet size through the complete spray. The most fundamental difference between PDA and Malvern is that PDA device measures in a very small volume rather than through the whole spray. Therefore, a comparison of results requires to convert the PDA data into line-of-sight spatially averaged data or the Malvern data need to be spatially resolved (conversion into point data). The first approach has been already performed by Jackson and Samuelsen [50] and the second approach can be found in the deconvolution method elaborated by Hammond [175] or different ways described by Yule at al. [429] and Lee and Reitz [249]. Although the first approach is considerably easier, it results in only one overall value for comparison, while the second method allows comparison through the spray. Considering the advantages of of the second method as well as capability of the Spraytech [1] software to perform the deconvolution conversion, the conversion of Malvern data has been performed in this work. The procedure of deconvolution is noticeably simplified for sprays which are axially symmetrical. SO and RSO sprays can not be described as axially symmetrical however since the Malvern measurements were performed on the spray centreline, the same approach as for symmetrical sprays could be applied. The spatial resolution of the deconvolution procedure has been determined and described in details by Dodge and his co-workers [114].

[1] Spraytech in the name of software serving the Malvern device used in this work.

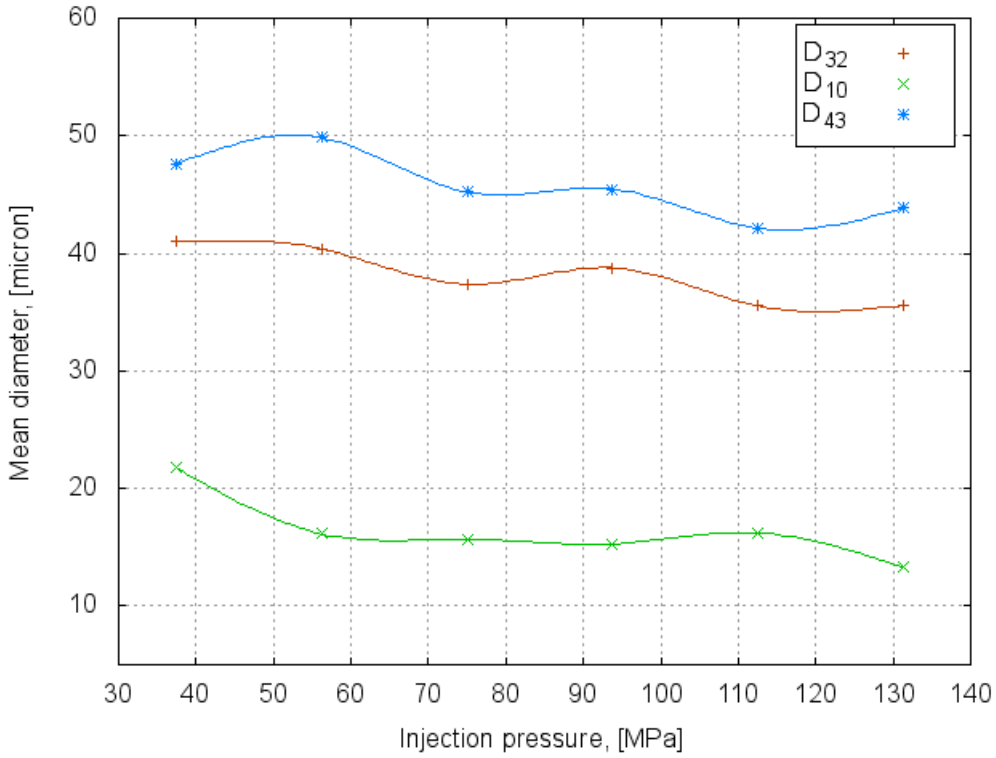

Figure 6.60: *Effect of injection pressure on RSO at 30°C and the ambient density of 45 kg/m*^{3}

A detailed comparison of the Sauter mean diameters for four different ambient densities is presented in Figure 6.67. The figure includes also the error bars indicating the maximum and minimum deviation from the mean values. As it can be seen for almost all measurements the presented values are within the error margins or are very close to these. Simply, the error bars of both experimental measurements are overlapping each other. As it can be seen from Figure 6.67 (a) and (b) the substantial differences between PDA and Malvern can be found approximately in a pressure range of 60-120 MPa. The diameter curves are significantly apart indicating the biggest D_{32} differences. It can be noticed that values of the lowest injection pressure are surprisingly consistent. As it has been already pointed out, at the lowest injection pressure RSO spray may be deteriorated and deformed hence expected inaccuracy and variation in size measurements. As the ambient density increases, deviation between PDA and Malvern results rises and it can be seen in Figure 6.67 (c). Presented curves exhibit the same trend of decreasing Sauter diameters with injection pressure although a difference between PDA and Malvern can be recorded particularly for the highest injection pressure. As the injection pressure and the ambient density increase it is expected that the drop population consist more readily of small droplets and number densities are high, particularly near the spray centre. Also, taking into account that the PDA system introduces aberrations which result in the counting of some drops, particularly

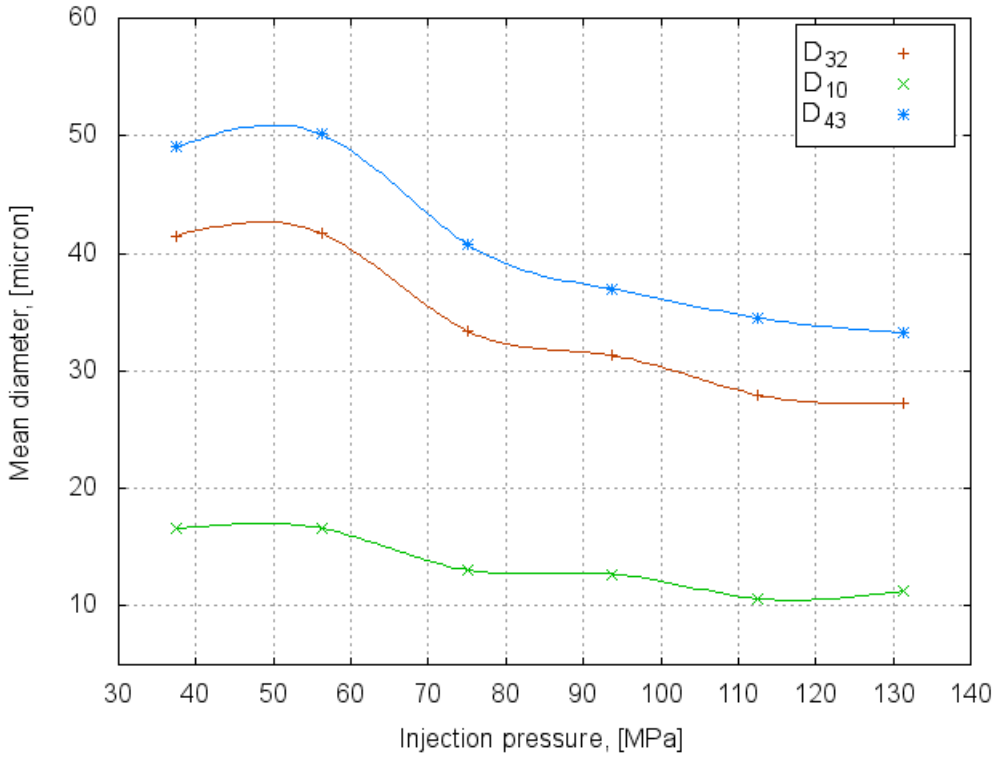

Figure 6.61: *Effect of injection pressure on RSO at 30°C and the ambient density of 60 kg/m*^{3}

larger ones, which are outside the proper measurement volume [1], it might be possible to detect preferentially the larger drops and miss some of the smaller drops passing the measurement volume. Thus, the highest Sauter values can be found in Figure 6.67 (c).

As it can be observed at each presented graph of Figure 6.67, the Malvern values between 60 and 130 MPa are lower than the results of PDA. A similar trend was observed by Cossali and Hardalupas [95] who found that the Sauter mean diameter measured by laser diffraction was 30% smaller than the line-of-sight estimates from the phase Doppler measurements in the petrol spray and 100% smaller in the diesel spray.

Some other factors influencing differences between PDA and Malvern are the sampling location and high spray density. The sampling locations of both methods are comparable and had been set up to be similar, but still are not identical. Also, the resolution of the PDA instrument is much finer than the Malvern unit. Malvern averages over much larger parts of the spray and accept the axial symmetry of spray.

High density of RSO spray cause errors in both methods, however the Malvern test suffers from the multiple-scattering effect, which may result in a systematic bias toward smaller average drop sizes. This has been widely reported by Felton et al. [141]. A comparison of the arithmetic mean diameters by the PDA and Malvern instruments was conducted according to the experimental details presented in the Sections 3.4 and 4.3. Results of the

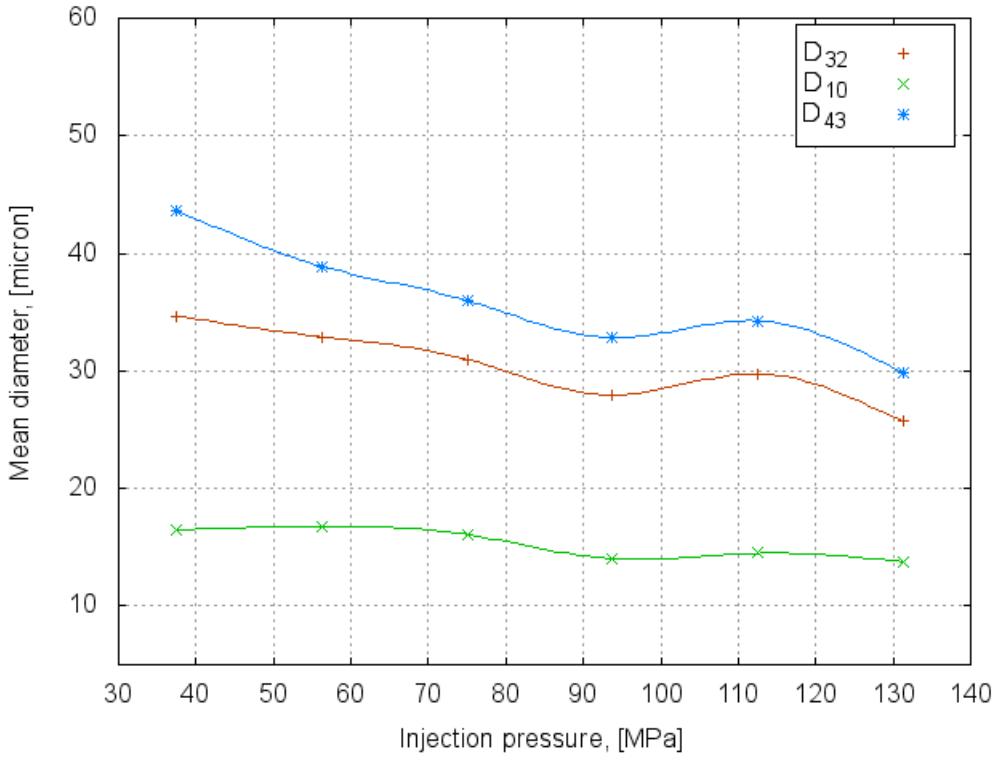

Figure 6.62: *Effect of injection pressure on RSO at 40°C and the ambient density of 15 kg/m*^{3}

comparison are presented in Figures 6.68. As it can be recognised that data presented in the graph have been derived from the two different droplet populations as those in Figure 6.67. A difference in distribution shape may be seen between the D_{10} and D_{32} values of the PDA and Malvern tests. It can be seen that the Sauter mean diameters compare more favourably than the arithmetic mean diameters. A similar results has been found by Dodge [114] who concluded that th effect was due to a difference in the width of the size distribution. Also, Lee and Reitz [249] performed a comparative study of three different fuels using laser diffraction and PDA. Their work showed a similar deviation of D_{32} values measured by both methods as presented in this section, however the largest differences were found for the most central and radial measurements. It has to be highlighted that Lee and Reitz used a different deconvolution method, which apparently might provide better accuracy. Differences in drop sizes and distribution shapes has been also reported by Jackson et al. [206] comparing PDA and Malvern results. The authors found differences qualitatively similar to those presented here. Nevertheless, comparison of the literature results and the present data indicates a clear differences between these two techniques. It can be stated that both instruments measure Sauter mean diameter with better repeatability than the arithmetic values as well as the PDA instrument may miss some of the small droplets, and Malvern overemphasise them [114].

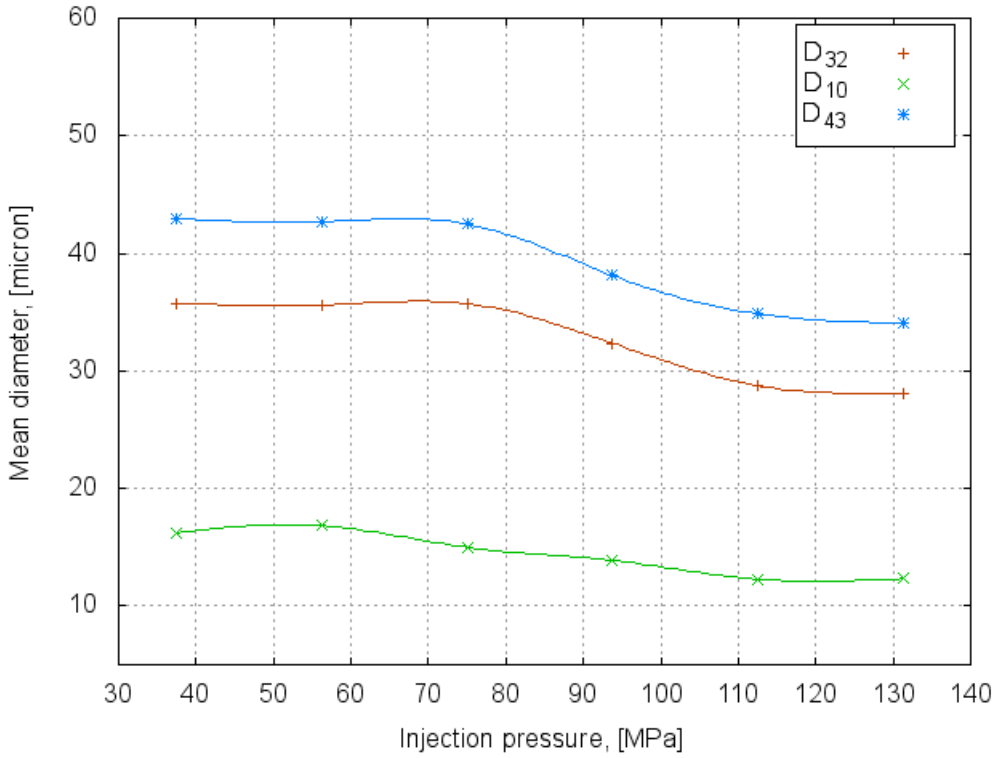

Figure 6.63: *Effect of injection pressure on RSO at 40°C and the ambient density of 30 kg/m*^{3}

A careful analysis and comparison of the PDA and Malvern results would require considerably more attention. The author states that each method features in advantages but in measurement of dense spray both are subjected to various drawbacks. Nevertheless, PDA and Malvern techniques can be considered as complementary and serve well in comparative studies of dense spray if they are carefully setup and the results are analysed with care [113; 395; 415]. Also, it is expected that the RSO measurements represent the most “difficult” experimental case. RSO spray is denser and more compact and, therefore, measurement of SO would naturally provide a better accuracy.

6.3.6 Effect of injection pressure on RSO droplets validation

High density sprays such as RSO, are particularly difficult to be characterised using laser techniques. RSO density and viscosity much higher than for the conventional diesel affect spray development by making sprays consisting of less spherical drops, very likely increasing the breakup length. This may result in reduced accuracy of PDA measurements as well as the number of validated drops. It has been recognised that attaining measurements of plant oils is challenging and requires vary precise tuning of the applied laser instruments. As it was recorded throughout the experiments, the injection pressure affected number

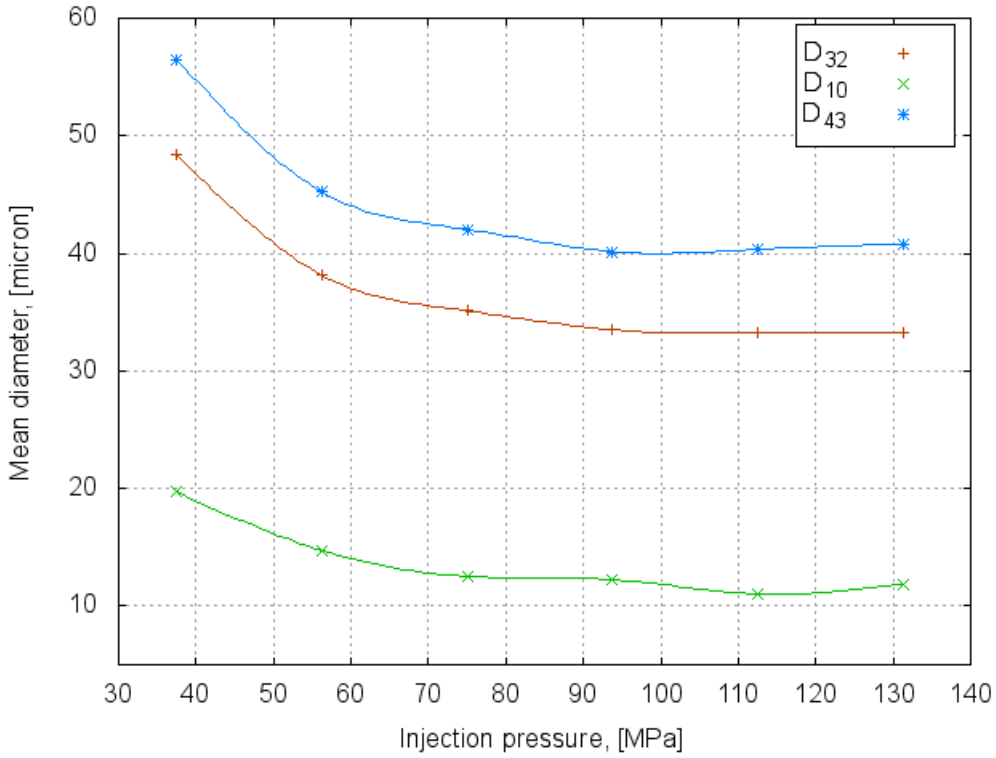

Figure 6.64: *Effect of injection pressure on RSO at 40°C and the ambient density of 45 kg/m*^{3}

of validated drops and caused variation in the accuracy. In this subsection the effect is presented in more detail. Despite it is not directly related to modification of CDI system, the author believes that this will provide essential information for those willing to study plant oil sprays using PDA.

The influence of the injection pressure on the number of validated drops is presented in Figure 6.69. The validated drops term refers to the percentage of validated drops within a studied population. The figure represent an average and typical trend recorded for RSO at two extreme ambient densities of 15 and 60 kg/m^3 at an oil temperature of 60°C. The validated drops were considered as those of meeting velocity (one component, U) and sphericity validation limits (see *Section 4.3*). As the injection pressure increase, validation decreases by almost 20% and 50% for 15 kg/m^3 and 60 kg/m^3 respectively. It is apparent that higher injection pressure creates more compacted (dense) spray, therefore the similar trend for both curves can be observed. A similar effect and trend was observed for SO test. Nevertheless, SO validation was significantly higher (by ∼15% on average).

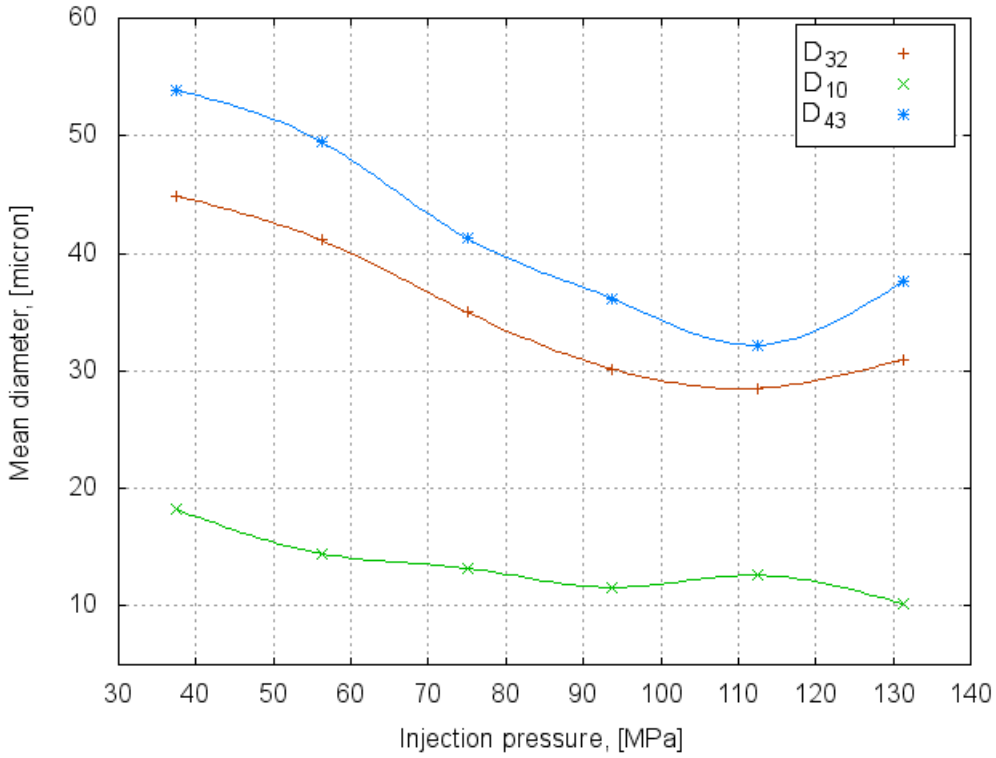

Figure 6.65: *Effect of injection pressure on RSO at 40°C and the ambient density of 60 kg/m*^{3}

6.4 Acoustic emission tests

Analysis of AE signal is very much based on the recognition of acoustic events and association of these event with the appropriate mechanical events. The process is often called as pattern recognition. The fundamental differences between CR and other DI nozzle injection patterns cause a great difficulty to perform the pattern recognition of a running engine. The reason is, the CR injection does operates according to the electric impulse produced and controlled by the ECU, rather than a mechanical governor. Strictly speaking, injection event do not follow a series of mechanical events in a way it takes place in conventional DI engines. For instance, the main injection, i.e. its start and duration is not a function of the crankshaft position, but rather a function of the position and other parameters like power demand, ambient temperature, acceleration etc.

One can suggest that if a ECU map is known, then the pattern recognition might be more feasible, although such recognition is not so straightforward. Simply, the ECU works as an intelligent set of adaptive function rather then a set of equations. A separate issue is a simultaneous measurement of AE and the ECU output, which was not possible in this work. For instance one of the most convenient way of monitoring would be recording of all mechanical signals associated with needle lift, valves etc. together with the output

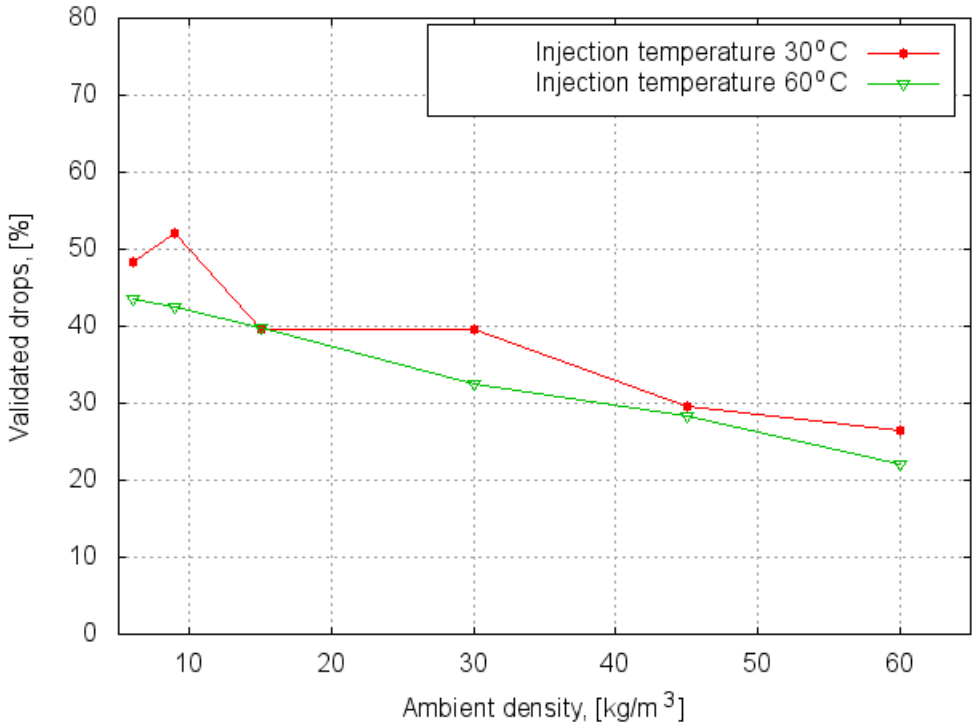

Figure 6.66: *Effect of ambient density on validated numbers of rapeseed drops.*

signals of the ECU. Such measurements was beyond the capabilities of the AE acquiring setup and also correlation amongst all these signals was rather to difficult to be included in this work.

Thus the AE signal pattern analysis was performed in this work using the signal processing methods presented in the Section 4.4 and deductive analysis of AE signal performed using standard diesel and RSO and a signal of a dry injector. The analysis was also supported by the available description of CDI Bosch injector [74; 203].

6.4.1 AE analysis of Common-rail injector signal

To understand AE Common-rail signal it is essential to learn how the injector operates. In general the injector's operation can be divided into four stages:

1. Injector remains closed but high pressure fuel is applied
2. Injector opens and injection starts
3. Fully opened injector
4. Injector closes and injection terminates

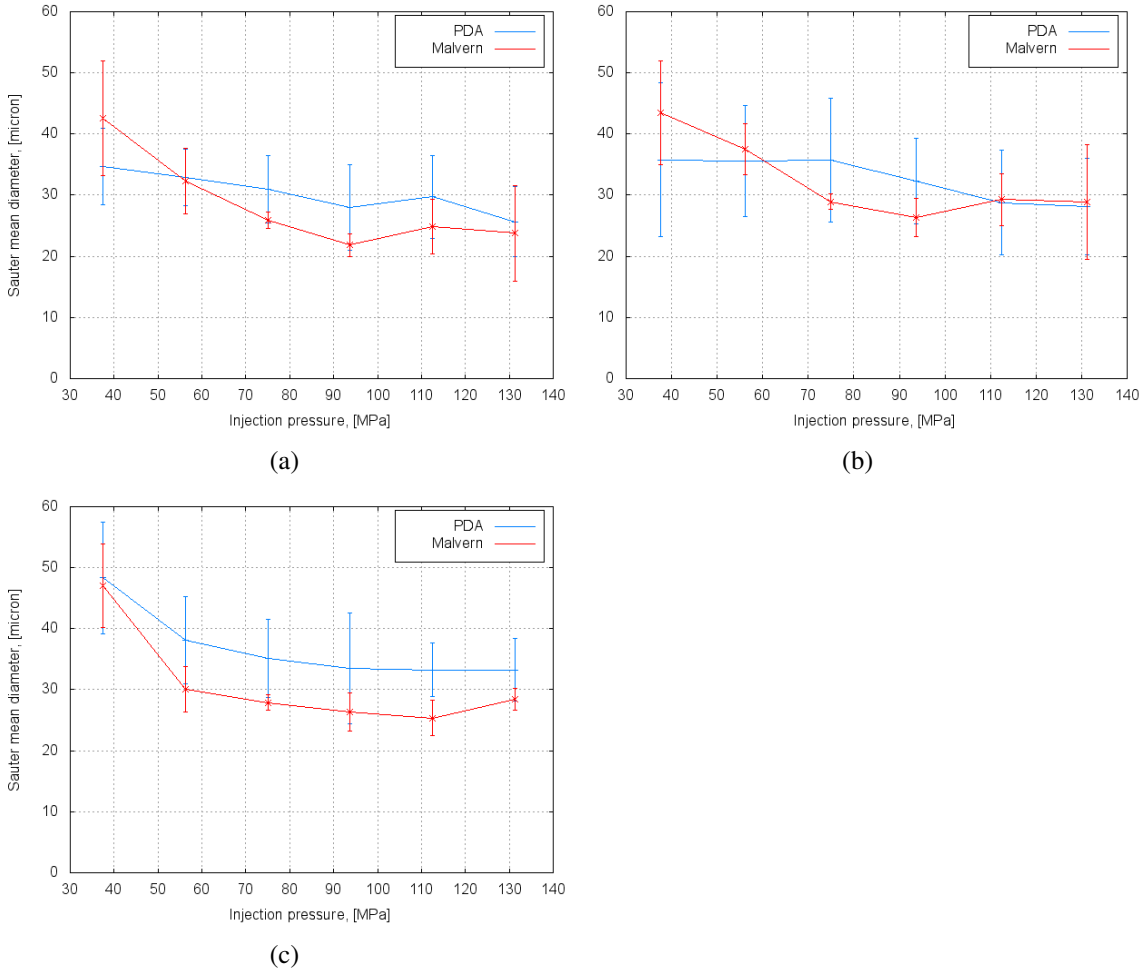

Figure 6.67: *Comparison of PDA and Malvern Sauter mean diameters measurements for RSO at the ambient density of. (a) 15 kg/m^3; (b) 30 kg/m^3; (c) 45 kg/m^3.*

Figure 6.70 depicts the resting position (left picture) and the fully opened injector. The main mechanical parts of the injector are outlined the picture showing the injector internals at resting and injection stage. These stages result from the distribution of the forces applied to the internal and external components of the injector, and hence causing acoustic emissions of various frequency and signal duration. These four stages only outline the major operational mechanical sequences, however do not directly reflect on the complex injector AE signal. Each of above stages are described below in more details for a fully operating injection (with pressurised fuel inside). Additionally, the stage description is depicted by the AE graph of almost not pressurised injector or not-fully pressurised being energised for 1 ms (Figure 6.71). This injector was investigated under a very low pressure of around 2 bars, which did not lead to spray nor flow of fuel out of the injector but allowed moving the control plunger and the needle. At this pressure the internal fuel movement is not picked up by the AE equipment. The pressure was recommended by engineers of Elsbett Company. Hence, Figure 6.71 present the major events without a

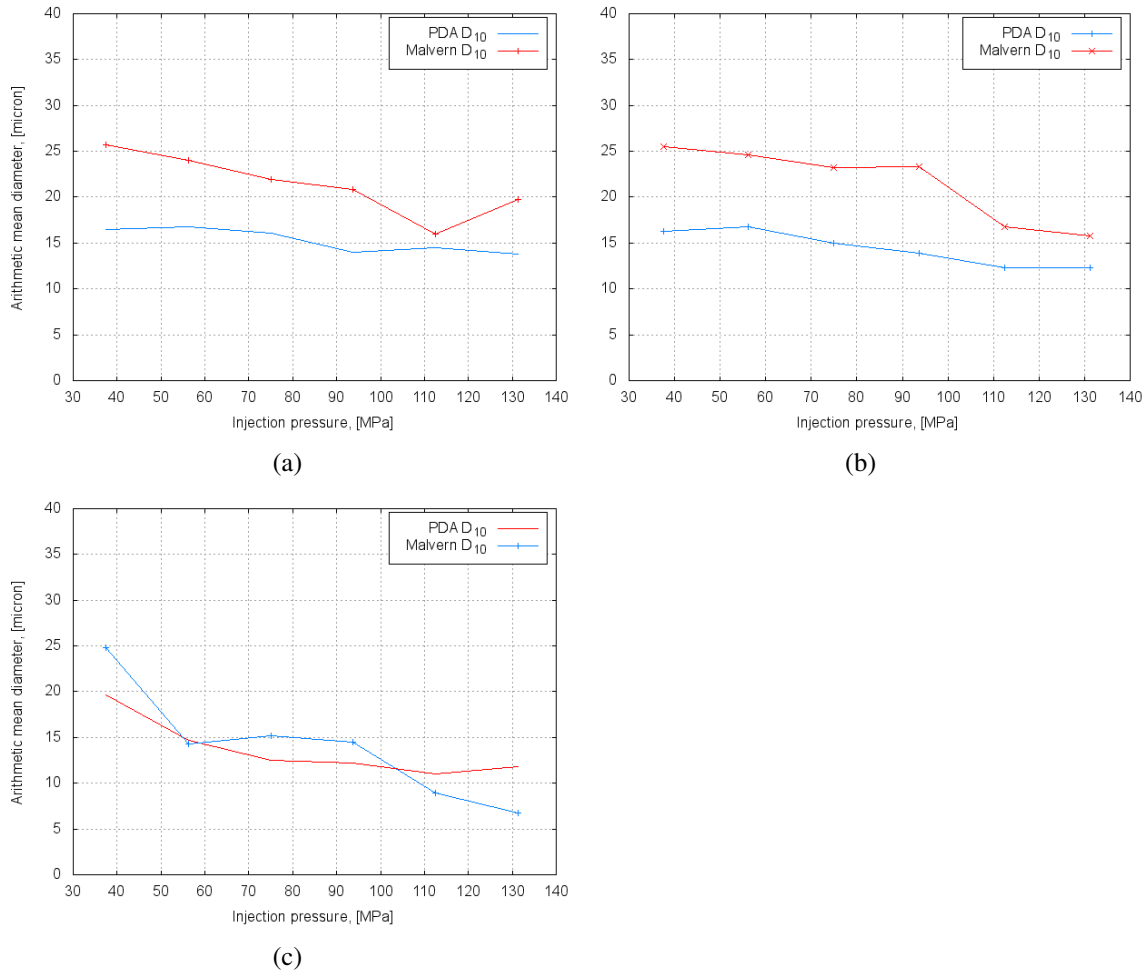

Figure 6.68: *Comparison of PDA and Malvern arithmetic mean diameters measurements for RSO at the ambient density of. (a) 15 kg/m^3; (b) 30 kg/m^3; (c) 45 kg/m^3.*

signal indicating the flow. The procedure was performed to collect an AE signal, which then could be compared to signals of fully pressurised nozzle. The major events of the AE signal were identified and associated with the operational staged described below.

Injector remains closed but high pressure fuel is applied - at this stage the solenoid valve is not energised and is closed. This is shown in Fig. 6.71 as a signal part before index "1". The valve spring forces the armature's metal ball against the bleed-orifice seat. The bleed-orifice remains closed. (In case of real injection pressure, the rail's pressure builds up in the valve control chamber, and the same pressure is also present in the nozzle chamber volume.) The rail pressure applied at the control plunger end face, together with the force of the nozzle spring, maintain the nozzle in the closed position. At this stage no significant detection of the AE should be seen, and it is represented by a signal part right up to the first peak in Figure 6.71. Some small amplitude changes can be seen and they are mostly related to the vibration of the injection system transmitted along the fuel lines.

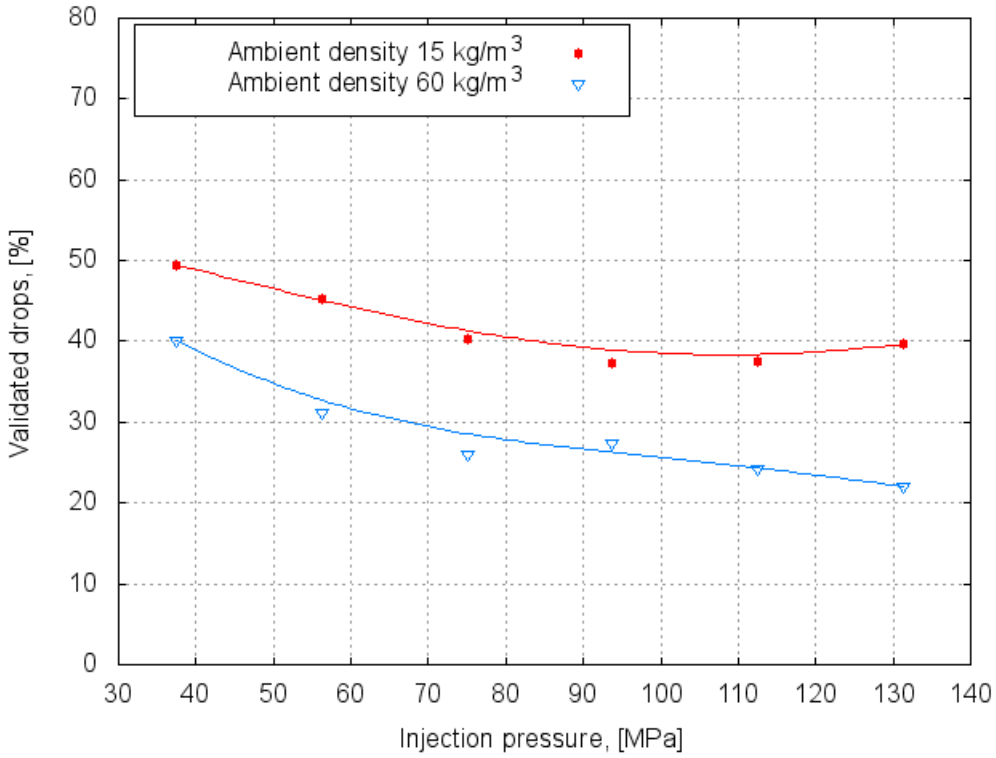

Figure 6.69: *Effect of injection pressure on validated numbers of rapeseed drops.*

Injector opens and injection starts - The injector armature remains at its resting position as indicated by index "1" (Fig. 6.71). The solenoid valve is energised with the pick-up current, which serves to ensure that it opens quickly. This can be seen as a noticeable AE peak, first in Figure 6.71 of the duration of ∼0.2 ms. The force exerted by the triggered solenoid now exceeds that of the valve spring and the armature opens the bleed orifice. Almost immediately, the high-level pick-up current is reduced to the lower holding current required for the electromagnet. When the bleed orifice opens, fuel can flow from the valve-control chamber into the cavity situated above it, and from there via the return to the fuel tank. The flow speed and hence the time of opening depends on the fuel pressure. The bleed orifice prevents complete pressure balance, and the pressure in the valve control chamber sinks as a result. This leads to the pressure in the valve-control chamber being lower than that in the nozzle's chamber volume, which is still the same pressure level as the rail. (In case of a higher fuel pressure, the reduced pressure in the valve-control chamber causes a reduction in the force exerted on the control plunger, the nozzle opens as a result, and the injection starts.) In the case of no fuel in the injection the opening of the bleed orifice and the flow from the valve-control chamber into the cavity is not detected and shown in Figure 6.71. The component of the first AE peak are herein mainly related to the solenoid valve movement and the smash of the armature plate against the solenoid

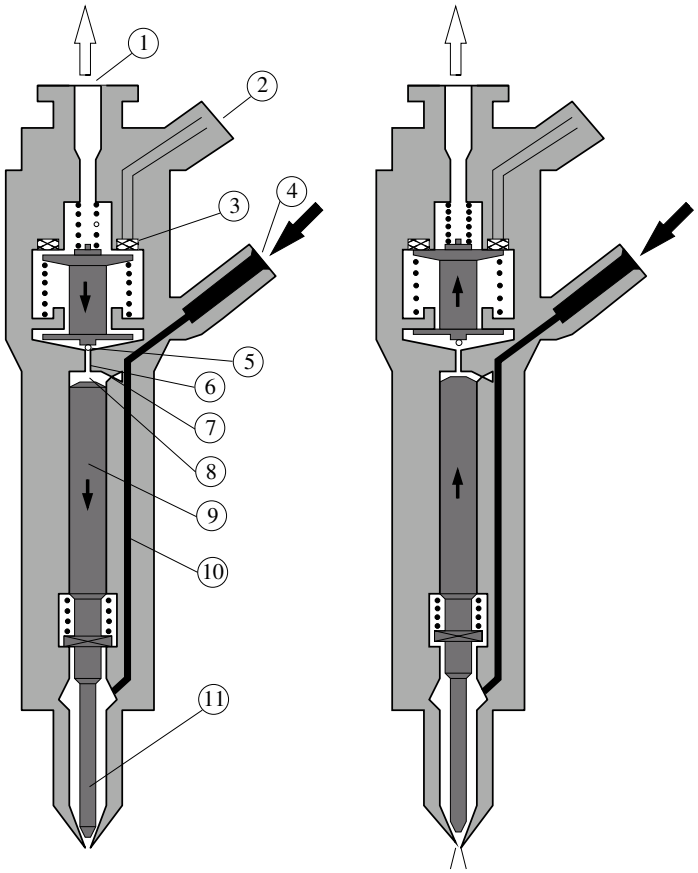

Figure 6.70: *Injector (schematic). (1) fuel return, (2) electrical connection, (3) solenoid valve, (4) fuel inlet from the rail, (5) valve ball, (6) bleed orifice, (7) feed orifice (connecting the fuel inlet with the valve control chamber (8) valve control chamber, (9) valve control plunger, (10) feed passage to the nozzle, (11) nozzle needle*

valve face and the minimal over-spring. It has to be noted that during the actual operation the nozzle needle opening speed is determined by the difference in the flow rate through the bleed and feed orifices.

Fully opened injector - The control plunger reaches its upper stop where it remains supported by a cushion of fuel which is generated by the flow between the bleed and feed orifices. The injector nozzle has now opened fully (part "2" in Fig. 6.71), and normally the fuel is injected into the combustion chamber at a pressure almost equal to that in the fuel rail. Force distribution in the injector is similar to that during the opening phase. Figure 6.71 does not show a distinctive AE response for this stage since there is no fuel spray. It is represented by an "empty" region of $\sim$0.9 ms. The pattern of this region is terminated with a small peak which has been described as "the artifact of the injector opened" ($\sim$1.25 ms) and is very likely an echo of the AE signal detected at the opening stage as well as the force distribution but of much low amplitude. It is very difficult to

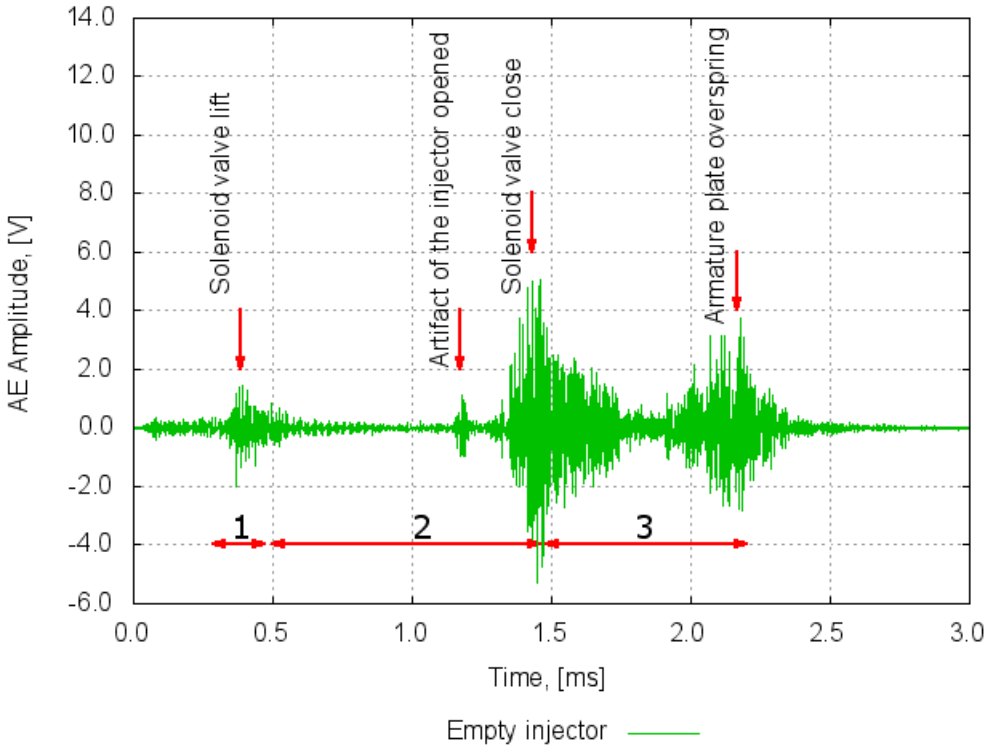

Figure 6.71: *Event analysis of the empty injector triggered with 1 ms opening signal.*

resolve the origin of the AE signal since the time domain of the events is very narrow and the AE detecting resolution is quite low. It is also expected that the AE sensor contributes in the signal by its own signal response. Nevertheless, it is assumed that the signal artifact it is not associated with the essential mechanical response of the injector.

Injector closes and injection terminates - As soon as the solenoid valve is no longer triggered, the valve spring forces the armature downwards and the ball closes the bleed orifice (signal part "3" in Fig. 6.71) . The armature is a 2-piece design. Here, although the armature plate is guided by a driver shoulder in its downward movement, it can "over-spring" with the return spring so that it exerts no downwards-acting forces on the armature and the ball. The closing of the bleed orifice leads to pressure buildup in the control chamber via the input form the feed orifice. This pressure is the same as that in the rail and exerts an increase force on the control plunger through its end face. This force, together with that of the spring, now exceeds the force inside the chamber volume and the nozzle needle closes. The nozzle needle closing speed is determined by the flow through the feed orifice. Injection ceases as soon as the nozzle needle comes up against the bottom stop again. The stage is distinctly depicted in Figure 6.71 started at $\sim$1.4 ms and lasting until

$\sim$1.75 ms, although the actual movement is taking place in a very narrow window around $\sim$1.45 ms. The signal tail represent a signal response appearing due to the strong impact on the AE sensor. It is quite noticeable that this stage is represented by a high amplitude and thus signal strength. As mentioned above the elements of the AE signal are complex and in a dry injector are mainly because of the hit of the armature against the injector body, the "over-spring", interaction between the armature and the valve ball and also changes of the current in the solenoid. It is expected that AE pattern in each stage will change in accordance with the fuel pressure and the flow.

The last AE signal element in Figure 6.71 is described as the armature over-spring although its interpretation can be very much speculative. One can notice that the signal structure resembles very much the AE signal of the closing injection and a time gap between the closing event and the actual signal corresponds very much to the time space between the solenoid valve lift and the first artifact. Therefore, the author accepted that the last AE peak is very much a consequence of post-interactions of the closing events but also could be a movement of the nozzle needle (11 in Figure 6.70). The needle does not travel together with the movement of the armature since there is not enough fuel in the valve control chamber, although it moves eventually and may contribute in the signal due to the plunger interacting with the plunger spring. Despite the cause of such AE detection it can be assumed that the pattern should be less noticeable at low fuel pressures (slower movement and the muting effect of the fuel) and more significant at higher injection pressures (greater impact of the plunger against the spring). Also, it can be assumed that the pattern can appear sooner at higher injection pressures due to faster interactions between the armature, the plunger and the needle.

The above signal analysis was performed for a not-fully pressurised nozzle. Figure 6.72 shows a comparison of a such empty injector with the signals for the minimum and maximum injection pressures (37.5 and 131.3 MPa respectively). All signals were taken at the same timing, however the signal patterns show a varying "gap" (lack of peaks) between the start (time=0.0) and the first peak representing a mechanical event. This can be explained by the fact that with increasing injection pressure the flow through the feed orifice enhances and the response of the injector becomes shorter. If the injection pressure increases the valve control chamber fills up quicker and also forces the internals to move quicker, hence the "gap" becomes shorter (filled with some peaks associated with the internal fuel flow) and the armature of the actual event stronger (higher impact). Therefore, for the highest injection pressure (the blue signal) the "gap" is the shortest, whereas for the non-spraying

injector the gaps is the longest.

The second noticeable difference is the signal shape after the closing event (depicted as the second strongest peak from the left for the not-fully pressurised signal). As for the dry injector there is a significant gap between the closing AE signal and the artifact, the same gap is getting filled up with various peaks whilst the injection pressure increases. This is is especially apparent for the highest pressure and is because of series of overspring of the armature as well as more violent flow through the closing bleed orifice and the valve control chamber. The same situation is not seen for the lowest injection pressure, which would suggest the muting effect of the fuel inside the aperture volume. Simply, the overspring is stifled by the fuel which has not been compressed and can absorb any mechanical waves occurring inside the volume.

The AE signal of the highest injection pressure is fundamentally different. Its strength is higher and the number of individual peaks is also higher (towards the end of the signal). The accumulation of peaks is assumed because of more intense mechanical impact of the armature including overspring as well as a collection of artifacts (echoes) and the overlapping sensor responses. Although, it can be seen that there is a significant AE peak representing the start of the valve closing. Since the presented signals of Figure 6.72

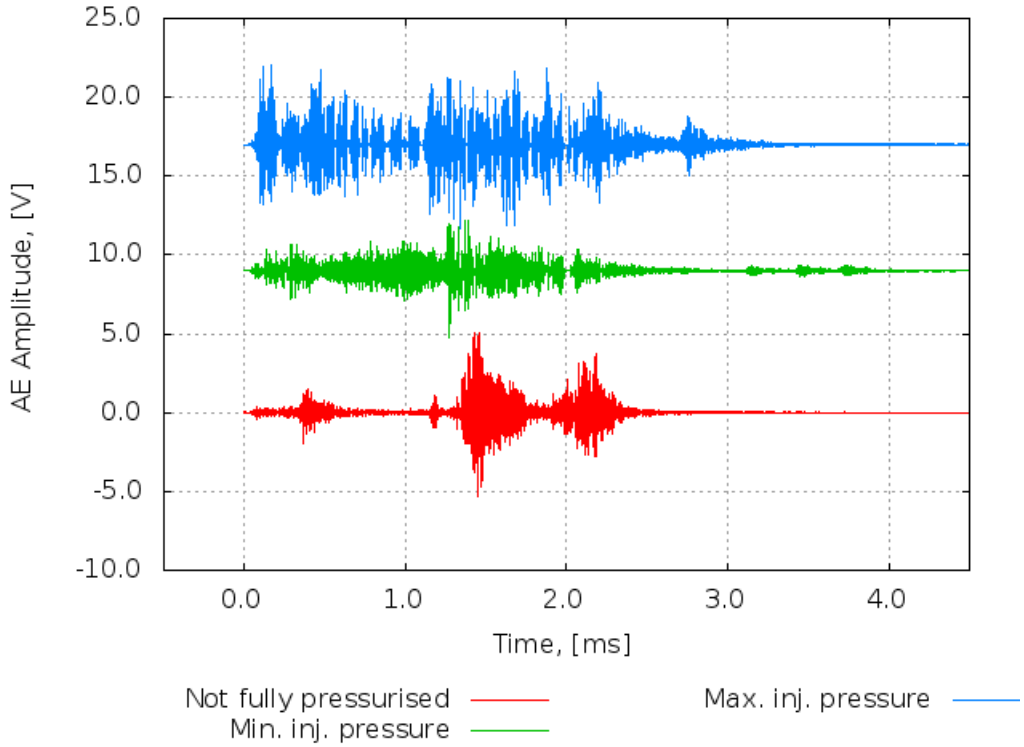

Figure 6.72: *Comparison of the AE signal of the not-fully pressurised injector with a typical AE signal for the minimum (37.5 MPa) and maximum (131.3 MPa) injection pressures accordingly*

were collected for injecting nozzles, the AE pattern consist of the AE response to the internal fuel flow. It can be easily recognised that the "wet" AE patterns consist of a series of AE peaks which are not present in the dry signal i.e. between the opening and closing peaks. Such a AE part is identified as an AE flow response. The Figure reveals that the amplitude of the flow pattern is increasing with pressure (higher for the highest injection pressure) and is having the raising and falling feature i.e. almost sinusoidally increases and drops. It can be also noticed that the rise part is shorter for the highest injection pressure and longer for the lowest injection pressure. The last observation which identifies the location of the flow pattern is the duration of the flow part, which is $\sim$1.75 ms.

It is essential to recognise injection pattern, which then can be used in comparative studies of the CDI injection system working on RSO and diesel.

Despite the above description seems to follow a logic, it requires a double check. Proper identification of the flow pattern is essential, and if done incorrectly may mislead and provide wrong conclusions. To identify correctly, a part of the AE signal strictly related to fuel flow, an additional AE signal analysis was performed using an actual acoustic analysis and Fourier Transform. The procedures are presented in the next subsection.

6.4.2 Preliminary injection pattern recognition

It can be seen already from Figure 6.72 that pattern recognition of AE CDI injections could be challenging. The signals can not be be only associated with the on/off signal triggering the injector. The rest of AE signals are inherently linked to various and dynamically changing mechanical events in the injector. Injection event is noticeably short and the expected effective flow is even shorter. Therefore, it is quite challenging to define the actual fuel flow by looking at AE signals. It was found during the experiments that operation of the injector is associated with characteristic sounds, which could be associated with moves of the solenoid valve and therefore with opening and closing of the injector. This finding was utilised to perform the acoustic analysis of signals by converting collected data into signal detectable by humans.

Basically, an AE signal was converted into an acoustic signal that could to be heard. Samples, were converted into audio files in the way that were not deformed but could be heard within a up-scaled time domain. Then, the files were introduced into a software,

which strengthened the acoustic events and played them. Figure 6.73 shows a screenshot of three AE converted signals i.e. no injection, injection at the lowest and the highest fuel pressure. It was confirmed that for the non-injecting signal mainly two characteristic click can be heard, i.g. the opening and closing of the injector. The grey part (top signal in Figure 6.73) between these two clicks cold indicate a place where normally injection takes place. For the other two signals, the middle and bottom one, a characteristic "low-frequency" noise originated in liquid flow through an orifice was heard. These regions were marked in grey. The presented procedure and the analysis as shown in Figure 6.73 allowed to establish a first guess of a time domain for injection (for all signals triggered for 1.0 ms and recorded using the same AE acquisition setup) as well as to select a range of frequencies, which can be associated with the flow. In the next subsection a method using the Fourier Transformation is applied to refine the frequencies of the injection flow pattern. It should be underlined that the use of audio files was considered as an additional and qualitative method prior to the analysis using Fourier transform.

6.4.2.1 Analysis of the injection pattern using Fast Fourier Transform and Time-Frequency Analysis

Features of the Fourier Transform offers a unique ability to analyse a signal in respect to frequency spectrum. Here the Fast Fourier Transform is utilised to perform an analysis of the fuel flow in side the CDI injector. Additionally, the simplified version of Fourier Transform is utilised together with a Hanning window specified for diesel and RSO AE signals.

Figure 6.74 represent the FFT graph of the injector operating without pressurised fuel i.e. when no injection occurs. It can be seen that the main frequency range within some events take place is from 0.07 to 0.4 MHz and a separate peak around 0.6 MHz. One can recognise five noticeable signal peaks i.e. around 0.1, 0.15, 0.2, 0.3 and 0.6 MHz. From a scaled part of Figure 6.74 it can be seen that the first two peaks have the highest (strongest) amplitude, and therefore it could be associated with some mechanical events taking place inside the injector, and as well as the event around 0.6 MHz. It was concluded that these frequencies are very much associated with opening and closing of the solenoid valve and the overspring. It was confirmed by listening to a signal as the opening and closing sounds have slightly different frequencies: the opening as higher sound that the closing,

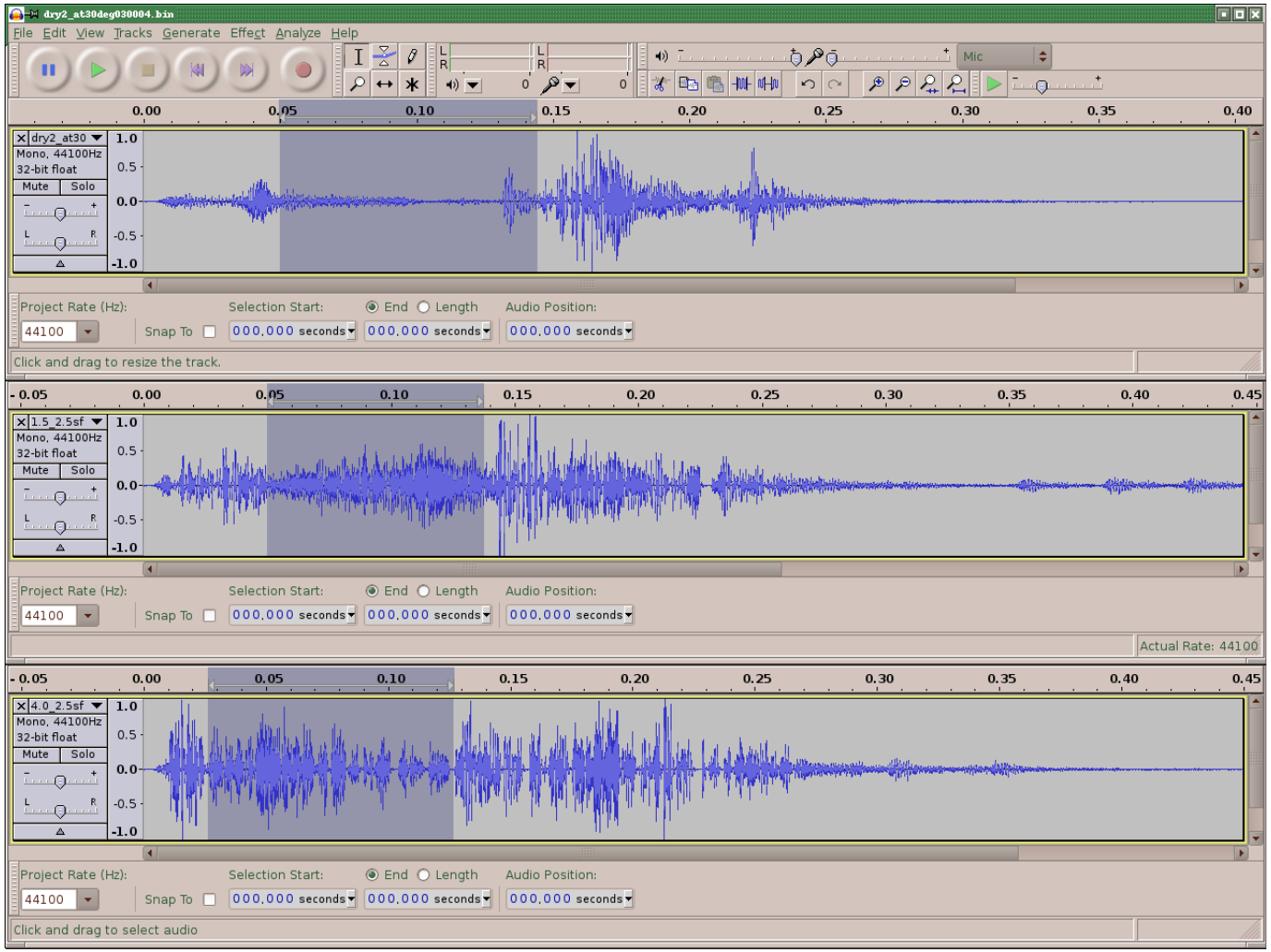

Figure 6.73: *Acoustic analysis of the AE signals. Non-injecting signal (left or top), the lowest (middle) and the maximum (right or bottom) injection signals. The grey region marks possible injection signal.*

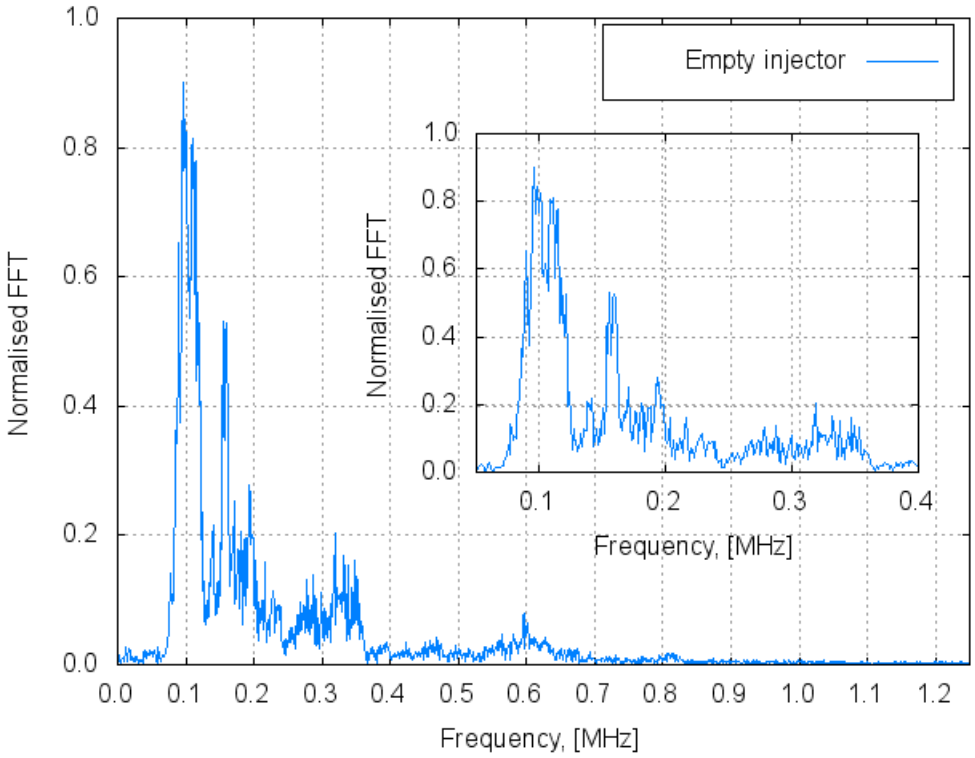

Figure 6.74: *The FFT pattern of the non-injecting nozzle injector.*

although the difference is just noticeable. The findings would indicate that the empty injector should feature of some peaks at low frequencies, preferably two have a frequency shift associated with the sound difference. Figure 6.74 shows that the frequencies should be found somewhere at the beginning of the X-axis. The frequency pattern clearly shows that presence of the two peak around 0.1 and 0.15 MHz.

Much better refinement can be made by comparing the FFT signals of empty and pressurised injectors. The comparison is presented in Figure 6.75, where the empty injection AE signal was compared with two AE signals of maximum and minimum injection pressures respectively. The figure show the main difference within the frequency domain, and those can be associated with the nozzle operation. It can be seen that the highest frequency component located between 0.05 and 0.2 MHz is reduced with increasing injection pressure. It can be explained that whilst the fuel injection increases the interaction amongst mechanical parts changes - higher pressure moves some parts faster. It is also noted that the strength of the mechanical impacts is higher at higher injection pressures and therefore the waves propagates pretty readily along the nozzle being subjected to all kind of effect known in acoustics. It is important to notice that the operating nozzle features of two frequency component which very likely are related to the fuel flow. They are present around 0.32

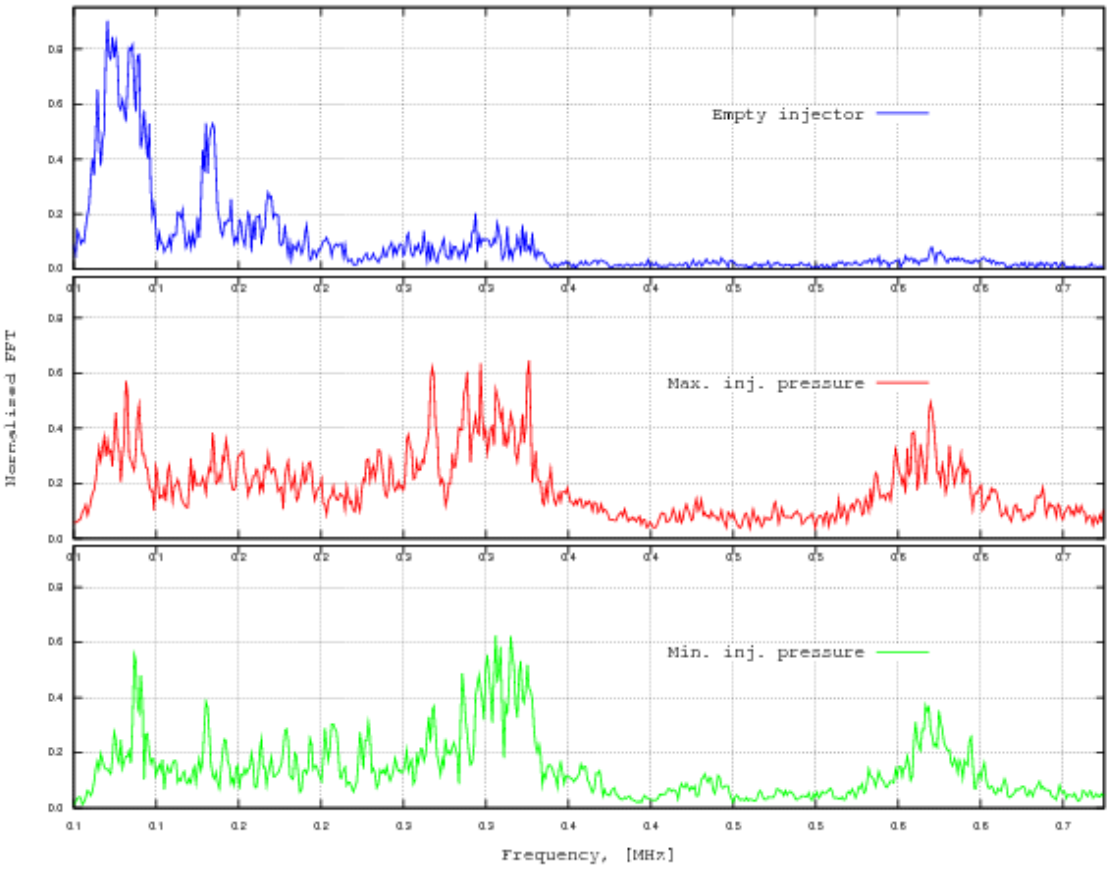

Figure 6.75: *Comparison of the FFT signals for the non-operating and operating nozzles at minimum (37.5 MPa) and maximum (131.3 MPa) injection pressures.*

and 0.6 MHz. The first component is increasing with pressure and characterises flow at relatively high frequency, whereas the second component, also increasing, could be related only to flow through a very small orifice, for instance the bleed orifice. Nevertheless, it is difficult to provide a solid statement and it should be accepted that both components needs to be analysed, whilst observing the fuel flow. More detailed variation of FFT's for various injection pressures can be seen in Figure 6.76. The graphs represent the normalised FFT of typical AE signal (not averaged) taken at various injection pressure for Diesel and at 25°C. One can see that all FFT plots feature the same pattern i.e. three distinctive peaks can be seen. Also, the amplitudes are not always identical, which could be explained by the fact that each plot consists of a non-averaged signal and as it was proved in Section 6.2 there is a difference from injection to injection. Therefore, the same injection pressure may results in different amplitudes due to more or less developed sprays. Also, the same injection pressure can produce slightly different spray pattern due to injection delay as well as two injection pressures can result in different delays and mechanical interactions

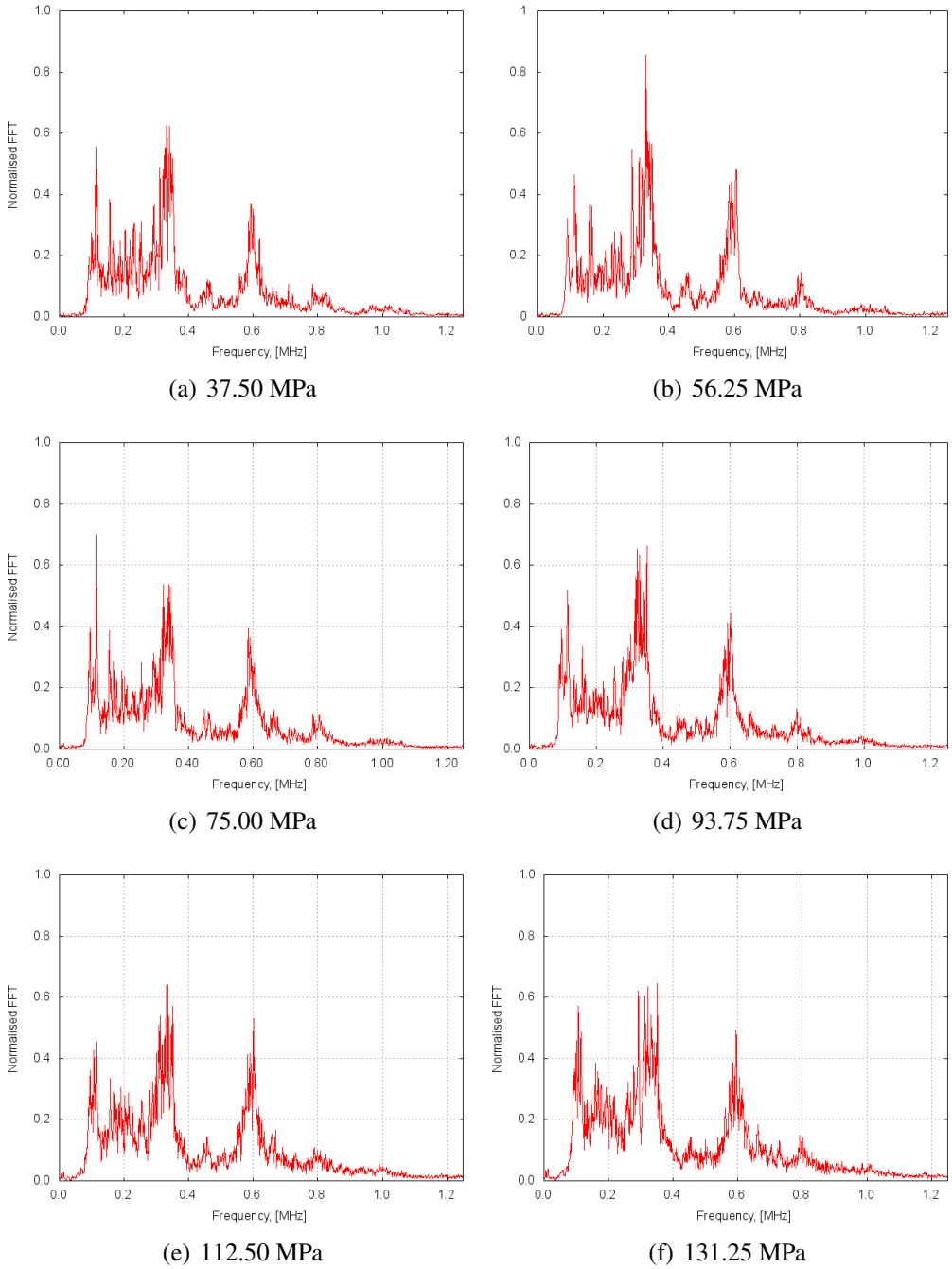

(a) 37.50 MPa (b) 56.25 MPa

(c) 75.00 MPa (d) 93.75 MPa

(e) 112.50 MPa (f) 131.25 MPa

Figure 6.76: *Presentation of FFT pattern for various injection pressures (in MPa): (a) 37.50 (1.5 V), (b) 56.25 (2.0 V), (c) 75.00 (2.5 V) (d) 93.75 (3.0 V), (e) 112.50 (3.5 V) and (f) 131.25 (4.0 V)*

inside injector. Using the AE technique for CDI injections, one should realised that its sensitivity will always result in signals which having a limited repeatability due to few reasons: internal injection interactions as well as ambient conditions. This should explain why the plots in Figure 6.76 presents signals of slightly different amplitudes within the same frequency domain.

6.4.3 AE energy of Diesel and RSO injection

Analysis of the Fourier Transforms of diesel AE signals in *Subsection 6.4.2.1* allowed to specify four main frequency range (bands), in which the energy of AE signal can be analysed. In principle the AE energy components was calculated for all event taking place for four energy ranges:

- Frequencies lower than 0.25 MHz (**frequency cut, FL**), which could represent events of armature movement, artifacts etc.
- Frequencies higher than 0.65 MHz (**frequency cut, FH**), which could represent very high fluid flows as well as event associated with the current flow,
- Frequency band of signals between 0.29 and 0.36 MHz (**low frequencies band, LFB**), which was assumed to occur when the internals of the injectors are moving, interacting e.g. the plunger movement,
- Hight frequency band of 0.56 to 0.65 MHz (**high frequencies band, HFB**), which from the Fourier Transform analysis was associated with the actual fuel flow.

The frequency ranges were chosen arbitrarily and are based on the frequency analsis presented in *Section 6.4.2*.

The AE energy term is used here as a calculated value of an event by integrating the area of the event within a given frequency band. Basically the AE energy represent the integrated area below a curve, which in this case is a curve of the AE amplitude. The method of AE energy calculation was presented in the work of Nivesrangsan [290].
It is expected that the calculated values would be proportional to injection pressure and would reflect very noticeably difference between diesel and RSO. Since the AE amplitude is proportional to the singal strength, it can be foreseen that the AE energy calculated for higher injection pressure would be higher than for the energy of lower injection pressure. Results of energy calculations for diesel are shown in Figure 6.77. One can clearly see the same trend for all frequency bands. In general, the AE energy components increase exponentially with injection pressure, and the highest energy can be found for the highest injection pressure of 131.25 MPa. The results are consistent and follow the expected behaviour, which indicates that for increased injection pressure the AE load is increasing due to higher mechanical impact inside the injector. The impact is a direct effect

of interactions amongst the internal parts, which move more violently once the injection pressure increases. This results in higher mechanical impact and, for instance, the plunger movement can be expected to be faster of a higher momentum and hence of higher AE response. The trends remains the same and it indicated that the injection events are having fixed frequency spectrum, although the amplitude is changing (increases) with injection pressure. It can be concluded that the CDI injection is characterised by a constant set of frequencies and the injection events vary only due to the mechanical impact. No significant

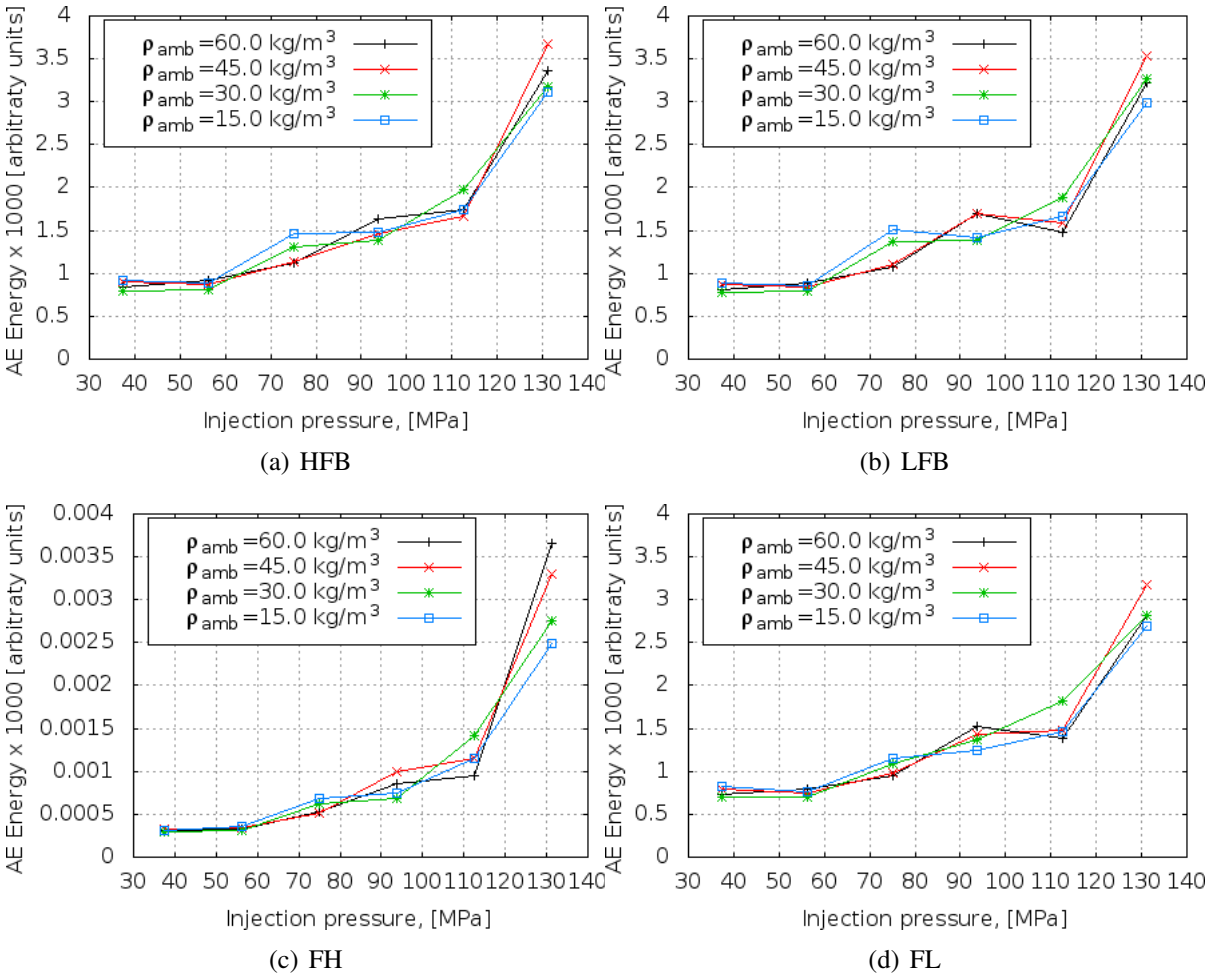

(a) HFB (b) LFB

(c) FH (d) FL

Figure 6.77: *Energy content for diesel at 30°C injected at various injection pressures and ambient pressures.*

effect of ambient pressure is present as seen in Figure 6.77. Each subfigure shows four curves that are associated with four different ambient pressures (i.e. ambient densities). Since the back pressure of the injection chamber is not affecting the internal flow of the injector, no ambient pressure effect on the AE energy is present. The effect is expected and consistent with the theoretical predictions, which simply indicate that the internal flow is only affected by the internal pressure and the effect of back pressure is negligible due to

the very small cross-section area of the injector orifices.

Figure 6.77 (c) shows the AE energy of the actual flow. It is very likely that the energy componets include also the AE signal of the propagated fuel jet inside the injection chamber. The trend is very similar to the rest of frequency bands, although the energy values are much lower i.e. 1000 times lower of order of magnitude. The results are somehow expected. The internal flow associated with the AE emission of the propagating jet is very low in comparison to the other mechanical events occurring inside the injector. Since the fluid flow is also a less intense event (the internal flow of fuel is milder) the AE energy results of Figure 6.77 (c) seems be logical.

The energy results of the FH are slightly affected by the ambient pressure, especially noticeable for the highest injection pressure. For the injection pressure of 131.25 MPa the AE energy is seen to decrease in the order of 60, 45, 30 and 15 kg/m^3. The result can be explained by the interaction between the ambient gas and the injected fuel jet. Since the jet penetration is deeper, the fuel jet is subjected to the highest friction and such friction increases with the ambient density. As it has been shown in *Section 6.2* where the effect of injection pressure was studied (*Subsection 6.2.1*), jet penetration for fuel injected at 131.25 MPa features the most compact penetration and hence the highest degree of gas-fuel interactions. The effect is mainly observed for the highest injection pressure and less pronounced at lower pressures It is concluded that the AE signal due to gas-fuel interactons is not only the main element of higher energy. It is expected that the highest injection pressure imposes higher internal flow, and therefore the higher leak through the ball valve (see Figure 6.70). Although the results follow the expected trend and can be logically interpreted, it has to be outlined that the detailed determination of the AE sources contributing in the FH energy would required more sophisticated methods including availability of a transparent CDI injector model.

Figures 6.78, 6.79 and 6.80 show the AE energy content calculated in a similar manner as for diesel but for RSO at 30°C, 40°C and 60°C respectively. Firstly, the graph presenting AE energy at RSO of 30°C is discussed here. Presented results clearly point out a difference between trends of diesel and RSO. The increasing trend of AE energies can be seen within the whole range of injection pressures and therefore one can conclude that the AE energy is strong function of injection pressure. The effect is much more pronounced than the situation present at diesel graphs, where the energy uprise was mainly detected for the highest injection pressure.

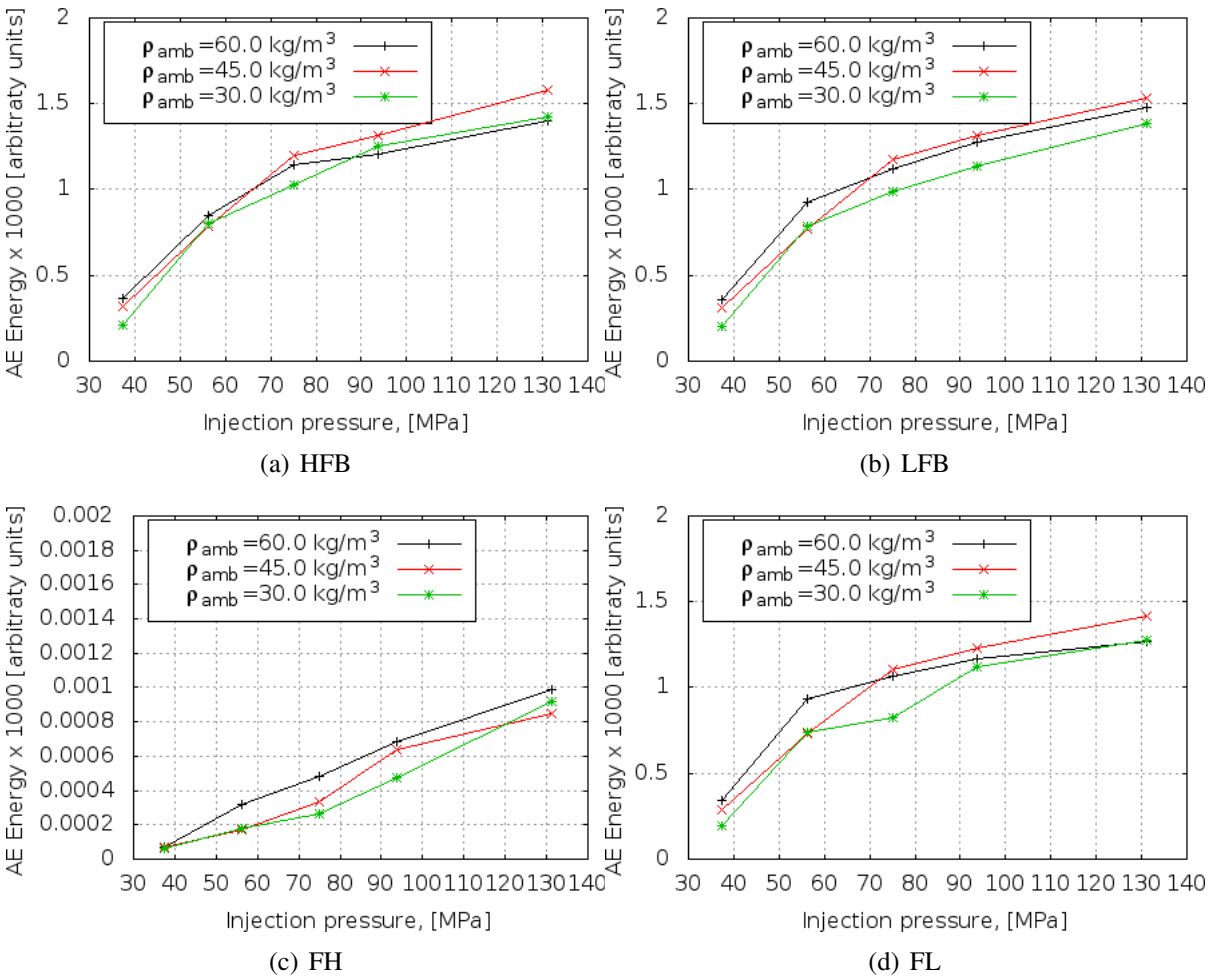

(a) HFB (b) LFB

(c) FH (d) FL

Figure 6.78: *Energy content for RSO at 30°C injected at various injection pressures and ambient pressures.*

Further and very noticeable conclusion is the magnitude of the AE energies recorded for various temperatures. Firstly, it can be seen that for the same temperature of 30°C. the energy values are lower than the recordings for diesel. It has been shown in the previous sections (*Section 6.2* and *Section 6.3*) that spray atomisation at temperatures close to 30°C is very much deteriorated by the RSO liquid properties, which reduce significantly the spray development and penetration. It is expected that a similar effect could be found for signals representing interactions of internal components of the injector subjected to the internal RSO flow. At 30°C the internal liquid flow remains very much reduced and any displacement of the internal elements e.g. the plunger is subjected to the hight viscosity of the liquid. This implies that any mechanical impacts and the shock propagations are noticeably reduced by stagnant and highly dense fluid (RSO). Analysis of the AE component for various frequency bands reveals a similar trend already observed for diesel i.e. the energies are having close values and following a similar trend.

6.4.3.1 Temperature effect on RSO AE energy (injection at 40°C and 60°C)

Since it has been shown that fuel temperature can improve jet atomisation and spray development (*Section 6.2* and *Section 6.3*), the elaboration of AE energy for two elevated temperatures (consistent with previous spray characterisation experiments) was performed. As it has been already discussed, RSO AE trends are significantly different than those observed for diesel in Figure 6.77. Figures 6.79 and 6.80, RSO at 40°C and 60°C, respectively, follow a similar trend observed in Figure 6.78 (RSO at 30°C). For all energy bands trends are increasing with injection pressure, which is particularly seen for the HFB, LFB and FL energy ranges. This behaviour reflects the findigs in *Section 6.2*, where a very strong effect of injection pressure on spray atomisation was found. The same observation is present here in Figure 6.79(c), which represents the AE energy with fuel flow and atomisation. It is interesting to observe that the maximum values of AE energies

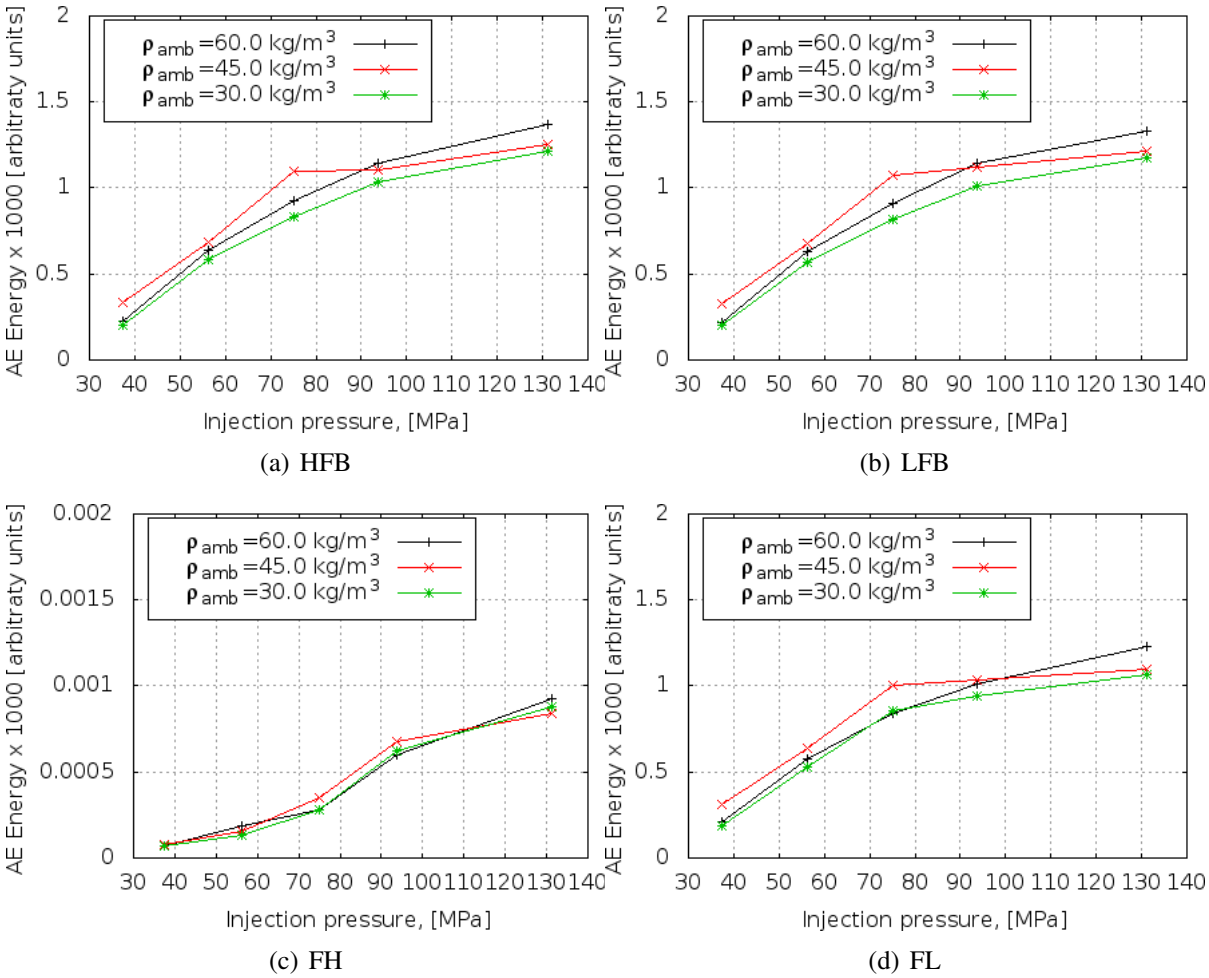

(a) HFB (b) LFB

(c) FH (d) FL

Figure 6.79: *Energy content for RSO at 40°C injected at various injection pressures and ambient pressures.*

reached at 40°C are still much below those recored at 30°C for diesel. The findings is

valid for the whole range of injection pressures and analysed frequency bands. Results are consistent with findings presented in *Section 6.2* and *Section 6.3* where RSO spray developmet and droplet sizes were still much deteriorated and higher than for diesel at 25°C respectively. The mechanism of spray development in a CDI injector is complex. It consists of internal flow development (here investigated using the AE technique) as well as of effects leading to droplet formation and development. The AE experiments show that insufficient internal flow can be associated with much lower AE energies and then backup findings of spray characterisation. AE energy data collected for RSO injected at 60°C is

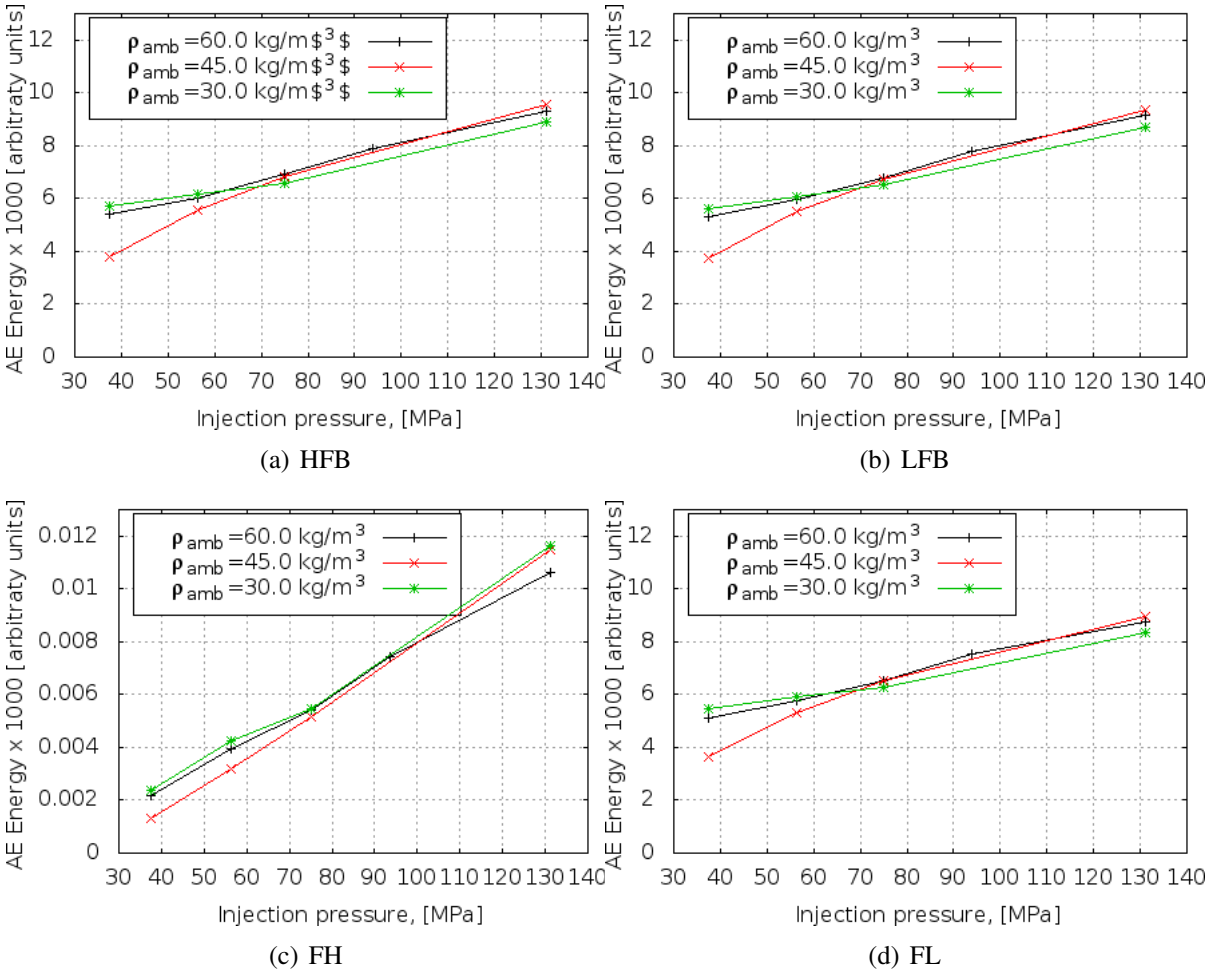

(a) HFB (b) LFB

(c) FH (d) FL

Figure 6.80: *Energy content for RSO at 60°C injected at various injection pressures and ambient pressures.*

shown in Figure 6.80, which displays some difference from the trend and results collected at 30°C and 40°C. In all frequency band cases, trends are very much linear with injection pressure. The AE energy lines are featuring almost the same curve slope (Figure 6.80 (a,b,d)), whereas the AE energy acquired for the FH band is increasing more noticeably and significantly different from the data presented for diesel at 30°C and RSO at 30°C and 40°C.

The major conclusion drawn from Figure 6.80 is that at 60°C RSO produces AE energies higher than diesel at 30°C. It can be seen that even at injection pressures around 40 MPa the AE energies are higher than for diesel, and that could imply that the injection temperature (the actual temperature of pre-heated fuel) is sufficient to ensure enhanced internal flow of RSO at 60°C. Previous discussion of RSO behaviour exposed to 60°C (*Section 6.1*) and changes of its density and viscosity can help to explain these results. The fundamental physical properities of RSO at temperatures around 60°C are still higher in comparison to density and viscosity of diesel at 30°C but already provide values of the same order of magnitude. This is especially important for viscosity (see Figure 6.2), which at 60°C is very much approaching the viscosity of diesel. Since, the viscosity is a major factor affecting flow properties it can be concluded that the performance of the CDI injector injecting RSO at 60°C could be very close to the operation on diesel. One can still arise a question why the AE energy values are higher, whilst the RSO flow properties are still reduced? An reasonable answer could be due to excellent lubricating properties of RSO, which in some cases is much better than it is of diesel. The issue was briefly presented in *Section 2.1.1* and some general explanations can be found in works of Asadauskas et al. [46], Masjuki and co-workers [259; 260], and Zaher et al. [430]. In all these publication authors confirmed very beneficial RSO lubricating properties and as result reduced wearing of bearings, cylinder and injectors.
It is known that CDI injector are particularly sensitive to fuel quality and its wearing properties [203]. Therefore it seems that RSO properities at 60°C are beneficial and can be expected to yield much better internal operation of injector elements (plunger movement, needle etc.). The better lubrication thus result in higher AE energies recorded in the measurements.

One can still discuss why the positively enhanced AE energy does not reflect on the better quality of RSO atomisation. As it was underlined above, the injection process is very complex and the observation of RSO spray development and droplet sizes are influenced by interactions with ambient conditions right after injection. Simply, despite the sufficient internal flow, spray formation is still sensitive to temperature, pressure and inside-the-spray interactions.
The above statement is particularly important for CDI modification: **the sufficient internal flow inside the injector may not result in the sufficient spray development and therefore both injectors and the combustion chamber (cylinder) must be pre-heated**.

6.5 CFD spray simulations

This section presents results of KIVA simulations of standard and RSO sprays taking place in a constant volume vessel as well as in the cylinder of a Volvo diesel engine. All simulations were carried out without combustion. Results of the constant volume runs are presented for the atmospheric ambient pressure because amounts of injected diesel and RSO were only measured at this presure (see *Subsection 6.1.4*). The values were then used to fit of the discharge coefficient for the KIVA model and provide amount of injected fuel. Author also performed calculations for higher ambient pressures, but results did not show good agreement with experiments due to discrepancies between injected amounts of the fuel.

The engine simulations follow the conditions listed in the Table 5.8 and 5.9 and were done only to compare trends of spray diesel and spray development in a small cylinder configuration. The Volvo configuration represents a much larger cylinder volume of 2 litres compare to the Mercedes CDI engine, but the cylinder geometry and the shape of the piston are very similar. Engine simulations did not use injected amount as input variable but an injection profile as it was defined originally for diesel.

Simulation of fuel sprays injected at high pressures are particularly difficult. Diesel spray studies thus can still be the focus of further research. The study of SO sprays is presented to verify whether the existing KIVA code was able to simulate the dense diesel sprays and provide a satisfactory agreement with experiments.

Results carried out in the constant volume geometry were compared with experimental data at selected injection and ambient conditions. Then, RSO simulations were presented. In the end results of RSO simulations performed in an engine-like conditions are shown. All results have been further analysed using user-own scripts. It has to be underlined that all KIVA simulations results were manually shifted to the same time position as corresponding experimental. The procedure was applied because KIVA simulations does not compensate a delay/hesitation time, which is normally seen in experimental data. The operation allowes starting both experimental and simulated curves at the same time.

As it was presented in the *Subsection 4.2.3*, the experimental penetration values were calculated based on the adaptive threshold method. The criteria for the determination of liquid penetration length was 95% accumulated liquid mass distance from the injector.

6.5.1 Preliminary SO simulations

In order to validate the existing KIVA results some preliminary SO spray simulations were made under selected constraints for which experimental data exist. Figure 6.81 represent a sample of a computational grid with an encapsulated SO spray. The calculation were carried out at conditions listed in Table 5.6, and using the Reitz-Diwakar (RD) and Reitz Kelvin-Helmholtz-Rayleigh-Taylor (KH-RT) breakup models. Results of spray tip penetrations are shown in Figures 6.82, 6.83 and 6.84. In Figure 6.82 the penetration

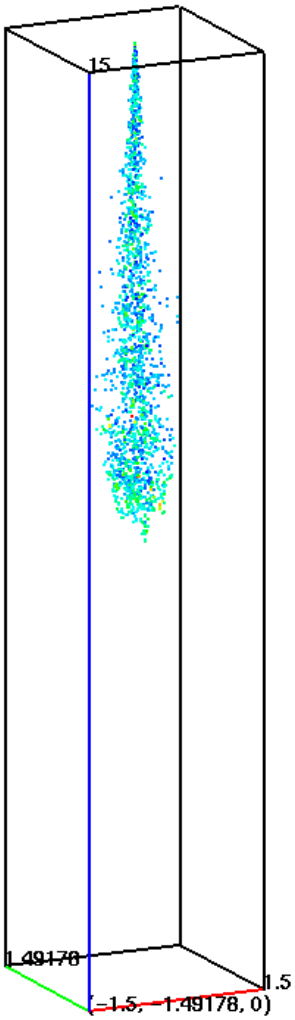

Figure 6.81: *A sample image of a 3D presentation of a SO spray in the computational rectangular volume (the cuboidal shape represent only the boundaries defined by the post-processing programme, whereas the the actual computational grid has been enclosed inside the cuboid).*

results based on simulations closely follow the experimental data. A higher deviation from the experimental values can be seen at the end of the penetration curve only. Both models presents acceptable agreement with the experiments, while the KH-RT model predicting the end of injection more accurately. The KH-RT curve follows more tightly the experimental trend. As it can be noticed, the calculated penetration curves tend to

reach a constant value quicker than the experimental line. It can be concluded that such trend is caused by higher calculated drag forces affecting spray development and therefore its distance. The KIVA models can, thus, lead to underestimated penetration values due to incorrect formulation of the shear forces effect. This can be also a consequence of higher momentum of the experimental spray due to the initial injection delay. The delay can be seen at the beginning of the penetration curves where the calculated values are higher than the experimental ones. As the experimental spray develops its momentum increases while the calculated spray shows deterioration. Deviation of the calculated values from the experimental data is also reported in the literature on modelling of high-pressure diesel sprays ([426] and [69]). Figure 6.83 refers to the penetration results collected

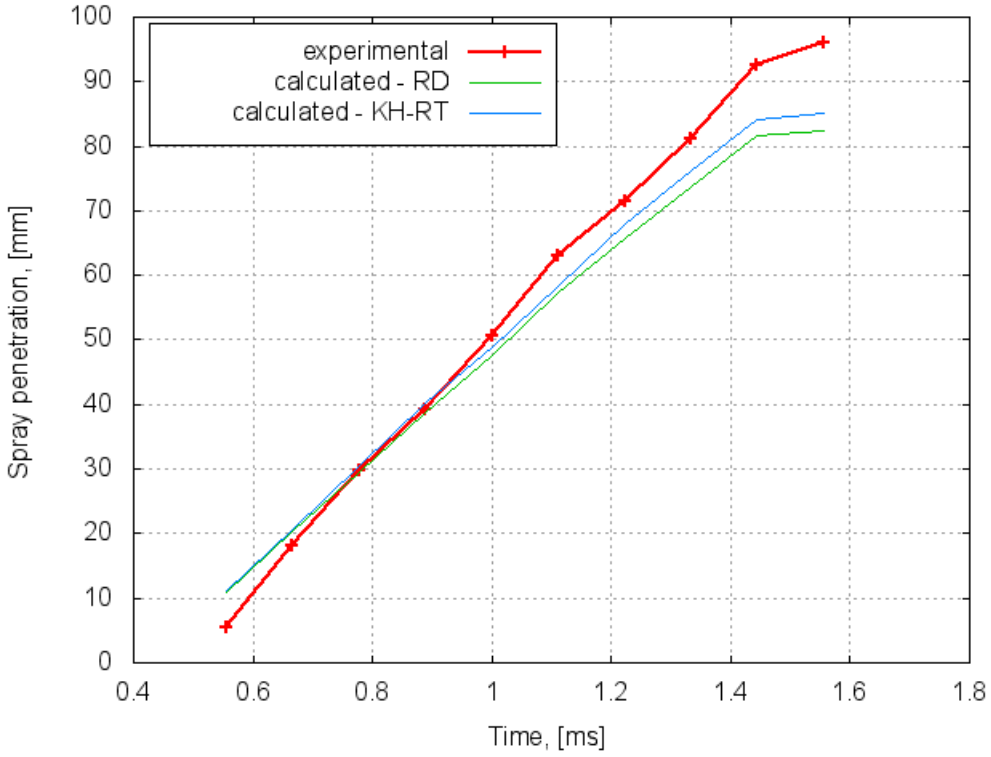

Figure 6.82: *Comparison of experimental and calculated spray tip penetration for SO at injection pressure of 56.25 MPa and ambient atmospheric pressure.*

and calculated for a higher injection pressure of 93.75 MPa. A similar trend as already observed for the previous case can be seen for the calculated data. Both penetration curves closely follow a similar almost initial linear trend. More noticeable differences, between the experimental and simulated data, can be seen at the beginning and at the end of the penetration period. The deviations are symmetrical i.e. are higher at the beginning and lowest at the end. Similar to the discussion of Figure 6.82, it can be noticed further spray development of the experimental results whereas the calculated values are quickly slowing

down shortly after 1.0 ms. A higher degree of differences between the experiment and simulation can be recorded for the beginning of the penetration, where the calculated values are higher. It is thought that such deviation is caused by higher injection delay between the experimental and calculated data. The experiment is still featured by an injection delay, however significantly reduced in the comparison to the data in Figure 6.82 The calculated penetration, unaffected by the delay, are higher from the very beginning of the penetration. It should be emphasised that the KIVA model does not account for the obstacles such as flow obstruction and pressure waves. Figure 6.84 represents results for an even higher

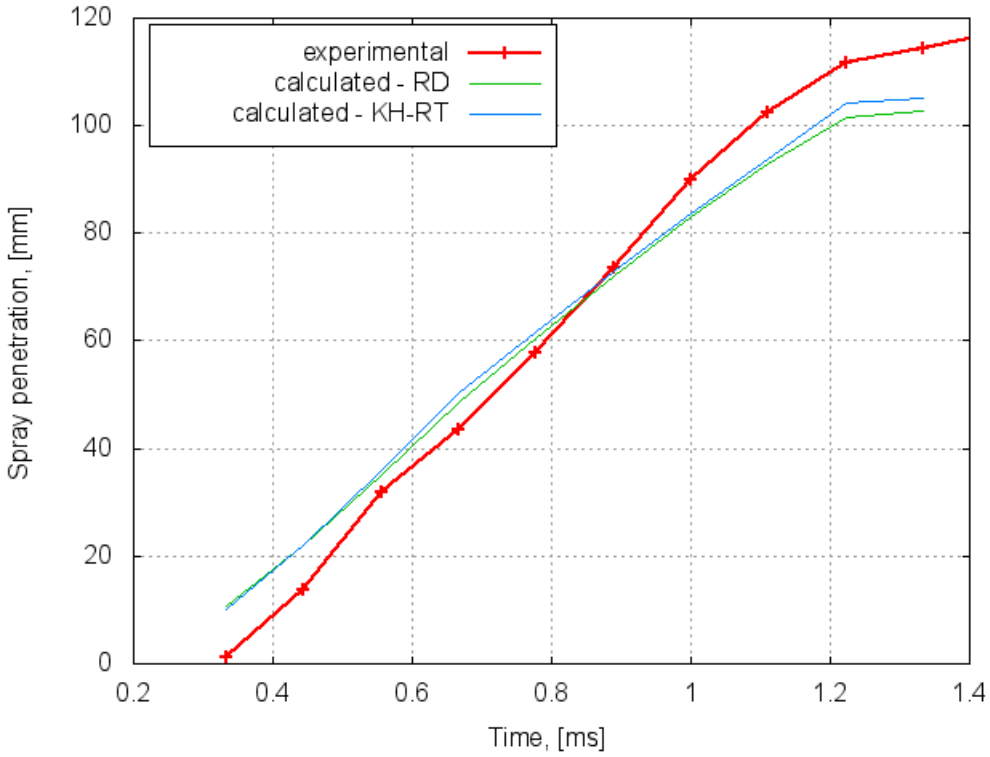

Figure 6.83: *Comparison of experimental and calculated spray tip penetration for SO at injection pressure of 93.75 MPa and ambient atmospheric pressure.*

injection pressure of 131.25 MPa. Once again the calculated values follow the similar trend and deviate from the experimental data at the start and towards the end of the injection. The difference of the initial stage for experimental and calculated values are noticeably reduced. The injection obstruction caused by the injection delay has much weaker effect on the experimental penetration hence the gap between the simulation and experimental curves is small. The presented calculated curves exhibit a significant difference comparing to the lower injection pressures. The calculated values are higher than experimental for the whole injection period of time. It can be concluded that the experimental data do not suffer form the drastic momentum changes and therefore the recorded data are

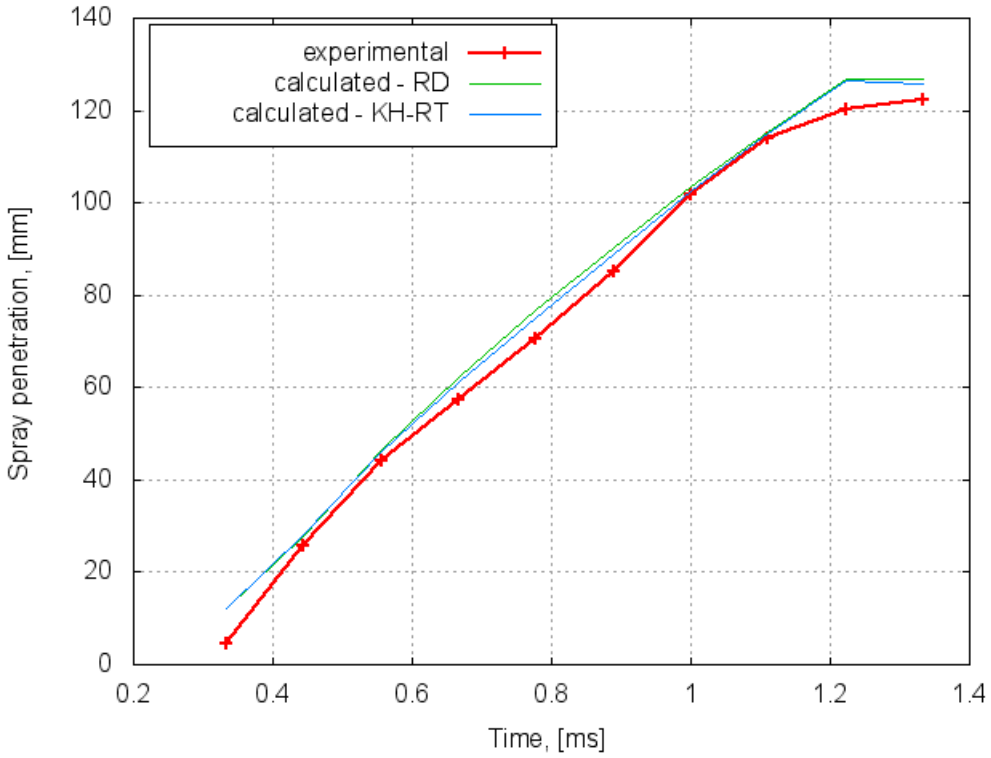

Figure 6.84: *Comparison of experimental and calculated spray tip penetration for SO at injection pressure of 131.25 MPa and ambient atmospheric pressure.*

lower. It is seen that although both models provide similar values, the KH-RT model follows the experimental curve a bit more closely in the middle of the injection curve. But generally the beginning and the end of penetration is described equally well by both models.

These results may indicate that the KIVA simulation does not accurately describe the whole injection process (spray penetration). This can be caused by the inefficient KIVA models as well as the experimental results being collected in a system with a certain degree of disruption (see the discussion in *Sections 4.2 and 4.3*) in comparison to the theoretical KIVA calculations carried out for an ideal and stable system. The differences of penetration at the beginning and at the end can be caused by a delay inside the injector and obstruction of the internal flow. This is particularly important when a cold and pulsed spray is measured. The delay causes lower initial penetration due to the effectively lower injected mass at the beginning then gradually rising as the injection progresses and a higher momentum is reached. It has to be stressed that the experimental delay varies with injection pressure and therefore a comparison of the initial penetration between experiments and calculations is not always consistent. Unfortunately, the injection delay and so called the "initial" or "border" flow conditions can not be included in KIVA runs. Additionally, the

KIVA simulations were performed for diesel whereas in the experiments SO had been used. Physical properties of both fuels are similar but SO is less volatile, which has had effect on the formation of a gas phase. Another possible reason is the way in which KIVA calculates the injected mass. It is accomplished using an average spray velocity instead of applying a real velocity profile for each nozzle and injection conditions. The calculated values could be improved by introducing a real injection profile rather than utilising an average velocity. Despite all these factors, the diesel simulations are to be satisfactory.

Analysis of the results does not clearly favour a single breakup model. But from the data presented above and the description of models, the Reitz Kelvin-Helmholtz-Rayleigh-Taylor approach seems be more suitable for high-pressure diesel spray simulations. The same conclusion can not be easily drawn for RSO and a similar analysis has been performed for RSO sprays in the following subsection.

6.5.2 RSO spray simulations

RSO penetration at 56.25 MPa and calculated results are shown in Figure 6.85. Both sets of calculated curves feature a noticeable offset from the experimental values. The trends represent a good agreement with the experiment nevertheless the calculated data are higher. All three curves are almost parallel and no deviation at the beginning or end can be observed. The calculated results of RD model describe the penetration of RSO with a higher accuracy than the hybrid model. The KH-RT model provides values by 20% higher than the experiment and approximately by 5% higher than the RD model. It can be seen that the existing curve trend of Figure 6.85 does not strictly follow SO data depicted in Figure 6.82. The situation seen in Figure 6.85 represents the greater agreement deficiency, however the the trend is common for both cases (Figures 6.82 and 6.85). As the injection pressure increases the simulated values do follow a different trend. The tendency can be seen in Figure 6.86, which presents the penetration data recorded at 93.75 MPa. Deviation between the experiment and simulations become more apparent at the beginning and the end of penetration. A difference at the beginning of the penetration is significantly high. Both calculated curves have a very similar initial trend whereas the experimental curve is more flatter which indicate the initial obstruction of the injection. The calculated values are almost linear whilst the experimental trend fits into a "S" like shape. The smoother trend can be explained by much slower development of the

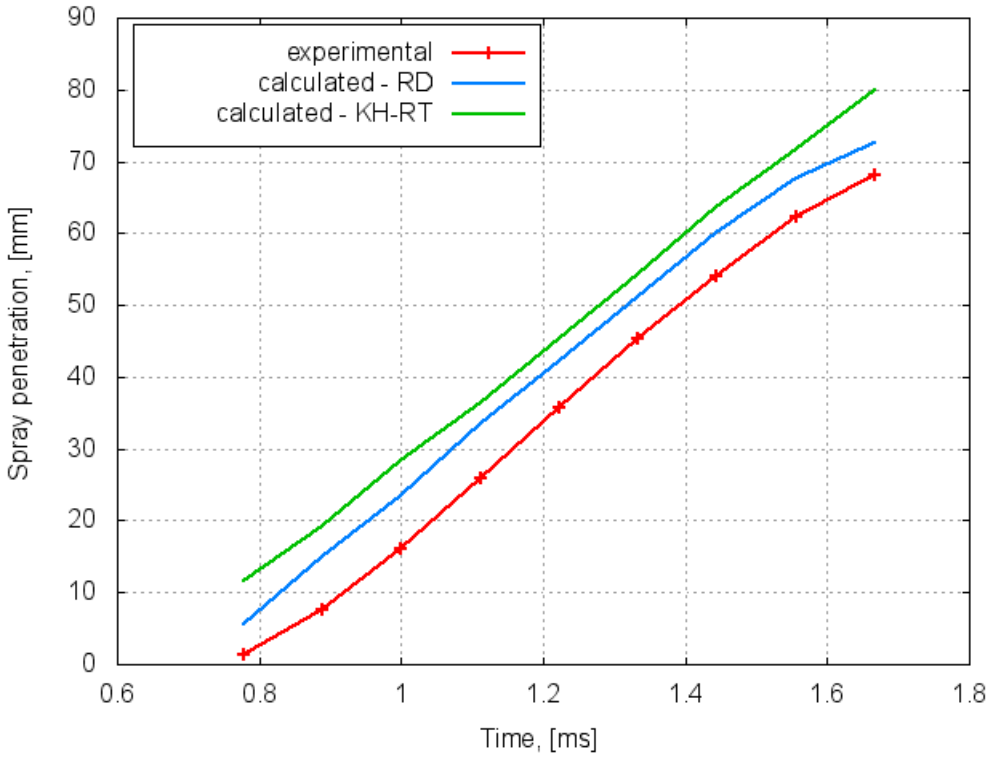

Figure 6.85: *Comparison of experimental and calculated spray tip penetration for RSO at injection pressure of 56.25 MPa and ambient atmospheric pressure.*

penetration at the beginning as well as the gradual slowdown of the fuel jet just before the injection is terminated. Nevertheless, it can be seen that all curves finish off in a similar manner described by a smooth, bend line. Assessment of the breakup model is disputable. The RD form describes the RSO penetration better from the beginning until the injection time equals 1.0 ms, whereas the rest of the experimental penetration curve is more likely followed by the KH-RT model until the injection time of ∼1.5 ms. As it can be seen the difference between the two both models is not substantial. The injection of 93.75 MPa was selected for a graphical comparison between the experiment and calculations (Figure 6.86). The experimental pictures have not been averaged but randomly picked up from a set of five consecutive injections of 93.75 MPa. Figure 6.87 shows a series of experimental and computational time-scaled snapshots of a half-spray in a comparative layout. Right images show computational sprays, whereas those in the left experimental images. Images correspond to the spray penetration data shown in Figure 6.86. Hence, a difference at the beginning and at the end of the injection can be expected. This can be clearly observed at 0.777 and 0.888 ms where the calculated spray tip penetrations are longer than those of the experimental spray images. A similar occurrence can be seen after 1.3333 s, whereas the middle of the penetration represents a better agreement.

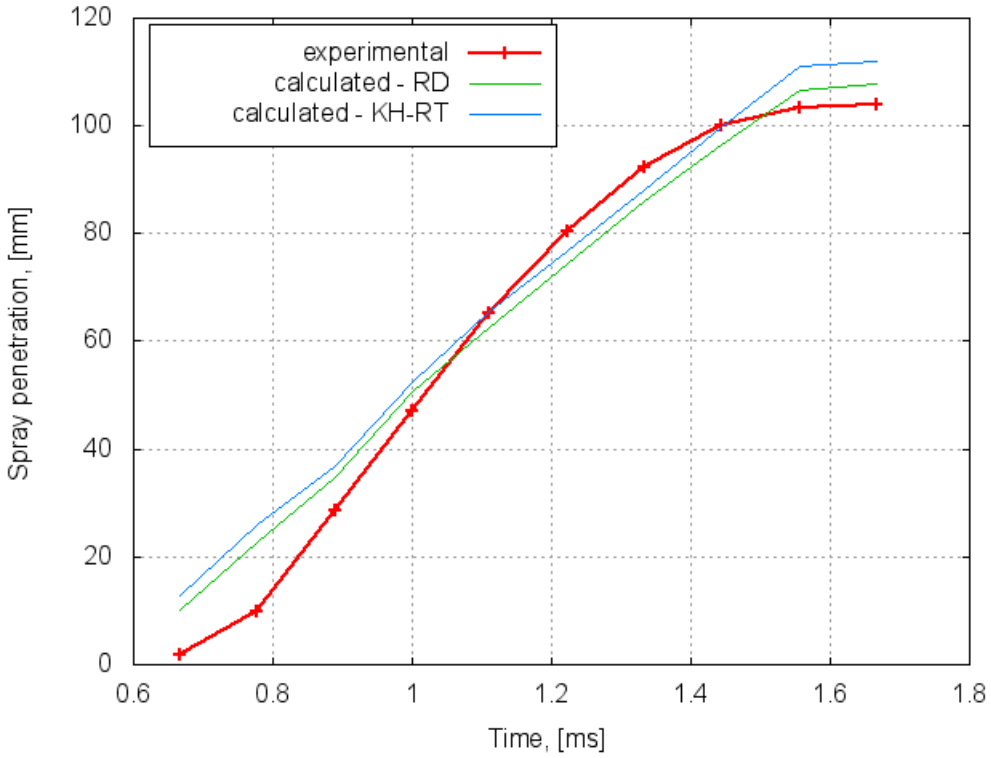

Figure 6.86: *Comparison of experimental and calculated spray tip penetration for RSO at injection pressure of 93.75 MPa and ambient atmospheric pressure.*

The graphical presentation allows to compare the shape of injected oil with time. As it can be seen, the calculated snapshot shapes fairly resemble the experimental spray outlines. However, it can be seen that the calculated shapes are fuller and wider. The calculated shape has rounded end with a wider and fuller middle part gradually narrowing up towards the injector tip. It can be noticed that both experimental and calculated shapes of RSO sprays are adequately described by similar contour. Figure 6.88 presents experimental and

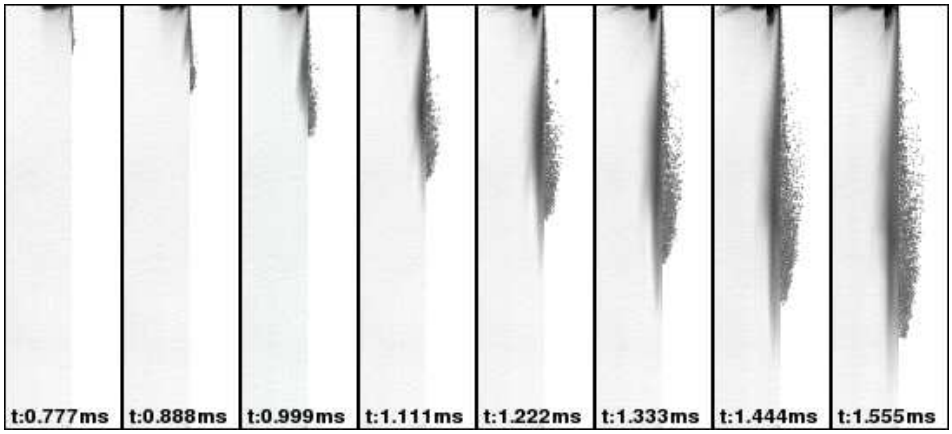

Figure 6.87: *Graphical presentation of the experimental and calculated spray development of RSO injected at 93.75 MPa. Right images - computed; Left images - experimental.*

calculated penetration of RSO injected at 131.25 MPa. High injection pressure results in a similar calculated trend as observed in Figure 6.86. The relation between the experimental and calculated values shows higher deviation at the beginning and lower at the end of penetration. The calculated values are almost identical at the initial stage of the penetration and are described by a straight line, whereas the experimental curve features a gradual initial increase then after 1 ms become more linear. Also, a difference at the end of the penetration can be observed where the KIVA models overcalculated the spray penetration. Nevertheless the curves reveal the same terminal shape.

The calculated values are essentially higher and decrease at the very end of the penetration (after 1.6 ms). It can be accepted that both mathematical models present the same level of agreement with the experiment. It is seen that the RD model follows more closely the experimental values especially at the end of the spray penetration. Figure 6.89 depicts

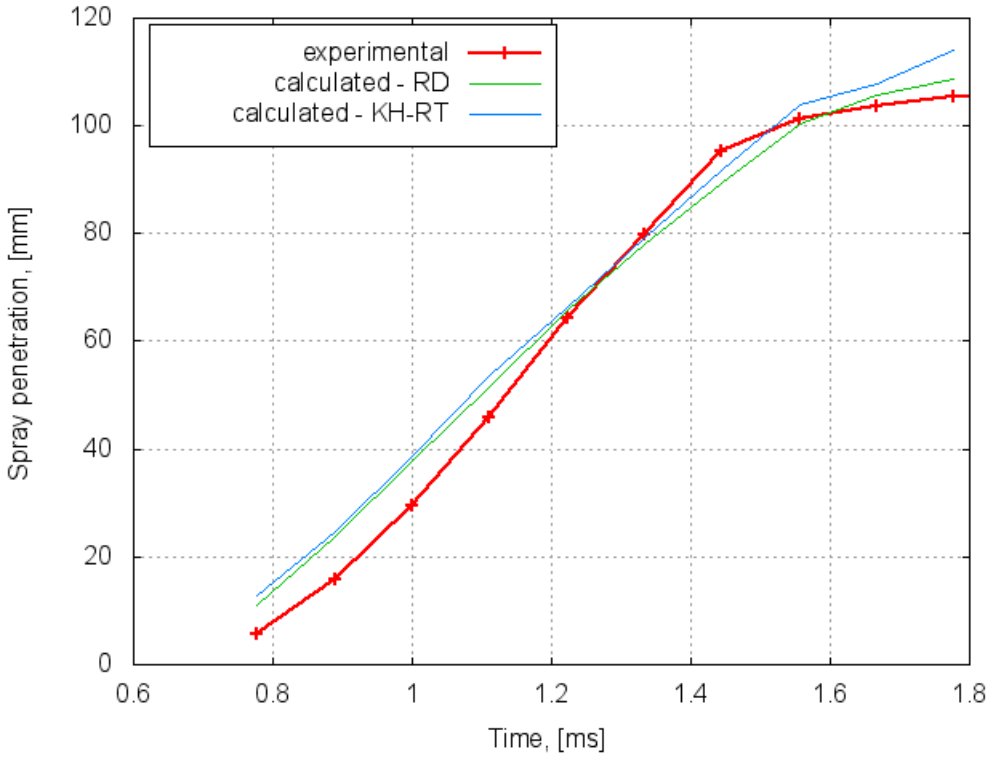

Figure 6.88: *Comparison of experimental and calculated spray tip penetration for RSO at injection pressure of 131.25 MPa and ambient atmospheric pressure.*

in a comparative manner experimental and simulated spray shapes of RSO injected at 131.25 MPa. As also depicted in Figure 6.88, the initial penetration reveals significant differences between the experiment and the simulation. The experimental spray shapes are a needle like, whereas the calculated spray shapes are fuller, rounder.

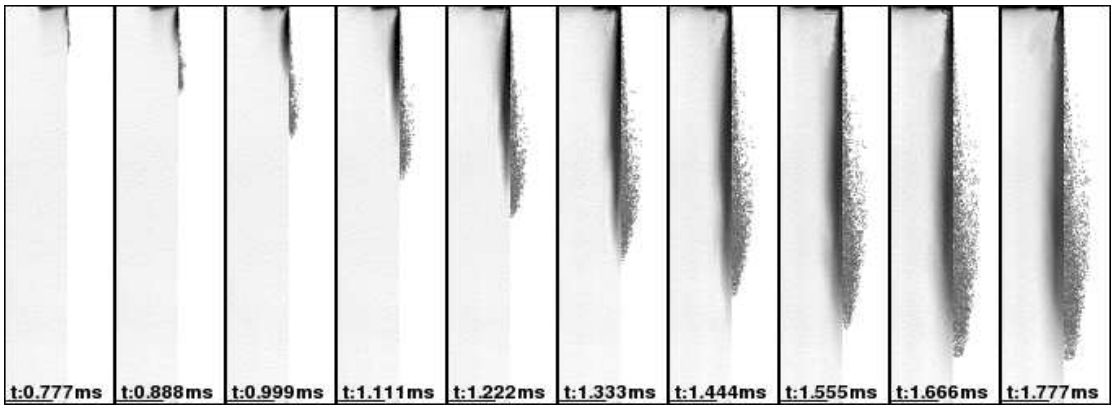

Figure 6.89: *Graphical presentation of the experimental and calculated spray development of RSO injected at 131.25 MPa*

6.5.3 RSO breakup using KH-RT and KH-DDB models

Presented results have shown the performance of the two breakup models on spray penetration. The models can be used to find out penetration as well as drop sizes. A comparison between experimental and numerical drop size distribution allows to select the most accurate breakup model for RSO simulations. It has been experimentally and numerically demonstrated that breakup and collisions have influence on the drop size distribution [69; 384] of diesel. The following analysis is based on a comparison of the experimental and calculated Sauter mean diameters of RSO at 40°C and atmospheric pressure (chamber) for different injection pressures. Based on findings of Payri et al. [315] and Coghe et al. [91], it has been assumed that the RSO Sauter mean diameter should be approximately constant along the radial direction as it has been found for diesel. Thus the comparison included the measured and calculated values of the mean diameter along the spray centreline. Figure 6.90 shows a comparison between experimental and numerical RSO drop size distribution. Although calculated values are different from the experiment, it can be seen that the average values are quite similar. The present results, closely resemble the SMD trend discussed by Kong et al. [224]. KIVA predicts larger drop diameters at lower injection pressures equally for both breakup models. According to the KIVA collision model, the probability of coalescing droplets is proportional to the ratio of the droplet diameters. At low injection pressures KIVA produces an intact RSO liquid core and some initial droplets, which having unequal sizes more likely to coalesce due to the lower initial momentum of the injected oil directly at the beginning of the injection. Hence, the number of large drops calculated at low injection pressures is higher than for the experiment. Once the injection pressure increases the mean diameters start to decrease. It can be seen that the magnitude of the reduction is

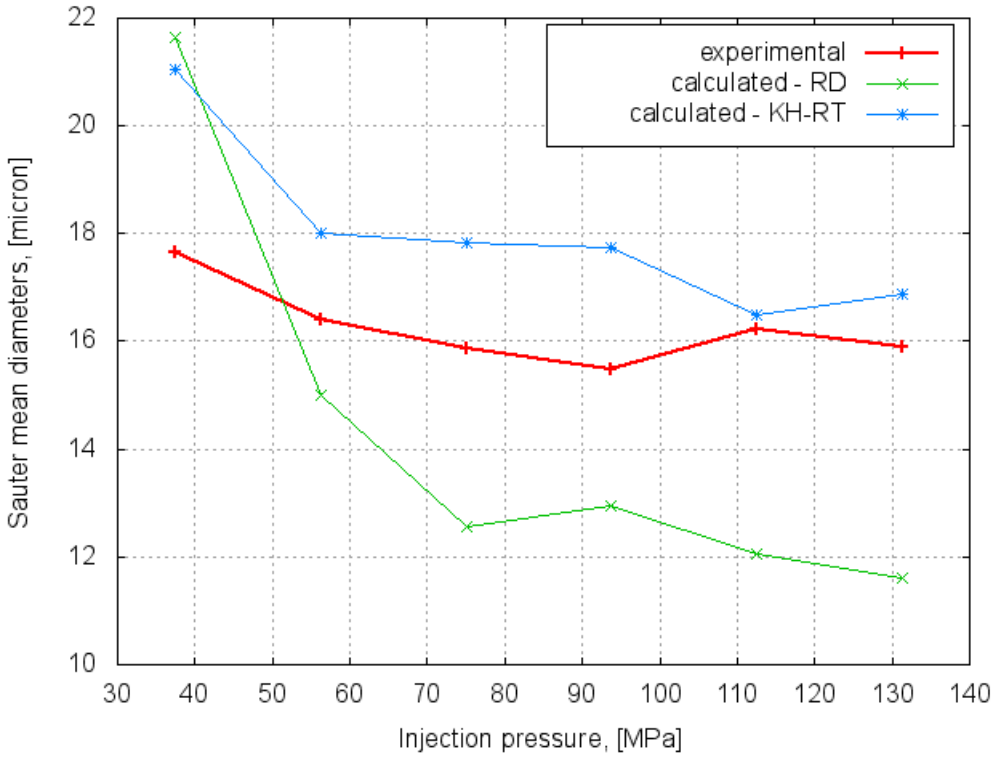

Figure 6.90: *Comparison of experimental and calculated Sauter mean diameter for RSO at 40°C injected at ambient atmospheric pressure.*

very much different for both models. The RD breakup model underestimate the diameters, whereas the KH-RT model tends to over predict the Sauter mean values. A gradual increase of accuracy is seen with the increasing injection pressure for the KH-RT model. As it has been outlined in the *Subsection 2.6.2*, the KH-RT model generally gives better accuracy and the results presented here confirm this for RSO too.

Inaccuracy of breakup models to calculate the Sauter mean diameter of diesel has been already reported by de Risi and his co-workers [102]. The underestimation of the RD model is expected to be improved by more detailed numerical implementation of the gas to liquid density ratio. As originally KIVA's code was developed for fuels of much lower density, the code applicability to RSO should be revised. The value of the breakup length calculated from the KH-RT model is based on the assumption of negligible liquid viscosity of the gas phase. This lead to the reduced expression of the breakup time (Equations (2.6.19) and (2.6.13)) used in KIVA code. It is proposed that the breakup models should be modified to include lower Weber numbers of RSO droplets and reduce the maximum growth of the wavelength, Ω, described by the Equation (2.6.12). The development of a new breakup model could be in a scope of the future work on RSO spray

simulations.

6.5.4 Engine simulations of diesel and RSO injections

Undoubtedly, the most interesting part of studies on RSO as diesel substitute is its performance under the engine operating conditions. The idea of investigating (by simulation) injection of RSO at engine conditions was very much inspired with the work of Raubold [336], and dictated by the fact that simulations are the fastest and the cheapest way to perform such studies. The aim of this PhD work was to establish differences between diesel fuel and RSO in spray development and air-fuel mixture formation under engine conditions with particular attention paid to the cold start and the injection event for the preheated RSO.

This section presents selected results from RSO spray simulations in a real engine setup compared with diesel. As mentioned at the beginning of this section simulations tended to compare only trends. Engine KIVA simulations were performed according to the setup outlined in *Subsection 5.2.5* in Tables 5.8 and 5.9. The KH-RT model was employed in all simulations. The injection profile was taken as originally used for diesel calculations and described in [386] therefore pre-defined injection pressure was not used. Using the injection profile it was estimated that the injection pressures was approximately 80 MPa.

Results are presented in a form of snapshots, which show changing volume between the cylinder top and the piston bowl. As spray development was symmetrical snapshot present only right side of the volume. All pictures show volume projections constructed as a cut through the spray centreline and the piston centre and perpendicularly to the view. Results were depicted with a series of cylinder snapshots within a range of crankshaft position just after the beginning of injection (-7.48°) and the end of injection (20.08°). The last included snapshot represent position of the crankshaft $\sim$8.3° prior to the ignition.

Various position of the crankshaft were used to present concentration of gaseous phase of injected fuel according to colour scale corresponding to the total mass fraction of vaporised diesel and RSO. Additionally, fuel concentration pattern was combined with a population of fuel droplets represented by dots. The droplets represent the fuel quantity which was not evaporated.

Figure 6.91 presents the diesel injection taking place at the cold start conditions where both engine and fuel temperatures are at 10°C. This case is described by parameters cor-

responding to the case ED1 in the Table 5.9. Such operational conditions are specific, rarely taking place in a real situation thus play here strictly comparative role. The highest concentration of diesel represents pink colour and the dark blue area characterises the ambient zero-diesel-concentration region. At the beginning of the injection the highest fuel concentration is located near the injection point and gradually expands across the injection volume. The snapshot taken at 7.51° presents an uniform highly concentrated fuel region tightly surrounding the cylinder volume closely to the centre of the piston bowl. As the injection terminates and the piston starts moving backwards the fuel region is getting aggressively disrupted by the increasing gas motion inside the piston bowl. The air-fuel mixture at 17.51° presents a typical pattern of intensively mixed environment. Presence of unevaporated diesel drops indicates that the diffusion process has been significantly terminated by the low fuel and ambient temperature. The last snapshot recorded at 20.08° shows the air-fuel mixture featuring a sufficient level of air entrainment and it can be expected it to allow efficient combustion. As it can be seen at the pictures taken between the crank angles of 7.51 and 17.51°, there is a significant number of satellite drops located mainly at the piston surface and the engine head. If the engine temperature is low the droplet residue can not be evaporated from the surface and contribute in the excessive soot buildup or the carbon deposit. Nevertheless, the droplets can be evaporated and ignited when the engine temperature rises and the mixing process intensifies. A similar diesel injection taken place at the elevated engine (227°C) and fuel temperature (60°C) is presented in Figure 6.92 (case ED2 of Table 5.9). The injection conditions represent real engine temperature recorded for a real diesel engine at a constant load and RPM. The presented snapshots resemble Figure 6.91 however the temperature effect is more pronounced. The enhanced fuel vaporisation can be already seen at the first snapshot and at -4.98° the air-fuel mixture becomes richer in diesel and the outer of the mixture region is more “diluted”. This is caused by extended spray penetration but moreover higher ambient and fuel temperature result in faster evaporation of the spray jet. The gaseous fuel penetrates the injection volume quicker as it can be noticed as wider green region representing the borderline between the pure air and the surroundings of the fuel spray. The snapshot taken at 5.02° describe the region of rich air-fuel mixture propagating outwards the cylinder bowl. The pictures at 10.0 and 12.5° of the crankshaft shows enhanced vapour mixing due to increasing swirl motion. The aerodynamic forces push the air-fuel mixture and increase air entrainment (15.0°). The picture in Figure 6.91 at 15.01° does not reveal such enhanced mixing and expanding mixture motion. The last snapshot of Figure 6.92

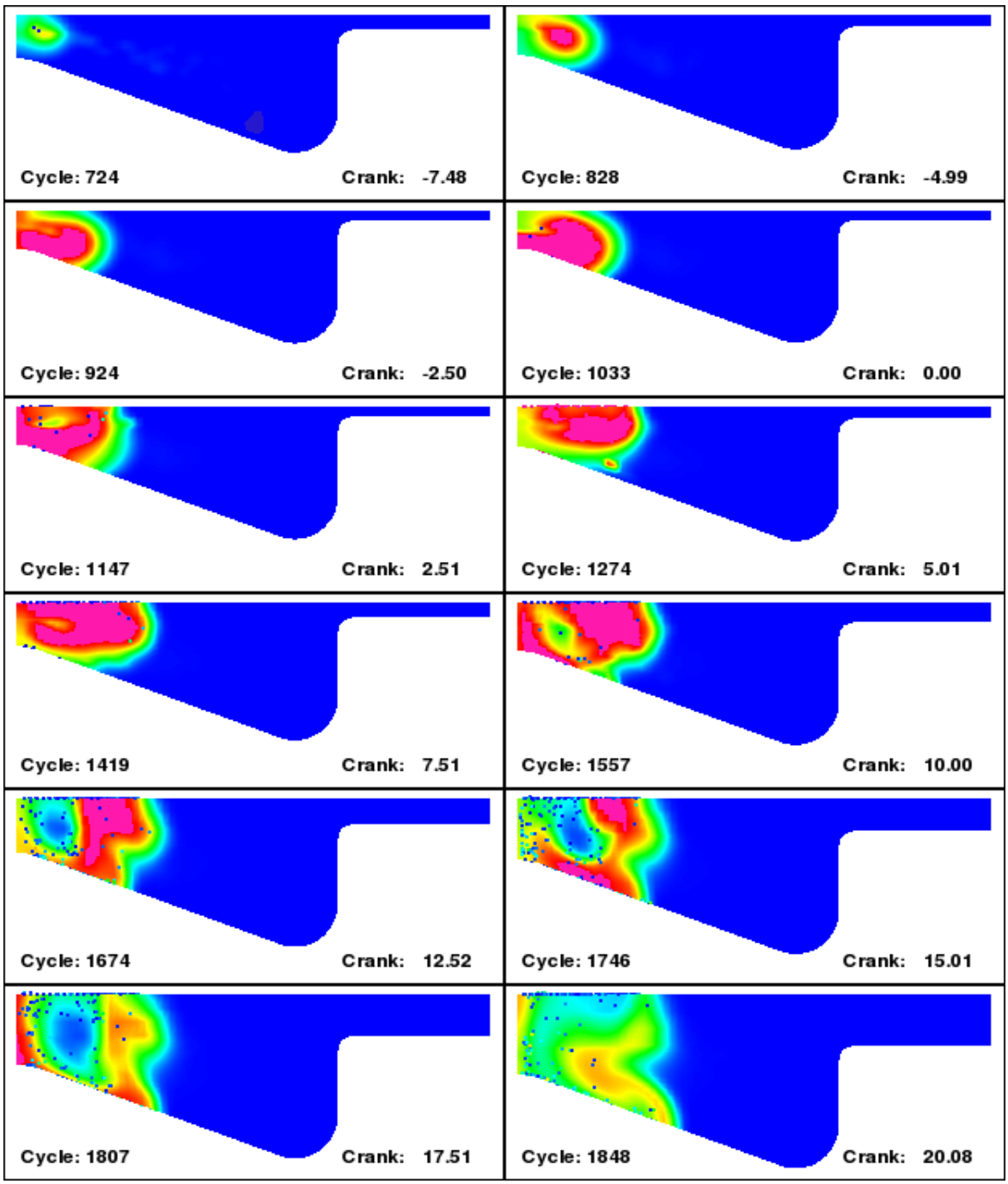

Figure 6.91: *Diesel injection at the cylinder and fuel temperature of 10°C.*

presents extensively mixed and developed air-fuel region. The highest fuel concentration described by the pink colour can be found only very close to the piston centre which may indicate some droplet residue. This distinguishes the mixing process from the final injection stage depicted in Figure 6.91. The presence of unevaporated droplets is common for both operational temperatures however the droplet concentration is lower at 227°C. It can be concluded that these drops can be readily evaporated and combusted.

From the presented pictures it can be concluded that diesel evaporation does not require significantly elevated cylinder temperature. Sufficient diesel atomisation and mixing enables expected combustion. It has to be pointed out that the diesel spray penetration at the presented conditions is appropriate for the fuel atomisation and formation a mixture with air. The cold start conditions were also employed to investigate RSO injection subjected to

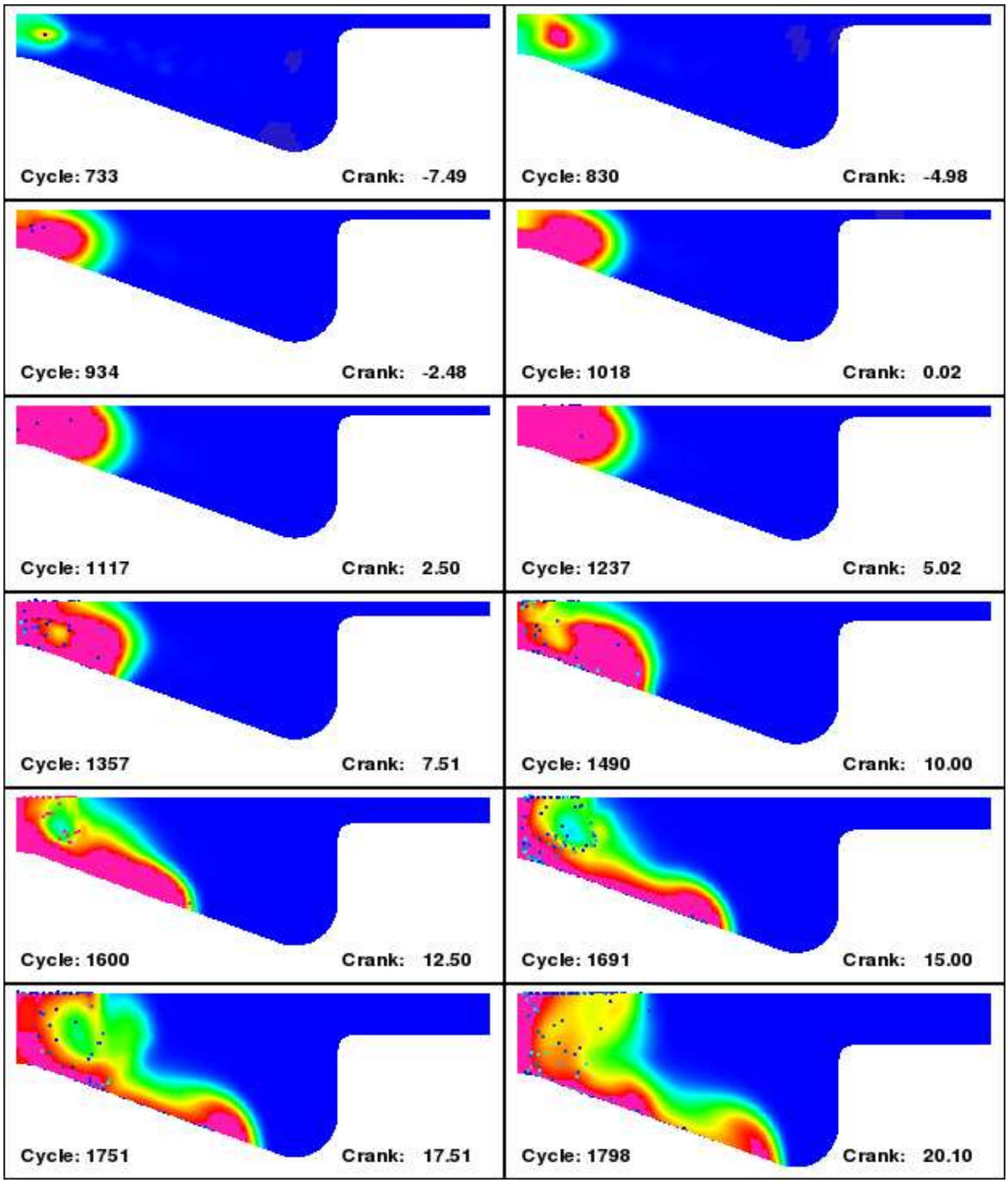

Figure 6.92: *Diesel injection at the cylinder temperature of 227°C and fuel temperature at 60°C.*

the engine and oil temperature of 10°C and operational conditions corresponding to the

case ERSO1. The results of simulation are presented in Figure 6.93. First three snapshots do not indicate presence of gaseous RSO oil or some isolated light blue patches indicate its very low concentrations. Apart from the low in-cylinder temperature, there are two main reason influencing formation of the air-RSO mixture. The first is very poor RSO atomisation and therefore the significant reduction of the dispersed RSO. At 10°C RSO viscosity noticeably reduces the oil flow and thus deteriorate the spray development. As already by observed from experimental RSO spray development measurements for different fuel temperatures in *Section 6.2*. Secondly, by comparing the snapshots with diesel simulation, it can be clearly seen that number of injected droplets is much lower, which results in slower RSO vaporisation and the fuel diffusion through the air. The picture at 2.51° of the crankshaft shows a buildup of RSO concentration on the piston bowl. This is caused by larger drops, which having higher momentum can reach the piston bowl much quicker. Furthermore, the distance from the cylinder centre to the piston bowl is too short for the effective RSO breakup and evaporation. The last four snapshots of in Figure 6.93 shows cumulation of RSO drops in a close position to the piston top. Location of the unevaporated drops is in the opposite region that for the diesel simulation shows in Figure 6.91. It can be concluded that the concentration of RSO drops close to the piston top can contribute to the unburned RSO buildup in the engine oil. The engine oil deterioration due to the excessive presence of RSO has been already confirmed in the literature [288].
The presented results clearly show that the temperature of 10°C significantly reduces air-fuel mixture formation and could lead to the incomplete RSO combustion. This supports the well know approach of pre-heating of the fuel prior to injection. The next computation case (Table 5.9 ERSO2) refers to the running engine temperature of 227°C (an elevated internal temperature of the combustion volume) and RSO injected at 10°C. The situation would take place in the case of dual fuel system at its startup when already warm engine switched to operate with RSO much colder than the engine cylinder block. It can be speculated that firstly an amount of not fully pre-heated cold RSO is injected, and then this amount is followed by the oil at higher (pre-heating) temperature. This is a common situation in the startup of an engine operating at a single tank mode (no auxiliary diesel tank for startup and shut down). In a such mode RSO remaining in fuel lines and injectors is not always fully pre-heated, and also it can not be recirculated back to the fuel tank nor preheated in a fuel pre-heater.

Figure 6.94 presents results of a KIVA simulation considering a case of RSO injected

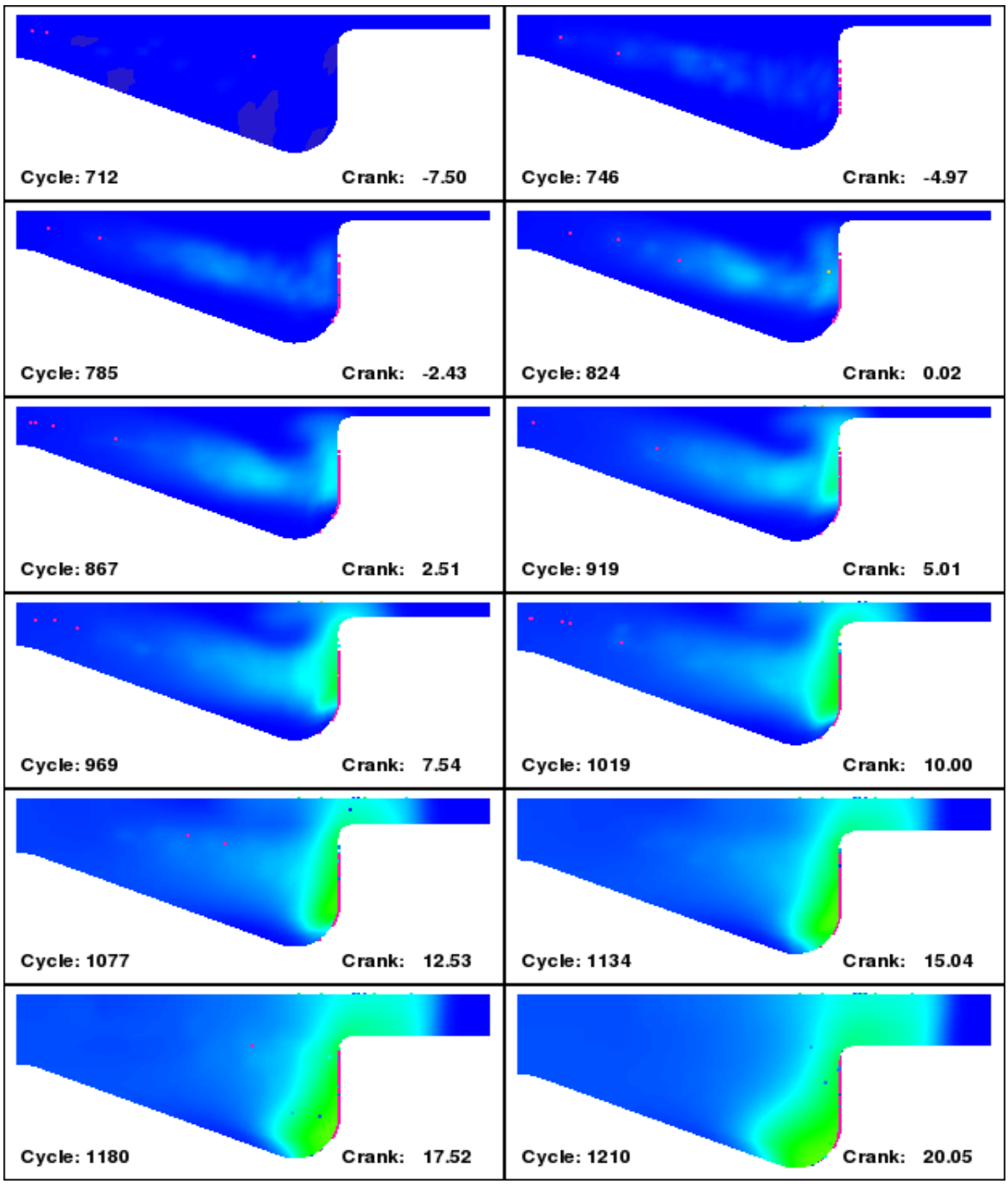

Figure 6.93: *RSO injection at the cylinder temperature of 10°C and fuel temperature at 10°C.*

at 10°C into a pre-heated cylinder at 227°C. At the beginning of the simulation the gaseous concentration of RSO is similar to this one shown for diesel in Figure 6.91. It can be expected that the similar droplet population travel across the cylinder however higher ambient temperature enhances quicker RSO evaporation. This can be found as larger light blue and green patches in the pictures of 0.03° up to 5.02°. Injected RSO amount forms large droplets readily travelling toward the piston bowl and accumulating on its

surface. This is indicated by the blue region in the middle of the volume and the light blue and green vertical patches along the outer piston bowl. Nevertheless, it can be noted decreasing number of droplet residue present in the piston bowl and the cylinder head. It can be concluded that the higher piston and cylinder temperature improves droplet vaporisation by reducing the number of oil droplets. High swirl enhances the breakup as well as improves the heat transfer from the cylinder wall into the volume. Comparison of Figures 6.93 and 6.94 does not reveal expected improvement to be more similar to Figure 6.92. It can be concluded that presented RSO concentration distribution may lead to slightly enhanced combustion but still could cause soot formation. However, it can be expected that oil accumulated on the cylinder and piston bowl will be redistributed and ignited once its viscosity is reduced. As it can be expected RSO combustion can be improved by enhancing its penetration through the air and formation of the air-fuel mixture. As it can be seen from the previous figures, cold RSO does not form the required air/fuel mixture even if the injection take place inside the warm environment. Therefore, it becomes more apparent that the oil should be injected at more elevated temperature. The next case (Table 5.9 ERSO3) considers injection of RSO at 60°C i.e. at the fuel temperature extensively studied in this research work and practically reachable through the engine modification. Results of the RSO spray penetration indicated that at 60°C RSO is expected to exhibit significantly enhanced atomisation and hence improved formation of the air-fuel mixture (see *Subsection 6.2.3*).

Figure 6.95 presents results of KIVA simulation at the engine temperature of 227°C with the pre-heated RSO (60°C). The initial analysis of the snapshots reveals their similarity to those shown in Figure 6.91. It can be seen that the spray development and RSO concentration follows diesel pattern recorded at 10°C. Pictures taken at -4.98 through -2.50, 0.01 and 2.5° show higher concentration of gaseous RSO formed very close to the injection point. Such behaviour was not found in the previous simulation where cold RSO was used (Figure 6.94). This can be recognised as a crucial improvement in the air/fuel formation for RSO. The pink region represents a rich RSO air-fuel mixture which gradually get enriched with air due to faster evaporation and the swirl motion. This occurs in the pictures at 10.0, 12.51 and 15.02° of the crankshaft. It can be seen that the air-fuel mixture is readily blended and forms a typical structure affected by the swirl motion. The mixing region occupies centrally the cylinder volume from its top down to the piston bowl (15.02 and 17.52°). As it can be seen at 15.02° there is a significant void which is not occupied by a RSO/air mixture. A possible explanation of this could be that at 60°C there is larger

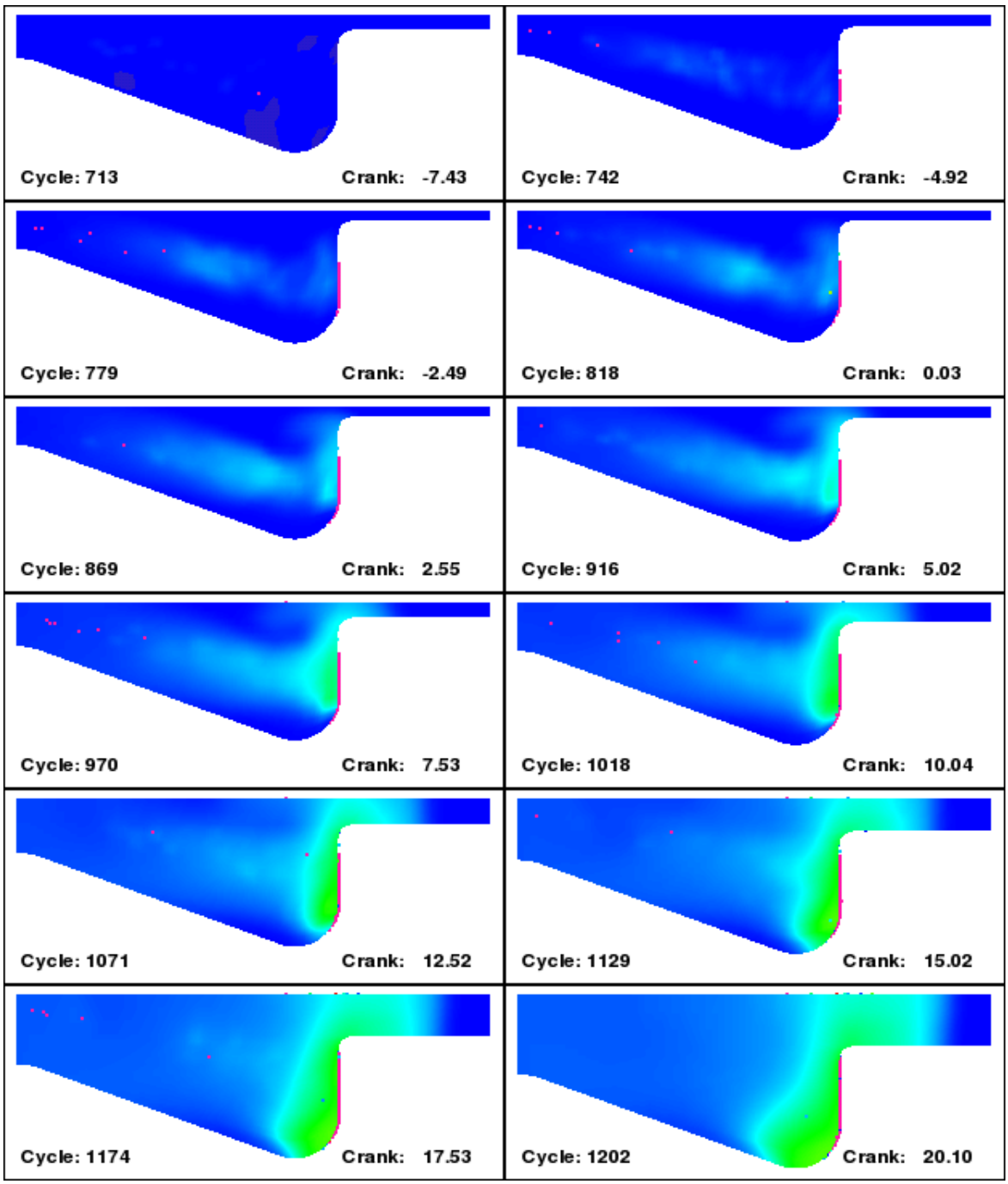

Figure 6.94: *RSO injection at the cylinder temperature of 227°C and fuel temperature at 10°C.*

number of small drops being injected, which follow the swirls and do not migrate to the outer side of the bowl. The last two snapshot indicate the presence of the unevaporated RSO droplets gathered at the cylinder head and piston surfaces. The same occurrence can be seen in the case of diesel simulations in Figures 6.91 and 6.92 and different from further radial droplet location in Figure 6.94. This indicates the complete evaporation of RSO droplets travelling towards the piston top. It can be expected that the unevaporated

droplets have the largest diameters of the injected population. The droplets are expected to be ignited and not to contribute in the engine oil deterioration. The final RSO simulations

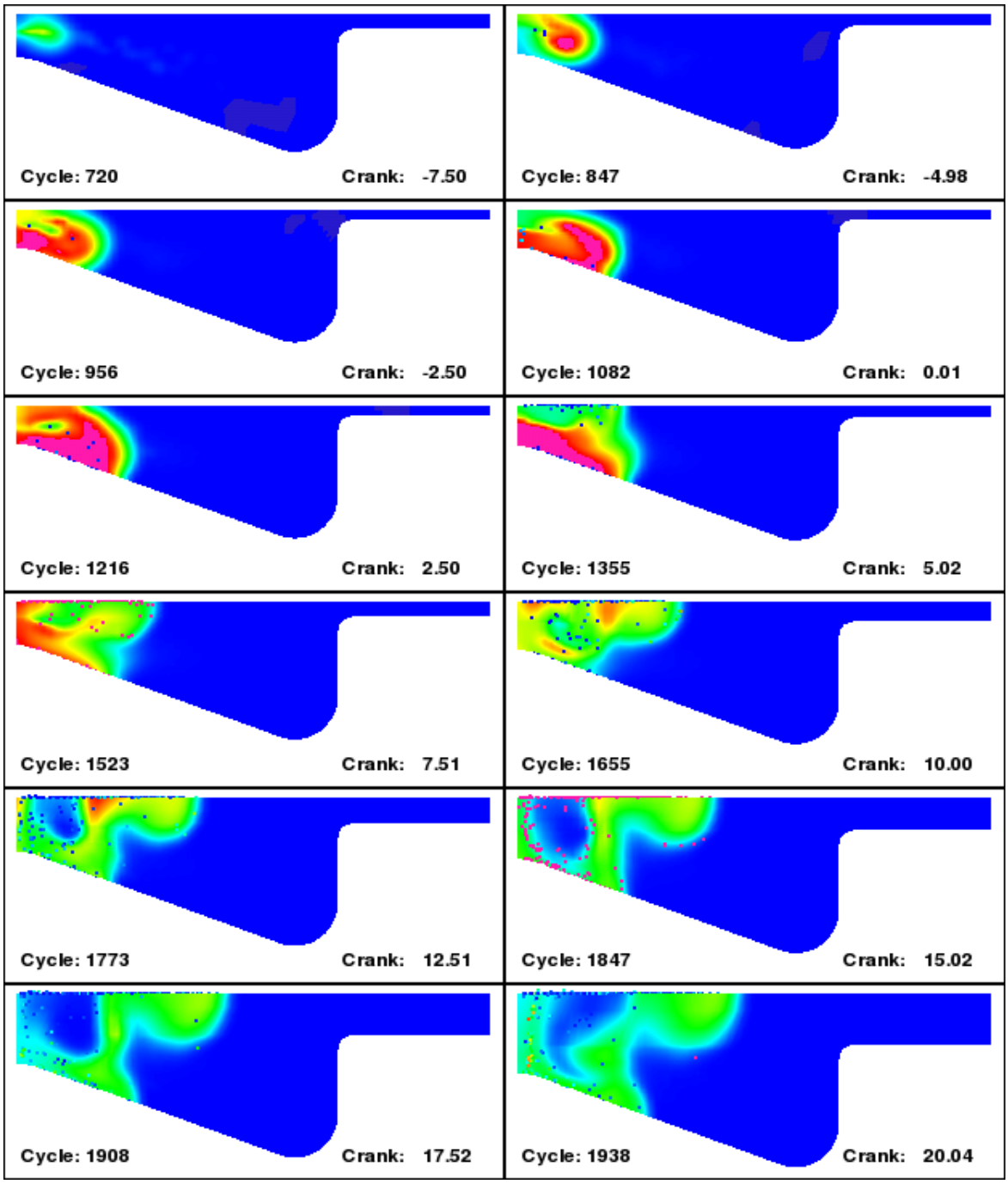

Figure 6.95: *RSO injection at the cylinder temperature of 227°C and fuel temperature at 60°C.*

included the identical engine thermal conditions however the injected RSO temperature risen upto 77°C. The fuel temperature refer to the performed CDI engine tests running on RSO where the oil temperature had been measured and found equal to 77°C. Hence 77°C reflect on the effective oil temperature present in the injector. Figure 6.96 depicts

graphically the results of the KIVA simulation under such operational conditions. The presented snapshots can be commented in the same manner as the results presented in Figure 6.95 with highly imposed RSO evaporation. Beginning of the injection can be characterised by the increased RSO evaporation and very high concentration of RSO in the air-fuel cloud indicated by the pink patch. Starting from the crankshaft position of 2.50° an increasing air entrainment due to swirl mixing is noted. The pink region becoming disrupted and includes yellow and green areas of more diluted gaseous RSO neatly filling the centre of the piston bowl. This indicates a typical formation of the air/fuel mixture and manifest a gradual preparation of a combustible gaseous mixture. The recorded changes started from 10.01° reveal gradual and effective mixing and dislocation of the fuel mixture to the centre of the piston bowl. The last pictures indicates the efficient creation of the air/fuel mixture of relatively small regions of highly concentrated in RSO vapour. Also, it can be seen that unevaporated RSO droplets remain still in the region of the reduced swirl motion as well as on the cylinder head.

6.6 Effect of modification to the engine system

This section utilised results presented above and the theory and experience of the CR technology to define a set of solutions which could be applied to modify a CR diesel engine to be able to operate on neat RSO. The solutions are described below and are results of the observations and conclusions drawn according to the results acquired in this work and the experience collected throughout the project. Some of suggested modifications were implemented in a Mercedes CDI engine and tests. Modifications were employed to overcome problems associated with the cold start (the short-term problems, see *Subsection 2.1.2.1*), but also problems of the long-term operation. This section shows the main changes which would be performed on a CDI system to operate problem-free on pure RSO in a single tank mode without a significant overall cost. As it was presented in a previous chapter (*Chapter 2*) where various attempts to run diesel engines were described, a suggested modification has to be feasible engineering wise and affordable by customers.

It is accepted that these modifications might not have provided an optimal and a final solution but to determine a quality and direction of the performed changes still subjected to further improvements. The second important goal of this section is also to recommend further changes by presenting and proving some technical prerequisites.

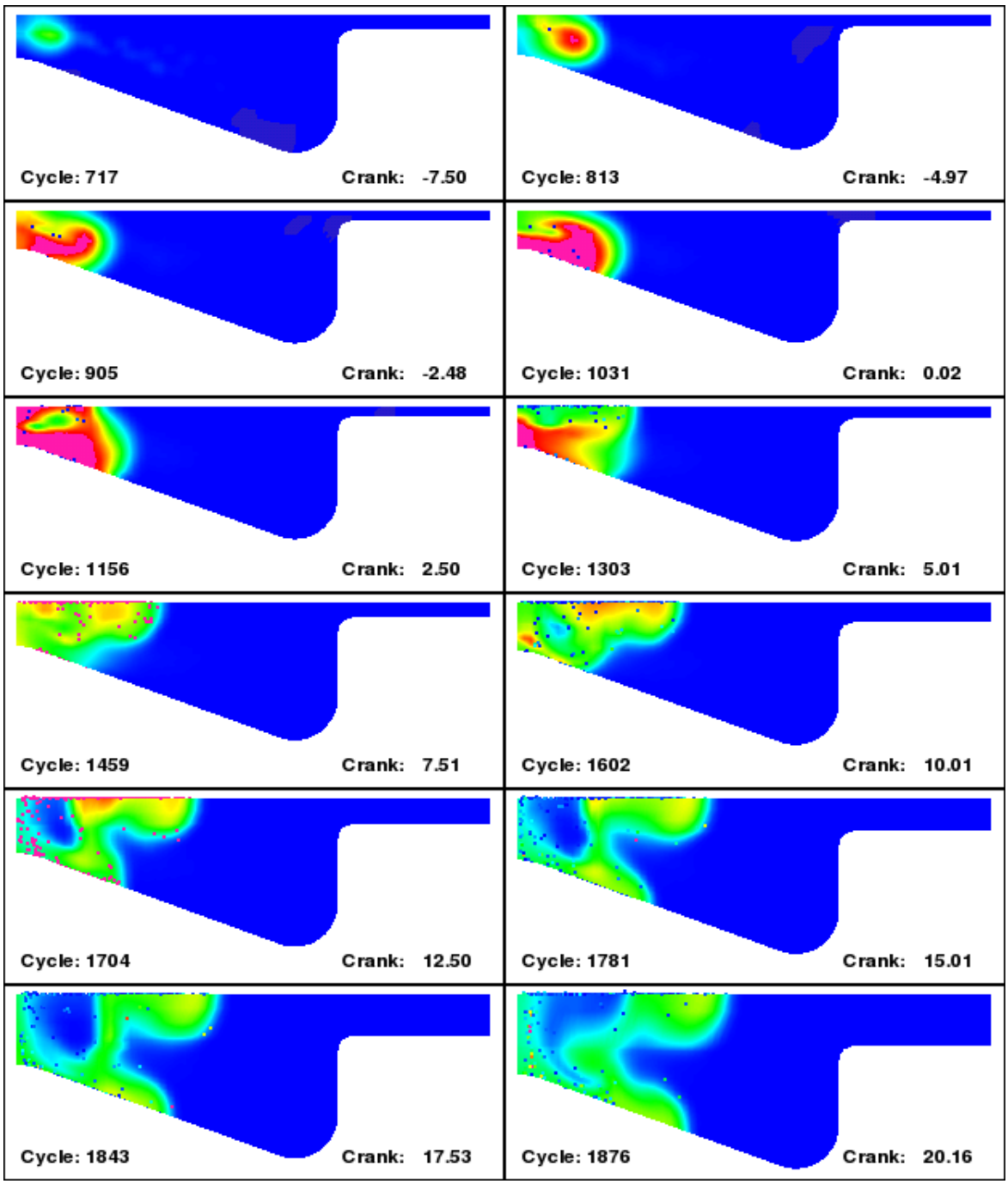

Figure 6.96: *RSO injection at the cylinder temperature of 227°C and fuel temperature at 77°C.*

6.6.1 Problem definition

Analysis of results of the previous chapters clearly indicate differences in physical properties, flow behaviour and spray development and characterisation between diesel and RSO. Reviews of the available resources on diesel engines modifications, the preliminary tests in which an unmodified CDI engine was operated [22], the analysis of the bench scale experimental results [187] and experimental results of this thesis allowed the author to

identified a set of prerequisites, which were consideter to be solved by modification:

1. **Quantities of injected** fuel limit performance of CDI system and result in overall engine effectiveness. Due to differences in viscosity, density and surface tension, injected volumes of RSO are different from diesel. The use of RSO in CDI poses a few challenges to injection system operation due to higher density and viscosity. The filter clogging and deteriorated RSO flow through fuel delivery parts are the common problems associated with different RSO liquid properties.

2. **Spray characteristic of RSO** is significantly different in terms of spray penetration, cone angle, and drop size distribution, as it has been shown in *Section 6.3*. The poorer spray atomisation is expected to be the main reason of incomplete combustion and engine oil deterioration.

3. **Fuel flow inside the injector** is sensitive to different fuel properties as originally designed for diesel. Higher viscosity and surface tension reduce fuel flow in the injector and therefore leads to the injection delay (hesitation) and shortening of the effective duration of injection. RSO flow reduces internal leaking but require higher energy input for faster and stronger interaction of the injection parts in a presence of high viscosity liquid.

4. It is expected that producing the RSO spray featuring a similar or the same spray characterisation as for diesel would improve combustion. RSO spray alteration can be done by changing its physical properties using injection pressure and fuel temperature.

The last statement is believed to be crucial and defines a direction of the modification. It can be recognised that the assumption of similar spray characteristics providing the same combustion quality can be overestimated. Different combustion kinetics as well as vaporisation mechanism of RSO is going to affect the combustion. Otherwise, two, same size droplets of diesel and RSO may behave in a different way as far as air/fuel mixture formation and combustion are concerned. Nevertheless, it can be recognised that the similar spray characteristics is a reasonable way to improve RSO combustion. Some general guidelines were considered by the author to modify the Mercedes CDI system and were based on the following assumptions:

1. The CDI engine is not started on conventional fuel. So there is not a solenoid control valve as normally used to switch to RSO once operating temperature is reached. The

engine is operating only on cold pressed RSO, preferably produced from the winter breed of rape seed.

2. Despite lower heating value of RSO the energy demand is supplemented by higher oil mass injected in the same injected fuel volume. Furthermore, the CR control unit is capable of the limited, but flexible, increase/decrease of injected fuel accordingly to the engine load.

3. The major factor governing the engine performance is the RSO spray development. It is assumed that an identical or a similar RSO characteristics to diesel should result in a RSO combustion characteristics that is very similar to that of diesel.

4. The ECU alters some injection parameters accordingly to the combustion output and signals gathered throughout the CDI engine.

5. The engine is filled up with appropriate engine oil suitable for diesel engines running on a pure plant oil.

6. Combustion product of RSO are biased or did not deteriorate in a noticeable manner the exhaust system. This is applied to the parts of exhaust system locating after the exhaust ducts including the catalyst, however the assumption is not applied to a possible soot buildup inside the cylinders.

7. The injection system is not purged of RSO once again operating on normal diesel before the engine is shut off.

8. A significant amount of waste heat is generated by the engine even in very cold ambient temperatures but also the battery capacity is sufficient to provide some extra energy for various heating elements.

Each statement above can be related to a specific, technical modification of the injection system. It was accepted that the final modification must comprise of a solution merging changes of: the delivery system (low-pressure loop), the high pressure system (high-pressure loop) and additional parts (e.g. heaters, fuel pumps etc.). Suggestions above prompt that alteration of RSO injection could be realised by a classical route of oil preheating. However, in the case of CDI perheating might not be sufficient due to varying injection pressure. Simply, the temperature effect is not sufficient at low injection temperatures to make the RSO spray similar to its diesel counterpart. On the other hand, the

operation of CDI system is too complex and not only governed mechanically. It was shown in *Subsection 2.2.5* that CDI controls injection pressure and timing independently of engine speed through the ECU and hence the ECU access is crucial. The system implements very sophisticated electronics and software hence any of its changes become highly difficult. It can be assumed that modifications of the injection regime or injection conditions should be performed in combination of the re-programming of the ECU or replacing the existing electronic components. An alternative way is to change mechanical components only being used to produce fuel spray. This is due to a lack of information of the ECU and limited level of user intervention offered by manufacturers. As a relatively new technology in the market, manufactures do not tend to make its technical documentation available even to researchers engineers, and unfortunately, the newest generation of the CR is even less friendly for developers.
During the time of the PhD work, the resources available to the author did not provide a method of tweaking the ECU. Therefore, modifications related to ECU changes were not applied. Some of the additional comments on the modification including limitation are given in the next chapter in *Recommendations for future work 8*.

Next subsections describe changes, which were possible to be made on the Mercedes CDI engine. Modifications were performed with the great assistance and help of Elsbett Company at their workshop.

6.6.2 Performed modification of the fuel delivery system

CDI delivery system (the low-pressure loop) plays a crucial role in pre-conditioning the fuel. A slight deterioration of the pre-pressure pump supply would affect the efficiency of the high pressure pump and thus the fuel metering. Also, during the cold start the flow of RSO significantly influences the performance of the other parts of the CDI, e.g. fuel filters. Thus, a modification of the delivery system to supply a stable and sufficient RSO flow was of a great priority.

The major, performed changes of the delivery system was the replacement of the existing fuel hoses by rubber tubes of larger diameter and positioned with automotive type hose clamps. This was essential especially at cold ambient conditions where the RSO viscosity degrades the flow and affects feeding of the high pressure loop.
Fuel lines were routed such that RSO could be drawn from the tank, through the heat

exchanger and the fuel filter at the minimal pressure drop. The diameter of hoses was selected in a way that even at low temperatures and varying RSO viscosity the clearance permitted relatively free flow through the hoses. The hoses were insulated along most of their path with prefabricated pipe insulation.

It has to be noted that the performed modification used a single fuel tank. There was no provision for heating the RSO within the fuel tank. Although, during the operation RSO inside the tank was mixed with the oil surplus returning from the high pressure pump and the rail. It was measured that an outlet average surplus temperature was about 55°C. The effect was desirable and enhanced lowering RSO viscosity and density.

There was no auxiliary tank serving a small quantity of the conventional fuel for the start-up and the engine shut-down. RSO was directly routed from the fuel tank to the low-pressure loop. A suction nozzle was modified and its metal mesh coarse filter was removed. The RSO outlet was positioned in the way to leave some space between the bottom of the fuel and the outlet, thus some space for sedimentation (wax residue) accumulation could be accommodated. This was done to prevent sediment from being drawn into the fuel outlet, which would otherwise cause premature fuel filter plugging and clog the fuel lines.

To utilise beneficial effect of RSO preheating engine's heat surplus was utilised by circulating the coolant through a RSO preheater. An aluminium fluid-to-fluid plate heat exchanger was fitted on a steel mounting place close to the fuel filter. The heat exchanger was approximately 9.5 cm in length, 6.0 cm in width and 6.0 cm in depth. Two nozzles of the heat exchanger were designed as inlet/outlet of RSO, and another two ports were used for the coolant inlet/outlet respectively. The engine coolant was directly withdrawn from the cooling system through a length of rubber hose connectors installed for this purpose. The coolant traveled in the opposite direction to RSO, so the heat exchanger worked in counter current mode for better utilisation of the waste heat. The inlet hose connected the coolant duct where the coolant was branched off to flow towards the engine block with the inlet port of the heat exchanger. The inlet hose was split into the original heater hose supplying coolant to the radiator. The outlet of the heat exchanger was directed to the coolant reservoir tank and practically the coolant works at atmospheric pressure. This coolant-oil heat exchanger concept provided primary heating and from this point of the fuel delivery system RSO was pre-heated up to approximately 70°C.

The original fuel filter was replaced by a fuel filter with a filtrating cartridge mesh around 3 μm. It was installed to trap larger particles and prevent possible injector plugging and obstructions of the fuel pump due to fine particles present in RSO. A second identical fuel filter was fitted alongside the first one to allow a flexible switch in case of unexpected clogging of the primary fuel filter. The second filter was fitted parallelly to the primary one and a simple valve was used to redirect the flow from one filter to another. Additionally, the filters were equipped with heating clamps, which provided appropriate heat flux to preheat a filter. The heating clamps were electric heaters powered from the battery through a control unit consisting of a relay, a temperature sensor and a connector including a 10 A fuse. The assembly was essential at cold-start and allowed quick pre-heating of filter's volume which normally is filled up with RSO left there after the engine is turned off. On average, the low pressure loop preheating lasted for 10-15 min prior to the start and sometimes was maintained until the engine coolant reading reached at least 50°C. An additional hand-pump was build in between the filter and the fuel delivery pump. Furthermore it has been found a problem of air entering the fuel system via different connections present in a modified system.

The last detail of the modification is a replacement of existing fuel tubes with a larger diameter hoses, between the filter set and the high-pressure pump.

6.6.3 Performed modification of the high pressure loop

As stated above modification to the ECU were not performed only some changes to the high-pressure loop are made.

After the filter the fuel pipes were insulated and replaced with larger diameter tubes. With the modification of the low pressure loop when fuel hit the high-pressure pump its temperature was around 65°C. It was accepted that RSO should be heated to a minimum of 70°C in order to reduce viscosity to less than 15 cP, a tolerable viscosity of most fuel injection pumps [68; 168]. Although, in practice RSO at 65°C was accepted by the CDI high-pressure pump without any operational problems [168; 295; 296] and it was concluded that 60-70°C was the optimum temperature range for RSO for diesel engines under moderate load versus full load [168; 253]. Since the coolant temperature is coincidentally maintained at approximately 90°C, RSO could be used as fuel by capturing waste heat from internal combustion through the heat exchanger.

As it was described in *Subsection 2.2.5*, the CDI rail was constructed of a thick wall steel tube of a significant heat capacity. Therefore, a next unavoidable change of the modification was to pre-heat and insulate the rail. Rail and injector pre-heating systems were combined together to heat those elements at the same time. Their integral part was a heating tape consisting of two heating metal elements placed at the top and at the bottom alongside the rail. The main purpose of the element was not to pre-heat RSO inside the rail but to maintain a temperature at which RSO could flow inside the rail.
It is known that any mechanical modifications of CDI injectors are difficult and therefore the opening pressure of injectors can not easily modified by changing their mechanical parts, Therefore a non-intrusive approach was applied. Each injector was equipped with a thin heating element which allowed heat up the injectors prior to the engine start. The heating elements were fitted alongside the injectors and were isolated from the cylinder block through a thin layer of insulation. The heating elements were powered from the battery and controlled jointly with the rail by a system of temperature sensors and relays. This allowed a very smooth and economic energy management and therefore to conserve the battery power. On average, the high pressure loop preheating lasted for 10-15 min prior to the start and sometimes was maintained until the engine coolant readind reached at least 50°C.
The last change made to the high-pressure loop was the replacement of the existing fuel return with tubes of larger diameter. The return fuel tubes were collecting fuel surplus and directtin it back to the fuel. Insulation of these tubes neither pre-heating was fount not to be essential.

6.6.4 Implementation of modification in a CDI engine

Modifications of the low and high pressure loops described above have been implemented in a CDI Mercedes E220 class and tested. The genuine parts of the high pressure loop remained unchanged and some new elements had to be incorporated assisting the alteration of the RSO temperature. The CR injection system of the Mercedes car was modified accordingly to the suggested changes and then certified by an authorised Mercedes service garage. The changes allowed operation on RSO in a single tank mode. The scale of the modification demonstrated commercial feasibility of the changes and also ensured a quick customer delivery.

6.6.5 Modification results

This section presents the results of quantitative and qualitative tests done on the modified CDI engine. The experimental procedures related to the results are presented in 4.5.

6.6.5.1 Emission tests results

Certain emissions are included in the standard engine tests, and these are CO, NO_x, HC, particulate matter (PM) and CO_2. These are normally expressed in grams per kilometre. In this work results or comparative tests between diesel and RSO are presented. Figure 6.97 shows percentage changes of emissions in a comparative manner. Results represent the averaged data and the worst emissions recorded throughout the tests in comparison to diesel emission. In the figure, values represent the RSO data relative to diesel (values for diesel are 100%.

Generally emissions can be affected by many factors like: engine age, maintenance of the engine, type of exhaust after-treatment technology and others. Nevertheless, presented results allow a cooperative analysis to be done and make general but crucial statements about the CDI emissions when RSO is used. The emission of carbon monoxide is found

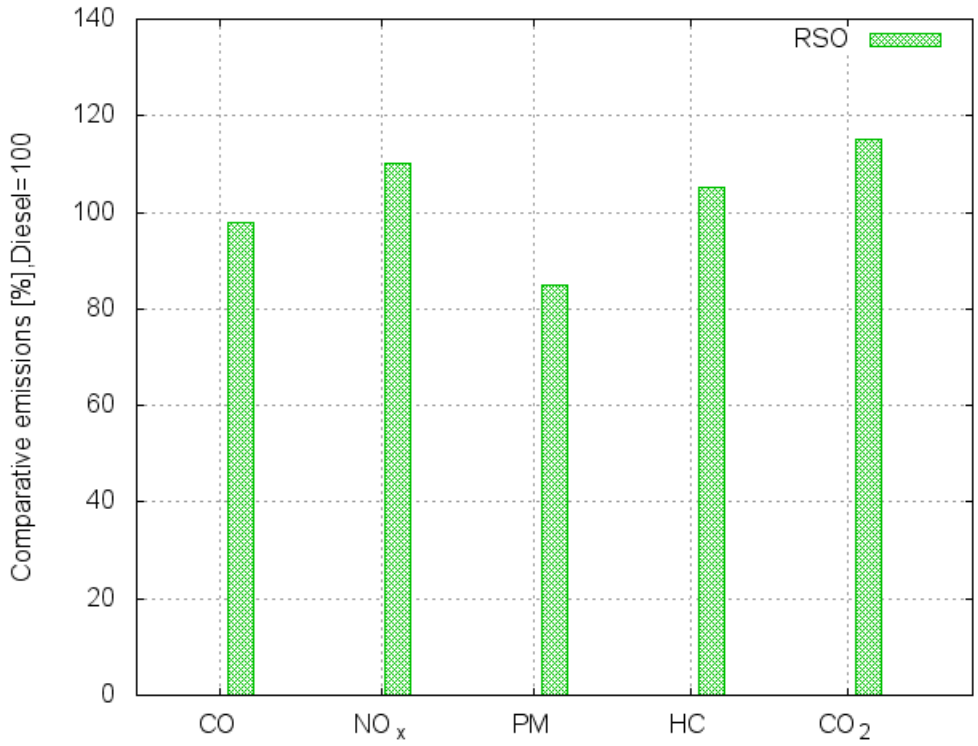

Figure 6.97: *Comparative results of emissions test for diesel and RSO*

to be slightly lower than for diesel. Although, the change is not significant is important

and can be explained that the overall carbon is better oxidised. This could be a results of higher amount of oxygen available in RSO than it is found for diesel (see Figure 2.2 in *Subsection 2.1.1.1*) and therefore it can contribute in combustion.

Carbon dioxide emissions from diesel engines operating on conventional diesel are lower than for equivalent petrol engines, due to the inherent efficiency of the diesel engines. Results of CO_2 emissions in Figure 6.97 proves this trend. It can be seen that the carbon dioxide emissions are higher almost by 10%. The fact can also explained the results of lower CO emission i.e. the CO was further converted into CO_2.

Although not always the case, in general it appears that the use of plant oils in diesel engines increases PM in exhaust emissions compared to those from conventional diesel. In some test PM emission were found to be lower than for diesel. The evidence from the figure shows that in these test the PM emissions were much lower than for diesel. The results can be questioned and only explanation of this could be that the measurements were did not include the engine start, where the majority of particulates is created. This PM measurement was performed at warm engine, when the catalyst and the particulate filter are working very efficiently. One can speculate that in this case the PM emissions should be close to diesel. The explanation of the lower PM emissions can be the decreased initial fuel injection (lower injected amounts due to lower injection pressure of the pilot and properties of RSO).
If the PM emissions are lower, the PM emission reduction by the use of RSO could assist in more rapid adoption of particulate traps. These end-of-pipe pollution control devices are widely proposed as a solution of diesel PM emissions, and are very effective. However, because of current emission levels, they tend to fill with trapped material and require maintenance more quickly than is desirable. A large reduction in the volume of PM reaching the trap would likely extend the maintenance interval considerably, thereby making the use of these devices more acceptable to diesel engine operators.

Literature prediction of NO_x emissions for plant oils match with experimental data well. The NO_x was increased and the soot was decreased according to the initial fuel injection duration was decreased. In Figure 6.97 the NO_x was increased and the soot was decreased very likely because the injection duration was shortened. As it was shown in the literature [201] the NO_x was increased as the initial injection pressure was increased.

A recent study of polycyclic aromatic hydrocarbons emissions generally concluded that, for the engine tested, neat RSO produced more unburned higher hydrocarbons than the conventional diesel fuel. RSO without a catalytic converter results in emissions are expected to be higher than that of the conventional diesel fuel. It is expected that a CDI engine combined with a catalyst will result in further emissions reduction. Although, there have been mixed reports in terms of exhaust emission when plant oil is used as diesel engine fuel. Nwafor and Rice [49] reported that hydrocarbon (HC) emission was lower for neat RSO compared with diesel. Kotsiopoulos and Yfantis used blends of waste olive oil and diesel and found that, with increasing percentage of waste olive oil, the Bosch smoke number (BSN) and HC and CO emissions increased, while NO_x emission decreased [229]. Prasad et al. obtained results that show that Jatropha and Pongamia oils give higher smoke emission but lower NO emission when compared with diesel [331]. Figure 6.97 shows a small increase of HC. Without appropriate gas analysis it is very difficult to assess the origin of the HC emission. It can be speculated that the emission consists of long-chain, unsaturated hydrocarbons readilly formed during the combustion of RSO. It is recommended to perform more detail studies or if the RSO combustion model is available perform relevant combustion simulations.

As it can be see from Figure 6.97 the emissions for RSO are very close to diesel. Although, to achieve Euro IV targets of emissions regulations for NO_x, it would be recommended to improve them. It is suggested that that a new combustion chamber design, EGR (Exhaust Gas Recirculation) system and newly developed CR fuel injection system for RSO would be needed to be adopted. A new combustion chamber design could decrease particularly the smoke of partial load for the strict PM target. EGR system was modified to optimise the EGR rate and uniform that of each cylinder [289].

6.6.5.2 Visible smoke and exhaust smell results

The next engine test was performed on visible smoke and exhaust smell. Visible smoke represents exhaust as it e.g. steam coming out of the exhaust system. The parameters which are not normally quantitatively assessed although their observation tells a lot about combustion. Also, the aspect of smog creation and general driveability are functions of these two parameters.

The smell of RSO exhaust is distinctive and it has often been characterised as having a

"fish and chips" smell. Despite most people reportedly find this to be more pleasant than the conventional diesel exhaust RSO exhaust can be very intense and cause eyes, nose and throat irritations. Visible smoke is one of the factors which can indicate the quality of combustion and also is considered as an important factor as far as the environmental impact is considered.
In these test visual observations of visible smoke emissions from the exhaust pipe were made while starting the engine at different ambient temperatures. Also, similar observations were conducted when driving the vehicle. Observations were made primarily by observing the amount of visible smoke released from the exhaust pipe under conditions that normally cause diesel engines to emit significant amount of visible smoke i.e. cold starts, hard acceleration from start and ascensions for steep grades. The observations were made in a comparative way between the conventional diesel and RSO.

Some amounts of visible smoke was produced when the engine was started at cold conditions with a little of pre-heating. The visible smoke emission was noticeable and higher than for diesel for a period of time until the engine reached its normal operational temperature. The time dependents on ambient conditions and the engine load. Also, hard acceleration up steep grades at cold weather and full power acceleration from a standing start led to noticeable amounts of visible smoke. Generally, if the heating procedure was applied the engine produced negligible amounts of smoke comparable to diesel emissions or amounts which were not different from diesel production.
However, it has to be pointed out that there is a difference in colour of visible smoke between diesel and RSO. The conventional fuel produces more blue smoke whereas combustion of RSO results in white smoke. This indicates reduction of black particulates (PM) normally present in diesel smoke. The conclusion is proved by results of PM presented in Figure 6.97.

6.6.5.3 Power output and fuel economy test results

The excellent power and economy characteristic provided by the combination of energy density of conventional diesel fuel, and the efficiency of the CDI engine is desirable and should not be sacrificed by using RSO. Power output of the diesel engine is very important to the driver and correspond to the successful assessment of the CDI modification. Horsepower and torque on RSO fuel would have to be very close to that of conventional

diesel for market acceptance of RSO as a fuel. Literature review provided examples that bio-diesel offers similar fuel economy to conventional diesel [6; 84; 235; 408] but much less information was found for RSO. Therefore, fuel economy tests of RSO are essential and need to be analysed.

To assess the power and engine performance the DynoStar kit was employed, which works like an electronic dynamometer. DynoStar allows to accurately measure the amount of power a car is putting on to the ground, which is an invaluable tool when doing after-market modifications. Figure 6.98 shows a typical graph representing a driving history of the unmodified engine running on diesel. The measurement were taken for 5 min and included acquisition of the CDI engine speed, power and torque as function of the driving time. Using the graph it is possible to analyse changes of the engine performance in accordance to speed. As it can be seen the characteristic represent parameters depending on the actual engine power output and RPM (speed). The results revealed a history of events i.e torque, power and speed following each other with time. It can be seen that the fluctuation of the torque and power are followed by the speed and the changes of first two allow the car change its speed quickly and smoothely.

A similar test had been performed for the modified engine running on RSO, however the direct, time independent, comparison of diesel and RSO operation engines is not possible. Despite a very similar driving pattern and the time scale, the conditions were not strictly the same. Therefore, the next figure, Figure 6.99 represents an relative comparison to diesel and can be assessed only qualitatively.

Figures 6.98 and 6.99 reveals minor changes in the engine performance. In general, the recorded pattern resembles the diesel measurements but with some changes. On average, a power drop can be observed for RSO in the almost whole range of speed, which can be expected if the same amount of fuel is injected. Almost the same power output (comparing diesel and RSO) can be observed at higher engine speed. It can indicate that higher speed frequently associated with the higher load utilises higher injection pressure of the injection regime (split injection). This may lead to accordingly higher quantities or RSO injected or effectively utilised (combusted), Thus, the engine output is almost the same. Analysis of the engine torque in relation to speed shows a similar trend for both fuels.

The analysis can prove that the RSO injection at higher injection pressures is more effective, providing more enhanced formation of air/fuel mixture as well as better combustion. It

would be recommended also to compare diesel and RSO in rolling test in addition to the driving test using DynoStar. Such test could provide results at different and constant loads lasting longer than the driving tests [72].

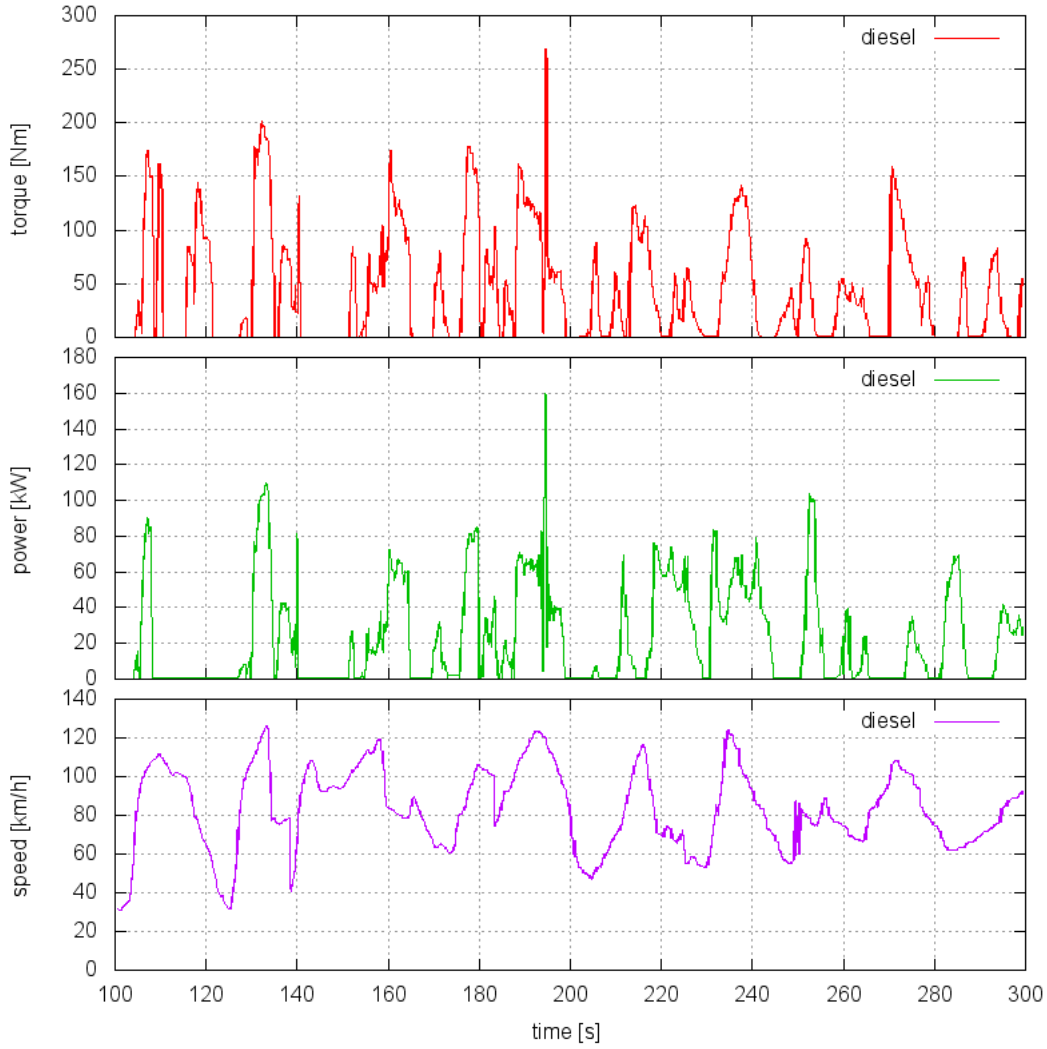

Figure 6.98: *Engine performance characteristic, when fuelled with diesel.*

6.6.5.4 Lubricating oil test results

Test of using a conventional, mineral type of lube oil and diesel fuel revealed [321; 322; 325; 326] that the fuel pushed to the oil pan by piston rings evaporates from the hot lubrication oil, whereas plant oil remains there and due to its acid structure it tends to esterify the lubricant. This changes the properties of the lube oil making it very thick so it can no longer be pumped to the lubrication passages. Therefore, the lube oil used in the car was replaced by the enhanced engine oil (PlantoMot, SAE 5W/40) suitable for diesel engines working on plant oils [21]. Apart form excellent lubrication properties, the

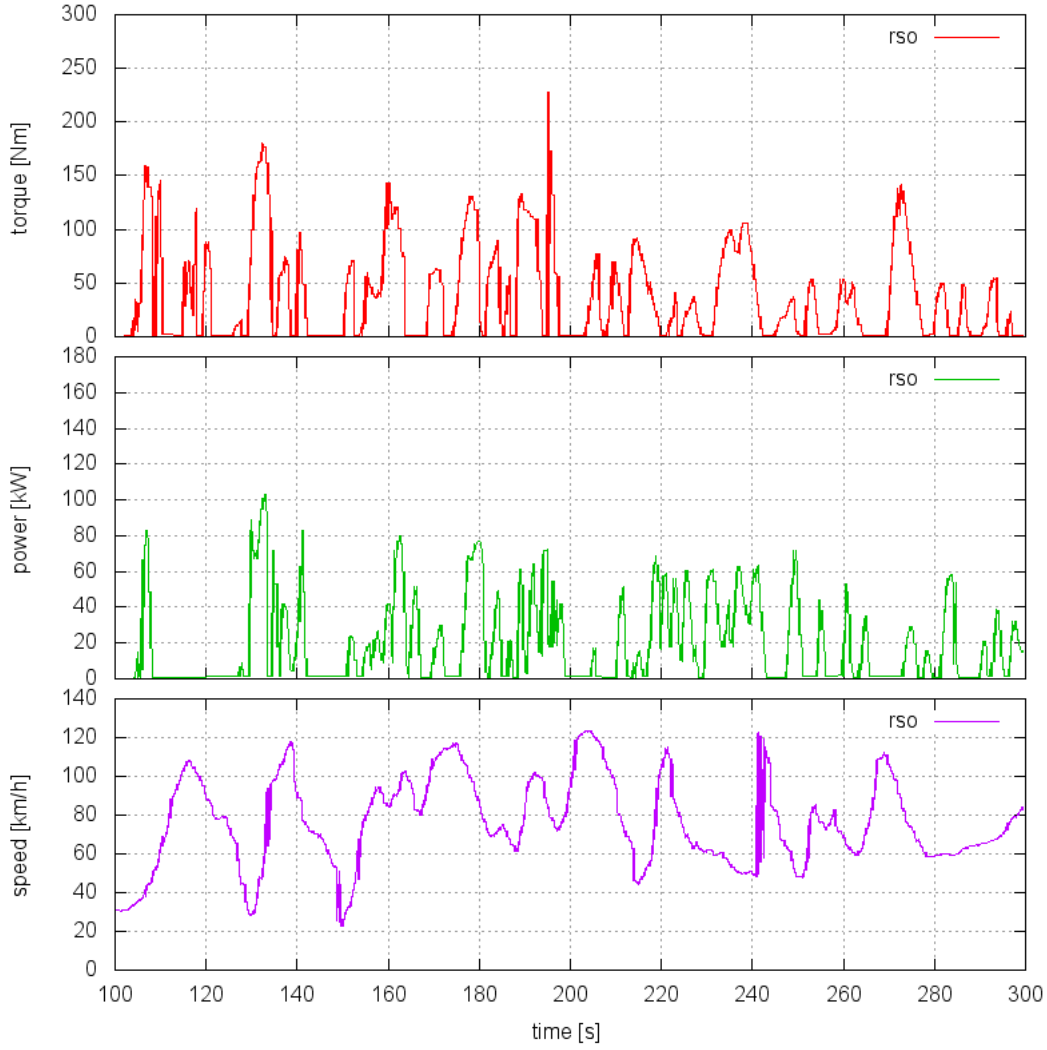

Figure 6.99: *Engine performance characteristic, when fuelled with RSO.*

utilisation of PlantoMot makes the modification more environmental friendly particularly if the oil composition does not cause water contamination.

The application of the oil helped to avoid the so called polymerisation of lubricants when mixed with free acid fuels like RSO for a much longer period compared to fossil based lubricants. However, it was recognised that the possibility that the RSO could be pushed to the oil pan was very low. This was concluded from the observations of the pan oil level which did not exhibit any abnormalities.

Table 6.1 presents results of density and viscosity test of samples of standard, synthetic lube oil and its enhanced counterpart. It can be seen that the results are not very different from each other and from their nominal values (of the fresh oil). It can be safely concluded that the changes from the nominal values are due to aging process of the oil rather to effect of the oil deterioration due to application of RSO as fuel.

Table 6.1: *Lubricating oil tests. In brackets the nominal values for fresh oils are given*

Properties	Synthetic 5W-40 Diesel Oil	PlantoMot, SAE 5W/40
Density at 15°C [kg/m^3]	856 (854)	927(923)
Viscosity at 100°C [mm^2/s]	15.3 (15.1)	15.2 (15.0)

6.6.5.5 Acceleration test, drive-ability and fuel consumption results

Diesel cars acceleration is considered to be barely adequate at its best. A stopwatch was used to record 0-100 km/h acceleration for standard diesel and RSO. Each test was performed once in each direction under calm conditions on a level, paved surface. Prior to each test the vehicle was driven for approximately five minutes at approximately 90 km/h. Table 6.2 presents results of 3 different runs/tests. Results are very similar for both fuels and it can be concluded that RSO acceleration times are very close to those for diesel.

Additional to the DynoStar measurements of a car, a build-in computer interface was

Table 6.2: *Acceleration test results of diesel and RSO.*

Test number	Diesel 0-100 km/h [s]	RSO 0-100 km/h [s]
1	15.3	15.6
2	15.2	15.7
3	15.3	15.6

used to readout of output under stable driving conditions. It has been found that at average speed of 95 km/hour the RSO fuel consumption was 7.2 litres/100km. This means that the real fuel consumption in 1 hour was 6.84 litres of RSO. This provided the average RSO consumption of 250 g/kWh (269 cm^3/kWh). Fuel economy calculations were based on vehicle logs for approximately 4 hrs driving. The driving cycle was a combination of approximately 50% local trips and 50% motorway trips. Paved roads with flat to moderate grades were selected.

6.6.5.6 Injector and cylinder inspection results

Fuel injector coking has been reported in [33; 147; 164; 209; 263], as a problem when diesel engines were operating on plant oils or pure bio-diesel over long periods of time. Deposit formation depends on the type of injector and fuel and generally it can be said that lacquer formation (due to polymerisation) and incomplete combustions are the main

reasons for injector coking. It was hypothesised that the start-up or shut-down cycle procedure, especially using bio-diesel or diesel, both of which are known to have a solvent cleaning effect on injectors, would solve the problem. The same cleaning effect can not be expected if a car runs incorrectly in a single tank mode on RSO. Thus inspection of the injection system is essential to assess a possible deposit buildup.
The diesel injector exhibited the amount of coking that would typically be expected for the conventional diesel and therefore by comparing it was possible to detect any unusual operation. Even though it was a qualitative observation, it was still considered to be a reliable indicator of any injector coking caused by RSO used under typical driving conditions. The inspection was performed after approximately 50000 km for diesel and 45000 km for RSO.

The injectors and the cylinder head were in very good condition almost free of deposit. Coking did not appear to be present on any of the injector nor on the cylinder head. A close inspection of the injector bores did not reveal passage blockage but only slightly noticeable partial narrowing. Results of the inspection are presented in Figure 6.100. An injector bore working on diesel is shown in Figure 6.100(a) and corresponding one operating on RSO (b) respectively. It can be seen that the bore exposed to RSO revealed a very low deposit buildup concentrated on its circumference. This resulted in a negligible reduction of the bore clearance by approximately 1 μm in comparison to the injector working on diesel as presented in Figures 6.100(d) and (c) respectively. It can be concluded that the revealed buildup due to RSO does not decrease the injector performance.

6.6.5.7 Cold weather performance results

Cold weather test were essential to assess a scale of short-term problems mainly related to the cold weather start. Normally, a short period of heating, up to 10 minutes, was required to advance engine start. Application of a block heater significantly helped to start up the engine. A 4.2 kW (full load) Webasto engine block heater was used for approximately 60 min as specified by the suppier. The measured coolant temperature was 80°C. After pre-heating the engine started up almost instantly without problems or significant differences from the diesel start.
The final test reveals that the modified system was able to run practically on 100% RSO down to -10°C. Also it has been shown that a 10% diesel blend improved the cold start ability at the ambient temperature of -20°C.

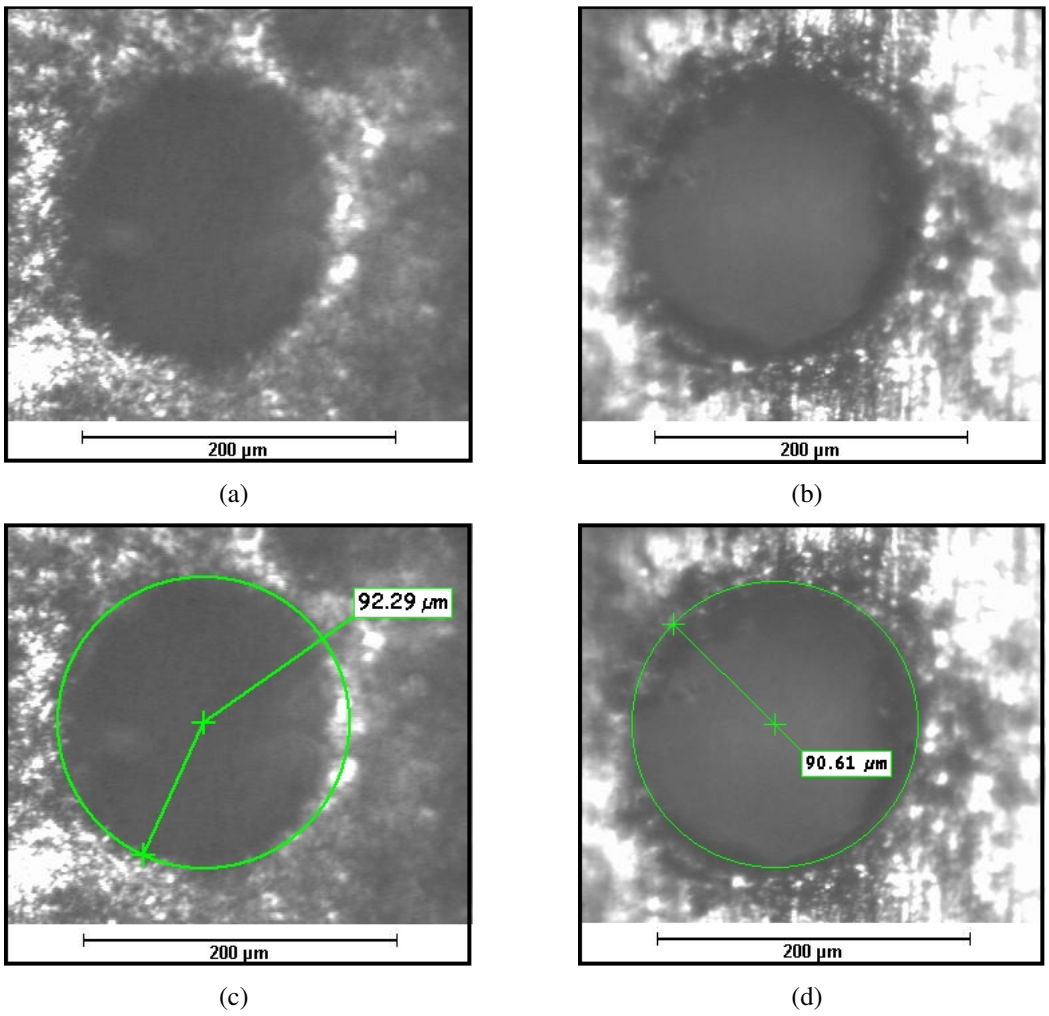

Figure 6.100: *Presentation of the CDI injector inspection showing clearances of injector bores: (a) running on diesel (b) running on RSO (c). Estimation of the effective bore cross section: (a) running on diesel (b) running on RSO (c).*

Chapter 7

Conclusions

Ex uno disce omnes

The investigation of CDI injection system operating on plant oils and particularly RSO can be elaborated on through various aspects. The topic of modification of a CDI system was analysed via feasibility and technical studies. In the first part, a general study of plant oil applications in diesel engines was presented, whereas the second part of the thesis concentrated on the technical and fundamental studies to compare the operation of a CDI system running on RSO with diesel. This part provided essential understanding of the differences between diesel and RSO spray produced in the CDI and then allowed to suggest and implement some of the modifications.

Due to the very extensive character of this thesis it is very difficult to withdraw concise set of conclusions. Thus this chapter provides a list of closing conclusions grouped independently for each important and major chapter or section of the thesis. It is believed that the layout results in a better and clearer demonstration of the main findings of this project.

7.1 Chapter 2: Plant oils as a diesel fuel substitute

Considering information presented in *Chapter 2*, the following conclusions can be drawn:

1. Neat plant oils are a considerable alternative substitute for diesel fuel offering a natural way to balance the CO_2 emission. Due to the difference from diesel physical and chemical properties, direct application of plant oils in diesel engines causes degradation of the injection process and in turn, adversely affects the diesel engine's performance. The fuel properties which affect the performance of a given injection

system include viscosity, specific gravity, and surface tension. Plant oils have substantial prospects as long-term substitutes for diesel fuels. The characterisation of plant oils provides some insight into mechanisms leading to the durability problems encountered when used as fuels for diesel engines. Recent investigation showed that the injection and combustion characteristics of plant oils in diesel engines are significantly different from diesel. Operational problems are common for all diesel engines, thus can be overcome by applying similar solutions to all diesel engines.

2. Short- and long-term problems seem to be related to the difference in physical and chemical characteristics of both plant oils and diesel fuel. Higher viscosity of plant oils interferes with the injection process and leads to poor fuel atomisation and disruption of the injection system. Studies of injection and spray characteristics are a key solution to successful application of plant oils. The tendency towards polymerisation and low volatility leads to deposit formation, carbonisation of injector tips, ring sticking and lubricating oil dilution and degradation. The combination of high viscosity and low volatility of plant oils causes poor cold engine start up, misfire and ignition delay.

3. Engine performance with plant oils is similar to that with diesel fuel. Application of various neat plant oils in diesel engines led to similar performance problems and emissions. NO_x emissions were lower, however are dependant on speed and load. In most cases the unburned hydrocarbon emissions were observed at partial loads. Excessively emitted CO and CO_2 can be balanced against CO_2 utilisation by the plants resulting in little or even a net loss in CO_2. Particulate emissions of plant oils were higher than for diesel fuel. Plant oils contain no sulphur, which would lead to a decreases in acid rain.

4. In spite of short- and long-term problems, literature verifies that plant oil can be used as a direct replacement for diesel fuel. The use of plant oils blended with diesel fuel reduces usual short- and long-term problems and improves engine durability. It is expected that CR diesel engines can run on plant oils as well, however modifications are needed before certain plant oil types can be safely recommended for longer use. In particular, modifications of the injection system are required to ensure good engine performance.

5. Successful substitution of mineral diesel with RSO needs a stable and secure oil market and easily accessible oil supply sources. Rapeseed oil has to be economically competitive with diesel fuel.

6. The resource base for RSO production is limited by a number of factors which include: the amount of land available for cultivation; seed yields per hectare; the impact of rapeseed growth on neighbouring crops; the economic advantages that can be enjoyed by cultivating oilseed rape rather than alternative crops and political restrictions.

7. Rapeseed oil used for fuel should be cultivated preferably on "set-aside" land as a non-food crop and its production supported by government subsidies. The production might be most successful for farmers who are diversified in both crop and livestock, especially in regions where a large spread exists between the price that farmers receive for their oilseed and the price they pay for protein meal. By processing rapeseed in the community - farm based plants, additional charges normally paid to other businesses might be eliminated giving RSO a competitive edge over conventional diesel. The community-based concept appears to present the best opportunity for success and requires less investment.

8. The economic viability of RSO is dependent on a reduction in excise duty levied by the government; the price of rapeseed; the value of the by-products and the cost of seeds processing.

9. Rapeseed oil production in rural communities has the potential to increase economic activity through job creation and an increased tax base. The production of RSO by farmers' cooperatives would be important in the development of rural economies based on local renewable resources.

7.2 Chapter 2: Diesel injection systems

1. There is a wide range of diesel engines distinguished by the way in which the fuel is injected. A vital component of all diesel engines is a mechanical or electronic governor, which limits the speed of the engine by controlling the rate of fuel delivery. Both mechanical and electronic injection systems can be used in either direct or indirect injection configurations.

2. Mechanically governed fuel injection system characterises the early group of diesel engines IDI. Older engines make use of a mechanical fuel pump and valve assembly which is driven by the engine crankshaft (usually from the timing belt or chain). Injection systems of the mechanically governed injection use a combination of springs and weights to control fuel delivery relative to both load and speed. Modern, electronically controlled diesel engines (DI) control fuel delivery and limit the maximum RPM by use of electronic devices (electronic control unit (ECU)).

3. Controlling the timing of the start of injection of fuel into the cylinder is a key to minimising emissions, and maximising fuel economy (efficiency). Governing injection of diesel fuel in IDI and DI had been optimised and is fuel specific, therefore complexity with the engine conversion to use neat plant oils increases with advancement of the injection system.

4. The principal advantage of CR is that fuel pressure is independent of engine speed. The other advantage is that the common pressurised fuel supply lends itself readily to ”pilot” and ”post” injection sequences (split injection).

5. Some older diesel engines (IDI engines) with mechanical injection pumps could be successfully run on neat plant oils. This is directly related to indirect formation of fuel-air mixture i.e. in a separate chamber, rather in a cylinder.

6. In Common-rail split, injection is the principal means of controlling diesel combustion noise and fuel economy, but poses as one of the main challenges of converting the system to operate on neat plant oils.

7.3 Chapter 3 and 4: Experimental systems and methods

1. A novel, standalone experimental rig was built to investigate the performance of a CR system. The rig comprised of the genuine CR parts and the modified Elsbett injection stand (see Figures 3.1, 3.6, 3.7).

2. Application of SF_6 allowed to mimic in-cylinder conditions at a relatively low ambient pressure. Hence, the use of SF_6 eliminated the need to maintain very high gas pressures inside the spray chamber.

3. The experimental rig was modified accordingly and utilised for a series of experiments involving several spray diagnostic techniques: high-speed camera spray characterisation, Phase Doppler Anemometry and Malvern laser for spray sizing and acoustic emission for non-intrusive spray flow diagnostic.

4. The setup of a high-speed camera and Phase Doppler Anemometry is essential for a correct and meaningfull analysis of dense spray. Additional application of Malvern laser allowed to assess and validate results of the Phase Doppler Anemometry measurements. The validity of the measurements was positively confirmed yielding an applicable although demanding, in terms of fine tuning, technique for dens spray studies.

5. Acoustic emission required a specific signal recognition procedure which would make it possible to recognise the consecutive peaks of a spray signal and correlate them to the characteristic events features of CR injection.

6. It was observed that spray-to-spray repeatability and symmetry can vary and also that the first injection shot exhibited the highest level of undevelopment. Thus, data from the first injection was always rejected and not processed.

7.4 Chapter 5 and 6: Simulation software and results

1. Numerical analysis of RSO spray characteristics can help to compare its performance in CDI engines with those of diesel. Simulations have to accommodate the high density feature of RSO spray.

2. Several fuel spray models for predicting liquid penetration and drop size distribution have been reviewed and discussed in relationship to RSO simulations. The available breakup models are capable of simulating a dense RSO spray. However, they require a careful experiment verification as the existing literature lacks in similar analysis.

3. A modified KIVA-3v Fortran code has been used to simulate spray. A novel *fuelib* module has been worked out to accommodate RSO simulations. Previous experimental penetration and sizing data were used to initiate spray penetration simulations. Additionally, a modified method of calculating the mean spray velocity has been provided. The method includes a variation of the discharge coefficient with the injection pressure and position of the injector needle.

4. The KH-RT and RD models were selected to simulate exclusive cases of the non-evaporating standard and RSO sprays corresponding to the previous experimental spray tests. The models performance was validated against the experimental data and it has been found that both models can be used to predict a dense RSO spray with almost the same accuracy.

5. Standard and RSO spray simulations were performed in a fully 3D rectangular mesh, where the geometry was optimised to accommodate different initial injection conditions.

6. A direct injection engine cylinder geometry has been used to investigate RSO and diesel air/fuel mixture formation under non-combustible conditions. Results revealed that successful combustion of RSO could be possible at elevated cylinder temperatures of 227°C and a fuel temperature of 60°C.

7. It has been recognised that better numerical assessment of the RSO performance in a CDI engine would require elaborated RSO combustion kinetics.

7.5 Chapter 6: Results of experimental spray studies

1. Density of RSO at 40°C is 1.2 times higher than diesel. High oil density affects the performance of the injection system high-pressure pump as well as fuel lines. Temperature of oil significantly reduces density of the oil; therefore heating can be used to bring the oil density as close as possible to diesel density. However, heating beyond 80°C is technically difficult to reach in a real injection system.

2. The most detrimental parameter of RSO is its higher viscosity, which is about 10 times higher than that of diesel fuel at 40°C. Values of surface tension are higher than normal diesel fuel. At 40°C, RSO surface values are about 30% higher in comparison to diesel fuel. The problem of higher density, viscosity and surface tension can be reduced by pre-heating the oil.

3. Values of RSO surface tension are higher than for normal diesel fuel. At 40°C, RSO surface values are about 30% higher in comparison to diesel fuel. Again, this will lead to poor nozzle performance, however deterioration of spray atomisation will also be affected by very high oil viscosity. Pre-heating of the oil can reduce high values of surface tension and viscosity.

4. It has been shown that injected quantities of standard and RSO remain different for the same injection conditions. This indicates a need for adjusting the injection system to provide the same energetic value of injected RSO. The most significant differences between diesel and RSO can be found at lower injection pressures.

5. It was observed that the performance of fuel filter and oil flow through the system is oil temperature dependant. Rapeseed oil requires more time to reach constant flow at the same heating conditions. Results showed that RSO temperatures lower than 40°C can noticeably deteriorate filter performance.

6. As was reported in previous studies, studied flow properties strongly affect the spray characteristics in diesel engines, and RSO shows different flow properties compared to standard diesel. Therefore it is recommended to investigate spray produced by CR injection system running on RSO before any modifications are applied.

7.6 Chapter 6: Preliminary modification test

1. A set of modifications has been defined and implemented on a CDI engine to operate on RSO in a single tank mode. These changes were applied mainly to overcome problems associated with cold starts (short-term problems) but also problems of long-term operation. The modifications were defined according to the problem definition and modification constraints.

2. Modifications concentrated on the temperature increase of RSO and therefore included the modification of: the fuel delivery pipes, fuel filter, injector preheating, fuel pumping and fuel distribution and re-distribution.

3. The existing standard synthetic oil was replaced with the PlantoMot bio-oil to reduce the possibility of oil polymerisation.

4. Performed changes were assessed through: an emission test of CO, NO_x, HC, particulate matter (PM) and CO_2, visible smoke and exhaust smell study, power output and fuel economy test, lubricating oil analysis, acceleration test and drive-ability, fuel consumption tests and injector and cylinder inspection. The test included cold-start conditions.

5. The emission results showed lower CO and PM production and higher CO_2, HC and NO_x emissions. The overall emission values were very close to those observed for diesel.

6. Investigation of power output, torque and accelerations showed a slight decrease for RSO. Power and torque patterns were very similar to those recorded for diesel. Measured acceleration was marginally lower than for diesel. Fuel consumption or RSO was slightly higher up to (5% on average).

7. The engine produced higher visible smoke, especially at cold-start and initial operation. The exhaust had a specific smell and was white-blue in colour.

8. Investigation of standard and modified lube oils of the RSO operating engine revealed that density and viscosity have not changed very much. It can be safely concluded that the changes from the nominal values are due to the aging process of the oil rather than the effect of the oil deterioration due to application of RSO as fuel. It is still recommended to use PlantoMot oil as a better environmental solution.

Chapter 8

Recommendations for future work

Malum consilium quod mutari non potest

The subsections of *Chapter 6* (*Section 6.6*) concentrated on basic modifications, which were performed within this PhD research ensuring their commercial feasibility. Modification of the CDI system would be complex and needs to be optimised. Partial modifications or selective changes only to some components may result in long term operation problems. In a recent AVL (AVL Group, GmbH) publication [189] it was suggested that the assessment of the future potential of diesel engine should be done only by taking the complete engine/vehicle system into consideration. However, crucial modification constraints (see *Section 6.6*) did not permit performing such analysis in this PhD research.

As it was presented in *Section 6.6* modification of the hight-pressure loop is the most challenging and technically difficult. The complexity of the ECU box and lack of adequate tools makes the modification of ECU an open problem for the future. More complex modifications were not performed due to financial and time constraints but can be recommended. Majority of performed modifications consisted of "technical shortcuts" to overcome the most obvious short- and long-term operational problems. However, the functional complexity of the CDI system needs to be carefully analysed taking into account all required changes to ensure that the system is properly modified and will not cause technical obstacles during various operational conditions.

Also, it has to be noted that apart form crucial elements like ECU, there are some other parts and functional features of the injection system, which significantly affect the functionality of the engine running on plant oils. They are not directly related to the modification but should also be looked into and taken into account when any modification is planned or

made.

This section presents some of the comments, future suggestions and recommends other modifications, which reflect on some important and unmodified (in this work) elements of the CDI system. The subsections below describe some technical aspects of modifications, which have not been investigated experimentally in this work and are left as recommendations for future consideration.

8.1 Recommendations for the high pressure loop modification

Subsection 6.6.3 already presented some implemented changes of the high pressure loop. This part of the CDI system remains the most difficult to be modified however, it is important for a successful modification of the injection system. The difficulty comes from the fact that injectors and the engine management systems are very compact. These parts were by default not designed to be modified or even repaired. It is accepted by the manufactures that the characteristics of the injected spray, its interaction with the wall of the piston-bowl, and the swirling air determine the efficiency of the combustion process, the concentration of exhaust gases, and particulate emissions. The same conclusion can be applied to any DI engine operating on RSO. Fuel atomisation reduces the cylinder wall-wetting, is effective in minimising the influence of fuel properties, improves the air/fuel ration controllability, and reduces engine HC emissions [182]. Thus, modification of the high pressure loop is the most crucial amongst the suggested changes, but also the most challenging to meet criteria of the Euro IV and V requirements.

It has been shown in *Section 6.2*, atomisation of RSO below 40.0 MPa and at oil temperatures below 20°C is extremely deteriorated and leads to a partly atomised spray and large RSO drops. Also, it can be seen that such fuel temperature is very likely taking place despite the efficient pre-heating system operating from engine start-up. This happens due to the oil residue, which is always present in places of the injection system where heating is retarded. Therefore, it can be suggested that the minimum injection pressure utilised to ensure more enhanced atomisation, and to avoid the combustion problem should be at least 50.0 MPa. The real opening pressures (the lowest injection pressures) are frequently

below 35.0 MPa, which is appropriate at start-up and practically no load conditions, when diesel fuel is used. Such low injection pressure is easy to produce and its creation does not consume a significant amount of engine power. The way how a CDI system could produce the minimum injection pressure of 50.0 MPa from the very start of the engine is challenging and remains an open issue.

As it has been previously recognised in *Chapter 6* the combination of elevated oil temperature and the injection pressure results in more enhanced RSO atomisation approaching droplet distribution of diesel. This is expected to improve the combustion of RSO and thus the CDI operation on RSO. From the presented results, it can be concluded that elevation of the injection pressure would be the most effective. Nevertheless, the injection pressure effect should be combined with elevated RSO temperature. The changes due to elevated temperature can be implemented through external RSO preheating, whereas the pressure effect can only be reached through changes of the ECU.

As far as geometrical changes are concerned, it is well known [247] that the smaller the inclination angle of the injector the more advantageous in reducing smoke by reducing spray-to-spray (hole-to-hole) deviation and more uniformly distributing injected fuel in a combustion chamber. Also, as it has already been shown in *Section 6.2* the RSO spray angles are generally smaller and thus a modification of the injector diameter would result in increased spray angle leading to the enhanced formation of the air/fuel mixture. It is believed that similar mechanical injector changes would significantly improve RSO atomisation. Such mechanical modifications of injectors are difficult and their feasibility would have to be assessed by manufacturer of the injector . In case if injector mechanical changes not be performed the most optimal way to modify CDI injection is to re-programm the ECU and EDC. This could be done by completely re-writing the existing injection algorithm according to the recorded changes of single injection of RSO under various injection and ambient conditions. It is recognised that the existing algorithm is build in a sequential way [203], i.e. by gathering crucial signals (information), and translating them into variables, which are substituted into numerical formulas defining the output variables directly controlling the injection. An ECU response is therefore created accordingly to the algorithm frequently called a map. The sequential way is understood as a step-by-step procedure of processing the incoming signals with respect to a memorised map and responses are carried over to a next stage of the injection algorithm. Every map works as a

transfer function, f_i of the kind reported in Equation 8.1.1 which associates to one or more input signals, x_n, a correction factor, C_{fi}, to the quantity of fuel to be injected according to the angular position of the accelerator , a, and to its time derivative, $\dot{a}$ [107].

$$f_i(x_1, x_2, ..., x_n) = C_{fi} \tag{8.1.1}$$

The total injected fuel per cycle q_{fuel} is calculated according to Equation 8.1.2:

$$q_{fuel} = q(a, \dot{a}) \prod_i C_{fi} \tag{8.1.2}$$

The transfer function is defined by a discrete set of points and its output value is obtained by a multidimensional interpolation routine executed via hardware. Therefore, changing the map means to change the set of discrete points which define the transfer function. Operating with the map settings it is also possible to vary the injection pressure and the injection timing with the engine speed. It is recognised that the injected fuel per cycle, the correction factors and the injection timing and pressure have to be optimised by taking into account the existing engine geometry to maximise performance and to reduce emissions [103]. The optimisation process and its verification has been successfully applied by De Risi and his co-workers to modify a CDI system to operate on natural gas as a dual fuel CDI engine [107] and could be done for RSO. Thus, by re-defining the existing procedures, a modification would serve as a new “recipe” on how to adjust the CDI injection system accordingly to a new type of fuel. Figure 8.1 presents operating-stage controller. The diagram represents the way how the ECU calculates the appropriate injected fuel quantity in order that the engine can operate with optimum combustion at every operating stage. Additionally, blue coloured boxes represent elements (functional algorithm elements), which have to be re-programmed if the ECU is to work on RSO. The changes could be the topic of an extensive future research project.

As it has been stated above the injection CDI map can be optimised by building a mathematical function and implementing findings from RSO spray experimental studies. A similar set of functions could be constructed to describe RSO flow, heat transfer, low- and high-pressure delivery. By combining these two sets of multi-objective functions it is possible to find the optimal solution using optimisation procedures already applied to diesel. Methods of complex optimisation of the CDI system were presented and utilised in several studies [104]. Parameters like injection pressure and duration, injection quantities,

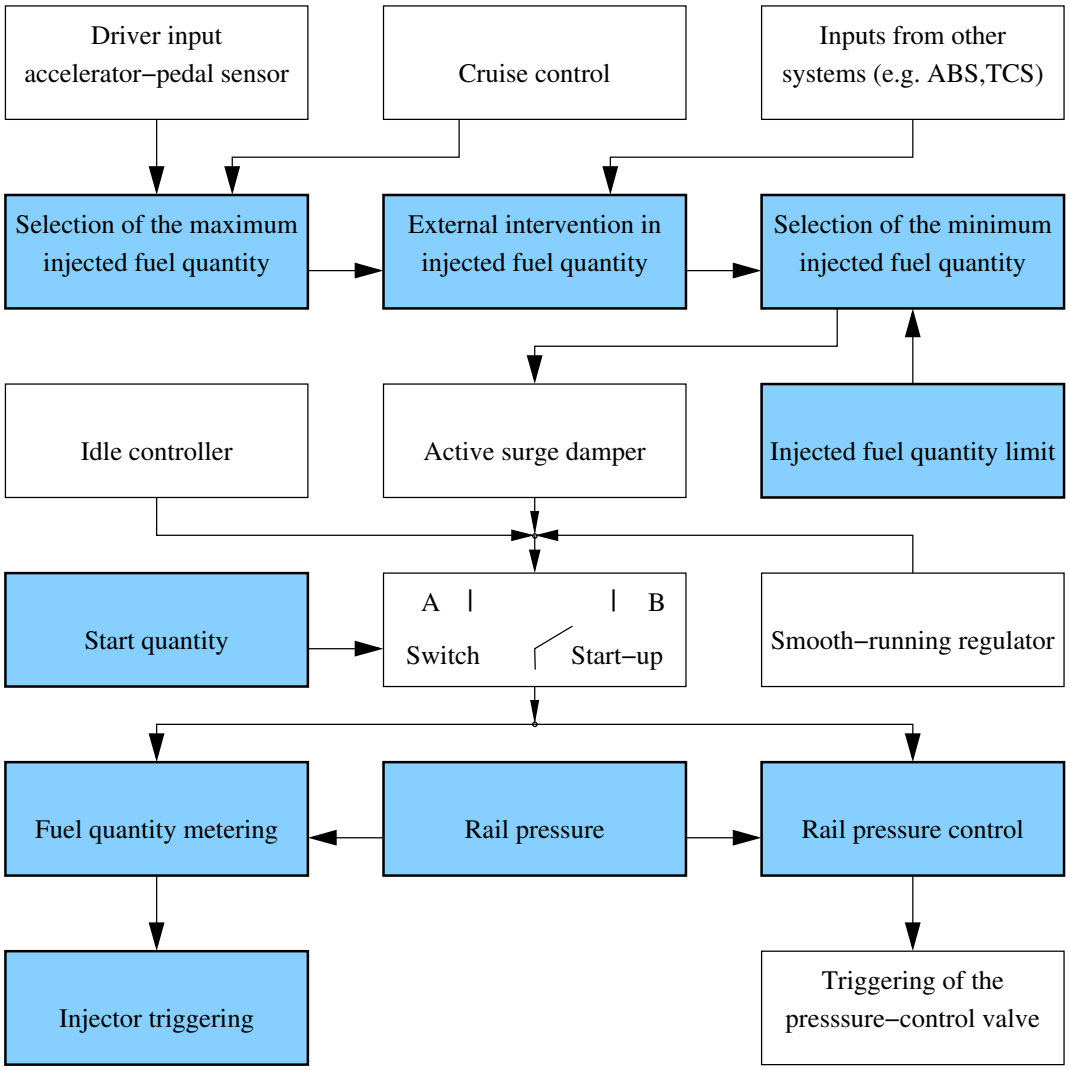

Figure 8.1: *A diagram representing a calculation in the ECU of the injected fuel quantity. Starting-switch position A: Start; starting-switch position B: Drive mode. [203]*

combustion parameters, noise and others were introduced into multi-objective algorithms to provide optimal operational parameters. It can be concluded that a similar approach can be applied to a CDI system operating on RSO. Complex modelling of the injection process or even the critical parts of the system (injector solenoid valves [71], injectors and injection pressure rail valve [198; 334], sensors and actuators [379], flow rates and injection timing [293] etc.) combined with sensitivity studies and influence of fuel properties can provide solutions for optimal RSO injection.

8.1.1 Recommendations for pilot and post injection modification

Because the injection pattern of CDI is much different from that of conventional in-line systems, it is considered that the desired operation conditions for cold start are also differ-

ent. In CDI injection pressure and timing can be controlled independently of engine speed and additionally the improvement of cold start-ability by using pilot injection [388; 401]. This leads to the advantage of using pilot injection in cold starts to improve the initial firing (compare to *Subsection 2.2.6*). Modification of the ECU must take into account these two injection modes.

It is known that pilot injection enhances the engine startup however the mechanism of pilot injection is quite specific, it requires very precise timing and metering of the pilot fuel quantity. Once injected fuel is atomised the fuel droplets absorb heat from the cylinder surroundings to evaporate. And it can be concluded that the larger quantity of fuel injected the more heat absorbed. As it can be seen, the temperature is considered to be the most important factor for initial firing in cold conditions the droplet evaporation affects the initial firing [64]. In some cases there is no firing because of the lower temperature. The described situation reflects on diesel fuel and thus the operation on RSO is expected to have even more serious difficulties. The advantage of pilot injection can only be maintained if the pilot fuel volume evaporates. In case of poor RSO evaporation, it is important to provide appropriate conditions to utilise the improvement of pilot injection. Otherwise, the system will not be fired and a gradual buildup of unburned RSO will take place. Initial timing as well as cylinder temperature after injection are every important for quick initial firing. Therefore, in the presence of RSO it is considered to modify the injection rate of even the way of injecting the pilot volume. There are two possible scenarios: one when the initial volume is reduced per injection, but injected in a couple of pilot injections. This approach utilises the CDI flexibility of multi-injection. And in the second case, when the injection timing is advanced and the injection pressure increased to ensure complete droplet evaporation. It was shown that advancing pilot injection timing causes pilot volume to disperse more readily [388] and thus it is highly desired. By increasing the time for initial firing in cold starts when the heating is problematic is expected to provide enough time for evaporation for the different RSO injection rate.

Both solutions feature advantages and drawbacks. Nevertheless, the modification of pilot injection should be taken into account. If the pilot injection is advanced, the combustion noise can increase for smaller pilot volumes less than 3 mm^3/stroke [388]. Again, such modifications can only be preformed by changing the ECU program and the final solution should be found by careful injection and combustion studies.

From the perspective of environmental protection it is extremely important to reduce

emissions of harmful components released during combustion of RSO. Especially the unburned HC from the engine during the start-up process is of a great concern. The problem lies in the fact that the formation of the HC is largely controlled by the temperature and the air/fuel mixture formation. With the conventional fuel, after the engine is started, the unburned HC emitted from the engine usually undergoes physical adsorption and desorption to the catalytic converter [184; 371]. In CDI engines with split injection strategy it is possible to reduce HC, soot and NO_x emissions simultaneously. This is possible by introducing post injection (described in details in *Subsection 2.2.6*). Post injection extends the combustion process and therefore the temperature drop is delayed and can provide a small amount of fuel utilised by the catalyst. As far as the first enhancement is understood the second case needs to be closely analysed if RSO is used.

Normally, the post injection quantities provide unburned diesel amounts, which after evaporation in the cylinder are evacuated together with products of the main injection. The mixture of exhaust gases and vaporised fuel travel towards catalyst where the catalytic combustion takes place. The process results in an almost complete decomposition of unburned HC. Although, results presented in *Subsection 6.6.5* did not reveal significant increase of unburned HC the problem can be more noticeable when the catalytic converter exceeds its lifetime. Furthermore, catalytic combustion takes place at low temperatures, hence NO_x formation is minimised. Quantities of post injection are relatively large (up to 20 mg/cycle [64]) and in the case of diesel the quantities are fully controlled and optimised by the ECU box. Utilisation of RSO imposes constraints on the idea of post injection. The chemical and physical constituency of RSO is basically different from diesel and it can be expected that RSO will not take part in catalytic combustion of the unburned HC. Simply speaking, if a small quantity of RSO is injected after the combustion process it is very likely that it will not completely evaporate and may reduce the efficiency of the catalyst. However, the presented theory has not been experimentally verified, but it is expected that the catalyst life may be affected by the post injected quantities of RSO. Therefore it is concluded that the post injection pattern should be revised and appropriate changes of the ECU program should be performed very possibly to avoid post injection. Again, it would required the unlimited access to ECU and very likely re-programming of its algorithms.

8.1.2 Recommendations for injection timing modification

For a diesel engine the sensitivity of the injection timing is a major parameter, which affects the engine performance, emissions and durability. Major NO_x concerns led to the search for possible ways of emission reduction by optimising injection timing as well as rate of injection. It has been recognised that retardation of injection timing is an effective way to reduce NO_x emissions. However, as NO_x is gradually increasing, fuel consumption increases radically and PM increases gradually. The deterioration of fuel consumption and the combustion are considered to increase the PM and this fact makes the adjustment of injection timing very complex. Although, the exhaust gas recirculation (EGR) system has been adopted as a way to reduce further levels of exhaust emissions [289] excessive buildup of NO_x is in the centre of attention for many engineers. Effects of injection timing on the influence of emissions are well recognised for conventional fuel as well as for diesel, but there is a need to analyse the influence of RSO on injection timing too.
The ignition delay and combustion characteristics are very sensitive to changes in injection timing at specific fuel properties. Moreover, plant oils are sensitive to the high temperatures at which they undergo chemical reactions such as thermal cracking of double-bond carbon chains and polymerisation [81; 351]. On the other hand it has been shown that a significant injection hesitation (delay) takes place when using RSO in comparison to diesel fuel (see *Subsection 6.2.5*) of a CDI system is used. A set of various factors is expected to affect the performance of CDI engines when RSO fuel is used, but a little has been done to explore the problem.

As it has been shown in *Subsection 8.1*, the injection CDI map can be optimised by building a mathematical function and implementing findings from RSO spray experimental studies. A similar set of functions could be constructed to describe RSO flow, heat transfer, low- and high-pressure delivery. By combining these two sets of multi-objective functions it is possible to find the optimal solution using optimisation procedures already applied to diesel. Methods of complex optimisation of the CDI system were presented and utilised in several studies [104]. Parameters like injection pressure and duration, injection quantities, combustion parameters, noise and others were introduced into multi-objective algorithms to provide optimal operational parameters. It can be concluded that a similar approach can be applied to a CDI system operating on RSO. Complex modelling of the injection process or even the critical parts of the system (injector solenoid valves [71], injectors and injection

pressure rail valve [197; 198; 334], sensors and actuators [379], flow rates and injection timing [293] etc.) combined with sensitivity studies and influence of fuel properties can provide solutions for optimal RSO injection. Some research presents different ways to optimise CDI system, [62; 65; 94; 117; 238; 317] but leading to almost the same results i.e. defining a set of operational or constructional variables, which need to be implemented for more efficient engine operation.

If the modification of CDI shall lead to emissions complying with Euro IV or V regulations, injection timing has to be adjusted to ensure acceptable emissions. From preliminary testing of the CDI engine it can be concluded that the CDI system applies the benefit of injection rate variation strategies and injection timing is adjusted automatically in accordance to new fuel, however NO_x emission remains higher than diesel (compare Figure 6.97). It is expected that to optimise the injection rate, the injected fuel amount during injection duration should be adjusted by the air swirl, engine speed and load and this can only be achieved by re-programming ECU. In general, to prevent the sharp increase of combustion pressure, initial injection rate should be low [289] but this collides with previous findings in *Section 6.2*,*6.3* and *6.5*, which show that elevated injection pressure should be applied. The task of injection timing optimisation is expected to be solved by more careful engine studies combined with the analysis of the ECU program.

One of the feasible injection and emissions control strategies is the optimisation of engine combustion with an improved combustion design and an adequate injection strategy. The effect of the combustion chamber shape (or the bowl geometry) on the diesel engine performance is very complex and frequently utilised to improve air/fuel mixture formation [70; 103; 151; 208]. The combustion chamber geometry influences not only the flow field, but also affects the wall impingement. The bowl geometry and dimensions, such as the pip region, the bowl lip area and the torus radius, are all known to have an effect on the in-cylinder mixing and combustion process. Construction of a new bowl geometry was utilised by Elsbett Company to design their DI diesel engine operating fully on RSO [168] by creating a unique high-swirl configuration. It has been shown that modification of the engine into a low heat rejection engine has improved the combustion of plant oil [331]. Combustion chamber optimisation should be performed for different fuel and operating conditions for many combinations using for instance KIVA code to optimise the combustion chamber geometry together with various engine operational input parameters. Similar work was already innitiated in *Chapter 5* where cold spray in a real CDI geometry was studied. The possible calculations could be based on re-designing the

high-swirl ports and re-entrant low-diameter bowl. The problem of impinging high velocity RSO observed in KIVA simulations could be overcome by exploring the effect of larger diameter bowls i.e. to allow more free spray travelling throughout the combustion chamber achieving an enhanced use of the oxygen and reducing the wall impingement [151]. It is expected that optimisation of the CDI cylinder is a way to minimise emissions and improve air/fuel mixture formation, which is essential in a case of RSO.

8.2 Recommendatios for additional future work

Throughout this PhD work it has been recognised that the study of the modification of CDI to operate on neat plant oils, represents a complex problem. As it was written in the *Introduction* the modification can be analysed by looking into technical and non-technical topics. Both groups require more detailed work, and in fact, should be accomplished separately. The text below encloses the main elements of study, which could be performed to widen the topic of the CDI modification and build up appropriate technical and non-technical know-how:

1. Studies on the availability of specific plant oils for various parts of the World and the long-term project of their prices in relation to crude oil prices, prices of food and local agriculture policy.

2. Analysis of the market of waste and fresh plant oils to establish the largest potential for plant oil supply. Evaluation of the cost to treat waste plant oils in order to bring them up to the required fuel standards would help to identify the competitiveness factor.

3. Consideration of single tank or two tank arrangement, which should be connected with the technical and economical assessement of the modification.

4. Investigation of the catalyst exposed to long-term engine tests and the impact of various oil types on it. Lifetime of the catalyst should be established and a possibility of eliminating the catalyst should be taken into account.

5. Extensive CDI engine test to be performed at various operational conditions and combined with measurements of engine performance, emissions and durability. The test should be performed on a long-term basis on different modification variants. The test should include records of servicing and engine tuning.

6. Investigation of wear and lubrication oil of the CDI engine subjected to a long-term driving and severe operational conditions.

In summary, it is believed that modification of the CDI engine can be performed successfully to ensure smooth operation and environmental friendliness. The main challenge is the implementation of the suggested modifications.

Literature

[1] *Dual PDA. Dantec UK Ltd. 1998.*

[2] Annual book of ASTM standards, part 23. Technical report, American Society for Testing of Materials, Philadelphia, 1979.

[3] *The KIVA-II computer program for transient multidimensional chemically reactive flows with sprays*. International Fuels and Lubricants Meeting and Exposition, November 1987.

[4] *The TAB method for numerical calculation of spray droplet breakup*, November 1987.

[5] Pilot project "Biodiesel": Summary. Technical report, Austrian Institute of Agricultural Engineering, Bundesanstalt für Landtechnik, Federal Institute of Agricultural Engineering, Wieselburg, Austria, 1991.

[6] Biodiesel performance trials: A final report. Technical report, Illinois Soybean Checko Board,Illinois Soybean Association, Bloomington, IL. International Energy Agency, 1994.

[7] *Experimental Study on a Diesel Spray of Multi-Stage Injection*, volume Proceedings of COMODIA 94, 1994.

[8] Kodak EKTAPRO HS Motion Analyser, Model 4540mx user manual., 1995.

[9] European energy to 2020. a scenario approach. Technical report, European Commision - DGXVII,Brussels, Belgium, 1996.

[10] Council directive to the quality of petrol and diesel fuel. Technical report, European Commission, January 2005 1997.

[11] Council directive to the quality of petrol and diesel fuel. Technical report, European Commission,Brussels, Belgium, 1997.

[12] Acea commitment on co_2 emissions reductions from new passenger cars in the Framework of an Environmental Commitment between the European Commission and ACEA. (available at www.acea.be/acea/co2emissionscars.html). Technical report, European Commission, 1998.

[13] Biodiesel 200. European Community Publications. Technical report, European Community Publications, 1998.

[14] Interim report on target standards for vehicle fuel consumption. Technical report, Japanese Ministry of Transport website, October 1998.

[15] Well-oiled: Europe's voracious appetite for oil burning cars is still spiralling. reported in fact of the week no. 136, july 17, 2000. Technical report, Automotive Industry Data Newsletter, No17,Office of Transportation Technologies, US Department of Energy, 2000.

[16] ETC spills technology database-oil properites database. Technical report, Environmental Technology Centre, 2001.

[17] United Kingdom oilseed and production. Technical report, Foreign Agricultural Service, 2001.

[18] DEFRA: Statistics website. Technical report, DEFRA, 2002.

[19] European commission announcement. Technical report, European Commission, Brussels, 2002.

[20] NFU publications. http://www.nfu.org.uk/pubs/sets.asp, 2004.

[21] Fuchs Petrolub AG-www.fuchs-oil.de (last accessed april 2006). Technical report, 2006.

[22] Private Communication. Technical report, ELSBETT Technologie GmbH, Summer 2002.

[23] IBM Research. *IBM Visualization Data Wxplorer Qucik Start Guide. Version 3 Release 1 Modification 4. SC34-3262-02*. IBM, 2002.

[24] A A Abdel-Rahman. On the emissions from internal-combustion engines: A review. *International Journal of Energy Research*, 22:483–513, 1998.

[25] Rafeef Abu-Gharbieh, John Persson, and Michael Försth. Compensating laser sheet images of optically dense sprays. In *Proceedings of the Swedish Symposium on Image Analysis, SSAB 1999*, 1999.

[26] Rafeef Abu-Gharbieh, John L Persson, Michael Försth, Arne Rosen, Andreas Karlström, and Tomas Gustavsson. Compensation method for attenuation planar laser images of optically dense sprays. *Applied Optics*, 39(8):1260–1267, 2000.

[27] R J Adrian. Particle-image technique for experimental fluid mechanics. *Ann Rev Fluid Mech*, 23:261–304, 1991.

[28] Kristina Ahlin. *Phd Thesis: Modelling of pressure waves in the Common Rail Diesel Injection System*. PhD thesis, Tekniska Högskolan i Linköping, 2000.

[29] S Ahmad. Oleochemicals and other non-food applications of palm oil and palm oil products. Technical report, PORIM, Kuala Lumpur, Malaysia, 1991.

[30] C A Allen and K C Watts. Comparative analysis of the atomization characteristics of fifteen biodiesel fuel types. *American Society of Agricultural Engineers*, 43(2):207–211, 2000.

[31] C W Allen and K C Watts. Experimental analysis of biodiesel atomization characteristics. *Canadian Agricultural Engineering*, 40:281–285, 1998.

[32] R Altin. *An experimental investigation on use of plant oils as diesel engine fuels*. PhD thesis, Gazi University Institute of Science and Technology, 1998.

[33] R Altin, S Cetinkaya, and H S Yucesu. The potential of using vegetable oil fuels as fuel for diesel engines. *Energy Conversion and Management*, 42(5):529–538, 2001.

[34] A A Amsden. The KIVA-3: A kiva program with block-structured mesh for complex geometries. Technical report, Los Alamos National Laboratory, 1993.

[35] A A Amsden. KIVA-3v: A block-structured KIVA program for engines with vertical or canted valves. Technical report, Los Alamos National Laboratory, 1997.

[36] A A Amsden. KIVA-3v, release 2, improvements to kiva-3v. Technical report, Los Alamos National Laboratory, 1999.

[37] A A Amsden, T D Butler, P J O'Rourke, and J D Ramshaw. KIVA: A comprehensive model for 2-d and 3-d engine simulations. *SAE Technical Paper*, 1985.

[38] A A Amsden, P J O'Rourke, and T D Butler. KIVA-II: A computer program for chemically reactive flows with sprays. Technical report, Los Alamos National Laboratory, 1989.

[39] A A Amsden, J D Ramshaw, L D Cloutman, and P J O'Rourke. Improvements and extensions to the KIVA computer program. Technical report, Los Alamos National Laboratory, 1985.

[40] A A Amsden, J D Ramshaw, P J O'Rourke, and J K Dukowicz. KIVA: A computer program for two- and three-dimensional fluid flows with chemical reactions and fuel sprays. Technical report, Los Alamos National Laboratory, 1985.

[41] R Aneja and J Abraham. How far does the liquid penetrate in a diesel engine: Computed results vs. measurements? *Combustion Science and Technology*, 138(6):233–255, 1998.

[42] F N Ani, M Lal, and A Williams. The combustion characteristics of palm oil and palm oil ester. *Proceedings of the Third International Conference on Small Engines and their Fuels for Use in Rural Areas*, 1990.

[43] L Araneo and A Coghe. Effect of injection conditions on penetration and drop size of HCCI Diesel sprays, 2002.

[44] L Araneo and C Tropea. Improving phase Doppler measurements in a Diesel spray. *SAE*, 3, 2000.

[45] C Arcoumanis, M Gaivaises, and B French. Effect of fuel injection processes on the structure of diesel sprays. *SAE*, (970799), 1997.

[46] Svajus Asadauskas, Joseph M Perez, and Larry J Duda. Oxidative stability and antiwear properties of high oleic vegetable oils. *Lubrication Engineering*, 52(12):877–882, 1996.

[47] ASAE. *Economics of on-farm production and use of plant oil for fuel*, August 1982.

[48] ASAE. *Evaluation of on farm press*. ASAE, 1982.

[49] ASAE. *The use of neat rapeseed oil in diesel engine*, April 1982.

[50] ASME, International Gas Turbine Conference and Exhibit, 30th. *Spatially resolved droplet size measurements*. ASME, March 1986.

[51] W D Bachalo and M J Hauser. Development of the Phase/Doppler spray analyser for liquid drop size and velocity characterisations. *Proc. AIIA/SAE/ASME 20th Joint Propulsions Conference*, 1984.

[52] Choongsik Bae, Jinsuk Kang, and Hang-Kyung Lee. Diesel spray development from VCO nozzles with common-rail. *American Society of Mechanical Engineers, Internal Combustion Engine Division (Publication) ICE*, 2001.

[53] S Baik, J Blanchard, and M Corradini. Development of micro-Diesel injector nozzles via mems technology and effects on spray characteristics. *Atomization and Sprays*, 13(5):211, 2001.

[54] J B Baisot and J Yon. Droplet size and morphology characterization for dense sprays by image processing: application to the Diesel spray. *Experiments in Fluids*, 39(6):977–994, 2005.

[55] A D Ball, F Gu, and W Li. The condition monitoring of diesel engines using acoustic measurements, Part 2: Fault detection and diagnosis. *SAE 2000 World Congress, Session: Noise & Vibration, Detroit, USA (SP-1514)*, 2000.

[56] S Bari, T H Lim, and C W Yu. Effect of preheating of crude palm oil (cpo) on injection system, performance and emission of a Diesel engine. *Renewable Energy*, 27(3):339–351, In press.

[57] S Bari, C W Yu, and T H Lim. Filter clogging and power loss issues while running a Diesel engine with waste cooking oil. *Proc Instn Mech Engrs, Part D: J Automobile Engineering*, 216(12):993–1001, 2002.

[58] D Bartholomew. Plant oil fuel. *JAOCS*, 58:286A–288A, 1981.

[59] R Basshuysen van, G Kromer, and R Brauder. Influence of swirl intensity and air flow on mean effective pressure and exhaust gas emissions of a small high speed DI Diesel engine. *IMechE*, 1982.

[60] Manfred Andreas Beeck and Werner Hentschel. Laser metrology-a diagnostic tool in automotive development processes. *Optics and Lasers in Engineering*, 34(2):101–120, 2000.

[61] Chehroudi Behrouz. Preliminary drop size and velocity measurements in a dense Diesel-type spray. *SAE Technical Paper Series*, 1990.

[62] P Belardini and C Bertoli. Multi-dimensional modeling of combustion and pollutants formation of new technology light duty diesel engines. *Oil And Gas Science and Technology Rev. IFP*, 54(2):251–257, 1999.

[63] R Bellman and R H Pennington. Effect of surface tension and viscosity on taylor instability. *Quarterly of Applied Mathematics*, 12:151–162, 1953.

[64] J Benajes, S Molina, and J M Garcia. Influence of pre- and post-injection on the performance and pollutant emissions in a HD Diesel engine. *SAE*, (0526), 2001.

[65] J Benajes, J V Pastor, R Payri, and A H Plazas. Analysis of the influence of Diesel

nozzle geometry in the injection rate characteristic. *Journal of Fluids Engineering, Transactions of the ASME*, 126(1):63–71, 2004.

[66] P Bergstrand and I Denbratt. Diesel combustion with reduced nozzle diameter. *SAE*, 2010, 2001.

[67] M T Bialkowski, T Pekdemir, M Brautsch, D Towers, and G Elsbett. Experimental analysis of rapeseed oil atomisation characteristics in a common-rail fuel injection system. *Proceedings of VAFSEP2004, Dublin, Ireland*, 2004.

[68] Michal Bialkowski. Private communication with Bosch GmbH and Delphi. Single hole injector., 2003.

[69] G M Bianchi, P Pelloni, E E Corcione, L Allocca, and F Luppino. Modeling atomization and drop breakup of high-pressure diesel sprays. *ASME Journal of Engineering for Gas Turbines and Power*, 123:419–42, 2001.

[70] G M Bianchi, P Pelloni, F E Corcione, E Mattarelli, and F L Bertoni. Numerical study of the combustion chamber shape for common rails H.S.D.I diesel engines. *SAE Paper*, 2000-01-1179, 2000.

[71] G M Bianchi, P Pelloni, F Filicori, and G Vannini. Optimization of the solenoid vlave behavior in common-rail injection systems. *SAE*, 2000-01-2042, 2001.

[72] Robert W Bilger. Advanced laser diagnostics in combustion for prototype and modelling development, 2000.

[73] Robert Bosch. *Diesel Fuel-Injection Systems Unit Injector System/Unit Pump System*. Bentley Publishers, 2000.

[74] Robert Bosch. *Diesel In-Line Fuel-Injection Pumps PE*. Robert Bosch, 2003.

[75] Robert Bosch. *Distributor-Type Diesel Fuel-Injection Pumps*. Bentley Publishers, 2003.

[76] Robert Bosch. *Diesel-engine Management*. Professional Engineering Publishing, 2004.

[77] Robert Bosch. Unit pump system (UPS)-web page. Technical report, Bosch GmbH, 2006.

[78] M Brautsch. The "Overall efficiency of supply" of various vegetable oils. *EuroSun'96 Proceedings*, 1996.

[79] G Bruneaux. Liquid and vapor spray structure in high-pressure common rail Diesel injection. *Atomization and Spray*, 11(5):533–556, 2001.

[80] J J Bruwer, B v.D Boshoff, F J Hugo, J Fuls, C Hawkings, A N Walt, A Engelbrecht, and L M du Plessis. Use of sunflower seed oil in diesel engined tractors. *Proceedings of the International Symposium on Alcohol Fuels Technology, Proceedings of the 4th International Symposium on Alcohol Fuels Technology*, 1980.

[81] T Callahan, T W Ryan III, L G Dodge, and J A Schwalb. Effects of fuel properties on diesel spray characteristics. *SAE Papers*, 1987.

[82] M Calvin. Fuel oils from higher plants. Technical report, Prepared for the U.S. Department of Energ, 1985.

[83] R Campanella, D Laforgia, A Ficarell, and V Damiani. Spray characteristics of five-hole VCO nozzles of a Diesel electro-injector. *SAE*, 103(3):100–119, 1994.

[84] Mustafa Canakci and Jon H Gerpen. Comparison of engine performance and emissions for petroleum diesel fuel, yellow grease biodiesel, and soybean oil biodiesel, 2001.

[85] Z M Cao, K Nishino, S Mizuno, and K Torii. PIV measurement of internal structure of Diesel fuel spray. *Experiments in Fluids*, 19:67–70, 1999.

[86] S P Carruthers, J S Marsh, P W Turner, F B Ellis, D J Murphy, T Slabas, and B A Chapman. Industrial markets for uk-produced oilseeds. *Research Review, Grown Cereals Authority*, 1995.

[87] T N Castro Dantas de, A C Silva da, and A A D Neto. New microemulsion systems using diesel and vegetable oils. *Fuel*, 80(1):75–81, 2001.

[88] S K Chen, A H Lefebvre, and J Rollbuhler. Factors influencing the effective spray cone angle of pressure-swirl atomisers. *Journal of Engineering for Gas and Turbines and Power*, 114(97):97, 1992.

[89] C P Chiu, Y P Chang, R F Horng, and W R Chen. Photographic study on air-assisted fuel spray in an optically-accessible cylinder of a test rig. *International Symposium COMODIA*, 1994.

[90] Chryssakis A Christos, Dennis N Assanis, Jee-Kuen Lee, and Keiya Nishida. Fuel spray simulation of high-pressure swirl-injector for DISI engines and comparison with laser diagnostic measurements. *SAE*, 01-0007, 2003.

[91] A Coghe and G E Cossali. Phase Doppler characterisation of Diesel spray injected in a high density gas under vaporization regimes, 1994.

[92] G S Collins, R C Griffin, and R D Lacewell. National economic implications of substituting plant oils for diesel fuel. Technical Report CONF-820860, Energy Citations Database, US, January 1982.

[93] Elsbett Company. Private Communications. Technical report, ELSBETT Technologie GmbH, 2003.

[94] Marco Coppo, Claudio Dongiovanni, and Claudio Negri. Numerical analysis and experimental investigation of a common rail-type diesel injector. *Journal of Engineering for Gas Turbines and Power*, 126:874, 2004.

[95] E Cossali and Y Hardalupas. Comparison between laser diffraction and phase Doppler velocimeter techniques in high turbidity, small diameter sprays. *Experiments in Fluids*, 13(6):414–422, 1992.

[96] Gianpietro E Cossali, Gianni Brunello, and Aldo Coghe. LDV characterization of air entrainment in transient Diesel sprays. *SAE Transactions*, 1991.

[97] R J Crookes, F Kiannejad, and M A A Nazha. Systematic assessment of combustion characteristics of biofuels and emulsions with water for use as diesel engine fuels. *Energy Convers. Mgmt.*, 38(15-17):1785–1795, 1997.

[98] C Crua, J C Evans, D A Kennaird, and M R Heikal. In-cylinder study of the formation, autoignition and soot production of Diesel sprays at elevated pressures, 2003.

[99] C Crua, D A Kennaird, S S Sazhin, M R Heikal, and M R Gold. Diesel autoignition at elevated in-cylinder pressures. *International Journal of Engine Research*, 5(4):365–374, 2004.

[100] N Damaschke, G Gouesbet, G Grehan, H Mignon, and C Tropea. Response of PDA systems to non-spherical droplets, 1997.

[101] T Dan, S Takagishi, N Ohishi, and Y Fujimoto. Spray structure in diesel fuel spray with high injection pressure. *Trans. Japan Soc. Mech. Eng.*, 1996.

[102] A de Risi and D Laforgia. Theoretical investigation on variable-density sprays. *Atomization and Sprays*, 12(1-3):363, 2002.

[103] A de Risi, D F Manieri, and D Laforgia. A theoretical investigation on the effects of combustion chamber geometry and engine speed on soot and no_x. *ASME*, 2001.

[104] Arturo de Risi, Paolo Carlucci, Teresa Donateo, and Antonio Ficarella. A combined optimization method for common rail diesel engines. *ASME*, 2002.

[105] Arturo de Risi, Gianpiero Colangelo, and Domenico Laforgia. An experimental study of high pressure nozzles in consideration of hole-to-hole spray abnormalities. *SAE*, (2000-01-125-), March 2001.

[106] Arturo de Risi, Raffaella Di Sante, and Gianpiero Colangelo. Optical characterization of a Diesel spray at high temperature and pressure. Technical report,

Dipartimento di Ingegneria dell'InnovazioneUniversità degli Studi di Lecce,, Lecce, 2004.

[107] Arturo de Risi and Domenico Laforgia. Preliminary results of the transformation of a car's DI Diesel engine in to a dual fuel one with common rail injection. *ASME*, 1999.

[108] E Delacourt, B Desmet, and B Besson. Characterisation of very high pressure Diesel sprays using digital imaging techniques. *Fuel*, 84(7-8):859–867, 2005.

[109] A Demirbas. Fuel properties and calculation of higher heating values pf vegetable oils. *Fuel*, 77(9-10):1117–1120, 1998.

[110] Ayhan Demirbas. Fuel properties and calculation of higher heating values oils. *Fuel*, 77(9-10):1117–1120, 1998.

[111] J Dent. A basis of the comparison of various experimental methods for studying spray penetration. *SAE*, 1971.

[112] J M Desantes, J V Pastor, R Payri, and J M Pastor. Experimental characterisation of internal nozzle flow and Diesel spray behaviour. Part II: evaporative conditions. *Atomization and Sprays*, 2005.

[113] Lee G Dodge. Calibration of the malvern particle sizer. *Applied Optics*, 23(14):2415–2419, 1984.

[114] Lee G Dodge, Deborah J Rhodes, and Rolf D Reitz. Drop-size measurement techniques for sprays: comparison of Malvern laser-diffraction and Aerometrics phase doppler. *Applied Optics*, 26(11):2144–2154, 1987.

[115] Lee G Dodge, Thomas W. III Ryan, and Michael G Ryan. Effects of different injector hole shapes on Diesel sprays. *SAE Technical Paper Series*, (SAE Paper), 1992.

[116] R Domann, Y Hardalupas, and A R Jones. A study of the influence of absorption on the spatial distribution of fluorescence intensity within large droplets using Mie theory, geometrical optics and imaging experiments. *Meas. Sci. Technol.*, 2002.

[117] Teresa Donateo, Arturo de Risi, and Domenico Laforgia. Optimization of high pressure common rail electro-injector using generic algorithms. *SAE*, SAE Paper 2001-01-1980, 2001.

[118] A Doudou. Turbulent flow study of an isothermal Diesel spray injected by a common rail system. *Fuel*, 84(2-3):287–298, 2005.

[119] R M Douglas, D A Hymers, J A Steel, and R L Reuben. Source identification of piston ring and cylinder liner interaction using acoustic emission. *Proceeding of the 17^{th} International Conference on Condition Monitoring and Diagnostic Engineering Management, COMADEM, Cambridge, UK*, 2004.

[120] R M Douglas, J A Steel, R L Reuben, and T L Fog. On-line power estimation of large diesel engines using acoustic emission and instantaneous crankshaft angular velocity. *Internaltional Journal of Engine Research*, 7(5):399–410, 2006.

[121] J A Duke. The quest for tolerant germplasm. crop tolerance to suboptimal land conditions. *ASA Special Publication,American Society for Agronomy*, 32:1–61, 1978.

[122] J K Dukowicz. A particle-fluid numerical model for liquid sprays. *J. of Computational Physics*, 35:229–253, 1980.

[123] J R Dunn and A Schneeberger. Economic implications for the potential development of a plant oil fuel industry. *Plant oil fuels, Proceedings of the International Conference on Plant and Plant Oils as Fuels*, 8:149–158, 1982.

[124] P D Dunn and W Jompakdee. Measurement of the rate of carbon build-up in diesel engines employing plant oil fuels. *Proceedings of the Third International Conference on Small Engines and their Fuels for Use in Rural Areas*, 1990.

[125] P D Dunn and E D I H Perera. The effect of viscosity and other properties of vegetable oil fuels on spray characteristics. *Proc 2nd International Conf. On Small Engines and their Fuels in Developing Countries*, 1987.

[126] Robert O Dunn and Marvin O Bagby. Low-temperature filterability properties of alternative diesel fuels from vegetable oils. *Fuel and Energy Abstracts*, 38(5):330–330, 1997.

[127] F Durst and M Zare. Laser Doppler measurements in two phase flows. *Proc. LDA-Symp., Copenhagen*, A76-45326 23-35:403–429, 1975.

[128] F Dust, A Melling, and J H Whitelaw. *Principles and practice of Laser-Doppler Anemometry*. Academic Press, 1981.

[129] J Dykyj, J Svoboda, R C Wilhoit, M Frenkel, and K R Hall. *Landolt-Boernstein:Vapor Pressure and Antoine Constants for Hydrocarbon, and Sulfur, Selenium, Tellurium, and Halogen Containing Organic Compounds*. Springer-Verlag, 1999.

[130] D L Dyne van, M G Blase, and K D Carlson. Industrial feedstocks and products from high Erucic Oil: Crambe and industrial rapeseed. Technical report, Univ. Missouri, Columbia, MO, 1990.

[131] D L Dyne van, J A Weber, and C H Braschler. Macroeconomic effects of a community-based biodiesel production system. *Bioresource Technology*, 56(1):1–16, 1996.

[132] A C Eckbreth. *Laser diagnostics for combustion temperature and species*. Gordon and Breach, 1996.

[133] F Eisfeld. Investigation of the penetration, the spreading, and the atomization of a Diesel injection jet using high speed cinematography. *Proceedings of 25th International Congress of High-Speed Photography and Photonics*, 2003.

[134] M S El-Beshbeeshy, J T Hodges, and M L Corradini. Image analysis of Diesel sprays. *SAE Transactions*, 101(33):1634–1647, 1992.

[135] M El-Ghamry, J A Steel, R L Reuben, and T L Fog. Indirect measurement of cylinder pressure from diesel engines using acoustic emission. *Mechanical Systems and Signal Processing*, 19(4):751–765, 2005.

[136] M H El-Ghamry, R L Reuben, and J A Steel. The development of automated pattern recognition and statistical feature isolation techniques for the diagnosis of reciprocating machinery faults using acoustic emission. *Mechanical Systems and Signal Processing*, 17(4):805–823, 2003.

[137] J L Emil and S Winnett. Biomass and global climate change: An overview. u.s. epa climate change division, washington, dc 20460, 1995.

[138] C R Engler, L A Johnson, W A Lepori, and C M Yarbrough. Effects of processing and chemical characteristics of plant oils on performance of an indirect-injection diesel engine. *Journal of the American Oil Chemists' Society*, 60(8):1592–1596, 1983.

[139] M Fangrui and A H Milford. Biodiesel production: a review. *Bioresource Technology*, 70:1–15, 1999.

[140] P V Farrell and M S Beckman. Vapor phase imaging of Diesel fuel sprays from a common rail injector. Technical report, Engine Research Center, University of Wisconsin-Madison, 2000.

[141] P G Felton, A A Hamidi, and A K Aigai. Measyrement of drop-size distribution in dense sprays by laser diffraction. *Proceedings, ICLASS-85, Third International Conference on Liquid Atomisation and Spray Systems (The Institute of Energy, London)*, 1985.

[142] E Ferchau. Equipment for decentralised cold pressing of oil seeds. Technical report, Folkecenter for Renewable Energy, Denmark, 2000.

[143] A Ficarella, D Laforgia, G Starace, and V Damiani. Experimental investigation of the sprays of an axi-symmetric nozzle of a common-rail high pressure electro-injector. *SAE*, 970054, 1997.

[144] FISITA. *Ambient temperature and fuel effects on DI and IDI diesel cold start emissions*, volume I. Proc. XXIII FISITA Congress, May 1990.

[145] T L Fog, E R Brown, H S Hansen, L B Madsen, P Sorensen, E R Hansen, J A Steel, R L Reuben, and P S Pedersen. Exhaust valve leakage detection in marine diesel engines. *Proceeding of the 11th International Conference on Condition Monitoring and Diagnostic Engineering Management, COMADEN, Australia*, 1998.

[146] T L Fog, L K Hansen, J Larsen, H S Hansen, L B Madsen, P Sorensen, E R Hansen, and P S Pedersen. On condition monitoring of exhaust valves in marine diesel engines. *Neural Networks for Signal Processing - Proceedings of the IEEE Workshop*, 1999.

[147] E F Fort and P N Blumberg. Performance and durability of a turbocharged diesel fuelled with cottenseed oil blends. *The International Conference on Plant and Vegetable Oils as Fuels, American Society of Agricultural Engineers)*, 1982.

[148] T A Fox and J Stark. Characteristics of miniature short-tube orifice flows. *Proc. Inst. Mech. Eng.*, 203(C5):351–358, 1989.

[149] Hajime Fujimoto, Dae Choi, Yuta Shima, and Jiro Senda. Two-dimensional imaging of fuel-vapour concentration by use of LIEF technique during mixture formation process in a DI Diesel engine. *Measurement Science and Technology*, 13:391–400, 2002.

[150] Z Gao and W Schreiber. The effect of EGR and split fuel injection on Diesel engine emission. *International Journal of Automotive Technology*, 2(4):123, 2001.

[151] M Gavaises, A Theodorakakos, and G Bergeles. Modelling wall impact of diesel sprays. *Int. J. Heat and Fluid Flow*, 17(2):130–138, 1996.

[152] T Gemci, J Hom, and N Chigier. Experimental study of evaporating full-cone spray by determining droplet temperature with rainbow refractometry and comparing with numerical simulation, 2000.

[153] Tevfik Gemci, James Hom, and Norman Chigier. Simulation of evaporating spray and comparison with droplet temperature measurement obtained by rainbow refractometer. *Proceedings of ASME Fluid Engineering Division*, 2000.

[154] P N Giannelos, F Zannikos, S Stournas, E Lois, and G Anastopoulos. Tobacco seed oil as an alternative diesel fuel: physical and chemical properties. *Industrial Crops and Products*, 16(1):1–9, 2002.

[155] J D Gill, R L Reuben, M Scaife, E R Brown, and J A Steel. Detection of diesel engine faults using acoustic emission. *Proceedings of the 2nd International Conference: Planned Maintenance, Reliability And Quality*, 1998.

[156] J D Gill, R L Reuben, M W Scaife, and J Asquith. A study of small HSDI diesel engine fuel injection equipment faults using acoustic emission. *Journal of Acoustic Emission (USA)*, 18:211–216, 2001.

[157] C E Goering, A W Schwab, M J Daugherty, E H Pryde, and A J Heakin and. Fuel properties of eleven vegetable oils. *Trans. ASAE*, 25:1472–1483, 1982.

[158] Carroll E Goering and Bob Fry. Engine durability screening test of a diesel oil/soy oil/alcohol microemulsion fuel. *JAOCS, Journal of the American Oil Chemists' Society*, 10(16):1627–1632, 1983.

[159] H J Goettler, R F Harwood, M Ziejewski, and H J Klosterman. On the thermal decomposition and residue formation of plant oils. *SAE, International Fuels and*

Lubricants Meeting and Exposition, 1986.

[160] V Golovitchev, N Nordin, R Jarnicki, and J Chomiak. 3-d diesel spray simulations using a new detailed chemistry turbulent combustion model. Technical Report 00FL-447, Chalmers University of Technology - Sweden, 2002.

[161] M A Gonzale, Z W Lian, and R D Reitz. Modeling Diesel engine spray vaporization and combustion. *SAE*, 920579, 1992.

[162] R C Gonzalez and P Wintz. *Digital Image Processing*. Wiley-Interscience, 1992.

[163] J W Goodrum and M A Eiteman. Physical properties of low molecular weight triglycerides for the development of bio-diesel fuel models. *Bioresource Technology*, 1996.

[164] M S Graboski and R L McCormick. Combustion of fat and vegetable oil derived fuels in diesel engines. *Progress in Energy and Combustion Science*, 24(2):125–164, 1998.

[165] G Grassi and T Bridgwater. Biomass for energy and environment, agriculture and industry in europe: A strategy for the future. Technical report, Commission of the European Communities, Directorate General for Science Research and Development, 1992.

[166] L V Griend, M E Feldman, and C L Peterson. Modelling combustion of alternative fuels in a DI diesel engine using kiva. *Transactions of the ASAE*, 33(2):342–350, 1990.

[167] Vander Griend, L M Feldman, and C L Peterson. Properties of rape oil and its methyl ester relevant to combustion. *ASAE Paper*, (88-6507), 1988.

[168] Elsbett Group. Elsbett GmbH Web Page - www.elsbett.com (accessed in may 2006). Technical report, Elsbett Company, 2004.

[169] GGA Group. GAA Performance Measuring Products, http://www.roadtune.co.uk/ (the last access may 2006). Technical report, GAA Performance Measuring Products, 2006.

[170] F Gu, A D Ball, and K K Rao. Prediction of injection parameters from monitoring vibration. *Proceeding IMechEng.*, 210(4):303–312, 1996.

[171] F Gu, W Li, A D Ball, and A y Leung. The condition monitoring of diesel engines using acoustic measurements, Part 1: Acoustic characteristics of the engine and representation of the acoustic signals. *SAE 2000 World Congress, Session: Noise & Vibration, Detroit, USA (SP-1514)*, 2000.

[172] M Gürü, U Karakaya, D Altiparmak, and A Alicilar. Improvement of Diesel fuel properties by using additives. *Energy Conversion and Management*, 43(8):1021–1025, 2002.

[173] D Gust. Why study photosynthesis? asu photosynthesis center, world wide web information page, 1995.

[174] M R Halder, S K Dash, and S K Som. A numerical and experimental investigation on the coefficients of discharge and the spray cone angle of a solid cone swirl nozzle. *Experimental Thermal and Fluid Science*, 28(4):297–305, 2004.

[175] D C Hammond Jr. Deconvolution technique for line-of-sight optical scattering measurements in axisymmetic sprays. *Applied Optics*, 20(3):493–499, 1981.

[176] Z Han, R D Reitz, F E Corcione, and G Valentino. Interpretation of k-epsilon computed turbulence length-scale prediction for engine flows. *Proceedings of 26th Symposium On Combustion, The Combustion Institute*, 1996.

[177] Y Hardalupas and S Horender. Phase Doppler anemometer for instantaneous measurements of droplet concentration, 2000.

[178] Y Hardalupas, A.M.K P Taylor, A.M.K.P, and J H Whitelaw. Characteristics of the spray from a Diesel injector. *International Journal of Multiphase Flow*,

18(2):159–179, 1992.

[179] Y Hardalupas, R F Tsai, and J H Whitelaw. Spray unsteadiness in coaxial arirblast atomizers. in heat transfer in fire and combustion systems. *ASME, HTD*, 1996.

[180] K J Harrington. Chemical and physical properties of plant oil esters and their effect on diesel oil performance. *Biomass*, 9(11):1–17, 1986.

[181] H J Harwood. Oleochemicals as a fuel: Mechanical and economic feasibility. *Journal of the American Oil Chemists' Society*, 61(2):315–324, 1984.

[182] F Hattori, K Takeda, T Yaegashi, and A Harada. Analysis of fuel and combustion behaviour during cold starting of SI gasoline engine. *JSAE Review*, 18(4):351–359, 1997.

[183] N Hay and J L Jones. Comparison of the various correlations for spray penetrations. *SAE*, 720776, 1972.

[184] Ronald M Heck and Robert J Farrauto. Automobile exhaust catalysts. *Applied Catalysis A: General*, 221(1-2):443–457, 2001.

[185] N Hemmerlein, V Korte, and H Richter. Performance, exhaust emissions and durability of modern Diesel engines running on rapeseed oil. *SAE Transactions*, SAE Paper 910848, 1991.

[186] W Hentschel and K P Schindler. Flow, spray and combustion analysis by laser techniques in the combustion chamber of a direct-injection Diesel engine. *Optics and Laser in Engineering*, 25(6):401–413, 1996.

[187] C Herrmann. Erprobung eines Common-Rail Einspritzsystems in Betrieb mit naturbelassenem Pflanzenol. Master's thesis, Fachhochschule Amberg-Weiden, 2003.

[188] M Herrmann. Modeling primary breakup: A three-dimensional eulerian level set/vortex sheet method for two-phase interface dynamics. *Center for Turbulence Research - Annual Research Briefs*, 2003.

[189] Peter L Herzog and Rainer R Cichocki. Will the HSDI Diesel engine meet the legislative challenges of EUROIII/IV? *Fisita World Automotive Congress. Paris, September 27-October 1*, 1998.

[190] T L Herzog and P Gutmann. EURO iv and the HSDI-An integrated vehicle approach. *Proceedings of The 15th Internal Combustion Engine Symposium (International)*, 1999.

[191] F Hildenbrand, C Schulz, J Wolfrum, F Keller, and E Wagner. Laser diagnostic analysis of no formation in a direct injection Diesel engine with pump-line-nozzle and common rail injection systems. *Proceedings of the Combustion Institute*, 2000.

[192] H Hiroyasu and M Arai. Fuel spray penetration and spray angle in Diesel engines. *Trans. SAE Japan*, 44(385):3208–3220, 1980.

[193] H Hiroyasu and M Arai. Structure of fuel sprays in Diesel engines. *Transactions of the SAE*, SAE 900475, 1990.

[194] Ki Bae Hong, Hong Sun Ryou, and Seong Hyuk Lee. The influence of breakup time constant and cavitation modeling on numerical simulation of high-pressure Diesel sprays. *ILASS-Asia, Annual Conference of Liquid Atomisation and Spray Systems, Tsukuba, Japan, 14-15 Dec. 2002*, 2000.

[195] H Hosoya and T Obokata. Effect of nozzle configuration on characteristics of steady-state Diesel spray. *SAE Special Publication - Diesel Combustion Processes*, 1993.

[196] Y Hotta, K Nakakita, M Inayoshi, T Ogawa, T Sato, and M Yamada. Combustion improvement for reducing exhaust emissions in IDI diesel engine. *JSAE Review*, 18(1):19–31, 1997.

[197] D T Hountalas. Available strategies for improving the efficiency of di diesel engines - a theoretical investigation. *SAE*, SAE Paper 2000-01-1176, 2000.

[198] D T Hountalas and A D Kouremenos. Development of a fast and simple simulation model for the fuel injection system of diesel engines. *Advances in Engineering Software*, 29(1):13–28, 1998.

[199] L P Hsiang and G M Faeth. Drop deformation and breakup due to shock wave and steady distrubances. *International Journal of Multiphase Flow*, 21(4):545–560, 1995.

[200] J S Hwang, J S Ha, and S Y No. Spray characteristics of DME in conditions of common-rail injection system(II). *International Journal of Automotive Technology*, 4(3):119124, 2003.

[201] J W Hwang, H J Kal, J K Park, M H Kim, Liu Shenghua, and J O Chae. A study on the effect of injection reate on emission characteristics of DI Diesel engines by a multizone model. *Proceedings of The 15th International Combustion Engine Symposium (International), Seul, Korea, July 13-16 1999*, 1999.

[202] E A Ibrahim, H Q Yang, and A J Przekwas. Modeling of spray droplets deformation and breakup. *AIAA Journal of Propulsion and Power*, 9(4):651–654, 1993.

[203] Ralf Isenburg, Micha Münzenmay, and H Kull. *Diesel accumulator fuel-injection system Common Rail*. Robert Bosch GmbH, 1999.

[204] N Ishikawa and L Zhang. A new observation technique for measuring airflow motion around the Diesel fuel spray. *Technical Nores/JASAE Review*, 20(3):425–427, 1999.

[205] A Isigigür, F Karaosmanoglu, H A Aksoy, F Hamdullahpur, and L Ö Gülder. Performance and emission characteristics of a diesel engine operating on sunflower seed oil methyl ester. *Applied Biochemistry and Biotechnology*, 45-46(1):93–102, 1994.

[206] T A Jackson and G S Samuelsen. Performance comparison of two interferometic droplet sizing techniques. *Proc. Photo-Opt*, A87-11045 01-35:73–79, 1984.

[207] J E Jimenez, C Mendez, F Castro, F V Tinaut, and B Gimenez. Experimental comparison between conventional and bio-derived fuel sprays. *SAE*, 2001-01-1072, 2001.

[208] R J R Johns. Calculation of diesel combustion in idealised chambers. *International Symposium COMODIA 94*, 1994.

[209] Sam Jones and Charles L Petersen. Using unmodified vegetable oils as a Diesel fuel extender - a literature review, 2002.

[210] R W Jorach, H Doppler, H Ressel, and W Scheibe. Common rail application for medium speed engines: the answer from the fuel injection system supplier on the customers' demands. *International Council on Combustion Engines*, not known.

[211] T Kaimai, H Tsunemoto, and H Ishitani. Improvement of SOF emission in a small direct injection Diesel engine. *JSAE Review*, 18(2):201–202, 1998.

[212] T Kamimoto. Diagnostics of transient sprays by means of laser sheet techniques. *International Symposium COMODIA 94*, 1994.

[213] J Kang, S Choi, and C Bae. Spray characteristics of high-pressure injectors for HSDI Diesel engines. *Proceedings of The 15th Internal Combustion Engine Symposium (International)*, 1999.

[214] F Karaosmanoglu, A Isigigur, F Hamdullahpur, O L Gulder, and A Aksoy. Used canola oil as diesel fuel alternative, 1993.

[215] J T Kashdan, J S Shrimpton, H J Booth, and A Whybrew. Assessment of particle characterisation via phase Doppler anemometry and automated particle image analysis techniques. In *10th International Symposium on Applications of Laser Techniquies to Fluid Mechanics*, volume 10, pages 1–13, 2000.

[216] M Kato, H Kano, K Date, T Oya, and K Niizuma. Flow analysis in nozzle hole in consideration of cavitation. *SAE Paper*, 970052, 1997.

[217] K R Kaufmann, M Ziejewski, G L Pratt, and H L Goettler. Fuel injection anomalies observed during long term engine performance tests on alternative fuels. *Society of Automotive Engineers*, 1985.

[218] H Kazunori, T Tetsuya, T Eii, and T Yoshihiro. Performance and emission characteristics of a swirl-chamber diesel engine with emulsified rapeseed oil fuels. *Nippon Kikai Gakkai Ronbunshu, B Hen/Transactions of the Japan Society of Mechanical Engineers*, 1997.

[219] D A Kennaird, C Crua, J Lacoste, M R Heikal, M R Gold, and N S Jackson. In-cylinder penetration and break-up of Diesel sprays using a common-rail injection system. *SAE*, 2002-01-1626, 2002.

[220] K D Kihm, D P Terracina, and J A Caton. Spray-tim droplet SMDs of intermittent high-pressure sprays of Diesel fuel compared with coal-water slurry sprays. *Journal of the Institute of Energy*, 1995.

[221] Y M Kim and T S Wang. Numerical studies on droplet breakup models. *Journal of Propulsion and Power*, 11(2):389–392, 1995.

[222] R J.H Klein-Douwel, M Douch, L M.T Somers, W A de Boer, and R S.G Baert. Visualization of Diesel fuel sprays in a high pressure, high temperature cell under engine-line conditions. *Proceedings of the European Combustion Meeting*, 2003.

[223] M Kondo, S Kimura, I Hirano, Y Uraki, and R Maeda. Development of noise reduction technologies for small direct-injection Diesel engines. *JSAE Review*, 21(3):327–333, 2000.

[224] S C Kong, P K Senecal, and R D Reitz. Developments in spray modeling in diesel and direct-injection gasoline engines. *Oil and Gas Science Technology*, 54(2):197–204, 1999.

[225] W Körbitz. Biodiesel production in europe and north america, an encouraging prospect. *Renewable Energy*, 16(1-4):1078–1083, 1999.

[226] R A Korus, J Jo, and C Peterson. A rapid engine test to measure injector fouling in diesel engines using vegetable oil fuels. *JAOCS*, 62(11):1563–1564, 1985.

[227] R A Korus, T L Mousetis, and L Lloyd. Polymerization of plant oils, 1982.

[228] H J Koss, A Wiartalla, and H Bäcker. Spray propagation, mixture formation, auto-ignition and soot formation of multi-component fuels in in a pressure chamber. *IDEA-EFFECT 2nd periodic report*, 1993.

[229] P N Kotsiopoulos and E A Yfantis. The behaviour of a small direct injection diesel engine using waste olive oil as a fuel supplement. *In Proceedings of 5^{th} International Conference on Small Engines, their Fuels and the Environment, 5-7 April 1995*, 1995.

[230] J Krahl, J Bunger, O Shroder, A Munac, and G Knothe. Exhaust emissions and health effects of particulate matter from agricultural tractors operating on rapeseed oil methyl ester. *JAOCS, Journal of the American Oil Chemists' Society*, 79(7):717–724, 2002.

[231] Jurgen Krahl, Axel Munack, Mufit Bahadir, Leon Schumacher, and Nancy Elser. Review: Utilization of rapeseed oil, rapeseed oil methyl ester or diesel fuel: exhaust gas emissions and estimation of environmental effects. *SAE*, SAE Paper 962096, 1996.

[232] H Kuniyoshi, H Tanabe, G T Sato, and H Fujimoto. Investigation on the characteristics of Diesel fuel sprays. *SAE*, 13(5):357–363, 1980.

[233] Koteswara Rao Kunkulagunta. Video imaging and analysis of common rail sprays in an optical engine using shadowgraphy technique. *SAE*, 109(3):1528–1537, 2000.

[234] T W Kuo. Evaluation of a phenomenological spray-combustion model for two open-chamber diesel engines. *SAE Paper*, 872057, 1987.

[235] W Kuorbitz. Utilization of oil as a biodiesel fuel. *CAB International*, 1995.

[236] K Kurachi, T Serizawa, K Wada, S Kato, and H Ito. Investigation of measurement of Diesel spray breakup length by using Doppler signals. *SAE*, -(24):5–8, 2001.

[237] Karl A Kusters, Johan G Wijers, and Dirk Thoenes. Particle sizing by laser diffraction spectrometry in the anomalous regime. *Applied Optics*, 30(33):4839–4847, 1991.

[238] X l Seykens, L M Somers, and R S Baert. Modelling of common rail fuel injection system and influence of fluid properites on injection process. *Proceedings of VAFSEP2004, 6-9 July 2004, Dublin, Ireland*, 2004.

[239] J Lacoste, C Crua, M Heikal, and D Kennaird. PDA characterisation of dense Diesel sprays using a common-rail injection system. *SAE Transactions*, 112(4):2074–2085, 2003.

[240] J Lacoste, D Kennaird, S Begg, and M R Heikal. Phase Doppler anemometry measurements of a Diesel spray, 2002.

[241] O Laguitton, M Gold, D Kennaird, C Crua, J Lacoste, and M Heikal. Spray development and combustion characteristics for common-rail Diesel injection systems, 2002.

[242] C C Landreth and R J Adrian. Electro-optical image shifting for particle image velocimetry. *Applied Optics*, 27:4216–4220, 1988.

[243] C C Landreth, R J Adrian, and C S Yao. Double pulse particle image velocimetry with directional resolution for complex flows. *Experiments in Fluids*, 6(2):119–128, 1988.

[244] P Le Gal, N Farrugia, and D A Greenhalgh. Laser sheet dropsizing of dense sprays. *Optics & Laser Technology*, 31(112):75–83, 1999.

[245] C S Lee and S W Park. An experimental and numerical study on fuel atomization characteristics of high-pressure Diesel injection sprays. *Fuel*, 81(18):2417–2423, 2002.

[246] Chang Sik Lee, Ki Hyung Lee, Chon Soo Mun, and Kim Sik Dae. Spray structure and characteristics of high-pressure gasoline injectors for direct-injection engine applications. *Atomization and Sprays: Journal of the International Institutions for Liquid Atomization and Spray Systems*, 11, 2001.

[247] H S Lee and K M Lee. Optimization of combustion system for heavy duty diesel engine equipped with common rail fuel injection system. *Proceedings of The 15th Internal Combustion Engine Symposium (International)*, 1999.

[248] J Lee, H Akiyama, and N Iida. Analysis of hight-pressure fuel injection and a micro-nozzle spray combustion using a rapid compression machine. *Proceedings of The 15th Internal Combustion Engine Symposium (International)*, 1999.

[249] K Lee and R Reitz. Investigation of spray charasteristics from a low-pressure common rail injector for use in homogenous charge compression ignition engine. *Measurement Science and Technology*, 15:509–519, 2004.

[250] S W Lee, J Kusaka, and Y Daisho. Spray characteristics of alternative fuels in constant volume chamber (comparison of the spray characteristics of LPG, DME and n-dodecane). *JSAE Review*, 2001.

[251] N Levy, S Amara, and J C Champoussin. Simulation of a diesel jet assumed fully atomized at the nozzle exit. *SAE*, 107(3):1642–1653, 1998.

[252] A B Liu, D Mather, and R D Reitz. Modeling the effects of drop drag and breakup on fuel sprays. *SAE Technical Paper*, 930072, 1993.

[253] G Lohmann. BioCar Web Page. www.biocar.de (last accessed on may 2006). Technical report, BioCar, 2006.

[254] B R Long and K D Boutin. Enhancing the process of diesel engine condition monitoring. *Proceeding of Technical Conference, American Society of Mechanical Engineers, Internal Combustion Engine Division, ICE*, 1996.

[255] H T C Machacon, S Shiga, T Karasawa, and H Nakamura. Performance and emission characteristics of a diesel engine fuelled with coconut oil-diesel fuel blend. *Biomass and Bioenergy*, 20(1):63–69, 2001.

[256] Andrew G MacPhee, Mark W Tate, Christopher F Powell, Yong Yue, Matthew J Renzi, Alper Ercan, Suresh Narayanan, Ernest Fontes, Jochen Walther, Johannes Schaller, Sol M Gruner, and Jin Wang. X-ray imaging of shock waves generated by high-pressure fuel sprays. *Science*, 2002.

[257] Milan Marcic. Diesel spray liquid phase measuring device. *Sensors and Actuators*, 2001.

[258] H Masjuki, M Z Abdulmuin, and H S Sii. Investigations on preheated palm oil methyl esters in the Diesel engine. *Proceedings of the Institution of Mechanical Engineers, Part A: Journal of Power and Energy*, 210(2):131–138, 1996.

[259] H H Masjuki, M A Kalam, M A Maleque, A Kubo, and T Nonaka. Performance, emissions and wear characteristics of an indirect injection diesel engine using coconut oil blended fuel. *Proceedings of the I MECH E Part D Journal of Automobile Engineering*, 215(3):393–404, 2001.

[260] M Masjuki, A M Zaki, and S M Sapuan. A rapid test to measure performance, emission and wear of a diesel engine fueled with palm oil diesel. *J. American Oil Chemist Society*, 70(10):1021–1025, 1993.

[261] D R McCubbin and M A Delucchi. The social cost of the health effects of motor-vehicle air pollution. Technical report, Institute of Transportation Studies, University of California at Davis, UCD-ITS-RR-96-3(11), 1996.

[262] C S McIntosh, R V Withers, and S M Smith. The economics of on-farm production and use of vegetable oil for fuel. *Proceedings of the International Conference on Plant and Vegetable Oils as Fuels*, 1982.

[263] Mediterranean combustion symposium. *Droplet vaporisation characteristics of vegetable oil derived biofuels*. stituto di ricerche sulla combustione, June 1999.

[264] A D Meister and R E Sims. Production and economics of rapeseed oil and tallow ester as alternative fuels for compression ignition engines. *Energy in Agriculture*, 3(3):223–232, 1984.

[265] L A Melton. Spectrally separated fluorescence emissions for Diesel fuel droplets and vapor. *Applied Optics*, 22(14):2224–2226, 1983.

[266] S S Merola and B M Vaglieco. Analysis on Common Rail Diesel engine combustion process by optical diagnostics, 2004.

[267] Steffen Meyer, Andreas Krause, Dirk Krome, and Günter P Merker. Ein flexibles Piezo-Common-Rail-System mit direktgesteuerter Düsennadel. *MTZ*, 2002.

[268] B H Miles, Paul E Sojka, and G B king. Malvern particle size measurements in media with time varying index of refraction gradients. *APPLIED OPTICS*, 1990.

[269] G A Mills and A G Howard. A preliminary investigation of polynuclear aromatic hydrocarbon emissions from a diesel engine operating on plant oil-based alternative fuels. *Journal of the Institute of Energy*, 56:131–137, 1983.

[270] T Minami. Reduction of Diesel engine NO_x using pilot injection. *SAE*, 1995.

[271] Masahiko Miyaki, Hideya Fujisawa, Akira Masuda, and Yoshihisa Yamamoto. Development of a new electronically controlled fuel injection system ECD-U2 for Diesel engines. *SAE*, 910252, 1992.

[272] N Miyamoto, H Ogawa, K Obata, and G Cao. Improvements of diesel combustion and emissions by addition of oxygenated agents to diesel fuels: influence of properties of diesel fuels and kinds of oxygenated agents. *Technical Notes JSAE Review*, 1998.

[273] Ali Mohammadi, Yoshiyuki Kidoguchi, Kei Miwa, and Tomoyuki Hirose. Effect of Diesel spray impingement on fuel-air mixing process in DI Diesel engines. *SAE*, 1999.

[274] P Monkhouse. Laser diagnostics in a Diesel truck engine. *Proceedings of 6^{th} Conference of Sustainable Energy Marie Curie Research Training Fellowship*, 2000.

[275] A Monyem and J H Gerpen van. The effect of biodiesel oxidation on engine performance and emissions. *Biomass and Bioenergy*, 20(4):317–325, 2001.

[276] R Morgan, M Gold, J Wray, and S Whelan. A study of the formation and break-up of a Diesel spray for HSDI Diesel engine combustion systems. *The Fifth International Symposium on Diagnostics and Modeling of Combustion in Internal Combustion Engines (COMODIA)*, 2001.

[277] R Morgan, J Wray, D A Kennaird, C Crua, and M R Heikal. The influence of injector parameters on the formation and break-up of a Diesel spray. *SAE*, 2001-01-0529, 2001.

[278] C K.M Msipa, C E Goering, and T D Karcher. Vegetable oil atomisation in a DI Diesel engine. *Transactions of the ASAE*, 26(6):1669–1672, 1983.

[279] C Muller, V Michel, G Scacchi, and G M Côme. Thergas: a computer program for the evaluation of thermochemical data of molecules and free radicals in the gas phase. *Journal de chimie physique*, 92(5):1154–1178, 1995.

[280] A Munack, O Schroeder, J Krahl, and J Bunger. Comparison of relevant exhaust gas emissions from biodiesel and fossil Diesel fuel. *Agricultural Engineering International: the CIGR Journal of Scientific Research and Development*, 2001.

[281] T Murayama, Y Fujiwara, and T Noto. Evaluating waste plant oils as a diesel fuel. *Proceedings of the Institute of Mechanical Engineers*, 214(D):141–148, 2000.

[282] Kwang-Jae Myong, Motoyuki Arai, Tomoyuki Tanaka, Jiro Senda, and Hajime Fujimoto. An experimental investigation and numerical analysis of multi-component fuel spray. *JSME International Journal, Series B: Fluids and Thermal Engineering*, 47(2):200–206, 2004.

[283] J D Naber and D Siebers. Effect of gas density and vaporisation on penetration and dispersion of Diesel sprays. *SAE*, 960034, 1996.

[284] K Nagai and T Seko. Trends of motor fuel quality in Japan. *JSAE Review*, -(96-99):1–4, 2000.

[285] N Nagel and P Lemke. Production of methyl fuel from miceoalgea. *Appl. Biochem. Biotechnol.*, 24-25(1):355–361, 1990.

[286] H Nakai, Y Konishi, and A Fukushima. An electronically controlled fuel injection system for new Diesel engines. *Technical Notes/JSAE Review*, 1997.

[287] D A Nehmer. Measurement of effect of rate shaped and split injection on Diesel engine soot and NO_x emissions. *SAE*, 1994.

[288] NewAuthor1 and M A Hanna. Vegetable oil fuels : International conference on plant and vegetable oils as fuels. *ASAE*, 1982.

[289] M Nishida, K Suginuma, A Roppongi, and Y Todo. Advances of engine technology to improve performance and emissions for medium-duty Diesel engine. *SAE*, 1999.

[290] Pornchai Nivesrangsan. *Multi-source, multi-sensor approaches to Diesel engine monitoring using Acoustic Emission*. PhD thesis, Heriot-Watt University, Edinburgh, Scotland, UK, 2004.

[291] Niklas Nordin. *Complex chemistry modeling of Diesel spay combustion*. PhD thesis, Chalmers University of Technology, 2000.

[292] Niklas Nordin. A mesh independent collision condition for lagrangian sprays. Technical report, Thermo and Fluid Dynamics Chalmers University of Technology, 2000.

[293] N Nouguchi, H Terao, and C Sakata. Performance improvement by control of flow rates and diesel injection timing on dual-fuel engine with methanol. *Bioresources Technology*, 56(1):35–39, 1996.

[294] W H Nurick. Orifice cavitation and its effect on spray mixing. *ASME J. Fluids Eng.*, 98:681–687, 1976.

[295] O M Nwafor. Effect of varying fuel inlet temperature on the performance of vegetable oil in a diesel engine under part-load conditions. *International Journal of Ambient Energy,*, 20(4):205–210, 1999.

[296] O M Nwafor. The effect of elevated fuel inlet temperature on performance of diesel engine running on neat vegetable oil at constant speed conditions. *Renewable Energy*, 28(3):171–181, 2003.

[297] O M Nwafor and G Rice. Performance of rapeseed oil blend in a diesel engine. *Applied Energy*, 54(4):345–354, 1996.

[298] O M Nwafor, G Rice, and A I Ogbonna. Effect of advanced injection timing on the performance of rapeseed oil in Diesel engines. *Renewable Energy*, 21(3-4):433–444, 2000.

[299] B Ofner, S Eisen, and F Mayinger. Performance of common-rail fuel injection systems in DI-Diesel-engines. *Proceedings of the 1st International Conference on Engineering Thermophysics (ICET '99)*, 1999.

[300] Hiroyuki Ohnishi, Tetsuya Yoshida, Takatomo Arifuku, and Toshikazu Kadota. Characteristics of fuel discharge in multihole VCO nozzle. *Nippon Kikai Gakkai Ronbunshu, B Hen/Transactions of the Japan Society of Mechanical Engineers*, 1995.

[301] M Okajima, M Kato, H Kano, S Tojo, and M Katagiri. Contribution of optimum nozzle design to injection rate control. *SAE Transactions*, 100(3):232–245, 1991.

[302] P J O'Rourke. *Collective drop effects on vaporising liquid sprays*. PhD thesis, Princeton University, Princeton Univ., Princeton, 1981.

[303] P J O'Rourke. Statistical properties and numerical implementation of a model for droplet dispersion in a turbulent gas. *J. of Computational Physics*, 1989.

[304] Frank A Ortega. *GMV General Mesh Viewer - User's Manual*. Los Alamos, 1995.

[305] M Oschwald, S Bechle, and S Welke. Systematic errors in PIV by realizing velocity offsets with the rotating mirror method. *Experiments in Fluids*, 18(5):329–334, 1995.

[306] F Ossler, S Agrup, and M Alden. Three-dimensional flow visualization with picosecond Mie scattering and streaking-camera detection. *Applied Optics*, 34(3):537–540, 1995.

[307] K Park and A P Watkins. Comparison of wall spray impaction models with experimental data on drop velocities and sizes. *International Journal of Heat and Fluid Flow*, 17(4):424–438, 1996.

[308] S W Park and C S Lee. Macroscopic structure and atomisation characteristics of high-speed diesel spray. *International Journal of Automotive Technology*, 4(4):157, 2003.

[309] Jose V Pastor, Jean Arregle, and Alberto Palomares. Diesel spray image segmentation with a likelihood ratio test. *Applied Optics*, 40(17):2876–2885, 2001.

[310] Jose V Pastor, Jose J Lopez, and Enrique Julia. Planar laser-induced fluorescence

fuel concentration measurements in isothermal Diesel. *Optics Express*, 10(7):309–323, 2002.

[311] M A Patterson. *Modeling the effects of fuel injection characteristics on Diesel combustion and emissions*. PhD thesis, University of Wisconsin-Madison, 1997.

[312] M A Patterson and R D Reitz. Modeling the effects of fuel spray characteristics on diesel engine combustion and emissions. *SAE Transactions*, 107(33):27–43, 1998.

[313] J Pauly, J L Daridon, J M Sansot, and J A Coutinho. The pressure effect on the wax formation in diesel fuel. *Fuel*, 82(5):595–601, 2003.

[314] F Payri, V Bermudez, R Payri, and F J Salvador. The influence of cavitation on the internal flow and the spray characteristics in Diesel injection nozzles. *Fuel*, 83(4-5):419–431, 2004.

[315] F Payri, J M Desantes, and J Arrègle. Characterisation of DI diesel sprays in high density conditions. *SAE*, 960774, 1996.

[316] Francisco Payri, Jose V Pastor, Alberto Palomares, and J Enrique Julia. Optimal feature extraction for segmentation of Diesel spray images. *Applied Optics*, 43(10):2102–2111, 2004.

[317] R Payri, H Climent, F J Salvador, and A G Favannec. Diesel injection system modelling. methodology and application for a first-generation common rail system. *Proceedings of the Institution of Mechanical Engineers, Part D: Journal of Automobile Engineering*, 2004.

[318] L A Perkins, C L Peterson, and D L Auld. Durability testing of transesterified winter rape oil (brassica napus l.) as fuel in small bore, multi-cylinder, dl, cl engines. *SAE Technical Paper Series,International Off-Highway and Powerplant Congress and Expostion*, 1991.

[319] C L Peterson. Plant oils as an agricultural fuel for the Pacific Northwest. Technical Report 598, University of Idaho, AES, 1981.

[320] C L Peterson. Carbon cycle for rapeseed oil biodiesel fuels. *Biomass and Bioenergy*, 14(2):91–101, 1998.

[321] C L Peterson, D L Auld, B L Bettis, K N Hawley, and T J Karsky. Potential use of vegetable oils as a diesel fuel replacement. *Fuel Alcohol USA*, 1982.

[322] C L Peterson, D L Auld, and R A Korus. Winter rape oil fuel for diesel engines: recovery and utilisation. *Journal of JAOCS*, 60(8):1579–1587, 1983.

[323] C L Peterson, M Feldman, R Korus, and D L Auld. Batch type transesterication process for winter rape oil. *Applied Engineering in Agriculture*, 7(6):711–716, 1991.

[324] C L Peterson, B J Hammond, S M Beck, D L Reece, and J Thompson. Processing, characterization and performance of eight fuels from lipids. *ASAE*, 13(1):71–79, 1994.

[325] C L Peterson, D L Wagner, and D L Auld. Vegetable oil substitutes for Diesel fuel. *Transaction ASAE*, 26(2):332, 1983.

[326] Charles L Peterson and Dick L Auld. Technical overview of vegetable oil as a transporation fuel. *FACT, Solid Fuel Conversion for the Transportation Sector, ASME*, 12:45–54, 1991.

[327] Charles L Peterson, Jack Brown, Daniel Guerra, David C Drown, and Russell V Withers. Rapeseed oil as diesel fuel. an overview. *Biodiesel*, 1:916–921, 1992.

[328] S E Plotkin. European and Japanese fuel economy initiatives: what they are, their prospects for success, their usefulness as a guide for US action. *Energy Policy*, 29(13):1073–1084, 2001.

[329] A A Pollock. Classical wave theory in practical AE testing. *Progress in Acoustic Emission III - JAP Society of Non-Destructive Testing*, 1986.

[330] C F Powell, Y Yue, R Poola, J Wang, M C Lai, and J Schaller. X-Ray measurements of high pressure Diesel sprays. *SAE*, 01-0531, 2001.

[331] C M Prasad, M V Krishna, C P Reddy, and K R Mohan. Performance evaluation of non-edible vegetable oils as substitute fuels in low heat rejection diesel engines. *Proc. Instn Mech. Engrs, Part D: J. Automobile Engineering*, 214(2):181–187, 2000.

[332] E H Pryde. Vegetable oil fuel standards. *Vegetable Oil Fuels: Proceedings of the International Conference on Plant and Vegetable Oils Fuels. St. Joseph, MI: ASAE*, 1982.

[333] E H Pryde. Plant oils as diesel fuels: overview. *JAOCS, Journal of the American Oil Chemists' Society*, 1983.

[334] C D Rakopoulos and D T Hountalas. A simulation analysis of a DI diesel engine fuel injection system fitted with a constant pressure valve. *Energy Conver. Mgmt.*, 37(2):135–150, 1996.

[335] Pekka Rantanen, Antti Valkonen, and Andreas Cronhjort. Measurements of Diesel spray with a normal size nozzle and a large-scale model. *International Journal of Heat and Fluid Flow*, 1999.

[336] W Raubold. Thermodynamic analysis of the engine internal process to determine the suitability of vegetable oils as alternative fuels for diesel engines. *Fuel and Energy Abstracts*, 38(2):105–105, 1997.

[337] R D Reitz. Mechanisms of atomization processes in high-pressure vaporizing sprays. *Atomization and Spray Technology*, 3:309–337, 1988.

[338] R D Reitz. Modeling atomization processes in high-pressure vaporizing sprays. *Atomization and Spray Technology*, 3:309–337, 1988.

[339] R D Reitz and F B Bracco. On the dependence of spray angle and other spray parameters on nozzle design and operating conditions. *SAE*, 790494, 1979.

[340] R D Reitz and F V Bracco. *Mechanisms of breakup of round liquid jets. Encyclopedia Fluid Mech.* 1986.

[341] R D Reitz and R Diwakar. Structure of high-pressure fuel sprays. *SAE Paper*, 870598, 1987.

[342] D R Rhim and P V Farrell. Effect of gas density and the number of injection holes on the air flow surrounding non-evaporating transient Diesel sprays. *SAE*, 0532, 2001.

[343] B Rice, A Frohlich, R Leonard, and W Korbitz. Bio-diesel production based on waste cooking oil: Promotion of the establishment of an industry in ireland. Technical Report XVII/4.1030/AL/77/95/IRL, Agriculture and Food Development Authority, September 1997.

[344] P Richards, M W Vincent, and S L Cook. Emissions characteristics of Diesel vehicles equipped with particulate filters and using fuel additive for regeneration. *SAE*, 2000.

[345] J B Riley and Y C Agrawal. Sampling and inversion of data in diffraction particle sizing. *Applied Optics*, 30(33):4800–4817, 1991.

[346] R Rinolfi, R Imarisio, and R Buratii. The potentials of a new Common Rail Diesel fuel injection system for the next generation of DI Diesel engines. In *Internationales Wiener Motorensymposium*, 1995.

[347] D Robart, S Breuer, W Reckers, and R Kneer. Assessment of pulsed gasoline fuel sprays by means of qualitative and quantitative laser-based diagnostic methods. *Particle and Particle Systems Characterization*, 18(4):179–189, 2000.

[348] S Romano. Plant oils - a new alternative, plant oil fuels., August 1982.

[349] R Rotondi, G Bella, C Grimaldi, and L Postrioti. Atomization of high-pressure Diesel spray: experimental validation of a new brekup model, 2001.

[350] G Rottenkolber, K Dullenkopf, and S Witting. Two phase PIV measurements inside the intake port if an IC-Engine. *Proceedings of VSJ-SPIE98*, 1998.

[351] T W Ryan and M O Bagby. Identification of chemical changes occurring during the transient injection of selected vegetable oils. *SAE*, 930933, 1993.

[352] A D Sagar. Automobiles and global warming: Alternative fuels and other options for carbon dioxide emissions reduction. *Environmental Impact Assessment Review*, 15(3):241–274, 1995.

[353] C Sarre von, S C Kong, and R D Reitz. Modeling the effects of injector nozzle geometry on Diesel sprays. *SAE*, 0912, 1999.

[354] S Sazhin, C Crua, D Kennaird, and M Heikal. The initial stage of fuel spray penetration. *Fuel*, 82(8):875–885, 2003.

[355] S S Sazhin, C Crua, and M R Heikal. Fuel spray penetration: modelling and experiments, 2003.

[356] A Schäfer. Pflanzenölfettsäure-Methyl-Ester als Dieselkraftstoffe/Mercedes-Bentz. *Proceedings Symposium Kraftstoffe aus Pflanzenöl für Dieselmotoren*, 1991.

[357] P Schihl, A Atreya, and W Bryzik. Development of a shear layer ignition model for application to direct-injection Diesel engines. *Combustion and Flame*, 121(33):453–470, not known.

[358] M L Schlick, M A Hanna, and J L Schinstock. Soybean and sunflower oil performance in diesel engine. *ASAE*, 31(5):1345–9, 1988.

[359] R Schmehl. Advanced modeling of droplet deformation and breakup for cfd analysis of mixture preparation, 2002.

[360] R Schmehl, G Klose, G Maier, and S Wittig. Efficient numerical calculation of evaporating sprays in combustion chamber flows, 1998.

[361] David P Schmidt and Christopher J Rutland. Reducing grid dependency in droplet collisions modeling. *Journal of Engineering for Gas Turbines and Power*, 127:227255, 2004.

[362] S Schultheis. Vibration analysis of reciprocating compressors. *Orbit*, 6:1–9, 1996.

[363] Leon G Schumacher, William G Hires, and Steven C Borgelt. Fueling diesel engines with methyl-ester soybean oil. Technical report, University of Missouri,Columbia, 1992.

[364] J Senda and H Fujimoto. Multicomponent fuel consideration for spray evaporation field and spray-wall interactions. *SAE*, 1071, 2001.

[365] J Shao, Y Yan, G Greeves, and S Smith. Quantitative characterization of Diesel sprays using digital imaging techniques. *Measurement Science and Technology*, 14:1110–1116, 2003.

[366] Amanda J Sharkey. Condition monitoring, diesel engines, and intelligent sensor processing. *Intelligent Sensor Processing (Ref. No. 2001/050), A DERA/IEE Workshop on*, 6971569:1/1–1/6, 2001.

[367] E G Shay. Diesel fuel form vegetable oils: status and opportunities. *Biomass and Bioenergy*, 4(4):227–242, 1993.

[368] T Shiraisho, M Fujieda, and M Oosuga. Influence of the spray pattern on combustion characteristics in a direct injection engine. *JSAE Review*, 17(4):435–435, 1997.

[369] M Shuster, D Combs, K Karrip, and D Burke. Piston ring cylinder liner scuffing phenomenon studies using acoustic emission technique. *Advances in Powertrain Tribology, SAE,*, 1782(SP-1548), 2000.

[370] Mark J.H. Simmons, Sohial H Zaidi, and Barry J Azzopardi. Comparison of laser-based drop-size measurement techniques and their application to dispersed liquid-liquid pipe flow. *Optical Engineering*, 39:505, 2000.

[371] Brett C Singer, Thomas W Kirchstetter, Robert A Harley, Gary R Kendall, and

James M Hesson. A fuel-based approach to estimating motor vehicle cold-start emissions. *Journal of the Air and Waste Management Association*, 49:125–135, 1999.

[372] S Sinha and N C Misra. Diesel fuel alternative from plant oils. Technical report, Exhibition and Communication Enterprises (India) Pvt Ltd., 1997.

[373] C Scott Sluder, Robert M Wagner, Samuel A Lewis, and John M Storey. High efficiency clean combustion in a Direct-Injection Diesel engine. Technical report, Oak Ridge National Laboratory Fuels, Engines, and Emissions Research Center, 2001.

[374] Gregory J Smallwood and Omer L Gulder. Views on the structure of transient diesel sprays. *Atomization and Sprays*, 10:355–386, 2000.

[375] N O Sonntag. Structure and composition of fats and oils. *Bailey's industrial oil and fat products*, 1979.

[376] S D Sovani, E Chou, P E Sojka, J P Gore, W A Eckerle, and J D Crofts. High pressure effervescent atomisation: effect of ambient pressure on spray cone angle. *Fuel*, 80(3):427–435, 2001.

[377] A Srivastava and R Prasad. Triglycerides-based diesel fuels. *Renewable and Sustainable Energy Reviews*, 4(2):111–133, 2000.

[378] W K Stephens. *Emissions must be cut to avert shift in climate, panel says. In Themes of the Times, a contemporary view of selected subjects from the pages of The New York Times*. Prentice-Hall, 1995.

[379] R K Stobart, A May, B J Challen, and T Morel. New tools for engine control systems development. *Annual Reviews in Control*, 23:109–116, 1999.

[380] K Stork, M Mintz, A Vyas, F Stodolsky, and R Cuenca. Another way to go?-Some implications of a light-duty diesel strategy, 1997.

[381] R C Strayer, J A Blake, and W K Craig. Canola and high erucic rapeseed oil as substitutes for diesel fuel: Preliminary tests. *JAOCS, Journal of the American Oil Chemists' Society*, 60(8):1587–1592, 1983.

[382] R C Strayer, W K Craig, and G C Zoerb. Engine deposit and pour point studies using canola oil as a diesel fuel., 1982.

[383] G Stumpp and M Ricco. Common rail - an attractive fuel injection system for passengers car DI Diesel engines. *SAE*, 960870, 1996.

[384] T F Su, M A Petterson, R D Reitz, and P V Farrell. Experimental and numerical studies of high pressure multiple injection sprays. *SAE*, 960861, 1996.

[385] S Subramaniam and P J O'Rourke. Numerical convergence of the kiva-3 codes for sprays and its implications for modeling. Technical report, Los Alamos National Laboratory, LAUR 98-5465, 1998.

[386] Marek Sutkowski. Private communication.

[387] M Tabata and M Arai. Atomization of high viscosity liquid by a Diesel nozzle. *Bulletin of JSME*, 29(252):1795–1802, 1986.

[388] H Tanaka, A Ando, and K Ishizaka. Study on pilot injection of DI Diesel engine using common-rail injection system. *JSAE Review*, 23:5–8, 2001.

[389] F X Tanner. Liquid jet atomization and droplet breakup modeling of non-evaporating diesel fuel sprays. *SAE,Transactions: Journal of Engines*, 970050, 1997.

[390] F X Tanner, M Brunner, and G Weisser. A computational investigation of water injection strategies for nitric oxide reduction in large-bore di diesel engines. *SAE*, 1069, 2001.

[391] F X Tanner and G Weisser. Simulation of liquid jet atomization of fuel sprays by means of a cascade drop breakup model. *SAE*, 980808, 1998.

[392] Franz X Tanner, Guang Sheng Zhu, and Rolf D Reitz. A turbulence dissipation

correction to the k-epsilon model and its effect on turbulence length scales in engine flows, 2001.

[393] Pertti Taskinen. Modeling of spray turbulence with the modified rng k-epsilon model. Technical report, Energy and Process Engineering, Tampere University of Technology, 2004.

[394] G I Taylor. The shape and acceleration of a drop in a high speed air stream. Technical Report AC 10647/Phys. C69, The Scientific Papers of G. I. Taylor, University Press, Cambridge, 1993.

[395] T Tedjojuwono, T Asakura, and Y Kawase. Measurements of particle number density using the variable fringe-spacing laser Doppler velocimeter. *Applied Optics*, 23(15):2554–2558, 1984.

[396] Paul J Tennison, Thierry L Georjon, Patrick V Farrell, and Rolf D Reitz. An experimental and numerical study of sprays from a Common Rail injection system for use in an HSDI Diesel engine. *SAE Paper*, 980810, 1998.

[397] P Thomas. Canola growers manual. Technical report, Canola Council of Canada, Winnipeg, 1984.

[398] T C Tow. Reduction particulate and NO_x emissions by using multiple injection in a heavy duty DI Diesel engine. *SAE*, 940897, 1995.

[399] Dave P Towers. Private communication. Private communication with D.P.Towers about setting up the PDA system., 2003.

[400] M Tulej, B Bougie, T Dreier, P Beaud, G Knopp, P P Radi, T Gerber, and N J Dam. Investigations of Diesel spray injections under non-reactive and reactive conditions using high pressure high temperature test rig, 2003.

[401] T Ueda, L Zhang, and M Gabe. Improvement of the cold startability of common-rail injection system by pilot injection in a HD Diesel engine. *Proceedings of The 15th Internal Combustion Engine Symposium (International)*, 1999.

[402] N B Vargaftik. *Tables on the Thermophysical Properties of Liquids and Gases*. John Wiley and Sons, 1975.

[403] G Vellguth. Performance of plant oils and their monoesters as fuels for diesel engines. *SAE*, 952061, 1983.

[404] C A Vernavas. Studies of diesel engine combustion using a multidimensional computer simulation. Master's thesis, University of Illinois at Urbana-Champaign, 1990.

[405] T Wakisaka, Y Shimamoto, Y Isshiki, S Akamatsu, and K Ibaraki. Improvement in droplet break-up model for numerical analysis of fuel sprays,. *JASE Review*, 18(1):3–10, 1997.

[406] T Wakisaka, Y Shimamoto, Y Isshiki, and T Noda. Numerical analysis of spray phenomena in fuel injection engines. *International Symposium COMODIA*, 1994.

[407] Y Wakuri, M Fuji, R Amitani, and R Tsumeaya. Studies on the penetration of fuel sprays in a Diesel engine. *Bull. Jap. Soc. Mech. Engrs.*, 3:123–130, 1960.

[408] K C Walker. Biodiesel from rapeseed. *Journal of the RASE*, 155:43–44, 1994.

[409] Kerr C Walker and Werner Korbitz. Rationale and economics of a british biodiesel industry. Technical report, British Association for Biofuels and Oils, January 1994.

[410] M P Walsh. Global trends in diesel emissions control. *SAE*, 0107, 1999.

[411] T C Wang, J S Han, X B Xie, M C Lai, N A Henein, E Schwarz, and W Bryzik. Parametric characterization of high-pressure Diesel fuel injection systems. *Transactions of the ASME*, 125(2):412–427, 2003.

[412] X F Wang and A H Lefebvre. Mean drop size from pressure-swirl nozzles. *Journal of Propulsion and Power*, 3(1):11–18, 1987.

[413] Z W Wang, L S Zhong, and F C Zhuang. Experimental investigation of the spray characteristics of pressure AT, 1994.

[414] J A Weber. The economic feasibility of community-based biodiesel plants. Master's thesis, University of Missouri, Columbia. 108 pp., 1993.

[415] John F Widmann, Cary Presser, and Stefan D Leigh. Improving phase Doppler volume flux measurements in low data rate applications. *Meas. Sci. Technol.*, 12:1180–1190, 2001.

[416] G Wigley, J Heath, G Pitcher, and A Whybrew. Experimental analysis of the response of a PDA system to a partially atomized spray, 2000.

[417] Graham Wigley, Graham K Hargrave, and John Heath. High power, high resolution LDA/PDA system applied to gasoline direct injection sprays. *Particle and Particle Systems Characterization*, 16(1):11–19, 1999.

[418] A M Williamson and O Badr. Assessing the viability of using rape methyl ester (rme) as an alternative to mineral diesel fuel for powering road vehicles in the uk. *Applied Energy*, 59(2-3):187–214, 1998.

[419] M Wilson. Soybeans by the tankful. *Prairie Farmer*, 1993.

[420] Yuri M Wright, Thomas Gerber, Stephan Kunte, Alexios-Paul Tzannis, Thomas Koch, and K Boulouchos. Pflanzenoel-simulationen. Technical report, ETH Zurich, Laboratory for I.C. Engines and Combustion Systems, 2001.

[421] K J Wu, D A Santavicca, and F V Bracco. LDV measurements of drop velocity in Diesel-type sprays. *AIAA Journal*, 22:1263–1270, 1984.

[422] Zhijun Wu, Zhen Huang, and Lijun Hao. An image-shifting technique based on grey-scale classi cation for particle image velocimetry. *Optics and Laser in Engineering*, 2002.

[423] T Yatsufusa, K Nishida, T Yoshizaki, and H Hiroyasu. Spray development and ignition processes under split injection in a DI Diesel model combustion chamber. *Proceedings of The 15th Internal Combustion Engine Symposium (International)*, 1999.

[424] C Yeh and H Z Cummins. Localised fluid flow measurements with a He-Ne laser spectrometer. *Appl. Phys. Lett.*, 4:176–178, 1964.

[425] C Nan Yeh, T Kamimoto, H Kosaka, and S Kobori. Quantitative measurements of 2D fuel vapor concentration in a transient spray via Laser Induced Fluorescence Technique. *SAE Paper*, 103(4):1156–1167, 1994.

[426] J K Yeom. A study of the behaviour characteristics of Diesel spray by using a high pressure injection system with common rail apparatus. *KSME International Journal*, 17(9):1371–1379, 2003.

[427] J Yu and C Bae. Dimethyl ether (DME) spray characteristics in a common-rail fuel injection system. *Proc. Instn. Mech. Engrs. Part D: J. Automobile Engineering*, 217(12):1135–1144, 2003.

[428] J Yu, J Lee, and C Bae. Dimethyl ether DME spray characteristics compared to Diesel in a common-rail fuel injection system. *SAE*, 2898, 2002.

[429] A J Yule, Ah Seng, P G Felton, A Ungut, and N A Chigier. A study of vaporizing fuel sprays by laser techniques. *Combust. and Flame*, 44:71–84, 1982.

[430] Ferial A Zaher, Ola A Megahed, Kinawy El, and S Omayma. Utilization of used frying oil as diesel engine fuel. *Energy Sources*, 25(8):819–826, 2003.

[431] Y Zhang, T Ito, K Nishida, and T Yoshizaki. Quantitative measurement of liquid and vapor phase concentrations in a split injection Diesel spray by processing ultraviolet and visible laser images. *JSAE*, -(61-01):5–8, 2001.

[432] Yuyin Zhang and Keiya Nishida. Effect of injection temporal splitting on the characteristics of fuel-air mixture formation in a common rail Diesel spray. *Proceedings of*

the Institution of Mechanical Engineers, Part D: Journal of Automobile Engineering, 218(3):323–331, 2004.

[433] G S Zhu and R D Reitz. Engine fuel droplet height-pressure vaporisation modelling. *Transactions of the ASME*, 2000.

[434] M Ziejewski, H Goettler, and G L Pratt. Comparative analysis of the long-term performance of a Diesel engine on vegetable oil based alternative fuels. *SAE*, 860301, 1986.

[435] M Ziejewski and H J Goettler. Comparative analysis of the exhaust emissions for vegetable oil based alternative fuels. *Alternative Fuels for CI and SI Engines, SAE*, (900):65–73, 1992.

[436] M Ziejewski and H J Goettler. Design modifications for durability improvements of diesel engines operating on plant oil fuels. *Int. Off-Highway & Powerplant Congress & Exposition SAE*, 921630, 1992.